责任编辑：金　怡　陈丽茹
封面设计：张育智　吴晨迪

南京水利科学研究院

PROCEEDINGS OF PIANC SMART RIVERS 2022

ISBN 978-7-5630-7719-9
定价：189.00元

PROCEEDINGS OF PIANC SMART RIVERS 2022

Yun Li,Yaan Hu,Philippe Rigo,Francisco Esteban Lefler,Gensheng Zhao

河海大学出版社

PROCEEDINGS OF PIANC SMART RIVERS 2022

Chief Editors

Yun Li

Yaan Hu

Philippe Rigo

Francisco Esteban Lefler

Gensheng Zhao

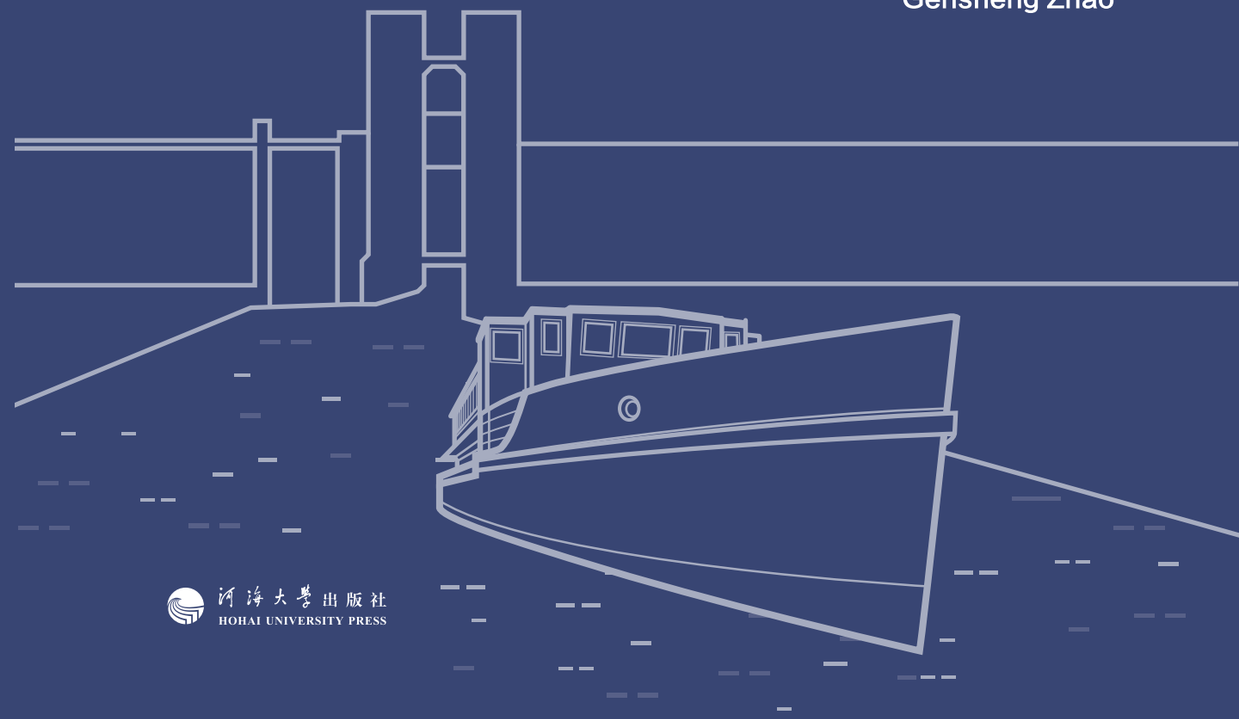

河海大学出版社
HOHAI UNIVERSITY PRESS

PROCEEDINGS OF PIANC SMART RIVERS 2022

Chief Editors

Yun Li

Yaan Hu

Philippe Rigo

Francisco Esteban Lefler

Gensheng Zhao

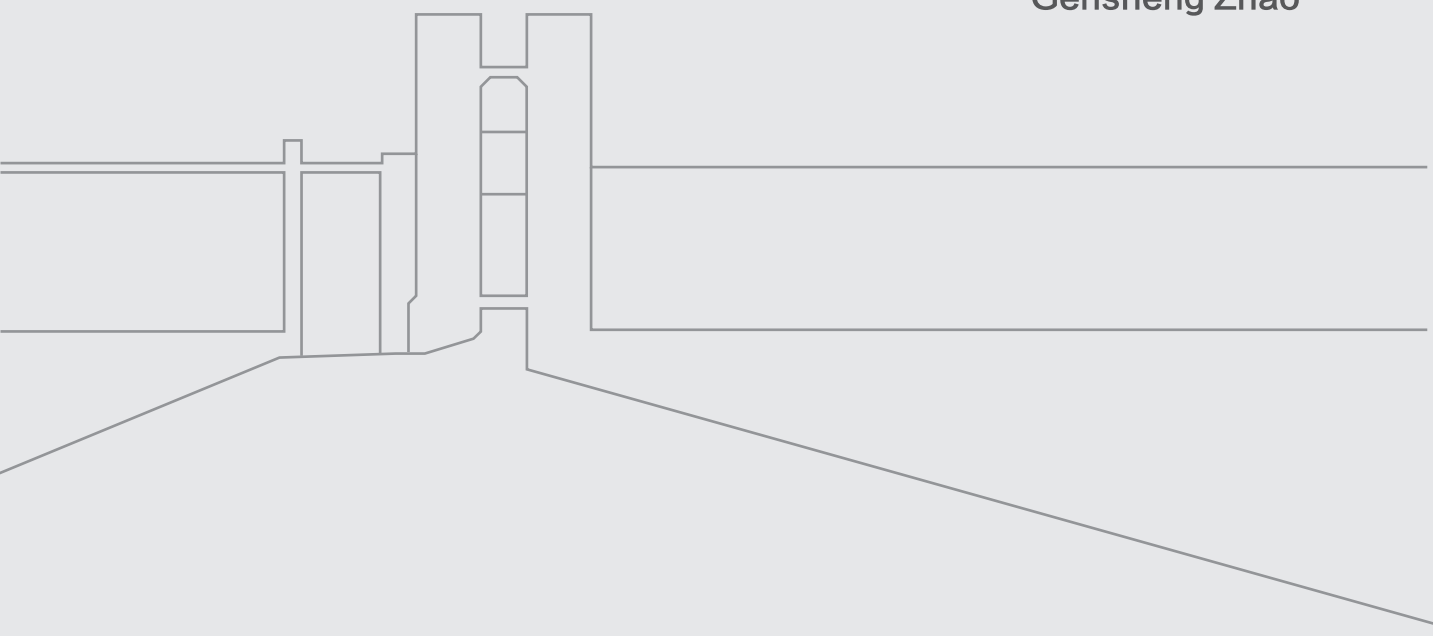

河海大学出版社
HOHAI UNIVERSITY PRESS
·南京·

图书在版编目(CIP)数据

国际航运协会第10届内河航运国际学术会议论文集 = Proceedings of PIANC Smart Rivers 2022 : 英文 / 李云等主编. -- 南京 : 河海大学出版社, 2022.10
ISBN 978-7-5630-7719-9

Ⅰ. ①国… Ⅱ. ①李… Ⅲ. ①内河运输—国际学术会议—文集—英文 Ⅳ. ①U6-53

中国版本图书馆CIP数据核字(2022)第182260号

书　　名	国际航运协会第10届内河航运国际学术会议论文集 Proceedings of PIANC Smart Rivers 2022
书　　号	978-7-5630-7719-9
责任编辑	金　怡　陈丽茹
特约编辑	岳盈娉　杨　洋
特约校对	杨　曦　朱梦媛
封面设计	张育智　吴晨迪
出版发行	河海大学出版社
地　　址	南京市西康路1号(邮编:210098)
网　　址	http://www.hhup.com
电　　话	(025)83737852(总编室)　(025)83722833(营销部)
经　　销	江苏省新华发行集团有限公司
排　　版	南京布克文化发展有限公司
印　　刷	江苏凤凰数码印务有限公司
开　　本	787毫米×1092毫米　1/16
印　　张	27.5
字　　数	886千字
版　　次	2022年10月第1版
印　　次	2022年10月第1次印刷
定　　价	189.00元

Contents

Topic 1
Waterway Infrastructure

Experimental study on discharge capacity of emergency ship lock

Wei Wang[1], Xianzhong Chen[2], Weichun Qiu[3], Honghao Fan[4], Zhongshan Tong

[1] Nanjing Hydraulic Research Institute, Nanjing, China. e-mail: suiningwangwei@163.com
[2] Changshan River Waterway Development and Construction Headquarters, Quzhou, China
[3] Changshan Dingyang Shipping Construction and Development Co., Ltd., Quzhou, China
[4] Dept. of Hydraulic Engineering, Nanjing Hydraulic Research Institute, Nanjing, China. e-mail: 776051686@163.com

Abstract: Emergency ship lock is the first hub building in the construction of Changshan River shipping hub. Its function orientation is: participating in flood discharge in flood season and shipping in dry season. It can effectively solve the layout conflict between flood discharge buildings and shipping projects in the existing flood channel. The emergency ship lock is composed of upper lock head, lock chamber and lower lock head, and the internal shape of the lock is complex. There is no research result on discharge capacity for reference, so the emergency ship lock study should be on its discharge capacity characteristics first, which is directly related to the flood safety of the river in flood season. In this paper, a cross-section model of emergency ship lock with a geometric scale of 1∶30 is established based on a shipping hub in Changshan River. Combined with the existing overall model test data, the discharge capacity and its influencing factors of emergency ship lock are studied, especially the influence of lateral shrinkage and submergence coefficient of emergency ship lock. Through dimensional analysis and multi-parameter optimization, combined with the model test results, the recommended equation of emergency ship lock flow coefficient is given, and the error calculation equation of emergency ship lock flow or water level under different flooding degrees is obtained. The results show that when the upstream water head is small, the discharge increment of emergency ship lock is obvious, and with the increase of upstream water head, the discharge increment of emergency ship lock decreases gradually.

Keywords: Emergency ship lock; Discharge capacity; Submergence coefficient; Flow coefficient

1 Introduction

Channel resources and hydropower resources as important parts of basin water resources development, interact and restrict each other. Setting navigation locks in the

river channel of the navigational river construction hub power station or the built power station will affect the flood discharge safety and flow conditions of the river channel. To solve this problem, Zhejiang Institute of Communications Co., Ltd. and Zhejiang Design Institute of Water Conservancy and Hydro-electric Power Co., Ltd. proposed emergency ship locks in the construction of Changshan River cascade hubs. On the one hand, in order to meet the flood discharge requirements of the hub during the flood season, the emergency ship lock needs to participate in flood discharge. On the other hand, emergency navigation is required in the case of large and medium repair of the lock and accidents. The emergency ship lock chamber is equipped with gate, water conveyance system, drainage and other facilities. The lock chamber is long and the shape is complex. The thickness of weir crest/water head before weir is >10, which is the short channel flow. The traditional calculation equation of weir discharge capacity is difficult to meet the calculation requirements of emergency navigation gate discharge capacity. In this paper, theoretical analysis and physical model test are used to study the discharge capacity of emergency ship lock.

2 Project profile

The layout of the hub project from left to right is: ship lock, emergency ship lock, flood sluice and power station. A total of 17 holes are arranged in flood sluice and sediment flushing sluice, and the net width of single hole is 14 m. The total net width of discharge is the same as that of the scheme, which is still 252 m. The top elevation of the bottom plate of the flood sluice is 66 m, and the top elevation of the threshold of the emergency ship lock is 66 m. The main powerhouse of the power station is arranged on the right side of the sluice. Due to the construction of the ship lock, some rivers are occupied. In order to ensure that the flood section area of the river after the construction of the sluice is roughly equal to that of the original river and to facilitate flood discharge, the power station needs to be properly advanced to the right bank and dredge the downstream right bank beach.

The main length of the emergency ship gate is 221 m, of which the head of the upper lock head is 25 m, the length of the gate chamber is 165 m, the head of the lower lock head is 31 m, and the width of the upper and lower lock heads and gate chamber mouth is 14 m. The upstream approach channel is arranged in an open-type. The right side of the ship lock gate is arranged with a diversion pier, and the right side of the downstream approach channel is arranged with a diversion wall. The length is about 70 m, and the net width of the approach channel is 14 – 20 m.

3 Experimental design

The emergency ship lock section model adopts the normal model with geometric scale of 1∶30 and is designed according to F_r similarity criterion. The upper, chamber and lower heads of emergency navigable gates are all made of organic glass. The roughness of organic glass is 0.008,0, and it is converted to the prototype at about 0.014,1 according to the resistance similarity, which basically meets the requirements of resistance similarity. For the convenience of observation, the emergency ship lock section model was tested in glass flume.

In order to ensure the inflow similarity, the upstream topography of emergency navigable lock section model is simulated to about 150 m before the entrance of emergency ship lock, and the downstream topography is simulated to about 180 m downstream of emergency ship lock, so as to meet the requirements of stable similarity of upstream and downstream flow. The model consists of water supply system, water measurement control system, model test section, and water return system. The flow rate is measured by standard rectangular weir; water level measuring points S1 and S2 are measured by water level measuring needle, and the accuracy is 0.1 mm. In order to ensure the accuracy of the test data, the test was repeated several times. For the section model layout diagram, see Fig.1.

4 Analysis on discharge capacity of emergency ship lock

The emergency ship lock is composed of upper lock head, lock chamber and lower lock head, and the internal shape of the lock is complex. There are many factors that affect the emergency ship lock. The main geometric dimensions include the width B of the upstream weir, the length L of the weir body along the flow direction, the height P of the weir body, and the form of the weir crest. The factors that affect the discharge capacity include the total water head H_0 on the weir, the water depth h_s behind the weir, the gravity acceleration g, the flow velocity U, and the density ρ of water. The functional relationship is Eq. (1).

Eq. (2) can be obtained by the π law of the scaling analysis method.

Assuming $f_3\left(\frac{B}{P},\frac{L}{P},\frac{h_s}{H_0}\right)=m_1$ is the comprehensive flow coefficient, it can be seen that the flow coefficient is a function of $\frac{B}{P},\frac{L}{P}$ and $\frac{h_s}{H_0}$, and $\frac{h_s}{H_0}$ is the ratio of the water depth behind the weir to the water head before the weir, which is called the

submergence degree. Fig. 2 shows the relationship curve between the submergence degree and the comprehensive flow coefficient fitted according to the experimental data. Eq. (5) is the formula of inundation and comprehensive flow coefficient obtained by fitting test data. It can be seen from Fig. 2 that when $\frac{h_s}{H_0} < 0.70$, $0.461,0 \leqslant m_1 \leqslant 0.467,8$, the comprehensive flow coefficient m_1 changes little with $\frac{h_s}{H_0}$, and the maximum comprehensive flow coefficient of emergency navigation lock is about $0.467,8$; when $\frac{h_s}{H_0} > 0.80$, the comprehensive flow coefficient m_1 changes greatly with $\frac{h_s}{H_0}$. Assuming that $\frac{h_s}{H_0} < 0.70$, $m_1 = 0.464$, $Q = 0.464B\sqrt{g}H_0^{\frac{3}{2}}$, the maximum error between the calculated value of Eq. (7) and the experimental value is about 0.8%. Therefore, when the submergence after the emergency navigation ship lock is less than 0.70, the flow coefficient can be calculated as 0.464.

Let $m_2 = \frac{\sqrt{2}}{2} m_1 = m\sigma\varepsilon$, σ be submerged coefficient, ε be coefficient of side contraction and m be flow coefficient. According to the empirical equation (Eq. (9)) recommended by *Hydraulics*, when the water depth is shallow and the flow velocity approaches 0, the coefficient of side contraction and submerged coefficient approaches 1, $\frac{\sqrt{2}}{2} m_1 = m$, and the maximum flow coefficient m is 0.331. Assuming $m = 0.331$, the equation for calculating the submerged coefficient of emergency navigable lock is shown in Eq. (8).

Fig. 3 is the relationship between $\frac{h_s}{H_0}$ and comprehensive flow coefficient m_1 of emergency navigable ship lock section model and overall model. Fig. 3 shows that the comprehensive flow coefficient m_1 of emergency navigable ship lock section model is greater than that of the unitary model. The unitary model of emergency navigable ship lock and the section model of emergency navigable ship lock are the same, the flow coefficient m and the coefficient of submergence σ of the unitary model and the section model of emergency navigable ship lock are the same, and the coefficient of side contraction of the emergency navigable ship lock section is greater than that of the unitary model.

5 Using the template for several components

5.1 Equations

$$f_1(B,L,P,H_0,h_s,g,U,\rho) = 0 \tag{1}$$

$$f_2\left(\frac{B}{P},\frac{L}{P},\frac{h_s}{H_0},\frac{g\,H_0}{U2}\right)=0 \tag{2}$$

$$U=\sqrt{gH}f_3\left(\frac{B}{P},\frac{L}{P},\frac{h_s}{H_0}\right) \tag{3}$$

$$Q=B\sqrt{g}H_0^{\frac{3}{2}}f_3\left(\frac{B}{P},\frac{L}{P},\frac{h_s}{H_0}\right) \tag{4}$$

$$m_1=0.467,8-1.57\times10^{(-6)}\times e^{(12.44\frac{h_s}{H_0})} \tag{5}$$

$$Q=(0.331-0.708\times10^{(-6)}\times e^{(12.44\frac{h_s}{H_0})})B\sqrt{2g}H_0^{\frac{3}{2}} \tag{6}$$

$$Q=0.461B\sqrt{g}H_0^{\frac{3}{2}}\ ,\quad \frac{h_s}{H_0}<0.70 \tag{7}$$

$$\sigma=1-2.14\times10^{(-6)}\times e^{(12.44\frac{h_s}{H_0})} \tag{8}$$

$$\varepsilon=1-0.2[(n-1)\zeta_0+\zeta_k]\frac{H_0}{nb} \tag{9}$$

5.2 Figures

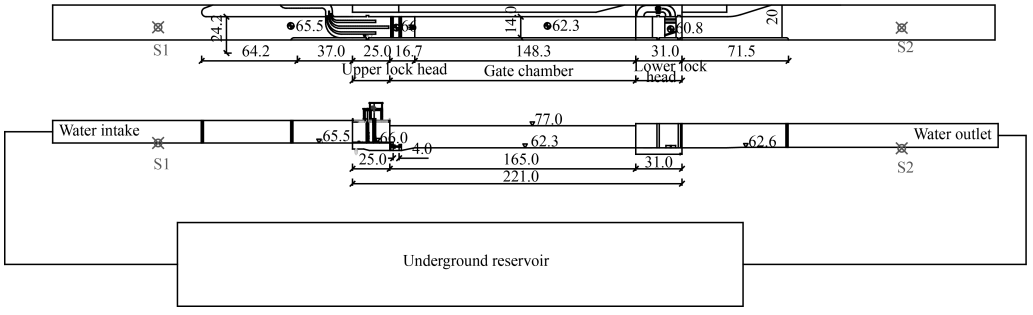

Fig. 1. Section model layout diagram.

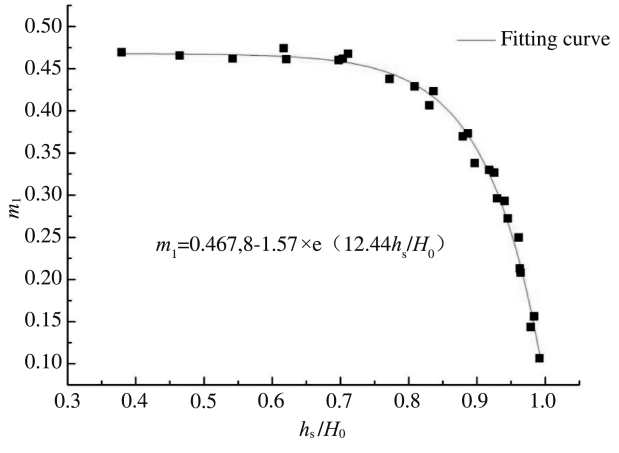

Fig. 2. Relationship between the submergence degree and the comprehensive flow coefficient.

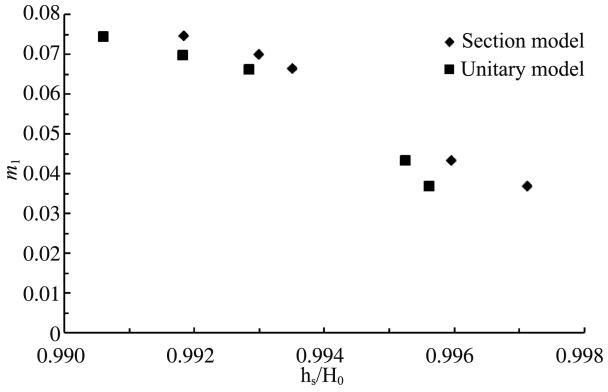

Fig. 3. The relationship between h_s/H_0 and comprehensive flow coefficient m_1 of emergency navigable ship lock section model and unitary model.

5.3 Footnotes

In this paper, H_0 is the total head in front of emergency navigable lock ship, h_s is the water depth behind the weir of emergency navigable lock ship. m_1 is the comprehensive flow coefficient. ζ_0 is pier coefficient. ζ_k is side pier coefficient. n is number of sluices.

6 Conclusion

In this paper, the normal physical model with a geometric scale of 1∶30 is established based on a shipping hub in Changshan River. The results show that comprehensive flow coefficient is related to submergence and the coefficient of submergence. when $\frac{h_s}{H_0} < 0.70$, the comprehensive flow coefficient m_1 changes little with $\frac{h_s}{H_0}$, and the maximum comprehensive flow coefficient of emergency navigation lock is about 0.467 8; when $\frac{h_s}{H_0} > 0.80$, the comprehensive flow coefficient m_1 changes greatly with $\frac{h_s}{H_0}$. Therefore, when the submergence after the emergency navigation ship lock is less than 0.70, the flow coefficient can be calculated as 0.464.

Acknowledgements

Thanks for the project support provided by Changshan River Waterway Development and Construction Headquarters.

Reference

Zhejiang Institute of Communications Co.,Ltd. and Zhejiang Design Institute of Water Conservancy and Hydro-electric Power Co.,Ltd. Feasibility study report of Changshan River (Huibu-Shuanggang) navigation and power hub project.

Nanjing Hydraulic Research Institute. Model test of the Changshan River shipping project in the upper reaches of Qujiang River—Report on the results of physical model test of Zhaoxian Hub.

Peng X.M., Cui G.T., Jia S. B. Study on discharge capacity of labyrinth weir. Journal of Tianjin University,2003,36(6):727-730.

Guo X.L.,Yang K. L.,Xia Q.F.,et al. Discharge capacity characteristics of Piano Key weir. Journal of Hydraulic Engineering,2014,45(7):867-882.

Li J.X., Zhao Z. X. Hydraulics. Nanjing: Hohai University Press,2001:14-23.

Planning studies on inland waterway in Tianjin

Yanhua Yang[1], Jing Qu[2], Huaguo Li[3],
Mingjin Zhang[4], Huaqian Qiao[5]

[1,2,3,4,5] Tianjin Research Institute for Water Transport Engineering, Tianjin, China. e-mail: kaixinqujing@sina.com

Abstract: As the main sea gate of the river systems in the Beijing-Tianjin-Hebei region and even in North China, Tianjin is rich in inland river resources and has the basic conditions to realize the coordinated development of marine transportation and inland river transportation. Due to the limitation of water resources and the rise of transportation methods such as roads and railways, the inland waterway in Tianjin has been suspended for several years, and the development space of inland water transportation has not been considered during the construction of some bridge facilities. Compared with inland waterways in other regions, there are more restrictive factors for inland waterways in Tianjin. Considering the water resources conditions and the facilities that obstruct navigation, the functional orientation, development direction and planning layout of the inland waterway in Tianjin is re-examined. This paper conducts the planning studies on inland waterways in Tianjin, and starting from the development history of inland waterway shipping in Tianjin and the current conditions of inland waterways, combined with the conditions of hydrology and water resources, the ideas, goals and framework plans for the development of inland navigation in Tianjin are studied. By sorting out all the river channels in Tianjin, comprehensively considering the water resources conditions, the situation of obstruction facilities, and the results of regional navigation requirements, 10 inland water channels in Tianjin are proposed, with a total length of 451 km. The research in this paper is helpful to clarify the status quo of inland waterway resources in Tianjin, and plays an important supporting role in the protection of inland waterway resources in the future.

Keywords: Tianjin; Inland river; Waterway; Navigation; Planning

1 Introduction

Tianjin is located in the northeastern part of the North China Plain, with the Bohai Sea in the east and the Yanshan Mountain in the north. With the relatively low terrain, the basin is a typical fan-shaped Haihe River system, where many rivers merge into the sea, which is called "the lower tip of the nine rivers" (Ding et al., 2016; Ren, 2015). Tianjin is prosperous because of water transportation. In the

1960s, there were 14 navigable rivers in Tianjin, with a navigable mileage of 555 km, and a 3,000-ton seagoing vessel could go directly under the Jiefang Bridge.

Affected by the limitation of the water resources of Haihe River (Wang et al., 2015) and the rise of roads, railways and other transportation methods, the waterway in Tianjin has been suspended for several years, and the original planning level has been greatly controversial in urban construction. With the acceleration of construction in Tianjin, in the construction of some bridge facilities the reserved space for the development of inland water transportation was not taken into account, causing damage to the inland waterway.

From the geographical location of Tianjin, as the main sea gate for river systems in the Beijing-Tianjin-Hebei region and even in North China(Su et al., 2016; Xu et al., 2019; Zang et al., 2017), Tianjin has the basic conditions to realize the coordinated development of marine transportation and inland water transportation. At the same time, Daqing River and Duliujian River can directly connect with Xiong'an New Area, which is very important for promoting the development and construction of cultural belt of the Grand Canal (Chen et al., 2018; Liu et al., 2019) and the Xiong'an New Area. Therefore, it is necessary to re-examine the functional positioning, development direction and planning layout of Tianjin inland waterway.

2 Current status of inland waterways in Tianjin

2.1 Current status of the riverway

There are many river systems in Tianjin, which is known as "the lower tip of the nine rivers". There are 19 flood channels (1,100 km) and 109 main drainage channels (1,896 km), and Tianjin's water area reaches 1,256 km^2. The river network is densely distributed, and the inland river resources are rich.

Tianjin is located in the Haihe River Basin. The main stream of the Haihe River is 73 km long from below the Jingang Bridge. There are five major tributaries including the North Canal, Yongding River, Daqing River, Ziya River, and South Canal in the upper reaches, and more than 300 large tributaries extending in all directions, starting from the Taihang Mountains in the west, leaning on the southern edge of the Inner Mongolia Plateau in the north, and spanning Beijing, Tianjin, Hebei, Shanxi, Shandong, Henan, Liaoning and Inner Mongolia.

The whole territory of Tianjin is located in the Haihe River Basin, accounting for 3.73% of the total area of the basin. According to the river system division principle of the Haihe River Basin, Tianjin is divided into six river systems in the Haihe River

Basin, namely Beisan River, Yongding River, Daqing River, the main stream of Haihe River, South Zhangwei Canal and Heilonggang-Yundong area. Among them, the Beisan River system includes three main rivers, i.e. the North Canal, the Chaobaixin River and the Jiyun River, with the drainage area of 6,745 km^2 in Tianjin; the northern part of the Yongding River system is bounded by the Beisan River system, and the southern part is connected with the Daqing River system and the main stream of the Haihe River, with the drainage area of 327 km^2 in Tianjin; the northern part of the Daqing River system is bounded by the Yongding River system and the main stream of the Haihe River, and the southern part is connected with the Heilonggang-Yundong area system, with drainage area of 2,783 km^2 in Tianjin; the northern part of the main stream system of the Haihe River is connected with the Yongding River system, and the west and south parts are connected with the Daqing River system, all within the territory of Tianjin, with drainage area of 2,012 km^2; the main channel of the South Zhangwei Canal is not in Tianjin except the South Canal, 44 km from Jiuxuan Gate to the Eleventh Port, and the Machangjian River, 40.3 km from Jiuxuan Gate to Wanjia Wharf, with drainage area of 8 km^2; the north of the Heilonggang-Yundong area system is bounded by the right embankment of the Ziyaxin River and is connected with the Daqing River system, and the south is bounded by the city, with drainage area of 45 km^2.

2.2 Current status of waterway class

In October 1999, the Ministry of Communications, the Ministry of Water Resources and the State Economic and Trade Commission decided to approve the Classes Ⅰ to Ⅳ waterways in inland rivers of China, excluding the rivers in Tianjin. In 1999, the provincial people's governments and the competent transportation departments completed the examination and approval of Classes Ⅴ-Ⅶ waterways and other waterways beyond classes respectively. According to "The Reply of the Tianjin Municipal People's Government on Approving the Designation of Daqing River and Other Inland Waterways as Class Ⅵ Inland Waterways", the technical classes of Tianjin North Canal, Daqing River, Ziya River and Xinkai Jinzhong River are determined to be Class Ⅵ. In 2002, the Ministry of Transport began to investigate the national inland waterways, and released "The Second National Inland Waterway Census Atlas" in 2005, including 8 inland waterways in Tianjin, with total length of 412 km. In 2013, the State Council approved "The Comprehensive Plan for the Haihe River Basin (2012—2030)", which proposed that the Beijing-Hangzhou Canal and the main stream of the Haihe River should be used as the skeleton with other waterways as supplement, in-

cluding five inland waterways in Tianjin, with total length of 338 km. Based on the above three documents, the current waterway management in Tianjin covers all the above-mentioned planning areas, involving a total of 8 rivers with total mileage of 560 km, as shown in Table 1.

Table 1 Current class of major inland waterways in Tianjin.

S/N	River name	Starting and ending points	Class
1	Haihe River	Jingang Bridge to Guanghua Bridge	Class Ⅵ
		Guanghua Bridge to Erdao Gate	Class Ⅳ
		Erdao Gate to Damp Proof Gate	Class Ⅲ
2	Jizhou Canal	Jiuwangzhuang to Jingshan Railway Bridge	Class Ⅵ
		Jingshan Railway Bridge to Beitang	Class Ⅳ
3	Xinkai Jinzhong River	Erdao Gate to Jinzhong River Gate	Class Ⅵ
4	North Canal	Qujiadian to Sancha River Mouth	Class Ⅵ
5	Daqing River	Taitou to the Sixth Port	Class Ⅵ
6	Ziya River	Xiaohe Gate to Jingang Bridge	Class Ⅵ
7	South Canal	Jiuyi Gate to the Eleventh Port	Class Ⅲ
8	Machangjian River	Jiuyi Gate to Wei Gate	Class Ⅲ

2.3 Current status of waterway transportation in Tianjin

Tianjin inland passenger transport currently only retains the navigation function for short-distance tourism, involving the Haihe River and the Ziya River. Among them, the sections from Jingang Bridge to Lishunde Wharf (6 km) and from the Ziya River Yangliuqing Wharf to Sancha River Mouth in the upper reaches of the Haihe River are open to seasonal tourism, and the section from the Bund Park to Xingang Ship Lock in the lower reaches of Haihe River is open to tourism throughout the year.

As of the end of 2018, there were 17 cruise ships with 1,566 seats in Haihe River. Among the Haihe River cruises, the passenger capacity of a single cruise is 30 passengers at the minimum and 200 passengers at the maximum. Among the 17 operating ships, the proportion of medium-sized ships with 60-90 passengers is the highest. Since 2010, the total number of tourists received has reached nearly 5.3 million, which has increased from 388,000 in 2010 to 872,900 in 2018, with an average annual increase of more than 10% (Table 2). For Haihe River cruise scenery, see Fig. 1.

Table 2 Tourist reception of Haihe River cruises.

Year	2010	2011	2012	2013	2014	2015	2016	2017	2018
Number of people(10,000)	38.80	42.03	44.80	50.10	54.60	62.00	67.00	84.00	87.29

Fig. 1. Haihe River cruise scenery.

2.4 Analysis of navigation obstruction facilities

In 2017, the national per capita water resource was 2, 074.5 m^3, while the water resources in Beijing-Tianjin-Hebei region and North China were only 7% of the national level, even lower than that in the Middle East. Tianjin's per capita water resources are the lowest in China at 83.4 m^3. At present, the main rivers in the Haihe River Basin are facing serious dry-off, and the average annual dry days of the main rivers are close to 200 days. A large number of sluices and dams have been built in the Haihe River Basin to block the incoming water as much as possible to ensure the demand for water for production and domestic use, which has caused great difficulties for navigation. According to the survey data and the actual measurement data of the hydrological station, many rivers in Tianjin are even in a dry state before the rainy season in May, or just preserve the water volume of the urban landscape. Due to the shortage of water resources, there are many sluices and dams obstructing navigation on the rivers in Tianjin. Taking the Haihe River as an example, there are 5 bridges that obstruct navigation along the rivers above the Erdao Gate of the Haihe River.

3 Research on waterway planning scheme in Tianjin

3.1 Regional development requirements

The Tianjin section of the Grand Canal is an important area connecting the north and south of the Grand Canal. It starts from Muchang Gate in Wuqing District in the north to Jiuxuan Gate in Jinghai District. The total riverway length in Tianjin is about 181 km. Starting from Tianjin, it can directly reach the sub-center of Tongzhou District in Beijing in the north, and connect Beijing with the provinces along the Grand Canal such as Hebei and Shandong in the south. After the establishment of the

Xiong'an New Area in 2017, Tianjin Port has become the most convenient outlet for the Xiong'an New Area. The route consisting of Daqing River and Duliujian River can directly connect Xiong'an New Area and Tianjin Port. This route can become an important part for serving the Xiong'an New Area. Therefore, the development of inland waterway shipping in multiple rivers in Tianjin can further enrich the coordinated development of Beijing-Tianjin-Hebei region and realize the coordinated connection of various transportation modes.

3.2 Planning principles

Compared with inland waterways in other regions, there are more restrictive factors for inland waterways in Tianjin. Considering the water resources conditions and the facilities that obstruct navigation, the principles for formulating the waterway planning scheme in Tianjin are put forward as follows:

(1) Judging from the water source conditions of the basin, the conditions for large-scale restoration of inland waterway shipping are not available in the near future.

(2) From the perspective of inland water transportation demand, Tianjin inland water transportation is only suitable for medium and long-distance transportation of large-volume and low-time-sensitive materials close to the river in terms of freight transportation and mainly suitable for short-distance tourism and other recreational water transportation activities in terms of passenger transportation.

(3) In terms of geographical location, Tianjin is still the inland water transportation hub in North China. From the perspective of protecting the amount of waterway resources, the main inter-provincial waterway shipping functions will be retained and the resumption of navigation will be gradually realized when conditions permit.

3.3 Planning scheme

Tourism navigation should take the national promotion of the protection, inheritance and utilization of the Grand Canal culture and the development and construction of the Xiong'an New Area as an opportunity to speed up the construction of tourism infrastructure, improve the quality of waterfront space, and further enhance the popularity of Tianjin inland tourism in the domestic tourism market. Freight navigation needs to be combined with the construction progress of Beijing Tongzhou Sub-center and Xiong'an New Area, meet the upper-level strategic requirements, scientifically and comprehensively evaluate the relationship between the capital investment of cargo shipping and external benefits, limitedly develop important segments and wharf ancillary facilities with high value, and get the most out of investment to serve the social

and economic development of the Beijing-Tianjin-Hebei region.

By sorting out all the river channels in Tianjin, comprehensively considering the water resources conditions, the situation of obstruction facilities, and the results of regional navigation requirements, 10 inland water channels in Tianjin are proposed, with a total length of 451 km. The specific channel mileage is shown in Table 3.

Table 3 Tourist reception of Haihe River cruises.

S/N	Channel name	Starting and ending points	Mileage(km)	Planning class	Functional orientation
1	Haihe River	Jingang Bridge to Guanghua	8	Class Ⅵ	Tourism
		Guanghua Bridge to Erdao Gate	26	Class Ⅵ	Tourism
2	Jizhou Canal	Beitang to Jinshan Railway Bridge	21	Class Ⅵ	Tourist transportation
		Jinshan Railway Bridge to Jiuwangzhuang	131	Class Ⅵ	Tourist transportation
3	Daqing River	Taitou to the Sixth Port	15	Class Ⅲ	Cargo-based, long-term development of tourism transportation
4	Duliujian River	The Sixth Port to Damp Proof Gate	69.8	Class Ⅲ	Cargo-based, long-term development of tourism transportation
5	Ziya River	Xiaohe to the Sixth Port	47.2	Class Ⅵ	The upstream of the Sixth Port is the inter-provincial waterway
		The Sixth Port to Jingang Bridge	28.8	Class Ⅵ	Tourism-based
6	Xinkai Jinzhong River	Erdao Gate to Jinzhong River Gate	37	Class Ⅵ	Urban landscape river-way
7	Yongdingxin River	Qujiadian to Damp Proof Gate	67	Class Ⅵ	Freight transport
8	North Canal	Muchang Gate to Beihekou	89.8	Class Ⅵ recommended	Obey the national inland waterway planning
9	South Canal	Wangshanzheng to the Eleventh Port	44	Class Ⅵ recommended	Obey the national inland waterway planning
10	Heilonggang River	Donggang Gate to the Eighth Control Gate	36	Class Ⅵ recommended	Obey the national inland waterway planning
11	Chaobaixin River	Zhangjiazhuang to Ningchegu Damp Proof Gate	81	Class Ⅵ	Tourism-based
12	Jintang Canal	Zaojia Ship Lock to Qinglongwan Old Road	22.5	Class Ⅵ	Tourism-based

References

Chen, Y., Yan, J., 2018. Research and protection of the settlement pattern of San-

chahe estuary canal in Tianjin. Huazhong Architecture(3): 105-108.

Ding, Y.K., Zhang, H., Shang, B.,2016. The spatial distribution and evolution trend of rivers in Hai River Basin. Acta Scientiae Circumstantiae, 36(1): 47-54.

Liu, Y.T., Yang, W.C., Yang, L., et al.,2019. Practical exploration of water ecological restoration and protection in the North Canal Watershed. Beijing Water (3): 57-62.

Ren, Y.L.,2015. Remediation of Haihe River and remodelling of Tianjin's urban environment in modern times. Fujian Tribune, The Humanities & Social Sciences(5): 94-99.

Su, Z.D., Shang, Y.,2016. Tianjin "coast outlet" effect under the background of Beijing-Tianjin-Hebei economic integration—concurrent discuss of the role of Tianjin free trade zone of promoting coordinated development of Beijing, Tianjin and Hebei. Journal of International Trade(10): 108-118.

Wang, C.S., Chen, R., 2015. Haihe conservancy and temporal-spatial variation of the channel in modern times. Acta Scientiarum Naturalium Universitatis Pekinensis, 51(6): 1141-1148.

Xu, Y., Zhao, B.Y.,2019. Business environment optimization measures of Tianjin port—from the perspective of Beijing-Tianjin-Hebei cooperative development. China Business and Market, 33(5): 30-37.

Zang, X.Y., Wang, K.Y.,2017. Path of promoting the urban function of Tianjin under the framework of coordinated development strategy of Beijing, Tianjin and Hebei. Theory and Modernization(4): 19-26.

Research on lock health monitoring based on 3D laser scanning technology

Fang Cheng[1,2]

[1] Nanjing Hydraulic Research Institute, Nanjing, China;

[2] College of Water Resources and Hydropower, Hohai University, Nanjing, Jiangsu, China. e-mail: fangcheng9804@foxmail.com

Abstract: As a navigable building, the locks bear an important task in shipping, and their operation safety issues are related to the shipping function of the river basin. In complex waters, the opening and closing of the lock herringbone gate is frequently affected by a variety of vibration sources, the stress concentration phenomenon and the impact of the passing ships on the lock during the navigation process will have a damaging impact on the lock structure; when the bottom plate of the lock is impervious to the bottom plate, the lock as a water barrier building will have seepage phenomenon, and the water transmission system that transmits water to the pilot channel of the lock will also leak; the lock is a discontinuous navigable building, and the silt accumulation makes the mouth of the lock not reach the draft depth of the ship, causing the ship to stop navigation, and traffic bottlenecks will be formed. The above three situations will lead to a decrease in the navigability of the locks, so in order to ensure the safe, stable and orderly navigation of the locks, the use of three-dimensional laser scanning technology to monitor the structural state of the locks in real time, can quickly and clearly obtain data, process the data and then reconstruct the data in three dimensions, intuitively judge the operating state of the locks according to the reconstruction model, and use the evaluation theory to analyze and evaluate the safety of the locks, providing a reference for the health monitoring and analysis of the locks. It has high engineering application value.

Keywords: Locks; Health monitoring; 3D scanning technology

1 Introduction

As an important part of the integrated transportation system, inland waterways not only play their basic role, but also play an important role in promoting the development of modern industry and agriculture, improving people's lives, promoting economic transformation and promoting cultural exchanges. At present, the state monitoring methods for locks generally include manual detection, stress deformation moni-

toring and vibration monitoring. Manual testing is measured by manually using the traditional tools, mainly including inspection and visual inspection. Stress deformation monitoring mainly uses strain sensors to monitor the bearing capacity and deformation of the structure in real time. Vibration monitoring mainly uses acceleration sensors to monitor the real-time vibration of the gate, and the method monitors a single amount. There is a certain error in manual detection, and it cannot be monitored in real time.

Guided by finite element analysis and based on vibration monitoring, Wang Xianlong developed a monitoring method for multi-sensor information fusion. In practical engineering applications, it is proved that the system can grasp the operating status of the gate in real time.

Based on the technical advantages of distributed optical fiber sensing in the monitoring of large-scale engineering structures, it is applied to the safety and health monitoring of the hydraulic structure of the lock, and the stress and strain process of the internal concrete and steel reinforcement of the lock head structure under the dual action of the heat release process of concrete hydration and the upper load are analyzed according to the monitoring data, and the feasibility of distributed optical fiber sensing technology in the safety monitoring of the lock is verified.

Chen Minghua solves the structural damage and accumulation damage caused by the long-term operation of the lock herringbone gate, and proposes a remote real-time monitoring technology scheme for the health status of the lock herringbone based on optical fiber Bragg grating. Solve the drawbacks of regular suspension of navigation for manual maintenance.

Many scholars have introduced modern measurement technology into the health monitoring of locks to solve the errors and drawbacks of traditional manual monitoring methods. The three-dimensional laser scanning technology provides a new method and means for the acquisition of space three-dimensional information, and its measurement and acquisition data has high accuracy, fast speed, simple and convenient operation, and has great efficiency and cost advantages. Three-dimensional laser scanning technology is widely used in civil engineering, construction and other industries, but the application of lock health monitoring is still in its infancy. Research and promotion of three-dimensional laser scanning measurement technology in the application of lock health monitoring will help promote the daily health monitoring of locks to information, intelligent development.

2 Three-dimensional laser scanning technology

2.1 Fundamentals of 3D laser scanning technology

The components of the 3D laser scanning system can be simply considered to be composed of three main parts, the first is the laser emitting device; the second is the light source receiving device; and the third is the rotation device that controls the direction of the laser. As shown in Fig. 1 below, the simple scanning principle of the three-dimensional laser is described. The 3D laser scanning system itself exists in this spatial coordinate system, with the center of the scanner as the coordinate origin, and then specifies the direction of the X axis, Y axis, and Z axis, which are perpendicular to each other. There is a laser ranging principle, you can quickly obtain a certain position on the target object P and the distance L to the instrument, and then through the internal calculation of the instrument you can get the lateral scanning angle alpha and vertical scanning angle beta, through Eq. (1) you can get the three-dimensional coordinates of the P point.

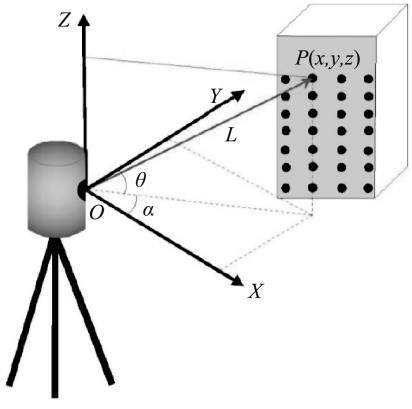

Fig. 1. Principles of 3D laser scanning.

$$\begin{cases} X = L\cos\theta\cos\alpha \\ Y = L\cos\theta\sin\alpha \\ Z = L\sin\theta \end{cases} \tag{1}$$

The three-dimensional laser scanner adopts the TOF (Time of Flight) pulse ranging method, which is the main ranging method for the current three-dimensional laser scanner. The distance to the target is obtained indirectly by measuring the time difference between the emission and reception of the laser pulse signal. As shown in Fig. 2 below, the laser transmitter emits a pulse signal to the target, reaches the re-

ceiving system after diffuse reflection of the target, sets the measurement distance to S, the speed of light is c, and the time difference between the measured laser signal and the round-trip propagation is Δt , then there is: $S = c\Delta t/2$. At the same time, the laser scans up and down from left to right to obtain a series of data.

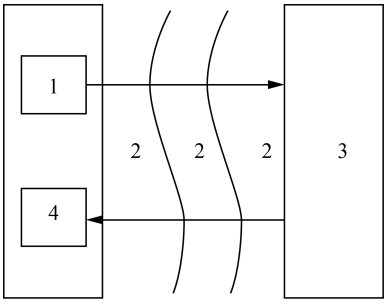

(1— Scanner emits laser pulse signal system; 2— Propagates the medium atmosphere; 3— Target under test; 4— Scanner receives laser pulse signal system)

Fig. 2. Schematic diagram of laser pulse ranging.

2.2 3D laser scanner technology advantages

Compared with traditional monitoring methods, 3D laser scanning technology is faster (more efficient), higher (high precision) and stronger (non-contact, all-weather operation), and has a wider range of applications. 3D laser scanning technology offers the following advantages:

(1) High efficiency

Traditional measuring instruments can only measure one data point at a time, which makes them cumbersome and time-consuming. 3D laser scanning, as the laser moves on an object or terrain surface, can record thousands to tens of thousands of data points per second. For the working nature of the lock, the lock is washed by the current at every moment, which has a certain impact on the structure of the lock, and the efficiency of the monitoring data directly affects the accuracy of the health evaluation of the lock.

(2) High precision

Depending on the environment of the scanning area and the specifications of the 3D laser scanner, its accuracy can reach millimeter-level or even sub-millimeter accuracy.

(3) Non-contact

Since 3D laser scanning is an optical-based technology, the scanner does not need to touch objects. For operation in large scene environments, it can meet the contactless observation of targets within 100 meters.

(4) 24/7 work

3D laser scanner is an active scanning technology. It is based on the laser principle to measure the distance, so its dependence on ambient light is almost zero, and it can work in most environments throughout the day.

3 Health monitoring of locks

3.1 Lock health monitoring indicators

The core of monitoring is the establishment of monitoring indicators. Monitoring indicators must be based on the analysis of large amounts of monitoring data and a large number of theoretical calculations and engineering analogies.

According to "Lock Prototype Observation Design" in "Code for Design of Hydraulic Structures of Shiplocks" (JTJ 307—2001), the lock hydraulic buildings are divided into general prototype observation and specialized prototype observation.

General observation items include: pilotage and lock chamber water level observation, foundation lift pressure and groundwater level monitoring behind the wall, vertical displacement, horizontal displacement, settlement and tilt observation of structures, fracture and settlement fracture observation, and backfill soil subsidence observation.

Lock specialization observations can be carried out as needed, including structural observations, such as earth pressure, concrete stress, etc.; deep observation of foundation and backfill soil; structural temperature field and temperature stress observation; and seepage observation.

For the working locks, the silt accumulation of the pilot channels affects the normal passage of the locks, so the silt accumulation is listed as a monitoring indicator. Based on 3D laser scanning technology, this paper monitors the deformation of the lock structure.

3.2 Health monitoring of ship locks based on 3D laser scanning technology

The application of 3D laser scanning technology to the health monitoring activities of the locks mainly adopts the rapid scanning of high-precision 3D point data of the measured object, which can effectively achieve the goal of approximate replication of the measured object. In the actual application process, it can provide high-density full coverage of the locks and associated entities including key deformation points, completely changing the limitations of the traditional measurement method to replace the deformation of the whole lock structure with key point deformation data,

and the observation results are more accurate and reliable, and the data results are very extensive.

3D laser scanning measurement technology in monitoring activities can help people obtain a high-density three-dimensional point cloud data, and through the monitoring data information, you can quickly and efficiently establish DEM data model, and successfully reproduce the lock entity ground true three-dimensional space. There are two main ways to carry out health monitoring based on 3D laser technology:

① The point cloud is processed and then detected; ② The combined point cloud and photo data are processed and then health detection is carried out by image processing. For cracks, maps of locks are produced, while for other monitoring indicators, cloud data are analyzed.

4 Conclusions

In the traditional lock monitoring, most of the locks use the lead line method and the line of sight method, which can only reflect the change data of the key monitoring points of the locks, but it is difficult to establish the overall deformation information of the macro structure of the locks. The application of 3D scanning technology is based on the laser ranging principle, and its application in lock monitoring can quickly build a 3D model of the target to be measured, and has the advantages of fast, efficient and contact-free application, so it is worth promoting.

Acknowledgements

This work was supported by Jiangsu Provincial Water Conservancy Science and Technology Project(2021026) and Fundamental Research Funds of Nanjing Hydraulic Research Institute(Y721001).

References

Zhang, S., Weng, Y.Z., Xiong, Z. N. Navigation safety assessment of port channels and terminals. Journal of Dalian Maritime University, 2006(4): 43-47.

Wang, X. L., Wu, P., Wang, P., et al. Research on gate condition monitoring system with multi-sensor information fusion. Water Transport Engineering, 2022(1): 157-164.

Song, Z. P., Fang, H. D., Zhang, D., et al. Study on monitoring of hydraulic structure of ship locks based on DFOS. Water Conservancy and Hydropower Engi-

neering,2014,45(9):35-38.

Chen, M. H. Remote monitoring system for health status of ship lock herringbone gate based on fiber bragg grating. Water Transport Engineering, 2020(2):143-147.

Wang, C. Y., Liu, H. Y., Zhou, J. Y. Safety monitoring technology and design of lock engineering. Hydropower Automation and Dam Monitoring, 2014, 38(5): 21-24.

Chen, J. F., Huang, G., Chen, G. R. Ship surveying technology based on 3D laser scanning. China Ship Repair, 2020, 33(3): 22-24.

Zhang, H., Yao M. B. Health monitoring of waterway bridges based on 3D laser scanning. China Water Transport (Second Half of the Month), 2012, 12(7): 196-197+216.

Study on aimed river pattern of waterway regulation

Wanli Liu[1], Weiyan Xin[2]

[1,2] Tianjin Research Institute for Water Transport Engineering, Tianjin, China. e-mail: tjtgliuwanli@163.com

Abstract: The concept of aimed river pattern of waterway regulation is put forward based on the analysis of riverbed evolution in the long river reach, and the aimed river pattern implies three-fold meanings. First, the concept refers to historical and recent river pattern with reasonable beach layout, excellent depth condition, the same flow direction for mid and low flow and micro bending thalweg. Second, the quantities of channel regulation would be economical if the favorable opportunity is seized to make the aimed river pattern through effective engineering measures. Third, the reach is more at risk of obstructing-navigation in dry season when the channel is relatively stable, and the proper channel condition in dry season is optimal for aimed river pattern. The study shows that the aimed river patterns of distinct reaches are different, which makes project layouts different. It is different from the meaning of basic alluvial river pattern for aimed river pattern which is closely combined with the beach layout and channel conditions of the studied reach and used to guide the layout of channel regulation works of the studied reach. For example, the overall project should be implemented by stages, and possible great changes should be implemented in the early stage to create an advantageous beach pattern. If the channel condition of a studied reach is poor and its beach layout and depth condition are much worse than that of aimed one, further measures of channel regulation works should be taken.

Keywords: Aimed river pattern; Waterway regulation; Beach layout

1 Introduction

Scholars at home and abroad have carried out a lot of studies on the advantageous river pattern. Schumm(1973) believes that the river will develop into a curved river in the term of a great gradient to have its length increased and the gradient reduced. According to the extreme value principle of energy consumption rate, various variables in the system will be adjusted constantly to make the movement of the system meet the minimum of energy loss (energy consumption rate) per unit river length in addition to meeting the conservation of mass and energy (or momentum) when the fluid or multiphase fluid mixed with solid moves under certain boundary conditions(Petit et al.,

2005). The assumption that the work of flow per unit weight along the way reaches the minimum value allowed by local conditions can be met in two ways or a combination of them, namely: ① increasing the river length and reducing its gradient, ② increasing the river width and reducing the flow velocity. The river will develop into a meandering one if the river mainly increases its length and reduces its gradient, and it will develop into a bifurcated or braided one if the river width is mainly increased, which still depends on the anti-scour performance of river bank (Xin, 2018). For straight rivers with banks constrained, width and length not increased, the requirements can only be met through the bending of main flow path (staggered side bars are formed on both banks).

It is inevitable that the straight river with movable boundary will be transformed into meandering flow, which is the internal rule that the flow tends to bend, and a meandering river is more stable than straight one. Jenks (1975) has proved that straight rivers are unstable compared with meandering ones from a statistical point of view. At the same time, the anti-scour ability of the bank of straight river is much greater than that of meandering or bifurcated one, and they can maintain the straight pattern due to the strong anti-scour ability (Liu, 2015).

The above studies on advantageous river pattern are not combined with the study on beach layout and channel conditions of the studied reach. Therefore, it is necessary to study the advantageous beach layout of reaches of distinct river pattern, and put forward the aimed river pattern for waterway regulation, so as to guide the layout of waterway regulation works of river.

2 The implication of aimed river pattern

2.1 The concept of aimed river pattern

The concept of aimed river pattern of waterway regulation is put forward based on the analysis of riverbed evolution in the typical long river reach, and the aimed river pattern implies three-fold meanings (Liu, 2020):

(1) The concept refers to historical and recent river pattern with reasonable beach layout, excellent depth condition, the same flow direction for mid and low flow and micro bending thalweg.

(2) The quantities of channel regulation would be economical if the favorable opportunity is seized to make the aimed river pattern through effective engineering measures.

(3) The reach is more at risk of obstructing-navigation in dry season when the

channel is relatively stable, and the proper channel condition in dry season is optimal for aimed river pattern.

It can be seen that the implication of aimed river pattern is different from that of basic river pattern of alluvial river from the above concept of aimed river pattern for waterway regulation. It is closely combined with beach layout and waterway conditions of the studied river reach to guide the layout of waterway regulation works of the studied reach.

For example, the beach layout and channel depth conditions of a studied reach are quite different from that of aimed river pattern. The overall project should be implemented by stages. The beach protection project with reasonable location and great possible changes should be implemented in advance, so as to create an advantageous beach pattern, and waterway regulation works should be taken further.

2.2 The principle of aimed river pattern selection

The selection of aimed river pattern depends on certain conditions, especially the hydrodynamic conditions and the geological conditions of bank and bed, etc. The aimed river patterns of beach sections of distinct river patterns differ greatly, so the project layouts of them are also different.

(1) The transformation of flow from straight to meandering is inevitable due to the internal rule that the flow tends to bend for the straight reach. The location of both banks and the boundary of beach should be stabilized with possible great changes, and it should be stabilized into a slightly curved low flow channel pattern. We should try to avoid a pattern of multiple transitions for thalweg.

(2) For the meandering reach, which is more stable than the straight one, the bent one is also unstable, that is, the straight and the bent are both unstable. The river reach is relatively stable with a 5 – 10 km curvature radius according to existing studies, and the meandering reach should have an enough length to make it stable. That is, the stability of meandering channel needs a reasonable radius curvature and sufficient length. It is necessary to protect the reasonable bank slope position in terms of the poor anti-scourability of meandering bank.

3 Selection of aimed river pattern for waterway regulation in typical reach

3.1 Study on the aimed river pattern of waterway regulation of Jiangxinzhou-Wujiang reach in the lower reaches of the Yangtze River

There are many shoals from Jiangxinzhou to Wujiang in the lower reach of the

Yangtze River, where the flow is bifurcated, the mainstream of the inlet reach is unstable and the navigation channel often swings greatly in history. The water depth of some reach is only about 5 m during the period of channel swinging, and the channel conditions are poor. At present, the overall river regime and the riverbed evolution of the reach are relatively stable, and the channel conditions are good except for the crossing of the head of Xiaohuangzhou. There are some specific performances in the reach, for example, the channel of Jiangxinzhou has been a slightly meandering pattern, the main and branch channel of Xiaohuangzhou reach has been relatively stable through years of regulation, and the channel conditions have been in good condition since Fanjiaji waterway became the main channel.

In the view of current river regime and channel conditions, the key to waterway regulation of Jiangxinzhou-Wujiang reach is to stabilize the mainstream of the inlet reach further, consolidate the relatively complete beach pattern, and maintain the current slightly meandering and branching pattern of Jiangxinzhou waterway. The transverse, curved and narrow flow conditions of the crossing of the head of Xiaohuangzhou should be properly regulated.

Based on the above analysis, the overall goals of waterway regulation of Jiang-Wu reach is: ① to take engineering measures to stabilize Jiangxinzhou into a slightly curved channel pattern with good navigation conditions, ② to make the channel of Wujiang and Fanjiaji stable and be bifurcated with obvious main branches and good channel conditions, ③ to change and adjust the inflow conditions of the crossing of Xiaohuangzhou head, broaden the navigation channel, improve the navigation conditions of the crossing of Xiaohuangzhou head fundamentally, and the good channel scale of the main channel of the Jiang-Wu reach, the left branch of Xiaohuangzhou and the channel of Wujiang can be maintained for a long time. According to the regulation goal, we selected the river pattern in January 2002 as the aimed one for regulation (see Fig. 1).

The favorable opportunity should be seized for channel regulation to shape the reach into a pattern similar to the aimed one through effective engineering measures. At the same time, the studied reach is long and the upper and lower are linked. The shaping of aimed river pattern through channel regulation and the grasp of the opportunity should be implemented by stages and from upper to lower gradually (Liu, 2011).

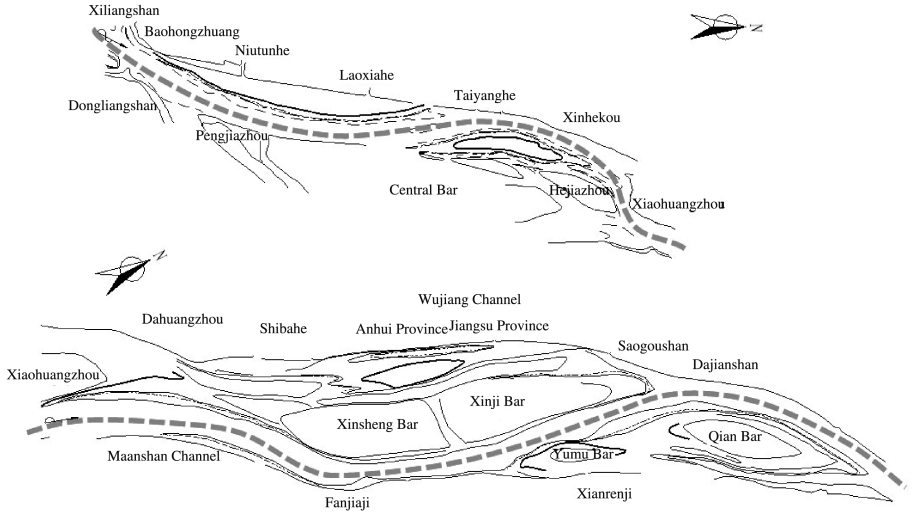

Fig. 1. The aimed pattern of Jiang-Wu reach (topographic map of January 2002).

3.2 Channel regulation aimed river pattern of Daijiazhou reach in the middle reaches of the Yangtze River

3.2.1 The selection of navigable main channel

The Daijiazhou reach of the middle reaches of the Yangtze River is a slightly curved bifurcated reach, the left branch is a circular channel and the right branch is a straight one. Based on the comprehensive comparative analysis of the current conditions, the area of channel scale, river pattern characteristics of the left and right branches, the right branch which is the optimal route for ship navigation with the shortest path, wider area and temporary bad channel conditions, is selected as the main navigation channel in dry season (Liu et al., 2012).

3.2.2 The selection of aimed river pattern

The right branch, which is straight, is selected as the main navigable branch, the aimed pattern is the layout of riverbed and beach expressed in the map in March 1998 (Fig. 2) according to the above concept of channel regulation aimed river pattern, combined with the topographic observation data and understanding of topographic characteristics of the studied river reach in recent 30 years.

In view of great differences between the layout of beach and channel, depth conditions, etc. of studied reach above and that of aimed river pattern, the overall project should be implemented by stages. And the beach protection project with reasonable location and possible great changes should be implemented in advance to create an

advantageous beach pattern, and then further waterway regulation works should be taken (Liu et al., 2009).

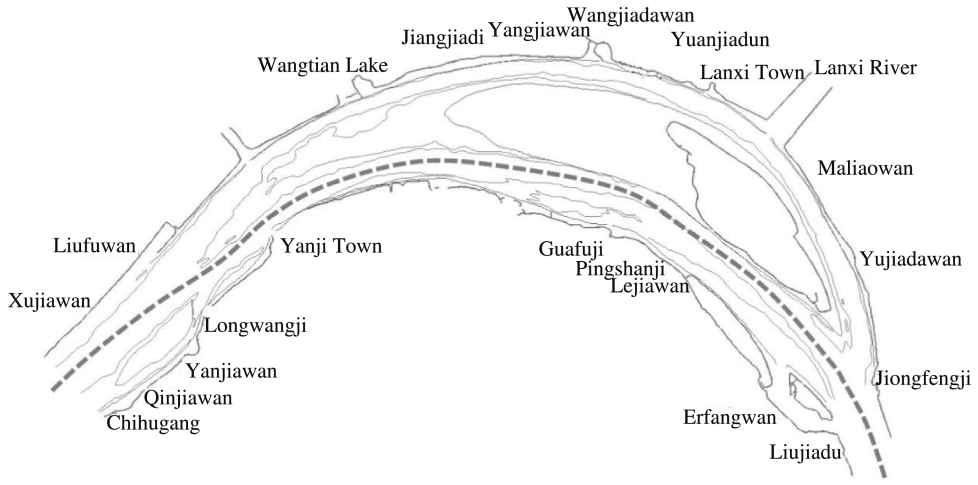

Fig. 2. The aimed pattern of Daijiazhou reach (topographic map of March 1998).

3.3 Channel regulation aimed river pattern of Shashi reach in the middle reaches of the Yangtze River

The Sanba beach of Shashi reach divides the channel into left and right branches. The convex bank is the side bar of Lalinzhou and the concave bank is the side bar of Yanglinji (Fig. 3).

According to the recent topographic data and analysis of the river reach, river pattern in November 2005 shall be a very suitable aimed river pattern for channel regulation if the waterway regulation project of Shashi reach needs to be implemented immediately without bridge. Due to the existence of the bridge, this kind of river pattern cannot be used as the aimed one for waterway regulation of Shashi reach. Therefore, the advantages and characteristics of this river pattern will not be analyzed here.

The river pattern at the end of flood season in 1992 is selected as the aimed one for channel regulation according to the analysis of relevant study results (Fig. 3). The typical feature of this river pattern is that the diversion ratio of right branch of Sanbatan is relatively small, about 20% (Li, 2007).

From the choice of flow path, we believe that the trend of "south channel" of Taipingkou central bar and "north branch" of Sanba beach is more reasonable, because it conforms to the principle of "slight bending". The trend of "south channel" of Taipingkou central bar is compatible and harmonious with that of upstream dynamic

axis.

Considering the large difference between the river pattern and the aimed river pattern during the implementation of the channel regulation project, the main project should be implemented first to create a favorable beach situation, and then further channel regulation projects should be taken to protect it.

In view of great differences between the river pattern before regulation project and aimed one, the main project should be implemented first to create an advantageous beach pattern which could be protected by waterway regulation works taken further then.

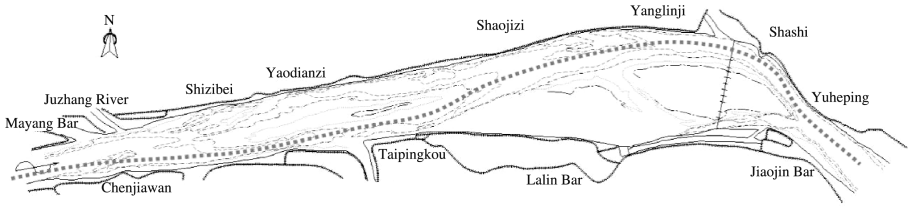

Fig. 3. The aimed pattern of Shashi reach (topographic map of November 1992).

4 Conclusions

(1) The concept of aimed river pattern of channel regulation is put forward. The aimed river pattern refers to historical and recent pattern with reasonable beach layout, excellent depth condition, the same flow direction for mid and low flow and micro bending thalweg. The favorable opportunity should be seized for waterway regulation to make the aimed river pattern through effective engineering measures.

(2) The aimed river pattern is closely combined with the beach layout and channel conditions of the studied reach, which is used to guide the layout of channel regulation works of the reach.

(3) The shaping of aimed river pattern through channel regulation should be implemented by stages and from upper to lower gradually.

(4) The overall project should be implemented by stages if the beach layout and channel depth conditions, etc. of a studied reach are quite different from that of aimed river pattern. The beach protection project with reasonable location and great possible changes should be implemented in advance, so as to create an advantageous beach shape, and waterway regulation works should be taken further.

Acknowledgement

This work was financially supported by National Key R & D Plan (2018YFB1600400), and basic research funding of National Commonweal Research Institutions (TKS20210403).

References

Jenks, W. N.,1975. Some considerations of straightness in channel form relating to the estuary of the Maclennan river, South Otago (New Zealand). Journal of Hydrology, 24(1-2): 89-109.

Liu, W. L.,2015. Systematic treatment technology of bifurcated reach in the middle and lower reaches of the Yangtze River. People's Communications Publishing House Co., Ltd.: 114-128.

Liu, W. L.,2020. Guiding restoration technology and practice of main navigable branches in the bifurcated reach of the middle and lower reaches of the Yangtze River. People's Communications Publishing House Co., Ltd.: 86-87.

Liu, W. L.,2011. Macro analysis report on riverbed evolution of Jiangxinzhou-Wujiang reach in the lower reaches of the Yangtze River. Tianjin, Tianjin Research Institute for Water Transport Engineering.

Liu, W. L., Li, Y. B., 2012. Discussion on branching selection of typical slightly curved branching reach in the middle reaches of the Yangtze River. Water Transportation Engineering(8):141-144.

Liu, W. L., Zhu, Y. D.,2009. Discussion on channel regulation of Daijiazhou reach in the middle reaches of the Yangtze River. Water Transportation Engineering, 30 (1):31-36.

Li, W.,2007. Some thoughts on the technical problems of waterway regulation in the middle and lower reaches of the Yangtze River. Waterway Port(12):418-424.

Petit, F., Gob, F., Houbrechts, G., et al.,2005. Critical specific stream power in gravel-bed rivers. Geomorphology, 69(1-4):92-101.

Schumm, S.A., Parker, R.S., 1973. Implications of complex response of drainage systems for quaternary alluvial stratigraphy. Nature Physical Science, 243(128): 99-100.

Xin, W. Y., Xu, H. J., Bai, Y. C.,2018. River pattern discriminant method based on resistance parameter and activity indicators. Geomorphology(303):210-228.

Topic 2

Inland Navigation Structure

Analysis on the contribution and countermeasures of the Pinglu Canal construction in the economic development of Qinzhou City

Xiaolei Liu[1], Yang Liu[2], Siyuan Wang[3], Fang Liu[4], Qilong Huang[5]

[1,2,3,4,5] China Academy of Transportation Science, Beijing, China. e-mail: 6868915@qq.com, 1109431747@qq.com, 674548349@qq.com, 24585460@qq.com, 1046852307@qq.com

Abstract: Based on the research results of Western Land-Sea New Corridor Canal (the Pinglu Canal) on the economic and social impact of Qinzhou City and countermeasures, this paper analyzes the influence of the Pinglu Canal on the freight channel pattern. By applying economic methods, the paper quantitatively analyzes the contribution rate of the Pinglu Canal to the economy of Qinzhou, and puts forward the development ideas and countermeasures of the transportation system along the river, which promotes the construction of the Pinglu Canal.

Keywords: Pinglu Canal; Qinzhou City; Contribution; Countermeasures

1 Introduction

The Pinglu Canal is a new channel for water transportation from the Xijiang River system to the Beibu Gulf coast. It is an important part of "The Overall Plan for the New Western Land-Sea Channel". The construction of the Pinglu Canal will not only directly enhance the river-sea linkage capability of Qinzhou City, but also improve the comprehensive transportation system, the layout of industries along the river, the development and upgrading of tourism, the comprehensive utilization of water resources, the ecological and environmental protection, and is of great significance to stimulating economic growth, industrial transformation and upgrading, social employment, and promoting regional coordinated development. Compared with the previous studies, this paper applies the input-output method to analyze the contribution rate of the Pinglu Canal to the economic and social development of Qinzhou City. Countermeasures such as terminal layout, collection and distribution system, and river-sea

combined transport route are proposed, which provides support for the compilation of Qinzhou's national economic and social development planning outline.

2 Analyse the contribution of the Pinglu Canal to Qinzhou City

2.1 Overview of the Pinglu Canal

The planned Pinglu Canal starts from the Xijin Reservoir area, and crosses the watershed between the Shaping River and the Jiuzhou River, and goes southward along the Qinjiang River to enter Qinzhou Port. It is planned to be constructed in Ⅰ-class channel.

The Pinglu Canal directly connects the Xijiang and Qinjiang water systems. The upper is connected to the Xijiang shipping trunk line. It goes westward through Nanning, Baise, Chongzuo and reaches Yunnan. It goes eastward to reach Guangdong-Hong Kong-Macao Greater Bay Area. It goes northward through Qianjiang, Liujiang, Hongshuihe, Duliujiang and reaches Liuzhou, Laibin and Guizhou. It goes southward to the sea. The middle and upper of the Xijiang shipping trunk line will go to sea from Qinzhou Port via the Pinglu Canal, which will be significantly shorter than the current voyage.

The construction of the Pinglu Canal will construct a new inland shipping network and form a new logistics channel. It is of great significance to promote regional economic growth, industrial transformation and upgrading, and is expected to form an economic belt along the river.

2.2 Contribution rate calculation

2.2.1 Direct economic contribution

The direct economic contribution refers to the economic added value created by related transportation activities. This paper only estimates the added value generated by inland shipping, and does not consider port production. It can be calculated by using the production method and the income method.

The production method is to first calculate the total output of each department, and then deduct the intermediate consumption, which can be denoted as: Value added = total output − intermediate input.

The income method is to first calculate the value-added of each department, and then accumulate them to obtain the total value-added, which can be denoted as: Value added = depreciation of fixed assets + labor compensation + net production tax + operating surplus.

In this paper, the production method is used. The intermediate input is calculated based on the ship operation case data of general routes, and the total output is calculated by taking the value of the total transportation cost of the predicted transportation volume.

Note: According to "New Western Land-Sea Channel Canal (The Pinglu Canal) Shipping Plan", the upper limit of the freight volume of the Pinglu Canal in 2035 will be 71 million - 113 million tons. And in 2050, it will be 82 million - 125 million tons. The inland water transportation mileage is within the range of 100 - 200 km, and the unit freight rate is 0.08 yuan/t · km.

(1) The total output

High scheme

2035: 113, 000×137×0.08=1, 238, 480 thousand yuan

2050: 125, 000×137×0.08=1, 370, 000 thousand yuan

Low scheme

2035: 71, 000×137×0.08=778, 160 thousand yuan

2050: 82, 000×137×0.08=898, 720 thousand yuan

(2) The intermediate input

The entire length of the canal is 137 km. Assuming that 1-ton materials need to be transported and the ship is fully loaded, it will take 3 days for one round trip. The basic data of ship operation are shown in Table 1. Therefore, the transportation cost for one trip is:

Fuel cost: 2.5×8, 500=21, 250 yuan

Ship maintenance: 25, 000÷(30÷3)=2, 500 yuan

Table 1 Basic data of 3000-ton ship operation.

Ship deadweight (ton)	Fuel consumption (ton/trip)	Oil price (yuan/ton)	Number of sailings (trip)	Daily maintenance (yuan/month)
3, 000	2.5	8, 500	3, 000	25, 000

Note: The data is collected according to typical data.

Based on this case, the estimated intermediate inputs in 2035 and 2050 are:

High scheme

2035: 113, 000×137×387÷10, 000=599, 114.7 thousand yuan

2050: 125, 000×137×387÷10, 000=662, 737.5 thousand yuan

Low scheme

2035: 71, 000×137×387÷10, 000=376,434.9 thousand yuan

2050: 82, 000×137×387÷10, 000=434,755.8 thousand yuan

2.2.2 Indirect economic contribution

The indirect economic contribution reflects the closeness of the forward and backward links between the water transport of the Pinglu Canal and other industries, and its promotion effect on consumption. It is an important indicator to measure its external economy, including the forward push and backward pull contribution to the upstream and the downstream industry, and the consumption-induced contribution under the multiplier effect.

According to the latest input-output table of Guangxi in 2017(Table 2), the input-output method is used to calculate the direct and indirect contributions of the canal to the economy. The input-output method is to arrange a series of internal departments input sources and output destinations into an input-output table, and calculate the consumption coefficient to conduct economic analysis and prediction.

Table 2 Input-output table of Guangxi in 2017 (million yuan).

Intermediate input	Intermediate usage						
	Agriculture	Industry	Architecture	Transportation	Commercial Catering	Other service	Total intermediate Usage
Agriculture	63,715.87	171,539.40	4,947.74	665.66	8,251.43	2,758.57	251,878.66
Industry	76,221.83	109,4161.53	345,663.06	44,629.78	37,159.87	146,677.31	1,744, 513.39
Architecture	292.49	2,066.16	17,708.25	188.94	866.09	4,361.28	25,483.21
Transportation	10,053.94	81,762.13	28,153.22	31,308.53	13,978.80	23,598.86	188,855.47
Commercial catering	10,662.22	87,285.62	21,056.40	7,181.92	10,204.31	46,432.39	182,822.86
Other service	12,459.65	109,582.28	79,961.03	40,608.25	55,657.98	256,823.58	555,092.76
Total intermediate input	173,406.00	1,546,397.11	497,489.70	124,583.07	126,118.48	480,651.98	2,948,646.34
Total value added	296,465.00	582,293.00	162,994.81	95,570.00	172,363.00	538,773.19	1,848,459.00
Total investment	469,871.00	2,128,690.11	660,484.51	220,153.07	298,481.48	1,019,425.17	4,797,105.34

Intermediate input	Final use					
	Total consumption	Capital formation	Export	Total final use	Others	Total output
Agriculture	105,102.98	13,150.51	10,547.31	267,675.55	0	469,871.00
Industry	292,420.98	187,979.64	147,181.78	1,237,642.37	0	2,128,690.11
Architecture	0	671,080.20	975.94	942,679.95	0	660,484.51
Transportation	37,688.12	−5,214.90	993.89	87,718.25	0	220,153.07
Commercial catering	76,282.13	20,957.73	747.59	193,976.37	0	298,481.48
Other service	539,049.78	48,492.82	948.84	651,003.91	0	1,019,425.17
Total intermediate input	1,050,544.00	936,446.00	161,395.35	3,380,696.39	0	4,797,105.34

According to the table, the matrix of direct consumption, complete consumption and value-added coefficient can be obtained.

Direct consumption matrix A: $a_{ij} = \frac{x_{ij}}{x_j}(i,j = 1,2,\cdots,n)$, refers to the direct consumption value of per unit department products of output value.

Complete consumption matrix C: c_{ij} refers to the direct and indirect consumption of the final product of a product j to another product i, that is, the complete consumption. The first round of consumption of a product to another product is direct consumption, and the consumption after the first round is indirect consumption, and the sum of direct consumption and indirect consumption is complete consumption, which refers to $C = (I-A)-1-I$.

Value-added coefficient matrix: $Z = (z_1, z_2, \cdots, z_n), z_j = g_j/x_j (j = 1,2,\cdots,n)$, refers to the value-added that can be created by adding one unit of output in department j.

According to the input-output table, select industries of agriculture, coal mining, metal ore mining, construction, transportation, accommodation and catering to calculate A_j. On the basis of A_j, through $(I-A)-1-I$, the complete consumption matrix C that fully reflects the connection of various sectors of the national economy is obtained.

Calculate value-added coefficient matrix:

$$Z = (0.630\ 95, 0.273\ 55, 0.246\ 78, 0.434\ 11, 0.577\ 47, 0.528\ 51) \tag{1}$$

Indirect economic contributions of the canal:

$$E_p = E_b + E_f + E_c \tag{2}$$

Where, E_p is the indirect economic contribution; E_b is the canal backward sweep contribution; E_f is the canal forward sweep contribution; E_c is the consumption-induced contribution.

According to the direct economic contribution value E_d, the economic value-added coefficient z and the complete consumption matrix C, the increase in the shipping output value ΔX of the canal can be obtained, and then the economic value-added of other departments in the downstream of the industrial chain can be calculated. Therefore, the canal backward sweep contribution is:

$$E_b = z(I-A)^{-1}\Delta X - \Delta X = z^T C \Delta X \tag{3}$$

The development of canal shipping drives the development of other departments of the regional economy in the upstream of its industrial chain, and the canal forward sweep contribution is:

$$E_f = z\Delta X' + zC\Delta X' \tag{4}$$

Bringing the data into the equation, the forward and backward sweep contribution under the high scheme in 2035 is obtained:

$$E_b + E_f = z^T C\Delta X + z\Delta X' + zC\Delta X' = 3.9 \text{ (billion yuan)} \tag{5}$$

The direct and indirect economic contributions of the canal expand the production of related departments and increase the income of workers. The consumption of these incomes will increase the final social demand, resulting in the consumption-induced contribution.

$$E_c = (E_d + E_b + E_f) \times c \times \frac{1}{1-c} \tag{6}$$

Where, c is the consumption multiplier.

In this paper, $c = 0.353,3$, and consumption-induced contribution under the high scheme in 2035 is:

$$E_c = (E_d + E_b + E_f) \times c \times \frac{1}{1-c} = 2.5 \text{ (billion yuan)} \tag{7}$$

The opening of the Pinglu Canal will surely drive the development along the river. According to the above calculations, under the high scheme, in 2035, the forward and backward sweep contribution will reach about 3.9 billion yuan, and the consumption-induced contribution will be about 2.5 billion yuan. In 2050, the forward and backward sweep contribution will reach about 4.3 billion yuan, and the consumption-induced contribution will be about 2.7 billion yuan. Under the low scheme, in 2035, the forward and backward sweep contribution will reach about 2.4 billion yuan, and the consumption-induced contribution will be about 1.6 billion yuan. In 2050, the forward and backward sweep contribution will reach about 2.8 billion yuan, and the consumption-induced contribution will be about 1.8 billion yuan.

2.3 The influence on the industry and urban development of Qinzhou City

2.3.1 Promote the upgrading of industries along the Pinglu Canal

One is to promote the construction of the agricultural system along the river. The Pinglu Canal will promote the optimization of agricultural spatial layout, such as the core of modern urban agricultural development, the characteristic agricultural linkage development axis, the north-south agricultural linkage development axis, and the northern mountainous characteristic agricultural area. It will promote the formation of riverside industrial agglomeration areas such as grain, livestock breeding, fruit, tea, sugar cane, marine fishery, and forestry. The second is to promote the construc-

tion of the industrial system along the river. Relying on the Pinglu Canal, it will improve the layout of petrochemical, equipment manufacturing, electronic information, new energy, and biomedicine industries. And it can promote the development of Lingshan Luwu Lingang Industrial Park, Qinzhou High-tech Industrial Development Zone, Huangma Industrial Park, Zhongma Industrial Park, Qinzhou Lingang Industrial Park and other riverside industrial areas in the South District. The third is to promote the development of the service industry along the river. In terms of tourism, it will build the Jiuzhou Museum, develop cruise tourism projects, innovate leisure tourism products, promote the integration of travel and tourism, strengthen supporting facilities and industrial development, and create characteristic tourism brands. In the logistics industry, it will accelerate the construction of logistics infrastructure, promote the deep integration of the transportation and logistics industry, build a comprehensive logistics service information platform, guide and cultivate logistics enterprises to become bigger and stronger, and deepen cooperation with upstream and downstream enterprises in the supply chain. In terms of ship and crew services, it will build a supporting service area for inland shipping, explore the establishment of a ship emergency rescue base, and support crew medical and training services.

2.3.2 Promote the development of Qinzhou City

First, it can promote coordinated regional development. The construction of the Pinglu Canal will stimulate new ideas for urban development in Qinzhou, adjust the administrative divisions in a timely manner in light of the actual management, actively promote the revitalization of rural industries, and enhance Qinzhou's role as a hub and gateway in the Pinglu Canal area. Second, it can promote greater emphasis on ecological and environmental protection. By controlling the ecological and environmental protection red line, we can develop green and smart inland waterway shipping, and minimize the impact of the construction and operation of the Pinglu Canal on ecological and environmental protection. Third, we pay more attention to the protection of drinking water sources along the Pinglu Canal to ensure the safety of relevant drinking water sources in Qinzhou during the construction and operation periods of the Pinglu Canal.

3 Analysis of countermeasures

3.1 The wharf layout

The Pinglu Canal mainly flows through Lingshan County and Qinbei District (Qinnan District), which are the most populous and economically large counties (dis-

tricts) in Qinzhou City, and there is nearly 60% of the population and 54% of the GDP. The two counties are not directly adjacent to the sea. The construction of the Pinglu Canal will create a more economical and environmentally friendly transportation method for the transportation of materials needed for the economic and industrial development of the two counties and urban construction, and will generate direct transportation demand for the Pinglu Canal. In order to promote the development of industries along the Pinglu Canal, combined with the layout of towns and key industrial parks along the Pinglu Canal, it is planned to consider Shaping Town, Luwu Town, Pingji Town, Huangma Industrial Park and Jiulong Town to construct port terminals and related supporting service facilities. Combine railway, waterway and highway transportation networks to realize the future three-dimensional transportation of the canal, and build transportation ports and industrial parks along the river to stimulate the economy along the route. Thus, the society will develop rapidly and healthily, and the Pinglu Canal Economic Belt will be formed.

3.2 The collection and distribution channel system

Focusing on the Pinglu Canal and the docks along the line, actively promote the construction of the collection and distribution system along the river. According to "The 14th Five-Year Development Plan for Comprehensive Transportation in Qinzhou City", focus on promoting the construction of freeway and first-grade highway.

In terms of freeway construction, continue to construct the section from Nanning to Zhanjiang to form a horizontal passage from the northwest of central Qinzhou to the southeast, and connect with Pinglu Canal crossing. The freeway from Liujing to Qinzhou Port has been built, which is parallel to the Pinglu Canal, forming the main north-south channel from Nanning in central Qinzhou to Qinzhou Port via Qinzhou. Start to construct Hengxian-Qinzhou Port Freeway, which becomes the north-south passage from Hengxian County in central Qinzhou to Qinzhou Port via Qinzhou, effectively connecting wharves and industrial clusters along the Pinglu Canal area. Start to construct freeway from Yulin to Pubei, which will become a fast channel for collection, distribution and transportation from Yulin and other Guidong cities to the Pinglu Canal, and promote the rapid distribution of passenger flow and logistics.

In terms of first-grade highway construction, start to construct Shaping-Qinzhou North Highway, Lingshan-Beihai Pingnan-Maotian section, Pubei-Lingshan Shaping section, Pubei-Luwu Highway. Continue to construct Shaping-Luwu-Pingji Highway, Lingshan Shaping-Nali Highway, Lingshan Ring Highway. These first-grade highways will serve the construction of the Pinglu Canal Wharf, cargo collection and distribution and emergency support, and form a collection and distribution system which

benefits neighboring cities such as Pubei County, Lingshan County, Qinzhou City and Yulin City along the canal.

3.3 River-sea combined transport system of the Pinglu Canal

3.3.1 River-sea combined transport scheme

According to the economic analysis of the ship type, combined with the current situation and planning of the waterway and ship type in the Xijiang River Basin, drawing on the experience, the river-sea combined transportation of the Pinglu Canal adopts the navigable ship type of the Xijiang shipping trunk line. After loading in Qinzhou Port or coastal ports, inland water ships enter the Xijiang trunk line, Zuojiang River, Youjiang River, Liuqian River, Hongshui River, Xianggui Canal and other inland river terminals for unloading. After loading in inland ports, inland ships descend directly to Qinzhou Port or coastal ports for unloading.

3.3.2 Route selection for river-sea combined transport

According to the current situation and planning of shipping in the Xijiang River Basin, combined with the forecasted traffic volume and flow direction of the Pinglu Canal, the main river-sea combined transportation routes of the Pinglu Canal are as follows:

- Route 1: Xijiang Main Line—Pinglu Canal
- Route 2: Zuojiang—Xijiang Main Line—Pinglu Canal
- Route 3: Youjiang—Xijiang Main Line—Pinglu Canal
- Route 4: Liuqian River—Xijiang Main Line—Pinglu Canal
- Route 5: Hongshui River—Xijiang Main Line—Pinglu Canal
- Route 6: Xianggui Canal—Xijiang Main Line—Pinglu Canal

3.3.3 Implementation plan of river-sea combined transport

According to the planned ship type of the Pinglu Canal and the predicted ship type of the sea area to the port, combined with the current flow and flow direction of various cargo types in the Pinglu Canal and the river-sea combined transport port area, considering the berths/shorelines of the river-sea combined transport in each port area, the river-sea combined transport of the Pinglu Canal will be implemented. The plan is as follows:

① Grain, cement, bauxite: Legou operation area

② Coal: Guozishan operation area of Jingu Port

③ Metal ore (excluding bauxite): Fangchenggang Daxiaodonggua Port

④ Container: Dalanping operation area and Dalanping South operation area

⑤ Other types of cargo: Dalanping operation area

4 Conclusions

4.1 Promote the integration of Qinzhou into the new western land-sea channel

The construction of the Pinglu Canal connects the main shipping line of the Xijiang River and the Beibu Gulf Port in Guangxi, and promotes the connection between Qinzhou City and the vast hinterland markets such as Chongqing, Hunan, Guizhou, and Yunnan, and accelerates the integration of Qinzhou City into the new western land-sea channel. According to "Qinzhou Port Master Plan", the cargo throughput of Qinzhou Port will reach 256 million tons in 2030, and the cargo collection and distribution volume will reach 512 million tons.

4.2 Significantly improve the industrial development of Qinzhou

The Pinglu Canal promotes the primary, secondary and tertiary industries, especially in the construction of demonstration zones, such as Qinzhou Modern Agriculture Demonstration Zone, near-port industrial park, near-port tourism and cultural area. A new industrial chain pattern will be formed, which will help to comprehensively accelerate the transformation and upgrading of Qinzhou's industrial economy. According to the preliminary calculation conclusion, under the high scheme, the annual added value will reach about 3.9 billion yuan in 2035, and will reach about 4.3 billion yuan around 2050.

4.3 Promote river-sea combined transport system

After the completion of the canal, it is expected to form a river-sea combined transport route with a fixed schedule through the transportation organization modes such as river-sea combined transportation and river-sea direct transportation, and give full play to the economic benefits of long-distance water transportation and large transportation capacity, expand the radiation radius of Qinzhou Port, and form a two-way inside and outside transport pattern. According to "Western Land-Sea New Channel Canal (the Pinglu Canal) Shipping Plan", the freight volume of the Pinglu Canal will reach 113 million tons in 2035 and 125 million tons in 2050.

4.4 Port and shipping service system of the Pinglu Canal

Based on the shoreline conditions and industrial foundation, it is recommended to arrange riverside docks in Shaping Town, Luwu Town, Pingji Town, Huangma Industrial Park and Jiulong Town, equipped with collection and distribution system. In

terms of freeway construction, construct Nanning-Zhanjiang section, Liujing-Qinzhou Port section, etc. to form a north-south channel and a horizontal channel to support the Pinglu Canal. In terms of first-grade highway construction, construct Shaping-Qinzhou North section, Lingshan-Beihaiping North-Maotian section, etc. to build a transportation network between the Pinglu Canal and the industries along the river.

Acknowledgements

Thanks to the research team for their persistence and efforts in the development of this project. Yang Liu provided systematic ideas in the research. Siyuan Wang made major contributions to the calculation of the contribution rate. Fang Liu gave an analysis on the tertiary industry. Qilong Huang gave an analysis of the social development of the region.

References

Ji, X.T., Su, J.B., He, L.D., et al. Summary of water saving technology of Panama Canal ship lock. Water Transportation Engineering, 2021(1): 111-117.

Wang, W.H. The construction of "smart port" is stable and far-reaching—the importance of smart port construction of Shanggang group under the new situation. Port Vertical and Horizontal, 2020(7): 23-25.

Xu, H. Study on the economy of mixed container liner routes of northern sea route and Suez Canal channel. Containerization, 2020(5): 1-8.

Wang, C., Liu, C. High quality development strategy of Zhejiang inland water transportation under the cultural belt of the Grand Canal. China Water Transport, 2020(6): 15-17.

Shi, M.C., Wang, Y. Countermeasures of Guangxi participating in the construction of a new land sea channel in the West. Port Aspect, 2020(12): 16-19.

Yang, H.B., Fan, S.Y., Yang, H.H., et al. Fuzzy comprehensive evaluation of navigation safety of Jianghan Canal. Water Transportation Management, 2020,42 (2/3): 23-27.

Zhang, W.L. Location of liner transport hub port considering the influence of canal. Dalian: Dalian Maritime University,2020.

Geng, W.N., Zhang, L.X., Li, B., et al. Discussion on the application of air rail in Qianwan Port area of Qingdao Port. Water Transportation Engineering, 2020 (8): 87-90.

Zhuang, C.Y. Analysis on port prosperity index of Shanghai international shipping

center. Water Transportation Management, 2020,42 (5): 52-57.

Yue, Y. Study on the development strategy of transportation system in the new land sea channel in the West. Urban Transportation, 2020,18 (3): 97-102.

Yang, M.Y., Yu, D.Y., Qin Y.G. Concept of the grand canal between Hunan and Guangdong. China Water Transportation, 2020(1): 55-57.

Zhao, G.H., Zhu, G.S., Wang, T. One belt, one road, international development of land and sea trade. Logistics Technology, 2019,38(7): 5-13.

Qiu, X. M. Shipping economic development of Hangzhou Ningbo Canal. Water Transportation Management, 2017,39(4): 15-17.

Ma, H.Y., Hu, Z.H., Zhou, Y. Based on the Three Gorges: building a new land water transportation channel for Northwest Logistics. Comprehensive Transportation, 2010(12): 41-44.

Su, P.C. Research on social evaluation of "four to three" channel upgrading project of Sunan Canal. Nanjing: Hohai University,2008.

Shen, X.R., Ji, X.Y., Mao, Z.X. Preliminary analysis on the combination of three major projects: Hangzhou Ningbo Canal, Cao'e River mouth gate and Fuchun River Diversion. Zhejiang communications Technology, 2002(2): 36-39.

Zhang, K.J. Enlightenment of Singapore Port development on China's port reform. Zhanjiang Port Authority of Guangdong Province,2000.

Calculation and correction of motion trajectory of flowing water tongue

Chenguang Sun[1], Fangfang Wang [2], Taolin He[3], Tao Yan[4], Ang Gao[5], Jie Luo[6]

[1,2,5,6] State Key Laboratory of Hydrology-Water Resources and Hydraulic Engineering, Nanjing Hydraulic Research Institute, Nanjing, China. e-mail: cgsun@nhri.cn, ffwang@nhri.cn, agao@nhri.cn, jluo@nhri.cn

[3] Power China Huadong Engineering Co., Ltd., Hangzhou, China. e-mail: he_tl@hdec.com

[4] Dayu College, Hohai University, Nanjing, China. e-mail: 2019010136@hhu.edu.cn

Abstract: In order to calculate the motion trajectories of the upper and lower edges of the water tongue, and reduce the amount of calculation, select the 35° and 20° pick angles as the research object, compare the trajectory curves of the model test and theoretical calculation, and correct them by the speed coefficient and angle coefficient. The results show that when the angle of the pick angle is 0°- 35°, the hydraulic loss along the route does not need to be considered, and the calculation method of the flow velocity at the ridge can be simplified; during the falling process of the water tongue, the upper edge is greatly affected by air resistance, and the lower edge of the water tongue is affected by the surface tension of the water body, so the velocity coefficient V_p and the angle coefficient θ_p are used to correct it; the correction coefficient has a threshold. For the research object of this paper, the threshold correction coefficient is: $V_p = 0.88$, $\theta_p = 1.2$. The research results can help designers quickly analyze the air trajectory of the water tongue to avoid the atomization effect caused by the collision of the water tongue, and at the same time, it can locate the landing area of the water tongue and do a good job in the protection of this area.

Keywords: Water tongue motion; Oblique throw equation; Trajectory correction; Model test

1 Introduction

There are many hydropower stations at home and abroad, including large, medium and small hydropower stations. Different hydropower stations have different energy dissipation methods. The more common ones are underflow energy dissipation, swirl energy dissipation, and dam body discharge holes. There is a greater requirement for the depth of the water cushion of the downstream water cushion pond. Once

the area where the water tongue acts on the bottom plate is a position with shallow water cushion and weak foundation, it will have a great impact. At the same time, in terms of flood discharge and atomization, the landing point of the water tongue also has a greater impact on the trend of atomized water mist. If the landing point is close, the atomization effect will easily spread to the power plant room, control room and other places where there are staff. If two water tongues collide in the air, it will easily aggravate the effect of atomization. Therefore, it is very necessary to study the trajectory of the water tongue in the air.

At this stage, experts and scholars at home and abroad have relatively more researches on the properties of the water tongue. Based on model tests and theoretical analysis, Ning Jinghao et al.(2017) summed up the calculation method of the water-lifting tongue distance and the factors affecting the water-lifting distance, and compared the characteristics of the water-lifting tongue with different body types. And improve the energy dissipation rate, the water tongue after aeration changes its three-dimensional diffusion trajectory, thereby reducing the scouring of the water tongue on the riverbed. Aiming at the problem of spraying and atomization, this paper analyzes the scouring, atomization and scouring of the discharge structure, and the relationship between the characteristics of running water tongue. Further recommendations are made for the study of water-bending tongues. Lian Jijian et al. (2004) established the differential equation of motion of aerated water tongue under the action of gravity, buoyancy and resistance, and obtained its numerical solution by the fourth-order Runge-Kutta method. Liu Shihe et al. (2002) studied the pick distance of plane fully aerated spallation jet, and obtained the water tongue pick distance equation considering the influence of aeration and air resistance. Liu Xuanlie et al. (1989) and others regarded the movement of the water tongue in the air as the oblique throwing motion of the water-gas two-phase flow under gravity and air resistance. The expressions of the movement trajectory, shooting distance, water entry angle, water entry speed and curve length of the aerated water tongue are obtained. Compared with the prototype observation, it is found that the water tongue is in good agreement. Rouse(1936) used the particle parabola equation in physics to study the jet trajectory, and found that when the initial flow velocity of the water flow increased, the deviation also increased. It can be seen from the previous research results that the calculation of the motion trajectory of the water tongue requires a large workload, which is difficult for the front-line designers. Compared with the theoretical calculation results, the water tongue trajectory was corrected by the velocity coefficient and angle coefficient, and the degree of agreement and relative error were used as the judgment criteria for the correction effect. The research results can help people estimate the movement trajec-

tory of the water tongue in the design stage of the flow-dissipation and energy dissipation, and provide certain technical support for the design of the discharge structure.

2 Trial overview

2.1 Test model

The model test selected a hydropower station as the research object, selected the model scale L_r, designed according to the gravity similarity criterion, followed "Specification for Normal Hydraulic Model Test" (SL 155—2012), and determined the relevant physical quantity scales as shown in Table 1. The schematic diagram of the model is shown in Fig. 1, including the upstream reservoir, arc gate, WES weir surface, inverse arc section, and flap nose, in which the upstream of the origin of the weir crest is an elliptic curve, the downstream of the origin is a power curve, and the weir surface curve and the downstream inverse arc. The sections are connected by dam slopes of 1∶0.75, and the bottom of the reverse arc is followed by a nose sill, the width of the nose sill is B, and the angle θ of the nose is 35° and 20°, respectively.

Table 1 The similar scale of each logistics flow in the model test.

Physical quantity	Symbol	Scale
Horizontal scale	L_r	L_r
Flow rate scale	V_r	$L_{r0.5}$
Flow scale	Q_r	$L_{r2.5}$
Roughness scale	n_r	$L_{r1/6}$
Time scale	t_r	$L_{r0.5}$

2.2 Test instrument

Model design, model production and installation, testing instruments and testing methods are all carried out in accordance with the requirements of "Specification for Normal Hydraulic Model Test" (SL 155—2012). The upstream and downstream water levels of the model are measured and controlled with a stylus with an accuracy of 0.1 mm; the model flow is measured and controlled by an electromagnetic flowmeter (DN type) with an accuracy of 0.01 l/s; the water surface line and air trajectory of the water tongue in the chute are measured with ruler.

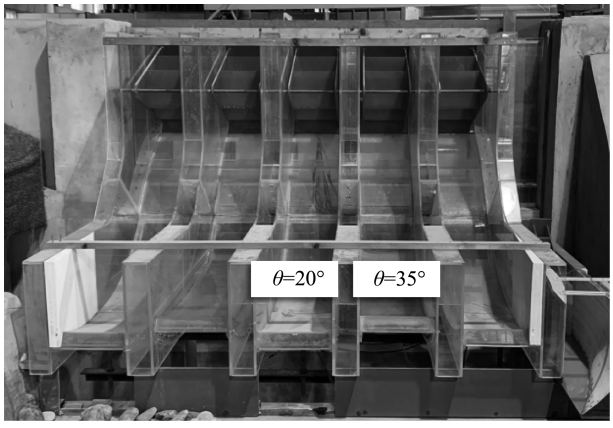

Fig. 1. Model diagram.

2.3 Test results

Under the check condition (single-hole flow rate Q_L = 103 l/s), the upper and lower edges of the water tongue (shown in Fig. 2) are tested for the trajectory measurement of the model. The measurement range of the water tongue trajectory is from the water tongue to the nose. It starts at the ridge and ends when the tongue enters the water. The aerial motion trajectories of the water tongue with pick angles of 35° and 20° are shown in Table 2 and Table 3, respectively.

Table 2 Motion trajectory of water tongue with a pick angle of 35° (check condition, Q_L=103 l/s).

Upper edge		Lower edge	
Pile number under the dam (m)	Elevation (m)	Pile number under the dam (m)	Elevation (m)
92.00	3,329.33	92.00	3,324.23
104.00	3,337.52	104.00	3,329.76
116.00	3,341.76	116.00	3,332.76
128.00	3,340.44	128.00	3,332.64
140.00	3,337.68	140.00	3,332.31
152.00	3,333.60	152.00	3,326.76
164.00	3,327.36	164.00	3,318.96
176.00	3,319.26	176.00	3,310.36

Table 3 Motion trajectory of water tongue with a pick angle of 20° (check condition, Q_L=103 l/s).

Upper edge		Lower edge	
Pile number under the dam (m)	Elevation (m)	Pile number under the dam (m)	Elevation (m)
92.00	3,325.24	92.00	3,321.04
104.00	3,330.51	104.00	3,323.76
116.00	3,332.28	116.00	3,324.36
128.00	3,329.46	128.00	3,323.16
140.00	3,326.40	140.00	3,320.76
152.00	3,321.75	152.00	3,315.48
164.00	3,314.80	164.00	3,309.36

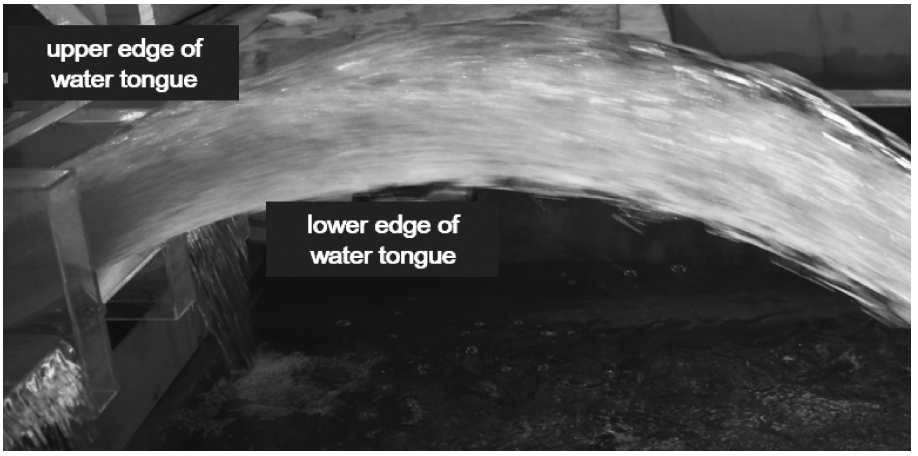

Fig. 2. Schematic diagram of the upper and lower edges of the water tongue.

3 Theoretical calculation

3.1 Calculation of flow velocity out of the threshold

Theoretical calculation assumes that the motion of the micro-element water body in the water tongue is the oblique throwing motion of the particle. According to this assumption, the micro-element water body on the upper and lower edges of the water tongue is selected to calculate the motion trajectory of the water tongue under different protruding angles. Since the gravitational acceleration in the vertical direction is g, without considering the air friction and the surface tension of the water body, the missing item in the solution of the oblique throwing trajectory of the particle is the water tongue exit velocity V_0. In this paper, two methods are used to calculate the sill

flow velocity V_0.

Method 1:

① Hydraulic radius $R = A/x = W \times h/(W + 2h)$

② Xie Cai coefficient $C = 1/n \times R^{1/6}$

③ Loss coefficient along the way $\lambda_h = 8 \times g/C^2$

④ Loss along the way $h_f = \lambda_h \times L/4R$

⑤ Flow velocity coefficient $\lambda_q = 1/(1 + h_f)$ 0.5

⑥ Energy conservation equation: $Z_1 + P_1/\rho g + V_{12}/2g = Z_0 + P_0/\rho g + (V_0')2/2g$, from the energy equation, it can be deduced that the flow velocity at the flap outlet $V_0' = [(H_1 - H_2 - 0.5h) \times 2g]^{1/2}$

⑦ Calculate the initial flow velocity $V_{01} = \lambda_q \times V_0'$

In the equation: the length of the overflow weir is L, the normal water depth h, the vertical water depth $h\cos\theta$, the roughness n, the single width W, the water level in the reservoir area H_1, and the outlet elevation H_2.

Method 2:

The basic method for calculating the cross-section flow velocity, the flow velocity at the flap outlet $V_{02} = Q/S = Q/W \times h\cos\theta$.

The model parameters are shown in Fig. 3. Substitute the parameters of the experimental model to obtain two groups of V_0 shown in Table 4. It can be seen from Table 4 that when the deflecting angle is 40°-50°, the difference between V_{01} and V_{02} is large, and the relative errors of 50°, 45°, and 40° are 12.65%, 6.68%, and 3.14%, respectively; when the angle is 0°-35°, the difference between V_{01} and V_{02} is small, and the relative error is within 1%. In this paper, the model table hole deflecting angle range is 20° and 35°, and V_0 can be calculated directly by applying Method 2.

Table 4 Method 1 and Method 2 V_0 (check condition, Q_L = 103 l/s).

θ(°)	V_{02}(m/s)	λ_q	V_{01}(m/s)	Difference(m/s)	Relative error (%)
50	31.78	0.98	27.76	4.02	12.65
45	30.25	0.98	28.23	2.02	6.68
40	29.63	0.98	28.70	0.93	3.14
35	29.17	0.98	29.13	0.03	0.10
30	29.49	0.98	29.57	−0.08	0.27
25	29.85	0.98	29.97	−0.11	0.37
20	30.19	0.98	30.35	−0.15	0.50
15	30.65	0.98	30.70	−0.05	0.16
10	30.96	0.98	31.04	−0.08	0.26

continue

θ(°)	V_{02}(m/s)	λ_q	V_{01}(m/s)	Difference(m/s)	Relative error (%)
5	31.17	0.98	31.36	−0.19	0.61
0	31.65	0.98	31.67	−0.03	0.09

Note: Relative error = $[(V_{02} - V_{01})/V_{02}] \times 100\%$

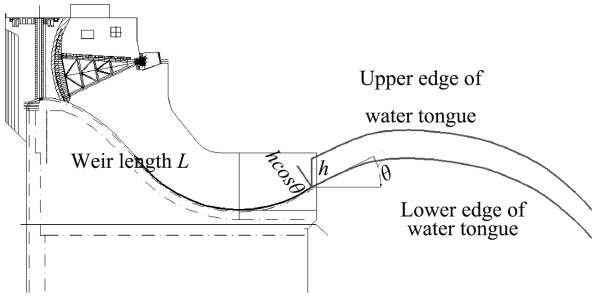

Fig. 3. Model parameters.

3.2 Water tongue trajectory drawing

After obtaining V_0 in 2.1, take a mass point on the upper and lower edges of the water tongue, and take 0.5 s as an interval to draw the movement position of each time point during the oblique throwing movement. Take the movement position at 0 s as the starting position, and take the movement position at 6 s as the end position, and the movement track of the water tongue can be obtained by connecting it with a smooth curve. Taking a pick angle of 35° as an example, the particle properties of the water tongue at each time point are shown in Table 5. The trajectory of the water tongue with a pick angle of 0°-50° is shown in Fig. 4. It can be seen from Fig. 4 that under the check condition the pick angle is in the range of 0°-50°, the higher the pick angle, the higher the water crown height of the water tongue, and the farther the pick distance.

Table 5 Movement process of water tongue with 35° pick angle (check condition, Q_L = 103 l/s).

T	x	y	V_x	V_y	V
0.00	0.00	3,327.70	20.43	24.35	31.78
0.50	10.21	3,338.65	20.43	19.44	28.20
1.00	20.43	3,347.14	20.43	14.54	25.07
1.50	30.64	3,353.18	20.43	9.63	22.58
2.00	40.86	3,356.77	20.43	4.73	20.97
2.50	51.07	3,357.91	20.43	−0.18	20.43
3.00	61.29	3,356.59	20.43	−5.08	21.05

continue

T	x	y	V_x	V_y	V
3.50	71.50	3,352.82	20.43	−9.99	22.74
4.00	81.71	3,346.60	20.43	−14.89	25.28
4.50	91.93	3,337.93	20.43	−19.80	28.45
5.00	102.14	3,326.80	20.43	−24.70	32.06
5.50	112.36	3,313.23	20.43	−29.61	35.97
6.00	122.57	3,297.19	20.43	−34.51	40.11

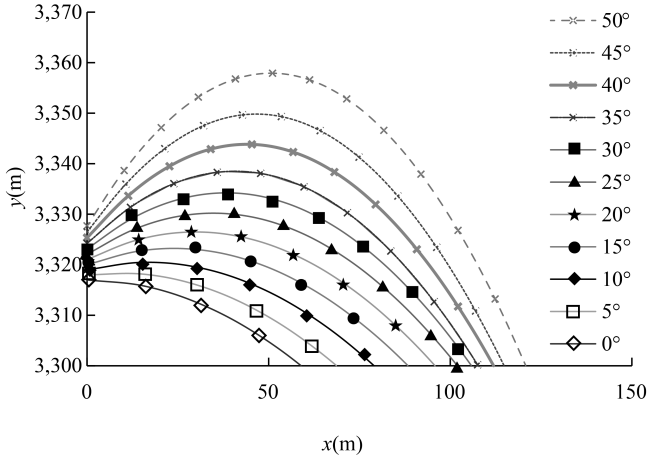

Fig. 4. Theoretical calculation of 0°−50° water tongue movement trajectory.

4 Results and analysis

4.1 Comparison between test and calculation of water tongue trajectory

The trajectory of the upper edge of the water tongue obtained from the test and theoretical calculation is shown in Fig. 5. It can be seen from Fig. 5 that there is a certain difference between the model and the theoretically calculated trajectory of the upper edge of the water tongue: in the process of the rising of the water tongue, the trajectory of the upper edge of the water tongue obtained by theoretical calculation and model test has the same movement trend, the error is small, but during the falling process of the water tongue, the theoretical curve is quite different from the experimental curve. The author believes that the reason for the difference is that the theoretical calculation does not consider the surface tension of the micro-water body and the air resistance it receives (Fig. 6: F_{air}, F_{water}), so the trajectory of the water tongue needs to be corrected from these two aspects. For the air re-

sistance, in order to simplify the correction difficulty, correct the flow velocity V_0 of the water tongue; and for the surface tension of the water body, it is corrected by the outlet angle θ out of the water tongue.

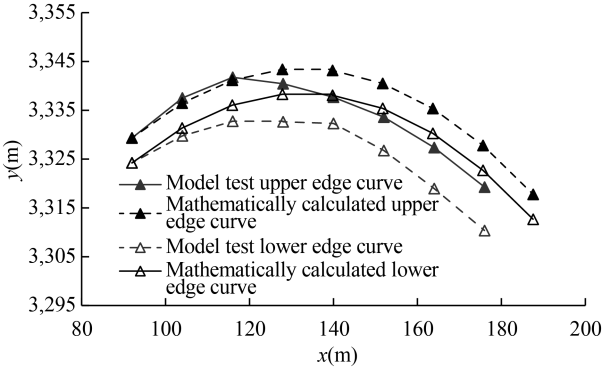

Fig. 5. Model test and theoretical calculation of water tongue trajectory (35°).

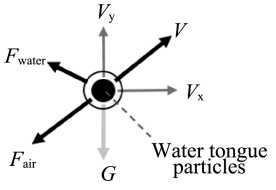

Fig. 6. Schematic diagram of the force of micro-element water body.

4.2 Water tongue trajectory correction

It can be seen from Fig. 5 that the curve of the upper edge of the water tongue in the model experiment is close to the calculated value, indicating that during the rising process of the water tongue, the air resistance received by the water tongue is relatively small, and the surface tension of the micro-element water body has an effect on the movement trajectory of the upper edge of the water tongue. The influence is small, so the calculated curve can be used for the upper edge trajectory of the water tongue during the rising process; during the falling process of the water tongue, the difference between the test and the calculated curve is large, and the upper edge of the water tongue has obvious diffusion and fragmentation during the falling process. So it can be considered that the surface tension of the water body on the upper edge of the water tongue is small during the falling process. The influencing factor is the air resistance on the upper edge of the water tongue, which can be corrected by the velocity correction coefficient V_p. After several corrections, the correction coefficient $V_p = 0.88$ was finally determined as the threshold correction coefficient. The trajectory of the upper edge of the water tongue after correction is shown in Fig. 7. It can be seen from

Fig. 7 that when the calibration coefficient is 0.88, the calculation and the trajectory curve of the model during the falling process are very consistent (maximum relative error < 0.1%). In the estimation of the water tongue trajectory in the subsequent process, the theoretical calculation curve is selected for the rising process of the water tongue upper edge, and the $V_p = 0.88$ correction curve is selected for the falling process of the water tongue upper edge, which can better restore the actual water tongue upper edge movement trajectory.

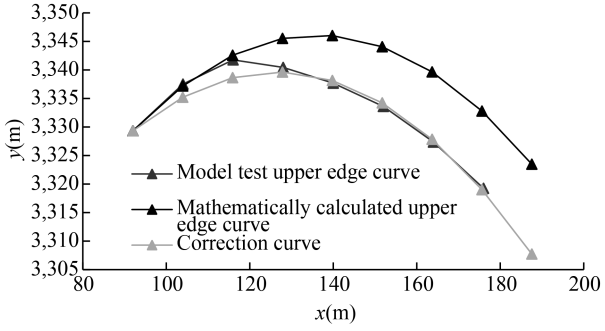

Fig. 7. Correction curve of the upper edge of the water tongue(35°).

The analysis shows that in the flow process of the chute, the lower edge of the water tongue produces friction with the side wall of the model, plus the influence of its surface tension, the angle coefficient θ_p is used to correct it, and the curve of the lower edge of the water tongue after correction is shown in Fig. 8. It can be seen from Fig. 8 that when $\theta_p = 1.2$, the calculated curve and the model test curve can achieve a good agreement (maximum relative error <0.1%), whether it is the ascending segment or the descending segment, so the calculated water tongue $\theta_p = 1.2$ is selected. The curve can be used as the actual water tongue movement trajectory.

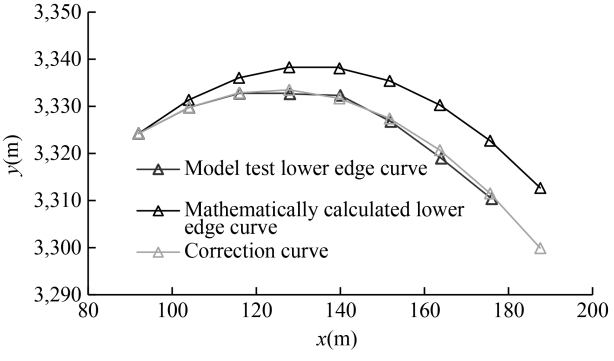

Fig. 8. Correction curve of the lower edge of the water tongue(35°).

4.3 Correction factor verification

V_p and θ_p are used to correct the trajectory of the theoretically calculated 35° pick angle water tongue. In this section, the 25° pick angle water tongue is selected to verify the accuracy and applicability of the above correction coefficients. Fig. 9 shows the upper and lower edge curves of the water tongue from the theoretical calculation and model test with a pick angle of 20°. Compared with Fig. 5 and Fig. 9, it is found that the difference trend of the trajectory of the water tongue between the test and the calculated water tongue with a pick angle of 20° is the same as that of the water tongue with a pick angle of 35°.

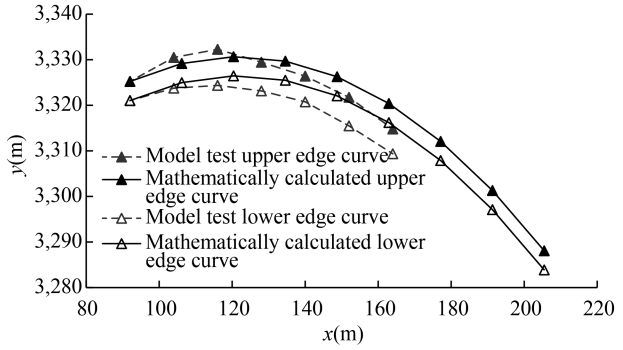

Fig. 9. Model test and theoretical calculation of water tongue trajectory (20°).

After using the same correction coefficient ($V_p = 0.88$, $\theta_p = 1.2$), the trajectory curves of the upper and lower edges of the water tongue are obtained as shown in Fig. 10. It can be seen from Fig. 10 that the trajectory of the water tongue with the same correction coefficient is the same as that of the 35° pick-up angle water tongue.

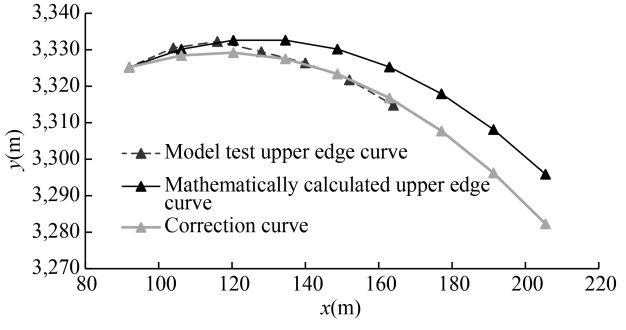

(a) Upper edge correction

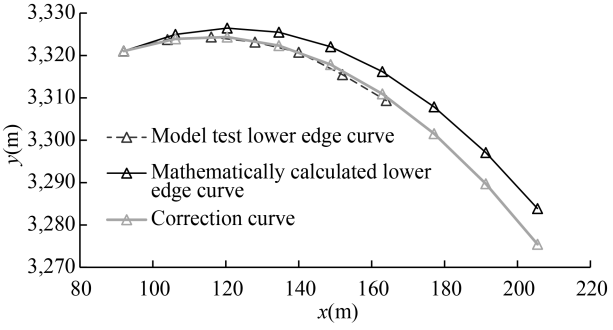

(b) Lower edge correction

Fig. 10. The trajectory correction of the upper and lower edges of the water tongue (20°).

5 Conclusions

(1) When the angle of the pick angle is 0°-35°, the calculation method of the flow velocity at the sill can be simplified ($V_{02} = Q/S = Q/W \times h\cos\theta$), and the hydraulic loss along the way does not need to be considered; when the pick angle is greater than 35°, it is necessary to consider the hydraulic loss along the route, and use the energy conservation to solve the problem.

(2) During the rising process of the water tongue, the air resistance has little influence on the trajectory of the water tongue, and the calculated trajectory of the water tongue is consistent with the test trajectory. During the falling process of the water tongue, the upper edge is greatly affected by the air resistance, and the lower edge is greatly affected by the surface tension of the micro-element water body, so the velocity coefficient V_p and the angle coefficient θ_p are used to correct it.

(3) The analysis results show that the correction coefficient has a threshold. For the research object of this paper, the threshold correction coefficient is: $V_p = 0.88$, $\theta_p = 1.2$.

Acknowledgements

This research is funded by the Science and Technology Support Program of Jiangsu Province (Grant No. BK20190142) and the National Natural Science Foundation of China (Grant No. 51909169). The authors gratefully acknowledge these financial supports.

References

Liu, X. L., Liu, J., Yao, Z. D., et al., 1989. The moving orbit and the horizontal

length of aerated jet flow in open air. Journal of Tianjin University (2): 23-30.

Liu, S. H., Qu, B., 2002. Investigation of plane aerated jet. Journal of Hydrodynamics, 17(3): 376-381.

Ning, J. H., Ning, L. Z. ,Ning, B. B., et al., 2017. Characteristics of the trajectory nappe and its influence. Journal of Engineering of Heilongjiang University, 8(4): 1-6.

Rouse, H., 1936. Discharge characteristics of the free overfall: Use of crest section as a control provides easy means of measuring discharge. Civil Engineering, 6(4):257-260.

Zhang, H., Lian, J. J., 2004. Differential equation of aerated jet motion and its numerical solution. Water Resources and Hydropower Engineering, 35(5): 46-48.

Coherent structure identification in a pressured backward-facing step flow

Fangfang Wang, Zhenxing Sun, Chenguang Sun, Gufei Fan, Weile Zhang, Jiayi Xu

Nanjing Hydraulic Research Institute, Nanjing, China. e-mail: ffwang@nhri.cn

Abstract: Vortex plays an important role in self-sustained turbulent processes and in the various transfer processes found in natural and engineering flows. However, vortex identification is an unsolved problem as no clear definition of a vortex is currently universally accepted, which brings big resistance for turbulence investigation.

Backward-facing step flow is taken as a study case to quantitatively obtain and identify the coherent structures (CS) caused by step separation. The CS shown by streamlines is consistent with the phenomenon of flow visualization. Based on the planar velocity matrix, a Q method is improved (a normalization is employed on the velocity matrix before calculation for the Q value) to identify those CS that are consistent with the streamlines. The identified CS can reflect their position and shape, even smaller ones that are not easy to be found by streamlines.

This work may contribute to further quantitative analysis for the CS in these flows.

Keywords: Vortex identification; Coherent structures; Backward-facing step; Improved Q method; Streamlines

1 Introduction

Vortex plays an important role in self-sustained turbulent processes and in the various transfer processes found in natural and engineering flows (Chen et al., 2015). And it's often viewed as "the sinews and muscles of turbulence" (Küchermann,1965). Therefore, vortex is the key to understanding and controlling turbulence flow. However, no definition of a vortex is currently universally accepted, despite the fact that fluid dynamicists continue to think in terms of vortexes (Chakraborty et al., 2005). As the important role of vortex in turbulent flow, it is particularly important to accurately define and identify a vortex.

Lugt (1972) defined a vortex as "A vortex is the rotating motion of a multitude of

material particles around a common center". This definition is consistent with some simple vortex phenomena and people's intuition. It emphasizes two features: one is rotational motion, and the other is a common center of rotation. Robinson (1991) further defined a vortex as "A vortex exists when instantaneous streamlines mapped onto a plane normal to the vortex core exhibit a roughly spiral pattern, when viewed from a reference frame moving with the center of the vortex core" (in a frame of reference moving with the center of vortex core, the instantaneous streamlines have a torus or helical shape when projected to a plane perpendicular to the vortex core), this definition, in addition to the above two features, refers to use of streamlines to describe vortexes, which is similar to the concept in fluid mechanics (a closed-form or spiral pattern of streamlines is called a vortex or spiral). Although the definition of vortex differs in the dynamic mechanism, the description of the kinematic characteristics of a vortex is basically the same. However, the inability to know in advance the orientation and motion of the center of rotation makes such a definition that seems consistent with our visual perception intractable (Zou, 2006).

Due to the lack of a clear definition, some methods based on different features are used for vortex identification and detection in flow analysis, including methods based on the velocity gradient tensor, pattern recognition method, pattern matching method and rigid body rotation vorticity method, etc. The latter several methods are non-local identification methods based on the topological structure of flow field. The first method is based on the velocity gradient tensor, which needs to calculate the characteristic quantities of gradient tensor and satisfy the Galileo Transform Invariance.

Backward-facing step (BFS) flow is fundamental in geometry and design, and it's widely seen in numerous project applications. For example, a step is usually designed in the ship lock water conveyance corridors and high-speed valve flow system. Then local energy dissipation and flow pattern adjustment generally happen there. Perturbation of the step generates a separation and reattachment flow with successive coherent structure (CS) there (Kostas et al.,2002; Hu et al., 2016; Wang et al., 2019). Therefore, it's also a good case for vortex studying.

BFS flow is taken as a study case in this study. We aim to quantitatively obtain and identify the CS caused by step separation, and discuss the definition and identification of a vortex.

2 Research methods

In this study, a pressured BFS water tunnel flow model is built and a particle image velocimetry (PIV) system is used to measure velocity field (Fig. 1).

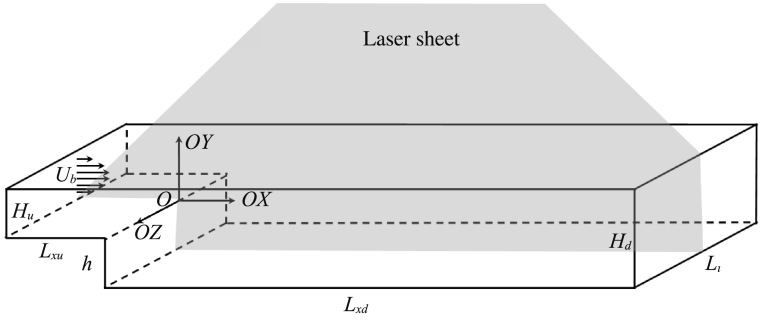

Fig. 1. Schematic of the test section with a PIV system.

The configuration parameters for the test section are listed in Table 1. A rectangular pressured tunnel with a vertical step ($h = 50$ mm) at the bottom surface is set. The expansion ratio, $E_r = H_d / H_u = 2$, where H_d and H_u are respectively water depth upstream and downstream of the step. The tunnel width, $A_r = L_z / h = 10$ is set. The channel lengths of upstream and downstream the step were $L_{xu} = 44\ h$ and $L_{xd} = 50\ h$, respectively. Honeycomb tubes are set near the inlet of the channel to obtain fully developed turbulent flow before the step.

Table 1 Configuration parameters of the BFS model.

Parameters	Values	Units
h	50	mm
L_{xu}	2,220	mm
L_{xd}	2,500	mm
H_u	50	mm
H_d	100	mm
L_z	500	mm
i	0	°
E_r	2∶1	—
A_r	10∶1	—

The flow tunnel is made of transparent PMMA (polymethyl-methacrylate) to provide a clear view for the PIV system. The PIV system mainly consisted of laser module, image acquisition module, and control module. The laser module generates a planar laser sheet with thickness of about 1 – 2 mm. The laser power energy is 10 W. The image acquisition module is made of a charge-coupled device (CCD) camera with a resolution about 5, 000 pix × 2, 000 pix. Hollow sphere glass particles are seeded into the water with an average diameter of 15 μm. The measurement accuracy was within 1% of the maximum velocity.

The experiment is carried out with a constant water head. The Reynolds number, $Re_h = U_b h/\nu$, is defined by the step height and the averaged velocity (U_b) located at 1 h upstream of the step, and ν is the kinematic viscous coefficient of water at 20 ℃. Table 2 shows flow conditions in the experiment.

Table 2 Flow conditions in the experiment.

h (cm)	U_b(m/s)	E_r	A_r	Re_h	X_r/h
5	0.088	2∶1	10	4,400	6.1

3 Results and discussions

3.1 Coherent structures

Fig. 2(a) shows the aluminum-powder pictures of streamlines for the step of 5-centimeter height, the exposure time being 0.5 seconds. The picture of short exposure reveals the intermingling of distinct CS behind the step, which is consistent with something shown by the instantaneous streamlines. As a comparison, the instantaneous streamlines obtained in this experiment (Fig. 2(b)) is also shown. These results are based on the same step height with turbulent water flow, and two figures show highly similar phenomena, although methods and proposers are different. In the figures, the main flow streamlines diffused smoothly, attached to the bottom wall after a certain distance, and formed a backflow zone at the downstream of the step. About 3-5 CS could be clearly seen there with maximum vortex scale of the same order of magnitude as the step height.

(a) Aluminum-powder picture (By Anti et al., 1961, exposure time is 0.5 seconds)

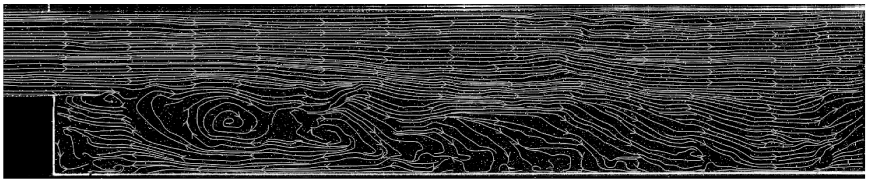

(b) PIV picture with streamlines

Fig. 2. Instantaneous flow over a BFS.

To study the CS, results shown by streamlines are consistent with what is seen in the flow visualization. The concept of vortex shown by streamlines is also consistent with current popular viewpoints. Therefore, in this study we define the CS shown by the two-dimensional instantaneous streamlines. However, the streamlines still only show the qualitative knowledge, so further quantitative identification is needed.

By analyzing the CS represented in streamlines, they are approximately considered to be elliptic, and the center of the streamlines is the vortex center. Therefore, some characteristic parameters are defined to describe the CS. Fig. 3 shows the CS represented by instantaneous streamlines. The CS is surrounded by spiral streamlines and it revolves around a common rotating center. The source of the streamlines (red point) is defined as the vortex center $Z(x, y)$, and the diameter along the X and Y directions is D_x and D_y respectively, with the average diameter $D = 0.5 \times (D_x + D_y)$, representing the length-height ratio D_x/D_y of the shape of the CS. The blue point between CS is called the saddle point.

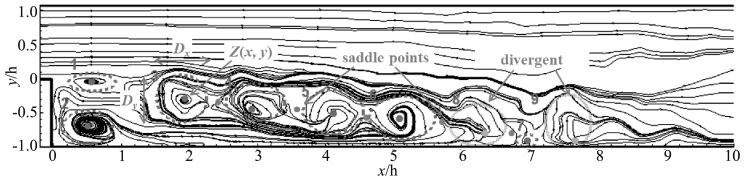

D_x— diameter in X direction, D_y— diameter in Y direction, $Z(x, y)$ — vortex center coordinates

Fig. 3. Schematic diagram of characteristic parameters of CS.

There are some typical CS forming behind the step as shown in Fig. 3. Their shape is mainly elliptic, and sometimes spiral, divergent and semi-circular. Number 1#-7# CS have obvious vortex center and rotation shape, while streamlines of Number 8#-9# CS are stellated without obvious boundary, which may be caused by their stronger three-dimensionality. The rotation direction of Number 2# CS is different from the others, which is counterclockwise and located in the step corner, where a second flow is induced by the reflux. Number 1#, 3#-7# CS develop in the shear layer behind the step with maximum length scale of the step height. Number 1# CS is smaller in size and formed in the early stage. Number 7# CS is close to the lower wall surface. These CS are connected by saddle points.

3.2 Identification method improvement

Considering the characteristics of backward step flow, it is characterized by the free shear layer and the bottom wall shear layer. As Q method considers both rotary strength and shear strength, it should be more suitable for the BFS flow. In this sec-

tion, the identification method of CS is further improved based on the Q method.

The Q method based on two-dimensional velocity tensor is derived here. From the second-order tensor properties, the characteristic equation of the local velocity gradient tensor ∇V of the incompressible fluid can be written as:

$$\lambda^3 + Q\lambda - R = 0 \tag{1}$$

If λ_1 , λ_2 , λ_3 are its three roots, there are three independent invariants between them:

$$P = \lambda_1 + \lambda_2 + \lambda_3 = div\boldsymbol{V} = 0 \tag{2}$$

$$Q = -\frac{1}{2}(e_{ij}\, e_{ji} + \Omega_{ij}\, \Omega_{ji}) = \frac{1}{2}(\Omega_{ij}\, \Omega_{ji} - e_{ij}\, e_{ji}) = \frac{1}{2}(\|\boldsymbol{\Omega}\|^2 - \|\boldsymbol{E}\|^2) \tag{3}$$

$$R = \lambda_1\, \lambda_2\, \lambda_3 = \frac{1}{3}(e_{ij}\, e_{jk}\, e_{ki} + 3\Omega_{ij}\, \Omega_{jk}\, \Omega_{ki}) \tag{4}$$

Where: e_{ij} , Ω_{ij} are the strain rate tensor and vorticity tensor, respectively.

Considering two-dimensional velocity components u and v, the velocity gradient matrix of two-dimensional flow field is defined as:

$$\nabla \boldsymbol{u} = \begin{bmatrix} \dfrac{\partial u}{\partial x} & \dfrac{\partial u}{\partial y} \\ \dfrac{\partial v}{\partial x} & \dfrac{\partial v}{\partial y} \end{bmatrix} \tag{5}$$

Q is defined as:

$$Q = \frac{1}{2}(\|\boldsymbol{\Omega}\|^2 - \|\boldsymbol{s}\|^2) \tag{6}$$

Where,

$$\boldsymbol{\Omega} = \frac{1}{2}[\nabla \boldsymbol{u} - (\nabla \boldsymbol{u})^T] \tag{7}$$

$\boldsymbol{\Omega}$ is the rotation rate matrix corresponding to the pure rotational motion in the flow, and is the antisymmetric part of the velocity gradient matrix;

$$\boldsymbol{S} = \frac{1}{2}[\nabla \boldsymbol{u} + (\nabla \boldsymbol{u})^T] \tag{8}$$

$\boldsymbol{S}$ is the strain rate matrix corresponding to the pure shear motion in the flow, and is the symmetric part of the velocity gradient matrix.

Based on the above definition, the two-dimensional CS region is usually shown as $Q>0$. However, in fact, there is no clear boundary between vortex and background flow. Usually, a threshold is set to identify the most important part of vortex structure (Jeong et al., 1995; Chakraborty et al., 2005), and the selected threshold should

consider the objective flow characteristics (Chen, 2014).

Fig. 4 compares the CS shown by streamlines and Q method. The identification result by the Q method is obviously different from that shown in streamlines. It's also hard to distinguish the difference of the free shear layer vortex and wall induced vortex. For this reason, the shear strength is relatively larger in BFS flow than that in a near-wall turbulent flow in open channel. Especially, the shear strength is even greater than the rotational strength at the near-wall and step separation, so it is difficult to reflect the vortical rotational motion. Moreover, the selection of threshold value is very sensitive to the result. Therefore, in order to obtain the CS shown in streamlines, it is necessary to improve the current Q method.

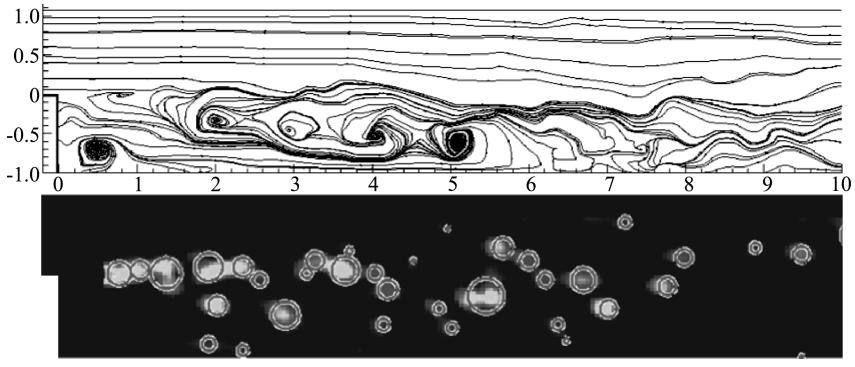

Fig. 4. Comparison between the CS shown by streamlines and Q method.

Vortex structure characterized by streamline is mainly determined by rotation strength, while Q method reflects the difference between rotation strength and shear strength. Therefore, the velocity matrix can be normalized firstly to improve the rotation strength and reduce the shear strength, so as to improve the recognition of CS. Specifically, velocity component matrices are normalized by Eq. (9) and Eq. (10) respectively, and then Q value is calculated according to the above method. Fig. 5 shows the process chart of the improved Q method.

$$\tilde{u} = \frac{u}{\sqrt{u^2 + v^2}} \tag{9}$$

$$\tilde{v} = \frac{v}{\sqrt{u^2 + v^2}} \tag{10}$$

Fig. 6 compares the CS shown by streamlines and improved Q method. The CS identified by the improved Q method accord well with those shown in streamlines, and they can reflect the CS's position and shape, even smaller one that is not easy to be found in the streamlines. Therefore, the improved Q method provides a powerful tool for the CS identification. It makes it possible to further investigate their rules of

distribution, shape, scales, etc.

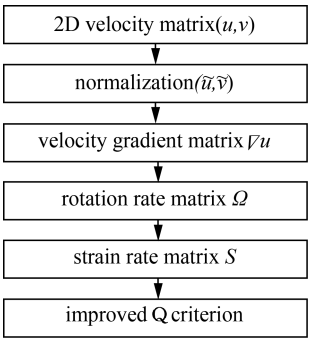

Fig. 5. Process chart of the improved Q method.

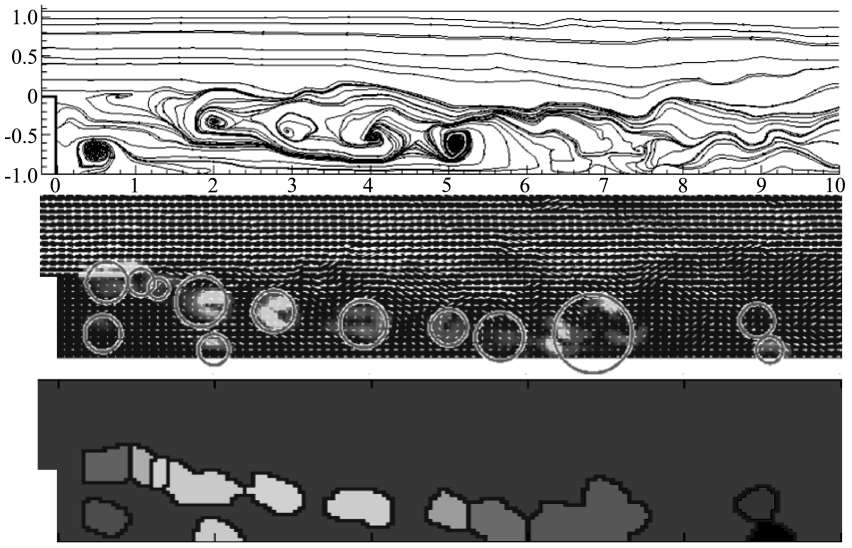

Fig. 6. Comparison of the CS shown by streamlines and improved Q method.

3.3 Discussion

Besides the Q method, identification methods based on velocity gradient tensor also include the vorticity (w) method, the $\triangle$ method, the λ_{ci} method, the λ_2 method and the streamline method. Comparisons and discussions are made in this section: (a) w method: In the early days, researchers defined a vortex as a structure carrying vorticity based on the vortex dynamics theory, and used w to represent a vortex (Bisset et al., 1990). w is twice the average rotational angular velocity of unit fluid element. It reflects the average rotation of the unit fluid element. Usually, a vortex is equivalent to the vorticity in the flow field. But the vorticity field is different from the vortex structure represented by the streamlines. Vorticity cannot reflect the rotation of fluid

elements and cannot reveal various vortex structures (Tian et al., 2017). For example, in a parallel shear flow, the vorticity is not zero, but intuitively the flow field does not have a rotating streamline; in a strong shear flow such as wall turbulence, the vorticity cannot distinguish the vortex structure from the shear layer background. Therefore, despite this criterion is widely used, it has big limitations (Li et al., 2014). (b) $\triangle$ method: The discriminant $\triangle$ of the characteristic equation of the velocity gradient tensor is used, and the region with $\triangle > 0$ is defined as the vortex region (Chong et al., 1990). (c) λ_{ci} method: The imaginary part λ_{ci} of the conjugate complex eigenvalue of the velocity gradient tensor is used, and the region where $\lambda_{ci} > 0$ is defined as the vortex region, which is called the rotation intensity method by Zhou et al. (1999). (d) λ_2 method: The second eigenvalue λ_2 of the Hessian Matrix of pressure is used. When $\lambda_2 < 0$, the Hessian Matrix of pressure has two negative eigenvalues, indicating that the pressure is determined by two negative eigenvalues. Local minima appear in the plane spanned by the corresponding eigenvectors, and Jeong (1995) defined a flow structure with this characteristic as a vortex. (e) Streamline method: Zou et al. (2006) proposed to use the local bending characteristics of streamlines to identify a vortex. By analyzing the streamline shape, the streamline patterns are usually divided into the patterns of the streamline itself and the relative relationship between streamlines. It is pointed out that the former is represented by velocity, curvature and torsion, while the latter requires new discriminant parameters. Finally, the C_0 criterion for vortex region identification and the three-parameter criterion $\{C_0, C_1, C_2\}$ for vortex core region identification are proposed. This method is similar to the vortical concept defined by Robinson (1991) from viewpoint of streamline, but it has not been extended.

For the Q method, it uses the second invariant Q of the velocity tensor, which means the difference between the rotation rate and the strain rate, and its value reflects the relationship between the rotational motion and shear motion. Hunt et al. (1988) defines the region where $Q > 0$ as a vortex region. And this improved Q method has increased the rotational intensity and emphasized the rotational motion. Therefore, it can show the rotational vortical structure that is consistent with what is shown by streamlines.

Chen Qigang (2014) compared $\triangle$ method, λ_{ci} method, λ_2 method and Q method when identifying CS in open channel turbulent flow. He believed that $\triangle$ method, λ_{ci} method, λ_2 method and Q method could all effectively identify vortex structure contained in flow field in two-dimensional flow field. Especially for those CS with large intensity, the results of different methods are consistent with those obtained by Chakraborty et al. (2005) in the three-dimensional flow field under the condition of

using appropriate thresholds. However, the BFS flow has significant differences from the near-wall flow. BFS flow has a strong free shear layer and is also attached by the wall. The CS formed in the free shear layer is different from that in the near-wall shear boundary layer, and the reattachment flow makes the vortical structure more complex. Therefore, the current methods cannot represent those vortical structures shown by streamlines, but a good result was obtained by the improved Q method.

4 Conclusions

The following conclusions can be drawn:

(1) The CS shown by streamlines are consistent with the phenomenon of flow visualization. This paper supports the vortical concept shown by streamlines, especially in the BFS flow.

(2) The improved Q method provides a powerful tool for the CS identification. The identification result accords well with those shown by streamlines, and they can reflect the CS's position and shape, even smaller one that is not easy to be found by streamlines.

Acknowledgements

This research is funded by the Science and Technology Support Program of Jiangsu Province (Grant No. BK20190142) and the National Natural Science Foundation of China (Grant No. 51909169). The authors gratefully acknowledge these financial supports.

References

Bisset, D. K., Antonia, R. A., Browne, L. W. B., 1990. Spatial organization of large structures in the turbulent far wake of a cylinder. Journal of Fluid Mechanics, 218(218):439-461.

Chakraborty, P., Balachandar, S., Adrian, R. J., 2005. On the relationships between local vortex identification schemes. Journal of Fluid Mechanics(535): 189-214.

Chen, Q. G., 2014. High-frequency measurement of vortices in open channel flow with particle image velocimetry. Tsinghua University.

Chong, M. S., Perry, A. E., Cantwell, B. J., 1990. A general classification of three-dimensional flow fields. Physics of Fluids, 2(5):765-777.

Chen, Q., Zhong, Q., Qi, M., et al., 2015. Comparison of vortex identification criteria for planar velocity fields in wall turbulence. Physics of Fluids, 27 (8):085101.

Hu, R.Y., Wang, L., Fu, S., 2016. Investigation of the coherent structures in flow behind a backward-facing step. International Journal of Numerical Methods for Heat & Fluid Flow, 26(3/4):1050-1068.

Hunt, J., Wray, A.A.,Moin, P., 1988. Eddies, streams, and convergence zones in turbulent flows. Center for Turbulence Research.

Jeong, J., Hussain, F. ,1995. On the identification of a vortex. Journal of Fluid Mechanics, 285(285):69-94.

Kostas, J., Soria, J., Chong, M., 2002. Particle image velocimetry measurements of a backward-facing step flow. Experiments in Fluids, 33(6):838-853.

Li, Z., Zhang, X.W., He, F., 2014. Evaluation of vortex criteria by virtue of the quadruple decomposition of velocity gradient tensor. Acta Physica Sinica, 5(63): 701-704.

Lugt, H.J., Gollub, J.P., 1984. Vortex flow in nature and technology. New York: Wiley-Interscience: 305.

Robinson, S.K., 1991. Coherent motions in the turbulent boundary layer. Annual Review of Fluid Mechanics, 23(1):601-639.

Tian, S., Gao, Y., Dong, X., et al., 2017. A definition of vortex vector and vortex. Journal of Fluid Mechanics, 849.

Wang, F.F., Gao, A., Wu, S.Q., et al., 2019. Experimental investigation of coherent vortex structures in a backward-facing step flow. Water.

Zhou, J., Adrian, R.J.,Balachandar, S., et al., 1999. Mechanisms for generating coherent packets of hairpin vortices in channel flow. Physics of Fluids, 387(10): 353-396.

Zou, W.N., 2006. On the vortex in fluid flow.

Zou, W.N., Zhao, Y., Dong, H., 2006. Vortex detection based on streamline analysis.

Distribution uniformity at diversion port of equal inertia filling and emptying system for hydro-floating ship lift

Jun Li[1], Feifei Sun[2], Qianyu Deng[3], Guangde Li[4]

[1,4] China Energy Engineering Group; Guangxi Electric Power Design Institute Co., Ltd., Nanning, China. email: 791796032@qq.com; 285533504@qq.com

[2] Design & Consulting Corp. NHRI, Nanjing, China. email: 810561975@qq.com

[3] Nanjing Hydraulic Research Institute; Key Laboratory of Navigation Structure Construction Technology, Ministry of Transport, PRC. Nanjing, China. email: 591727515@qq.com

Abstract: The paper conducts a study on the uniformity of flux distribution in the equal inertia filling and emptying system of hydro-floating ship lift, this paper introduces the characteristics of the equal inertia filling and emptying system and analyzes the main impact factors of the non-uniformity of branch flux, compares the influence of different lengths of straight pipe sections in front of each level of branch on flux distribution through mathematical models, and obtains the influence of spatial arrangement conditions on the uniformity of flux distribution in the equal inertia filling and emptying system.

Keywords: Hydro-floating ship lift; Equal inertia filling and emptying system; Flux distribution; uniformity

1 Introduction

The hydro-floating ship lift drives the balancing weight to lift and lower through the filling and emptying system, fills and discharges water to the shaft, and then drives the ship chamber to run through the wire rope. The hydraulic characteristics of the water flow in the hydraulic drive system directly affect the synchronization of each counterweight and the stationarity of the ship chamber operation, so it is important to study the characteristics of the water flow in the hydraulic drive system.

2 Characteristics of equal inertia hydraulic drive system

The hydraulic synchronous system used in the completed and operating Jinghong

hydro-floating ship lift consists of equal inertia filling and emptying system and 16 independent shafts. The geometric structure of the equal inertia filling and emptying system is completely symmetrical, and the inertia length from the water inlet to the outlet branch at the bottom of each shaft is equal. The first and second diversions are arranged on the plane, and the third and fourth diversions are carried out on the elevation (the third and fourth diversions are arranged in the load-bearing structural walls). The water flow through each level of diversions changes the flux direction into the next diversion using right-angle bends, and through four diversions, the water flows in the upstream main are distributed to each independent shaft.

Equal inertia filling and emptying system pipeline diversion structure is shown in Fig. 1. The filling and emptying system in the horizontal direction is a primary diversion and secondary diversion, and in the vertical direction is a three-stage diversion and four-stage diversion. The length of the straight pipe section before one to four-stage diversion is L1, L2, L3, L4, respectively, and the final branch length is L5.

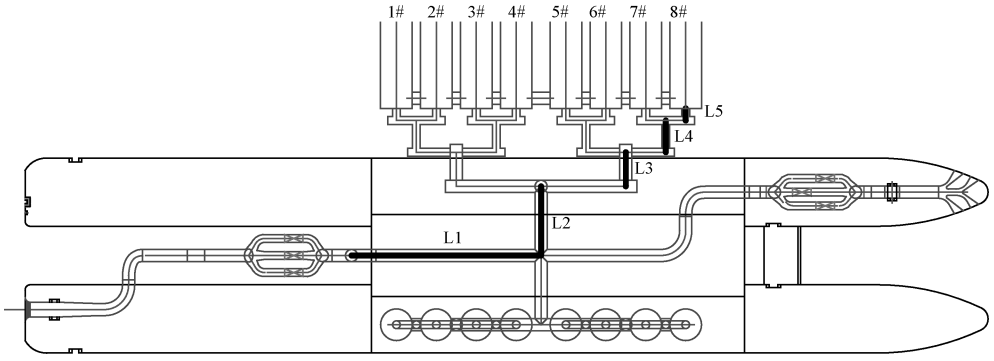

Fig. 1. Equal inertia filling and emptying system diversion piping layout.

The geometric structure of the equal inertia filling and emptying system is symmetrical, but each branch flux is different, mainly for the following reasons: on the one hand, the constraints of the spatial arrangement conditions exist, the length of the straight pipe section in front of the manifold at all levels is short, the flux velocity distribution in the pipe before the manifold is not uniform, and there is the phenomenon of undesirable flow, resulting in uneven manifold flow at all levels; on the other hand, due to the effect of turbulence and construction accuracy, the flux distribution at each manifold is not completely equal. The above factors lead to uneven the last outlet branch flux and difference of water level between the shafts.

The branch flux in the equal inertia filling and emptying system is uneven, and each shaft is independent of the other, resulting in the inability to eliminate the water level difference of each shaft in time. Although there is a connecting corridor at the

bottom of the shafts, the water level between the shafts changes quickly, under the inertia of water flow, the connecting corridor has limited effect on the timely adjustment and equalization of the water level difference of the shaft. Previous research results have shown that with the increase of flow rate and flow velocity in the filling and emptying system, the unevenness of outflow will also be further intensified.

Therefore, it is necessary to analyze the influence of spatial factors on the uniformity of the diversion of the equal inertia filling and emptying system, and the research results are important for optimizing the design of the hydro-floating ship lift drive system and analyzing the applicability of the equal inertia filling and emptying system.

3 Calculated working condition

In this paper, based on the Jinghong ship lift project, the characteristics of the branch flux of the hydraulic drive system of "independent shaft + equal inertia filling and emptying system" are calculated and analyzed through mathematical model tests, and the influence of the length of the branch pipes in front of the diversion manifold at all levels on the uniformity of the diversion is studied.

In order to explore the influence of the length of the branch pipe before the diversion manifold at each level on the uniformity of the diversion, the length of the straight pipe before the tertiary and quaternary diversion manifold (L3 and L4) and the length of the branch pipe at the final stage (L5) were increased to 5 times the pipe diameter, and the uniformity of branch flux before and after the adjustment was compared. The calculated working conditions are shown in Table 1, and the process line of the water delivery flow for the calculated working conditions is shown in Fig. 2.

Table 1 Calculated working conditions for the analysis of the effect of branch length on manifold uniformity.

Working condition	Length of straight pipe section before the three-stage manifold (L3) (m)	Length of straight pipe section before the four-stage manifold (L4) (m)	Length of end-stage branch pipe (L5) (m)
zg00	7.0	6.5	2.5
zgL3	12.5(5 times tube diameter)	6.5	2.5
zgL4	12.5(5 times tube diameter)	8(5 times tube diameter)	2.5
zgL5	12.5(5 times tube diameter)	8(5 times tube diameter)	8(5 times tube diameter)

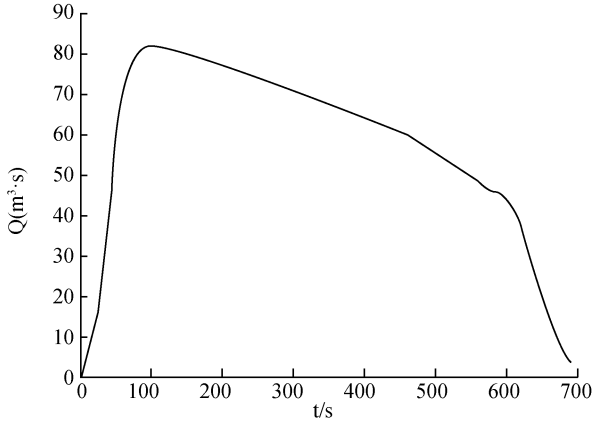

Fig. 2. Process line of water delivery flow in the calculated working conditions.

4 Analysis of manifold uniformity

The longitudinal velocity vector distribution of the hydraulic drive system at a typical moment (maximum flow rate) is shown in Fig. 3. As shown in the figure, the water flow in the equal inertia filling and emptying system reaches each stage of the diversion manifold for diversion after a right-angle turn to change direction. The length of the straight pipe section in front of the vertical three-stage and four-stage manifold is short, and the flux velocity distribution in the pipe is asymmetrical, with obvious phenomenon of undesirable flow, which affects the uniformity of the manifold.

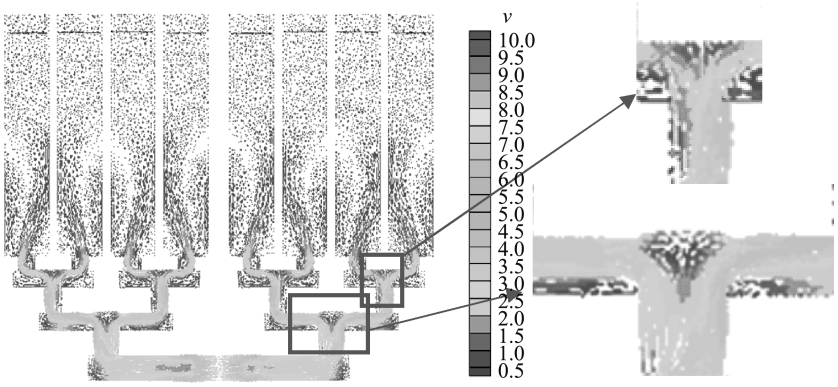

Fig. 3. Typical moment longitudinal profile flow velocity vector diagram.

The relative deviation (the ratio of the deviation to the average flow) was used as an index to analyze the flux deviation generated by the diversion at each level of the manifold, and to study the influence of the length of the straight section in front of the manifold on the uniformity of diversion. The statistical results are shown in

Table 2. Among them, the deviation of secondary diversion is the deviation of the total branch flux 1－4# and 5－8#, the deviation of tertiary diversion is the deviation of the total branch flux 1－2# and 3－4#, 5－6# and 7－8#, and the deviation of quaternary diversion is the deviation of branch flux 1# and 2#, 3# and 4#, 5# and 6#, 7# and 8#.

Mathematical model calculation results show that: increasing the length of the straight pipe before the three-stage manifold can improve the uniformity of the manifold at the two-stage and three-stage manifolds, and increasing the length of the straight pipe before the four-stage manifold can improve the uniformity of the manifold at the three-stage and four-stage manifolds; the more the number of stages, the greater the deviation accumulated by the manifold.

Table 2 Influence of branch length on the uniformity of the manifold.

Working condition	Secondary deviation	Tertiary deviation	Fourth level deviation
zg00	1.0%	5.0%,4.5%	14%,13%,11%,10%
zgL3	0.6%	4.0%,2.0%	14%,13%,12%,12%
zgL4	0.8%	2.5%,2.0%	7.5%,5.5%,4.5%,4.0%
zgL5	0.7%	2.1%,1.7%	4.5%,4.0%,3.0%,2.5%

The standard deviation of the branch flux (S_q) responds to the degree of dispersion of the flow. The process line of the change of the standard deviation of branch flux for the four groups of working conditions in the water filling process is shown in Fig. 4. As shown in this figure, the length of the straight pipe section in front of the diversion manifold of the equal inertia filling and emptying system is increased to 5 times the pipe diameter, which can significantly improve the uniformity of the branch flux, and the standard deviation of the branch flux is reduced by about 70%.

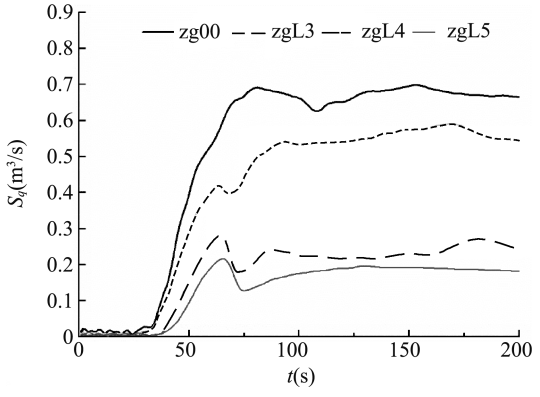

Fig. 4. Influence of the length of the straight pipe section in front of the manifold on the uniformity of branch flux.

5 Conclusions

Constrained by the space arrangement conditions, the length of the straight pipe section in front of the diversion manifold in the project is usually less than 5 times the pipe diameter, resulting in uneven diversion. If the lifting height increases, the water flow rate and flow velocity will be further increased, which will aggravate the unevenness of the diversion of the equal inertia filling and emptying system, thus affecting the synchronization of the water level of the shaft and the stationarity of the ship chamber operation. Therefore, the hydraulic drive system arrangement type of "equal inertia filling and emptying system + independent shaft" needs further analysis and demonstration when applied to the hydro-floating ship lift with large lifting height.

References

Xue, S. Hydraulics of hundred-meter scale hydro-floating ship lift. Doctor thesis, Hohai University,2017.

Hu, Y. Basic research and application of hydro-floating ship lift. Doctor thesis, Nanjing Hydraulic Research Institute,2011.

Hu, Y., Xuan, G.X., Li, Z.H. Key technology research of hydraulic floating ship lift for Jinghong Hydropower Station on Lancangjiang River in Yunnan. Nanjing Hydraulic Research Institute,2008.

Zhang, R. Research on operating characteristics of HFSL. Beijing: China Institute of Water Resources and Hydropower Research, Hydraulics and River Dynamics,2007.

Effect of cross-river navigation obstruct bridge on navigable flow conditions and river regulation technology

Chen Xianzhong[1], Wang Yu[2], Weichun Qiu[3], Honghao Fan[4], Jianjun Zhao[5], Ming Zhang[6]

[1] Changshan River Waterway Development and Construction Headquarters, Quzhou, China

[2,5,6] State Key Laboratory of Hydrology-Water Resources and Hydraulic Engineering, Nanjing Hydraulic Research Institute, Nanjing, China. e-mail: wangy@nhri.cn

[3] Changshan Dingyang Shipping Construction and Development Co., Ltd., Quzhou, China

[4] Quzhou Jiujiang River Shipping Construction and Development Co., Ltd., Quzhou, China

Abstract: The construction of cross-river bridges was limited by many conditions such as river channels and construction, which might cause the deterioration of the navigable flow conditions and affect the navigation safety of ships. The pier distance for Quzhou-Jiujiang Railway Old Bridge on Changshan River could not meet the navigation requirements, and Quzhou-Jiujiang Railway Old Bridge and New Bridge ran in parallel, which contributed to more complicated flow conditions in the bridge area. This paper adopted 1/60 hydraulic model to numerically and experimentally propose route adjustment measures considering river regime, immigration, and railway on basis of the numerical simulation of the initial layout of navigable flow conditions. Engineering measures such as river dredging in the bridge area were adopted to reduce the intersection angle between the mainstream across the bridge and the railway bridge and effectively reduced the longitudinal and lateral flow velocity according to navigable flow conditions of new ship route. It had been verified that the optimized flow conditions could meet the navigability with $Q<650$ m^3/s, which significantly improved the navigable standard. The self-propelled ship model test showed that ship maneuvering parameters were all within the required range. The research results could be used as a reference for related projects.

Keywords: Navigation obstruct bridge; River regulation; Navigable flow conditions; Changshan River

1 Introduction

With the development of modern transportation, cross-river bridge construction solved the problem of connection of land transportation. Route direction and naviga-

tion need to be comprehensively considered for the selection of bridge sites. Depending on navigable width and flow conditions, the waterway passing through the bridge area also guaranteed a certain length of excessive straight section. However, there were all kinds of obstructions that cannot meet the requirements of all aspects. If a new bridge was built closer to the existing bridge, navigation obstruction effect on the navigation safety was more evident for the bridge group composed of two or more bridges comparing with a single bridge (Zhao et al., 2012).

The navigable flow conditions of the river segment with bridge group were influenced by the bridge spacing and bridge span, and more factors should be considered in the selection of bridge sites (Chen et al., 2012). The simulation of the three-dimensional mathematical model noted that the construction of the bridge pier group would raise the upstream flood level, and the hydrodynamic conditions also resulted in river bed deformation (He et al., 2007). Numerical simulation of the effect of angle between the axis of the pier group and the flow direction on flow field demonstrated that this effect increased with the increase of angle, and it was concluded that the staggered arrangement of piers could better reduce the adverse effects on the river flow field caused by the excessively large angle (Wu et al., 2009).

According to "Navigation Standard of Inland Waterway" in China, the normal direction of the bridge axis should be consistent with the flow direction of the water flow as much as possible, and the declination angle should be less than 5°. However, for the case of poor flow conditions in the curved river and bridge area, flow direction and the normal direction of the bridge axis were generally greater than 5°. In addition, the straight section of the upstream channel was short, which influenced the navigation safety (Chen et al., 2001). Shoji et al. (1986) proposed that if the distance between bridges was less than 8 times the ship length in the straight channel or the span of the main navigation hole was less than 2 to 3 times the ship length, the risk probability of the ship hitting the bridge would increase. Cheng et al. (2005) developed a calculation method for the net width of bridge navigation holes from the perspective of ensuring the safe navigation of the bridge area. Zhang et al. (2016) formulated the relationship between the bridge spacing and the bridge span on the river section of curved bridge group.

Obstructing navigation in bridge area could generally adopt a combination of regulating structures and river dredging (Hu et al., 2005). Furthermore, the waterway remediation in the bridge area of curved river should mainly concentrate on adjusting the river situation and flow path, and the regulation methods such as curving cut-off and plain-cutting were employed for obstructing navigation during the dry season (Xu et al., 2004). Among the current cross-river bridges on the Changshan River, only

Quzhou-Jiujiang Railway Old Bridge, 3 km upstream from the Zhaoxian Junction, could not meet the navigation requirements. For the initial layout, the angle between the centerline of the waterway and the centerline of the Quzhou-Jiujiang Railway Bridge (Old Bridge) is about 60°; and the net width between two piers of the old bridge was only about 27 m. It was difficult to control the rudder when the ship passed through the bridge hole, which was prone to collision pier accident and safety hazard. Therefore, it was necessary to conduct research on optimization and adjustment of the waterway layout of the Quzhou-Jiujiang Railway Bridge area, and explore corresponding river dredging and remediation measures to ensure the safety of ship navigation.

"Navigation Standard of Inland Waterway" stipulated that the control indicators of flow conditions in the entrance area of approach channel of the ship lock were longitudinal velocity, lateral velocity and inverse velocity $\leqslant$ 2.0 m/s, 0.3 m/s and 0.4 m/s for Class Ⅲ waterway, respectively. Here, the control index of the bridge area is implemented according to the above standard due to the complicated navigation conditions of the bridge area.

2 Project summary

The Quzhou-Jiujiang Railway Old Bridge, located in the micro-bend river section in vicinity of Wangjiayu Village about 3 km upstream of the Zhaoxian Junction, was parallel to Quzhou-Jiujiang Railway New Bridge and located upstream from the new bridge with the worst navigation conditions in the Changshan River channel. The piers distance of the Quzhou-Jiujiang Railway Old Bridge was about 34 m and the bridge was a 32 m simply supported beam. The designed maximum navigable water level was 75.8 m, and the navigable net height was 9.5 m. For the initial layout, the angle between the centerline of waterway and the centerline of old bridge was about 60° and the net width between the navigation holes of the old bridge was only about 27 m, as shown in Fig. 1. In order to ensure the safety of ships crossing the bridge, the route in the bridge area should be perpendicular to the axis of the railway bridge. Therefore, the route in the bridge area was S-shaped, and straight segment was short for the routes upstream and downstream of the railway bridge due to terrain restrictions. Additionally, the right bank of the bridge area was Wangjiayu Village, and the reconstruction of waterways and bridges should consider immigration issues.

3 Experiment and numerical simulation methodology

The test model was designed at the geometric scale of 1/60 on basis of Froude

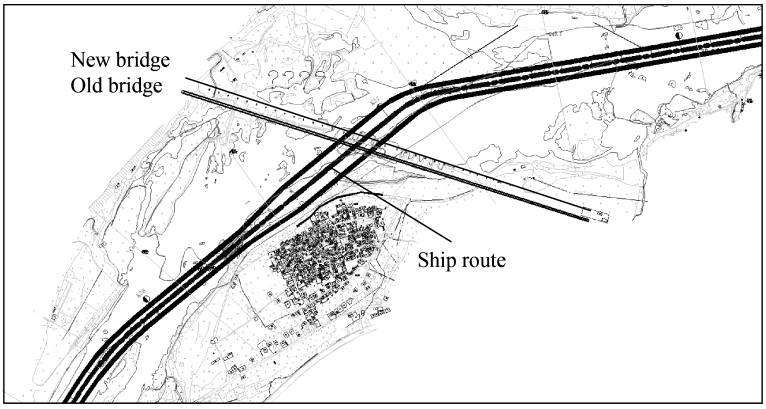

Fig. 1. Status quo of Quzhou-Jiujiang Railway area.

similarity criterion according to the similarity law of model, the terrain conditions of junction upstream and downstream and the laboratory site. There were curves upstream from railway bridge, therefore, the upper boundary of physical model was arranged at about 1.6 km upstream of railway taking account of the smooth inflow and navigable flow conditions, and the lower boundary of physical model should be taken at 1.6 km downstream from railway bridge.

The section method is used for terrain production, and the triangulation wire system is employed for plane stakeout where the triangle closure error hardly exceeded ±1′. The model elevation was measured by a level and checked during the production process, and the installation elevation error of the section was controlled by ±1 mm. For complex terrain, the intensive section was added and processed separately in order to improve the production accuracy. The junction, including sluice, ship lock and power station, was made of PMMA. The surface of the river was made of cement mortar. The overall model was photographed in Fig. 2.

The flow velocity measurement adopted the acoustic Doppler flow meter produced by Nortek Company with a range of 0.1 – 400 cm/s. The flow discharge was measured by a standard rectangular thin-walled weir with an error of less than 1%; the velocity was measured by a water level stylus with an accuracy of 0.02 mm.

On basis of hydrodynamic simulation software, numerical simulation constructs a two-dimensional flow numerical model of Quzhou-Jiujiang Railway Bridge area taking account of factors such as river dredging and the arrangement of bridge piers and anti-collision piers, as shown in Fig. 3. The upper boundary adopted the corresponding flow discharge, and the relationship between the water level and flow discharge of Zhaoxian Junction was used as the lower boundary.

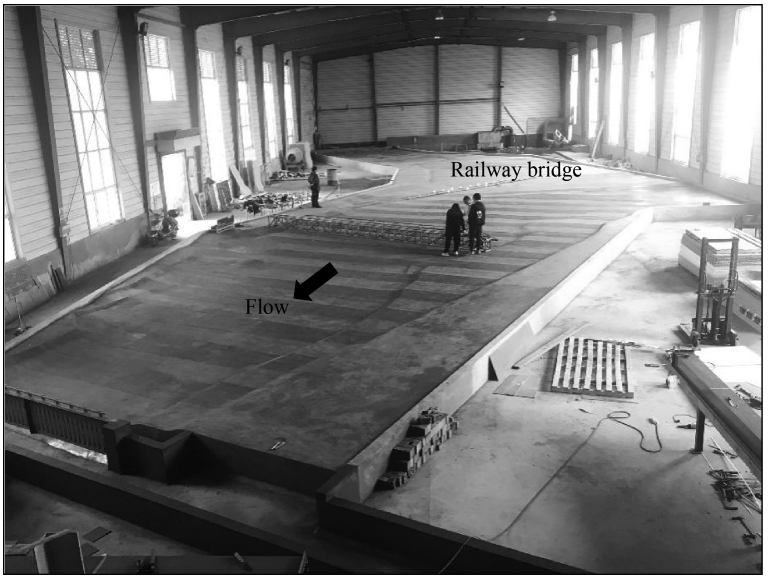

Fig. 2. Model photo of Quzhou-Jiujiang Railway Bridge area.

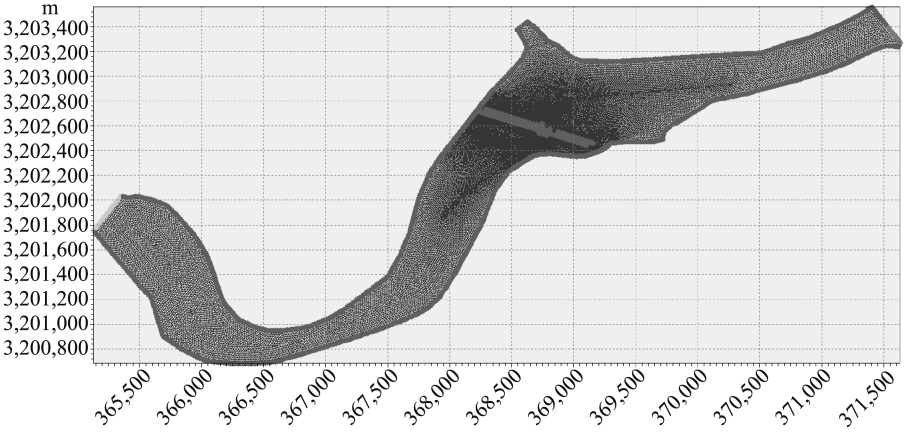

Fig. 3. Two-dimensional flow numerical model of Quzhou-Jiujiang Railway Bridge area.

4 Proposal comparison and optimization measures

In order to improve the safety of ships passing through the navigation piers of the Quzhou-Jiujiang Railway Bridge, the shipping route should be arranged perpendicular to the centerline of the old bridge. Therefore, the adjustment of the navigation layout of Quzhou-Jiujiang Railway Bridge area was plotted in Fig. 4, including two adjustment proposals. Proposal Ⅰ: The upstream route of the bridge site was arranged inside the existing river bank embankment; Proposal Ⅱ: The upstream route of the

bridge site is arranged outside the existing river bank embankment. For these two proposals, the center of the waterway in the bridge site area was basically perpendicular to the bridge. However, Proposal Ⅰ involved resettlement and demolition, and the embankment on the right bank should be retreated. The waterway elevation was 69.1 m.

(a) Definition sketch of Proposal Ⅰ

(b) Definition sketch of Proposal Ⅱ

Fig. 4. Definition sketch of ship route adjustment.

4.1 Proposal selection

On basis of waterway layout in Fig. 4(a), the results of numerical simulation demonstrated the maximum lateral flow velocity was calculated as 0.5 m/s in vicinity of the bridge site, and the lateral flow velocity was massively greater than 0.3 m/s

(see Fig. 5) for $Q=1{,}000$ m^3/s in Proposal Ⅰ. For $Q=500$ m^3/s, the maximum lateral velocity calculated in vicinity of bridge site was about 0.35 m/s. Therefore, flow conditions for Proposal Ⅰ hardly met the navigation requirements.

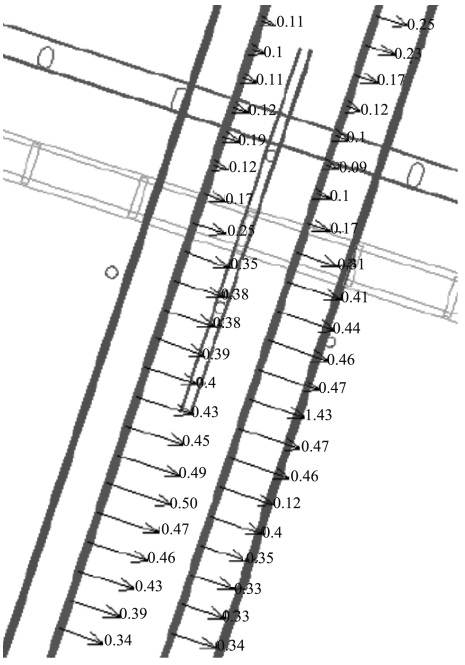

Fig. 5. Numerical simulation of lateral flow velocity for Proposal Ⅰ ($Q=1{,}000$ m^3/s).

On basis of waterway layout in Fig. 4(b), the results of numerical simulation demonstrated the maximum lateral flow velocity was calculated as 0.54 m/s in vicinity of the bridge site (see Fig. 6(a)) for $Q=500$ m^3/s in Proposal Ⅱ. Fig. 6(b) experimentally plotted lateral flow velocity in railway bridge area for $Q=500$ m^3/s. Affected by the flow rate and the overall river situation, the angle between the mainstream and the route at the bridge area was about 55°, the maximum lateral velocity of the left route was 0.41 m/s, and the maximum lateral velocity of the right route was 0.34 m/s. In summary, the combined results of numerical simulation and physical model test showed that flow conditions in the bridge area for $Q=500$ m^3/s hardly met the navigation requirements.

Fig. 6(c) gave the lateral flow velocity distribution at railway bridge area for $Q=400$ m^3/s. The overall flow regimes at the bridge area was smooth with an average flow velocity of about 0.3 m/s. The angle between flow direction and ship route was about 50°, the maximum lateral velocity of the left route was 0.25 m/s, and the maximum lateral velocity of the right route was 0.27 m/s. Therefore, navigable flow conditions meet the navigation requirements for $Q=400$ m^3/s.

Generally speaking, Proposal Ⅱ could meet the navigation requirements for $Q \leqslant 400\ m^3/s$, hence, Proposal Ⅱ was recommended as the preliminary proposal of route adjustment and further measures were proposed for optimization as Proposal Ⅰ required larger resettlement and the embankment on the right bank of the river should be retreated.

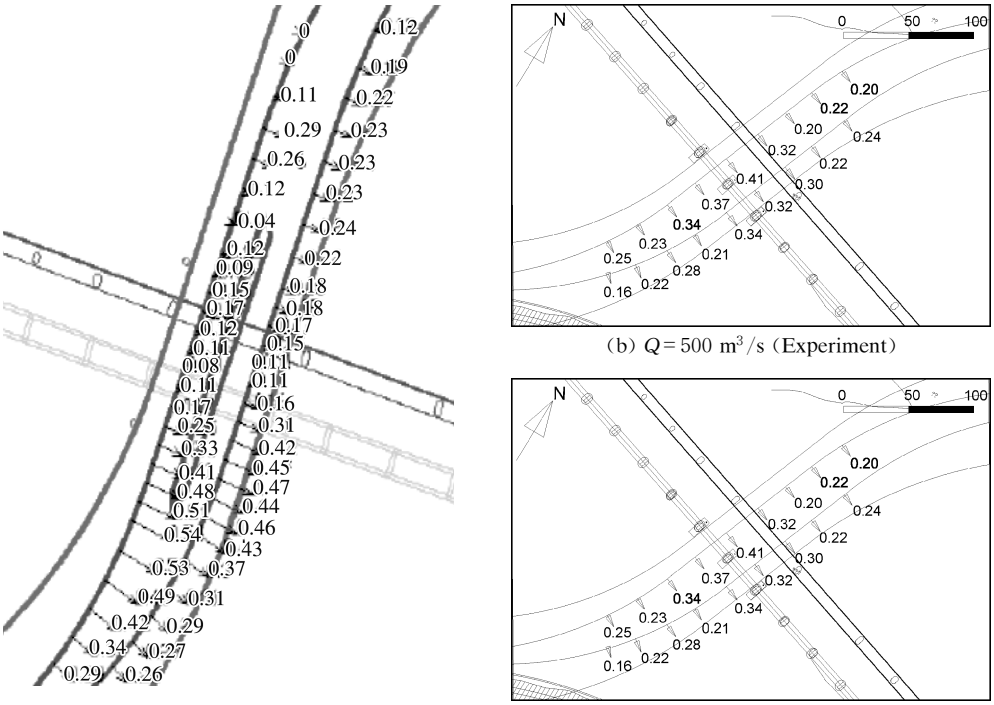

(a) $Q = 500\ m^3/s$ (Numerical simulation)

(b) $Q = 500\ m^3/s$ (Experiment)

(c) $Q = 400\ m^3/s$ (Experiment)

Fig. 6. Lateral flow velocity for Proposal Ⅱ.

4.2 Dredging measurement

Considering flood plain on the railway bridge area upstream and downstream, dredging could be employed on the left side of river to optimize the maximum navigable flow discharge. On basis of the dredging range and flood plain elevation, the flood plain dredging was carried out within 1 km upstream and 300 m downstream of the railway bridge. The definition sketch of dredging was shown in Fig. 7. The dredging elevation was 69.1 m, which was consistent with the waterway elevation.

Fig. 8 and Fig. 9 plotted the lateral velocity distributions at railway bridge areas for $Q = 650\ m^3/s$ and $800\ m^3/s$, respectively. It could be seen that the average flow velocity was about 0.42 m/s for $Q = 650\ m^3/s$ and dredging the upstream of the railway bridge could optimize the flow velocity. The angle between the main stream and ship route at the bridge area was about 40°. The maximum lateral flow velocity of the

Fig. 7. Dredging measurement for Proposal Ⅱ.

left and right route was all 0.29 m/s; therefore, flow conditions met the navigation requirements for $Q=650$ m^3/s.

The average flow velocity was about 0.50 m/s for $Q=800$ m^3/s, and the angle was about 40° between the mainstream and ship route at the bridge area. The maximum lateral velocity on the left route and right route was 0.38 m/s and 0.36 m/s, respectively. Therefore, navigable flow conditions for $Q=800$ m^3/s were slightly beyond the navigation standard, which hardly met the navigation requirements.

To sum up, flow conditions meet navigation requirements for $Q\leqslant 800$ m^3/s within dredging the terrain of the bridge area to 69.1 m.

5 Self-propelled ship model test

According to the proposal of shipping route, the ships passed through the old bridge by two routes on the left and right. The self-propelled ship model test had respectively verified the navigation index of the ship for going up and down along different routes. For the upgoing ships along the left route (see Fig. 10(a)), maximum steering angle, maximum drift angle and maximum roll angle were 20°, 8° and 1.0°, respectively. For the upgoing ships along the right route (see Fig. 10(b)), maximum speed of the opposite bank, maximum steering angle, maximum drift angle and maxi-

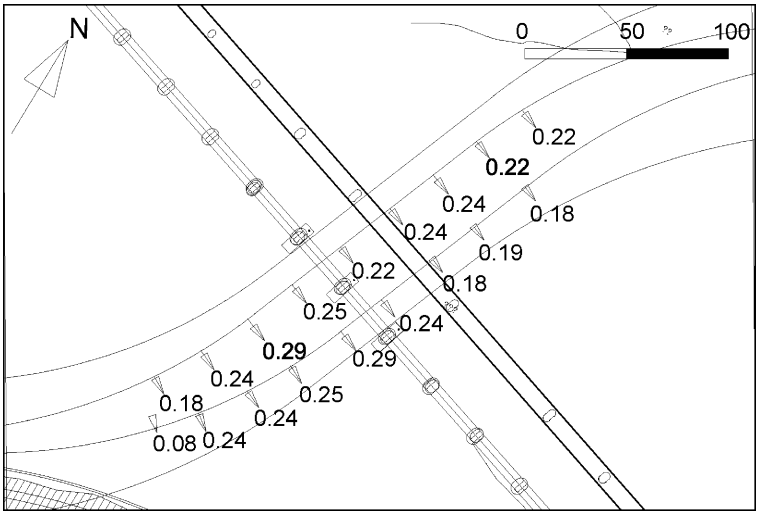

Fig. 8. Lateral flow velocity for Proposal Ⅱ (Q=650 m³/s).

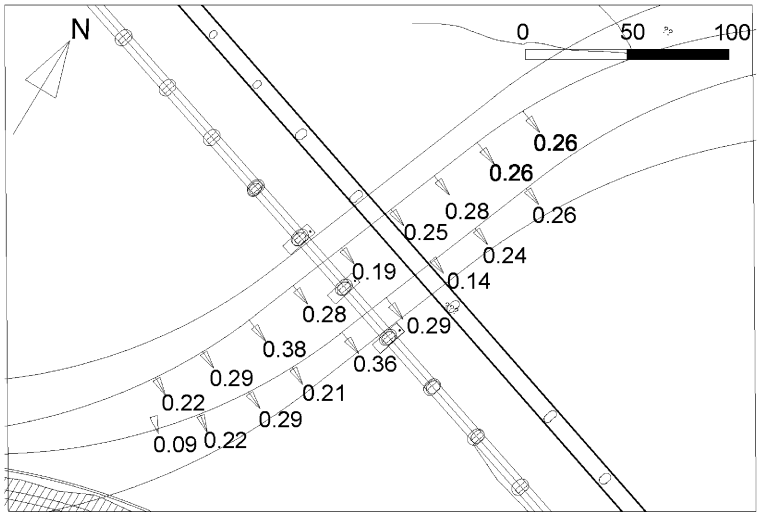

Fig. 9. Lateral flow velocity for Proposal Ⅱ (Q=800 m³/s).

mum roll angle were 1.8 m/s, 20°, 10° and 1.0°, respectively.

For the downgoing ships along the left route (see Fig. 11(a)), maximum steering angle, maximum drift angle and maximum roll angle were 15°, 10° and 1.0°, respectively. For the downgoing ships along the right route (see Fig. 11(b)), maximum steering angle, maximum drift angle and maximum roll angle were 20°, 10° and 1.0°, respectively.

For the upgoing ships along the left route and the downgoing ships along the right route, the control difficulty increased due to the short upstream straight section of the

right route and the downgoing poor rudder efficiency of going down.

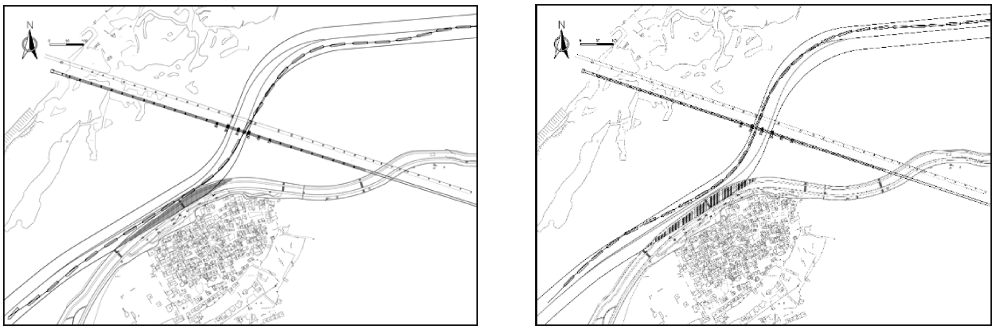

(a) Along left route (b) Along right route

Fig. 10. Ship track line and sailing attitude in bridge area (upgoing).

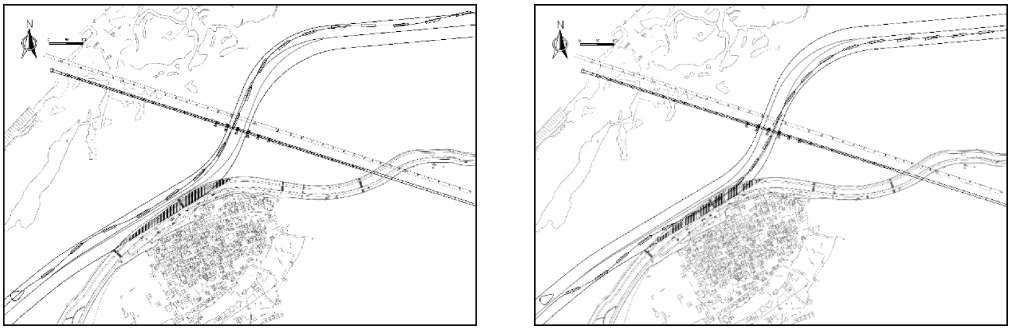

(a) Along left route (b) Along right route

Fig. 11. Ship track line and sailing attitude in bridge area (downgoing).

6 Conclusions

(1) In order to ensure the safety of ships crossing the bridge, the shipping route in the bridge area should be perpendicular to the axis of the railway bridge. By comparison and selection, Proposal Ⅱ without immigrants was determined as the preliminary proposal.

(2) Numerical simulation and physical model test research showed that Proposal Ⅱ could meet the navigation requirements for $Q \leqslant 400$ m^3/s, and the maximum navigable flow discharge 650 m^3/s could be met with river dredging measures.

(3) Self-propelled ship model test verified that the ships could pass through the railway bridge safely and smoothly, and the maneuvering parameters were within the required range. It was recommended that upgoing ships choose the right route and downgoing ships choose the left route.

Acknowledgements

This research has been financially supported by the National Natural Science Foundation of China (Grant No. 52009083), and the Natural Science Foundation of Jiangsu Province (Grant No. BK20200159).

References

Chen, M., Chen, M.D., Yang, B., et al., 2012. A review of navigation conditions and navigation safety along bridge group reach. Hydro-science and Engineering(4): 29-33.

Chen, M.D., Wang, D.Y., 2001. An approach to the navigable clearance dimensions and navigation safety guarantee measures for crossing-river bridge. Port & Waterway Engineering(4): 42-43.

Cheng, Y.Z., Xu, X.Y., Shen, X.X., et al., 2005. Calculation method of clear width of bridge on bend navigable waterway. Port & Waterway Engineering(1): 58-61.

He, G.J., Fang, H.W., Fu, R.S.,2007. Three-dimensional numerical analysis on water flow affected by piers. Journal of Hydrodynamics (Ser. A), 22 (3): 345-351.

Hu, X.Y., Ou, Y.F., Shen, X.X., et al., 2005. A review of studies on navigation problem of the area near a bridge and its countermeasures. Journal of Waterway and Harbor(3): 167-171.

Shoji, K., Wakao, T., 1986. On the ship's waterways passing through bridges. Water Forum: World Water Issues in Evolution, ASCE, 530-537.

Wu, F., Gan, M., 2009. Numerical simulation research on the effect by the bigger angle between the middle-line of the piers group and the river flow. Journal of North China Institute of Water Conservancy and Hydroelectric Power, 30 (1): 11-14. (in Chinese)

Xu, Z.H., Zhao, Z.Z., Chen, J.Q., et al., 2004. Waterway regulation scheme for curved river section with bridge. Port & Waterway Engineering(9): 53-55.

Zhang, Y.L., Chen, M., Wei, P.L., et al., 2016. Relationship between bridge distance and span at bridge group reach in mountainous rivers. Port & Waterway Engineering(4): 136-140.

Zhao, Z.Z., Chen, M.D., Lin, Q., et al., 2012. Navigation condition experiment of Caiyuanba bridge group reach of the Yangtze River. Journal of Chongqing Jiaotong University (Natural Science), 31 (6): 1240-1243.

Experimental study on comprehensive optimization of navigation flow condition of Pak Beng Hydropower Station in Mekong River

Changhai Han[1], Kaiwen Yu[2], Kang Han [3], Yu Yang[4], Zhiguang Yu[5]

[1,2,3,4] Nanjing Hydraulic Research Institute, State Key Laboratory of Hydrology Water Resources and Hydraulic Engineering, Nanjing, China. e-mail: kaiwyu@163.com

[5] Hubei Institute of Water Resources Survey and Design, Wuhan, China

Abstract: Pak Beng Hydropower Station is characterized by curved river sections, a large number of units and sluices, and large total discharge, so the contradictions between flood discharge, power generation and shipping are very prominent. In this paper, the hydraulic model with a scale 1 : 100 is used to study the flood discharge and navigation flow condition. The navigation flow condition of the upstream approach channel with floating navigation embankment and the pier-plate navigation embankment, and the navigation flow condition of the downstream approach channel with permeable section were tested. The structural types of the upstream and downstream navigation buildings are optimized and the maximum navigable discharge is determined. In addition, an optimal scheduling scheme is proposed to consider energy dissipation and anti-scouring comprehensively. The results show that the navigable guarantee rate can reach more than 95% under the discharge of 10,000 m^3/s, so 10,000 m^3/s is determined as the maximum navigable discharge. Under the maximum navigable discharge, when the upstream navigation wall adopts the floating navigation dike, the downstream adopts the navigation wall and additional permeable piers, and the number of units is more than half, not only the navigation flow condition can be met, but also the outflow velocity of the stilling basin is not greater than the anti-scour flow velocity of the riverbed.

Keywords: Pak Beng Hydropower Station; Navigation flow condition; Flood discharge and energy dissipation; Optimized operation

1 Introduction

The navigation flow condition at the entrance area of the approach channel can affect the navigation of ships, which is jointly affected by multiple factors such as ter-

rain, layout, and operation scheduling (Li et al., 2011; Yu, 2014; Li et al., 2015). At the entrance area of the approach channel, bad flow patterns are easy to appear, such as oblique flow, transverse circulation and backflow, which seriously affect the navigation safety of ships (Ma et al., 2011; Wei, 2012; Wang et al.,1998). Besides, for the project with a large number of generator units and discharge sluices, the impact of operation scheduling modes on the navigation flow condition is also prominent (Wu et al., 2006; Wu, 2016).

The flow characteristics of the approach channel are important technical indexes for navigation safety evaluation of navigable buildings. According to "Code for Master Design of Shiplocks" (People's Communications Press,2001), for IV ship lock, in the navigation section and adjustment section of the approach channel, the flow pattern should be still water; in the anchorage area of the approach channel, the longitudinal flow velocity and transverse velocity should be less than 0.5 m/s and 0.15 m/s respectively; in the entrance area, the longitudinal flow velocity, transverse flow velocity and backflow velocity should be less than 2.0 m/s, 0.3 m/s, and 0.4 m/s, respectively.

Pak Beng Hydropower Station is composed of non-overflow dams on both banks, flood-discharging and sand-sluicing gates, power station buildings, ship locks and fishways, as shown in Fig. 1. The crest length, the maximum dam height and the normal water level are 899.5 m, 69 m, and 340 m, respectively. Powerhouse section is located in the left main river channel with 18 generator units; 14 discharging sluices with the size of 15 m×23 m are arranged in the dam section of flood discharge and sand sluice, and the sluices are divided into Zone 1, 2 and 3 from left to right, where there are 3 holes in Zone 1 and Zone 2 and 8 holes in Zone 3; the ship lock dam section arranged on the right bank is designed according to the standard for 500 t navigation ship, and the effective size of the lock chamber is 120 m×12 m×4 m (length×width×threshold depth). The original designed maximum discharge is 13, 200 m^3/s.

Pak Beng Hydropower Station is located in the continuous turning section, the upstream water depth of which is large. The entrance area of the downstream approach channel is arranged on the convex bank of the bend, where the navigation flow condition is easily affected by the oblique flow and the bent flow, making the flow condition too complex to meet the navigation requirements. In addition, Pak Beng Hydropower Station is characterized by a large number of units and sluices, and large total discharge, so the contradictions between flood discharge, power generation and shipping are very prominent. Therefore, it is necessary to conduct experimental research on the shape of navigation wall, navigation flow conditions and scheduling methods. Based on 1∶100 hydraulic model test, reasonable layout of approach chan-

nel and scheduling methods of the hydro-junction are proposed, and the maximum navigable discharge is demonstrated and determined.

The overall model is designed according to the gravity similarity criterion. The total length of the simulated river channel is 5.4 km, including 2.7 km above the dam axis and 2.7 km below the dam axis.

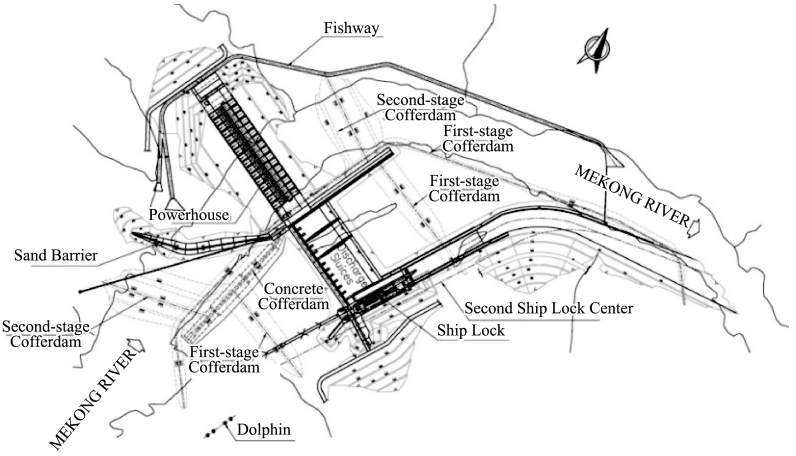

Fig. 1. General layout of Pak Beng Hydropower Station.

2 Experiment on navigation flow condition of upstream approach channel

In order to put forward a reasonable layout scheme of the navigation wall of the upstream approach channel, a comparative test was conducted between floating navigation embankment and the pier-plate navigation embankment. As shown in Fig. 2, for the pier-plate navigation embankment, the pile number of the navigation wall, the length of the navigation wall, the normal water level and the draft depth are 0 -250, 226.5 m, 340 m and 10 m respectively. For floating navigation embankment, the pile number, the length, the width of the navigation wall, and the draft depth are 0 - 265, 241.5 m, 9.4 m and 3 m respectively. Experimental results of upstream navigation flow conditions are shown in Table 1 and Fig. 3.

For pier-plate navigation embankment scheme, under the discharge of 13,200 m^3/s with the even opening of discharge sluices in Zone 3, the flow velocity in the upstream approach channel is obvious, which is far beyond the requirement of static water stipulated in the code, and the transverse flow velocity in the entrance area of approach channel is also greater than 0.3 m/s. Under the discharge of 13,200 m^3/s with the even opening of discharge sluices in Zone 1 and 2, the flow velocity in the upstream approach channel and the transverse flow velocity in the entrance area exceed

the standard. Under the discharge of 5,771 m^3/s and the power station generating at full load, the flow velocity near the ship lock can meet the navigation requirements. Therefore, the pier-plate navigation embankment scheme is only feasible under the full load condition of the power station.

For floating navigation embankment scheme, under the discharge of 13,200 m^3/s with the even opening of discharge sluices in Zone 1, the maximum velocity in the upstream approach channel is 0.88 m/s and a backflow area with the flow velocity of 0.49 m/s is within 100 m of the approach channel, so the flow velocity of the upstream approach channel cannot meet the navigation requirements. Under the discharge of 13,200 m^3/s with the even opening of discharge sluices in Zone 1 and 2, the maximum velocity in the upstream approach channel and a backflow velocity also exceed the navigation requirements. Under the discharge of 10,000 m^3/s with the even opening of discharge sluices in Zone 1 and 2, the flow velocity in the upstream approach channel decreases to 0.29 m/s, so the flow condition in the approach channel basically meets the requirements.

According to hydrological statistics, the navigable guarantee rate of 10,000 m^3/s discharge can reach more than 95%. By considering the test results of upstream navigation flow condition, it is appropriate to take 10,000 m^3/s as the maximum navigation discharge. At the same time, it is reasonable and feasible to adopt the floating navigation embankment scheme in the upstream approach channel.

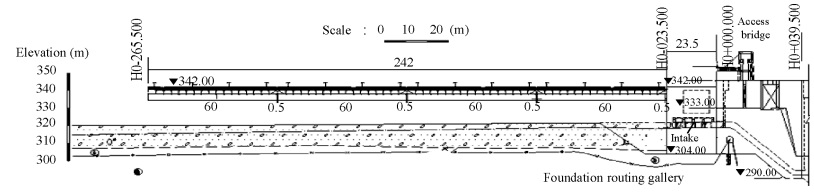

(a) Pier-plate navigation embankment

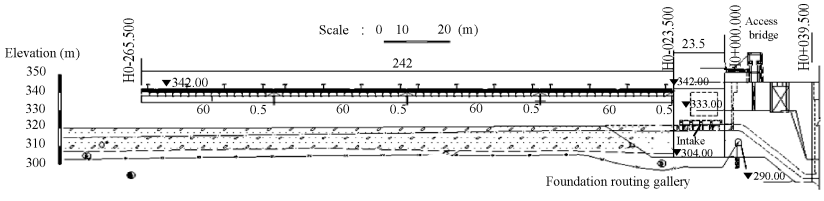

(b) Floating navigation embankment

Fig. 2. Layout of the upstream navigation wall.

Table 1 Navigation flow condition in different layout of the navigation wall of upstream approach channel.

Navigation wall scheme	Discharge (m^3/s)	Operation methods of power station/ discharge (m^3/s)	Scheduling methods of discharge sluices	The flow velocity (m/s)				
				In approach channel		In the entrance area		
				Longitudinal	Backflow	Longitudinal	Transverse	Backflow
Pier-plate	13,200	Full/5,771	Zone 3	1.40－1.88	0.00	2.04	0.36	0.00
	13,200	Full/5,771	Zone 1 and 2	0.60－0.85	0.38	1.99	0.44	0.00
Floating	13,200	Full/5,771	Zone 1	Max 0.88	0.49	1.74	0.16	0.63
	13,200	Full/5,771	Zone 1 and 2	Max 0.93	0.38	1.77	0.15	0.38
	10,000	Full/5,771	Zone 1 and 2	Max 0.29	0.29	0.76	0.13	0.29
Control index						≤2.00	≤0.30	≤0.40

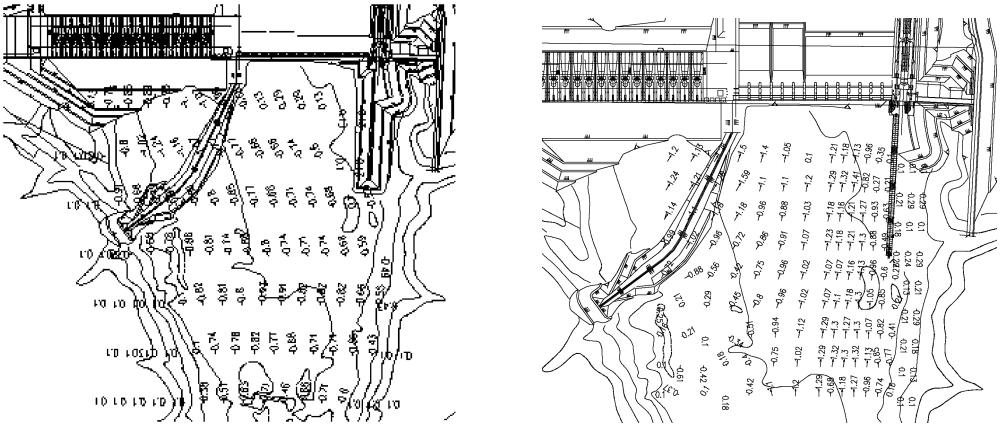

(a) Pier-plate navigation embankment with discharge of 5,771 m^3/s

(b) Floating navigation embankment with discharge of 10,000 m^3/s

Fig. 3. Velocity distribution of upstream approach channel(m/s).

3 Experiment on navigation flow condition of downstream approach channel

3.1 Originally designed scheme

In the originally designed scheme of the downstream approach channel, the test conditions and results of navigation flow condition at the entrance area are shown in Fig. 4 and Table 2. Under the discharge of 13, 200 m^3/s, there is a backflow zone in the entrance area of the downstream approach channel resulting from the flow around the embankment head. The backflow velocity in the right channel reaches 0.57～0.85 m/s and the longitudinal velocity exceeds 2.0 m/s, so the navigation flow condition at the entrance area seriously exceeds the standard. Under the discharge of 10,000 m^3/s,

the maximum backflow velocity in the right channel is 0.46 m/s, and the navigation flow condition at the entrance area does not completely meet the navigation requirements. Under the discharge of 5,771 m^3/s, the characteristic velocity within 300 m of the entrance area can meet standard except that the backflow velocity of some points in the entrance area of the right channel reaches 0.49 m/s. Under the condition of minimum navigation discharge (1,650 m^3/s), the flow velocity of downstream approach channel can meet the navigation requirements except transverse velocity of a few points on the left line of the channel.

It can be concluded that when the discharge is not higher than the full discharge of 5,771 m^3/s of the power station, the flow condition at the entrance area can basically meet the specification requirements. However, under the condition of the designed maximum navigable discharge (10,000 m^3/s), the longitudinal flow velocity and backflow velocity cannot meet the requirements of the specification. Therefore, it is necessary to further optimize the layout scheme of the navigation wall of the downstream approach channel.

Table 2 Characteristic velocity of the entrance area in original design scheme of downstream navigation wall.

Discharge (m^3/s)	Upstream water level (m)	Operation methods of power station/ discharge(m^3/s)	Scheduling methods of discharge sluices	Maximum velocity measurement(m/s)		
				Longitudinal	Transverse	Backflow
13,200	340	Full/5,771	Zone 1 and 2	2.24	0.28	0.85
10,000	340	Full/5,771	Zone 1 and 2	1.88	0.15	0.46
5,771	340	Full/5,771	Closed	1.78	0.28	0.49
1,650	335	5 units	Closed	0.83	0.37	0.32
Control index				≤2.00	≤0.30	≤0.40

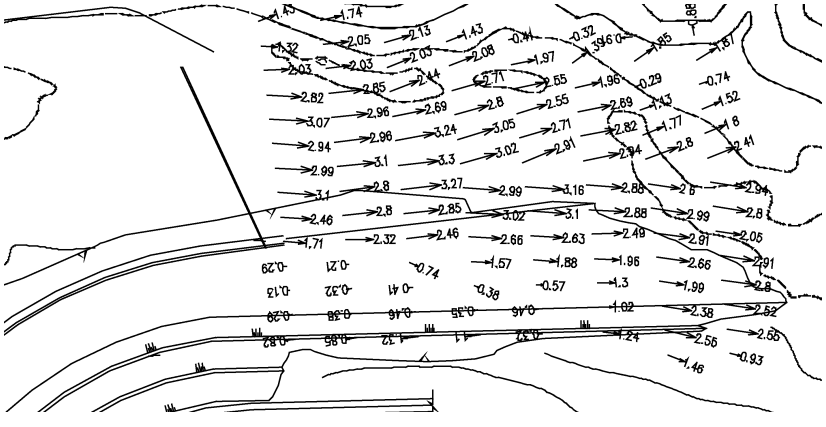

Fig. 4. Velocity distribution in downstream river and the entrance area of approach channel with the discharge of 10,000 m^3/s in original designed scheme (m/s).

3.2 Optimized layout scheme of navigation wall

3.2.1 Optimized scheme 1

Because the downstream entrance area is located on a narrow riverbed, it is possible to move the entrance area up to a slightly wider river channel to reduce the flow velocity of the river channel. Optimized scheme 1 is proposed according to the actual situation of the river channel, in which the downstream navigation wall is shortened by 100 m and the entrance area is moved up to a slightly wider river channel. 4 test conditions of the original scheme are repeated and the results are shown in Table 3.

Under the discharge of 13,200 m^3/s, the longitudinal velocity on the left line of the approach channel at 200 m in the downstream entrance area exceeds the standard, and the backflow velocity on the right line of the approach channel exceeds the standard. Under the discharge of 10,000 m^3/s, the backflow velocity on the right line of the approach channel exceeds the standard, and the maximum backflow velocity on the route is 0.68 m /s. Under the discharge of 5,771 m^3/s or 1,650 m^3/s, the flow velocity at the entrance area of downstream approach channel can meet the navigation requirements except for some points on the right line of the approach channel.

In order to meet the navigable feasibility of 13,200 m^3/s and 10,000 m^3/s as far as possible and reduce the influence of backflow on navigation, the layout of the navigation wall of the downstream approach channel needs to be further optimized.

Table 3 Characteristic velocity of the entrance area in optimized scheme 1 of downstream navigation wall.

Discharge (m^3/s)	Upstream water level (m)	Operation methods of power station/ discharge(m^3/s)	Scheduling methods of discharge sluices	Maximum velocity measurement(m/s)		
				Longitudinal	Transverse	Backflow
13,200	340	Full/5,771	Zone 1 and 2	2.18	0.17	0.85
10,000	340	Full/5,771	Zone 1 and 2	1.88	0.09	0.68
5,771	340	Full/5,771	Closed	1.31	0.19	0.46
1,650	335	5 units	Closed	0.65	0.10	0.54
Control index				≤2.00	≤0.30	≤0.40

3.2.2 Optimized scheme 2

The main problem of optimized scheme 1 is that the backflow velocity on the right line of the approach channel exceeds the standard. Studies show that supplying water to the approach channel by means of permeable piers can effectively reduce the effect of backflow. Therefore, on the basis of the optimized scheme 1, an additional permeable pier of 84 m is set up, as shown in Fig. 5. Two working conditions of 13,200 m^3/s and 10,000 m^3/s of the original layout scheme were repeated, and the re-

sults are shown in Fig. 6.

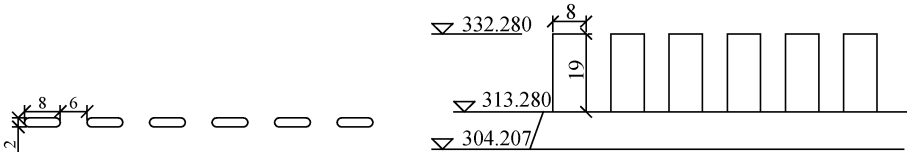

(a) Plane layout (b) Facade layout

Fig. 5. Schematic diagram of permeable pier (m).

Under the discharge of 13,200 m^3/s, the flow velocity on the navigation route can basically meet the standard except that the backflow velocity of a few points at 300 m from the right line of the approach channel exceeds the standard. Under the discharge of 10,000 m^3/s, the flow velocity at the entrance area can basically meet the navigation standard except for the longitudinal velocity and transverse velocity of a few points at 300 m from the right line of the approach channel.

It can be concluded that when the navigation wall of the downstream approach channel is shortened by 100 m and an additional permeable pier of 84 m is set up on the basis of the originally designed scheme, the navigation flow condition can meet the requirements under the maximum navigable discharge (10,000 m^3/s).

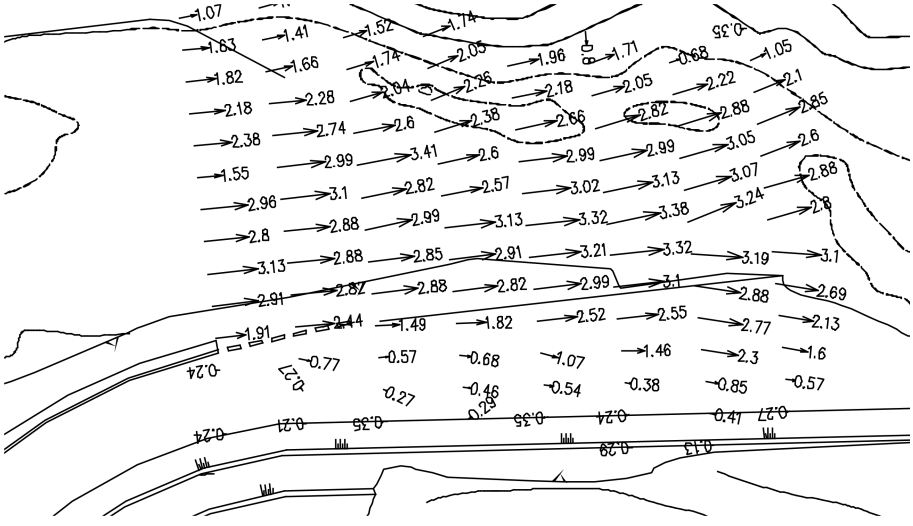

Fig. 6. In optimized scheme 2, velocity distribution in downstream river and the entrance area of approach channel with the discharge of 10,000 m^3/s (m/s).

4 Reasonable operation and scheduling methods of the hydro-junction

In the previous navigable tests, the conditions considered are that the power station generates at full capacity with the discharge of Q = 5,771 m^3/s, and the remaining flow is discharged through the sluices in Zone 1 and 2. Further, under the condition that the power station is full and the opening of the discharge sluices gradually increases to the side of the ship lock, it is necessary to clarify the navigation flow condition in the upstream approach channel and know how to schedule the sluices when half of the units of the power station are shut down. The following scheduling schemes are formulated, shown in Table 4.

Table 4 The scheduling methods of the discharge sluices in model test.

Operation condition	Upstream water level(m)	Discharge (m^3/s)	Operation methods of power station	Scheduling methods of discharge sluices
1	340	10,000	16 units are full	Evenly open 6 holes in Zone 1 and 2
2			16 units are full	Evenly open 6 holes in Zone 1 and 2 and 2 holes on the left side of Zone 3
3			16 units are full	Evenly open 6 holes in Zone 1 and 2 and 3 holes on the left side of Zone 3
4			The 8 units on the left are full and the 8 units on the right are closed	Evenly open 14 holes
5			The 8 units on the left are full and the 8 units on the right are closed	Evenly open 6 holes in Zone 1 and 2 and 2 holes on the left side of Zone 3
6			The 8 units on the left are full and the 8 units on the right are closed	Evenly open 6 holes in Zone 1 and 2

4.1 Flow conditions in the approach channel under different scheduling methods

The velocity distributions in the approach channel under different operation scheduling methods are shown in Fig. 7. For operation condition 1, the maximum velocity in the upper approach channel is 0.29 m/s, and the flow condition at the entrance area of the approach channel can basically meet the requirements. For operation condition 2, there is a backflow velocity of 0.32 m/s in the upstream approach channel 150 m away from the entrance area, while the flow conditions at the entrance area of approach channel basically meet the specification requirements. For operation condition 3, there is a longitudinal velocity of 0.66 m/s in the approach channel 100 m away from the entrance area of the upstream approach channel, but the flow

conditions at other locations in the approach channel can basically meet the specification requirements. For operation condition 4, the flow velocity is about 1.2 m/s, which cannot meet the navigation requirements. For operation condition 5 and 6, the flow velocities in the upstream approach channel are 1.0 m/s and 0.6 m/s, respectively. And they also cannot meet the navigation requirements.

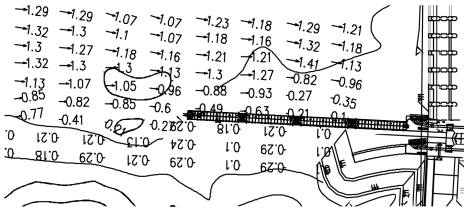

(a) Operation condition 1

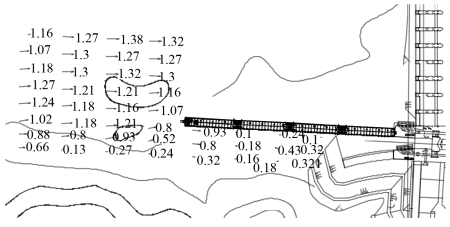

(b) Operation condition 2

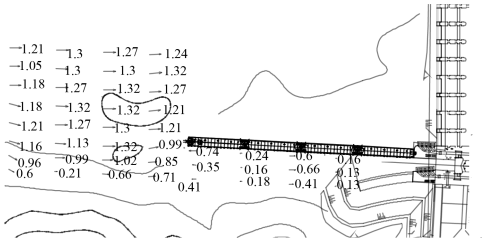

(c) Operation condition 3

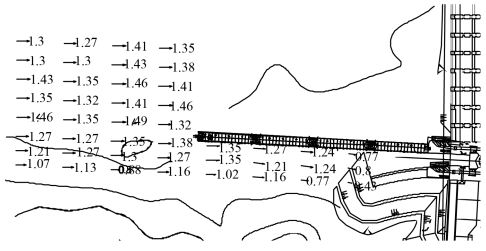

(d) Operation condition 4

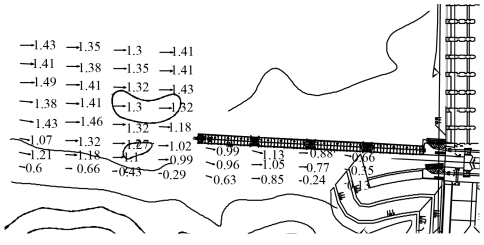

(e) Operation condition 5

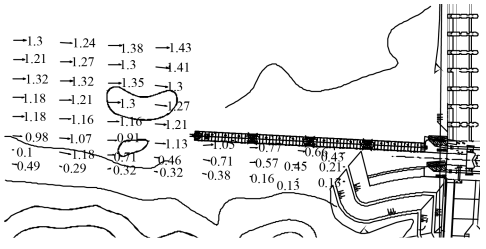

(f) Operation condition 6

Fig. 7. Velocity distribution of upstream approach channel and the entrance area(m/s).

It can be seen that under the condition that the discharge is 10,000 m^3/s and power station is full, the discharge sluices can be operated with 8 holes on the left at most to ensure that the flow condition of the upstream approach channel can meet the navigation requirements. Under the condition that the discharge is 10,000 m^3/s and half of the units are in operation, the flow velocity in the upstream approach channel cannot meet the navigation requirements whatever the scheduling is, which means that under the condition of 10,000 m^3/s flow discharge, the number of operating units must reach more than half to ensure the navigation of the hydro-junction.

4.2 Flow velocity distribution of stilling basin under different scheduling methods

The scheduling schemes have an important influence on the energy dissipation and the outflow velocity downstream of the stilling basin. Therefore, in the above operation conditions, flow velocity of the stilling basin and its downstream in Zone 1 was measured to predict the possible scouring downstream.

The results are shown in Fig. 8. The outflow velocities in operation conditions 1－3 are all below 4.0 m/s. The outflow velocity in operation condition 4 is the smallest, which is 3.27 m/s, and the outflow velocity in operation condition 6 is the maximum reaching 6.61 m/s. Since the anti-scour velocity of the downstream river channel is 5.0 m/s, the scheduling condition that the 8 units are full and the opening of discharge sluices is 6 holes on the left should be avoided under the discharge 10,000 m^3/s.

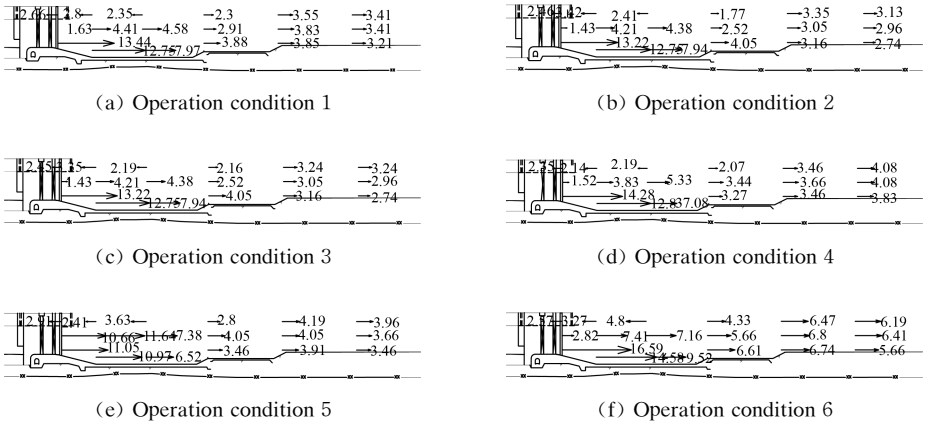

(a) Operation condition 1　(b) Operation condition 2

(c) Operation condition 3　(d) Operation condition 4

(e) Operation condition 5　(f) Operation condition 6

Fig. 8. Velocity distribution of stilling basin under various operation conditions(m/s).

5 Conclusions

In this paper, based on the 1∶100 overall hydraulic model, a comprehensive study on the layout and navigation hydraulics of the Pak Beng Hydropower Station was carried out, and the optimal layout schemes were proposed. The comprehensive analysis of the test results shows that:

(1) According to hydrological statistics, the navigable guarantee rate of discharge 10,000 m^3/s is more than 95%, so it is feasible to determine 10,000 m^3/s as the maximum navigable discharge. Under the maximum navigable discharge, when the upstream navigation wall adopts a floating embankment with a length of 265 m, and the downstream navigation wall adopts the scheme of shortening the navigation wall by

100 m compared with the original scheme and adding an 84 m permeable pier, the navigation flow condition can meet the requirements.

(2) Not only can the navigation flow condition in the approach channel meet requirements, but also the outflow velocity of the stilling basin is not greater than the anti-scour velocity of the river bedrock by reasonable scheduling. Under the discharge of 10,000 m^3/s when the power station generates at full capacity, the discharge sluices can be operated with 8 holes on the left at most, and the number of operating units must reach more than half to ensure that the navigation flow conditions meet the requirements.

References

Li, J. T., Pu, X. G., Zhang, M., 2011. On improvement laws of flow conditions at the entrance of ship approach channel in narrow continuous meandering river by diversion pier. Port & Waterway Engineering(6): 100-105.

Yu, Z.G., Han, C.H., Peng, C.B., 2014. Overview of bent waterway navigation hub layout research. Pearl River, 35(06):102-105.

Li, Q.X., Han, C.H., Li, Y.F., 2015. Influence of riverbed material excavating field on entrance area navigation conditions. Hydro-Science and Engineering(6): 47-53.

Wu, X.R., 2006. Research on the navigation flow condition of hydro-junction. Port & Waterway Engineering(9):52-55.

Wu, Z.Y., Jiang, C.B.,Jie, C., 2016. Influence of sluice gate opening mode on navigation flow condition. Advances in Science and Technology of Water Resources, 36(03): 73-77+82.

Ma, D.G., Liu, X., Zhao, J.Q., 2011. The research of navigation flow conditions and improvement measures on entrance area and connecting reach of Dahua Lock in Hongshui River. Advanced Materials Research, 250-253:3624-3629.

Wei, X., Song, G.C., Feng, J., 2012. Analysis of shiplock arrangement and navigation flow condition at Yujiang Laokou hinge. Western China Communication Science & Technology(8): 144-146+152.

Wang, L., Chen, Y., 1998. Hydraulic model test on navigation flow condition and ship prototype investigation for Wuqiangxi Project. Journal of Yangtze Riverentific Research Institute(3): 30-34.

Ministry of Transport of the People's Republic of China. Code for Master Design of Shiplocks: JTJ 305—2001,2001, Beijing: People's Communications Press.

Experimental study on downstream navigable flow condition optimization with emergency navigable locks effect

Weichun Qiu[1], Yu Wang[2], Jiaoguo Ye[3], Jintao Fang[4], Jianjun Zhao[5], Jinde Gu[6], Xiujun Yan[7], Xingwei Zheng[8]

[1] Changshan Dingyang Shipping Construction and Development Co., Ltd., Quzhou, China

[2,4,5,6,7] State Key Laboratory of Hydrology-Water Resources and Hydraulic Engineering, Nanjing Hydraulic Research Institute, Nanjing, China. e-mail: wangy@nhri.cn

[3] Quzhou Communications Investment Group, Quzhou, China

[8] Quzhou Jujiang River Shipping Construction and Development Co., Ltd., Quzhou, China

Abstract: The addition of emergency navigable locks at Tianma Junction located in Changshan River changed the original boundary conditions. Considering the influence of the downstream river topography, flow conditions in entrance area and connecting section of the approach channel were significantly different from the original layout. Based on the 1/100 hydraulic physical model, this paper compared the characteristics of flow longitudinal and lateral velocity distribution in the downstream entrance area and connecting section of the approach channel with and without emergency navigable lock, and developed an optimal layout with the adjustment of downstream separation levee. The results showed that the addition of emergency navigable locks will deteriorate the navigable flow conditions downstream of the ship lock. By modifying the 90 m end of the downstream separation levee into 4 diamond-shaped diversion piers, flow conditions in the entrance area and the connecting section were significantly improved, which could satisfy the normal operation of ship locks. This study could provide a reference for the construction of the emergency navigable lock in the later stage.

Keywords: Emergency navigable locks; Navigable flow condition; Entrance area

1 Introduction

With the development of water transportation industry in China, it is necessary to add emergency navigable locks so as to improve the navigation guarantee rate thanks to ensuring navigation during the maintenance period of the ship lock. Furthermore, emergency navigation locks could meet the requirements of flood dis-

charge, and better cope with emergencies (to meet the simultaneous entry and exit of two rescue ships). Emergency navigation lock could spill flood in flood season, whereas it could ensure navigation in the maintenance period of the ship lock.

The projects to add emergency navigable locks could refer to the construction of the second-line ship locks. At present, many scholars studied the impact of the construction of the second-line ship locks on the navigable flow conditions of the first-line ship locks. Wang et al. (2016) noted that the embankment effect of separation levee of second-line ship lock increased lateral velocity on the approach channel of the first-line ship lock for the Mengli Junction on Beijiang River. Wang et al. (2021) pointed out that the construction of the second-line ship lock narrowed flow cross-section, which led to obvious oblique flow in entrance area. Based on Jingnan Junction, Wang et al. (2021) made clear that the construction of the second-line ship lock in the curved narrow-trough river section will generate oblique flow in entrance area of the first-line ship lock. Moreover, the first and second-line ship locks would influence each other. Li et al. (2013) analyzed Zhuzhou Junction to demonstrate that the excavation of the second-line ship lock caused severe oblique flow to approach channel of first-line ship lock.

It could be seen that the adverse impact of second-line ship lock on first-line ship lock mainly embodied that flow conditions would keep away the intense oblique flow in entrance area of first-line ship lock, which could provide a reference for the research in this paper. Compared with the second-line ship lock, the emergency navigable lock was relatively small in scale and navigable capacity, and met flood discharge requirements. The addition of an emergency navigable lock on the junction is the first in China, and there was no literature to study its impact on the navigable water flow conditions of the ship lock. Therefore, it was necessary to carry out model tests to study the characteristics.

2 Project summary

Tianma Junction, the second cascade project of the Changshan River cascade development in the upper reaches of the Qiantang River, was located in Changshan County of Zhejiang Province. The junction layout, located in the upper section of the large-angle curved river section, was the power station, sluice and ship lock from right to left, as exhibited in Fig. 1. The sluice baseboard and width were 76.50 m and 196 m with 14 holes, respectively. Normal water level was 84.00 m. The power station employed two generator sets with 4.0 MW installed capacity. The size of lock chamber was 180 m×23 m×8 m (length×width×water depth on sill). Downstream

approach channel was composed of a 195 m berthing section, a 100 m navigation section, and a separation levee of 60 m width and 312 m length. The emergency navigable lock, a renovation project, was added between the sluice and the ship lock with a net width of 14 m. In daily work, its function was the same as that of the sluice (it could be regarded as one hole of the sluice).

The addition of emergency navigable locks at Tianma Junction would definitely change the original boundary conditions. In addition, the entrance area and connecting sections of downstream approach channel were on the convex bank of the river with a sharp bend greater than 90°. The large intersection angle between main flow and shipping routes caused adverse hydraulic phenomena such as serious oblique flow velocity, backflow, and swirling (Huang et al., 2017). The ship crossed the river channel obliquely when it transited to the concave bank (Yu et al., 2014). The ship was difficultly navigated due to the influence of flow in the bend, so it was necessary to further demonstrate and optimize the navigable flow conditions.

According to "Code for Master Design of Shiplocks" (JTJ 305—2001) in China, longitudinal velocity, lateral velocity and inverse velocity $\leqslant$ 2.0 m/s, 0.3 m/s and 0.4 m/s for Class Ⅲ waterway, respectively.

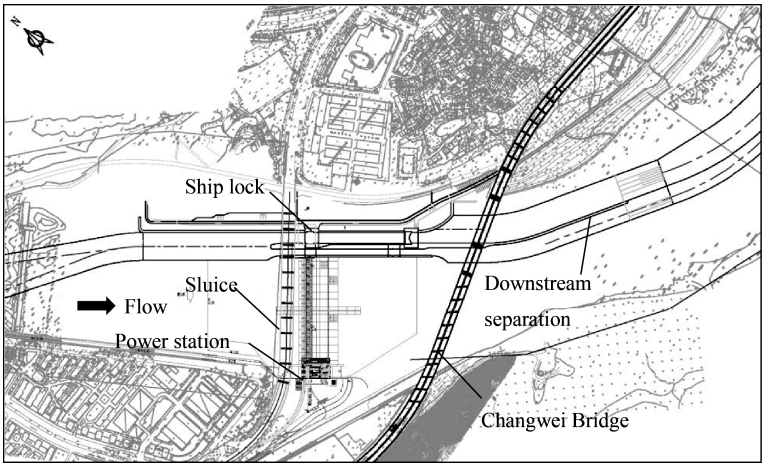

Fig. 1. General layout of Tianma Junction.

3 Experimental setup and methodology

3.1 Experimental setup

The test model was designed at the geometric scale of 1/100 on basis of Froude similarity criterion according to the similarity law of model, and simulated the up-

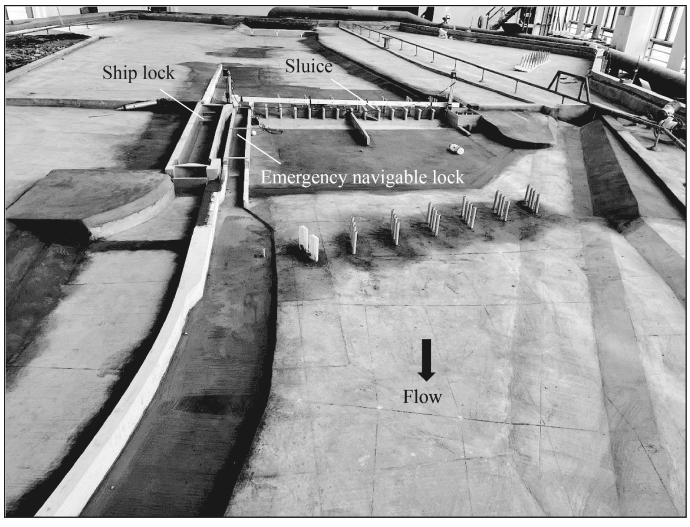

Fig. 2. Hydraulic model of Tianma Junction (mirror image).

stream and downstream river channels, navigable buildings and upstream and downstream approach channels with mirror image. The upper boundary of physical model was arranged at about 1.6 km upstream of sluice, taking into account the smooth inflow and navigable flow conditions. The presence of curves in the sluice downstream contributed to complex flow conditions. Consequently, the lower boundary of physical model should be taken to 900 m downstream of curve.

The section method was used for terrain production, and the triangulation wire system was employed for plane stakeout where the triangle closure error hardly exceeded ±1′. The model elevation was measured by a level and checked during the production process, and the installation elevation error of the section was controlled by ±1 mm. For complex terrain, the intensive section was added and processed separately in order to improve production accuracy. The junction, including sluice, ship lock and power station, was made of PMMA. The surface of the river was made of cement mortar. The overall model was photographed in Fig. 2.

The flow velocity measurement adopted the acoustic Doppler flow meter produced by Nortek Company with a range of 0.1 – 400 cm/s. The flow discharge was measured by a standard rectangular thin-walled weir with an error of less than 1%; the velocity was measured by a water level stylus with an accuracy of 0.02 mm.

3.2 Experimental cases

Table 1 listed the experimental cases for navigable conditions of Tianma Junction. During the test, the discharge of power station was 116 m^3/s. Additionally, the water level of downstream of sluice was controlled on basis of the numerical simula-

tion of stage-discharge relation curve.

Table 1 Experimental cases of Tianma Junction.

Cases No.	Flow discharge (m^3/s)	Water level (m)	Discharge of power station (m^3/s)
1	1,008	80.34	116
2	800	79.90	116
3	600	79.48	116
4	116	78.56	116

4 Flow conditions without emergency navigable lock

Table 2 Velocity measurements of downstream approach channel entrance and connecting section.

Discharge (m^3/s)	Maximum longitudinal velocity (m/s)	Maximum lateral velocity (m/s)	Sluice operation
116	0.25	0.07	Closed
600	0.67	0.17	1.2 m opening for #2, #4 and #6
800	0.88	0.20	1.1 m opening for #2—#6
1,008	1.11	0.22	1.7 m opening for #2—#6

The preliminary experiment showed the opening of left sluice could easily contribute to oblique flow and backflow in downstream approach channel since ship lock was arranged on the left bank. Therefore, the opening of right sluice should be better employed. The measurements of the flow velocity of the downstream approach channel were displayed in Table 2. Table 2 noted that, velocity indexes of downstream approach channel within 200 m from the gate (3 times the maximum ship length) met the navigation requirements within the flow discharge of 116 - 1,008 m^3/s.

5 Flow conditions with emergency navigable lock

5.1 Flow conditions of downstream approach channel

Sluice operation referred to previously recommended operation in Table 2 for each condition with the addition of an emergency navigable lock, and some operation adjustments were made in combination with changes in the junction layout.

The experiment measured velocity distribution of the downstream approach channel. The results demonstrated that there was obvious lateral flow within 100 - 250 m downstream from the sluice for Q = 1,008 m^3/s, and the maximum lateral velocity was 0.49 m/s on the section 200 m downstream from the head of separation levee. Moreo-

ver, obvious lateral flow occurred on the section 100 – 200 m downstream from the head of separation levee for $Q = 800$ m^3/s. For $Q \leqslant 600$ m^3/s, the lateral velocity was less than 0.3 m/s, and longitudinal velocity and backflow velocity met the specification requirements simultaneously. Fig. 3 photographed flow regime in downstream entrance area, and a large range of backflow was observed for $Q = 1{,}008$ m^3/s.

The reasons for the above-mentioned large lateral flow lied in: 1) The addition of emergency navigable lock increased the cross-sectional area of approach channel, and the intensity of lateral flow in the entrance area increased with the increase in the proportion of the approach channel in the river channel (Huang et al., 2016). Secondly, the addition of emergency navigable lock increased the lateral distance between ship lock and sluice, which resulted in the large intersection angle between flow direction and the axis of ship lock. 2) The backflow was formed in downstream approach channel owing to the phenomenon of stream on the head of separation levee (Qiu et al., 2019; Cheng et al., 2016) and the shear effect of hydrostatic fluid in approach channel and mainstream (see Fig. 3). The flow in the edge of the backflow area contributed to obvious lateral flow due to its own lateral diffusion and the traction of the backflow. 3) The downstream approach channel was located on the convex bank where the sand was easily deposited, which contributed to a large angle between the centerline of the downstream approach channel and the mainstream of the river channel. A variety of reasons were superimposed to cause a large-scale cross-flow in the entrance area of the downstream approach channel.

Fig. 3. Flow regime in downstream entrance area for $Q = 1{,}008$ m^3/s.

5.2 Revised case of downstream approach channel

The severe flow regime should be optimized due to large lateral flow velocity for

$Q \geqslant 600$ m^3/s. Therefore, downstream separation levee was adjusted taking account of the effect of the length variation of separation levee in suppressing the lateral flow (Jiang et al., 2014; Huang et al., 2016), the discharge capacity after sluice moving and downstream dredging.

5.2.1 Revised case Ⅰ

Fig. 4 plotted the separation levee which was lengthened 90 m for revised case Ⅰ. The deflection position of the mainstream moved downstream by extending separation levee, which weakened the influence of the sluice discharge on flow in the approach channel and reduced the lateral flow velocity. The data demonstrated that the maximum lateral velocity was 0.44 m/s for $Q = 1{,}008$ m^3/s, and the peak lateral velocity decreased compared with the original layout. However, circulation flow was enhanced within the extension of separation levee, which resulted in lateral velocity exceeding navigable standard in the right range of the channel centerline from 100 to 300 m. Therefore, revised case Ⅰ could not meet navigable requirements.

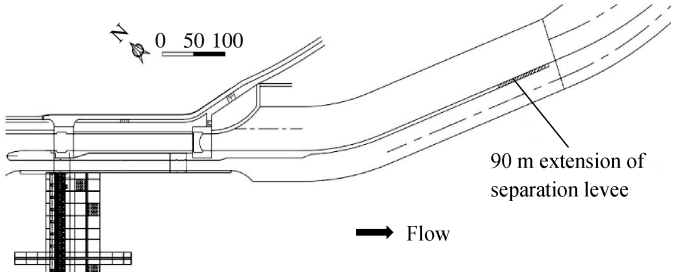

Fig. 4. Definition sketch for revised case Ⅰ.

5.2.2 Revised case Ⅱ

Fig. 5 showed the downstream separation levee shortened by 90 m based on the original layout for revised case Ⅱ. By shortening downstream separation levee, the position of entrance area moved up, and its distance from the downstream large-angle bend increased. The data of flow velocity showed that the maximum lateral flow velocity was 0.41 m/s for $Q = 1{,}008$ m^3/s. The observation exhibited that the lateral diffusion space increased, and the overall lateral flow velocity improved compared with revised case Ⅰ. Nevertheless, the lateral flow velocity still exceeded standard, so scheme 2 could not meet the navigation requirements.

5.2.3 Revised case Ⅲ

From the comprehensive revised case Ⅰ and revised case Ⅱ, it could be seen that extending or shortening the partition wall barely changed the influence range of the lateral flow and didn't significantly improve the lateral flow amplitude and gradient in the entrance area. Therefore, other optimization measures needed to be taken.

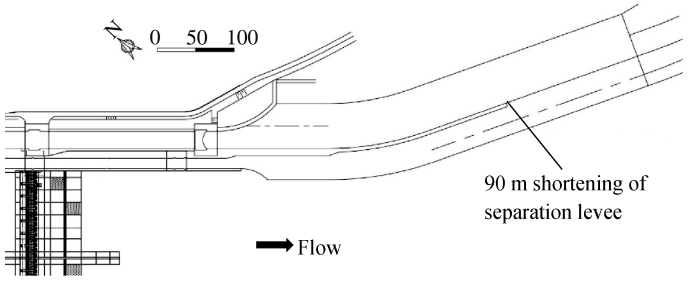

Fig. 5. Definition sketch for revised case Ⅱ.

Considering that the blocking effect of the diamond-shaped diversion pier reduced the flow momentum of entering the entrance area (Li et al., 2011), revised case Ⅲ added 4 diamond-shaped diversion piers with an overall length of 90 m at the end of the downstream separation levee (see Fig. 6). The angle between the diversion piers and the parallel line of the channel center line was 23°, and the center distance of the diversion piers was 22 m (see Fig. 7). The observations showed that the maximum lateral flow velocity in the entrance area was 0.33 m/s for $Q = 1,008$ m^3/s. Thanks to the characteristics of adjusting flow for the diamond-shaped diversion piers, the lateral velocity in entrance area was obviously improved. In fact, the lateral flow velocity in the right part of the channel centerline exceeded navigable standard. Therefore, revised case Ⅲ could not meet the navigation requirements.

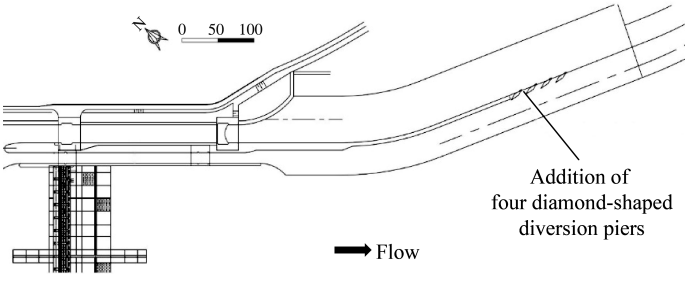

Fig. 6. Definition sketch for revised case Ⅲ.

5.2.4 Revised case Ⅳ

The lateral flow velocity of few measured points exceeded the standard in a small part for revised case Ⅲ and the scope of lateral flow for revised case Ⅱ was significantly reduced compared with revised case Ⅰ. Hence, revised case Ⅳ changed the 90 m at the end of downstream separation levee to four diamond-shaped diversion piers (see Fig. 8), and the number, size, and layout of the diversion piers were consistent with those in revised case Ⅲ. The flow velocity showed that the maximum lateral flow velocity in entrance area was 0.31 m/s (see Fig. 9). Therefore, the longitudinal and

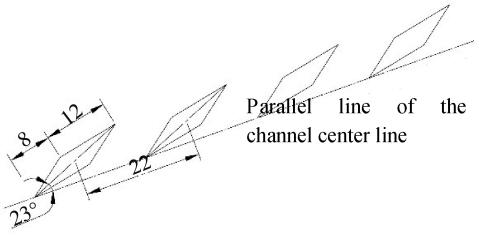

Fig. 7. Definition sketch for revised case Ⅲ.

lateral flow velocity in entrance area basically met the navigation requirements for Q = 1,008 m^3/s. Shortening the length of separation levee, moving the diamond-shaped diversion piers forward and appropriately introducing flow into entrance area of downstream approach channel could reduce the influence of lateral flow. Here the revised case Ⅳ was preferred as the final remediation case.

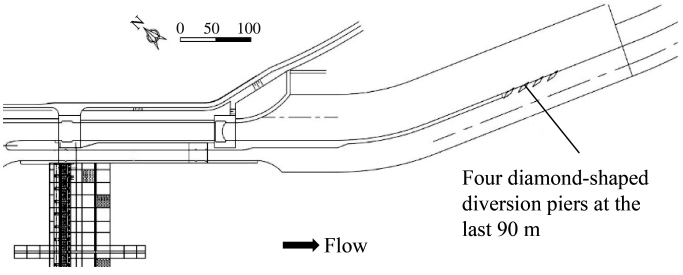

Fig. 8. Definition sketch for revised case Ⅳ.

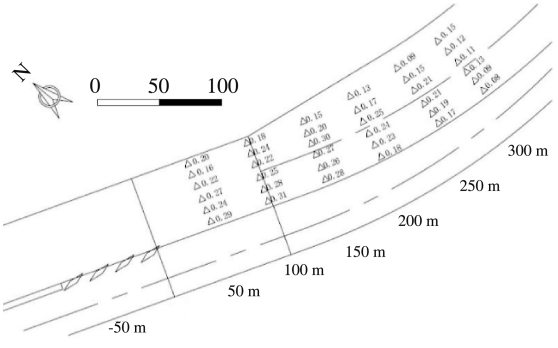

Fig. 9. Lateral velocity distribution in entrance area of downstream approach for revised case Ⅳ (Q=1,008m^3/s).

6 Conclusions

1) Downstream navigable flow conditions met navigation requirements without emergency navigable lock for Tianma Junction. The addition of emergency navigable lock changed the original boundary conditions, and obvious lateral flow and circulation flow superposition contributed to large lateral velocity in the entrance area and connecting section as downstream entrance area was located on the convex bank of the river channel with a large angle and a sharp bend.

2) Extending or shortening the length of separation levee downstream of Tianma Junction only changed the influence scope of lateral flow; the arrangement of the diversion pier was an economical and convenient engineering measure to effectively improve downstream regime.

Acknowledgements

This research has been financially supported by the National Natural Science Foundation of China (Grant No. 52009083), and the Natural Science Foundation of Jiangsu Province (Grant No. BK20200159).

References

Cheng, L., Zhao, J.J., Gu, J.D., 2016. Navigation condition at entrance of approach channel of low-head hydro-junction in S-shaped curved river. Port & Waterway Engineering(12): 106-112.

Huang, M.H., Han, W.W., Wu, P., 2016. Layout of guard wall of locks. Port & Waterway Engineering(11): 162-166.

Huang, J., Zhao, J.J., Gu, J.D., 2017. Navigation flow condition at great angle bend. Port & Waterway Engineering(4): 146-150.

Jiang, C., Zhao, J.J., Gu, J.D., 2014. Experimental studies on flow condition for navigation of Qingtian hydroproject located at Oujiang River. Hydro-Science and Engineering(2): 74-80.

Li, J.T., Pu, X.G., Zhang, M., 2011. On improvement laws of flow conditions at the entrance of ship approach channel in narrow continuous meandering river by diversion pier. Port & Waterway Engineering(6): 100-105.

Li, J.T., Hao, Y.Y., 2013. Influence of second-line lock construction on navigation condition of first-line lock on Zhuzhou navigation power junction in Xiangjiang

River. Port & Waterway Engineering(6): 103-107.

Ministry of Transport of the People's Republic of China. Code for Master Design of Shiplocks: JTJ 305—2001,2001. Beijing: People's Communications Press.

Qiu, S.X., Liu, D., Liu, Z.F., et al., 2019. Experimental research on navigable flow condition of the lower approach channel of the ship lock reconstruction and expansion project of the Jiantan Hydro-junction. Guangdong Water Resources and Hydropower(7): 11-16.

Wang, Y.L., Sun, G.D., Li, Y., et al., 2016. Experimental research on navigation flow conditions in upper approach channel of Beijiang Mengli Hydro-junction. Port & Waterway Engineering(4): 105-112.

Wang, J.P., Liu, C., Zhang, S.B., et al., 2021. Experimental research on navigation flow condition in upstream entrance area of Fengguang Hydro-junction's expanded locks. Port & Waterway Engineering(1): 156-161.

Wang, B., He, F.F., Wang, X.Y., et al., 2021. Study on navigable flow conditions of multi-lane lock in curved narrow channel section. Port & Waterway Engineering(4): 108-115.

Yu, Z.G., Han, C.H., Peng, C.B., et al., 2014. Overview of Bent Waterway Navigation Hub Layout Research. Pearl River, 35 (6): 102-105.

Experimental study on navigation flow condition of Gedi Hydro-project in Changshanjiang River

Kaiwen Yu[1], Kang Han[2], Changhai Han[3],
Jianjun Zhao[4], Zhiguang Yu[5]

[1,2,3,4] Nanjing Hydraulic Research Institute, State Key Laboratory of Hydrology Water Resources and Hydraulic Engineering, Nanjing, China. e-mail: kaiwyu@163.com

[5] Hubei Institute of Water Resources Survey and Design, Wuhan, China

Abstract: Changshanjiang River is a mountain stream river with common characteristics of mountainous rivers, so the flow conditions at the entrance area of the approach channel are complicated. Gedi Hydro-project is one of the navigation cascade development projects in the mainstream of Changshanjiang River, which is located in the middle of the S-shaped curved river. The upstream approach channel is located in the main channel of the concave bank adopting the semi-open approach channel. Due to the influence of the narrow channel and bend flow near the dam, it is prone to form oblique flow and backflow in the entrance area of upstream approach channel. The entrance area of downstream approach channel is located on the convex bank of the bend, and the angle between the mainstream flow direction and the approach channel is large, so the velocity indexes of the entrance area of downstream approach channel are difficult to meet the navigable safety requirements. Based on the overall hydraulic model with a scale of 1∶80, the navigation flow characteristics of the entrance area of the upstream and downstream approach channel were studied, and the optimized schemes and reasonable scheduling methods were proposed. The results show that: (1) The maximum navigable discharge can be significantly increased by excavating the upstream left bank. (2) Reasonably dredging the convex bank of the downstream channel and adjusting the route layout of approach channel can effectively improve the flow conditions at the entrance area of approach channel to make the velocity indexes meet the navigation requirements. (3) For scheduling methods of discharge sluices, priority should be given to opening the discharge sluices in the left area and when the discharge is greater than 800 m^3/s, the number of discharge sluices opened should be 6.

Keywords: Gedi Junction; Curved rivers; Approach channel; Entrance area; Navigation flow condition

1 Introduction

On the curved rivers in mountainous areas, navigation-power junction projects

have the common characteristics of "many curves, many beaches, and short straight sections", which makes the navigation flow condition at the entrance area of approach channel too complex to meet the requirements for ships entering and leaving the entrance area of approach channel (Han et al., 2014; Han et al., 2013). Based on the characteristics of mountain rivers, semi-open and open approach channels are widely used (Yu et al., 2014), and the unfavorable flow patterns at the entrance area of approach channel have been effectively improved through engineering measures such as diversion piers, and submerged spurs (Yang et al., 2016; Wei et al., 2012; Hao et al., 2004; Li et al., 2014). However, due to the complexity and particularity of the problems, many navigable problems of navigation-power junction projects still need to be researched by physical model test. The Changshanjiang River is a mountain-river with a large water surface slope, shallow water, many beaches, many bends and short straight sections. The Gedi Junction is one of the projects of cascade development of shipping on the mainstream of the Changshanjiang River, which is located on the S-shaped curved channel. The upstream approach channel located in the main channel of the concave bank adopts a semi-open approach channel. Oblique flow and backflow zone are likely to be formed in the entrance area of the approach channel due to the influence of narrow channels and bend flow near the dam area, which will adversely affect navigation. The entrance area of the downstream approach channel is located on the convex bank of the lower curve, where the angle between the direction of the main flow and the approach channel is relatively large, so the flow conditions at the entrance area are complicated and will affect the safety of navigation. In this paper, the navigation flow condition is studied and the optimized scheduling methods and layout schemes are proposed.

2 Project overview

The overall layout of Gedi Hydro-project is illustrated in Fig. 1. The power station, flood discharge gate and ship lock are arranged in sequence from left to right, including 2 power stations with an installed capacity of 4.5 MW and 20 flood discharge sluices numbered 1#-20# from right to left with a total net width of 238 m. The discharge sluices are divided into left and right zones by longitudinal guide walls. The ship lock is located on the right side of the project, with a design operating head of 6.0 m. The effective size of the lock chamber is 180.0 m × 23.0 m × 4.0 m (length × width × threshold depth), which is designed to be navigable for 500 t ships. The geometric scale of the model is 1∶80, which is designed according to the gravity similarity criterion. The upstream river channel, the hub buildings, the upstream and

downstream approach channels are all included. In the model, the upstream boundary is arranged 500 m upstream of the upper bend (about 1.9 km from the dam axis) and the downstream boundary is about 1.7 km downstream of the dam, so a 3.6 km long river section is simulated.

The bottom flow velocities are measured by a DPJ propeller current meter with an incipient velocity of 1 cm/s and an accuracy of 0.01 cm/s.

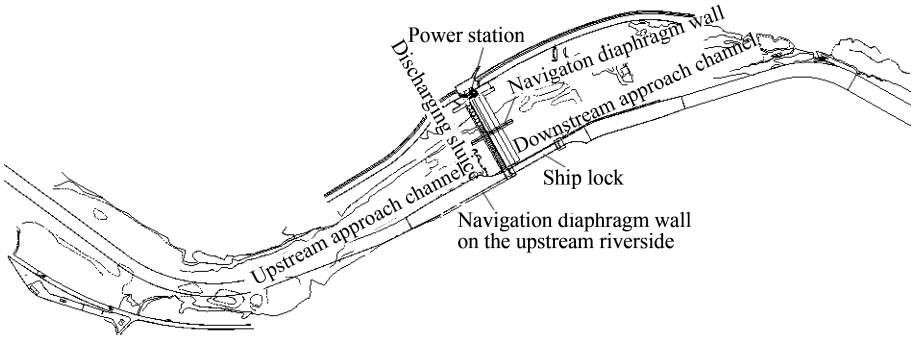

Fig. 1. The overall layout of Gedi Hydro-project.

According to "Code for Master Design of Shiplocks" (Ministry of Transport of the People's Republic of China, 2001), for Ⅳ ship lock, in the navigation section and adjustment section of the approach channel, the flow pattern should be still water; in the anchorage area of the approach channel, the longitudinal flow velocity and transverse velocity should be less than 0.5 m/s and 0.15 m/s respectively; in the entrance area, the longitudinal flow velocity, transverse velocity and backflow velocity should be less than 2.0 m/s, 0.3 m/s, and 0.4 m/s, respectively.

3 Navigation flow condition of upstream approach channel

3.1 Original design scheme

The upstream approach channel located in the main channel of the concave bank adopts a semi-open approach channel, which means that there is no navigation diaphragm wall on the upstream riverside. The total length of the approach channel is 320.0 m, including a 220.0 m long anchorage area and 100.0 m long navigation section, and the bottom width is 60.0 m.

The maximum navigable discharge of the Gedi project should be comprehensively determined according to the actual hydrological conditions, the navigation standards of the downstream established projects, the layout, and the hydraulic model test. So,

tests on the navigation flow condition and scheduling methods are carried out with the discharge of 600 m^3/s, 800 m^3/s, 1,062 m^3/s and 1,234 m^3/s. The operation conditions and results are shown in Table 1 and Table 2 respectively.

Table 1 Test conditions of upstream navigable flow condition.

Operation condition	Discharge (m^3/s)	Upstream water level(m)	Downstream water level(m)	Operation methods of power station	Scheduling methods of discharge sluices	Relative opening of sluices
1	600	78.5	74.68	Full	4#-8#	0.22
2	600	78.5	74.68	Full	13#-17#	0.22
3	800	78.5	75.16	Full	4#-8#	0.35
4	800	78.5	75.16	Full	13#-17#	0.35
5	1,062	78.5	75.75	Full	13#-17#	0.48
6	1,234	78.5	76.09	Full	13#-18#	0.44

Table 2 Characteristic velocity at the entrance area of upstream approach channel of the original design.

Operation condition	Maximum velocity measurement(m/s)								
	The entrance area			The anchorage area			The navigation section		
	Longitudinal	Transverse	Backflow	Longitudinal	Transverse	Backflow	Longitudinal	Transverse	Backflow
1	0.71	0.16	0.00	0.75	0.18	0.05	0.59	0.16	0.10
2	0.70	0.11	0.00	0.45	0.12	0.09	0.06	0.09	0.09
3	0.87	0.19	0.00	0.88	0.15	0.10	0.79	0.20	0.10
4	0.87	0.15	0.00	0.56	0.14	0.09	0.00	0.04	0.09
5	1.18	0.13	0.00	0.80	0.24	0.09	0.09	0.13	0.11
6	1.40	0.21	0.00	0.91	0.23	0.10	0.22	0.11	0.15
Control index	≤2.00	≤0.30	≤0.40	≤0.50	≤0.15	/	Still water area		

When discharge sluices numbered 4#-8# in the right area are opened, under the discharge of 600 m^3/s - 800 m^3/s, the characteristic velocity in the navigation section and the anchorage area cannot meet the requirements, as shown in Fig. 2.

When discharge sluices numbered 13#-17# in the left area are opened, under the discharge of 600 m^3/s, the navigation section of the upstream approach channel is a still water area, and there is a weak backflow in the anchorage area. The flow velocity indicators of the entrance area of the upstream approach channel can meet the navigation requirements. Under the discharge of 800 m^3/s, the navigation section of the upstream approach channel is basically a still water area, and in the anchorage area, the flow velocity in other anchorage areas is not greater than 0.5 m/s except that the maximum velocity of the centerline of the most upstream channel is 0.58 m/s. The flow velocity indicators at the entrance area basically meet the navigation require-

ments. When the discharge is greater than 800 m^3/s, the maximum longitudinal and transverse velocity of the anchorage area cannot meet the navigation requirements, as shown in Fig. 3. Therefore, it is necessary to take engineering measures to increase the maximum navigable discharge.

Besides, it also can be seen from the results that the discharge sluices in the left area should be opened for flood discharge to meet the navigation flow condition of the upstream approach channel.

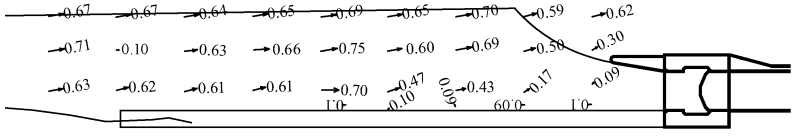

(a) Operation condition 1

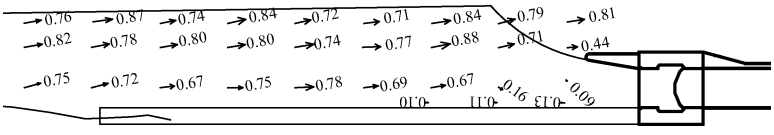

(b) Operation condition 3

Fig. 2. Plane velocity distribution of the upstream approach channel when discharge sluices numbered 4#-8# in the right area are opened(m/s).

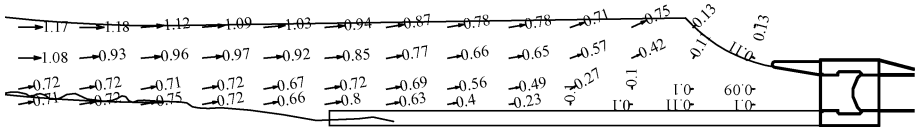

(a) Operation condition 5

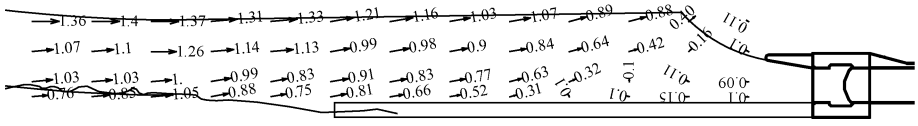

(b) Operation condition 6

Fig. 3. Plane velocity distribution of the upstream approach channel when discharge sluices numbered 13#-17# in the left area are opened(m/s).

3.2 Optimized scheme

Considering the obvious narrowing of the reach at 0.5 km-1.0 km upstream of Gedi Junction, excavation and dredging are carried out on the upstream left bank to expand the cross-sectional area of the water and reduce the velocity of the upstream approach channel. The range of excavation and elevation is shown in Fig. 4.

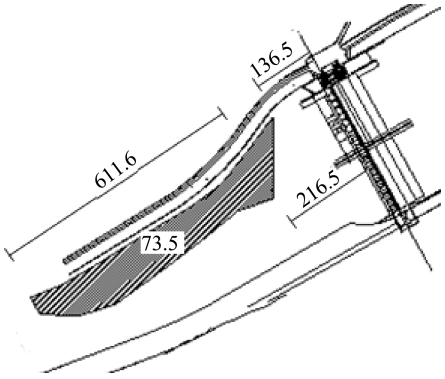

Fig. 4. The range of excavation and elevation on the upstream left bank(m).

Navigation flow condition of upstream approach channel has been significantly improved after excavation. What can be seen from Table 3 is that when the discharge is less than 1,062 m^3/s, the velocity indicators of the entrance area of upstream approach channel basically meet the navigation requirements. However, under the discharge of 1,234 m^3/s, the characteristic flow velocity of the navigation section exceeds the design specification requirements. Therefore, the discharge of 1,062 m^3/s can be considered as the maximum navigable discharge in the upstream approach channel.

Table 3 Characteristic velocity at the entrance area of upstream approach channel of the optimized scheme.

Discharge (m^3/s)	Maximum velocity measurement(m/s)								
	The entrance area			The anchorage area			The navigation section		
	Longitudinal	Transverse	Backflow	Longitudinal	Transverse	Backflow	Longitudinal	Transverse	Backflow
600	0.52	0.08	0.00	0.36	0.08	0.09	0.08	0.08	0.09
800	0.70	0.11	0.00	0.47	0.10	0.09	0.00	0.04	0.09
1,062	0.70	0.13	0.00	0.53	0.14	0.09	0.00	0.06	0.09
1,234	1.10	0.15	0.00	0.69	0.33	0.11	0.17	0.30	0.15
Control index	≤2.00	≤0.30	≤0.40	≤0.50	≤0.15	/	Still water area		

4 Navigation flow condition of downstream approach channel

4.1 Original design scheme

Restricted by the river terrain, the entrance area of the downstream approach channel is located on the convex bank of the lower bend. At the same time, the angle between the direction of the main flow and the approach channel largely results from the influence of the central beach of the river channel on the current bifurcation,

which is detrimental to the navigation flow condition. In order to ensure the safety of navigation, the discharge of 116 m^3/s (full power discharge) and 1,062 m^3/s are selected to carry out the experimental study on the navigation flow condition at the entrance area of the downstream approach channel. Among them, operation method of the discharge of 1,062 m^3/s is that when the power station is full, the remaining water is discharged by evenly opening the 5 discharging sluices on the far left.

In the entrance area, the max longitudinal flow velocity, transverse flow velocity and backflow velocity are 2.33 m/s, 0.81 m/s, and 1.41 m/s respectively under the discharge of 116 m^3/s. And under the discharge of 1,062 m^3/s, the max longitudinal flow velocity, transverse flow velocity and backflow velocity are 3.97 m/s, 1.88 m/s, and 1.64 m/s, respectively. Results show that the flow velocity of the entrance area of the downstream approach channel far exceeds the navigation requirements, whether it is a large discharge or a small discharge.

4.2 Optimized scheme

In order to solve the problem that the navigation flow at the entrance area is concentrated and the angle between the flow and the route is relatively large (as shown in Fig. 5, the arrow indicates the direction of the main flow), it is necessary to adjust diversion route and excavation of the downstream beach to disperse the downstream flow and improve the flow condition at the entrance area. 3 optimized schemes are proposed, as shown in Fig. 6. Results of the flow velocity are shown in Table 4.

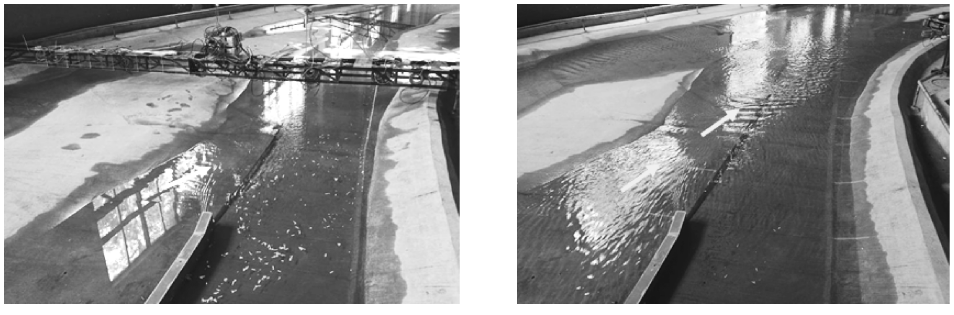

(a) Under the discharge of 116 m^3/s (b) Under the discharge of 1,062 m^3/s

Fig. 5. The flow pattern at the entrance area of the downstream approach channel in the original scheme.

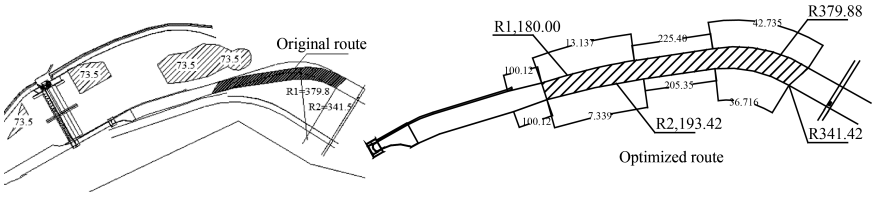

(a) Optimized scheme Ⅰ

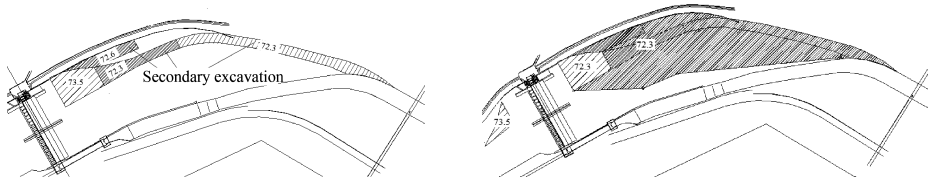

(b) Optimized scheme Ⅱ (c) Optimized scheme Ⅲ

Fig. 6. The optimized schemes of downstream approach channel.

Table 4 Characteristic velocity at the entrance area of downstream approach channel of the optimized scheme.

Optimized scheme	Discharge (m^3/s)	Maximum velocity measurement(m/s)		
		Longitudinal	Transverse	Backflow
Ⅰ	1,062	1.59	0.49	0.45
Ⅱ	116	0.80	023	0.35
	1,062	1.59	0.59	0.61
Ⅲ	600	1.05	0.32	0.10
	800	1.22	0.36	0.32
	1,062	1.46	0.37	0.31
Control index		≤2.00	≤0.30	≤0.40

In optimized scheme Ⅰ, we excavate and dredge the downstream area of the power station, the entrance area of the downstream approach channel and the high terrain on the left side of the channel to the elevation of 73.50 m, and arrange the downstream route as far as possible to the right bank, as shown in Fig. 6 (a). Under the discharge of 1,062 m^3/s, the navigation flow conditions within the 200 m range of the downstream approach channel entrance area are not obviously improved, where the lateral velocity and backflow velocity exceed the specification requirements.

In optimized scheme Ⅱ, we carry out the secondary excavation of the original beach on the downstream river channel on the basis of the optimized scheme Ⅰ, as shown in Fig. 6 (b). Under the discharge of 116 m^3/s, the characteristic flow velocity at the entrance area of the downstream approach channel meets the specification requirements. Under the discharge of 1,062 m^3/s, the maximum lateral velocity and backflow velocity still exceed the specification requirements within the 200 m range of the downstream approach channel entrance area.

In optimized scheme Ⅲ, we excavate and dredge all the downstream river channels to the elevation of 72.3 m on the basis of the optimized scheme Ⅱ, as shown in Fig. 6 (c). In this scheme, the flow conditions at the entrance area have been significantly improved, the flow at the entrance area and the connecting section is stable, and the fluctuation of the water surface is small. Under the discharge of 600 m^3/s –

1,062 m^3/s, the characteristic flow velocity at the entrance area of the downstream approach channel meets the specification requirements.

To sum up, the flow condition at the entrance area of the downstream approach channel has been effectively improved by reasonably dredging and adjusting downstream route, which makes the navigation requirements met under the discharge 116 m^3/s - 1,062 m^3/s.

5 Optimized scheduling methods of discharge sluices

Under different scheduling methods of discharge sluices, the flow condition not only needs to meet the navigation requirements of the upstream approach channel, but also meet the requirements of downstream flood discharge and energy dissipation, which means that the downstream flow velocity should be evenly distributed and a slight submerged hydraulic jump should be formed under the sluices to make full use of the stilling basin for energy dissipation. Therefore, on the basis of scheduling methods that can meet the navigation flow condition of the upstream approach channel, the flow velocity distribution and energy dissipation characteristics of the downstream discharge sluices are studied to further optimize the operation and scheduling methods of discharge sluices. The results are shown in Table 5, Fig. 7 and Fig. 8.

Under different discharges, a stable hydraulic jump can be generated downstream, and the backwater at the beginning of the hydraulic jump is close to the end of the floodgate pillar. Under the discharge of 800 m^3/s, the velocity at the bottom of the stilling basin is greater than that at the surface, and the average velocity at the end of the apron is about 2.6 m/s, which is evenly distributed along the vertical direction. Under the discharge of 1,062 m^3/s, the velocity at the bottom of the stilling basin is less than that at the surface. The average velocity at the end of the apron is about 3.2 m/s, and the velocity at the bottom is greater than that at the surface along the vertical distribution. So, the number of discharge sluices opened should be greater than 5 under the discharge of 1,062 m^3/s.

Table 5 Characteristic velocity at the entrance area under different scheduling methods of discharge sluices.

Discharge (m^3/s)	Upstream water level (m)	Operation methods of power station	Scheduling methods of discharge sluices	Relative opening of sluices	Average velocity(m/s)		
					Outlet of sluices	Top of tailrace sill	The end of the apron
800	78.5	Full	13# - 17#	0.35	9.0	5.0	2.6
1,062	78.5	Full	13# - 17#	0.48	8.8	5.2	3.2

From the review of the test result, it can be seen that in order to meet the requirements of navigation and energy dissipation, the discharge sluices in the left area

shall be opened for flood discharge, and when the discharge is greater than 800 m^3/s, the number of discharge sluices opened should be 6.

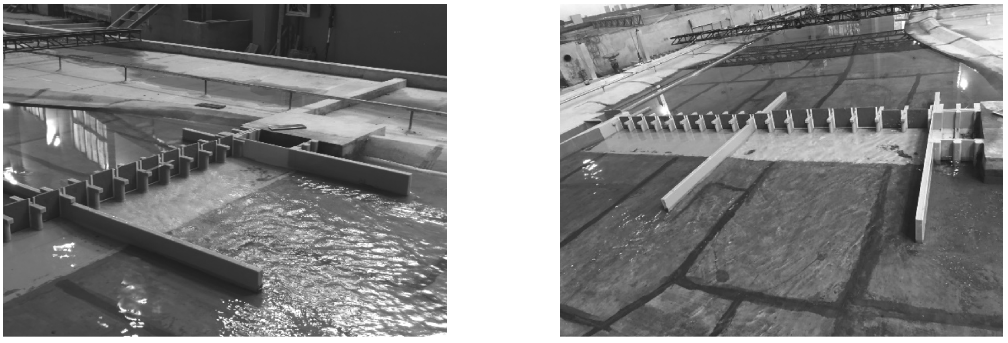

(a) Under the discharge 800 m^3/s (b) Under the discharge 1,062 m^3/s

Fig. 7. Flow pattern of the stilling basin under different scheduling methods.

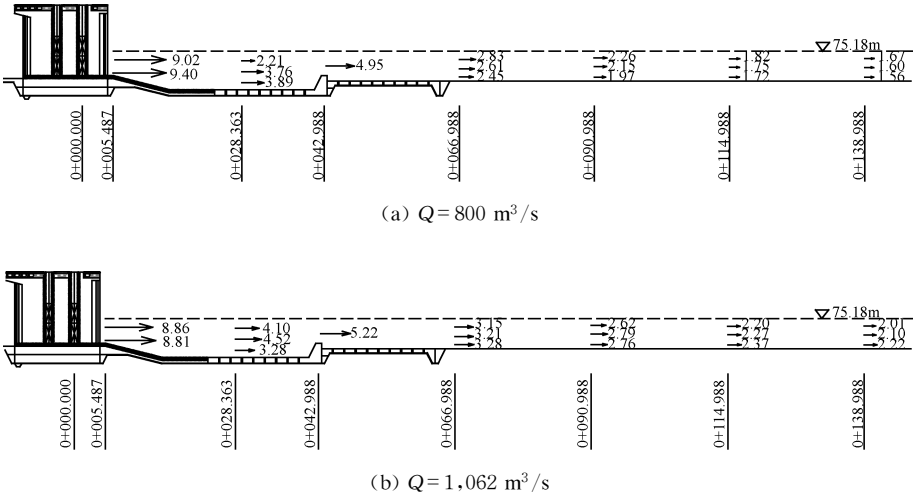

(a) $Q=800$ m^3/s

(b) $Q=1,062$ m^3/s

Fig. 8. Flow velocity distribution downstream of No. 15 discharge sluice.

6 Conclusions

The navigation flow condition at the entrance area of approach channel intensively affects the navigation safety of ships, which has been thought of as a key factor in navigation safety. A physical experiment was conducted to study navigation flow condition at the entrance area of approach channel of Gedi Hydro-project and propose optimized measures. The research results indicate the following:

(1) Under the originally designed scheme of the upstream approach channel, the maximum navigable discharge in the upstream is 800 m^3/s, which cannot meet the de-

signed navigation requirements. However, the maximum navigable discharge in the upstream has been increased from 800 m^3/s to 1,062 m^3/s through excavation and dredging of the upstream left bank, which makes the navigable discharge in the upstream basically meet the designed requirements.

(2) Under the originally designed scheme of the downstream approach channel, the flow velocity indicators of the entrance area of the downstream approach channel are far beyond the navigation requirements regardless of the large discharge or the small discharge. However, the maximum navigable discharge downstream has been increased to 1,062 m^3/s by dredging the beach on the convex bank of the river channel and adjusting the position of the downstream route.

(3) In order to meet the requirements for the navigation of the upstream approach channel and the energy dissipation of stilling basin, the discharge sluices in the left area should be opened for flood discharge, and when the discharge is greater than 800 m^3/s, the number of discharge sluices opened should be 6.

References

Han, C. H., Yang, Y., Li, Y. F., 2014. Layout of navigable channel of navigation-power the convex bank with slightly bended river junction on section. Port & Waterway Engineering (10): 121-125.

Han, C. H., Yu, Z. G., Yang, Y., 2013. Plan arrangement optimization of navigation structures of the Xiaoxitan Junction. Port & Waterway Engineering (6): 99-102.

Yu, Z. G., Han, C. H., Peng, C.B., 2014. Overview of bent waterway navigation hub layout research. Pearl River, 35(06):102-105.

Yang, Y., Li, Y. F., Han, C. H., 2016. Experimental study on navigation flow condition of Chengjing hydro-power station in Guizhou Qingshui River. Port & Waterway Engineering (12): 126-131.

Wei, J., Song, G. G., Jiang, F., 2012. Analysis of shiplock arrangement and navigation flow condition at Yujiang Laokou hinge. Western China Communications Science & Technology (8): 144-146.

Hao, P. Z., Li, J., Xu, G. B., 2004. General layout and experimental study on navigable condition the optimization of navigation-power junction at slightly curved braided reach. Port & Waterway Engineering (11): 66-69.

Li, Y. F., Yang, Y., Han, C. H., 2014. Optimal experiments of layout of an approach channel for Sanxikou navigable power project. Hydro-Science and Engineering (2): 89-94.

Ministry of Transport of the People's Republic of China. Code for Master Design of Shiplocks: JTJ 305—2001,2001, Beijing: People's Communications Press.

Research and application of key technologies of a restricted waterway project of an inland river in Northern Zhejiang based on BIM

Zuopeng Niu [1], Song Zheng[2, 3], Yanchun Zou[1], Luyi Liu[3], Tao Wang[2]

[1] CCCC Second Harbor Consultants Co., Ltd., Wuhan, China. email: 30874050@qq.com

[2] Jiaxing City Ganghang Management Service Center, Jiaxing, China

[3] Jiaxing Port and Waterway Construction Development Co., Ltd., Jiaxing, China. email: 393550014@qq.com

Abstract: BIM refers to the process, method and technology that create and utilize digital models to manage and optimize the whole process of design, construction and operation of construction projects. Compared with the construction field, the application of BIM technology in inland waterway engineering lags behind, and there is a lack of supporting tools and methods specifically for BIM application, as well as a lack of component model library and localized sample files. In view of the application of BIM technology in inland waterway restricted engineering, this paper studies key technologies and applications such as BIM model creation, BIM model delivery and BIM + GIS integration of inland river restricted waterway engineering. Based on a restricted waterway project in northern Zhejiang, Autodesk BIM platform and SuperMap 3D GIS platform, the author conducted BIM model creation, BIM model delivery and application verification of BIM + GIS and other key technologies for inland river restricted waterway projects, realized multi-source BIM data visualization, convenient delivery without plug-ins, and linkage between business data such as drawings, progress, changes, quality and safety and BIM model. The research results can promote the transformation of the design, construction and maintenance management of inland river restricted waterway engineering to three-dimensional and whole-life management, achieve the fine construction goal of inland river restricted waterway engineering, and provide reference for the application of BIM technology in inland river restricted waterway engineering.

Keywords: Inland waterway; BIM; Model; Integration

1 Introduction

Building Information Modelling (BIM), as the carrier of digital information inte-

gration of construction engineering, is an information model covering the whole life cycle of construction engineering. With the continuous development and progress of modern information technology, the landing and in-depth application of BIM, GIS and other technologies in the traditional construction engineering industry has been accelerated. As one of the important means and ways to improve the digital level of infrastructure engineering construction, BIM is of great significance in promoting the deep integration of traditional engineering industry and new generation information technology, so as to realize the informatization, digital construction and management of construction projects in the whole life cycle. BIM plays an important role in the process management and optimization of construction project planning, design, construction and operation and maintenance management and control.

Compared with the mature application of BIM in the construction field, the application of BIM in the field of inland waterway engineering is still in the primary stage, but industry experts have also carried out BIM application research in waterway engineering. Li Guojie and others focused on the BIM technology route, key technologies and application contents in the whole life cycle of the waterway regulation project in order to solve the problems of difficult implementation of BIM technology in the waterway regulation project. Guo Tao summarized the characteristics of channel engineering in the stages of design, construction, operation and maintenance, and discussed its application in each stage of channel engineering from the perspective of combining the advantages of BIM technology. Wang Wei and others introduced Autodesk series BIM software in the design of inland waterway, replacing the traditional CAD drawing tools, and significantly improving the parametric design efficiency of inland waterway revetment engineering and dredging engineering. Xu Maoxing and others studied the general idea and technical route of the application of BIM technology in waterway regulation according to the advantages and disadvantages of the traditional management mode of engineering projects.

To sum up, there is more and more research on the application of BIM in the field of waterway engineering, and preliminary results have been achieved. It is of great significance to carry out the application of BIM in inland waterway engineering construction projects. Based on a restricted inland waterway project in Northern Zhejiang, this paper will study and summarize the key technologies of the application of BIM in the restricted inland waterway project, so as to provide reference for similar inland waterway construction projects.

2 Application status of BIM in inland river restricted channel engineering

2.1 Characteristics of restricted inland waterway engineering

The characteristics of restricted inland waterways are mainly reflected in the types of waterways with small section scale, regular section shape, narrow water surface as a whole and restrictive factors on ship navigation. Most restricted inland waterways are concentrated in China's river transportation and areas with relatively developed social economy, such as Northern Zhejiang plain and southern Jiangsu. There are obvious differences between inland restricted channels and natural rivers, which can be regarded as a semi-natural ecosystem to a great extent. The riverbed is relatively flat, the water flow is relatively stable, the water level variation is small, the section scale is small, and the section shape is regular. The section scale of inland restricted channels is generally determined according to the minimum scale necessary for ship navigation.

2.2 Problems in BIM application of restricted inland waterway engineering

Foreign BIM technology is applied earlier, and its supporting software functions are relatively complete. Typical BIM software includes Autodesk, Bentley and Dassault, as well as Archicad, Tekla and other BIM software to solve local needs or professional applications. At the same time, China also has a number of domestic BIM software applied in different fields, such as Yingjianke, Explorer, Hongye, etc., but most of them come from secondary development or technical integration based on foreign open BIM software.

Due to the particularity and professionalism of the restricted inland waterway project, which is quite different from the construction, municipal and other engineering fields, and the existing BIM products on the market are not developed for the restricted inland waterway project, the existing BIM technical scheme and supporting software tools cannot meet the standards and requirements of design and application, and the popularity of BIM in the restricted inland waterway project is relatively low. As a result, the number of standardized component libraries in this industry is small and the precision is low.

Therefore, it is necessary to systematically study the key technologies of BIM application in all stages of the life cycle of inland restricted channel project in combination with the characteristics of inland restricted channel project and BIM application, so as to provide technical support for fully integrating the application of inland re-

stricted channel project and promote the application and promotion of BIM technology in inland restricted channel project.

3 BIM application of restricted inland waterway engineering

The first mock exam of BIM technology in inland waterway restricted channel is to solve the problem of fragmented business in its design, construction and operation stages, and solve the problem of information data transmission and sharing. In order to integrate project information, management information and resource information into a unified model, the project's management mode is integrated into a unified model by using parameterized and standardized BIM model components as the carrier. In this paper, based on the application requirements of an inland river restricted channel project in Northern Zhejiang, BIM technology application research is carried out. The general technical route of the research is shown in Fig. 1.

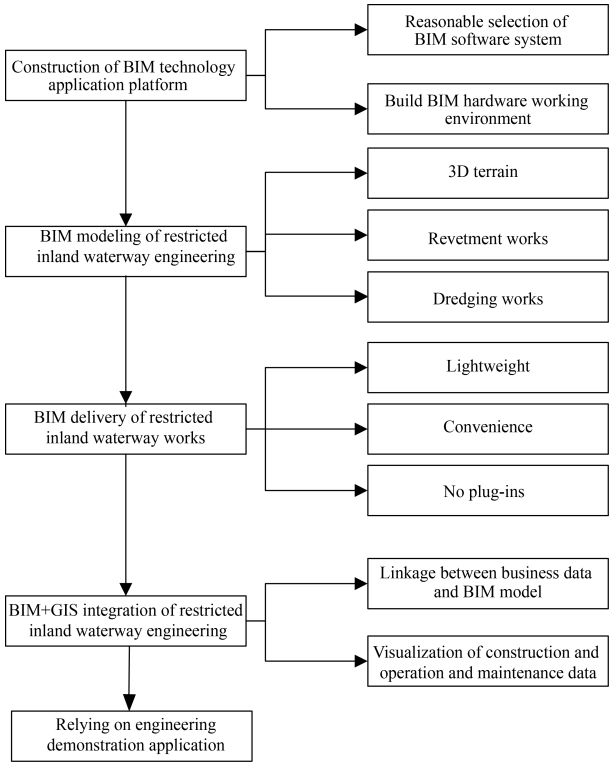

Fig. 1. General technical route of BIM application research of inland restricted channel engineering.

3.1 BIM modelling of restricted inland waterway engineering

The restricted inland waterway construction project has the characteristics of

small section scale and regular section shape. Therefore, it is necessary to solve the functional applicability of BIM software in the construction of inland waterway engineering in combination with the characteristics of restricted inland waterway engineering, put forward the BIM digital technical solution for waterway engineering system, and determine the creation method of professional BIM models such as topography, revetment and dredging in the construction project of inland waterway.

(1) BIM forward design

The Autodesk series BIM design software Civil 3D has powerful 3D collaborative design function, which can realize the design of "typical section" components with attribute information based on the advanced component editor in Civil 3D, and provide a design platform for the fine design of revetment, road and other ribbon projects. Based on the advanced component editor in Civil 3D, the design attribute information can be fused with the model, and the section design, engineering quantity statistics and other work can be handed over to the Civil 3D software, and the design section can be defined by inputting values to realize the forward design.

By comprehensively analyzing the special requirements of the revetment design of the restricted inland waterway project, and combining Civil 3D and the component editor, this paper puts forward the forward design idea of the revetment BIM of the restricted inland waterway project (Fig. 2). At the same time, in view of the heavy workload of creating the revetment infrastructure model, the author carries out the secondary development based on Civil 3D, and realizes the batch rapid modelling of the revetment infrastructure, which greatly improves the work efficiency.

(2) BIM secondary development

Civil 3D software provides rich APIs (Application Programming Interfaces) for secondary developers to call. By calling relevant interfaces, secondary developers can expand the functions and uses of Civil 3D according to their needs. The author carried out secondary development based on Civil 3D to realize batch rapid modelling of revetment infrastructure, which greatly improved work efficiency. The technical route is shown in Fig. 3.

3.2 Delivery of BIM model of restricted inland waterway project

At present, in the design stage, the application of BIM technology is mainly reflected in the fields of scheme adjustment, scheme comparison and selection, visual expression, performance analysis and so on. Due to the comprehensive use of a variety of BIM software for the establishment of BIM model and the high requirements of BIM software on computer performance, the BIM model is mostly delivered or displayed in the form of renderings or roaming video during the actual communication of

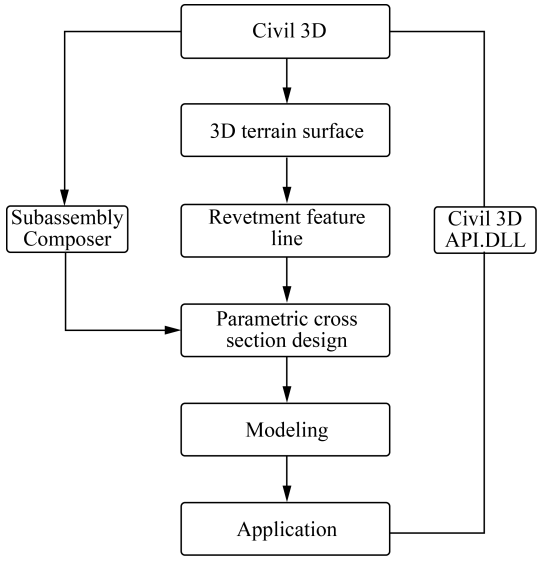

Fig. 2. Forward design idea of bank revetment BIM.

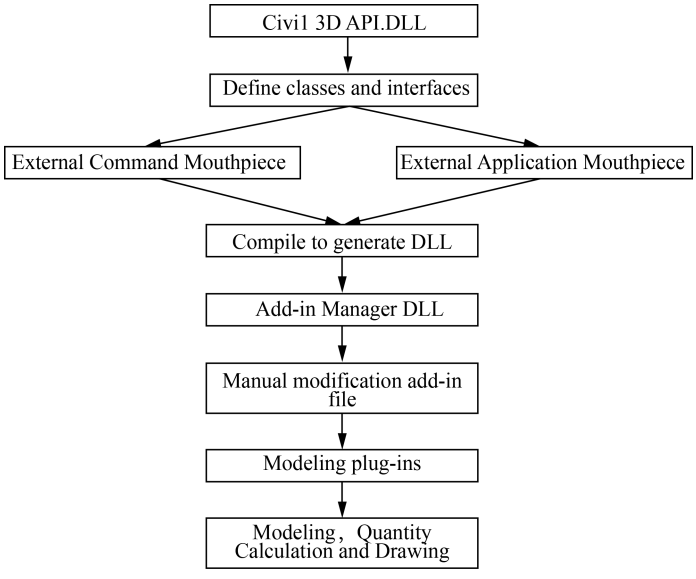

Fig. 3. Technical route of secondary development of Civil 3D.

the project, and the BIM model and its information data are not fully utilized. Therefore, on the basis of unified multi-source BIM data, BIM information can be effectively transmitted and shared in real-time in the whole life cycle of the project, so as to play the core role of BIM technology and truly realize the visualization of BIM design data and the convenience of BIM model delivery.

This paper will be based on the expression of all elements of the business scenario of the restricted inland waterway engineering, and take the data information mounting as the main line to realize the digital delivery of multidimensional, multivariate and heterogeneous data, such as basic geographic information, three-dimensional model data, transportation management business data, real-time perception data, and further promote the intelligent simulation, accurate decision-making, and digital delivery of the restricted inland waterway engineering industry.

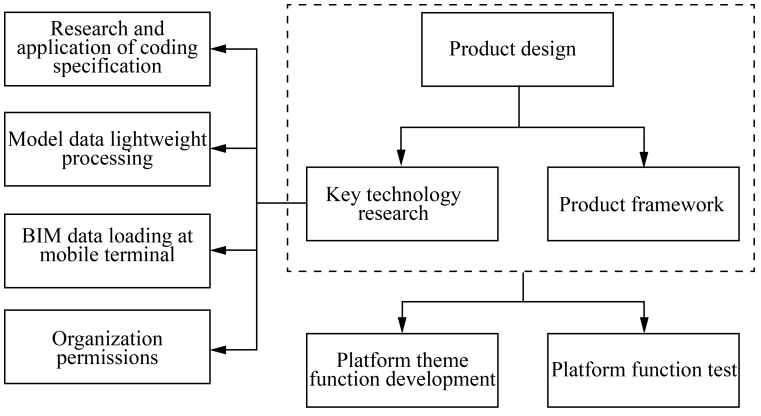

Fig. 4. BIM delivery technical route.

3.3 BIM + GIS integration of restricted inland waterway engineering

The application of BIM and GIS integration technology in the construction, operation and maintenance management stage of restricted inland waterway projects can improve the whole area monitoring and management ability of waterway and regional construction operations. This paper proposes a JSON-based public data model data integration method to improve the effective utilization of data resources and realize the integration and association of BIM model and business data. On this basis, a BIM + GIS project management system during the construction period is formed to realize the multi-dimensional and multi-level pattern of the combination of GIS-based overall macro control and BIM-based project bid section refined management, so as to meet the requirements of digital control in the construction process. It can also provide data support for the owner to carry out construction project operation and maintenance management in the later stage.

In this paper, JSON is selected as the public data model. Each type of data is processed in JSON. A virtual view is constructed, and finally mapped and bound with JSON intermediary data to complete the format conversion from the source database to the target database. See Fig. 5 for specific data format conversion process.

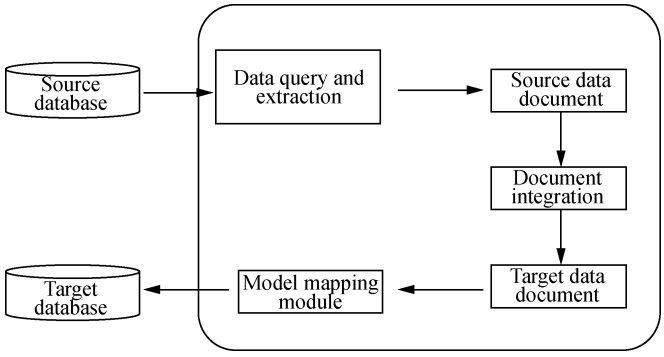

Fig. 5. Data format conversion process.

After the data format is unified, the data integration model is used for conditional filtering, compression and encryption, and persistent storage of data, providing a unified data interface for later data analysis calls. The data integration model adopted in this paper consists of three parts: interface, condition rule base and data processing. See Fig. 6 for the description of data integration structure.

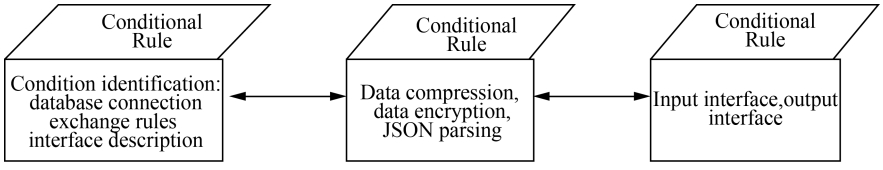

Fig. 6. Data integration structure description graph.

4 Engineering cases

Taking an inland restricted channel project in Northern Zhejiang as an example, this paper studies the key technologies of BIM application in the whole life cycle of inland restricted channel project. The supporting project starts from Zhapuzha bridge, which passes through Zhapu town, and finally ends at the junction of Jiaxing Port Area and Pinghu Lake. The channel mileage is 5.01 km and the reconstruction mileage is 5.67 km. It is implemented according to the restrictive class Ⅲ standard of inland river, in which the water depth is $\geqslant$ 3.2 m (the channel is deepened to 4.0 m along the slope), the bottom width is $\geqslant$ 45 m and the bending radius is $\geqslant$ 280 m.

Based on BIM technology, this paper realizes the creation and delivery of BIM models such as project 3D terrain model, revetment project and dredging project, and realizes the linkage and integration of project business data and BIM model through BIM + GIS, so as to realize the combination of overall macro control of the whole line

based on GIS and fine management of project bid section based on BIM.

4.1 BIM model creation

(1) 3D terrain

The original data of the three-dimensional terrain model of the restricted inland waterway project can be elevation point data, DWG topographic map or GIS data. The three-dimensional terrain model (terrain surface) can be generated based on the Civil 3D surface function, as shown in Fig. 7. Then, the satellite remote sensing images with coordinate information superimposed on the terrain surface are imported into the SuperMap 3D GIS platform to view the terrain status of the whole project scope.

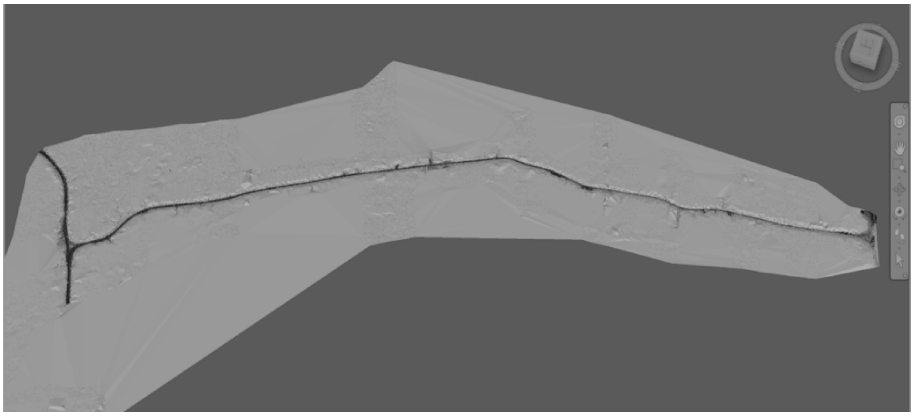

Fig. 7. 3D terrain model.

(2) Revetment works

Combined with the characteristics of the revetment project relying on the project, this paper establishes the BIM model of inland restricted channel revetment project by using Civil 3D, and improves some functions of Civil 3D through secondary development to realize the solid stretching and cutting of pile foundation, as shown in Fig. 8.

(3) Dredging works

Combined with the characteristics of the dredging project relying on the project, this paper uses Civil 3D to determine the centerline and profile (Fig. 9), sweeps along the centerline to generate new surfaces and entities, and establishes the BIM model of inland restricted channel dredging project (Fig. 10).

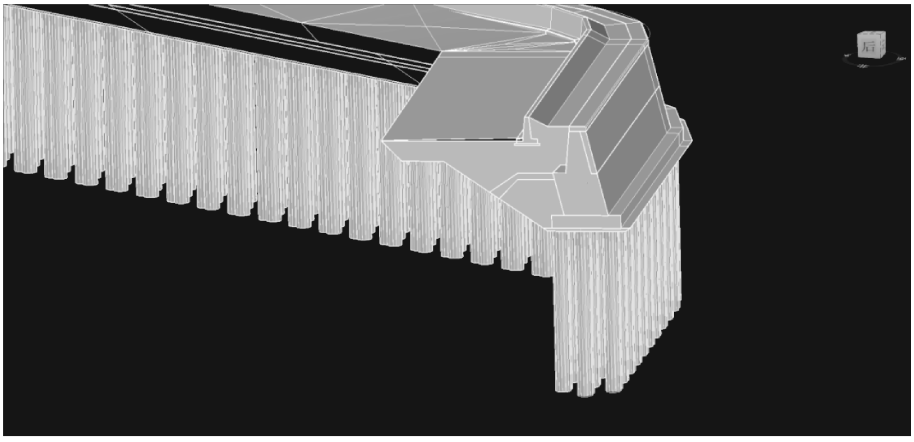

Fig. 8. Revetment engineering model.

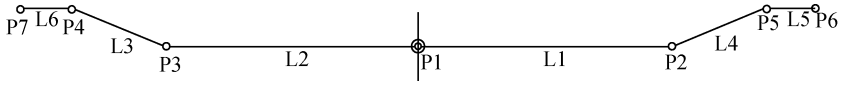

Fig. 9. Section design of dredging works.

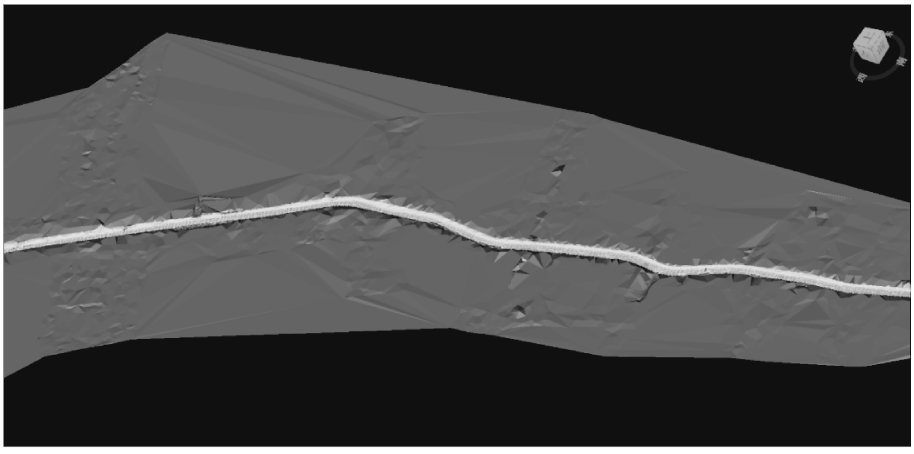

Fig. 10. Dredging engineering model.

4.2 BIM model delivery

See Fig. 11 for the implementation of multi-source GIS model, multi-source GIS model and data fusion based on BIM model and SuperMap 3D GIS plug-in.

4.3 BIM + GIS integrated application

Based on the project digital construction management and control and later oper-

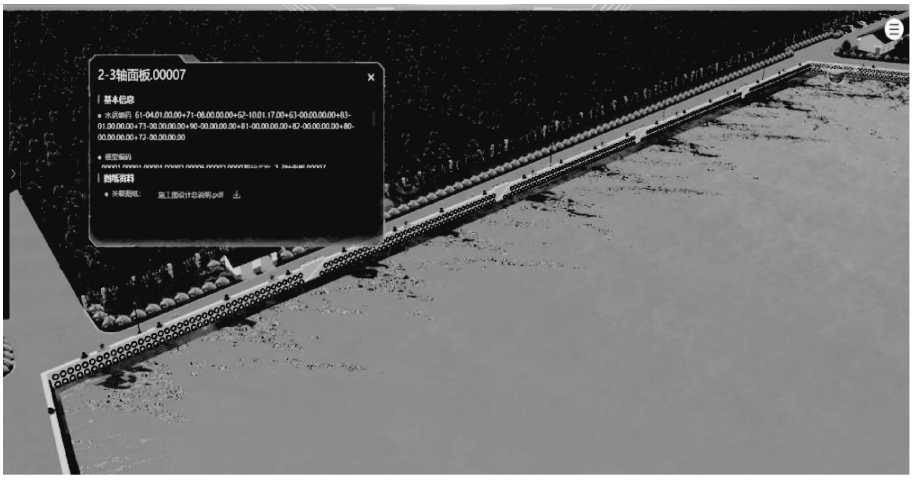

Fig. 11. BIM model delivery display.

ation and maintenance requirements, this paper realizes the linkage between business data and BIM model, supports the visual display of project construction and operation and maintenance data (Fig. 12), and multi-level management based on "BIM + GIS".

Fig. 12. BIM+GIS integration based on SuperMap.

5 Conclusion

The BIM software and tools used in this paper are all products of Autodesk. The GIS platform introduces the SuperMap 3D GIS technology of hypermap, a domestic

geographic information system software manufacturer, and studies the modelling and delivery technology of inland restricted waterway engineering based on BIM, so as to realize the convenient delivery of BIM model.

This paper realizes the linkage between business data and BIM model based on BIM+GIS, realizes the whole line macro control based on GIS and the fine management of project bid section based on BIM, and meets the needs of digital construction control and later operation and maintenance of the project.

During the construction of restricted inland waterway, the introduction of BIM+GIS technology improves the project construction efficiency and information management level, and plays a vital role in the whole process life cycle management of the project. The research results of this paper can provide reference for the application of BIM technology in similar projects.

References

Li, G.J., Liu, S., Guo, T., et al., 2018. Application of BIM technology in the whole life cycle of waterway regulation project. Water transportation engineering (8): 118-122.

Guo, T., 2018. Role of BIM technology in channel construction. Water transportation engineering (12): 21-25.

Wang, W., Yang, Z., 2019. Application of BIM technology in inland waterway design. Water transportation engineering (7): 193-197.

Xu, M. X., 2019. Application of BIM technology in waterway regulation engineering. Pearl River water transportation (8): 74-75.

Research on optimization of navigable water flow conditions for the complex bridge site section of the Changshan River

Ming Zhang[1], Xianzhong Chen[2], Honghao Fan[3], Xingwei Zheng[4], Qing Leng[5]

[1,5] Key Laboratory of Navigation Structures, Nanjing Institute of Hydraulic Sciences, Nanjing, China. e-mail: zhangm@nhri.cn

[2] Changshan Forestry and Water Conservancy Bureau, Quzhou, China. e-mail:780638054@qq.com

[3,4] Quzhou Xin'an Shipping Construction Development Co., Ltd., Quzhou, China. e-mail: 93344239@qq.com

Abstract: After the level of the Changshan River channel is upgraded, the water flow conditions in the bridge area of the bridge across the river need to meet the requirements of the regulations to ensure the safety of navigation. At present, the clear width of the navigation holes across the Changshan River Bridge on the Quchang Railway is only about 32.0 m. Considering the ship's maneuvering and navigation safety, it is appropriate that the angle between the centerline of the channel and the centerline of the bridge is orthogonal. Under this arrangement, the centerline of the channel near the upstream of the bridge site forms an angle of about 40° with the main flow of the channel, and the ship almost crosses the main flow from the right bank to the left bank, resulting in excessive lateral flow velocity in the channel. The floodplain is distributed in the bridge site area, and the river terrain is relatively open. There are objective conditions to improve the flow field characteristics of the river section through the improvement of the river terrain. The channel on the left side of the bridge site is dredged simultaneously with the channel at 69.1 m. When the maximum navigable flow is 800 m^3/s, the maximum calculated lateral velocity of the bridge site navigation hole is 0.3 m/s, and the water depth is 4.06 m, which meets the requirements of navigable water flow conditions.

Keywords: Bridge site navigable water flow conditions; Lateral flow velocity; Route optimization; River dredging

1 Introduction

At present, the clear width between navigation holes of Quzhou Changzhou Rail-

way crossing Changshan River Bridge is only about 32.0 m. After the grade of Changshan River channel is improved, considering ship handling and navigation safety, it is necessary to study the navigation flow conditions of the navigation section of the bridge site. Jiujingqu Railway bridge site has floodplain distribution and relatively open river terrain. There are objective conditions to improve the flow field characteristics of the river section through river terrain regulation. According to the layout of Jiujingqu Railway bridge project and the measured topography of Changshan River channel, the two-dimensional flow numerical model of Jiujingqu Railway bridge navigation section, navigable river regulation, route adjustment and other measures is constructed, and the flow conditions of ICBC in the navigation section of the bridge site are studied.

2 Project overview

The Changshan River is the southern source of the Qiantang River, originating from Xiuning County, at the northern foot of the Dajianshan Mountains in Anhui Province. At present, there are many beaches in the Changshan River, with rapid flow in flood season, less water in dry season, and poor waterway conditions. Only part of the voyage section can pass a 20-ton wooden boat, which is an external waterway. According to the "Changshan River Shipping Plan on the Upper Qujiang River" (draft for approval), "the Changshan River channel will be planned according to the standard of the Ⅳ-level channel after the cascade channelization." It is divided into six levels of development, from downstream to upstream: Huangtang Bridge, Hangbu, Zhaoxian, Gedi, Tianma and Baihutan cascade hubs, constructed in accordance with the standard of natural and channelized grade Ⅳ waterways, and the size of the waterway can meet the requirements of 1,000-ton ships navigation. Channel size: 3.4 m×60 m×480 m (water depth×navigation width×bending radius).

The research object of this paper, the Quchang Railway crossing Changshan River Bridge is located on the Changshan River between Wangjiayu Village and Pukou Village in Zhaoxian Town, between Changshan River Cascade Gedi Junction and Zhaoxian Junction, and is about 3.2 km away from Zhaoxian Junction. It is a 32 m simply supported beam. In this study, after the level of the Changshan River channel was upgraded, the water flow conditions of the bridge site can ensure the safety of ships crossing the bridge, and an optimization plan for channel regulation and route layout is proposed.

According to the latest topographic map, the distance between the left and right dams of the river section where the Quchang Railway crossing Changshan River Super

Bridge is located is about 950 m. The floodplain is distributed in the river channel, and the terrain is relatively open. Due to the sand excavation, the river channel terrain varies in depth. The angle between the mainstream in the river and the bridge centerline is about 40°.

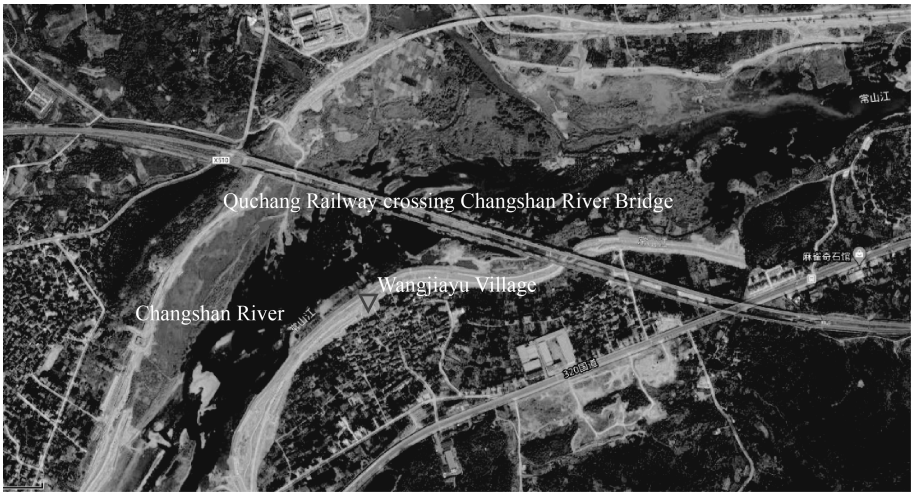

Fig. 1. Image of Quchang Railway crossing Changshan River Bridge.

3 Preliminary layout plan of the route and water flow conditions

3.1 Preliminary layout plan of the route

On a topographic map with a scale of 1∶10,000 , according to the embankments on both sides of the river, the topography of the river, and the combination of water flow conditions, the route is roughly arranged along the flow trend of the river, as shown in Fig. 2 below.

3.2 Preliminary layout scheme of water flow conditions

3.2.1 Computational model

According to the bridge layout of the Quchang Railway across the Changshan River and the measured topography of the upper and lower reaches of the bridge site, a numerical simulation model of water flow is constructed, and the navigable water flow conditions under the preliminary layout plan of the bridge site and waterway are simulated and calculated. Combined with the characteristics of the project's layout, and to ensure the accuracy of numerical simulation, this two-dimensional simulation range is shown above, where the downstream Gedi hub and the downstream Zhaoxian

Fig. 2. Schematic diagram of the route layout of the Quchang Railway across the Changshan River Bridge.

hub dam site are bounded, and the length is about 10 km. A total of 47,509 computing grids are generated in the simulation area, with an average grid size of 20 m, and the grids in the navigation hole area of the bridge site are locally refined with a grid size of 5 m.

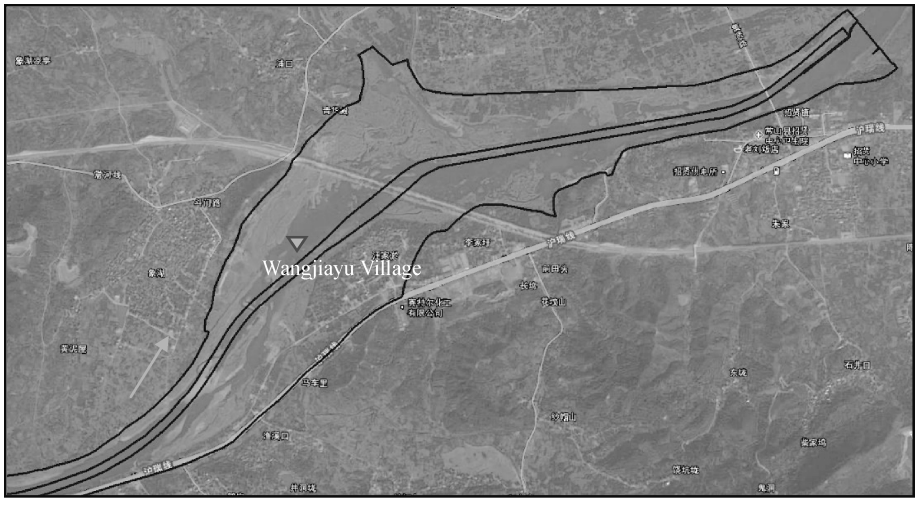

Fig. 3. Model calculation area.

3.2.2 Calculation method

The basic control equation of the two-dimensional water flow numerical simulation adopts the shallow water two-dimensional hydrodynamic equation system in the orthogonal rectangular coordinate system, including the water flow continuity equation and the water flow equation in x, y direction, which can be expressed as the following form.

Water flow continuity equation:

$$\frac{\partial h}{\partial t}+\frac{\partial U}{\partial x}+\frac{\partial V}{\partial y}=s_0 \tag{1}$$

The water flow equation:

$$\frac{\partial U}{\partial t}+\frac{\partial}{\partial x}\left(\frac{U^2}{h}\right)+\frac{\partial}{\partial y}\left(\frac{UV}{h}\right)+gh\frac{\partial h}{\partial x}+gh(J_{fx}-J_{0x})=0 \tag{2}$$

$$\frac{\partial V}{\partial t}+\frac{\partial}{\partial x}\left(\frac{UV}{h}\right)+\frac{\partial}{\partial y}\left(\frac{V^2}{h}\right)+gh\frac{\partial h}{\partial y}+gh(J_{fy}-J_{0y})=0 \tag{3}$$

where h is the water depth; s_0 the source term; U and V are the single-width discharges: $U=uh$, $V=vh$, u, v are the flow velocity in the x, y direction, respectively; J_{0x} and J_{0y} the bottom slope in the x direction, $J_{0x}=-\frac{\partial Z}{\partial x}$, $J_{0y}=-\frac{\partial Z}{\partial y}$, Z the river bottom elevation; J_{fx} and J_{fy} are respectively the friction gradient in x, y directions: $J_{fx}=\frac{n^2u\sqrt{u^2+v^2}}{h^{4/3}}$, $J_{fy}=\frac{n^2v\sqrt{u^2+v^2}}{h^{4/3}}$, n is the Manning roughness coefficient.

This model is solved by using the finite volume method.

3.2.3 Calculation results of water flow

In order to analyze the navigable water flow conditions of the upstream and downstream sections of the bridge site under the preliminary channel layout plan, combined with the possible maximum navigable flow range of this section, the 637 m^3/s, 743 m^3/s, 800 m^3/s, 1,000 m^3/s and 1,200 m^3/s flow conditions under different flow rates are calculated, and the lateral flow velocity, longitudinal flow velocity and water depth distribution of the channel upstream and downstream of the bridge site are analyzed.

Under the conditions of the preliminary design and layout of the channel, the statistical parameters of the water flow under different working conditions of the bridge site section are shown in Table 1. The flow field characteristics of the upstream and downstream channels of the bridge site correspond to different flow rates, which is shown in Fig. 4, and the transverse flow velocity of the channel centerline is shown in Fig. 5.

It can be seen from Table 1 that under the design channel parameters, when the flow rate of this section does not exceed 1,000 m^3/s, the maximum lateral flow velocity of the channel centerline near the upstream and downstream of the bridge site does not exceed 0.3 m/s, and the flow rate is 1,200 m^3/s, with a few statistical points slightly exceeding 0.3 m/s. Under different flow rates, the longitudinal velocity of the channel shall not exceed 0.8 m/s, and the water depth of the channel shall not be less than 4.0 m. The preliminary layout plan of the channel meets the requirements of navigable water flow conditions.

Table 1 Statistics on characteristic parameters of navigable water flow conditions in the 400 m segment upstream and downstream of the bridge site.

	Different flow rates under design channel conditions (m^3/s)				
	637	743	800	1,000	1,200
Transverse velocity (m/s)	0.06 – 0.19	0.08 – 0.21	0.09 – 0.23	0.11 – 0.27	0.14 – 0.32
Longitudinal velocity (m/s)	0.35 – 0.53	0.40 – 0.60	0.43 – 0.64	0.53 – 0.77	0.61 – 0.88
Channel depth (m)	4.00 – 5.91	4.02 – 5.93	4.04 – 5.95	4.10 – 6.01	4.17 – 6.09

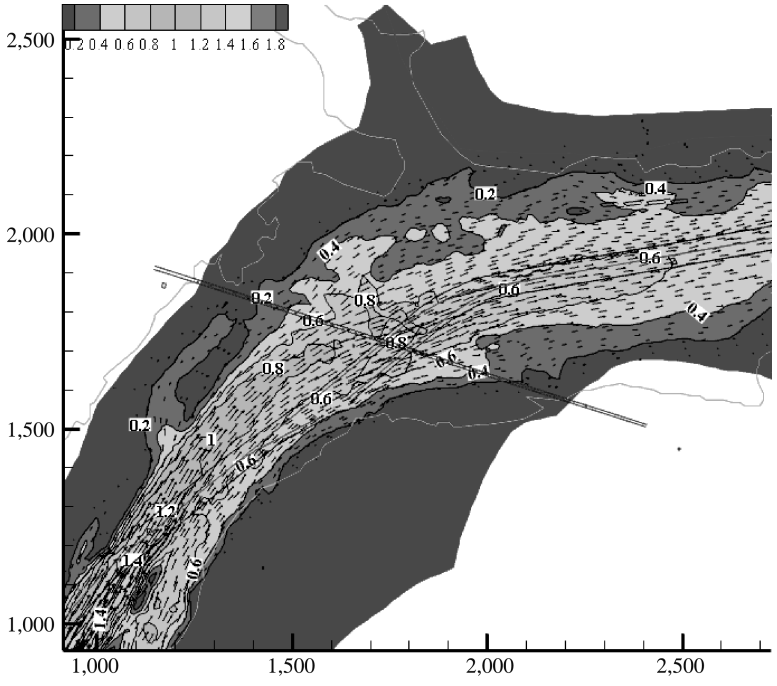

Fig. 4. Distribution map of the flow field at the bridge site (flow: 1,000 m^3/s).

Under this preliminary channel layout plan, although the lateral flow velocity in the channel in the bridge site area meets the requirements of navigable water flow conditions at a flow rate of 1,000 m^3/s, the angle between the centerline of the channel and the centerline of the Jiujingqu Railway Bridge (old bridge) is about 60°, and the net width between the navigation holes of the old bridge is only about 32 m. Thus, it is not easy to control the rudder when the ship passes through the bridge holes, since it is easy to hit the pier, and there is a potential safety hazard. Therefore, the channel layout of the bridge site segment needs to be further adjusted.

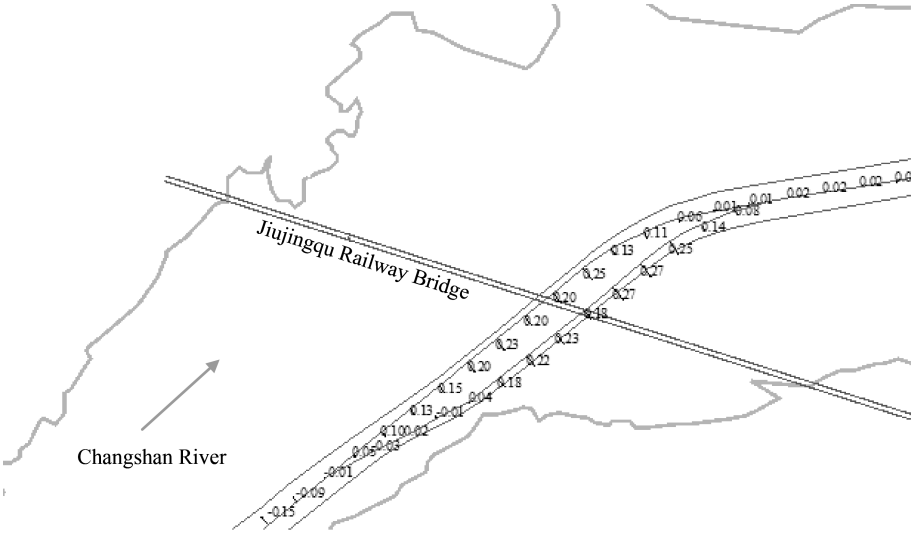

Fig. 5. Transverse flow velocity of channel centerline (Q=1,000 m³/s).

4 Optimization of water flow conditions for the bridge site section

4.1 Channel layout adjustment plan

In order to improve the safety of ships passing through the navigation hole of the old bridge of Jiujingqu Railway Bridge, the route should be arranged perpendicular to the centerline of the old bridge. Therefore, the route layout of the Jiujingqu Railway Bridge section is adjusted as shown in Fig. 6 below, including two adjustment schemes. Scheme Ⅰ: The upstream route of the bridge site is arranged outside the existing river bank embankment. Scheme Ⅱ: The upstream route of the bridge site is arranged along the inner side of the embankment. In these two schemes, the centerline of the waterway in the bridge site area is basically perpendicular to the centerline of the bridge. Scheme Ⅰ involves resettlement demolition, and the flood control embankment on the right bank of the river needs to be withdrawn.

Considering the channel dredging control elevation of 69.1m, the plane two-dimensional numerical simulation model is modified, and the navigable water flow conditions of the channel under the two adjustment schemes are calculated and statistically analyzed.

Under the condition of adjustment of Scheme Ⅰ, when the flow rate is 1,000 m³/s and 500 m³/s, the maximum lateral flow velocity is 0.5 m/s and 0.35 m/s near the bridge site. In this scheme, the centerline of the channel at the bridge site forms an angle of

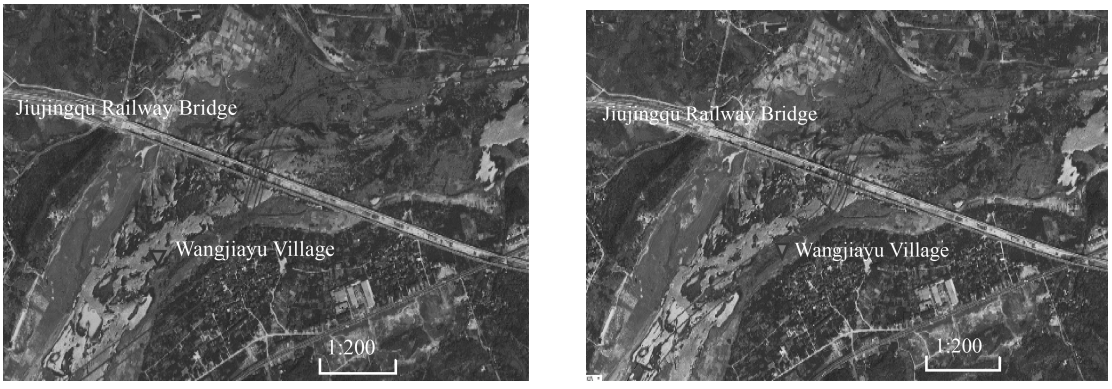

(a) Scheme Ⅰ (b) Scheme Ⅱ

Fig. 6. Channel layout adjustment schemes.

about 40° with the main flow of the river, and the ship almost crosses the main flow from the right bank to the left bank, resulting in excessive lateral flow velocity. Under the condition of route adjustment Scheme Ⅱ, even if the flow rate is 500 m^3/s, for the same reason, the maximum calculated lateral flow velocity in the bridge area is still as high as 0.54 m/s, which does not meet the requirements of the specification that the flow velocity in the channel does not exceed 0.3m/s.

4.2 River dredging and regulation and diversion scheme

In the bridge site area of the super bridge across the Changshan River on the Quchang Railway, the floodplain is distributed, and the river terrain is relatively open. There are objective conditions to improve the flow field characteristics of the river section through the improvement of the river terrain. As mentioned above, the waterway adjustment Scheme Ⅰ involves the demolition of resettlements, and the flood control embankment on the right bank of the river needs to be withdrawn. The river channel is dredged on the left side, and the dredging scope is shown in Fig. 7 below. The dredging control elevation is 69.1 m, which is consistent with the dredging elevation of the channel. Considering the safety of the piers, no dredging is required within 30 m upstream and downstream of the piers.

Considering the different discharge volumes of the upstream Gedi Project and the water level in front of the dam of the downstream Zhaoxian Project, the corresponding working conditions are designed for simulation calculation. The simulation results are shown in Table 2 below.

From the simulation results, the following conclusions can be drawn: the dredging of the channel on the left side of the bridge site and the channel at the same time of 69.1 m can improve the navigable water flow conditions of the bridge site. When

the maximum navigable flow is 800 m^3/s, and the water level in front of the dam of the downstream Zhaoxian Project is the corresponding maximum navigable water level of 73.0 m, the maximum lateral flow velocity of the bridge site navigation hole is 0.3 m/s and the water depth is 4.06 m, which meets the requirements of navigable water flow conditions.

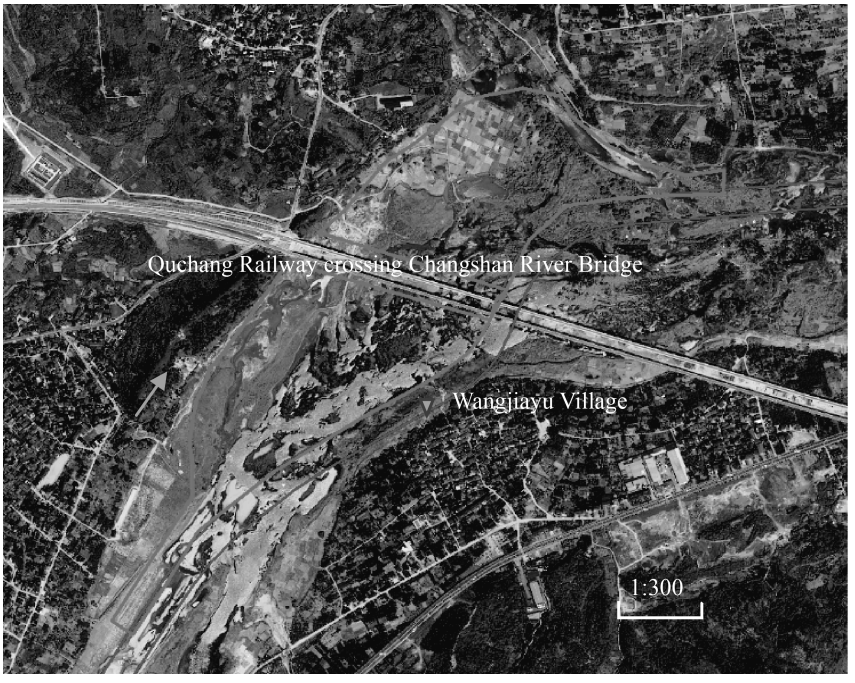

Fig. 7. Schematic diagram of the dredging range on the left side of the bridge site.

Table 2 Simulation calculation conditions and results.

Working condition	Flow (m^3/s)	Downstream water level (m)	Maximum transverse velocity (m/s)	Maximum longitudinal velocity (m/s)	Channel water level (m)	Channel depth (m)	Dredging control elevation (m)
1	500	73	0.20	0.47	73.06	3.96	69.1
2	800	73	0.30	0.74	73.17	4.06	69.1
3	1,000	73	0.37	0.90	73.26	4.16	69.1

The maximum navigable flow is 800 m^3/s, and the water level in front of the downstream Zhaoxian Dam is the highest navigable water level of 73.0 m. The centerline flow field and lateral flow velocity of the bridge site channel are shown in Fig. 8 and Fig. 9, respectively.

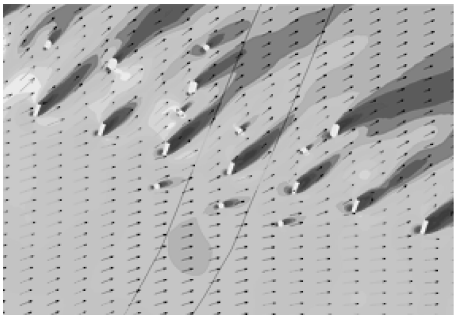

Fig. 8. Schematic diagram of the flow field of the bridge site channel.

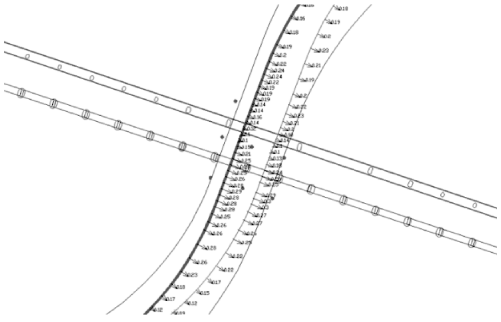

Fig. 9. The lateral velocity distribution of the bridge site channel centerline.

5 Conclusions

The Quchang Railway crossing Changshan River Bridge is a simply supported beam with a bridge span of 32 m. After the Changshan River waterway level is upgraded, the water flow conditions in the bridge area must meet the requirements of the regulations to ensure the safety of navigation. The calculation results of the water flow conditions in the bridge area show that, under the preliminary arrangement of the channel, although the lateral flow velocity in the channel in the bridge site area meets the requirements of the navigable water flow conditions with a maximum navigable flow of 1,000 m^3/s, the centerline of the channel and the centerline of the bridge form an angle of about 60°, and the net width of the navigation holes of the old bridge is only about 32.0 m, which is prone to collision with piers and has potential safety hazards. After the route adjustment, the centerline of the channel and the centerline of the bridge are approximately orthogonally arranged, which is beneficial for ships to pass the bridge. The offset of the right bank to the left bank results in the calculated lateral flow velocity being too large, which cannot meet the requirements of navigable water flow conditions. Considering that the channel on the left side of the bridge site is dredged simultaneously with the channel at 69.1 m, and when the maximum navigable flow is 800 m^3/s, the maximum calculated lateral velocity of the bridge site's navigation hole is 0.3 m/s, and the water depth is 4.06 m, which meets the requirements of navigable water flow conditions.

Acknowledgements

This study is financially supported by the National Key R&D Program of China (2021YFC3200302).

References

Qu, Z. H., 2014. Research on Qujiang Channel navigation condition. Hangzhou: Zhejiang University.

Zhang, M., Hu, Y. A., Fan, Z. W., et al., 2016. Optimization of operation mode of cascade hub based on integration of navigation-power junction. Port & Waterway Engineering (12): 113-119.

Pre-feasibility study report on flood discharge sluice project of hydropower station of Changshan River main stream (Huibu Intersection of two ports) navigation power junction project, Zhejiang Water Resources and Hydropower Survey and Design Institute Co., Ltd., 2019.

Pre-feasibility study report of Changshan River (Huibu-Intersection of two ports) avionics hub project, Zhejiang Shuzhi Jiaoyuan Technology Co., Ltd., 2019.

One of the relevant model test research reports of Qujiang (Quzhou section) navigation development project hub and ship lock in the middle and upper reaches of Qiantang River, one-dimensional numerical simulation of flow and sediment in the whole river, Nanjing Institute of Hydraulic Sciences, 2010.

Channel regulation model test of Yangfushan new port area of Oujiang River, Nanjing Institute of Water Resources, 2012.

Numerical simulation study on flow and sediment of channel regulation project in the engineering feasibility stage of Oujiang (Wenzhou section) shipping development project, Nanjing Institute of Hydraulic Sciences, 2013.

Study on numerical simulation of one-dimensional flow and sediment in the whole reach, Nanjing Institute of Hydraulic Sciences, 2009.

Research on the backflow characteristics of downstream navigation lock entrance area in sharp bends

Shouyuan Zhang[1], Chunhui Yu[2], Rongrong Wang[3], Hongyu Cheng[4], Gensheng Zhao[5]

[1,3,5] State Key Laboratory of Hydrology-Water Resources and Hydraulic Engineering, Nanjing, China. e-mail: oliviatungyur@outlook.com, rrwangnhri@outlook.com, gszhao@nhri.cn

[2] Quzhou Highway, Navigation and Transportation Management Center, Quzhou, China. e-mail: chyuHNTMC@outlook.com

[4] College of Harbour Coastal and Offshore Engineering, Hohai University, Nanjing, China. e-mail: hychenghhu@outlook.com

Abstract: When a navigation lock is located in the upstream of a sharp river bend, the large backflow in the downstream entrance area affects the navigation safety. This paper analyzed the different factors affecting the backflow features in the entrance area by computing the generalized numerical model which was established on the characteristics of the downstream entrance area in sharp bends. The influencing factors in backflow length of the entrance area including the broadening ratio, flow velocity, water depth and the relative position between the diversion dike and the bend were also investigated. Besides, a calculation formula of the backflow length in horizontal direction of the ship lock downstream entrance area was derived. A two-dimensional numerical model based on a hydropower junction located in the convex bank with a 90-degree sharp bend was built to verify the formula and further explore the effect of the diversion dike length on the flow conditions in the entrance area. The results indicated that the entrance backflow length in the horizontal direction was positively proportional to the broadening ratio, flow velocity and water depth. Moreover, the backflow area was divided into three sections, including the non-influenced section which was far away from the entrance, turbulent diffusion section and the reversing flow section. Besides, choosing suitable length of the diversion dike could effectively improve the navigation flow conditions of the entrance area and ensure the ship to pass the ship lock safely. This paper presents a method for analyzing the backflow characteristic of the downstream entrance area in similar hydropower junctions.

Keywords: Sharp bend; Entrance area; Diversion dike; Backflow length in horizontal direction; Backflow characteristics

1 Introduction

The flow condition of the entrance area in the junction between the ship lock approach

channel and the river channel plays an important role in efficiently passing ship locks (Li et al., 2013). Due to numerous river bends in the mountain area, sometimes the downstream entrance is designed in the bending section of the river channel. Affected by the diversion dike and the bend, the high-speed backflow occurred in the entrance area will interfere with the navigation (Han et al., 2021). Existing researches on the backflow in the entrance area mainly focus on two aspects, including theoretical analyses based on the generalized model and improvement measures combined with actual engineering operations. In case the water body in the approach channel is regarded as stationary, and the approach channel is long enough to make the water flow transited smoothly, the water flow in the entrance area can be approximately regarded as a unilateral sudden-expansion flow. In Cheng et al.'s research (1992), measured data based on the minimum energy consumption principle indicated that the length of the backflow was positively proportional to the Froude number, expansion rate and water depth, while inversely proportional to the roughness coefficient. Besides, an empirical formula for the length of the unilateral sudden-expansion flow in the straight river channel was derived. Zheng et al. (2014) built a two-dimensional numerical model to analyze the relationship between the spur length and the backflow length. Results showed that the spur length was positively proportional to the width and length of the backflow area. Zhong et al. (2017) analyzed the influence of various geometric scales and inflow discharges in the double step-shaped spur dikes on the backflow by applying a 3D numerical model of water flow. Li et al. (2013) built a straight water tank numerical model to analyze the influence of broadening ratio, flow velocity and water depth on the backflow length of the downstream approach channel. Jiang et al. (2020) took the JH Power Station as the research subject and proposed an empirical formula for the backflow length of the entrance area in the downstream approach channel based on the two-dimensional numerical model. Li et al. (2016) analyzed the backflow velocity, the transverse and longitudinal flow velocity in laboratory model tests, and proposed setting deflector piers and navigation walls outside the approach channel to improve the flow conditions.

Although researches above have made great progress in certain aspects, the simulation and investigation on the backflow were mostly conducted on the straight river channel, which were unable to fully demonstrate the backflow characteristics in the entrance area under sharp river bends of the mountain area. In order to further study the backflow characteristics in the entrance area of the downstream approach channel, a generalized numerical model was established to analyze the backflow under the sharp bend and the effects of broadening ratio, flow velocity and water depth on the backflow. Besides, the backflow characteristics were analyzed, and the backflow area was divided. An empirical formula of the backflow length in horizontal direction was also put forward. In addition, a hydropower junction located on the convex bank with a 90-degree sharp bend in the downstream entrance

area was taken as a research subject. A two-dimensional numerical model was built to analyze the backflow characteristics in entrance area, verify the empirical formula of the backflow length, and determine the most suitable length of the diversion dike for the junction.

2 Calculation and analysis of generalized numerical model

2.1 Generalized numerical model

A generalized numerical model was established on the basis of the Navier-Stokes equation to simulate the flow characteristics in entrance area of the downstream approach channel in wide-shallow river channel under the sharp bend. The viscous dissipation in the water body is neglected. Besides, the water body is regarded as an incompressible fluid and obeys the hydrostatic pressure distribution. The model was solved by the finite volume method, and the mesh was subdivided using the triangular finite element discretization technology. This model included the following continuous equations and motion equations (Fu, 1995).

Continuous equation:

$$\frac{\partial h}{\partial t}+\frac{\partial q}{\partial x}+\frac{\partial p}{\partial y}=0 \tag{1}$$

Momentum equation:

$$\frac{\partial q}{\partial t}+\frac{\partial}{\partial x}\left(\frac{qq}{h}\right)+\frac{\partial}{\partial y}\left(\frac{qp}{h}\right)=-gh\frac{\partial(h+z_b)}{\partial x}+\frac{1}{\rho}\left[\frac{\partial}{\partial x}\left(\varepsilon_t\frac{\partial q}{\partial x}\right)+\frac{\partial}{\partial x}\left(\varepsilon_t\frac{\partial q}{\partial y}\right)\right]-\tau_{xb} \tag{2}$$

$$\frac{\partial p}{\partial t}+\frac{\partial}{\partial x}\left(\frac{qp}{h}\right)+\frac{\partial}{\partial y}\left(\frac{pp}{h}\right)=-gh\frac{\partial(h+z_b)}{\partial x}+\frac{1}{\rho}\left[\frac{\partial}{\partial x}\left(\varepsilon_t\frac{\partial p}{\partial x}\right)+\frac{\partial}{\partial x}\left(\varepsilon_t\frac{\partial p}{\partial y}\right)\right]-\tau_{yb}$$

where h is the water depth, m; g is the acceleration of gravity, m/s^2; q is the discharge per unit width in the water flow direction, m^2/s; p is the discharge per unit width in the normal direction of water flow, m^2/s; z_b is the bed elevation, m; ρ is the water density, kg/m^3; ε_t represents the dynamic viscosity coefficient; τ_{xb} and τ_{yb} are the bottom frictional resistance, kN.

2.2 Design and verification of the model

A straight tank model was built to simulate the flow field and the backflow length in the unilateral sudden-expansion for verification. The total width of the water tank B is 20 m, the total length is 150 m, and the bottom slope i is 0.000 1. The length of the inflow stabilization section is 60 m, the width of the inlet B' is 15.7 m, the width of the simulated entrance area b is 3.5 m, and the width of the dike width Δ is 0.8 m. The size and features of the model designed for verification are shown in Fig. 1(a).

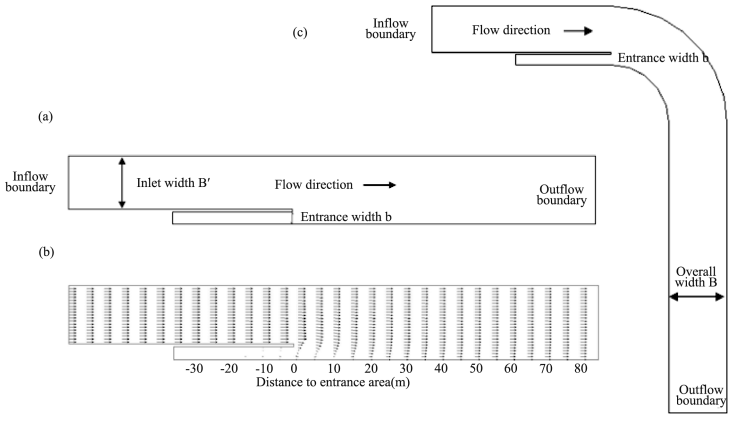

Fig. 1. Generalized numerical model (a) Numerical model for verification. (b) Unilateral sudden-expansion flow field in verification model. (c) Schematic diagram of the generalized numerical model under the sharp bend.

In calculating, the inflow and outflow boundaries are both permeable boundaries, and the rest are impervious boundaries. The inflow velocity is 0.64 m/s, the water depth is 1.0 m, and the simulation time is 1 hour. The unilateral sudden-expansion flow field is shown in Fig. 1(b). The calculated length of backflow in the unilateral sudden-expansion flow field is 8.2 m, which is close to the 8.4 m length of backflow calculated by the empirical formula proposed by Cheng et al. (1992), with a difference of 2.4%. Meanwhile, it is 4.8% different from the 7.8 m length of backflow calculated by Li et al. (2013). Under the calculation conditions with the inflow boundary velocity of 0.5 m/s and the water depth of 1.0 m, the length of backflow is 7.3 m. The calculation results are basically consistent with those calculated by Li's formula, with a difference of 0.9%. Thus, it is obvious that the established straight water tank model can well simulate the actual flow field. In order to demonstrate the water flow characteristics in entrance area of the downstream approach channel under the influence of sharp bends appropriately, a 90-degree bend is installed in the entrance area of the above-mentioned straight model. And the outflow boundary is set 100 m away from the bend, so as to make the water flow fully developed in the bend without the effect of the outflow boundary. The generalized numerical model for the downstream entrance area under sharp bends is shown in Fig. 1(c).

2.3 Calculation results and analyses of the model

2.3.1 The effect of broadening ratio

The water flow cross-section area suddenly increases due to the sudden change of the river channel when the water flow passes through the diversion dike, where a long

and narrow backflow area will be formed due to the water flow separation. The increase of the water flow cross-section area between the front and the back of the diversion dike will affect the backflow range. Since the water depth is a constant value in the generalized model, the alteration rate of the cross-section area is equal to the broadening ratio of the river width. The broadening ratio is displayed in the following formula.

$$\delta = \frac{B}{B'} = \frac{B}{B - \Delta - b} \tag{3}$$

where B is the total width of the water tank, m; B' is the width of the water inlet, m; b is the width of the entrance, m; Δ is the width of the diversion dike, m.

In order to study the effect of the broadening ratio, simulation of the backflow length under different broadening ratios was conducted when the model depth, the flow velocity and the location of bends were constant. During the calculation, the inflow velocity is 0.64 m/s, the water depth is 1.0 m, and the beginning of the bend is 3.0 m away from the dike head. The calculation results are shown in Fig. 2.

Simulation results indicated that under certain conditions of water depth, flow velocity and bend position, with the increase of the broadening rate, the backflow length of the downstream entrance area increased gradually, which was consistent with the variation tendency of the backflow caused by the unilateral sudden-expansion flow in Li and Cheng's study. Owing to the increasing broadening ratio, the proportion of the entrance in the river width was larger, which made the velocity of the mainstream flow increase as well as the backflow length due to the gradually increasing recovering distance of water flow. However, with the increase of broadening ratio, the rate of backflow length growth reduced gradually. When the broadening ratio increased from 1.17 to 1.21, the increasing range of the backflow length was about 23.96%. But the increasing range reached only 9.97%, when the broadening ratio increased from 1.29 to 1.33. This revealed that the backflow range did not increase proportionally with the increasing broadening ratio, and the oblique flow in the bend section affected the development of the backflow in certain ways, which was different from the simulation results of straight river channel in Li's research (2013). In straight channel, the backflow could fully develop along the way, and the backflow length was positively proportional to the increasing broadening ratio. But in the bend section, when the broadening ratio increased, the velocity of the mainstream flow and the oblique flow in the dike head area were faster, while the angle between the axis of the oblique flow and the vertical line was smaller. When the broadening ratio reached 1.17, the maximum oblique flow velocity in entrance area was 0.38 m/s. And when

the broadening ratio increased to 1.33, the maximum oblique flow velocity was 0.62 m/s. The oblique flow restricted the development of the backflow.

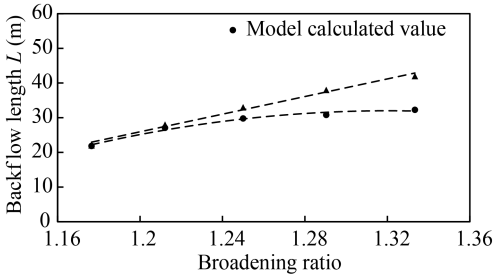

Fig. 2. Broadening ratio influence factor.

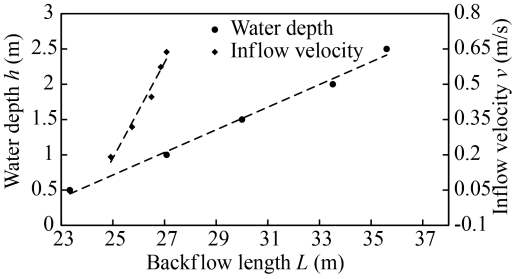

Fig. 3. Flow velocity and water depth influence factor.

2.3.2 The effect of flow velocity and water depth

When analyzing the influence of water depth on the backflow length, the broadening ratio is 1.21, the inflow velocity is 0.64 m/s, and the water depth is set as five different situations including 0.5 m, 1.0 m, 1.5 m, 2.0 m, and 2.5 m, respectively, for simulation and calculation. Besides, when analyzing the flow velocity factor, the broadening ratio is 1.21, the water depth is 1.0 m, and the flow velocity is set as 0.19 m/s, 0.32 m/s, 0.44 m/s, 0.57 m/s and 0.64 m/s, respectively. The calculation results under these two factors are shown in Fig. 3. Results showed that under the influence of the water depth and flow velocity as independent argument, the backflow length was positively correlated with each factor. Notably, the backflow length was more sensitive to the variation of water depth. When the factors were at the same variation rate, the change of water depth played a more important role in the backflow length. Under the influence of a single factor, the fitting formula of the backflow length is as follows.

$$\text{The effect of water depth:}\quad L = 6.19h + 20.9 \tag{4}$$

$$\text{The effect of flow velocity:}\quad L = 4.70v + 24.1 \tag{5}$$

where L represents the backflow length, m; h is the water depth at the inflow boundary, m; v is the inflow velocity, m/s.

2.3.3 The effect of relative position between the diversion dike and the bend

Since the water flow enters the bend after passing the diversion dike, the mainstream flow direction moves generally towards the convex bank. Under the influence of the concave bank boundary, the more the dike head extends into the bend, the less the cross-section area is, and the faster the overall flow velocity is. The velocity of oblique flow in dike head area becomes faster and its direction is more inclined to the convex bank. The relative positions between the diversion dike and the bend affect the backflow length in horizontal direction of the entrance area. The relative position

can be displayed in the following formula:

$$t = \frac{T}{b} \tag{6}$$

where t is the dimensionless coefficient which represents the relative position; T represents the distance from the dike head to the beginning of the bend, m; b is the width of the entrance, m. When the diversion dike head is in the straight section, t is negative. And t is positive, when the diversion dike head is in the bend.

In order to study the relationship between the relative position and the backflow length in horizontal direction, the backflow near the diversion dike in different positions is simulated when the broadening ratio, water depth and flow velocity are kept as fixed value. During the calculations, the inflow velocity is 0.64 m/s, water depth of inflow boundary is 1.0 m, water depth of outflow boundary is 0.9 m, and the broadening ratio is 1.21. The coefficient t and the calculation results are shown in Table 1.

Table 1 The calculation results of outside backflow length in horizontal direction.

T (m)	t	Backflow length (m)	T (m)	t	Backflow length (m)
7.00	−2.0	6.80	1.75	0.5	5.71
5.25	1.5	6.75	3.50	1.0	3.80
3.50	−1.0	6.80	5.25	1.5	3.31
1.75	−0.5	6.77	7.00	2.0	3.00
0	0	6.80			

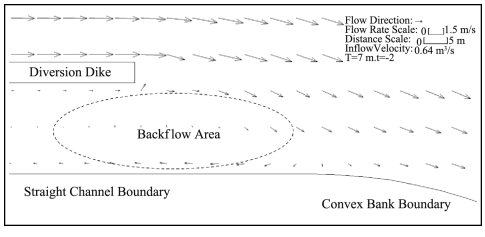

Fig. 4. Flow field in entrance area. ($t=-2$)

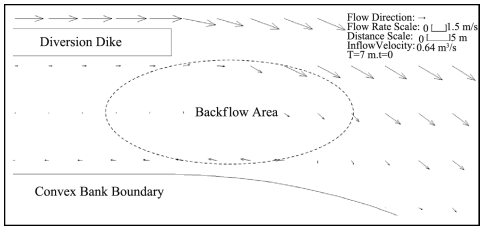

Fig. 5. Flow field in entrance area ($t=0$).

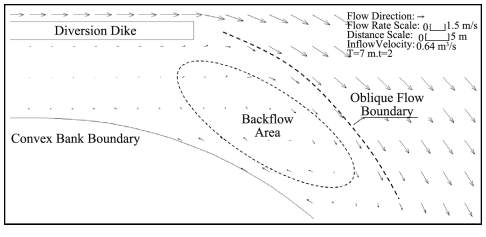

Fig. 6. Flow field in entrance area. ($t=2$)

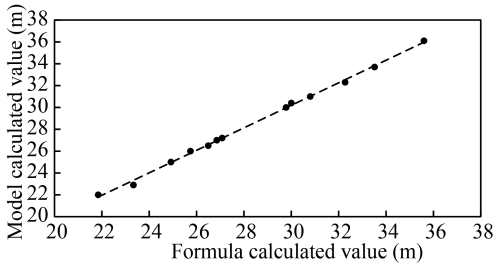

Fig. 7. The comparison between model and formula.

The calculated backflow length outside the entrance showed that when the dike head was in the straight river section, the backflow length was not affected by the relative position. Besides, backflows were within the straight section of the channel (see Fig. 4). When the dike head was aligned with the beginning of the bend, the backflow was not affected by the oblique flow, and the length was basically consistent with that when the head was in the straight section (see Fig. 5). When the division dike extended into the bend, with the coefficient t increasing, the backflow length outside the entrance decreased obviously, and the rate of the outside backflow length shortening reduced gradually. For instance, the backflow length shortened the most distinctly when the division dike extended 1 time wider of the entrance. At this time, the maximum oblique flow velocity reached 0.84 m/s, and the backflow area passed down from the bend to the boundary of the concave bank. What's more, when the division dike extended 2 times wider of the entrance, the maximum oblique flow velocity was 0.91 m/s (see Fig. 6). The backflow length inside the dike was basically consistent under nine kinds of calculating conditions. The fitting formula of the backflow length outside the entrance in horizontal direction is as:

$$\frac{L_{out}}{b} = 0.33\,t^2 - 1.16t + 1.91 \tag{7}$$

where L_{out} is the backflow length outside the entrance, m; t is dimensionless coefficient which represents the relative position.

2.3.4 Analyses of the backflow characteristics

Affected by the oblique water flow in the entrance area, the dynamic water outside the diversion dike causes the movement of the still water within the dike. Because of the shrinking or the spreading in water bodies, the water flow separation phenomenon appears and the friction force will be generated on the separation surface of the water flow. Under the friction force, the water body near the separation surface with the mainstream will move to the downstream. In order to fill the gap, the water body near the boundary will be replenished to form a closed backflow system. According to the calculation results of numerical simulation, the downstream backflow near the dike head in the diffusion section of the entrance area can be divided into the following three sections.

Section Ⅰ: Non-influenced section which is far away from the entrance. The water flow far away from the entrance is basically unaffected by the turbulence of the interface.

Section Ⅱ: Turbulent diffusion section. This section is the interface of water turbulence.

Section Ⅲ: Reversing flow section. The flow velocity in this section is relatively small, and flow velocity in the boundary of this section is 0 m/s. Unlike the backflow in the straight channel, the zero-value isopleth affected by the bend is not straight. However, when the entrance is located on the side of the convex bank, the zero-value isopleth is a curve and points to the convex bank.

According to the calculation results of the generalized numerical model, various factors affecting the backflow length were fitted by the curve. Considering the influence of the relative position between the dike and the bend on the backflow length, the empirical formula was obtained as follows:

$$L = (K_1 \delta^2 + K_2 \delta) b F_r \left(\frac{\delta h}{B}\right)^{1.5} + K_3 b(-1.13t + 4t) \tag{8}$$

where K_1 and K_2 are coefficients which need to be determined by experiments; b is the width of the entrance, m; Fr is the Froude number; h is the inflow depth, m; B is the total width of the river, m; δ is the channel broadening ratio; t is the coefficient of relative position. When the dike head is in the straight section, t is 0. And t is a positive value, when the diversion dike head is in the bend section. K_3 is the correction coefficient.

The comparison between the calculated results according to this formula and the numerical simulation results was shown in Fig. 7. It revealed that the calculated results fit well with the numerical simulation results, which proved that the formula could well demonstrate the calculation results of the model.

3 Navigation flow conditions in the downstream entrance area

In order to explore the practical application of the calculation results from the generalized numerical model in the entrance area of the sharp bend, a hydropower junction with the downstream entrance area in the convex bank was selected as the research subject in the present study. Moreover, the applicability and accuracy of the formula to calculate the horizontal backflow length as well as the backflow flow characteristics in the entrance area were also verified. The hydropower junction is in a wide-shallow river with a 90-degree sharp bend whose overall riverbed is flat and the channel grade is Class Ⅳ. The total width of the river channel is 344 m, the width of the diversion dike is 5 m, and the width of the downstream entrance area is 60 m. A two-dimensional numerical model is established based on the topographic data of the hydropower junction and the actual hydrological data, where the viscous dissipation in the water body is ignored.

The broadening ratio of river width in the entrance area of this hydropower junction is 1.20. In the calculation, the diversion dike lengths were set as 280 m, 330 m, 380 m and 430 m, respectively. The outflow boundary water level was 86.00 m, and the inflow boundary velocity at the flood gate was 0.88 m/s. Moreover, the inflow boundary velocity at the power station was 0.98 m/s and the simulation time was 6 hours. Fig. 8 shows the flow velocity and flow pattern in the entrance area of the 280-m long diversion dike.

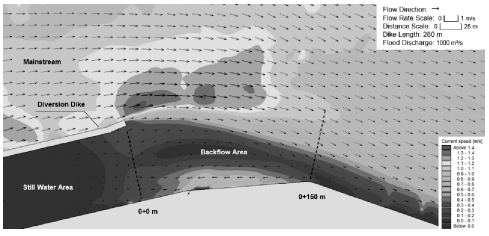

Fig. 8. Flow in entrance area (280 m).

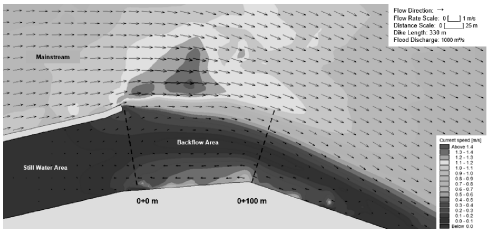

Fig. 9. Flow in entrance area (330 m).

When the diversion dike length was 280 m, the coefficient t was about 1.2. The results indicated that the backflow length was about 210 m, and the backflow length outside the entrance area was about 155 m. The maximum backflow velocity in the entrance area was 0.57 m/s. And the maximum transverse flow velocity in the entrance area was 0.57 m/s, which occurred 0+73 m away from the entrance. The high-speed flow area was about 126 m long and 80 m wide. The high-speed transverse flow area had a greater overlap with the channel layout. Class Ⅳ waterway stipulates that the maximum longitudinal flow velocity in the entrance area should not exceed 2.0 m/s, the maximum transverse flow velocity should not exceed 0.3 m/s, and the maximum backflow velocity should not exceed 0.4 m/s. Compared with the regulation, the backflow velocity and the transverse flow velocity in the entrance area both exceeded the limited value. The high-speed backflow and transverse flow near the dike head have an impact on ships entering the downstream approach channel. For example, excessive transverse flow will make it difficult for ships to enter the restricted waterway from the open water, and ships even have the risk of hitting the dike head. When the diversion dike was 330 m long, the dike head was flush with the beginning of the bend, and the angle between the dike head axis and the tangent line of the bend was smaller. Calculation results showed that the total transverse length of the backflow was about 247 m. The maximum backflow velocity in the entrance area was about 0.37 m/s. Compared with the design of the 280 m long diversion dike, the high-speed area caused by the dike head reduced obviously. In the bend, the maximum transverse flow velocity was less than 0.3 m/s and located in 0+220 m. The maximum longitudinal flow velocity was also less than 2.0 m/s. Furthermore, the flow conditions meet

the requirements for navigation. Fig. 9 demonstrates the flow velocity and flow field in the entrance area.

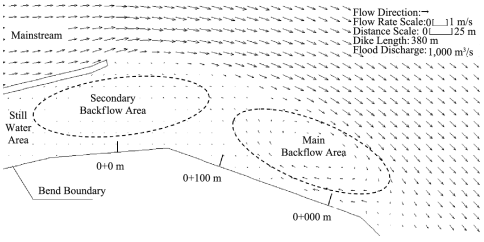

Fig. 10. Flow field in entrance area (380 m).

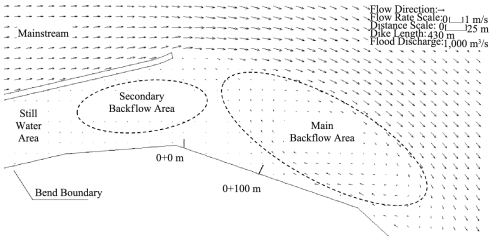

Fig. 11. Flow field in entrance area (430 m).

When the diversion dike was 380 m long, the coefficient t was about 1.2. Moreover, there were two backflow areas including the main backflow and the secondary backflow outside the entrance area. The main backflow length was about 117 m. Besides, the flow velocity in the river channel exceeded the standard, and the maximum backflow velocity reached 0.46 m/s. The secondary backflow was close to the entrance, 150 m long, whose extent was obviously weaker than the main backflow. The overhanging arrangement of the diversion dike caused a large area of high-speed flow, but that would not affect the flow conditions of the channel. When the coefficient t increased to 2.4, the main backflow was located within 0 + 81 m—0 + 270 m with a maximum backflow velocity of 0.48 m/s. The area of the main backflow was larger with the diversion dike extending farther into the bend. The area between the mainstream and the bank boundary expanded, and the backflow area also expanded. The flow conditions of the dike extending into the bend were shown in Fig. 10 and Fig. 11.

Based on the simulation results, the parameters of the formula were calculated. The formula for calculating the backflow length for this hydropower project is as follows.

$$L = 1.92(-466\delta^2 + 1231\delta)b\,F_r\left(\frac{h}{b}\right)^{1.5} - 0.58b(-1.13\,t^2 + 4t) \tag{9}$$

When the dike head was in the straight channel, the backflow length in the horizontal direction was 228 m, which was about 7.51% different from the calculated value. When the dike head extended in the bend and the coefficient t was 1.2, the backflow length in the horizontal direction calculated by the empirical formula was 125 m, and the difference was about 0.35%. When the coefficient t was 2.4, the length reached 101 m, and the difference was about 1.34%. It can be seen that the formula has good applicability. The results of backflow area division are basically consistent with the analysis results of the generalized numerical model. For this hydropower junction, the length of the downstream diversion dike should be set as 330 m.

4 Conclusions

Nowadays, more and more hydraulic junctions have been built to meet the increasing transportation capacity. The navigation flow conditions of the downstream entrance area cannot be ignored. In this paper a generalized numerical model was established based on the flow conditions of the downstream entrance area in sharp bends to analyze the sudden-expansion flow under the sharp bend. What's more, an empirical formula of the backflow length in the horizontal direction was derived, and verified by building a two-dimensional numerical model based on the actual hydraulic junction conditions.

Results showed that the broadening ratio, the flow velocity, the water depth and the relative position between the diversion dike and the bend all had influences on the backflow length. The backflow length would increase with the broadening ratio rising, while the increasing rate decreased gradually. Additionally, the backflow length was positively proportional to the flow velocity and the water depth. When the diversion dike was in the straight section, the backflow length was not affected by the location of the dike head. However, the backflow development in the horizontal direction was suppressed when the diversion dike extended inside the bend. Furthermore, the backflow of the downstream entrance area in the diffusion section was divided into three sections, including the non-influenced section, the turbulent diffusion section and the reversing flow section. The zero-value isopleth was the upper boundary of the reversing flow area, which is a curve and points to the bank. After comparison and verification, the error rate of the formula from the generalized numerical model was less than 8%, which is applicable. In addition, the flow field distribution in the generalized numerical model and the characteristics of the zero-value isopleth in the two-dimensional numerical model were both verified. Through calculation, the recommended length of the diversion dike in the downstream of this hydraulic junction was 330 m. The results above provide scientific references for future studies about the backflow characteristics of the downstream entrance area in the similar hydropower junction.

References

Cheng, T.J., Xie, B.L., 1992. Research on the backflow structure of unilateral sudden expansion and shallow water. Chinese Journal of Hydrodynamics (4):396-402.

Fu, G. Y., Ding, L. M., 1995. Experimental study on one side abruptly widening sand-laden water flow. Journal of Water Resources and Water Engineering(1):55-59.

Han, K., Yu, K. W., Zhao, J. J., et al., 2021. Experimental study on navigation flow condition and scheme optimization of Gedi junction in Changshan River. Port & Waterway Engineering (8):139-144.

Jiang, Z. W., Xu, G. X., 2020. Research on the water flow recovery distance of different discharge modes of the hub. Hydro-Science and Engineering (2):79-84.

Li, W., Zhang, B. H., 2013. Characteristics of circumfluence and improvement measures for entrance of lower approach channel. Port & Waterway Engineering (8):160-164.

Li, X. L., Chen, Y. Y., 2016. Navigable flow conditions in entrance area of lower approach channel of curved reach. Port & Waterway Engineering (2):127-130.

Zheng, Y., Wei, W. L., Liu, Y. L., 2014. Influence of spur-dike length on the recirculation scale by numerical simulation. Journal of Shenyang Agricultural University,45(2):195-199.

Zhong, L., Sun, J. Y., Liu, J. J., et al., 2017. Analysis on law of backflow around step-shaped spur dike. Hydro-Science and Engineering(5):9-17.

Research on the berthing conditions and control standards of ship locks with miter gate opening

Duoquan Li[1], Zhonghua Li[2], Jianfeng An[3], Shouyuan Zhang[4]

[1] College of Harbour Coastal and Offshore Engineering, Hohai University, Nanjing 210098, China. e-mail: tazenlee@hhu.edu.cn

[1,2,3,4] Nanjing Hydraulic Research Institute, State Key Laboratory of Hydrology-Water Resources and Hydraulic Engineering, Key Laboratory of Navigation Structure Construction Technology, Ministry of Transport, China, Nanjing 210029, China. e-mail: zhli@nhri.cn, jfan@nhri.cn, oliviatungyur@outlook.com

Abstract: The miter gates of the ship lock may be operated under the different water level between the inside and outside of the chamber under the influence of the over filling(emptying) water level fluctuation in approach channel and other potential factors. These factors will cause water surface slope in chamber when the miter gates open. The slope will increase the hawser force of the ship under the hydrodynamic pressure. In this paper, the formula between ship hawser force and water surface slope was derived. The effects of chamber water depth, water head difference value and miter gates operation schedule on water surface gradient were researched through laboratory model tests. In addition, a calculation method for the mooring force was carried out during the miter gates operation when the inside and outside water level were different. The results show that the mooring force is positively associated with the water surface gradient and the ship displacement, and the water surface gradient is the dominant factor affecting the mooring force in this case. The mooring force is a positive associated with the 1.5th power of the initial chamber water depth and the 1st power of the water head difference value. Besides, it has negative correlation with the 1st power of the miter gates opening speed and cross-sectional area of the chamber water at the midship. Based on the mooring force calculation formula, the reference value of miter gates operation schedule and the water head difference value were suggested to ensure the safety of vessels in the lock chamber.

Keywords: Lock chamber; Mooring force; Water surface gradient; Miter gates operation schedule; Water head difference value

1 Introduction

In recent years, inland water freight volume has increased significantly, and the

trend of large-scale ships passing through locks will become more obvious. With the continuous development of the trend of large-scale ships, the displacement of ships will be greatly increased. Even a small water level difference between the inside and outside of the lock might generate a huge mooring force when the miter gates are opening, which will endanger the berthing safety of ships passing through the lock. Many ship locks have had an accident in which the miter gates were opened by the reverse action of the water head, and the hawser was broken due to excessive mooring force. One of the key issues in the design and operation of the ship lock is to ensure the opening process of the miter gates of the large ship lock and the safety of the ships docked in the lock chamber.

In this paper, combined with the opening process of the miter gate of a large lock, the complex water flow and flow changes in the lock chamber and the force characteristics of the ship under the action are studied. The influence of the mooring force of the ship is established. The calculation method of the mooring force of the ship under the condition of the water level difference of the miter gate of the large ship lock is established.

2 Hydrodynamic characteristics when the miter gates open

When the miter gate is opened under the condition of water level difference inside and outside the lock chamber, the mooring force of the ship is a macroscopic reflection of the temporal and spatial variation of the water flow structure of the lock chamber. In view of the restraint of the ship by the cable, the translation and rotation of the ship in the plane direction are limited, and due to the small turning moment of the ship, the pitch and roll of the ship can be ignored. So the ship has six The DOF movement which can be simplified as a single DOF movement, that is, the lifting movement. A large number of physical tests have shown that under the condition of water level difference inside and outside the lock, the miter gate is opened by dynamic water, and the longitudinal propulsive wave is the main reason for the longitudinal mooring force, while the longitudinal mooring force is the main controlling factor that determines the starting mode of the miter gate.

2.1 Influence of flow rate change on ship mooring force

Under the condition that there is a water level difference between the inside and outside of the lock chamber, the miter gate is opened by dynamic water. It is assumed that: (1) There is only longitudinal water flow in the lock chamber, and it is considered that the longitudinal acceleration of the water flow is much greater than the ver-

tical and lateral acceleration; (2) The flow velocity distribution of the cross section in the lock chamber; (3) The pressure is distributed according to the hydrostatic pressure; (4) The ship does not move in any horizontal direction, and the effect of the dynamic water mass and damping force is ignored; (5) The vertical displacement of the ship does not affect the horizontal direction of the mooring rope. The force on the lock chamber and the motion of the ship can be expressed by the following equations: Continuity Equation:

$$\frac{\partial Q}{\partial x}+\frac{\partial}{\partial t}(A_k-A_m)=0 \tag{1}$$

Equation of motion:

$$\frac{\partial Q}{\partial t}+\frac{\partial}{\partial x}\left(\frac{Q^2}{A_k-A_m}\right)+g(A_k-A_m)\frac{\partial h}{\partial x}+g\frac{Q|Q|}{c_0^2(A_k-A_m)R}=0 \tag{2}$$

In the formula:

A_k = Bh, is the cross-sectional area of the lock chamber;

c_0 is Chezy coefficient;

R is the hydraulic radius.

The longitudinal mooring force F of the ship in the lock chamber during the opening process of the water level difference of the miter gate is the longitudinal mooring force of the ship caused by the shallow water long wave. The resistance and frictional resistance are very small and regarded as secondary factors, so there is:

$$F\approx-\frac{\partial h}{\partial x}W \tag{3}$$

In the formula:

$W=\rho\nabla$, is the displacement of the ship, and ∇ is the underwater volume of the ship in still water.

It can be obtained from Formula (3):

$$-\frac{\partial h}{\partial x}=\frac{1}{g(A_k-A_m)}\left[\frac{\partial Q}{\partial t}+\frac{\partial}{\partial x}\left(\frac{Q^2}{A_k-A_m}\right)+g\frac{Q|Q|}{c_0^2(A_k-A_m)R}\right] \tag{4}$$

For this study, the flow rate generated by the water level difference between the inside and outside of the lock chamber is small, and the rate of change of the flow rate along the longitudinal direction of the lock chamber is constant. Therefore, the second and third terms in the right side of Formula (4) are approximated as constants, and the differential form is rewritten as a differential form, considering that the length of the ship (fleet) is less than the length of the lock chamber, and it is berthed at any position in the lock chamber. The mooring force coefficient D is introduced, and combined with Formula (4), the longitudinal mooring force of the ship is ex-

pressed as:

$$F \approx \frac{DW}{(A_k - A_m)} \frac{\Delta Q}{\Delta t} + C \tag{5}$$

where $\Delta Q/\Delta t$ is the average flow rate increase in the range of the ship; D is the mooring force coefficient related to the size of the ship and the berthing position.

Therefore, the change rate of the flow rate in the lock chamber $\Delta Q/\Delta t$ during the opening process of the water level difference of the miter gates, the displacement W of the ship, the cross-sectional area of the midship A_m, and the cross-sectional area of the lock chamber A_k are the main factors that affect the berthing of ships in the lock chamber.

2.2 Influencing factors of longitudinal mooring force

When the water flows into (out of) the lock chamber through the gap of the miter gate, the water flow pattern is very complex, mainly composed of two parts which are below the water surface of the lock chamber and above the water surface of the lock chamber. Therefore, at any time t, the flow rate of the water delivery through the door gap is:

$$Q_t = Q_1 + Q_2 = \mu_d A_t \sqrt{2gH_t} + \frac{2}{3}\mu_d B_t \sqrt{2gH_t} \tag{6}$$

When the water flows into the lock chamber from the gap of the miter door:

$$\left.\begin{aligned} A_t &= B_t(H_1 - H_t) \\ Q_t &= \mu_d B_t \sqrt{2gH_t}(H_1 - \frac{1}{3}H_t) \end{aligned}\right\} \tag{7}$$

When water flows out of the lock chamber:

$$\left.\begin{aligned} A_t &= B_t h \\ Q_t &= \mu_d B_t \sqrt{2gH_t}(H_1 + \frac{2}{3}H_t) \end{aligned}\right\} \tag{8}$$

In the formula:

Q_t is the flow rate of water conveying through the door gap at time t, m^3/s;

Q_1 is the flow rate of water conveying through the door gap below the water surface of the lock chamber at time t, m^3/s;

Q_2 is the flow rate of the water conveyed by the part of the door above the water surface of the lock chamber at time t, m^3/s;

H_t is the water level difference between the upper and lower lock chambers at time t, m;

μ_d is the water flow coefficient of the miter gate seam, approximately 0.55;

B_t is the width of the gate slit at time t, m;

H_1 is upstream initial water depth, m;

h is initial water depth downstream, m.

The width of the miter gate B_t is a known function with time t as a variable, then according to the water balance equation, we can get:

$$\begin{cases} \Omega_1 dh_1 = \Omega_2 dh_2 = Q_t dt \\ dh_1 + dh_2 = -dH_t \end{cases} \tag{9}$$

For the single-stage ship lock in this test, C = Ω. Considering that the maximum water level difference in this experiment is only 0.5 m, and the leveling time is shortened after the miter gate is opened, in order to simplify the calculation, the water level difference between the inside and outside of the gate can be regarded as the first stage of segmented water delivery. Integrate Eq. (1) in Eq. (9):

$$\int_0^t Q_t dt = -\Omega \int_{h_1}^{h_2} dH_t \tag{10}$$

Based on theoretical analysis and physical experiments, the author gives the function relationship between the width B_t of the miter gate and the time t in another paper:

$$B_t \approx U\left(\frac{P_{\max}}{t_v}t\right)^2 + V\left(\frac{P_{\max}}{t_v}t\right) \tag{11}$$

In the formula:

U and V are constants;

$P_{\max}$ is the maximum stroke of the piston rods;

t_v is the speed of the miter gate opening.

Combining Formulas (7)-(11), and omitting the high-order infinitesimals, the mooring force of the ship can be obtained when the water is poured and discharged.

When the water flows into the lock chamber from the gap of the miter door:

$$F \approx \frac{DW}{(A_k - A_m)}\mu_d\left[2U\left(\frac{P_{\max}}{t_v}\right)^2 t + V\left(\frac{P_{\max}}{t_v}\right)\right]\sqrt{2g(h-h_2)}\left(\frac{1}{3}h + \frac{2}{3}h_2\right) + C \tag{12}$$

when water flows out of the lock chamber:

$$F \approx \frac{DW}{(A_k - A_m)}\mu_d\left[2U\left(\frac{P_{\max}}{t_v}\right)^2 t + V\left(\frac{P_{\max}}{t_v}\right)\right]\sqrt{2g(h_2-h)}\left(\frac{1}{3}h + \frac{2}{3}h_2\right) + C \tag{13}$$

introducing the comprehensive coefficient of mooring force, and simplifying the mooring force of ships during irrigation and drainage:

$$F \approx \frac{DWh\Delta h}{(A_k - A_m)} \frac{\sqrt{gh}}{t_v} + C \tag{14}$$

Let $k = \frac{Wh\Delta h}{(A_k - A_m)} \frac{\sqrt{gh}}{t_v}$, Fig. 1 shows the relationship between the maximum longitudinal mooring force F and k when the miter gates are operated under the condition of different displacements, different water level inside and outside the lock room, different opening time of the miter gates, and different threshold water depths.

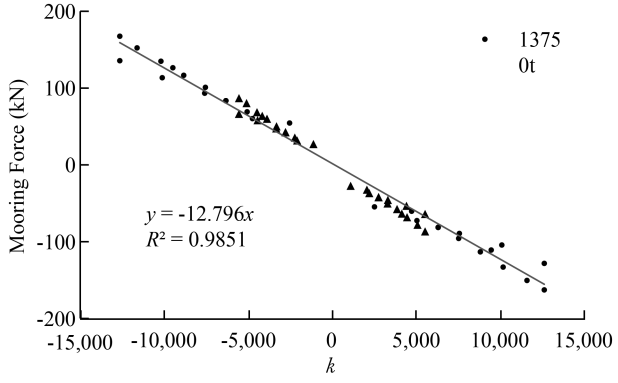

Fig. 1. Relationship between longitudinal mooring force and k.

It can be seen that when the miter gate is opened under the condition of different water level inside and outside the lock chamber, the maximum longitudinal mooring force F of the ship in the lock chamber is basically linear with $\frac{Wh\Delta h}{(A_k - A_m)} \frac{\sqrt{gh}}{t_v}$. It can be obtained that when the miter gate is opened under the condition of different water level inside and outside the lock chamber, the maximum longitudinal mooring force F of the ship has the following relationship:

$$F = -12.796 \frac{Wh\Delta h}{(A_k - A_m)} \frac{\sqrt{gh}}{t_v} \tag{15}$$

3 Standard control of miter door operation

At present, there are no clear specification requirements for the opening of the miter gate under the condition of different water level inside and outside the lock, and the berthing conditions of ships in the lock room when the miter gate opens under different water levels. Table 1 shows the mooring force values of ships with different door opening speeds and different water levels under the condition that the threshold water depth is 5 m for a 3000-ton ship calculated according to the formula in this paper.

Table 1 Longitudinal mooring force control standard of 3000-ton ship.

Hydraulic head (m)	Longitudinal mooring force (kN)								
	t_v=60	t_v=90	t_v=120	t_v=150	t_v=180	t_v=210	t_v=240	t_v=270	t_v=300
0.05	18.84	9.42	6.28	4.71	3.77	3.14	2.69	2.36	2.09
0.10	37.69	18.84	12.56	9.42	7.54	6.28	5.38	4.71	4.19
0.15	56.53	28.27	18.84	14.13	11.31	9.42	8.08	7.07	6.28
0.20	75.37	37.69	25.12	18.84	15.07	12.56	10.77	9.42	8.37
0.25	94.22	47.11	31.41	23.55	18.84	15.70	13.46	11.78	10.47
0.30	113.06	56.53	37.69	28.27	22.61	18.84	16.15	14.13	12.56
0.35	131.91	65.95	43.97	32.98	26.38	21.98	18.84	16.49	14.66
0.40	150.75	75.37	50.25	37.69	30.15	25.12	21.54	18.84	16.75
0.45	169.59	84.80	56.53	42.40	33.92	28.27	24.23	21.20	18.84
0.50	188.44	94.22	62.81	47.11	37.69	31.41	26.92	23.55	20.94

The standard for the berthing conditions of a ship depends on the ultimate tensile force that the mooring lines can withstand. Based on the current ship construction code and the actual situation in China, referring to the ship lock design code, the allowable cable tension of ships above 3,000 t is about 46 kN. It can be seen from Table 1 that for 3,000 t ships, if the opening speed of the miter door is 1 min, the different water level when opening the door must be less than 0.15 m; if the opening speed is 1.5 min, the different water level when opening the door is controlled within 0.25 m to meet the requirements of parking conditions; if the door is opened, the different water level can strictly meet the existing control standards, then from the perspective of ship berthing in the lock chamber, the opening speed should not be less than 2 min.

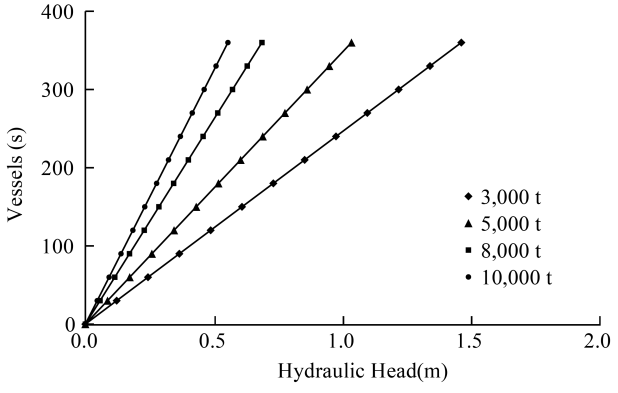

Fig. 2. Relationship between vessels and hydraulic head.

Referring to the design code of the ship lock, the allowable value of mooring force for ships of other tonnages is preliminarily proposed, and the allowable value of

the opening speed of the gate and the allowable value of the difference between the internal and external water levels are given. Fig. 2 is the critical curve of the opening rate of the miter gate and the different water level between the inside and outside of the lock, which is drawn using the corresponding longitudinal mooring force of ships of different tonnages as the control standard. The longitudinal mooring force of the ship berthing in the lock chamber during the opening of the miter gate under the condition of different water level between the inside and outside of the lock chamber for this tonnage ship is less than that allowed by the specification. It can be seen from this curve that the opening rate of the miter gate has a linear positive correlation with the different water level between the inside and outside of the lock. The increase of the different water level between the inside and outside of the gate increases the opening rate of the miter gate to ensure the safety of ships in the cabin.

The research results show that: under the condition that the threshold water depth is 7 m, the different water level between the inside and outside of the lock should not exceed ±0.2 m, while the opening speed of the miter gate should not be less than 90 s, and the opening rate of the miter gate should not be less than 120 s; for a 10,000-ton ship under the condition that the threshold water depth is 8 m, the different water level between the inside and outside of the lock should not exceed ±0.2 m, and the miter gate should open. The rate should not be less than 150 s.

4 Conclusions

In this paper, based on the test data of the ship mooring force under different opening and closing modes of the miter gate of a large ship lock, the influencing factors of the ship mooring force and the estimation of the mooring force during the opening process of the miter gate under the condition of different water level are studied. Formulas (12) and (13) are derived for calculating the mooring force of the ship in the lock chamber when the door is opened. In the design of the ship lock, the mooring force calculation formula established in this paper can be used, combined with the maximum mooring force of the ship allowed by the design, to quickly determine the reasonable opening time of the miter gate and the allowable opening different water level.

References

Wang, Z.G., 1992. Design of ship locks. Beijing: Water Conservancy and Electric Power Press.

Hu, Y.A., Li, Z.H., Lai, D.L., 2016. Influence of the opening and closing mode of the ship lift compartment lying down door on the bollard force of the ship in the compartment. Water Transport Engineering(12):148-152.

Wang, J., Yang, B., 2014. A review of the research on the bollard force of ships in lock chambers. Waterway Port, 35(5):527-531.

Zhou, H.X., Liu, Q.J., Zheng, B.Y., et al., 2006. Discussion on the application conditions of the formula for calculating the bollard force of ships in the pilotage of locks. Waterway Port(5):311-316.

Study on the influence of pier structure layout on navigation safety and scheduling efficiency in ship lock approach channel

Ning Lin[(1)], Jiahui Chen[(1)], Wenyuan Ji[(1)]

[(1)] Guangxi Xijiang Development & Investment Group Co., Ltd., Wuzhou, China. e-mail:6120506@qq.com, 395964563@qq.com, Wilson0813@sina.cn

Abstract: In the ship lock project, the layout of pier structure is an important part of ship lock design, since the number and configuration of the pier directly affect navigation safety, scheduling efficiency and through ability of lock. Taking Changzhou four-lane ship lock project as an example, this paper studies the influence law of the number and layout of pier structure in the approach channel of ship lock on navigation safety and scheduling efficiency based on operational statistics and mathematical simulations. In this paper, by comparing the effects of increasing the number of piers and the layout of single and double piers on the efficiency and through ability, a scheduling plan suitable for large multiple-lane lock group is proposed. The study shows that the layout of pier structure should be based on the navigation environment of the locks, with safety as the priority and efficiency as the consideration. A compromised scheme should be adopted for the layout of single-side and double-side piers for Changzhou four-line locks, that is, the number of right side piers should be appropriately increased, while the left side piers should be kept, so that more ships can berth on the right side temporarily. The downstream ship entering the approach channel has priority to dock at the right side pier. When the upstream ship is out of the lock, the ship on the left side piers has priority to enter the lock. At this time, the ship on the right side can be moved to the left side piers. This paper provides a reference for the layout of pier structure in the approach channel of ship lock, and also provides a strong basis for engineering design and scheduling management.

Keywords: Ship lock; Pier structure; Safety; Scheduling efficiency

1 Preface

The ship pier is an auxiliary navigation building set on both sides of the upstream and downstream approach channel of the lock, to guide ships to smoothly enter and exit the lock and dock while other ships are passing the lock. Its layout is not only

closely related to the design requirements of the level, lines, design fleet and passing capacity of the lock, but also depends on terrain, geology, current, sediment and upstream and downstream channels. Many researches, on the layout of the pier of lock approach channel, have been carried out by domestic scholars and engineers. Ji D.P. (1981) introduced the plane layout, structural type and foundation design of the upper and downstream navigation wall and adjacent piers of Gezhou Dam No.2 lock. Optimized analysis, on the layout scheme of the cascade lock of Beijing-Hangzhou Canal, has been made by Xu Y.Z. et al.(2021). Qi J.L. et al.(2019) studied the layout of the navigation facilities in the one-way mode of ship lock of the Three Gorges and Gezhou Dam ship locks for the purpose of shortening the operation time and increasing passing capacity. It follows that the layout of the ship pier is mostly studied from the design and construction of navigable buildings. The layout of the pier of lock approach channel directly affects the operation and scheduling efficiency of the lock, especially the multi-line lock group. However, few studies on this area have been reported. Changzhou four-line ship lock taken as an example, this paper analyzes quantity and arrangement of the pier and the influence of the passage capacity of the passage channel, based on the operation statistics and mathematical simulation.

2 Basic situation and operation characteristics of Changzhou Lock

2.1 Basic situation and dispatch difficulties of Changzhou Lock

The dam site of Changzhou hydro-junction lies on Xunjiang River, a branch of Xijiang River, 12 km upstream of Wuzhou City, Guangxi. Changzhou hydro-junction is the most downstream of Xijiang shipping trunk cascade reservoirs. The four-line lock is tied on the right bank, from left to right; the first-line lock is 2,000 t, the second-line lock is 1,000 t, and the third-and-forth-line lock is 3,000 t. Since 2020, the four locks have shipped more than 150 million tons for two consecutive years, making it the largest natural inland river lock group at home and abroad.

The distribution of navigable buildings of Changzhou four-line lock group is shown in Fig. 1. From the upstream anchorage to the lock, a railway bridge and a highway bridge are continuously distributed in about 4,500 m of water. The distance between the two bridges and the lock gate are about 2,400 m and 3,000 m respectively, and there are only two navigable holes. Q shows the incoming ship flow, and Q' shows the outgoing ship flow. Among them, Q_1, Q_2, Q_3 and Q_4 correspond to K_1, K_2, K_3 and K_4 respectively, that is, the corresponding first line to forth line lock. Q_{12} and Q_{34} indicate the ship flow into the first and second line gate group and the third

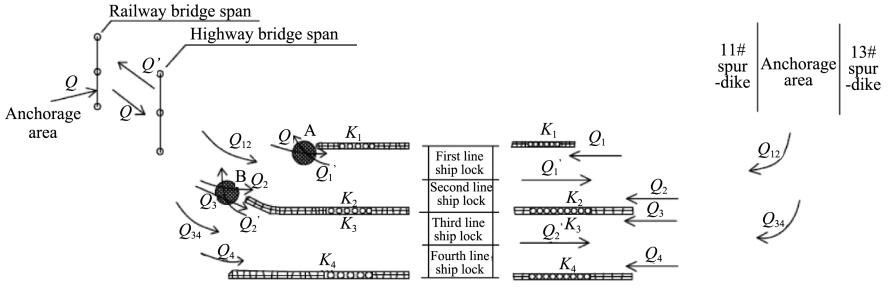

Fig. 1. Schematic diagram of ship traffic flow between upstream and downstream anchorage of Changzhou Junction.

and fourth line gate group, respectively. A and B are the areas of possible conflicts between the upper and lower vessels. The route of descending ships through this water is an arc of three points and one line. Due to the close distance of the three navigable buildings and low degree of freedom of the ships, the width of the navigable waters are significantly reduced. For the downstream of the hub, with the channel less limited, ships may only meet with a small amount in the vast waters far away from the lock, about 15 km away from the lock. The upstream ships pass through the bridge area in the form of continuous flow, and through the lock in the form of discontinuous flow, influencing and interacting with each other, which makes the navigation scheduling become a joint scheduling problem of the bridge and the lock. By formulating corresponding dispatching rules and reasonably arranging ship piers, it can effectively avoid ship crossing in possible conflict areas and ensure the safety of navigation, which will also bring different effects on the operation and scheduling efficiency of the lock.

2.2 Regulations of scheduling the general navigation

The navigation conditions of the upstream section of the hub are more complex. In order to improve the safety of ship navigation, make the ships operate properly, improve the operation and dispatching efficiency of the ship lock, and provide the possibility of joint dispatching of the bridge gate, it is necessary to conduct special control on the ships passing through this section. Bridge area control regulation: Usually, the navigable holes in the bridge area are single navigable and follow the right line rule. In special circumstances, two bridge holes can be temporarily allowed to pass upward ships or downward ships at the same time. Regulations of ship lock: The first and second line locks run in reverse, and the third and fourth line locks run in reverse. The first and second line, the third and fourth line locks operate staggerly. After the implementation of navigation control in the bridge gate waters, the ships on

the channel will form the ship alignment system of separate navigation system. That is, the upward and downward ships are required to sail in accordance with a certain route to avoid encounters. Ships traveling in the same direction will sail separately according to the ship type and driving characteristics to reduce the influence between each other. After the setting system, the number of possible conflict areas change from multiple to two, and the spatial location is determined. That is, in the upper gate area of the approach channel, the navigation route has been standardized and simplified.

3 Influence of pier structure layout on navigation safety

By analyzing the traffic flow into and from the ship lock gate, we found that two-way docking piers were set on the inside of the first, second, third and fourth line sluice channels. During the operation of the lock, two conflict zones at the gate of the approach channel would be caused by the incoming and outgoing ship. That is, the zones A and B in Fig. 1. There are three possibilities: Q_1 and $Q_{1'}$; Q_2 and $Q_{2'}$; Q_3 and $Q_{2'}$.

If the single side pier is used, that is, the first, second, third and fourth line gate groups are only set on the right side pier, only one conflict zone at the gate of the channel would be caused during the operation of the lock. That is, the area B in Fig. 1. There is only one possibility of crossover, namely, Q_2 and $Q_{2'}$. According to the analysis, the conflicts corresponding to the different landing pier setting methods are shown in Table 1. Therefore, it is safest to lay a single side pier in the first to the fourth line lock diversion channels.

Table 1 Position of pier and safety.

Layout of piers	Number of conflict zones at the gate of the channel	Number of possible crossings
1# and 2#, 3# and 4# both double sides	2	3
1# and 2#, 3# and 4# both single side	1	1
1# and 2# single side, 3# and 4# double sides	1	2
1# and 2# double sides, 3# and 4# single side	2	2

4 Influence of pier structure layout upstream on scheduling efficiency

Ship lock scheduling is always carried out around safety and efficiency. To ensure the navigation safety of multi-line lock dispatching, it is necessary to make the upstream and downstream ships not cross the possible conflict zone in the entrance area

of approach channel. Under the premise of safety, to ensure the efficiency of the ship lock operation, it is necessary to keep the ship on the pier, where ships are always waiting for the lock. The core problem of the study on the influence of pier layout on the scheduling efficiency is whether the time of evading cross-meeting ships in the conflict zone at the entrance affects the time of dispatching ships from anchorage to filling in the lock next to pier within a certain period. The following is the operation statistics of locks in recent years.

Table 2 Average operating parameters of locks from 2019 to 2021.

Number of ship lock		1#	2#	3#	4#
Running time per lock period(min)		52	46	61	61
Time of gate opening and closing(min)		4.5	4	5	5
Irrigation time(min)		10	10	12	12
Number of ships passing through lock at one time		8	5	14	14
Upstream	Time of sailing in(min)	17	15	22	22
	Time of sailing out(min)	15	13	18	18
Downstream	Time of sailing in(min)	18	15	22	22
	Time of sailing out(min)	15	13	17	17
	Time when a ship passes through the conflict zone(min)	10	7	16	16

Table 3 Time rule table of possible conflict zone for upstream ships passing through the entrance of lock on each line.

Number of ship lock	Time without upstream ships (min)	Time with upstream ships (min)	Unidirectional operation cycle (min)
1# 2#	43	9	52
3# 4#	49	12	61

4.1 Layout of double sides piers

Four lines ship lock are taken as a whole to be demonstrated. The upstream and downstream operation time are included in one operation cycle. Since the operation time of each lock is different, the longest of four lines ship lock operation time is calculated as the operation time. When $t=0$, the upstream gate of the first line lock and the third line lock have been opened, and the upstream and downstream locks of each line will have a demand to enter the lock within 122 min, that is, the number of four-lock ships should be issued from the anchorage to complement the berthing piers within 122 min. For upstream, the worst case scenario is that there is no overlap in the passage times of upbound vessels through the gate conflict zone. According to Table 3, the sum of the time for four locks of upbound ships to pass through the conflict

zone is $12\times2+9\times2=42$ min. According to Table 2, the time interval between the two ships before and after taking anchor lifting is 1 min, and it takes $1\times14\times2+1\times8\times2=44$ min to send downbound ships with four locks from the anchorage, and the cumulative time for these downbound ships to pass through the conflict zone is also 44 min. However, when $t=104$ min, one up-and-down cycle of first-line lock, the first-line and second-line lock groups start to leave the ship again. When $t=114$ min, the running time of the upper ship in the approach channel of the first and second line lock is 10 min, the leading ship begins to pass through the conflict zone, and when $t=122$ min, there are still upstream ships passing through. It can be seen that in this 122 min, the time for the unaccompanied ship to pass through the conflict zone is $114-42=72$ min$>$44 min. Therefore, the safe time is enough for the downstream ship to pass through the conflict zone and replenish the piers in time.

4.2 Layout of single side piers

In the same way, the four-line lock is demonstrated as a whole. For any 122-minute bidirectional cycle of the forth-line lock, there is a demand for the upstream and downstream of each line lock. That is, the number of four sluice boats issued from the anchorage within 122 min is required to supplement the ship pier. For upstream, according to Table 1, the sum of the time that ships pass through the gate conflict zone is $12\times2=24$ min. According to Table 2, four descending trips from the anchorage require $1\times14\times2+1\times8\times2=44$ min. The cumulative time of these ships to pass the conflict zone is also 44 min. $122-24=98$ min$>$64 min. Therefore, there is enough safe time for ships to replenish the piers.

4.3 Comparison and optimization of the scheme

By comparing the two pier layout schemes above, we can find that for double sides piers, the replenishment of ship to piers can still be performed during any bidirectional operation cycle, but the operating safety margin is relatively less. For the single side pier, the replenishment time is relatively more sufficient, and the safety and reliability are increased.

Taking safety as the priority and taking efficiency into account, the compromise scheme of the above two schemes can be considered. That is, piers on the right side should be increased appropriately while being retained on the left side, so that more ships can park on the right side, or dock temporarily. This arrangement makes it more like a single-sided scheme. At the same time, it is stipulated that the ships entering the approach channel have priority to dock on the right side of the pier. When the upper ship leaves the gate, the left ship on the ship pier can enter the gate first.

At this point, the ship on the right side can move to the left side on the pier. In this way, it can operate according to the single-side dock pier scheme. In the actual operation, in the upstream of the Changzhou lock, a row of adjacent piers are added on the right bank of the upstream approach channel as the dispatching berthing area. This is similar to compromise scheme mentioned above.

5 Conclusion

This paper analyzes the influence of the pier layout of the approach channel on the operation safety and dispatching efficiency. It provides a reference for the layout of the approach channel by the lock, and also provides a strong basis for the engineering design and dispatching operation.

References

Ji, D.P., 1981. Design of the upper and downstream navigation wall piers of Gezhou Dam No.2 lock. Yangtze River (6):18-22.

Xu, Y., Zhou, T.T., 2021. Optimization analysis of the layout scheme of the approach channel of the step lock of Beijing-Hangzhou Canal. Water Transportation of Pearl River (3):95-96.

Qi, J.L., Zhou, T.T., Ran, X.J., et al., 2019. Layout of the navigation facilities in the one-way mode of the Three Gorges and Gezhou Dam ship locks. China Water Transport (8):16-19.

Topic 3
Smart Shipping

Application of BIM+GIS+oblique photography in Shuangqiao navigation junction project

Liyuan Zhang[1], Rongqing Jiang[2], Shuai Wang[3]

[1,3] Plan and Design Institution of Waterway Transportation, Beijing 100007, China. e-mail: zhangliyuan@pdiwt.com.cn

[2] State Power Investment Corporation, Beijing 277800, China. e-mail: jiangrongqing@spic.com.cn

Abstract: BIM, GIS and tilt photography contribute independently in engineering field. Practice of technical integration is not enough. BIM technology focuses on building information on engineering scale, GIS technology focuses on resource information on urban and watershed scale, and tilt photography aims to reflect the real scene of a specific area with high precision. Technical integration will effectively expand the radiation range of engineering construction information, effectively assist engineering decision-making, help optimize the construction plan and improve the quality of engineering construction.

The author carries out a research on the integration of BIM technology, GIS technology and tilt photography, analyses their application status, technical characteristics and application fields, and describes hardware and software platform needed, key technology calculation method during integration. Finally, five conclusions are drawn:

1. The integration of BIM, GIS and tilt photography can be divided into four steps: BIM model creation, 3D real scene model creation, data fusion and achievement application.

2. The creation of BIM model usually needs to be completed by professional software. The 3D real scene model needs high-definition image data obtained by tilt photography to be formed through a series of operation processing, such as control measurement, spatial encryption, triangulation, texture mapping and so on. BIM model and 3D real scene model are used as data sources to realize the integration on GIS platform.

3. BIM model needs to be lightweight and the real scene model needs to apply three-dimensional cache technology and generate corresponding configuration files before integrated on GIS platform.

4. The integration of BIM, GIS and tilt photography technology can effectively combine macro scene and micro engineering, show the construction effect of the project, and significantly improve the visualization of the scheme. At the same time, linking construction information with the model enhances the intensity of information management and is conducive to the decision-making and implementation of the project.

5. In the application of layers and maps it should be used reasonably, and appropriate mosaic methods should be selected to improve the quality of final results.

Based on the key water junction project of Shuangqiao, the match of BIM model, diorama and spatial data, model data visualization display and interaction, engineering roaming are realized with the GIS platform. This will provide a demonstration experience for the application of BIM, GIS and tilt photography in waterway engineering and give support for the realization of urban and watershed level digital project management.

Keywords: BIM; GIS; Tilt photography; Navigation junction

1 Overview

With the rapid development of China's economy, the trend of large-scale and complex engineering construction is obvious, and the difficulty of design, construction and management is increasing. The use of information technology to integrate data throughout the life cycle of a project can significantly improve the efficiency and value of the project.

BIM technology (Building Information Modelling), first introduced into the engineering and construction industry in 2002, is now widely recognised around the world. A relatively complete definition of BIM comes from the US National BIM Standard, which states that BIM is a digital representation of the physical and functional characteristics of a facility, a shared knowledge resource, and a process for sharing information about the facility to provide a reliable basis for all decisions made throughout the facility's life cycle, from concept to demolition. At this stage, BIM technology has been widely used in the engineering design to construction process, and the vast amount of construction information integrated in BIM models has been deeply applied to project management.

GIS (Geographic Information System) is a technical system for collecting, storing, managing, computing, analysing, displaying and describing data about geographical distribution in the space of the whole or part of the earth's surface (including the atmosphere) with the support of computer hardware and software. GIS technology is able to store topographical features, land use and other macro-spatial environmental features at the urban scale, and can integrate map visualization and analysis of geographic information, and digital processing and statistical management of geographic distribution data. At present, the application areas of GIS mainly include resource management and resource allocation, urban planning and management, land information system and cadastral management, ecological and environmental management, and emergency response.

As BIM technology is mostly used to serve individual projects, it is difficult to reflect the spatial and temporal span of engineering projects and complex surrounding

scenes due to the limitation of model volume. GIS technology can precisely assist BIM models to build large scenes of surrounding geographical environment and improve the integrity of building information of BIM models. The integration of BIM and GIS is conducive to information integration and supervision of engineering construction, and is an important development direction of informationization in the field of engineering construction. After years of practice, BIM + GIS has accumulated a lot of experience in the construction fields of highways, railways, bridges and water conservancy, etc. The main application directions include route selection at the planning stage, scheme review and optimization at the design stage, construction simulation at the construction stage, and earthquake mitigation at the operation and maintenance stage.

As a new technology, tilt photogrammetry has the characteristics of portability, ease of use, labor saving and high model accuracy. The principle of this technology is to use UAVs with multi-lens tilt photographic image sensors for terrain mapping, together with automated modelling systems, thus effectively increasing the efficiency of model production. Especially in the creation of city-level models, economic and time costs can be significantly reduced. The combination of tilt photography technology and BIM + GIS can provide highly accurate current topographic data in the periphery of engineering construction, assist in analysing the impact of engineering construction on the periphery, and evaluate the technical and economic rationality of construction solutions.

The purpose of this paper is to study the technical route of combining BIM + GIS technology with tilt photography, and to test the effect by combining typical cases of waterway improvement projects, so as to lay the foundation for the construction of larger scenarios such as BIM + GIS + VR and BIM + GIS + Internet of Things, and to provide support for the realisation of digital project management at city level and watershed level. In this paper, we choose to use Bentley platform as the BIM model creation platform, DaJiang Jingwei M300 RTK + DG3PSDK UAV to obtain tilt photography data, WIT3D to create 3D realistic models, and Supermap platform for data fusion.

2 BIM + GIS data fusion methods and technologies

BIM + GIS technology fusion application is divided into four steps: BIM model preparation, 3D realistic model preparation, data fusion, results application and output.

2.1 BIM model preparation

At present, BIM model creation has been technically mature when specialist software is used for specialist area. Taking the Bentley platform as an example, the specialist modelling software is shown in Table 1.

Table 1 Professional software used in BIM modelling (Bentley platform).

Serial No.	Software	Applied specialties
1	MicroStation V8i / Connect	(Public)
2	MR-Geo	Geology
3	ShipLock Designer	Hydrolic Structure
4	OpenPlant Modeler Connect	Process Pipeline
5	BRCM	Electricity
6	OpenBuildings Designer	Architecture
7	OpenRoads Designer	Road
8	Project Wise	(Collaboration)

It should be noted that according to the standard specification, the BIM models created by each profession need to be assembled in the order of "model file—structural assembly—professional assembly—individual sub—assembly—project assembly" in a reference manner step by step and finally form the general assembly file.

2.2 3D realistic model preparation

The preparation of the 3D realistic model is divided into 8 steps, as shown in Fig. 1.

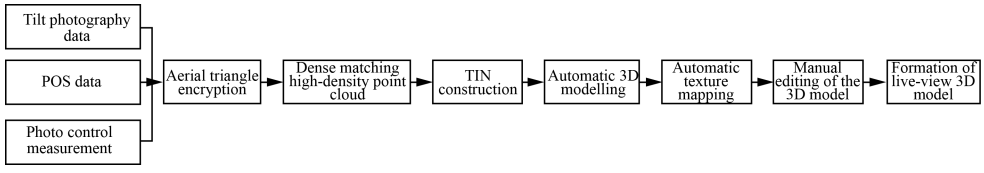

Fig. 1. 3D realistic model preparation process.

(1) Tilt photography measurement, POS data acquisition, ground photo control data

Tilt photography uses UAV low-altitude photogrammetry to achieve centimetre-level navigation and positioning and high-definition images, and the current image resolution is up to 1.5 cm.

POS is a positioning system, and the UAV images acquired during flight operations usually carry POS data.

The purpose of the photo control survey is to provide geodetic coordinates of the

image control points and the position of the stabbing points for the resolution of the aerial triangulation, linking the aerial photography data with the geodetic results, and the image measurement has the same mathematical relationship as the ground measurement. The accuracy of the image control point measurement directly affects the accuracy of the digital product. Therefore, it is necessary to make detailed provisions for the laying and measurement of photo control points according to the requirements of the specification.

(2) Aerial triangle encryption

Encrypt the control points through indoor operations to obtain the elevation and plane position of the encrypted points in order to further improve the accuracy of the terrain.

(3) Dense matching high-density point cloud

Form point clouds of the same name with spatially accurate positions based on the spatial relative relationship of images to form DSM (Digital Surface Model), DEM (Digital Elevation Model) and DOM (Digital Orthophoto Model).

(4) TIN construction based on point clouds

Form terrain triangulation networks based on point clouds.

(5) Automatic 3D modelling

Formation of terrain model based on triangulation network.

(6) Automatic texture mapping

Based on the spatial position of each triangle in the triangle network, the image with the best viewpoint is automatically mapped as the model texture.

(7) Manual editing of the 3D model

Fix problems such as gaps caused by blind spots in the filming viewpoint, or matching errors caused by image quality issues.

(8) Formation of live-view 3D model

The final results of the 3D live-view model are in OSGB data format, and a 12-layer Layered Display technology is used to ensure that feature models and building detail features are clearly displayed.

2.3 GIS platform data fusion

Data fusion in the GIS platform refers to the fusion of multi-dimensional data in the GIS platform, and this paper only discusses the fusion of BIM data and tilt photography data.

(1) BIM model data fusion

BIM model data fusion is to load BIM model files in GIS platform. At present, the data format and software interface of the BIM software platform represented by

Bentley are relatively close, and the geometric objects and their spatial relationships, attributes and materials are easily lost when data is interfaced through the intermediate format. This is why lightweighting tools are needed for this purpose. The role of lightweighting tools is to carry out BIM model analysis, model lightweighting, GIS data model reconstruction and unattended automatic export.

• BIM model analysis: Using shell extraction technology, the geometric model is extracted accurately and the .dgn file is deeply traversed to export the model's attributes and materials completely so that the model can be used for geometric operations and analysis on the GIS platform.

• Lightweighting of models: Use Level of Details (LOD) technology to resolve geometric models to different display accuracy and display details, significantly reducing the number of triangular slices and discarding non-essential information such as hidden features and constraint information of models, accelerating the speed of system graphics processing and rendering, and improving the browsing experience of models in GIS.

• GIS data model reconstruction: Reconstruct the data resolved from the design model in the GIS platform, restore the BIM model without loss and integrate the attribute information.

• Unattended automatic export: Without starting the relevant software of Bentley platform, as long as the reconstructed model is exported to the specified directory, the tool can monitor in real time and form 3D GIS files according to the user's setting parameters.

(2) Tilt photography data fusion

Tilt photography data fusion is to load the .osgb three-dimensional real-world model file in GIS platform. The volume of data files generated by tilt photography is large, often reaching tens or even hundreds of gigabytes. To display and process these graphic data on the GIS platform, 3D caching technology must be applied to load the graphic data smoothly and shorten the waiting time of users. Taking Supermap platform as an example, generating a 3D cache means splitting tilt photography data into different image collections according to different resolutions or scales and saving them under the corresponding folders, then establishing a spatial index file. The specific implementation process is shown in Fig. 2.

In the figure, the .osgb file is the tilt photography 3D data file, and the .xml file records the coordinate system and coordinate values of the tilt photography 3D data.

2.4 Application and output of results

The application of BIM + GIS can be applied throughout the whole life cycle of

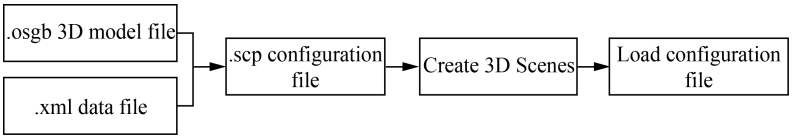

Fig. 2. The tilt photography data fusion process.

the project: In the planning stage, through the results of geospatial analysis, the amount of excavation works, the area of land acquisition and demolition, and the impact on existing buildings of different schemes can be compared. In the design stage, the smoothness of the connection between the dredged channel and the original river channel and the rationality of the structural scheme can be reviewed and the design scheme can be continuously optimised through visual presentation of the engineering scheme. In the construction stage, the construction process can be dynamically displayed based on the "progress BIM model" and "cost BIM model". In the operation and maintenance stage, the model is used to predict floods in combination with the topography and terrain, or further combined with monitoring data to monitor the water depth of the channel and the health status of the structures.

The results of the application of BIM + GIS technology in each stage can be displayed and output in different forms in multiple terminals, such as 3D virtual roaming videos, interactive models on the client side, interactive models on the web based on WebGL technology, etc.

3 Application examples

3.1 Project overview

The Tonghai Harbour Area-Tongzhou Bay Port Dredging Channel is a waterway formed by the New Jianghai River, the Dongzao New River and the Tonglyu Canal, which together form a waterway through the river to the sea. It is an important part of the "two vertical and five horizontal" Tongyang line in the main channel network planning of Jiangsu Province. Its geographical location is shown in Fig. 3.

In this paper, we take the Shuangqiao hub project located in the New Jianghai River, the Dongzao New River as an example to illustrate the effect of BIM + GIS application in the waterway improvement project.

The Shuangqiao hub is composed of a ship lock and a restraint lock, while the construction scale of the ship lock is 200 m × 23 m × 4.5 m, the middle hole of the restraint lock is 6 m wide, the side hole is 5 m wide, and the total net width is 16 m

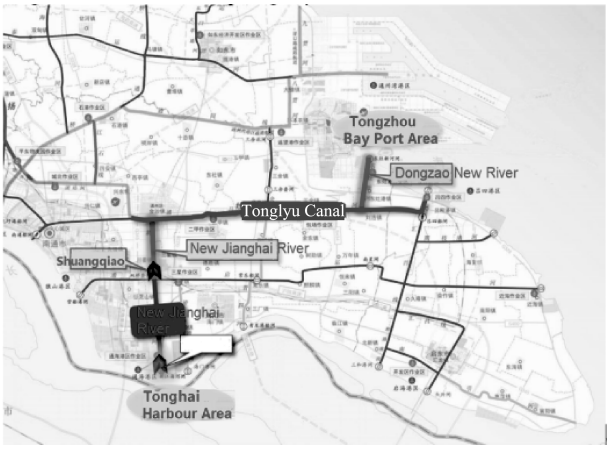

Fig. 3. Geographical location of the Tonghai Harbour Area-Tongzhou Bay Port Dredging Channel improvement project.

wide.

3.2 BIM+GIS integration results

3.2.1 BIM model results

The effect of BIM model creation is shown in Fig. 4-6. The modelling accuracy of the model is LOD200, and the applied software includes MicroStation, ShipLock Designer, ProjectWise and OpenBuildings Designer. See Table 1 in this paper for the description of each software.

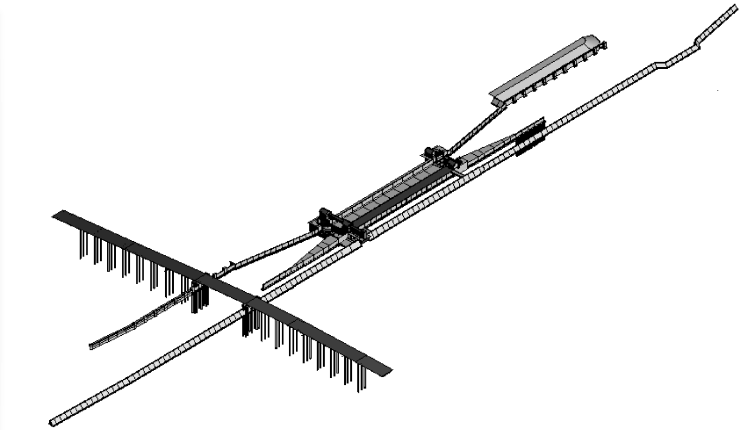

Fig. 4. Overall effect of the BIM model of the Shuangqiao hub.

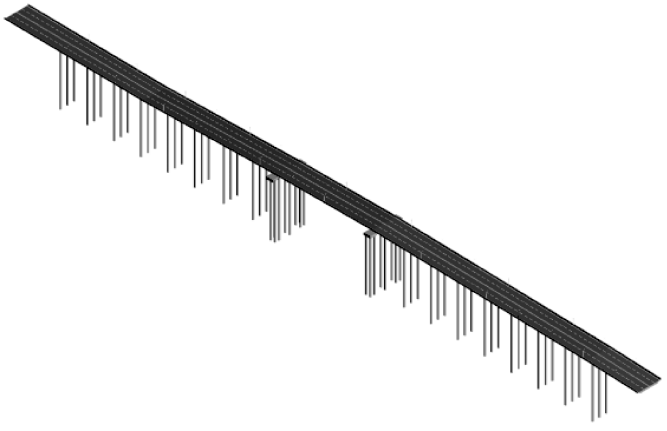

Fig. 5. BIM model of the bridge over the Shuangqiao hub.

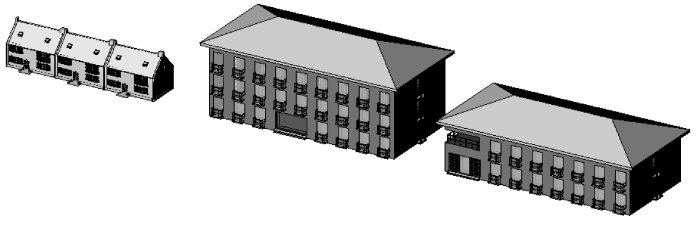

Fig. 6. BIM model effect of management area building of Shuangqiao hub.

3.2.2 3D realistic model

The 3D realistic model is constructed according to the following steps: based on the five-lens tilt aerial photography data, use the photo control measurement results for aerial triangulation, and secondary level aerial triangle encryption results according to the image control points; in order to ensure the absolute accuracy of the data results, finally use WIT3D tilt modelling software for realistic 3D model data production. Technical requirements are shown in Table 2, and the 3D realistic model generation effect is shown in Fig. 7.

Table 2 Technical requirements for the creation of the live-view model.

Work description	Requirement	Platform and software
Tilt photography measurement	Area of 5.4 square kilometers, resolution higher than 3cm	Airplane: Jingwei M300 RTK Camera: DG3PSDK
Photo control measurement	15,000 - 25,000 pixel intervals on the ground of the survey area	
3D realistic model creation	Plane error $<$0.4m; elevation error $<$0.3m	WIT3D, 3Dmax, Photoshop

Fig. 7. The effect of creating a 3D realistic model.

3.2.3 GIS platform integration application results

The fusion application results of BIM model and tilt photography model in GIS platform are shown in Fig. 8, in which area A represents BIM model, area B represents 3D realistic model, and area C shows the original sky map data file of GIS platform.

Fig. 8. BIM + GIS + tilt photography model fusion effect.

Fig. 9 shows the application effect of model feature query in GIS platform, the query content includes the main scale of the lock, the area of the left bank management area, etc. Fig. 10 shows the effect of the application of attribute display in the GIS platform, where the project attributes include ship lock class, annual passing capacity, design water level, land acquisition area, etc.

3.3 Analysis and discussion

As the BIM + GIS application is complicated, to improve the quality of integration, the following technical key points should be paid more attention to.

1. When BIM models are created, layers are used to manage model materials and

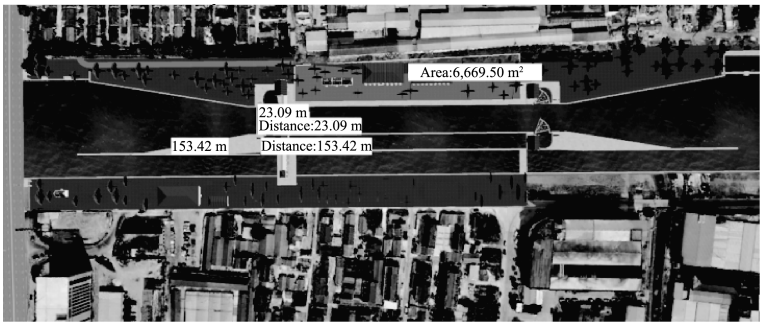

Fig. 9. GIS platform model attributes query effect.

Fig. 10. Effect of model attributes on GIS platform.

mapping is used to enhance model display effects.

BIM model creation often involves the site, structure, metal structure, electrical installation, water supply and drainage, and a variety of materials are used, such as concrete, steel, PVC plastic, etc. The same material may be classified into different specifications and grades. If layers are not properly used to classify and manage the models of different materials when modelling, it will be difficult to adjust the materials and textures of the models after the BIM models are integrated as a whole in the GIS platform later.

The use of mapping for ground traffic signs (such as signage lines, etc.) or road paving (such as playground runways, bicycle paths, etc.) can greatly increase the aesthetics of the model.

2. Reasonable choice of mosaic technology

There are three types of mosaic: ① planar overlay; ② fusion mosaic; ③ clear re-

placement. Planar overlay is to overlay the planarized data using the engineering BIM model after planarizing the features at the location of the proposed project. This method can reflect the process of demolition, site levelling, etc. Fusion mosaic is a method to retain a group of data sets while removing other groups of data sets when there are multiple sets of data sets in the same area. This method is often used to replace the current model with a proposed engineering model, replace low precision data with high precision data, or replace the current 3D terrain data with a user-created terrain model (often a TIN triangulation network). This method takes a long time and requires a high level of accuracy in the user-created triangulation network when fusing terrain, i.e., it must be complete and continuous. When there are holes in the middle of the triangulation, this creates a confusing interlacing of the terrain, as shown in Fig. 11.

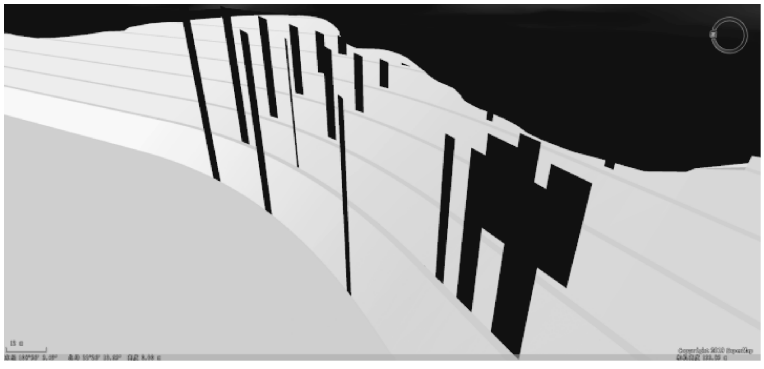

Fig. 11. Effect of fusion mosaic when triangulation is not continuous.

Clear replacement is used to determine the boundary of the proposed project and extract its boundary line. The original terrain data inside the boundary line will be cleared and replaced with the user-created model data, and the application scenario of this method is the same as the fusion mosaic. Due to its simple logic, eliminating the fusion operation in the boundary area, this method not only greatly reduces the amount of calculation, improves the calculation rate, but also significantly reduces the accuracy requirements of the triangle network terrain. The display effect is also significantly better than that of the fusion mosaic method.

4 Conclusions

The integration of BIM and GIS enables the exchange and interoperability of BIM information in the micro domain and GIS information in the macro domain, which enhances the depth of BIM application and expands the breadth of BIM appli-

cation.

This paper analyzes in detail the development and application status of BIM + GIS technology, describes the implementation process and key technologies for the creation of BIM model, tilt-photographic realistic model, and data fusion in GIS platform, and finally carries out engineering practice of Tonghai Harbour Area - Tongzhou Bay Port Dredging Channel Improvement Project. The application effects of BIM model creation, tilt photography realistic model, GIS platform-based scene roaming, engineering analysis, attribute query, etc. are demonstrated, which verify the feasibility and technical advantages of the whole set of technical processes. The research results of this paper provide a demonstration experience for the application of BIM + GIS in water transport projects, lay the foundation for the construction of larger scenarios such as BIM + GIS + VR and BIM + GIS + Internet of Things, and provide support for the realization of digital project management at city level and watershed level.

References

Shao, G.H. Research on the application of BIM technology in architectural design. Qingdao University of Technology,2014.

Li, Y. Research on BIM prediction method for construction schedule of construction projects. Wuhan University of Technology,2014.

Gan, L. Study on the application of BIM technology in construction project schedule management. Dalian University of Technology,2014.

Hu, Y. Geographic Information System (GIS) development history and prospect. China University of Geosciences (Beijing),2011.

Liu, X.Y., Zhong, P.F. A study on the evolution of land use and landscape pattern in Northwest China based on GIS analysis—Lanzhou City, Gansu Province as an example. Garden,2021,38(4): 89-97.

Ge, Z.G. GIS-based design of optimal spatial layout system for habitat ecosystem. Modern Electronics, 2021,44(8):128-132.

Hou, P.Z. Research on the application of GIS technology in the field of hydrogeology. Technology Wind,2021(11):129-130.

Liu, Y.H. Research on the application of railroad bridge project management based on BIM + GIS technology. Traffic World (Transportation. Vehicles), 2015(9): 30-33.

Xiong, X., Yang, K.H., Zhao, X.F., et al. Key technologies of BIM + GIS in the smart construction of highways. China Highway,2020(10):112-113.

Su, B.Q., Yu, D.H., Sun, B.D., et al. Research progress of water conservancy project informationization and BIM + GIS integration application. Journal of Qingdao University of Technology,2020,41(5):126-132.

Zhou, J. Key technology research of tilt photogrammetry in real-world 3D modelling. Kunming University of Technology,2017.

Guo, Z.L. Application of tilt photogrammetry technology in urban 1:500 topographic map measurement. Modern Mapping,2019,42(5): 58-60.

ArcMap-based visual analysis of erosion and deposition

Dongliang Lai[1], Hongwei Zhang[2]

[1,2] Zhejiang Design Institute of Water Conservancy and Hydroelectric Power Co., Ltd., Hangzhou, China. e-mail: laidl1992@163.com

Abstract: In order to realize the visualization analysis of the erosion and deposition changes, the basic process of establishing digital elevation model (DEM), calculating the erosion and deposition volume and visualizing the calculation results by using the conventional functions such as terrain grid generation and surface volume calculation in ArcMap is introduced with the actual topographic data of Qingshan Reservoir and the results of MIKE 21 erosion and deposition calculation. The analysis of Qingshan Reservoir erosion and deposition calculation shows that the siltation volume in Qingshan Reservoir from 2015 to 2018 is 1.91 million m^3, and the reservoir capacity is reduced by the corresponding volume. This method is simple and convenient, and the erosion and deposition results are visualized, which can be effectively applied to flushing and siltation analysis.

Keywords: GIS; Erosion and deposition; Visualization analysis; Reservoir capacity

1 Introduction

River channel flushing variation is a key issue to be analyzed in many major scientific researches and hydraulic projects, and how to visualize the flushing variation results is also a focus of researchers' attention. Hu Zhaoyang et al. (2015) applied the MIKE 21 pre- and post-processing module to visualize the riverbed siltation analysis. Wang Wei et al. (2014) combined DEM and CAD references to visualize the riverbed siltation changes in CAD. Zhang Ling et al. (2014) studied the visualization effect of riverbed siltation analysis from five aspects: data modelling processing, spatial resolution setting, graphic synthesis processing, display resampling setting, and graded color processing. Although good results have been achieved by using CAD and MIKE 21, the operation is complicated and not easy to promote.

In order to simplify the erosion and deposition analysis method, this paper uses the conventional functions of ArcMap such as terrain grid generation and surface volume calculation to establish digital elevation model (DEM), calculate erosion and deposition volume and visualize the calculation results. Taking Hangzhou Qingshan

Reservoir as an example and combining the results of MIKE 21 erosion and deposition calculation, a basic process of using ArcMap for siltation analysis is introduced to enrich the existing research tools.

2 Overview of Qingshan Reservoir

Qingshan Reservoir is located in Lin'an District, on the South Tiaoxi River which is the main stream of the East Tiaoxi River, about 40 km away from Hangzhou City. And this reservoir is a large water conservancy hub mainly for flood control, and also for irrigation and power generation. The reservoir controls a 603 km^2 basin above the dam site, accounting for 26.6% of the basin area of the East Tiaoxi River. The total reservoir capacity is 213 million m^3, which is a large reservoir. The mainstream of the river is 43.3 km long, with an average multi-year runoff of 475 million m^3 and an average multi-year flow of 15.1 m^3/s.

After the implementation of the reservoir improvement project in 2018, the responsible departments implemented immigration and resettlement, clarified the reservoir bank boundary and reservoir management authority, solved the historical problems of the Qingshan Reservoir, improved the reservoir management conditions, and effectively played the reservoir flood control function. Nowadays, due to the influence of water and sand coming from the upstream rivers such as South Tiaoxi River and Jinxi River, west of the tunnel at the end of Qingshan Reservoir, the end of the reservoir is silted up and swamped seriously, and a large amount of beach is exposed to the water surface.

The topographic data of Qingshan Reservoir are the actual measurement information of reservoir delimitation in 2015 and the numerical calculation results of Qingshan Reservoir hydro-sediment dynamics model for reservoir erosion and deposition in 3 years from 2015 to 2018.

3 Build terrain digital elevation model (DEM)

3.1 Generate terrain TIN mesh files

Extract the reservoir topographic elevation point data from the CAD topographic map. Set the elevation point file spatial coordinates in ArcCatalog to CGCS2000 3 Degree GK CM 120E, and add it to ArcMap layer. As shown in Fig. 2, use the Create TIN tool to create a TIN grid file for the reservoir topography, where the Elevation Field is selected for Height Field and Mass Points is selected for SF TYPE, and saved

to the work path. Following the method in Fig. 3 to extract the results of MIKE 21 erosion and deposition calculation, and generate the TIN grid file. The generated TIN grid files are shown in Fig. 4 and Fig. 5.

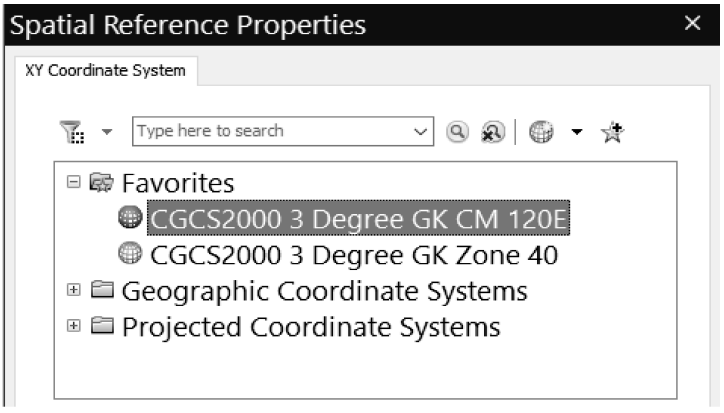

Fig. 1. Workspace projection settings interface.

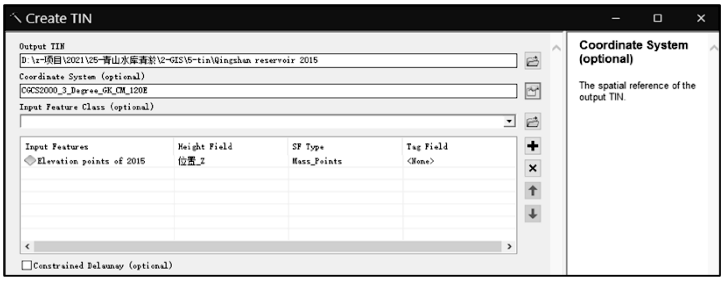

Fig. 2. Contour point to TIN grid file.

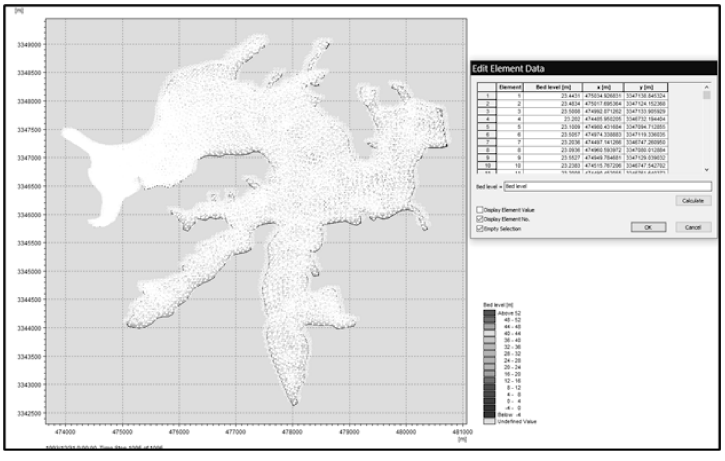

Fig. 3. Extract the results of MIKE 21 erosion and deposition calculation.

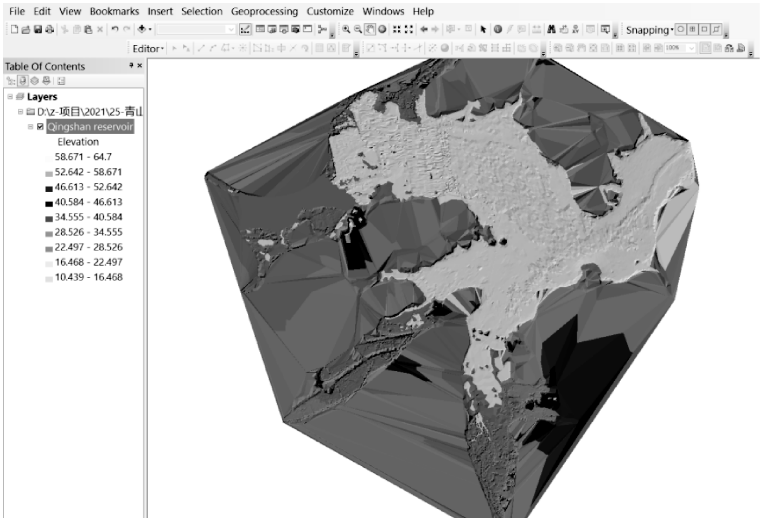

Fig. 4. Reservoir topography TIN grid file.

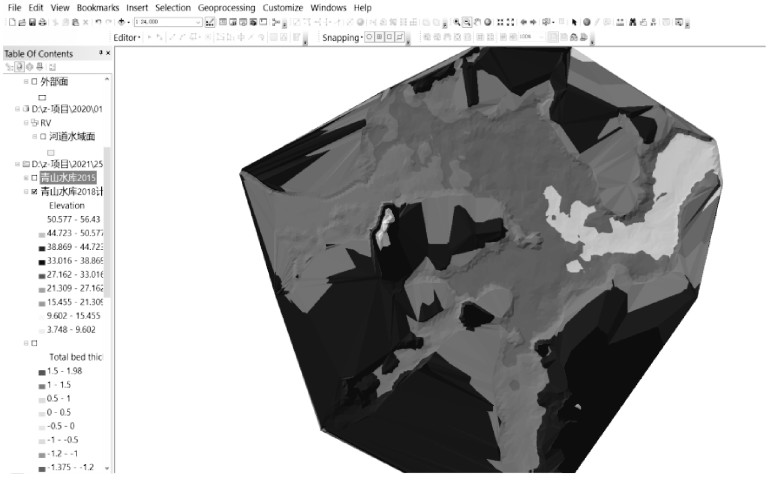

Fig. 5. TIN grid file of the results of the MIKE 21 calculation.

3.2 TIN grid file to DEM

The topographic digital elevation model (DEM) is generated from the topographic TIN grid file using the TIN to Raster tool, where the cell size is set to 10. Since the output file location is not a geographic database, the output file format needs to be set, and the file format can be bil, bip, img, etc. The output format is img here. Using the Clip tool to crop out the analysis area of the Qingshan Reservoir calculation, the results are shown in Fig. 8.

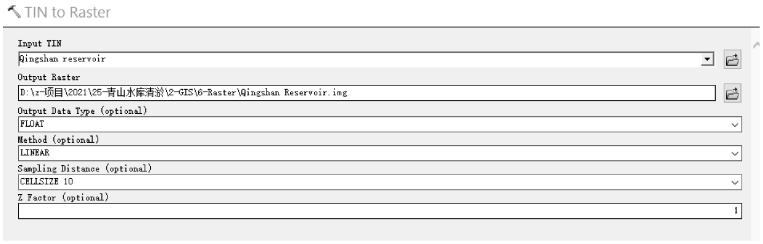

Fig. 6. TIN grid file to DEM.

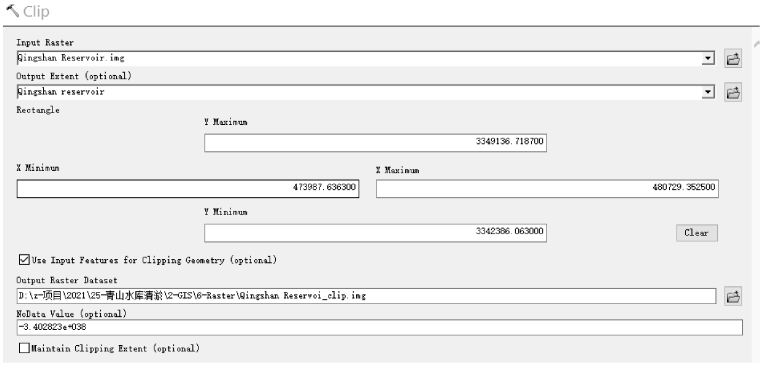

Fig. 7. Raster file Clip tool.

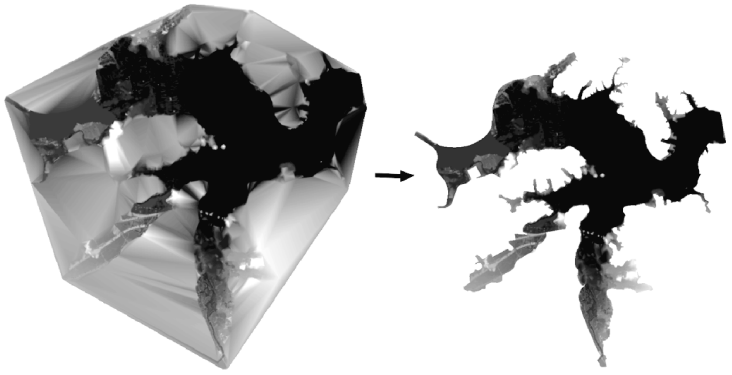

Fig. 8. Raster file Clip tool.

4 Reservoir erosion and deposition analysis

4.1 Erosion and deposition volume

Using Surface Volume tool, the volume between above 0 m elevation and reservoir

topography is calculated as shown below. The volume in 2015 is 285.57 million m^3 and the volume in 2018 is 287.48 million m^3, so the volume of siltation sediment in Qingshan Reservoir from 2015 to 2018 is 1.91 million m^3, and the corresponding reservoir capacity is reduced by 1.91 million m^3.

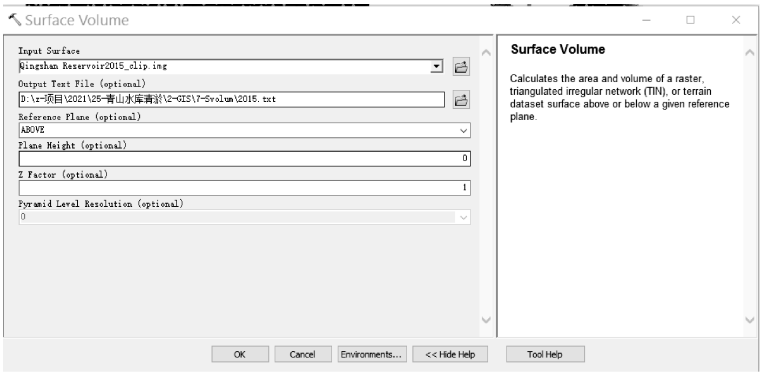

Fig. 9. Surface Volume tool.

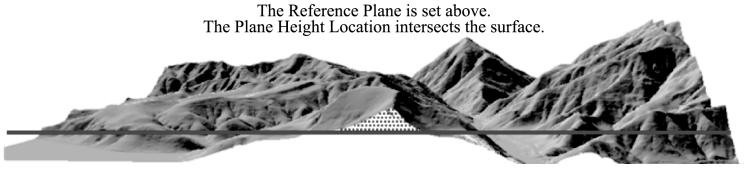

Fig. 10. Schematic diagram of reservoir capacity calculation.

4.2 Visualization of erosion and deposition changes

As can be seen from the Fig. 11, the Qingshan Reservoir is influenced by the upstream rivers, and there are more or less erosion and deposition at the end of the reservoir. The maximum erosion depth is −1.38 m in the erosion channel of the main inlet rivers, South Tiaoxi River and Jinxi River downstream for about 1.80 km. And deposition occurs on both sides of the channel with the maximum deposition height of 1.05 m. Until the middle of the reservoir, the flow velocity decreases, the sediment begins to settle, and some suspended particles continue to spread downstream.

5 Conclusion

In this paper, we combine the actual topographic data of Qingshan reservoir and the results of MIKE 21 siltation settlement to establish the digital elevation model (DEM), calculate the siltation volume and visualize the calculation results through the

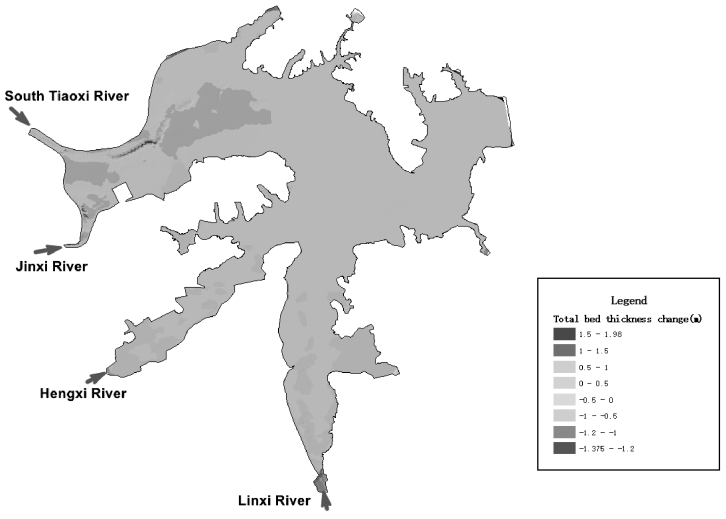

Fig. 11. Diagram of reservoir erosion and deposition.

conventional functions of ArcMap such as terrain grid generation and surface volume calculation. The analysis shows that the deposition volume in Qingshan Reservoir from 2015 to 2018 is 1.91 million m^3, and the corresponding reservoir capacity is reduced by 1.91 million m^3. The maximum erosion depth at the end of the reservoir is −1.38 m, which is located at about 1.80 km downstream of South Tiaoxi River. The maximum deposition height is 1.05 m at the end of the reservoir.

This method is simple and convenient to calculate the erosion and deposition volume, and the analysis of calculation results is intuitive, which can clearly show the distribution of reservoir erosion and deposition.

References

Hu, Z.Y., Wang, X.Q., Ye, L.Q., et al., 2015. Visualization analysis of riverbed erosion and deposition using MIKE 21 preprocessing and postprocessing modules. Water Resources and Power, 33(11), 143-146.

Wang, W., Chen, Z.F., Yuan, S., 2014. CAD visual analytics and its application in channel erosion and siltation. Yangtze River, 45(4), 99-101. https://doi.org/10.16232/j.cnki.1001-4179.2014.04.008.

Zhang, L., Cai, Z.L., Yin, H., et al., 2014. Visualization enhancement for erosion-deposition analysis in waterway. Bulletin of Surveying and Mapping, 11, 68-72. https://doi.org/10.13474/j.cnki.11-2246.2014.0366.

High-resolution simulation of hydraulic structures in a Typhoon Lekima induced coastal flood event

Yunsong Cui[1], Qiuhua Liang[1,2], Gang Wang[1], Xiong Yan[1], Jingchun Hu[3]

[1] Hohai University, Nanjing, China. e-mail: yunsong_cui@hhu.edu.cn; gangwang@hhu.edu.cn; xiongyan@hhu.edu.cn

[1,2] Loughborough University, Loughborough, England. e-mail: Q.Liang@lboro.ac.uk

[3] Zhejiang Institute of Hydraulics and Estuary, Zhejiang, China. e-mail: 13588843718@163.com

Abstract: Due to climate change and rapid urbanisation, urban flooding has become one of the most widespread natural hazards threatening people's lives and assets globally. Flood modelling now provides an indispensable tool to support flood risk assessment and management and to inform the planning of cities and the design of flood-resilient cities. Hydraulic structures such as sluice gates play an important role in urban flood risk management. However, direct simulation of hydraulic structures is not a current practice in high-resolution urban flood modelling. In this work, robust computational methods are developed to evaluate the effect of hydraulic structures in high-resolution urban flood modelling. The new model is applied to simulate and reproduce a flood event induced by Typhoon Lekima in 2019 in Yuhuan, Zhejiang Province, China. At 3 m resolution, the GPU-accelerated simulation is nearly 3.5 times faster than in real-time, demonstrating the model's efficiency and robustness. Further simulations are performed to systemically investigate the effect of pre-discharge of sluice gates on flood dynamics and associated risks, confirming the importance of directly considering hydraulic structures and their operations in urban flood modelling.

Keywords: Urban flood modelling; Sluice gates; Shock-capturing scheme; High-resolution; GPU

1 Introduction

The risk of flooding caused by extreme weather is expected to increase due to climate change and rapid urbanisation (IPCC, 2022). Urban flooding may lead to devastating consequences and affect sustainable development, especially in the highly urbanised areas. It is therefore vitally important to develop effective strategies to manage flooding risk and improve resilience.

Numerical modelling has become an indispensable tool for urban flood risk man-

agement and forecasting (Liang et al., 2015; Ming et al., 2020; Sanders, 2017). Significant efforts have been made during the last few decades to improve the accuracy and efficiency of urban flood models through advancing numerical methods to take advantage of high-performance parallel computing technologies (Liang et al., 2016; Wang et al., 2018; Xia et al., 2019; Xing et al., 2018). However, reliable prediction and forecasting of urban flooding remain to be a great technical challenge due to the complex urban structures and features that can predominate the flooding process but are difficult to be represented in the flood models. For example, hydraulic structures such as sluice gates may play an important role in urban flooding risk management (Cozzolino et al., 2015; Hailemariam et al., 2014). Despite of their importance, direct simulation of hydraulic structures has not yet become a common practice in 2D urban flood modelling. In recent years, some attempts have been made to consider hydraulic structures such as sluice gates in 2D urban flood modelling (Angeloulis et al., 2016; Dazzi et al., 2020; Morales-Hernández et al., 2013). Flux term and source term coupling approaches have been proposed and applied to benchmark tests or practical simulations. Cui et al. (2019) reported coupling strategies to use both of these approaches in a 2D shock-capturing shallow water equation model to investigate the effects of sluice gates in urban flooding. They demonstrated that sluice gates could be accurately simulated by integrating them into flux calculation.

In this paper, the flux coupling approach is further applied and tested for simulating hydraulic structures such as sluice gates in 2D high-resolution urban flood modelling. The improved flood model is implemented on GPUs to achieve high-performance computing to significantly improve computational efficiency. The model is tested by reproducing a multi-source flood event induced by Typhoon Lekima in Yuhuan city, China. It is then further used to systematically investigate and analyse the effects of pre-discharge of sluice gates on flooding process. The rest of the paper is organised as follows: Section 2 provides a brief introduction of the model and relevant components; Section 3 presents and discusses simulation results; and finally, brief conclusions are drawn in Section 4.

2 Model description

2.1 SWEs model

The fully two-dimension (2D) shallow water equations (SWEs) are derived by integrating, the 3D Reynolds-averaged Navier-Stokes equations based on the hydrostatic assumption, which can be written in a matrix form as:

$$\frac{\partial \mathbf{q}}{\partial t}+\frac{\partial \mathbf{f}}{\partial x}+\frac{\partial \mathbf{g}}{\partial y}=\mathbf{R}+\mathbf{S} \tag{1}$$

where t represents time; x and y are the Cartesian coordinates; $\mathbf{q}$ is the vector containing the flow variables; $\mathbf{f}$ and $\mathbf{g}$ are the flux vectors in the two Cartesian directions; $\mathbf{R}$ and $\mathbf{S}$ represent the vector of source terms containing the rainfall-runoff, bed slope and friction effect. The vectors are given by (Liang and Borthwick, 2009)

$$\begin{gathered}\mathbf{q}=\begin{bmatrix}\eta\\ q_x\\ q_y\end{bmatrix},\mathbf{f}=\begin{bmatrix}q_x\\ uq_x+g(\eta^2-2\eta z_b)/2\\ uq_y\end{bmatrix},\mathbf{g}=\begin{bmatrix}q_y\\ vq_x\\ vq_y+g(\eta^2-2\eta z_b)/2\end{bmatrix}\\ \mathbf{R}=\begin{bmatrix}r-f-s\\ 0\\ 0\end{bmatrix},\mathbf{S}_b=\begin{bmatrix}0\\ -g\eta\partial z_b/\partial x-\tau_{bx}/\rho\\ -g\eta\partial z_b/\partial y-\tau_{by}/\rho\end{bmatrix}\end{gathered} \tag{2}$$

where τ_{bx} and τ_{by} are the bed friction stresses that may be calculated from

$$\tau_{bx}=\rho C_f u\sqrt{u^2+v^2},\tau_{by}=\rho C_f v\sqrt{u^2+v^2} \tag{3}$$

Herein, η and z_b are water surface level and bed elevation above the datum, respectively; q_x and q_y are unit-width discharge in the two Cartesian directions; u and v are the corresponding depth-averaged velocity components; r, f and s are the rainfall intensity, infiltration rate and drainage loss, respectively; ρ is the water density; and $C_f=gn^2/h^{1/3}$ is the roughness coefficient with n being the Manning coefficient.

The above SWEs are solved using a finite volume Godunov-type scheme incorporated with the Harten, Lax, and van Leer approximate Riemann solver with the Contact wave restored (HLLC) to calculate interface fluxes on uniform grids (Liang, 2010; Liang et al., 2009; Yoro, 2001). To substantially improve the model's computational efficiency for large-scale and high-resolution simulations, Graphics Processing Unit (GPU)-based parallelisation is implemented via the NVIDIA CUDA (i.e. Compute Unified Device Architecture) framework (Liang et al., 2015; Xia et al., 2019).

2.2 Gate model

The flow conditions through the sluice gates usually depend on water levels η and gate opening e, which can be categorised into free and submerged flow in general. The corresponding formulations for gate discharge in open channels are derived from an Energy-Momentum (E-M) formula, which is given by Cozzolino et al. (2015)

$$q_s=\frac{\varepsilon}{\sqrt{1+\dfrac{\varepsilon e}{h_u}}}e\sqrt{2gh_u} \tag{4}$$

$$q_s = \sqrt{\frac{1-\frac{H}{h_u}}{1-\frac{\varepsilon e}{h_u}}}\frac{\varepsilon}{\sqrt{1+\frac{\varepsilon e}{h_u}}} e\sqrt{2gh_u} \tag{5}$$

where the flow depth H is defined by

$$H = h_u\left[\frac{2\left(\frac{h_u}{\varepsilon e}-\frac{h_u}{h_d}\right)}{\left(\frac{h_u}{\varepsilon e}\right)^2-1}+\sqrt{\left[\frac{2\left(\frac{h_u}{\varepsilon e}-\frac{h_u}{h_d}\right)}{\left(\frac{h_u}{\varepsilon e}\right)^2-1}-1\right]^2+\left(\frac{h_u}{h_d}\right)^2-1}\right] \tag{6}$$

where ε represents the contraction coefficient; h_u and h_d are the upstream and downstream flow depth, respectively; and $h_c = \varepsilon e$ is the flow depth at the vena contraction.

The flow conditions at the vena contraction are supercritical. With reference to h_c, the subcritical flow depth $h_c^{\sharp}$ is calculated using the Belanger's Equation:

$$h_c^{\sharp} = \frac{h_c}{2}\left(-1+\sqrt{1+8\frac{q_s^2}{gh_c^3}}\right) \tag{7}$$

The free flow conditions will be established when the depth h_d is smaller than the subsequent depth $h_c^{\sharp}$. The unit-width discharge through the sluice gate can be calculated using Eq.(4). Otherwise, the flow is submerged and the discharge is dependent on the downstream depth and calculated by the Eq.(5)-(6).

2.3 Coupled model

In this work, the flux coupling method (Morales-Hernández et al., 2013) is adopted and implemented to directly simulate the effect of sluice gates in the above 2D SWE model. The flow variables are updated to a new time step using the following time-marching scheme

$$\mathbf{q}_i^{n+1} = \mathbf{q}_i^n - \frac{\Delta t}{\Omega_i}\sum_{k=1}^{N}\mathbf{F}_k(\mathbf{q}_i^n)l_k + \Delta t(\mathbf{R}_i^n + \mathbf{S}_i^n) \tag{8}$$

where the superscript n denotes the time level; subscripts i is the cell index; Ω_i is the cell area; k represents the index of the cell edges ($N=4$ for Cartesian grids); l_k is the length of cell edge k; and $\mathbf{F}_k(\mathbf{q}) = \mathbf{f}_k(\mathbf{q}).n_x + \mathbf{g}_k(\mathbf{q}).n_y$ contains the interface fluxes normal to the cell boundary with the components of (n_x, n_y) defining the normal outward direction.

The coupling method is illustrated in Fig. 1, in which the red solid line represents a sluice gate, which is approximated in a stairs-case manner as indicated by the red dotted lines. In the current finite volume Godunov-type scheme, the approximate

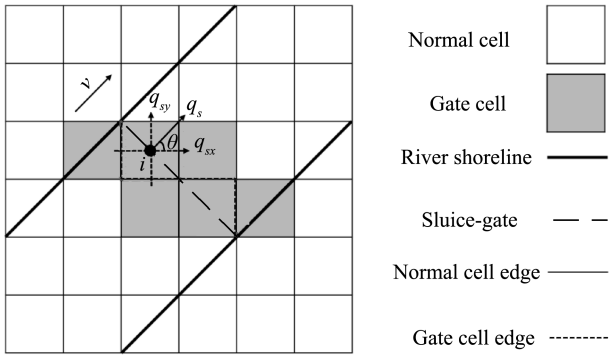

Fig. 1. Flux term coupling method for a sluice gate in the coupled model.

HLLC Riemann solver is used to calculate the interface fluxes in a "normal" cell. For the gate cells, the interface fluxes are calculated by

9. Under free flow:

$$\mathbf{F}_k(q_i)=\mathbf{F}_k(q_i)=\begin{bmatrix} q_{sx}^u-q_{sx}^d \\ u_u q_{sx}+\frac{1}{2}g(\eta_u^2-2\eta_u z_{bu})-u_c q_{sx}-\frac{1}{2}g(\eta_c^2-2\eta_c z_{bc}) \\ u_u q_{sy}-u_c q_{sy} \end{bmatrix} \tag{9}$$

10. Under submerged flow:

$$\mathbf{F}_k(q_i)=\mathbf{F}_k(q_i)=\begin{bmatrix} q_{sx}^u-q_{sx}^d \\ u_u q_{sx}+\frac{1}{2}g(\eta_u^2-2\eta_u z_{bu})-u_c q_{sx}-\frac{1}{2}g(\eta_H^2-2\eta_H z_{bH}) \\ u_u q_{sy}-u_H q_{sy} \end{bmatrix} \tag{10}$$

where the q_s is calculated using the Eq. (4)-(7) as introduced above.

It is worth mentioning that the above solution procedure is used for calculating the fluxes when the gate cell edge is aligned with the y-direction. The fluxes across an x-direction gate edge can be calculated similarly by manipulating Eq. (9)-(10). Detailed implementation of the numerical coupling method can be found in Cui et al. (2019).

3 Case study

In this work, the new coupled model is applied to reproduce a flood event induced by Typhoon Lekima in Yuhuan City, Zhejiang Province, China. Typhoon Lekima caused the death of 45 people, and economic loss of ¥45.38 billion (US $6.43 billion) in Zhejiang Province. As shown in Fig. 2, Yuhuan is a coastal city with its

western side open to the East China Sea and the other three sides surrounded by mountains.

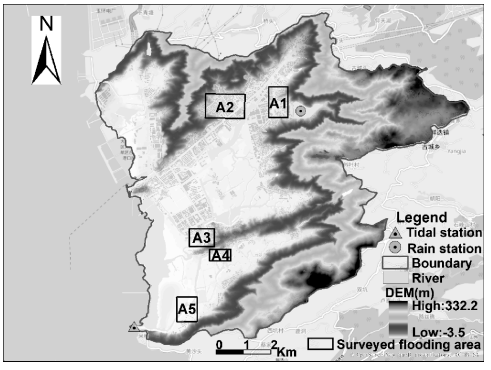

Fig. 2. Study area: DEM, gauge stations and surveyed flooding areas.

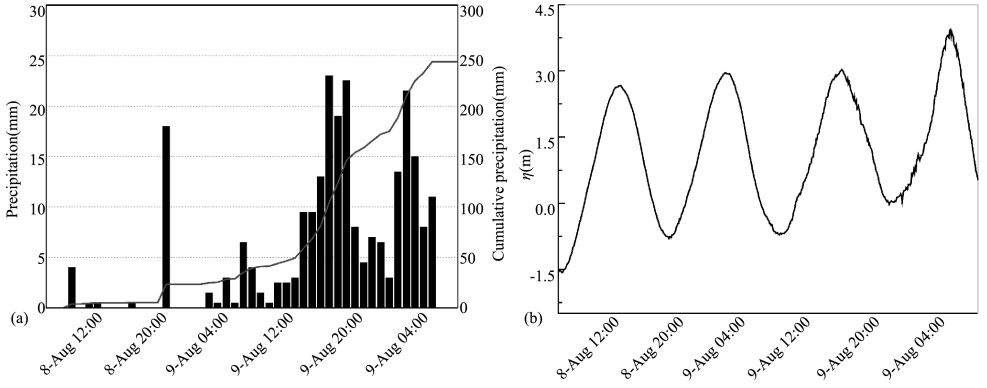

Fig. 2. flood drivers: (a) hourly and accumulated rainfall; (b) tidal level at the Qinglan Estuary.

The data available to support the simulation of the Typhoon Lekima induced urban floods include a high-resolution digital elevation model (DEM) (Fig. 2), the rainfall series and accumulated rainfall recorded in a rain station (Fig. 3(a)), the tidal level at the same time period (Fig. 3(b)) and the surveyed flooding areas as shown in Fig. 2. As shown in Fig. 4(a), the land-use type in the study domain may be divided into road, mountain, farm, river, building and other open built-up spaces. Field data including maximum inundation extent and flood depth in surveyed areas are available for validating the simulation results.

The model parameters (i.e., Manning coefficients, infiltration parameters and drainage capacity) are set according to land-use type and soil types extracted from land-use data. For the Manning coefficient, 0.02, 0.08, 0.035 and 0.05 is used respectively for roads, mountain areas, farmlands, rivers, buildings and other open built-up spaces. The infiltration parameters required by the adopted Green-Ampt

model include the hydraulic conductivity, wetting front metric potential and wetting front depth, which are set according to Rawls et al. (1983). The drainage loss is estimated according to the "Standard for Design of Outdoor Wastewater Engineering" (GB 50014—2021) adopted in Yuhuan. The location of sluice gates over the whole domain is shown in Fig. 4(a), and the details about each of the sluice gates are listed in Table 1. The total of twelve gates includes ten control gates and two tidal gates. A single-hole control gate is assumed to open as usual and the other control and tidal gates will be lifted to open if the upstream water level is higher than the downstream water level.

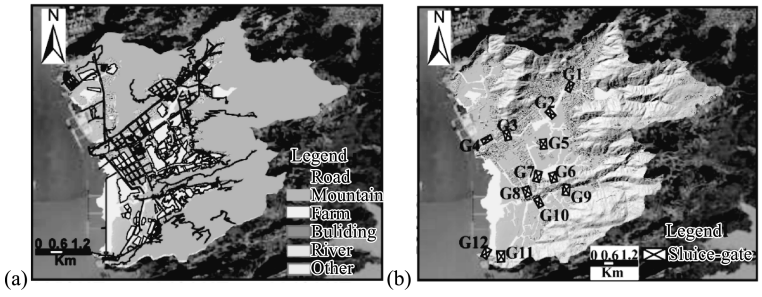

Fig. 4. Model parameters and inner boundary conditions are set according to: (a) land use type; (b) location of sluice gates.

Table 1 The information of sluice gates over the whole domain.

Description		Type	Size(n×B(m))
Label	Name		
G1	Gonglu	Control gate	4×3.0
G2	Chenyu	Control gate	1×3.0
G3	Longshan	Control gate	2×3.3
G4	Yongfu	Tidal gate	2×2.0
G5	Sangutang	Control gate	1×4.0
G6	Qinglannantang	Control gate	4×3.5
G7	Yongfeng	Control gate	2×2.8
G8	Changyu	Control gate	3×3.0
G9	Gushun(minor)	Control gate	1×3.0
G10	Gushun	Control gate	1×4.0
G11	Qingfeng	Control gate	2×2.5
G12	Mitongao	Tidal gate	5×4.0

The simulations are run on 3 m DEM, driven by the rainfall and tidal boundary conditions for the whole duration of the event (from 08:00 on the 8th to 08:00 on the 10th of August 2019). Fig. 5 shows the simulation results with and without pre-discharge of the sluice gates. It should be mentioned that the pre-discharge duration, i. e. ,

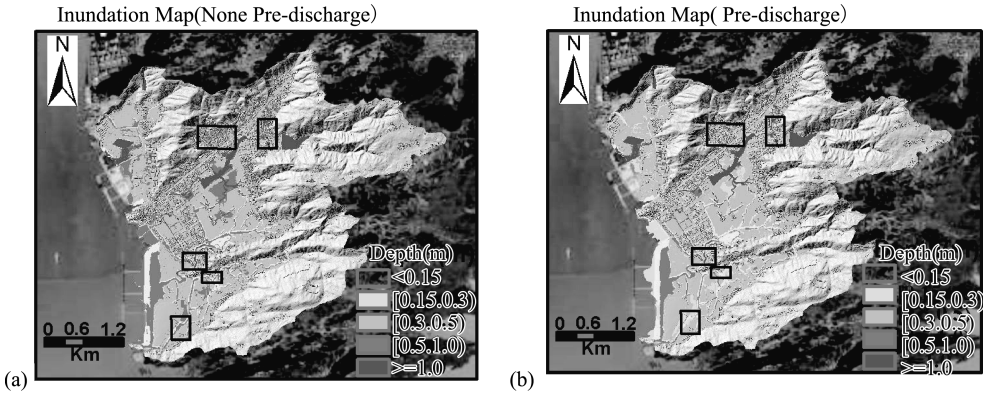

Fig. 5. Maximum inundation map under different scenarios: (a) none pre-discharge; (b) pre-discharge.

one hour, is set according to surveyed data. The inundation maps only display the inundation depth greater than 0.15 m, which is considered to impose negligible damage to objects (e.g., people, vehicles, buildings). The results clearly show the difference in the maximum inundation maps for the two cases, and the inundation extent in those surveyed flooding areas is significantly reduced after the pre-discharge of sluice gates is considered in the model. As listed in Table 2, the surveyed maximum flood depth at the gauge points inside the flooded areas (i.e., A1-A5) is used to evaluate the simulation results. The surveyed data is provided by the Zhejiang Institute of Hydraulics and Estuary in Hangzhou, China. The favourable comparison demonstrates the capability of the new coupled model in reproducing this urban flood event. The simulation results also indicate that considering the effect of pre-discharge of sluice gates better reflects the real-world reality and produces simulation results that agree better with the surveyed data.

Table 2 Comparison of the predicted maximum inundation depths with field datas.

Gauge	Inundation depth(m)/ Relative error(%)		
	Surveyed	Simulated (none pre-discharge)	Simulated (pre-discharge 1h)
GA1	>1.0	1.42/42.0	0.85/15.0
GA2	—	0.86/—	0.53/—
GA3	>1.0	1.68/68.0	1.11/11.0
GA4	0.4-0.6	0.81/35.0	0.68/13.3
GA5	0.5-1.0	1.34/34.0	0.92/8.0

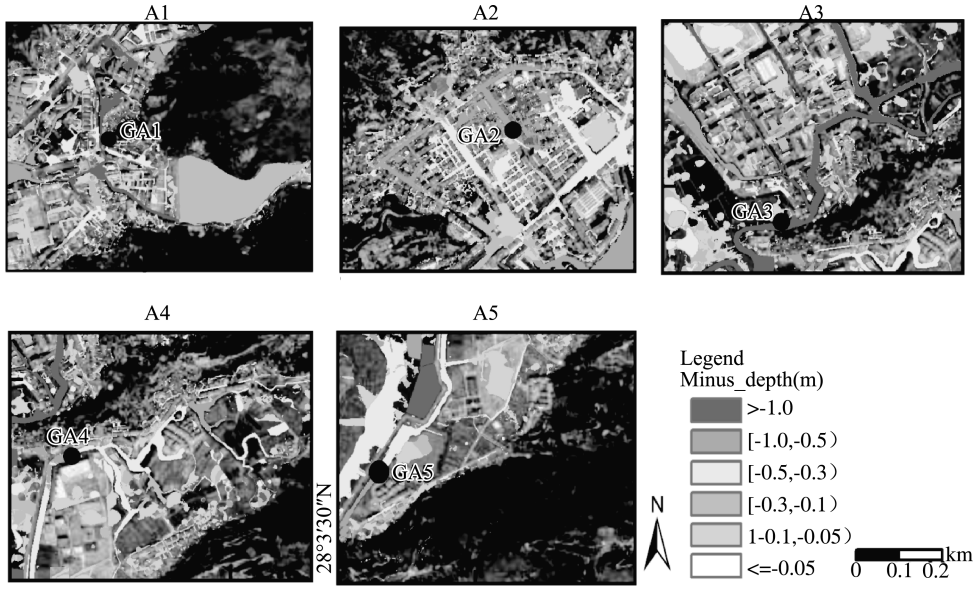

Fig. 6. The difference in inundation depth between two cases at the peak arrival time in each of the enlarged flooding areas.

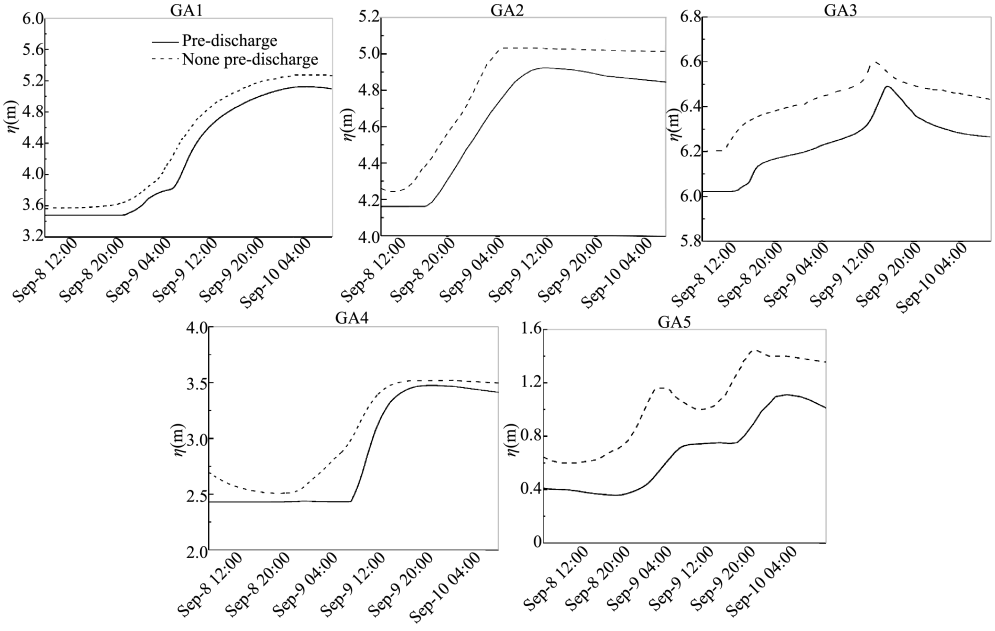

Fig. 7. Time series of water level at the gauge points in surveyed flooding area A1-A5.

To further investigate the function of sluice gates in flood control, the differences of inundation depth between two cases are plotted for the zoom-in flooding areas A1-A5 and shown in Fig. 6. Fig. 7 presents the time series of water level at the gauge

points in each of the flooding areas. As a whole, the effect of pre-discharge on the flood inundation is shown to be significant. This further confirms the importance of considering the effect of hydraulic structures in urban flood modelling. Associated with land-use type, the maximum depth difference tends to be more significant for the permeable objects (e.g., farmlands, rivers, mountain areas) and appears to be smaller for the impermeable objects (e.g., roads, buildings and facilities).

4 Conclusions

This paper presents a robust numerical method that can be used to directly simulate the effects of hydraulic structures in a 2D high-resolution urban flood model. The new fully coupled model is applied to reproduce the flood event induced by Typhoon Lekima in Yuhuan City, China. The simulation results are compared with field data. Satisfactory results demonstrate the accuracy and efficiency of the new model. Further simulations are produced to investigate the effect of the pre-discharge of sluice gates during the flood event. The difference in the inundation in the surveyed flooding areas is found to be significant for permeable objects (e.g., rivers and farmlands) but less obvious in impermeable objects (e.g., roads and buildings). The time series of water levels at gauge points are further examined to analyse the simulation results. Overall, the new model provides a potential tool for urban flood management and forecasting.

Acknowledgements

This work is partly supported by "The Fundamental Research Funds for the Central Universities" (B210202025) and "China Postdoctoral Science Foundation" (2021M690880).

References

Angeloudis, A., Falconer, R. A., Bray, S., et al., 2016. Representation and operation of tidal energy impoundments in a coastal hydrodynamic model. Renewable Energy (99): 1103-1115.

Cozzolino, L., Cimorelli, L., Covelli, C., et al., 2015. The analytic solution of the Shallow-Water Equations with partially open sluice-gates: The dam-break problem. Advances in Water Resources (80): 90-102.

Cui, Y., Liang, Q., Wang, G., et al., 2019. Simulation of hydraulic structures in 2D high-resolution urban flood modelling. Water (11): 2139.

Dazzi, S., Vacondio, R., Mignosa, P., 2020. Internal boundary conditions for a GPU-accelerated 2D shallow water model: implementation and applications. Advances in Water Resources (137): 103525.

Hailemariam, F.M., Brandimarte, L., Dottori, F., 2014. Investigating the influence of minor hydraulic structures on modelling flood events in lowland areas. Hydrological Processes (28): 1742-1755.

Liang, Q., 2010. Flood simulation using a well-balanced shallow flow model. Journal of Hydraulic Engineering (136): 669-675.

Liang, Q., Borthwick, A.G., 2009. Adaptive quadtree simulation of shallow flows with wet-dry fronts over complex topography. Computers & Fluids (38): 221-234.

Liang, Q., Smith, L.S., 2015. A high-performance integrated hydrodynamic modelling system for urban flood simulations. Journal of Hydroinformatics (17): 518-533.

Liang, Q., Xia, X., Hou, J., 2016. Catchment-scale high-resolution flash flood simulation using the GPU-based technology. Procedia Engineering (154): 975-981.

Ming, X., Liang, Q., Xia, X., et al., 2020. Real-time flood forecasting based on a high-performance 2-D hydrodynamic model and numerical weather predictions. Water Resources Research (56).

Morales-Hernández, M., Murillo, J., García-Navarro, P., 2013. The formulation of internal boundary conditions in unsteady 2-D shallow water flows: Application to flood regulation. Water Resources Research (49): 471-487.

Morales-Hernández, M., Murillo, J., García-Navarro, P., 2013. The formulation of internal boundary conditions in unsteady 2-D shallow water flows: Application to flood regulation. Water Resources Research (49): 471-487.

Rawls, W.J., Brakensiek, D.L., Miller, N., 1983. Green-Ampt infiltration parameters from soils data. Journal of Hydraulic Engineering (109): 62-70.

Sanders, B.F., 2017. Hydrodynamic modelling of urban flood flows and disaster risk reduction. Oxford Research Encyclopedia of Natural Hazard Science.

Toro, E.F., 2001. Shock-capturing methods for free-surface shallow flows. Wiley-Blackwell.

Wang, Y., Chen, A.S., Fu, G., et al., 2018. An integrated framework for high-resolution urban flood modelling considering multiple information sources and urban features. Environmental Modelling & Software (107): 85-95.

Xia, X., Liang, Q., Ming, X., 2019. A full-scale fluvial flood modelling framework based on a high-performance integrated hydrodynamic modelling system (HiPIMS). Advances in Water Resources (132): 103392.

Xing, Y., Liang, Q., Wang, G., et al., 2018. City-scale hydrodynamic modelling of urban flash floods: the issues of scale and resolution. Natural Hazards (96): 473-496.

The application of RS, GIS and GPS technology in waters digitization

Dongliang Lai

Zhejiang Design Institute of Water Conservancy and Hydroelectric Power Co., Ltd., Hangzhou, China. e-mail: laidl1992@163.com

Abstract: In order to promote the digital transformation of water supervision in Zhejiang Province, ensure waters play an important role in flood control, drainage, water supply, ecology and other aspects of the water, and comprehensively figure out the basic information and spatial data of waters, a way of establishing a water information geodatabase is introduced by applying RS, GIS and GPS technology, featuring dynamic updates. A way for enhancing water protection and efficient management is provided. This geodatabase contains 6 types of waters: rivers, reservoirs, lakes, mountain ponds, artificial waterways and other waters. Each type of water datasets includes management boundary line, water surface line, and waterfront line (the three lines). Water basic information in attribute tables contains: water name, code, location, basin, function, length, area, volume, etc.

Keywords: Water digitization; 3S; Water protection; Water management; Water information geodatabase

1 Introduction

Waters are important parts of the national land space, and "Zhejiang Waters Protection Measures", which came into effect on May 1, 2019, redefines the scope of waters and puts forward higher requirements for water space protection.

In order to establish a sound natural resource survey system, promote the digital transformation of water supervision in Zhejiang Province, ensure waters play an important role in flood control, drainage, water supply, ecology and other aspects of the waters, and comprehensively figure out the basic information and spatial data of waters, the paper introduced a way of establishing a water information geodatabase by applying RS, GIS and GPS technology, which features dynamic updates. A basis for enhancing water protection and efficient management is provided.

Geo-information Science and Technology, based on GIS (Geographic Informa-

tion System), GNSS (Global Navigation Satellite Systems), and RS (Remote Sensing), organically integrates the relevant parts of these three independent technologies to form a powerful technology system, which achieves rapid, dynamic, accurate and reliable collection, processing and updating of various spatial and environmental information. The geographic information transmission function, communication function, geographic expression function and spatial cognition function not only effectively describe the spatial morphological characteristics, spatial attribute characteristics and spatial relationship characteristics of geographic objects, but also visualize the mechanism and process of geographic phenomena and their development (Xie et al., 2022).

Therefore, the application of Geo-information Science and Technology provides a good working basis and technical means for the digitization of waters, and creates favorable circumstances for establishing a sound natural resource survey system and promoting the digital transformation of waters supervision in the province.

2 Technical approach to water digitization

2.1 Main workflow and requirements

The main work of water digitization includes data organizing and building a basic geodatabase, surveying and mapping, building a standard geodatabase and data importing. The workflow is shown in Fig. 1. The working base map requires the 1∶2000 topographic map, the 0.2 m precision satellite image map, and the third national land survey data. All spatial data should be based on the "1985 National Elevation Datum" and "China Geodetic Coordinate System 2000"(CGCS 2000) with Gauss-Kruger projection.

This water information geodatabase contains 6 types of water datasets, which are rivers (RV), reservoirs (RS), lakes (LK), mountain ponds (HP), artificial waterways (AC) and other waters (OW). Each type of water datasets includes 3 types of feature classes (the three lines), which are management boundary line, water surface line, and waterfront line. Management boundary line is the outer boundary of the management area set to protect the function of the water space. Water surface line is the outer edge of the water surface corresponding to the normal water level of rivers, lakes and other waters. Waterfront line is the outer edge of the functional area carrying the water. In addition, rivers include river centerline feature classes.

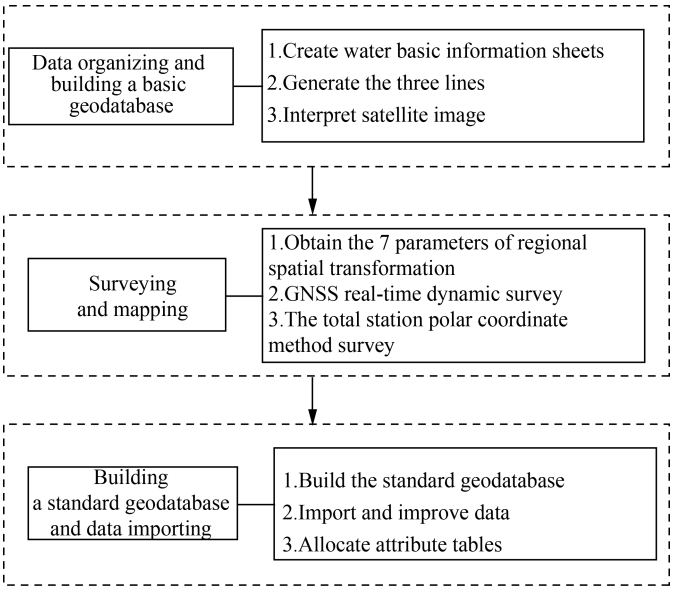

Fig. 1. Workflow diagram.

2.2 Data organizing and building a basic geodatabase

(1) Create water basic information sheets

Water basic information sheets include water name, code, location, basin, function, length, area, volume, etc. Complete these tables according to the existing information, and number all waters to ensure that the code is unique, so as to facilitate the connection with the spatial data of waters.

(2) Generate the three lines

Generate water surface lines of different waters based on the results of rivers, lakes, reservoirs, ponds and other land types in the 3rd national land survey. Extract water surface layer and river center line layer from the 1∶2000 topographic map to generate waterfront lines of different waters. As required by the river management regulations of Zhejiang Province, the waterfront lines will be expanded to generate water management lines. Build a basic geodatabase which contains 6 types of water datasets in GIS, and import the three lines above.

(3) Interpret satellite image

Import 0.2 m precision satellite image map into geodatabase, and check the rationality of the three lines. If necessary, adjust the three lines according to the satellite image.

2.3 Surveying and mapping

When the existing information and data can not meet the requirements of water digitization, obtain geographic data by surveying and mapping.

GNSS real-time dynamic survey method can be used to directly determine the three-dimensional coordinates of terrain and feature points for the measurement area with few surrounding high-rise buildings and little electromagnetic interference. Before the execution of this method, obtain the seven parameters of regional spatial transformation, and verify the 3D coordinates of two or more control points that are not involved in the solution. The difference of plane coordinates should be controlled within 2 cm, and the difference of elevation should be controlled within 3 cm(Shen, 2021). The total station polar coordinate method is used for areas with obvious vegetation cover and poor network signal. For areas with obvious vegetation cover and poor network signal, the total station polar coordinate method is applied.

2.4 Building a standard geodatabase and data importing

(1) Build the standard geodatabase

The standard water information geodatabase contains 6 types of water datasets. Each type of water datasets includes 3 types of feature classes (the three lines). Water surface line is a polygon feature class (a set of many-sided area features), and the other three are line feature classes. The attribute table of management boundary line, waterfront line and river centerline contains a unique water code corresponding to water surface line, while water surface line's attribute table contains water name, code, location, basin, function, length, area, volume, etc.

(2) Import and improve data

Import feature classes from basic geodatabase. Review and complement the three lines spatial data of each water based on the survey results. Perform topology check of spatial data and make sure to construct strict spatial topology relationship. The topology check includes spatial topology problems between line feature classes (lines must not overlap, must not intersect, must not have dangles, etc.), and polygon feature classes (polygon must not overlap, must not have gaps, etc.).

(3) Allocate attribute tables

Connect water basic information sheets to attribute tables of water surface lines by water code, and connect the length of river centerline to river surface line. Once the data is entered, digitization of water is done.

3 Example application

Changxing County belongs to Huzhou City, Zhejiang Province, with a total land area of 1,431.35 km^2, a water area of 92.39 km^2, and a current water surface rate of 6.45%.

There are 6 types of waters in Changxing County, which are rivers (RV), reservoirs (RS), lakes (LK), mountain ponds (HP), artificial waterways (AC) and other waters (OW). As shown in Fig. 2, the geodatabase consists of administrative boundary line dataset (BOU) in addition to water datasets. Fig. 3 shows that Changxing County is bounded by the West Tiaoxi River, with the Tiaoxi River Basin in the south and the Changxing Plain in the north. Fig. 4 shows the attribute table of river surface line, which contains basic information of rivers.

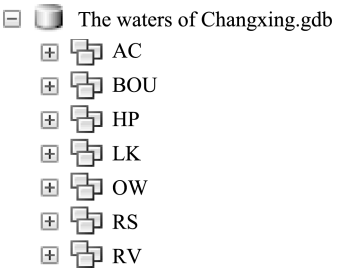

Fig. 2. The geodatabase of Changxing County.

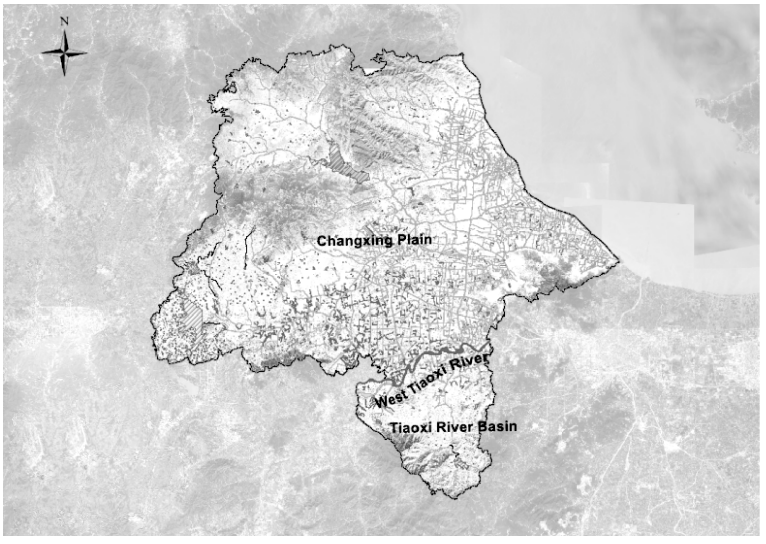

Fig. 3. The geodatabase of Changxing County.

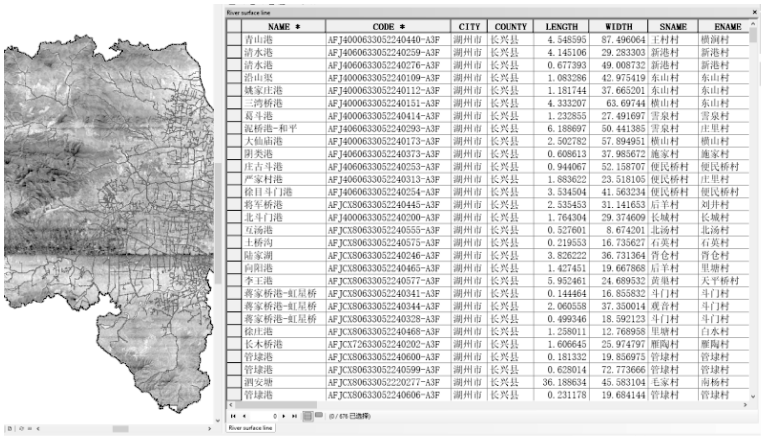

NAME *	CODE *	CITY	COUNTY	LENGTH	WIDTH	SNAME	ENAME
青山港	AFJ40006330522404 40-A3F	湖州市	长兴县	4.548595	87.496064	王村村	横涧村
清水港	AFJ40606330522402 59-A3F	湖州市	长兴县	4.145106	29.283303	新港村	新港村
清水港	AFJ40606330522402 76-A3F	湖州市	长兴县	0.677393	49.008732	新港村	新港村
沿山泉	AFJ40006330522401 09-A3F	湖州市	长兴县	1.083286	42.975419	东山村	东山村
姚家庄港	AFJ40006330522401 12-A3F	湖州市	长兴县	1.181744	37.665201	东山村	东山村
三跨桥港	AFJ40006330522401 31-A3F	湖州市	长兴县	4.333207	63.69744	横山村	东山村
葛斗港	AFJ40006330522404 14-A3F	湖州市	长兴县	1.232855	27.491697	雪泉村	雪泉村
泥桥港-和平	AFJ40606330522402 93-A3F	湖州市	长兴县	6.188697	50.441385	雪泉村	庄里村
大仙庙港	AFJ40006330522401 73-A3F	湖州市	长兴县	2.502782	57.894951	横山村	横山村
闭类港	AFJ40606330522403 73-A3F	湖州市	长兴县	0.608613	37.985672	施家村	施家村
庄古斗港	AFJ40606330522402 53-A3F	湖州市	长兴县	0.944067	52.158707	便民桥村	便民桥村
严家村港	AFJ40606330522403 13-A3F	湖州市	长兴县	1.883622	23.518105	便民桥村	庄里村
徐目斗门港	AFJ40606330522402 54-A3F	湖州市	长兴县	3.534504	41.563234	便民桥村	便民桥村
将军桥港	AFJCX80633052240445-A3F	湖州市	长兴县	2.535453	31.141653	后羊村	刘井村
北斗门港	AFJ40006330522402 00-A3F	湖州市	长兴县	1.764304	29.374609	长城村	长城村
伍汤港	AFJCX80633052240455-A3F	湖州市	长兴县	0.527601	8.674201	北汤村	北汤村
上桥内	AFJCX80633052240575-A3F	湖州市	长兴县	0.219553	16.735627	石英村	石英村
陆家湖	AFJCX80633052240246-A3F	湖州市	长兴县	3.826222	36.731364	晋仓村	晋仓村
向阳港	AFJCX80633052240465-A3F	湖州市	长兴县	1.427451	19.667868	后羊村	里塘村
李王港	AFJCX80633052240577-A3F	湖州市	长兴县	5.952461	24.689532	黄巢村	天平桥村
蒋家桥港-虹星桥	AFJCX80633052240341-A3F	湖州市	长兴县	0.144464	16.855832	斗门村	斗门村
蒋家桥港-虹星桥	AFJCX80633052240344-A3F	湖州市	长兴县	2.060558	37.350014	观音村	斗门村
蒋家桥港-虹星桥	AFJCX80633052240328-A3F	湖州市	长兴县	0.499346	18.592123	斗门村	斗门村
徐庄港	AFJCX80633052240468-A3F	湖州市	长兴县	1.258011	12.768958	里塘村	白水村
长木桥港	AFJCX72633052240202-A3F	湖州市	长兴县	1.606643	25.974797	雁陶村	雁陶村
管塘港	AFJCX80633052240600-A3F	湖州市	长兴县	0.181332	19.856975	管塘村	管塘村
管塘港	AFJCX80633052240599-A3F	湖州市	长兴县	0.629014	72.773666	管塘村	管塘村
洒安塘	AFJCX80633052220277-A3F	湖州市	长兴县	36.188634	45.583104	毛家村	南杨村
管塘港	AFJCX80633052240606-A3F	湖州市	长兴县	0.231178	19.684144	管塘村	管塘村

Fig. 4. The attribute table of river surface line.

4 Conclusions

In the context of the digital transformation of water supervision in Zhejiang Province, relying on geographic information science and technology, the work on water digitization has been studied from the district and county level. The application of Geo-information Science and Technology has the following advantages:

(1) GIS technology has powerful data analysis and processing functions, which can quickly query the spatial information and basic information of the waters, and offers an efficient and reliable technical way to supervise waters.

(2) The application of GNSS technology has not only improved the technical environment of surveying, but also improved the efficiency and quality of measurement, ensuring that the spatial data of waters meet the requirements of high accuracy.

(3) It is easy and quick to obtain the satellite image information of the whole district and county through RS technology, which is useful for region-wide watershed monitoring and historical change analysis.

References

Shen, J., 2021. Exploration of river topographic survey technology for water conservancy projects. Technical Supervision in Water Resources (11): 117-120,124.

Xie, H.L., Wen, J.M., Chen, Q.R., et al., 2022. Research progress of the application of geo-information science and technology in territorial spatial planning. Journal of Geo-information Science, 24(2): 202-219.

Topic 4
River System Management

Analysis of sediment pollutants adsorption and connecting factors at the typical Huaihe River confluence reach

Zhuoying Cang, Dongdong Jia

Key Laboratory of Port, Waterway and Sedimentation Engineering of Ministry of Transport, Nanjing Hydraulic Research Institute, Nanjing, China. e-mail: nkyzycang@163.com

Abstract: Water pollution is increasingly recognized as a serious concern in Huaihe River Basin, and confluence has always been the major component for water-sediment-pollutant transport in river network. The main purpose of this study is to investigate the forms of pollutant and relevant factors in typical confluence of Huaihe River. This paper assumes phosphorus as a main objective and measures other environmental factors like flow velocity, oxygen content, median particle size, water temperature and water depth. The methodological approach taken in this study is a mixed methodology based on long-term monitoring of water and sediment pollutant in the specific areas of the confluence of Huiji River and Guo River and data process by Statistical Product and Service Solutions (SPSS) nonlinear fitting. Results would seem to suggest that, based on temporal standard, pollutant enrichment is concentrated in spring and autumn due to the seasonal variation of temperature and oxygen, and adsorption capacity of phosphorus in sediment reaches the lowest in summer. And based on spatial standard, under the influence of hydrodynamic flow (especially falling flow), the deep pit near the right bank of the downstream is the primary area for pollutant enrichment, where sediment adsorption is enhanced with the increasement of water depth. Statistical tests reveal that compared with other environmental factors, temperature and oxygen have a more significant correlation with adsorption. In addition, in the typical hydrodynamic condition, water-sediment movement has considerable impact on pollutant mixing and transport in the confluence area. Graphic analysis results show that the phosphorus content of sediment begins with increasement and then declines after mixing, which means the hydraulic structure in confluence area improves adsorption in sediment.

Keywords: Confluence; Adsorption; Regression; Phosphorus; Sediment

1 Introduction

Water pollution is a typical and serious problem environmental problem in Huaihe River, China. It was also one of the first major rivers in China to carry out compre-

hensive treatment of water pollution. In recent years, with the point pollution treatment success, the structure of pollution factor in Huaihe River altered, and phosphorus was assumed as the major concern due to agricultural non-point pollution (Zeng et al., 2021). Phosphorus enrichment frequently contributes to the explosion of plankton, turbidity of water and reduction of biodiversity (Søndergaard et al., 2003) and sediment has affinity for phosphorus (Yu et al., 2004). Sediment can not only adsorb phosphorus as pollution sink to curb the deterioration of river environment but also release phosphorus as pollution source (Xu et al., 2003; Tang et al., 2014). In addition, confluence area is the major part for water-sediment-pollutant transport in river network. Complicated flow structure and obvious three-dimensionality of current contribute to the sediment desorption and readsorption. Therefore, this study offers some insights into sediment adsorption characteristics and factors in confluence area for Huaihe River water pollution treatment.

See Fig. 1, sampling site is located at the junction of Huiji River and Guo River. Guo River is the second largest branch of Huaihe River and Huiji River is the largest branch of Guo River. The selected junction faces Bozhou City on the east and west meets Luyi City. Hydrological data like flow velocity (FV), sediment phosphorus (PS), water phosphorus (PW), pH, oxygen content (O), median grain size (MGS), water temperature (WT) and water depth (WD) were collected from 2016 to 2017. The objective of this paper is to demonstrate the time and spatial pattern of sediment phosphorus and analyze connecting factors by curve estimation.

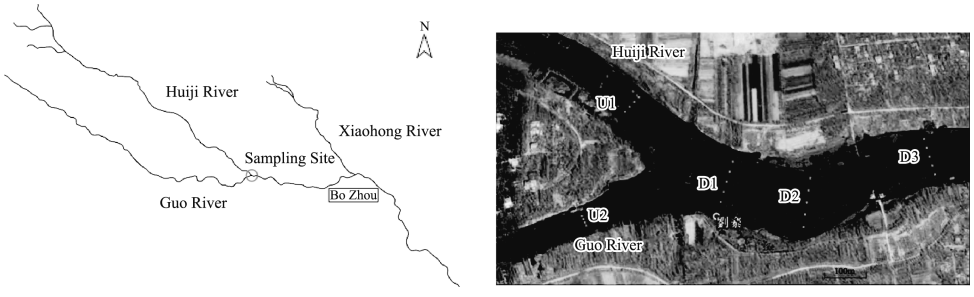

Fig. 1. Sampling sites in Huaihe River.

2 Time and spatial variation

See Fig. 2, the graph shows the variation of sediment phosphorus average value with time. Sediment phosphorus reached higher value in spring, dropped rapidly in summer, and slightly increased in autumn and winter. The max value is 1.286 mg/g and the minimum is 0.352 mg/g. It can be suggested that natural flow condition could

be a major factor for the variation of sediment phosphorus value due to the flow characteristics of Huaihe River. Flow quantity in Huaihe River differs obviously in rainy and dry season affected by climate reason and urban water issues (Shi et al. 2012), hence the maximum of pollutants frequently appears in dry season. On the other hand, engineering measures are frequently performed to control runoff in Huaihe River Basin to meet social and economic demands (Liu et al. 2003), which made the lowest flow quantity fall into 8 m^3/s in Guo River at non-flood season due to limitation of Mengcheng floodgate. Such engineering measures as sluice also result in the concentrated discharge of pollutants (Zhang et al. 2007), which contributes to the time difference of sediment phosphorus.

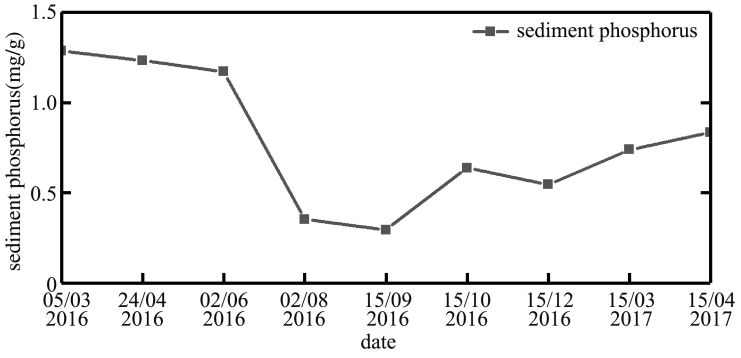

Fig. 2. Time variation of sediment phosphorus average in the confluence area of Huiji-Guo River.

Fig. 3 shows the longitudinal distribution of sediment phosphorus. See Fig. 3, the graph reveals that the average value of sediment phosphorus increased firstly and then decreased. A possible explanation for this might be that the flow structure and turbulence intensity in Y-shaped junction could have a close correlation with sediment phosphorus adsorption. The meeting of main stream and tributary brings about the flow collide and mixing, resulting in the redistribution of velocity (Feng et al. 2006), which generates acceleration zone in middle layer of river. In addition, the turbulence fluctuation intensity near river bed is much larger and the helical flow would be generated downstream along the river. In short, complicated and violent turbulence in D2 promotes sediment phosphorus adsorption, and adsorption decreases along the river due to turbulence weakening.

3 Univariate analysis

Fig. 4 shows the scatter and curve estimation between median particle size, water depth, velocity, water phosphorus, pH, water temperature, oxygen and sediment

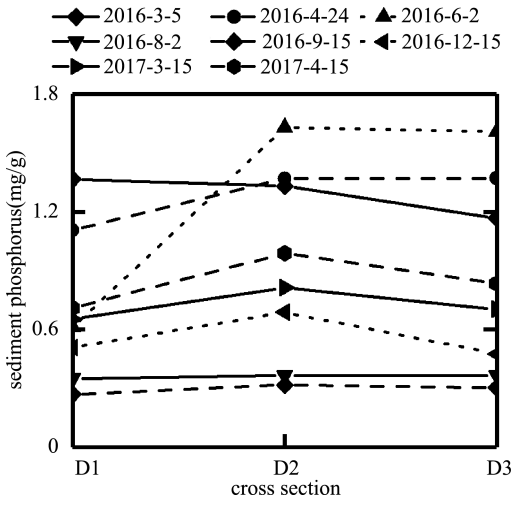

Fig. 3. Spatial variation of sediment phosphorus average in the confluence area of Huiji-Guo River.

phosphorus. All the functions pass the significance test of 0.01. However, ignorance of sediment aggregation effect could lead to inaccurate PS value (Tang, et al. 2017), which may affect the following results. See Fig. 4(a), there is a reciprocal relationship between median grain size and sediment phosphorus. Decrease of sediment grain size enhances the comprehensive adsorption capacity of sediment, which could be explained by the change of sediment specific surface area leading to variation of active component, thus affecting the amount of phosphorus adsorption. See Fig. 4(b), sediment phosphorus decreases at first and then rises with water depth growing. It can be suggested that tributary flowing into main stream results in backwater near upstream side (Yang et al., 2002). In the backwater zone, water depth increases and velocity decreases, which brings about retention effect in the confluence area. Consequently, water phosphorus can be fully adsorbed on the surface of sediment. Fig. 4(c) shows that sediment phosphorus goes up with flow velocity increasing. Increase of flow velocity means higher turbulence intensity , which causes more sediment to spread from riverbed into overlying water, breaking the phosphorus balance between sediment and water. Moreover, the dynamic flow enhances P retention on sediment because of the high penetration of oxygen and the higher probability of interactions of P and P reactants on sediment (Li et al., 2016). Fig. 4(d) shows a complex nonlinear outcome which seems discrepant compared with previous research that sediment phosphorus increases with water phosphorus growing. A possible explanation for this might be that the response relation between water phosphorus in river surface and sediment in riverbed is not obvious at the same sampling site. Firstly, bottom flow participates in the process of phosphorus exchange between water and sediment. Secondly, under dy-

namic water condition, surface water is not closely related to bottom water. Water samples are taken from the surface of river, thus a discrepant result is generated in Fig. 4(d). Fig. 4(e) reveals that both the alkalinity and acidity can promote sediment adsorption. See Fig. 4(f), both increase or decrease of temperature might result in the reduction of sediment phosphorus when at the point of 24.7℃. Fig. 4(g) shows that sediment phosphorus adsorption increases with oxygen content growing.

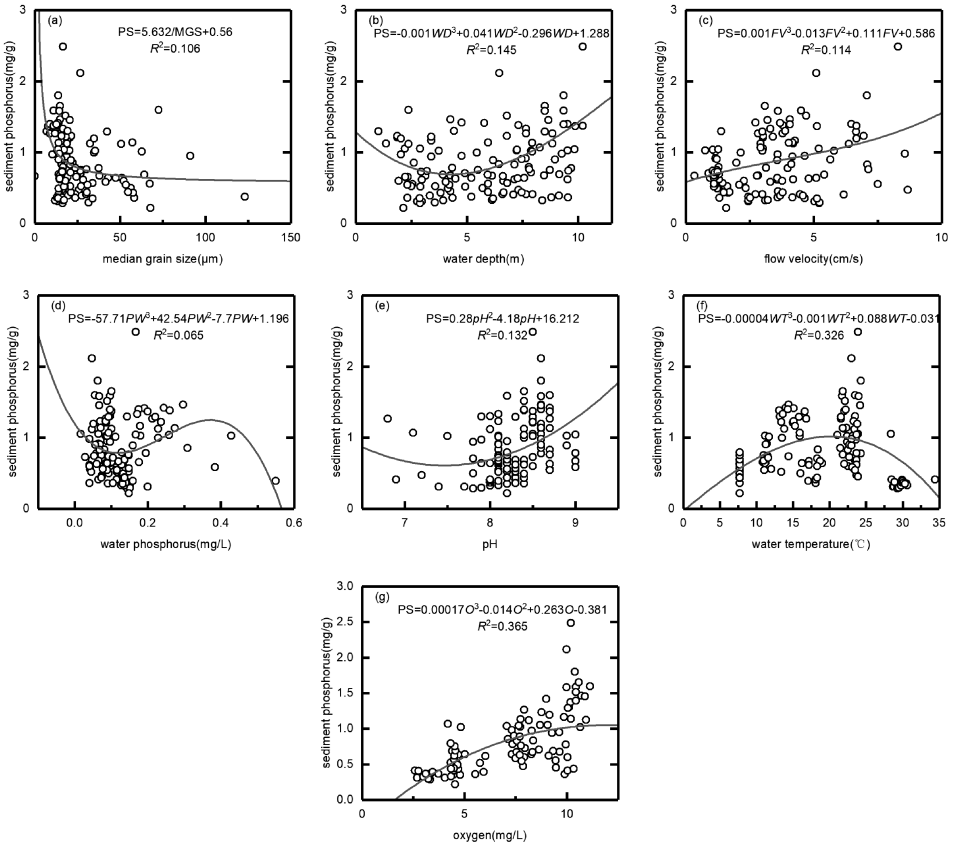

Fig. 4. Scatter plots and curve estimation between sediment phosphorus and median grain size(a), water depth(b), flow velocity(c), water phosphorus(d), pH(e), water temperature(f), oxygen(g).

4 Conclusion

Sediment phosphorus reached the maximum in spring, varied extremely in summer, and fluctuated upward in autumn and winter. It increased firstly and then decreased after the junction got affected by flow structure in the longitudinal direction along the river.

The increase of velocity and oxygen contributes to sediment phosphorus adsorp-

tion while the coarsening of sediment grain curbs adsorption. The effect of water depth, water phosphorus, pH, and water temperature on sediment phosphorus adsorption depends on their value range, where both water depth and pH have the minimum point of sediment phosphorus adsorption and water temperature has the maximum one.

Acknowledgements

The work presented in this paper is financially supported by the National Natural Science Foundation of China (Nos. U2040215 and 52079080).

References

Feng, Y.H., Guo, W.D., 2006. Numerical simulation of flow at Y-shaped open-channel junction. Hydroscience and Engineering (4): 34-40.

Li, Z., Tang, H., Xiao, Y., et al., 2016. Factors influencing phosphorus adsorption onto sediment in a dynamic environment. Journal of Hydro-Environment Research (10): 1-11.

Liu, Z., Shen, W.S., Wu, H.Z., 2003. The effects of water conservancy projects on ecoenvironment of Huaihe Water Area. Geography and Geo-information Science, 19(2): 77-81.

Shi, H.L., Hu, C.H., Wang, Y.G., et al., 2012. Variation trend and cause of runoff and sediment load variations in Huaihe River. Journal of Hydraulic Engineering, 43(5): 571-579.

Søndergaard, M., Jensen, J.P., Jeppesen, E., 2003. Role of sediment and internal loading of phosphorus in shallow lakes. Hydrobiologia, 506-509(1-3): 135-145.

Tang, H.W., Li, Q.X., Yuan, S.Y., et al., 2017. Effect of aggregation on the adsorption of phosphorus onto air-dried sediment in contrasting shear flow conditions. Journal of Soils and Sediments, 17(8): 2177-2186.

Tang, H.W., Yuan, S.Y., Xiao, Y., 2014. Effects of flow and sediment on the transport and transformation of pollutants in rivers: A review. Advances in Water Science, 25(1): 139-147.

Xu, Y.Q., Xiong, H.L., Zhao, X.L., 2003. The adsorption and release of phosphorus in sediment; A review. Chongqing Environmental Science, 25(11): 147-149.

Yang, S.F., Zhao, Z.Z., Yang, B., 2002. Study on the common boundary of the mainstream and the branch for numerical modelling. Journal of Chongqing Jiaotong

University, 21(2): 115-118.

Yu, X.Z., Zhong, D.Y., Li, J.X., et al., 2004. Review of studies on sediment in water environment. Journal of Sediment Research (6): 75-81.

Zeng, F.L., Yang, G., Wang, P., et al., 2021. Temporal and spatial variation of water quality and pollution trend of Huaihe River. Journal of Hydroecology, 42 (5): 86-93.

Zhang, Y.J., Xia, J., Wang, G.S., et al., 2007. Research on influence of dams/union dispatch on water quality in Huaihe River Basin. Engineering Journal of Wuhan University, 40(4): 31-35.

Contrast study on numerical simulation of pollutant diffusion methods

Xiangqian Wang[1], Jialing Hao[2], Yuan Zhong[3], Chaofeng Tong[4]

[1,2,3,4] College of Harbor, Coastal and Offshore Engineering; Hohai University, Nanjing, China. e-mail: 201303020040@hhu.edu.cn

Abstract: In the process of water flow, water flow state and water quality are more complex. The pollutants in the water flow diffuse in the action of water flow, which will have a certain impact on the water environment along the way. Therefore, the study of pollutant diffusion law in water flow has theoretical and practical value.

In this paper, the diffusion law of pollutants in the random walk model is studied with the ideal rectangular area as the research object. First, a two-dimensional hydrodynamic model is established and the hydrodynamic conditions of both are simulated to provide flow field data for further calculations. Then, based on the obtained rectangular regional flow field data, a convective diffusion model was established based on Euler's method, which simulated the distribution of pollution particles in a rectangular region of 160 m × 160 m, and then introduced a random walk model based on the Lagrange method. The convective diffusion model and the random walk model were used to simulate the distribution of pollution particles in the rectangular area of 160 m × 160 m after diffusion for 60 seconds respectively, and the characteristics of the two methods were analyzed by comparing the simulation results of the two methods.

Comparing the simulation process and simulation results of the two models, it can be seen that the principle of the convective diffusion model based on Euler's method is relatively simple, in which the programming is relatively easy, and it is suitable for simulating the diffusion of soluble pollutants; while the random wandering diffusion model under the Lagrange framework is relatively difficult to mathematically process and the amount of calculation is large, it can more directly observe the diffusion and distribution of particles, which has certain advantages in simulating insoluble pollutants.

Keywords: Hydrodynamic model; Random walk model; Convection diffusion model; Pollutant diffusion; Numerical simulation

1 Introduction

Basin economy is an important part of economic development in the world today, and China is no exception, of which the Yangtze River Basin economy is an important

pillar. However, along with the economic development, the environmental pollution problem has been intensifying. Water pollution has become one of the factors limiting economic growth and is also contrary to the theory of sustainable development. In this current situation, the importance of such issues as water pollution and water environmental quality should be further emphasized. Trying to accurately predict and control water environmental quality and water pollution, so as to take targeted preventive and protective measures, we first need to have a certain understanding of the diffusion characteristics of its pollutants. At present, scholars at home and abroad have made rich achievements in the study of pollutant dispersion (Li et al., 1993; Smith, 1983; Holley et al., 1970). For the study of wandering model, Liang applied it to the pollutant dispersion in open channel flow with submerged vegetation (Liang, 2014); Chen applied the stochastic wandering dispersion model to simulate oil spills in small watersheds such as rivers (Chen, 2016); Pan studied the pollutant migration characteristics of tide-sensitive rivers (Pan, 2007). In this paper, we take an ideal rectangular area as the research object to study the diffusion law of pollutants in the random walk model.

2 Ideal area hydrodynamic simulation

2.1 Boundary and mesh generation

The section of the actual water area is made up of an infinite number of consecutive points, which need to be converted into a finite number of points for easy calculation when performing numerical simulations.

Delft 3D uses finite difference method for discretization. This method is a more common method for numerical computing applications, and the length and width are maintained in a certain proportion when dividing the mesh, that is, when the contaminants move in one direction to the node downstream of the mesh, they are also mixed in the other direction (Liu, 2005).

In hydrodynamic simulation, a rectangular grid or orthogonal curve mesh is generally used to divide the calculation area. The advantage of a rectangular mesh is that it is easy to approximate the derivative by difference, and it is easier to determine the mesh node relationship, while the orthogonal curvilinear mesh can more accurately simulate the actual situation of the computed area with complex boundary. Rectangular meshing is used here to divide the calculation area.

The calculation area is ideal for a rectangular area of 160 m × 160 m, which is divided by a rectangular mesh of 16×16, as shown in Fig. 1.

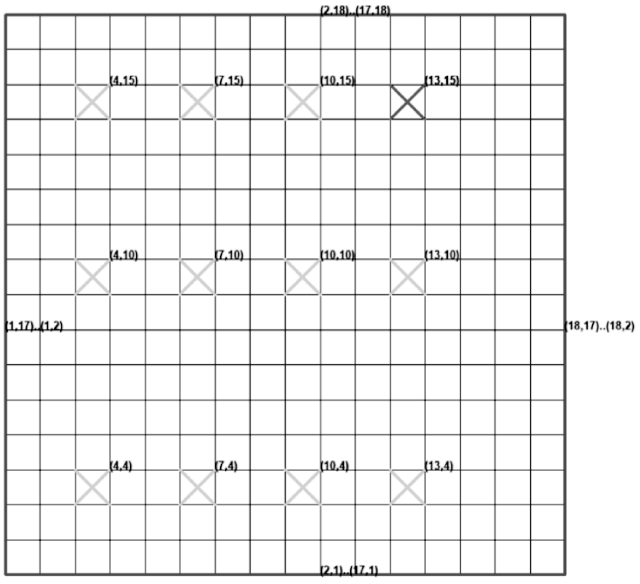

Fig. 1. Boundary, grid division and observation points.

2.2 Calculation and results

The simulated water level and depth average flow rate obtained are shown in Fig. 2.

The flow field data obtained from this simulation will be used as the basic information for water quality models in the next chapter to provide the flow field conditions for the model calculation.

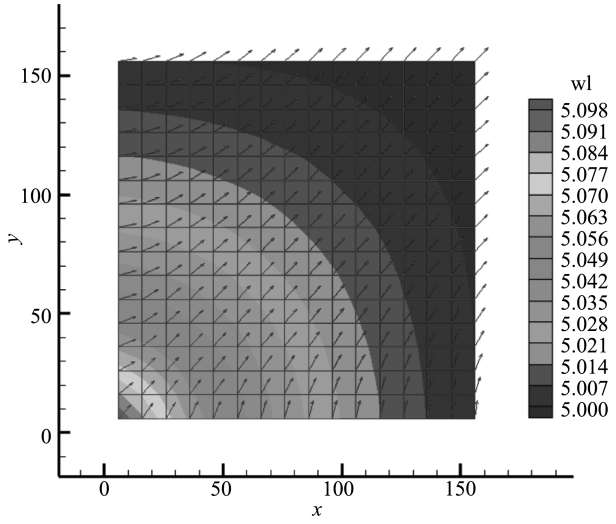

Fig. 2. Hydrodynamic simulation results of rectangular area.

3 Comparison of simulation methods for pollutant dispersion

3.1 Eulerian-based pollutant dispersion simulation

3.1.1 Model Principle

The mathematical model of pollutant transport can be expressed as a function against the pollutant concentration $C(x,y,z)$, which can describe the conservation of the pollutant during its motion. In the case of turbulent flow, assuming the validity of Fick's law and the Boussinesq approximation, an examination of the balance of the inflow and outflow masses in two cross-sections from a simple one-dimensional flow with velocity u reveals that:

$$\frac{\mathrm{d}c}{\mathrm{d}t}=\frac{\partial c}{\partial t}+\frac{\partial(uc)}{\partial x}=\frac{\partial}{\partial x}\left(D\frac{\partial c}{\partial x}\right)-\lambda c \tag{1}$$

where D is the vortex diffusion coefficient; λ is the attenuation coefficient.

The depth-averaged two-dimensional equation is:

$$\frac{\mathrm{d}c}{\mathrm{d}t}=\frac{\partial c}{\partial t}+\frac{\partial(uc)}{\partial x}+\frac{\partial(uc)}{\partial y}=\frac{\partial}{\partial x}\left(D\frac{\partial c}{\partial x}\right)+\frac{\partial}{\partial y}\left(D\frac{\partial c}{\partial y}\right)-\lambda c \tag{2}$$

3.1.2 Calculation and results

In the flow field obtained from the hydrodynamic simulation in the ideal region, the initial concentration of 150 kg/m^3 is added at the origin at the moment $t=0$, and no further concentration is applied. The turbulent diffusion coefficient is taken as $K_x=K_y=0.5$, the time step is $\Delta t=1\ s$, and the simulation duration is $t=60$ s. The simulation results are shown in Fig. 3.

From Fig. 3, it can be seen that at $t=60$ s, the center of the particle cluster is near (75, 80) and the concentration at the center is around 1.5 kg/m^3. The particle cluster is centered on the highest concentration point and has an elliptical distribution.

3.2 Simulation of pollutant dispersion based on random walk model

3.2.1 Model principle

The basic idea of the random walk model is that a large number of trackable particles are used to represent the pollutants, and the particles are released in the flow field to simulate a series of turbulent diffusion of the particle population by a random displacement process. The motion process is tracked, and finally the diffusion of the pollutants is derived by counting the distribution of the particle population.

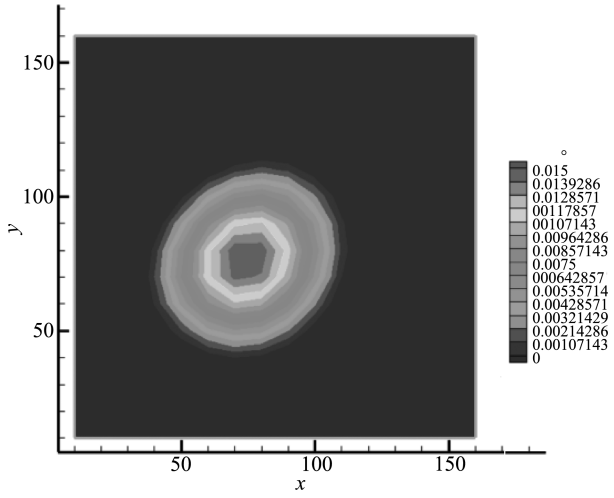

Fig. 3. Simulation results of concentration (C) based on Eulerian convective diffusion model.

As far as the diffusion process is concerned, the random wandering model treats turbulent diffusion as a random motion and simulates the diffusion process of particles by the stochasticity method.

3.2.2 Model building

Let N particles be released, where the coordinates of the i th particle at the moment $t = n\Delta t$ are (X_i^n, Y_i^n), then the coordinates of this particle at the moment $T = (n+1)\Delta t$ (X_i^{n+1}, Y_i^{n+1}) can be expressed as:

$$X_i^{n+1} = X_i^n + X_1 + f_x = X_i^n + udt + R_x \sqrt{2K_x\Delta t} \tag{3}$$

$$Y_i^{n+1} = Y_i^n + udt + f_y = Y_i^n + udt + R_y \sqrt{2R_y\Delta t} \tag{4}$$

where f_x, f_y is the random displacement component of the particle in the x, y direction caused by the turbulent process; K_x, K_y is the turbulent diffusion coefficient in the x and y directions; R_x, R_y is the standard normally distributed random number with mean 0 and variance 1 between $(-1,1)$.

Let the pollutant emissions be Q, then count the number of mass points n in each grid cell at the moment t. The concentration distribution of the pollutant at the moment t can be determined:

$$C_{i,j,k} = \frac{nQ}{N\Delta V} \tag{5}$$

where i, j, k is the number of the grid; ΔV is the volume of the grid.

Therefore, by determining the average value of the flow velocity and K_x, K_y, the distribution of the particles can be obtained by the two Eq. (3)-(4).

3.2.3 Calculation and results

In the flow field obtained from the ideal area hydrodynamic simulation, 5,000 particles are released instantaneously at the origin at the time $t = 0$. The grid spacing is $\Delta x = 10$ m, $\Delta y = 10$ m, the turbulent diffusion coefficient is $K_x = K_y = 0.5$, the time step is $\Delta t = 1$ s, and the simulation time is $t = 60$ s. The simulation results are shown in Fig. 4.

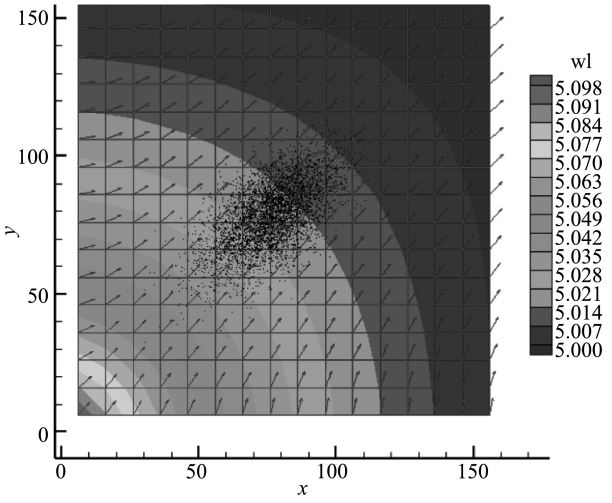

Fig. 4. Simulation results of random walk model.

4 Summary

The simulation results of the convective diffusion model based on Euler method and the random walk model based on Lagrange method are analyzed as follows:

From Fig. 4, it can be seen that at $t = 60$ s, the horizontal coordinates of the position of the center of the particle cluster are between 75–80 m and the vertical coordinates are between 75–80 m; meanwhile, 192 particles are distributed in the region by counting. The particles are elliptically distributed with the center of the region, which is more consistent with the distribution in Fig. 3.

Comparing the simulation process and simulation results of the two models, it can be seen that the principle of the convective diffusion model based on Euler's method is relatively simple, the programming is relatively easy, and it is suitable for simulating the diffusion of soluble pollutants, but when simulating insoluble pollutants, the motion process of the polluting substances cannot be displayed. Although the random wandering diffusion model under the Lagrange framework is relatively difficult to process mathematically and the amount of calculation is large, it can more directly ob-

serve the diffusion and distribution of particles, which has certain advantages in simulating insoluble pollutants.

References

Chen, L., Han L. X., Tan, J. Y., 2016. The application of random walk model on the oil spill accident in small rivers. China Water Transport, 16(6): 154-155.

Holley, E.R., Harleman, D.R.F., Fischer, H.B., 1970. Dispersion in homogeneous estuary flow. Hydraulic.Eng., 96(8):1651-1709.

Liang, D. F., Wu, X. F., 2014. A random walk simulation of scalar mixing in flows through submerged vegetations. Journal of Hydrodynamics, Ser. B, 26(3): 343-350.

Liu, X. L., 2005. Numerical simulation of the flow field and water quality of the two rivers confluence in Chongqing. Chongqing University.

Li, Y. L., Bian Z. J., Yu C. Z., 1993. Theoretical analysis and application of pollutant dispersion in tidal currents. Journal of Mechanics (4):394-403.

Li, Y. L., Zhou X. Y., Yu, C. Z., et al., 1993. Calculation of pollution mixing zone in tidal flow. Journal of Tsinghua University (Natural Science Edition) (2): 56-64.

Pan, H. B., 2007. Contaminator transport study of the tidal river based on the random walk model. Nanjing: Hohai University.

Smith,R., 1983. The contraction of contaminant distribution in reserving flows. Fluid Mech. (129): 137-151.

Determination and analysis of river ecological base flow(water level) in plain river network area

Xiaojun Ji[1], Yun Zhan[2]

[1] Water Conservancy Bureau of Nantong, Nantong, China, e-mail: 252144113@qq.com

[2] The Nantong Substation of the Hydrology and Water Resources Investigation Bureau in Jiangsu Province, Nantong, China. e-mail: 303781993@qq.com

Abstract: River ecological base flow (water level) is a basic indicator to maintain the ecological function of the river and control the development intensity of water resources. It is an important basis for coordinating the water consumption of life, production and ecology, and has a fundamental and important position in the allocation and scheduling of water resources. Nantong City is a typical plain river network area. In this paper, under the condition of mastering the river system of Nantong, the status quo of water resources development and utilization, and basic hydrological data, through method comparison, the annual minimum water level method was used to determine the ecological water levels of 13 rivers preliminarily including Jiuwei Port River and formulated corresponding safeguard measures with "one river, one policy". The ecological water level was assessed according to the "Technical Guidelines for Monitoring and Evaluation of Ecological Water Level (Flow) (Trial)". The management and control measures were put forward from four aspects, such as finding out the water resources and water ecology in the jurisdiction and determining the ecological water level (flow) target scientifically. The next step is to select the appropriate ecological flow (water level) calculation method according to the mobilization and operation of various water conservancy projects and the water intake of the river, and determine the target value of the ecological base flow (water level) of the river scientifically. The paper provides a reference to carry out the determination of river ecological base flow (water level) in the plain river network area.

Keywords: Plain river network area; Nantong City; Ecological base flow (water level); Management and control

1 Introduction

River ecological base flow (water level) is the basic index to maintain the ecological functions of rivers and lakes and control the intensity of water resources development and utilization, as well as it is an important basis for coordinating the "three life" water use, which plays a fundamental and prerequisite role in water resources al-

location and dispatching. Guaranteeing the ecological flow of rivers is related to the health of rivers, the construction of ecological civilization and high-quality development. The guiding opinions of determining and ensuring the ecological flow (water level) of rivers and lakes, and also the notice of determining and ensuring the list of key rivers and lakes (reservoirs) in Jiangsu province have been successively issued since 2019. It is required to select a number of key rivers and lakes (reservoirs) with important ecological functions, urgent requirements for water resources supervision, and typical demonstration which lead the important role in the determination and guarantee of ecological base flow (water level), and prepare the list of key rivers and lakes (reservoirs) for the determination and guarantee of ecological base flow (water level), and then determine the ecological base flow (water level) target in batches and levels so that can carry out guarantee work. The water control idea of "giving priority to water conservation, spatial balance, systematic governance and making efforts with both hands" has been actively implemented in Nantong. According to the guiding opinions, the determination and guarantee of ecological base flow (water level) of key rivers and lakes, and formulated the list of ecological base flow (water level) determination and guarantee of key rivers and lakes (reservoirs) has been fully implemented from 2020 to 2022 in Nantong. The ecological base flow (water level) of 13 rivers including Jiuweigang River has been determined successively, and the guarantee scheme has been formulated simultaneously with "one river and one policy". The ecological water level has been comprehensively and effectively controlled, which has laid a solid foundation for the construction of healthy rivers and lakes.

2 Regional overview

2.1 Physical geography

Nantong is located in the southeast of Jiangsu Province, in the lower reaches of the Yangtze River and Huaihe River Basins, across the river from Shanghai. It is the only city in Jiangsu with deep-water coastline along the river and coastal areas. It is an area with superior water resources conditions. Nantong has a land area of 8,001 km^2 and a sea area of 8,701 km^2. It belongs to the alluvial plain of the Yangtze River Delta and is located in the subtropical monsoon climate zone.

2.2 River system

The Nantong Plain is vast, with rivers, rivers and seas running through it, and the water network is densely covered. Nantong belongs to the two major water systems

of the Yangtze River and Huaihe River bounded by Tongyang Canal and Rutai Canal. To the south of Tongyang Canal (passing through Haian, Rugao and Dingyan line) and Rutai Canal (from Dingyan and Digang to Donganzha line), it belongs to the Yangtze River system, with an area of about 5,813 km^2; while the north is the Huaihe River system, covering an area of 2,188 km^2. The inland rivers in Nantong are divided into five levels, such as class Ⅰ River (dry river), class Ⅱ River (branch river), class Ⅲ River (big ditch), class Ⅳ River (medium ditch) and class Ⅴ River (small ditch). There are 12 first-class rivers, with a total length of 743.34 km; 111 secondary rivers with a total length of 1,901.04 km; The remaining rivers below class Ⅲ are composed of large, medium and small ditches, which are the ditch network on the surface and play the role of water storage, diversion, drainage and confluence. There are 53 rivers listed in the list of key rivers in Jiangsu Province, 2 river basins (Yangtze River and Tongyu River), 10 regional key rivers, and 41 important cross county rivers and important county rivers. The normal water level of Nantong inland river is generally 1.8 to 2.3 m, and that of some low-lying areas is about 0.8 to 1.3 m. The primary and secondary rivers are connected with the Yangtze River and the Yellow Sea, which play the role in regulating the whole river network and are the main project of waterlogging removal and irrigation in Nantong (Zhang et al.,2021).

2.3 Development and utilization of water resources

The average annual surface runoff was 2.56 billion m^3, precipitation infiltration recharge was 1.43 billion m^3, and total water resource reached 3.15 billion m^3 in Nantong excluding 840 million m^3 of double calculation of surface water and groundwater. According to the total population in 2020, the per capita share of local water resources was 414.6 m^3. However, the location advantage of water diversion along the river in Nantong can effectively make up for the shortage of local water resources. According to the statistics, the average annual water diversion of all gates along the river was 3.399 billion m^3 according to the calculated data from 1956 to 2019, during which the maximum annual water diversion was 5.992 billion m^3 in 1982, and the minimum annual water diversion was 1.429 billion m^3 in 1963. According to the water resources bulletin over the years, the water consumption of Nantong was basically stable between 3.583 billion m^3 and 4.096 billion m^3 from 2014 to 2020. From the analysis of water use structure, the domestic and urban public water use has increased from 308 million m^3 in 2014 to 487 million m^3, and the average annual growth reached 7.92%. While the industrial water consumption decreased from 1.418 billion m^3 in 2014 to 1.114 billion m^3, the average annual decrease is 3.94%; meanwhile, other water consumption was relatively stable as a whole.

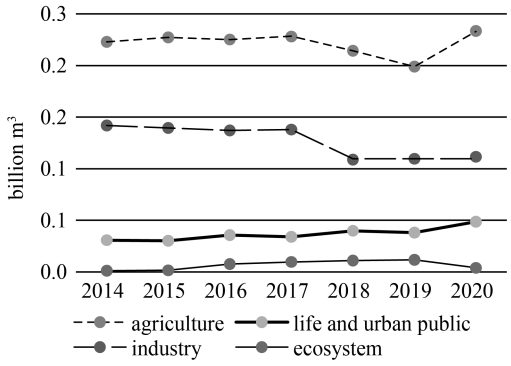

Fig. 1. The water structure diagram of Nantong City.

3 Determination of regional ecological water level (flow) targets

From 2020 to 2021, the ecological water levels (flow) of 13 rivers in Nantong City were successively determined as Jiuwei Port River, Tonglu Canal, Tongqi Canal, Yaowang Port River, Xinjianghai River, Ruhai Canal, Jiaogang River, Tongyang Canal Nantong Section, Bencha Canal, Beiling River, East section of Rutai Canal, Nanling River and Haimen River. And a guarantee plan was formulated simultaneously with "one river, one policy".

3.1 Materials and methods

At present, more than 200 methods for estimating river ecological base flow (water level) have been developed in the world, which can be classified into four categories: hydrology, hydraulics, habitat simulation and holistic (Tharme, 2003; Dong et al., 2020; Li et al., 2020)(Table 1). There are many rivers in Nantong City, the water network is dense, and the water conservancy engineering system is relatively complete. There are great technical difficulties in the determination of ecological flow (water level). Combined with the characteristics of the river system in the plain river network in Nantong City, and according to the current hydrological data, the annual minimum water level method in the hydrological method is selected as the research method. There are water level stations on the rivers, and the lowest annual water level with a 90% guarantee rate for at least 30 years is used as the ecological water level.

Table 1 Ecological flow calculation methods that are commonly used.

Classification of evaluation methods	Typical methods	Main principle	Advantages	Disadvantages
Hydrology	Tennant, flow duration curve, hydrological index method, 7Q10 method, annual minimum water level method, etc.	Based on the hydrological process of the river, a certain proportion of the annual average flow is selected as the minimum ecological base flow.	The algorithm is simple, and for areas lacking ecological data, the results can be quickly obtained based on the hydrological data records.	The hydrological change and ecological response mechanism is not involved, and the scientificity of the method is insufficient.
Hydraulics	Wet perimeter method, R2-Cross method, channel morphology analysis method, etc.	Select simple hydraulic parameters as the basis, such as wet cycle, maximum water depth, etc., and use measured data, hydraulic formulas to establish hydraulic parameter-flow relationship.	Taking into account biological habitat requirements to a certain extent.	When calculating hydraulic parameters, the selection of cross-section has a certain influence on the results, and it is necessary to analyze the actual situation of the river according to local conditions.
Habitat simulation	IFIM method, CASIMIR method, etc.	Based on the hydraulic model, habitat changes caused by changes in river flow are considered and combined with the habitat preference needs of the target species.	It has a good scientific basis for clarifying the ecological flow requirements of specific species.	The research method is more complex than the above two methods, focusing only on a certain species, failing to consider the overall needs of the river ecosystem.
Holistic	BBM method, DRIFT method, ELOHA method, etc.	Using historical data and monitoring data, through statistical analysis, the hydrology-ecological response relationship is established, and the ecological flow threshold is comprehensively determined after decision-making by stakeholders.	It has strong scientific and comprehensive function.	A large amount of hydrological and ecological data is needed, and the scientific community's recognition of the hydrological driving and ecological response mechanism is not perfect.

3.2 Release of ecological water level (flow)

The ecological water levels of 13 rivers including Jiuwei Port were released in 2021 (Table 2).

Table 2 The ecological water table of key rivers in Nantong.

Serial number	River name	Control section	Ecological water level (m)	Serial number	River name	Control section	Ecological water level(m)
1	Jiuwei Port River	Shigang water level station	1.04	8	Tongyang Canal Nantong Section	Dingyan water level station	0.86
2	Tonglu Canal	Huolong water level station	1.03	9	Bencha Canal	Xiaoyangkou (on the gate) water level station	0.33
3	Tongqi Canal	Changle Gate (on the gate) water level station	0.70	10	Beiling River	Xiaoyangkou (on the gate) water level station	0.33
4	Yaowang Port River	Shigang water level station	1.04	11	East section of Rutai Canal	Juegang water level station	0.82
5	Xinjianghai River	Changle Gate (on the gate) water level station	0.70	12	Haimen River	Haimen water level station	0.65
6	Ruhai Canal	Haian (pass) water level station	0.79	13	Nanling River	Xiaoyangkou (on the gate) water level station	0.33
7	Jiaogang River	Banjing water level station	1.09	Remarks: The water level base adopts the national elevation of 85			

4 Methods and results of the ecological water level (flow) assessment

According to the "Technical Guidelines for Monitoring and Evaluation of Ecological Water Level (Flow) (Trial)" issued by the Jiangsu Provincial Department of Water Resources, the duration of river evaluation is daily. The guarantee rate of river ecological water level (flow) is the percentage of the number of samples whose daily average water level (flow) is greater than or equal to the guarantee target in the evaluation period to the total number of samples in the evaluation period. It is generally assessed quarterly and annually. In 2021, the daily average water levels of the 13 rivers all met the minimum ecological water level requirements, and the water level compliance rates were 100%. The minimum water level value of each river control section in 2021 was greater than the determined value of the ecological water level.

Table 3 Comparison between the ecological water level and the annual minimum water level in the control section of each river.

River name	Control section	Ecological water level(m)	Lowest water level in 2021(m)
Jiuwei Port River, Yaowang Port River	Shigang water level station	1.04	1.793
Tongqi Canal, Xinjianghai River	Changle Gate (on the gate) water level station	0.70	0.903
Bencha Canal, Beiling River, Nanling River	Xiaoyangkou (on the gate) water level station	0.33	1.280
Ruhai Canal	Haian (pass) water level station	0.79	1.894
Tonglu Canal	Huolong water level station	1.03	1.653
Jiaogang River	Banjing water level station	1.09	1.922
Tongyang Canal Nantong Section	Dingyan water level station	0.86	1.837
East section of Rutai Canal	Juegang water level station	0.82	1.343
Haimen River	Haimen water level station	0.65	1.530

5 Suggestions for ecological water level (flow) control

Although we used the annual minimum water level method to calculate the ecological water level of the river, and the ecological water level also met the requirements after evaluation, the algorithm of the annual minimum water level method itself is relatively simple, and does not involve the hydrological change and ecological response mechanism, and the scientificity of the method is insufficient. The ecological base flow target of rivers and lakes is determined by factors such as the ecological rhythm of rivers and lakes, protection of rivers and lakes, and the degree of development and utilization of water resources. According to the new ideas of water control in the new era, the management and control of river ecological water level (flow) should be considered in the overall situation of water conservancy reform and development.

Taking the overall planning of life, production and ecology as the core, optimize and integrate all elements of the whole process of river and lake ecological flow management and control, such as theoretical methods, technical systems, and management mechanisms (Zheng, 2020), to form a more scientific and reasonable system of the ecological water level (flow) management and control.

5.1 Find out about clean water resources and water ecology

The rivers in Nantong belong to two major river systems, the Yangtze River and the Huaihe River. There are important wetlands, and unique and rare fishes in the rivers of the Yangtze River Basin. The main focus of the rivers in the Huaihe River Basin is to maintain river channels and maintain ecosystem health. Finding out the ecological background of Qingshui, especially the distribution of ecologically sensitive areas, can provide support for determining the ecological water level (flow) target scientifically.

5.2 Determine ecological base flow (water level) targets scientifically

Combined with the actual situation of Nantong rivers, on the basis of fully investigating and monitoring the existing water ecology, the mobilization and operation of various water conservancy projects, and the seasonal water demand of the river, partition, classify, and select appropriate ecological base flow (water level) calculation methods, such as hydraulic method, habitat simulation method and overall analysis method, etc., to determine the target value of river ecological base flow (water level) scientifically.

5.3 Improve monitoring and early warning mechanisms

At present, there are few real-time flow monitoring facilities in rivers in Nantong City. Combined with the layout of hydrological sites and gate and dam projects, ecological base flow (water level) monitoring facilities should be installed in important control sections to monitor the water level of key river sections on a daily basis and incorporate them into the water resources monitoring system. Once the monitoring information triggers the early warning threshold, emergency response will be initiated (Wang et al., 2019).

5.4 Improve the supervision and assessment mechanism

When determining the ecological base flow (water level) control objectives of key rivers, formulate the ecological base flow (water level) guarantee plan of key rivers with "one river, one policy", determine the assessment section, clarify the management and control responsibilities, and simultaneously implement water volume scheduling, early warning management and control, and water management and other safeguard measures (Zhang et al., 2019; Lin et al., 2020), further strengthen supervision, improve safeguard measures, and establish a sound evaluation and assessment mechanism.

6 Conclusion

This paper introduces the recent work of river ecological water level (flow) determination in Nantong City, and evaluates the currently determined ecological water level value. The guarantee rate is 100%, which meets the requirements of ecological management and control. However, the annual minimum water level method is relatively simple and has a single factor. It is necessary to further explore the ecological background of clean water resources and water resources based on the actual situation of the rivers in the river network area of the Nantong Plain, to select the appropriate ecological flow rate (water level) calculation method, and to determine the target value of river ecological base flow (water level) scientifically. The management and control of river ecological base flow is a brand-new task that requires continuous exploration and innovation (Luo et al., 2020; Peng et al., 2020). Guided by the water control ideas of "water saving priority, space balance, systematic governance, and two-handed efforts", we must adhere to "determined by water and acted according to the amount of water", and coordinate the water demand for "living, production, and ecology". We will promote the management and control of ecological base flow (water level) comprehensively and orderly , increase the ecological protection and restoration of rivers and lakes, continue to improve the ecological conditions of rivers and lakes, and provide water resources for the construction of beautiful Nantong and the high-quality economic and social development.

References

Dong, Z.R., Zhang, J., Zhao, J.Y., 2020. The scientific connotation of ecological flow. China Water Resources, (15):15-19.

Lin, Y.Q., Chen, Q.W., 2020. Research on issues related to ecological flow assurance. China Water Resources, 897(15): 26-28,19.

Li, Y.Y., Liao, W.G., Zhao, Z.N., et. al., 2020. General ideas and countermeasures to strengthen the management and control of river and lake ecological flow in the new era. China Water Resources, (15): 12-14.

Luo, H., Huang, L., Zhang, Q., 2020. Reflections on the goal of ecological flow assurance control and dispatch. Water Conservancy Planning and Design (6): 29-31.

Peng, W.Q., 2020. Analysis of five key issues of ecological flow. China Water Resources, 897(15): 20-25.

Tharme, R.E., 2003. A global perspective on environmental flow assessment: emerging trends in the development and application of environmental flow methodologies for rivers. River Res. Appl, 19(5-6): 397-441.

Wang, J.P., Li, F.P., Sun, J., 2019. Understanding and thinking about the guarantee of ecological flow in rivers and lakes. Water Conservancy Economy (4): 9-12.

Zhang, H.B., Yin, X., Li, W., 2019. Research on the countermeasure system of ecological flow protection of rivers and lakes in my country. Water Conservancy Economy (4): 13-16.

Zhang, Y., Zhang, S.T., 2021. Discussion on the determination and control measures of ecological flow of key rivers in Nantong City. Water Resources Development and Management, 70(11): 51-55.

Zheng, Z.Z., 2020. The practice of establishing a river and lake ecological flow guarantee system in Jiangsu Province. China Water Resources, 897(15): 66-67.

In-situ bioremediation of pollutants in Ghana, South Africa, Nigeria, and Egypt (Africa): A critical review

Maxwell Addae[1], Desmond Ato Koomson[2], Williams Kweku Darkwah [3]

[1] College of Civil and Transportation Engineering, Hohai University, Nanjing, China. e-mail: ingmaxwelladdae@gmail.com

[2] Key Laboratory of Integrated Regulation and Resource Development on Shallow Lakes, Ministry of Education, Environmental Engineering Department, College of Environment, Hohai University, Nanjing, China. e-mail: descy06@yahoo.com

[3] Research Center for Environment and Society, Department of Sociology, School of Public Administration, Hohai University, Nanjing, China. e-mail: williamsdarkwakwaku@yahoo.com

Abstract: Bioremediation, a new and exciting research field, is the environmental restoration process of making use of microorganisms to break down hazardous waste by speeding up the natural abilities of the microbes. The increase in regional pollution and the application of bioremediation technology have become of increasing global interest. A relatively new concept is the in-situ bioremediation applications in hazardous waste treatment. It is a fast-thriving technology in environmental administration where there are several accounts of in-situ bioremediation application domains in contaminated areas. Researchers in this new field hope it can be implemented in restoring all the different parts of the environment since there are microbes in almost every corner of our environment. Here, this critical review assesses the most contemporary advances in the in-situ bioremediation strategies and their function in some African countries. These four major countries, Ghana, South Africa, Nigeria, and Egypt, were selected due to their establishment as key geo-economical locations, the massive waste quantities they produce, and the unique in-situ bioremediation strategies implemented in their waste management system. This review further highlights novel strategies for remediation technology and then emphasizes the illustrated concepts for enhancing the environmental protection using in-situ bioremediation strategies. Researchers and engineers are required to be advised about relevant management and environmental evaluations that may warrant potential research into the production of suitable energy, oil, wastewater management, and environmental purification mechanisms. In-situ bioremediation technology has shown its capabilities as being among the best candidates suitable for environmental treatment. Further researches are essential to make full utilization of in-situ bioremediation technology. Hence, this review is significant for the considerable advancement of bioremediation technology.

Keywords: In-situ bioremediation; Africa; Polycyclic aromatic hydrocarbons; Wastewater treatment

1 Introduction

A worsening form of environmental pollution has been caused by the expansion of the populace and disparate anthropogenic actions. According to Kabanza and the team (Kabanza et al., 2013), in general, a huge populace imposes a strain on land-dwelling, which leads to the destruction and deterioration of nature and thus humanity's impoverishment. The bulk of anthropogenic events contributes to pollutant generation. These contaminants, both biological and non-natural, settle mainly in landfills and sediments.

For persistent organic and inorganic contaminants, sediments serve as sinks and secondary sources of contamination, serving as risks to the well-being of organisms inhabiting or feeding in those habitats (Cachot et al., 2007). Owing to the high hydrophobic nature and low degradation rate of these contaminants, in the aquatic systems (Perelo, 2010), solid-phase particulate matter is often adhered to and deposited into marine sediments (Hassan et al., 2018; Vane, Harrison, & Kim, 2007; Cuiping Wang, Sun, Chang, Song, & Qin, 2011; K. Zhang, Zhang, Li, & Zeng, 2011), which cause continuous particle binding, and sediment accumulation (Grosser, Friedrich, Ward, & Inskeep, 2000; Meng & Chi, 2015). Changes in environmental conditions leading to pollutant re-suspension in most African countries have been connected to secondary sediment emissions in aquatic ecosystems (Lu, Zeng, Liao, & Tong, 2012). Therefore sediments were identified as an essential reservoir and alternative causes of contamination in Africa (He & Chi, 2016). At present solid waste is disposed of at waste disposal sites in Egypt and these sites have critical recycling, processing, or reuse capacity (New Center for Integrated Studies of Land & Environment (NILE), 2013). Plastics, paper, and metals as solid waste under recycling are included in a 2013 report on recycled dry waste (New Center for Integrated Studies of Land & Environment (NILE), 2013).

However, by not collecting wet organic waste types that contribute to about 60% of total waste in Egypt (New Center for Integrated Studies of Land & Environment (NILE), 2013), many challenges remain outstanding. The 2013 year-end announcement on solid waste administration in Egypt by the New Center for Integrated Studies of Land & Environment (NILE) showed that municipal solid waste and agricultural waste generated in Egypt in 2012 tallied approximately 21 million tons and 30 million tons respectively (New Center for Integrated Studies of Land & Environment (NILE), 2013). In 2012, the total solid waste produced in Egypt was estimated at 89.28 million

tons (New Center for Integrated Studies of Land & Environment (NILE), 2013).

The most important environmental factor impacting Nigeria's urban and rural spaces is solid waste management. Nigeria is among the chief solid waste producers in Africa, with more than 170 million population. With each day that goes by, the solid waste volumes generated in Nigeria increase at an alarming rate, amid many policies and regulations. Nigeria in a year can produce more than 32 million tons of solid waste with only 20%–30% gathered for analysis. These figures suggest the urgency for more effective and efficient treatment of waste, such as bioremediation. These four major nations, Ghana, South Africa, Nigeria, and Egypt, are the continent's largest producers of solid waste. Their geo-economic relevance within Africa (i.e. Ghana and Nigeria to the West, Egypt to the East, and South Africa to the South) and their introduction of unique in-situ waste management bioremediation strategies have made these nations a critical priority for this study.

The term "bioremediation" is used to define the system of utilizing microorganisms purposefully to break down or remove hazardous components or waste from the environment (Brigmon, Camper, & Stutzenberger, 2002). To boost removal performance for a range of treatments and to curtail the biological clock costs of a restoration program. Bioremediation is a dependable and versatile technology (Molnaa, 1999). While a relatively recent idea, the implementation of bioremediation in hazardous waste treatment is becoming a rapidly developing environmental protection technology. Various inquiries have been organized on the use of polluted sites for bioremediation (Gavrilescu, 2004; Lavrova & Koumanova, 2011; Mittal & Singh, 2009; Seo, Keum, & Li, 2009; Yelton et al., 2013; Z. Zhao, Qin, Xia, Zhang, Mela, et al., 2019). Bioreactors, land farming, bioventing, biofilters, bioaugmentation, biostimulation, intrinsic bioremediation, composting, pumping, and curing are all examples of bioremediation processes (Boopathy, 2000). Industrial wastewater is created by mixing organic and inorganic contaminants and also discharging heavy metals as well as chromium, copper, cadmium, lead, and selenium. This industrial sewerage, comprising toxic metals, is periodically released into the land space without due treatment, contributing to a significant socio-environmental crisis worldwide (Gavrilescu, 2004; J. Wang & Chen, 2006). These are harmful contaminants that are not degradable. (Modoi, Roba, Torok, & Ozunu, 2014; Pavel, Diaconu, Bulgariu, Statescu, & Gavrilescu, 2012); thus they are stored in the food chain of their tenacity in nature. These contaminants reach dangerous levels in living systems over time, causing many diseases which include lung and digestive tract inflammation and cancer, low plant growth rates and animal death, and other health changes (Cheung & Gu, 2007; Orozco, Contreras, & Zaritzky, 2008).

In this critical review, some modern advances in the in-situ bioremediation strategies and their utilization in some African countries in the previous years are well presented. This review deliberates on the novel approaches for remediation technology and then emphasizes the concepts of enhancing the environment's protection using bioremediation strategies. Next, the general overview of bioremediation systems in Ghana, Nigeria, Egypt, and South Africa is summarized. Also, the applications, research challenges in bioremediation, plus perspectives in future research are advocated.

2 Polycyclic aromatic hydrocarbons (PAHs) as a pollution indicator in Africa

The global increase in industrial development, specifically in Africa, has become closely linked with severe complications of environmental pollution by hydrocarbons. Due to urbanization and industrial waste, polycyclic aromatic hydrocarbons (PAHs) are becoming increasingly pervasive contaminants in Africa's ecological space (Meng, Huang, Liu, & Chi, 2015). Several researchers have conducted their studies on soil PAHs (Nam, Song, Eom, Lee, & Smith, 2003) (Ma et al., 2005) (H. B. Zhang, Luo, Wong, Zhao, & Zhang, 2006) and sediments (Soclo, Garrigues, & Ewald, 2009) (Boonyatumanond, Wattayakorn, Togo, & Takada, 2006), and they can act as useful indicators of PAH pollution and risks for human exposures in Africa.

Soil is found to be the major environmental PAH sink (Yin, Jiang, Yang, Bian, & Wang, 2008) since these compounds are sparingly water-soluble, non-degradable, and readily absorbed by soil particles (Tang, Tang, Zhu, Zheng, & Miao, 2005). PAH sources are diverse and varied, ranging from domestic cooking, vehicular combustion of gasoline, coal usage by industrial plants and residences (Peng et al., 2011, 2013), coke products, creosote, and petroleum (Huang, El-Alawi, Penrose, Glick, & Greenberg, 2004) to a volcanic eruption, forest fires, and formation of sedimentary rocks (Zhen Wang, Chen, Yang, Qiao, & Tian, 2007). PAHs ingested into soil biological elements (Yin et al., 2008) (Chen, Zhang, Zhang, Li, & Zhou, 2018) by means highlighted above can then enter the water, atmosphere, and other medium and cause secondary pollution (Sarria-Villa, Ocampo-Duque, Páez, & Schuhmacher, 2016).

Some researchers have documented the existence of PAHs in the debris of lakes, rivers, and seas (Bouloubassi, Fillaux, & Saliot, 2001; Ghosh, Gillette, Luthy, & Zare, 2000; He & Chi, 2016) in African countries. Also, other studies have pointed out sediments as the second-most robust origin of PAHs after soils (Cachot et al., 2007; Z. Yang, Feng, Niu, & Shen, 2008; Z. Zhao, Qin, Xia, Zhang, Margaret, et al.,

2019) and 3-rings PAHs (e.g., phenanthrene) and 4-rings PAHs (e.g., pyrene) were mainly observed (Hassan et al., 2018; Y. Lin et al., 2016).

Most domestic effluents from urban areas in Africa are either released raw or after inadequate treatments into receiving nearby water bodies, commonly rivers that flow through large industrial or urban areas (Souza, Dziedzic, Cubas, & Maranho, 2013), hence polluting aquatic systems. Industrial and urban discharge, oil spills, atmospheric deposition, and fossil fuel burning are all part of the common pathways through which PAHs enter the aquatic ecosystem (Heemken, Stachel, Theobald, & Wenclawiak, 2000; Y. Lin et al., 2016), and get distributed into seawater, sediments, and organisms (Hong et al., 2016) (Tongo, Ezemonye, & Akpeh, 2017) (Xiang et al., 2018). Since PAHs are toxic, persistent, and may bio-accumulate in aquatic species, they have the potential to be transported over long distances and hence become widely distributed (Mari, Harrison, Schuhmacher, Domingo, & Pongpiachan, 2010). Benthic organisms (e.g., muscles, lobsters, clams) that are included in the human diet consume PAHs that are in sediments, thus exposing humans to sedimentary PAHs directly or indirectly when large predators (e.g., fish and squid), that also form part of the human diet, consumed these organisms (Abdel-Shafy & Mansour, 2016).

Densely populated cities are often accompanied by increased household garbage production, industrial wastes, and traffic pollution that cause an increase in the presence of PAHs and other contaminants by gradually being integrated into the soils within urban areas through the dry and wet mediums (Chun hui Wang et al., 2015). Anthropogenic factors are responsible for the higher concentration of PAHs in cities or bigger communities, while natural factors are mainly responsible for remote areas (Jiang et al., 2009; H. B. Zhang et al., 2006).

PAH soil pollution in Africa has created awareness due to its massive industrialization and urbanization over the past decades (Peng, Wang, Zhao, & Chen, 2016; Rose et al., 2015; X. Yang et al., 2015). Studies on PAHs pollution in soils from three major countries in Africa (namely, Ghana, South Africa, and Nigeria) characterized by a dense population, accelerated industrialization and urbanization, high rate of traffic congestion and large plants in the manufacturing sector have all reported severe environmental problems (Jiang et al., 2009; Liu et al., 2018; Tang et al., 2005; Chun hui Wang et al., 2015; Yin et al., 2008). Ignition of coal and fossil fuels, vehicular pollution, industrial processing, and coal tar (Callén, López, Iturmendi, & Mastral, 2012; Masih & Taneja, 2006; Nam et al., 2003; Orecchio, 2010; Peng et al., 2011; Wu et al., 2018), chemical production and oil leaks (Callén et al., 2012; Orecchio, 2010), solid waste emissions, and water irrigation (Yin et al., 2008)

were revealed as primary sources of PAHs in urban cities. Urban soils contaminated with pollutants directly influence the health of the entire population because pollutants are easily transferable through inhalation, ingestion, or dermal contact (Berretta, Bernardi, & Mercuri, 2000).

3 Remediation strategies

In our rivers, lakes, and seas, contaminants have polluted much of the sediments. Contaminated sediment can be associated with chronic and acute impacts on marine life (Margesin & Schinner, 2001). Sediments also constitute a significant source of bioaccumulative and recurrent hazardous chemicals, which may pose threats to ecological and human health.

These sediments, when polluted, subsequently become a source of pollution by chemical adsorption or ingestion of particles by biota. Sometimes, waves and high flows also disrupt and mix the elemental debris into the surrounding water, thereby increasing the contaminants released from the sediment into the overlying water. The remediation of polluted sediments has thus created a great deal of scientific and public interest worldwide, and different remediation strategies have been developed (D. Lin, Cho, Werner, & Luthy, 2014).

4 Principles of in-situ bioremediation technology and its strategies

Soil is often polluted by hydrocarbons such as gasoline, petroleum, and asphalt, and by recalcitrant polycyclic aromatic hydrocarbon (PAH) which results in a decrease in agricultural capacity over damages to soil worth, leaching, and erosion (Onwurah, Ogugua, Onyike, Ochonogor, & Otitoju, 2007; Otitoju, Onwurah, Otitoju, Ndem, & Uwah, 2011).

Since the most common physicochemical remediation path (evaporation, dissolution, usage of emulsifiers/chemical dispersants, and photo-oxidation) for these toxic waste tend to be eco-hazardous, bioremediation has been more promising (Admon, Green, & Avnimelech, 2001).

Bioremediation depends primarily on the mobilization of indigenous microorganisms' metabolic ability to degrade contaminants into less poisonous substances (Atlas & Bartha, 1973). This method thrives on the probability of the potential of these microbes to secrete different catabolic enzymes needed for the conversion to an environmentally acceptable level of precarious organic pollutants. Bioremediation is cost-effective, environmentally friendly, and can result in a significant reduc-

tion in the volume of pollutants.

The processes may take longer and are less predictable than conventional methods. However, if nutrients such as nitrate, phosphate, and microelements remain abundant, the microorganisms can continue working on the hydrocarbons adequately and will remain embedded in the polluted world (Seklemova, Pavlova, & Kovacheva, 2001). Many approaches have been developed to help sustain the supply of these essential nutrients. That includes the use of synthetic fertilizers, excrement of chicken, shells of periwinkle, compost products, liming, and soil cultivation (Ijah & Antai, 2003; Orji, Ibiene, & Dike, 2012). Inorganic fertilizers as a nutrient origin have been widely rolled out due to increased costs of remediation, soil, and plant toxicity, and the possibility of eutrophication, especially in the marine ecosystem. Some researchers are still of the view that the use of inorganic fertilizers can be beneficial. Bioremediation technology employs the following strategies:

1. Monitored natural recovery (MNR)
2. Biostimulation
3. Bioaugmentation
4. Phytoremediation

5 The Progress of in-situ bioremediation technology in Africa.

In-situ Bioremediation, compared to other known techniques for crude oil remediation, and polluted soil remediation such as physical isolation, degradation of chemicals, and photo-degradation, is a more attractive technique and is desired because of its comparative efficacy, advantages of low cost, and eco-friendliness (Perelo, 2010; Peter, 2011). In comparison to in-situ bioremediation, some other approaches yield byproducts that are equally harmful to the environment after they have successfully removed the contaminants they were intended to remove (Okoh & Trejo-Hernandez, 2006; Peter, 2011). In contrast, the bioremediation process can detoxify crude oil contaminants and result in the effective extraction of pollutants by removing them rather than moving them to other media (Okoh & Trejo-Hernandez, 2006; Peter, 2011). Environmental pollution is increasingly becoming a critical issue in Africa (Rizzo et al., 2016). Some researchers have shown bioremediation's effectiveness in the recovery of contaminated coastal environments, especially in Africa (Brown et al., 2017). Several studies concentrated in some countries in Africa such as Ghana, Nigeria, South Africa, Egypt, and Tanzania have shown how in-situ bioremediation technology is very efficient (Brown et al., 2017; Okoh & Trejo-Hernandez, 2006; Perelo, 2010; Peter, 2011).

5.1 In-situ bioremediation in Nigeria

A seminal report, prepared by UNEP in 2011, about the effect of oil on the environs of Ogoniland, Nigeria, demanded immediate recovery, beginning from Ogoniland, of the polluted ecosystem of the Niger Delta, Nigeria (UNEP, 2011). With a restoration program initiated in 2016, the government indicated a reinforced commitment to the restoration of the polluted environment in the Niger Delta (K. Sam & Zabbey, 2018; Kabari Sam, Coulon, & Prpich, 2017).

Over five decades, the advancement and extraction of crude oil have been the Nigerian economy's lifeline (Oghenero Okumagba & Okereka, 2013; OPEC, 2017). The region of the Niger Delta, which holds large oil deposits, is known to produce natural gas (192 trillion standard cubic feet) and oil (37.4 billion barrels), apart from being among the world's most biologically complex ecosystems (Oghenero Okumagba & Okereka, 2013; OPEC, 2017). A region of 112,000 km^2 is covered by the Niger Delta and covers several ecologically sensitive regions (Oghenero Okumagba & Okereka, 2013; OPEC, 2017).

Oil spills are reported to cause contamination of food chains and essential habitats that sustain life, including fish ponds, mangrove habitats, and streams and rivers, which makes the leakage of oil a significant issue for residents (Chinweze et al., 2012). The impact is people's deprivation of cultural and environmental benefits (Fentiman & Zabbey, 2015). Subsequently, there are apparent declines in other environmental systems in the country, such as timber production sites, fish breeding grounds, and mangrove forests (Feka & Morrison, 2017). Land pollution from oil production has numerous probable human health-related effects like cancer, congenital disabilities, mutations in genetics, and deformities in reproduction (Heubeck et al., 2003; Léopold et al., 2008; Park & Park, 2010), aside from the ecological effect, e.g., destruction of forest and wetland areas of mangroves; contamination of water (Elum, Mopipi, & Henri-Ukoha, 2016; Inam et al., 2016; John, Ntino, & Itah, 2016; Zabbey & Uyi, 2014).

A performance study of *Pseudomonas aeruginosa* on raw and treated Escravos of Nigeria has been done by researchers. As a soil contaminant, light crude oil can detail its efficacy and facilitate the use of this microbial pressure as an inexpensive and viable strategy of bioremediation (Ibrahim, Shuaibu, & Abdulsalam, 2016; Oluwafemi S. Obayori, 2012).

UNEP's (2011) study on Nigeria acknowledged current technologies being used in the regeneration of polluted land (UNEP, 2011). That being said, many of these techniques may leave environmental footprints, such as confinement, air stripping,

fixation, and incineration (Hou & Al-Tabbaa, 2014; Hou, Al-Tabbaa, & Guthrie, 2014), denying access to agricultural land and accelerating emissions of greenhouse gases (Hou & Al-Tabbaa, 2014; Hou et al., 2014).

Zabbey & Uyi's (2014) case studies and other studies by Wang et al. (2016), Abdulsalam et al. (2011), Adams et al. (2017), Rizzo et al. (2016), and Brown et al. (2017), revealed bioremediation efficiency in remediating coastal environments (Abdulsalam, Bugaje, Adefila, & Ibrahim, 2011; Adams, Niyomugabo, & Sylvester, 2017; Brown et al., 2017; Rizzo et al., 2016; Wang, Kuo, Hong, Chang, & Kao, 2016; Zabbey & Uyi, 2014). Bio-remediation is both economically feasible and socially appropriate. As a result of minimal environmental impact, it has the potential for jobs to be created and access to farmland is permitted and an environmentally friendly legacy is left behind.

5.2 In-situ bioremediation strategies in South Africa

Alegbeleye et al. (2017) run an experiment to analyze the event and ability of PAH degrading microorganisms that degrade acenaphthene and fluorine (PAH compounds) in the Western Cape as well as South Africa, two river systems (Alegbeleye, Opeolu, & Jackson, 2017). The findings showed the restoration of *Raoultella ornithinolytica*, *S. marcescens*, and *B. megaterium* polluted aquatic ecosystems when used on a more extensive and commercial scale, whereas *A. hydrophila* was unusable due to safety concerns, bigger commercial quantities needed to replenish PAH polluted river systems. It has also been shown to cause diseases in commercially important organisms like fish (Austin & Austin, 2012; Janda & Abbott, 2010). These researchers discovered that isolated PAH degrading microorganisms greatly decreased acenaphthene and fluorine concentrations throughout this analysis and can be used to bio-remediate PAH on a larger scale for contaminated water systems.

In South Africa, Sthembile and research colleagues investigated nitrosamines' prevalence, particularly N-nitrosodimethylamine (NDMA), within three separate water provisions. They made use of chloramines as cleaning agents and chlorine was connected to an upsurge of NDMA in the treatment of drinkable water (Kim and Clevenger, 2007; Alt, Sireesha, Akg, Sankar, & Lakshmi Tripura, 2014). Collected water tested and sourced within the treatment plant indicated the presence of NDMA. Fig. 1 shows the GC–MS water sample chromatograms obtained following chloramination and at the channels of distribution. High levels of NDMA after chloramination may indicate DMA presence, through which the response with monochloramine forms NDMA (Choi & Valentine, 2002). For a water sample, the aromatic identification and determination of compounds such as nitrosamines, limits of up to one part per bil-

lion (ppb), and gas chromatography (GC)/flame ionization detector (FID) can serve as the means of used to carry out the process (de Nardi, Zaiat, & Foresti, 2007; Fischer & Werner, 2000; Fraile et al., 2002; Zhendi Wang, Li, Fingas, Sigouin, & Ménard, 2002), GC/photoionization detector (PID) (Cunningham, Rahme, Hopkins, Lebron, & Reinhard, 2001; Dórea et al., 2007), GC/mass spectrometer (MS) (Disdier, Arfi, Pastor, Pauli, & Portugal, 1999) or GC/solid-phase microextraction (SPME) (Djozan, Pournaghi-Azar, & Bahar, 2004; Karac onji, Skender, & Karac 2006; Lee, Chang, & Dou, 2007) via headspace or by purging and trapping (Rosell et al., 2005; Rosell et al., 2003) depending on sample preparation methods. Studies performed in several research laboratories have demonstrated b-CD polymers' efficiency in removing organic compounds from samples of water (Mhlanga, Mamba, Krause, & Malefetse, 2007; Y. Wang et al., 2004).

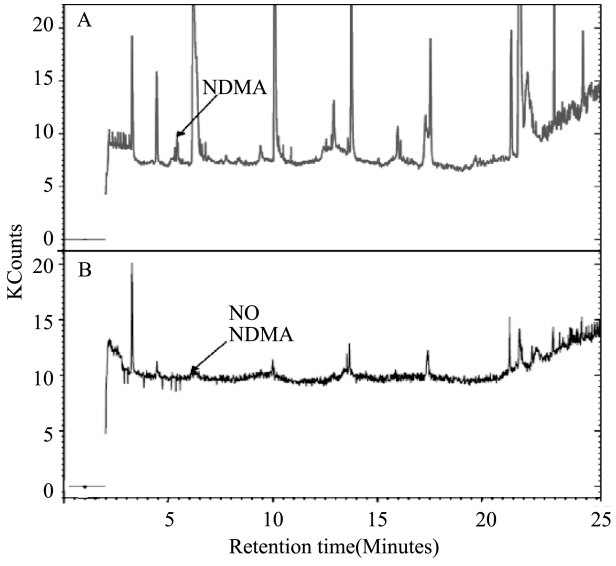

Fig. 1. GC-MS chromatograms of water samples containing NDMA collected from the distribution network at Bothaville: (A) before treatment and (B) reduced presence of NDMA after treatment.

Sthembile and the group detected a nearly 80% reduction in NDMA following polymer treatment (Mhlongo et al., 2009). The polymer showed the ability to extract NDMA and the potential, as seen in chromatograms, to absorb other species (Fig. 1B). Their conclusion from the studies was quantitative removal of NDMA (peak area-based) from water samples was performed, indicating the usage of nano-sponges in treating water could be used to mitigate trace pollutants such as NDMA (Mhlongo et al., 2009). Williams et al. (2014) noted the advanced biological management of the marine ecosystem with pollution as an economical and low-maintenance procedure (Williams et al., 2014), a bioreactor fixed-film pilot was intended for curtailing chro-

mium via a microbial population Enterobacter cloacae, Flavobacterium sp., and Ralstonia sp inclusive. The first up-scaled (24,000 L), is a practical illustration of a bioremediation system in South Africa which was an efficient biological Cr (VI) as represented in the research. It resulted in Cr (VI) (>99%) reduction. Slurry-phase, ex-situ system is another bioremediation strategy that controls the curing of soils in a bioreactor (Kulshreshtha, Agrawal, Barar, & Saxena, 2014).

5.3 The influence of bioremediation strategies in Tema Harbour and Adamus Resources Ltd. (ADL), Ghana

Chemical pollution, which is associated with ecological and socio-economic consequences such as the death of species, reduction of biodiversity, destruction of marine environments and contamination of food supplies, and deprivation of livelihoods as well as adverse effects on human health, is the main global environmental challenges in coastal marine ecosystems amongst other problems (Mestres, Sierra, Mösso, & Sánchez-Arcilla, 2010; Shahidul Islam & Tanaka, 2004). The organic pollutants of key interest as a result of their long-term environmental persistence, bioaccumulation along the food chain, long-range atmospheric transport, and adverse natural impacts such as endocrine interference, toxicity, genetic changes, reproductive abnormalities, and cancer are Polycyclic Aromatic Hydrocarbons (PAHs), dichlorodiphenyltrichloroethane (DDT), and hexachlorocyclohexane (HCH) (De Luca et al., 2004; King, Readman, & Zhou, 2004; Nyarko, Botwe, & Klubi, 2012; Shahidul Islam & Tanaka, 2004; X.-C. Wang, Zhang, & Chen, 2001; Willett, Ulrich, & Hites, 1998).

The coastal marine port of Ghana, Tema Harbour, lies along the Gulf of Guinea. It is an international harbour with significant fishing and shipping activities. Tema became Ghana's main industrial area, following the building of Tema Harbour in 1960 and the subsequent commencement of industrialization in the country. Tema's main industrial activities include: refining crude oil, smelting alumina, steel, paint, and manufacturing cement. Thus, anthropogenic activities from industrial, shipping, fishing, and other sectors have dominated Tema Harbour for nearly six decades.

Botwe and the team analyzed the pollution of DDTs, HCHs, and PAHs in sediments found in Tema Harbour (Ghana) and the related ecotoxicological threats (Botwe et al., 2017). Interpretations of DDTs, HCHs, and PAHs were by Soxhlet-extraction after Wang et al. (2001) and Fung et al. (2005), with a certain degree of changes (Fung et al., 2005; Wang et al., 2001). The foundational report indicated the presence of DDT, HCH, and the USEPA 16 priority PAHs (PAH16) in the sediments found in Tema Harbour. Different dispersion paths of ΣDDTs, ΣHCHs, and ΣPAHs in sediments were seen across the control sites: relatively more contamination by

ΣDDTs, ΣHCHs, and ΣPAHs, occurred at the most northeastern section of the harbour as indicated in Fig. 2.

Analysis of sediments polluted with PAHs to determine PAH distribution patterns has indicated less contamination by ΣPAH16 in the Main Harbour than those in the Fishing Harbour (see Fig. 3). Biodegradation of organic matter in sediments results from redox conditions (Caille, Tiffreau, Leyval, & Morel, 2003) and accumulates organic matter in sediments. A significant correlation (Maruya, Risebrough, & Horne, 1996; Wang et al., 2001; R. Yang, Jiang, Zhou, Yuan, & Shi, 2005) and a vigorous attachment of fine-grain carbon of organic background for organic contaminants and

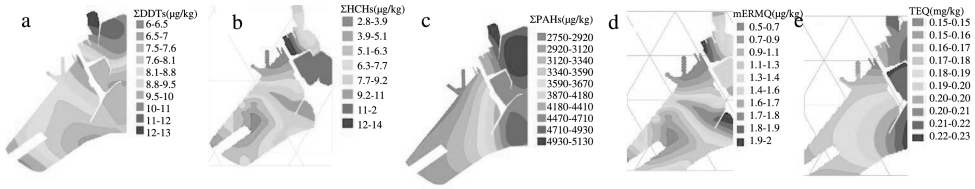

Fig. 2. Distribution patterns of (a) ΣDDTs, (b) ΣHCHs, (c) ΣPAHs, (d) mERMQ and (e) TEQ in Tema Harbour sediments.

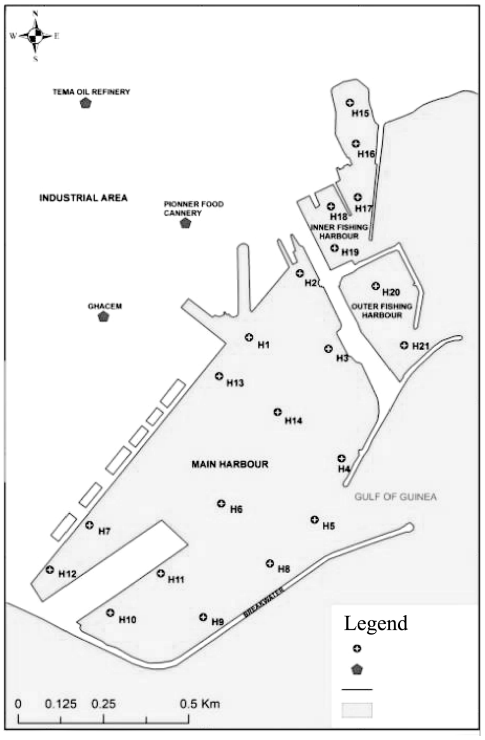

Fig. 3. Map of the Tema Harbour showing the monitoring stations. (Note: the Canoe Basin comprises H15-H17)

sediments (Hu et al., 2010; T. Lin et al., 2009) is required to normalize levels of organic contaminants using the TOC material to compare (Birch & Hutson, 2009; T. Lin et al., 2009). Botwe and group assessment on pollutant concentrations found that, γ-HCH in particular, is likely to pose high ecotoxicological risks in the harbour sediments (Botwe et al., 2017). Upon comparison with previous studies, their study points out a significant decrease in the levels of PAH pollution in Tema Harbour after the last big oil spill in 2007 as a result of the application of various bioremediation strategies employed by the Ghana government and other related agencies (Botwe et al., 2017).

Issah Abubakari also explored the application of bioremediation by Adamus Resources Ltd. (ADL), a mining-based establishment in Ghana (Western Region) as the critical method of treating soil contaminated with waste petroleum oil (Abubakari, 2013). The study involved the use of three separate biological nutrient substitutes, specifically Compost(C), Poultry droppings (PD), and natural Rubber processing sludge (RS), respectively, and three stages of nitrogen quantities of 0.2%, 0.4%, and 0.6%. Fundamental research to analyze the proportion of nitrogen and phosphorus in the soil was carried out and the three organic nutrient supplements showed the soils contained just 0.03% nitrogen and 0.12% phosphorus with a C∶N ratio of 80∶3, showing that the right amount of nitrogen is in deficiency by the soil for greater bioremediation to occur. Issah's conclusion was the addition of the organic nutrient supplements in the soil certainly aided the biodegradation of the petroleum hydrocarbons (Abubakari, 2013). In all three organic nutrient supplements, the 0.2 % N concentrations showed the best results and the poultry droppings were the best among the other modification products (Abubakari, 2013).

5.4 Application of in-situ bioremediation technology in Egypt

Oil spill pollution and remediation technologies such as bioremediation have increasingly gained global interest. To reduce hydrocarbon pollution, a significant source of environmental pollution, the production of extracellular bio-surfactant is among a few of the methods utilized to use microbes for degradation (Alt et al., 2014). Advances in this research line have significant usefulness for the preservation of our surroundings (Karsa, Bailey, Shelmerdine, & McCann, 1999; Meylheuc, Herry, & Bellon-Fontaine, 2001). Korayem and his team isolated the arid Egyptian soil Streptomyces interbreed, good in bio-surfactant output used for bioremediation (Korayem, Abdelhafez, Zaki, & Saleh, 2015). The impact of various hydrocarbons on bio-surfactant production has also been studied by other scientists (Chakraborty, Khopade, Kokare, Mahadik, & Chopade, 2009; Kokare, Kadam, Mahadik, & Cho-

pade, 2007).

Kokare et al. (2007) found that of all the oils and hydrocarbons tested, toluene (1% v/v) induced the highest bio-surfactant activity through Streptomyces sp. (Kokare et al., 2007). From the study, Korayem and the group suggested that treated molasses and peptone were the best carbon and nitrogen compounds added to starch nitrate medium compared to starch and KNO_3 to produce bio-surfactant (Korayem et al., 2015). Other physical and chemical parameters such as oxygen, temperature, and pH have been important to these variables due to their origins in carbon and nitrogen. Streptomyces sp. 5S, gotten from arid Egyptian soil, favoured molasses as a carbon source and peptone, as a nitrogen source, to produce bio-surfactant as reported by the study results.

Abo-State and group also separated indigenous bacterial species from infected samples of wastewater plus sludge with oil from petroleum belonging to Cairo Oil Refining Company (CORC), Mostorod, El-Qalyubiah, and Cairo, Egypt(Abo-State et al., 2018). Bacterial sp. of genera Achromobacter, Acinetobacter, Arthrobacter, Azoarcus, Brevibacterium, Cellulomonas, Corynebacterium, Flavobacterium, Marinobacter, Micrococcus, Nocardia, Ochrobactrum, Pseudomonas, Stenotrophomaonas, and Vibrio are accounted as hydrocarbon degraders (Chandra, Sharma, Singh, & Sharma, 2013; Foght, 2008; Mittal & Singh, 2009; Roy, Hens, Biswas, Biswas, & Kumar, 2002; Varjani, Rana, Jain, Bateja, & Upasani, 2015; Varjani & Upasani, 2016; Widdel & Rabus, 2001).

Naphthalene offers six intermediate products. Jia et al. (2008) have noted a pressure of Pseudomonas sp. that Naphthalene can reduce via the salicylate and phthalate channels.(Jia et al., 2008). Similar findings were recorded with Arthrobacter sp., although this strain or pressure is more described by its phthalic path than the salicylate path (Seo et al., 2009). In the biodegradation of Naphthalene by thermophilic Bacillus thermoleovorans, the role of both mechanisms was also suggested (Annweiler et al., 2000).

To deteriorate naphthalene to produce six transitional compounds. 1,2-Benzene dicarboxylic acid, 1, 2-Benzene dicarboxylic acid, Butyl-2, 4-dimethyl-2-nitro-4-pentenoate, 1-Nonen-3-ol, Eicosane, Nonacosane. Bordetella avium MAM-P22 was suggested after the GC/MS test was conducted. Abo-State and the team then concluded that isolated MAM-P22 was the best Naphthalene degrader.

1. Applications of in-situ bioremediations

Bioremediation, which includes employing microbes (bacteria and fungi) to convert pollutants into inert substances, has received growing publicity as an important biotechnological technique for the environmental cleanup of organic pollutants. It

presents numerous benefits, especially for diluted or evenly dispersed contaminants, over physical or chemical technologies. Bioremediation strategies are generally more advantageous than some means of treatment in the following aspects (Iwamoto & Nasu, 2001):

a. The processing speed can be changed from extremely aggressive to passive;

b. Incremental costs are lower than other alternatives for incorporating a bioremediation factor into most forms of treatments;

c. The method can be generalized from mass extraction to the creation of a movement barrier to fine grinding for a wide range of purposes;

d. With minimum site interruption, it can be achieved on-site;

e. It can be extended to pollutants that are concentrated or broadly diffused.

Despite the typical approval of bioremediation engineering it has its drawbacks and is also an immature technology for the removal of pollutants from the atmosphere. Heavy metals, radionuclides, some chlorinated compounds, and some chemicals have been found non-biodegradable. Additionally, achieving complete contaminant removal is not possible even though there may be a statutory authority beyond which rates of biodegradation are weak or marginal (Allard & Neilson, 1997).

2. Challenges and prospects in in-situ bioremediation technology

Studies on depletion of the substrate in combination with poisonous alternates and derivative products like salicylate and oxy-PAHs (PAH-ketones, quinones, and coumarins) are advanced as an explanation for a drastic decline in microbes populations (Bamforth & Singleton, 2005; Moscoso, Deive, Longo, & Sanromán, 2015; Moscoso, Teijiz, Deive, & Sanromán, 2012; Mrozik, Piotrowska-Seget, & Łabuzek, 2003). Such harmful intermediates and byproducts may have been processed and collected to induce bacterial death in the reactors.

Bacillus sp., *B. aryabhattai*, *B. marisflavi*, and *C. freundii* as isolates effectively deteriorated above 75% fluorene but did not sufficiently degrade acenaphthene and were therefore not perfect materials for the biodegradation process (Chenier et al., 2008). Because there is the same number of rings in both compounds, the explanation for this pattern cannot be confirmed. Neither compound could degrade some species of bacteria, and some were unable to withstand stress due to compound exposure. The reoccurrence of TCA would have been terminated for this metabolic rearrangement (Chenier et al, 2008). The metabolic network mentioned here enables the bacterium to generate energy, produce essential metabolites, and propagate with high levels of the compound when stressed.

While the potential for bioremediation is significant, its application has limitations, and only when sufficient attention is given to fundamental microbiological,

chemical, and engineering problems can these limitations be resolved. The following are some suggested solutions for the limitations in in-situ bioremediation:

- Accessibility and bioavailability of substrates to microorganisms
- The use of genetically engineered microorganisms
- The use of biostimulation and bioaugmentation
- The application of uses extracellular and cell-free enzymes

These proposed solutions are well documented and researched (Dey & Basak, 2015).

3. Conclusion

In-situ bioremediation, using microorganisms to efficiently remove on-site contaminants, is presumably lower cost, quicker and safer compared to traditional methods of treatment. This systematic review sums up the novel developments in the in-situ bioremediation strategies and their applications in some African countries to treat pollutants and environmental purifications. In-situ bioremediation technology has revealed its greatness by being among the best candidates suitable for environmental treatment. Hence, the considerable progress of in-situ bioremediation technology will progress soon. Given that, more studies are also necessary to make full use of in-situ bioremediation technology's excellent application strategies.

References

Abdel-Shafy, H. I., & Mansour, M. S. M., 2016. A review on polycyclic aromatic hydrocarbons: Source, environmental impact, effect on human health and remediation. Egyptian Journal of Petroleum, 25(1): 107-123. https://doi.org/10.1016/j.ejpe.2015.03.011

Abdulsalam, S., Bugaje, I. M., Adefila, S. S., & Ibrahim, S., 2011. Comparison of biostimulation and bioaugmentation for remediation of soil contaminated with spent motor oil. International Journal of Environmental Science and Technology. https://doi.org/10.1007/BF03326208

Abo-State, M. A. M., Riad, B. Y., Bakr, A. A., & Abdel Aziz, M. F., 2018. Biodegradation of naphthalene by Bordetella avium isolated from petroleum refinery wastewater in Egypt and its pathway. Journal of Radiation Research and Applied Sciences, 11(1): 1-9. https://doi.org/10.1016/j.jrras.2017.10.001

Abubakari, I., 2013. Effects of poultry droppings, compost & natural rubber sludge on bioremediation of petroleum hydrocarbon contaminated soil. 1-22.

Adams, F. V., Niyomugabo, A., & Sylvester, O. P., 2017. Bioremediation of crude oil contaminated soil using agricultural wastes. Procedia Manufacturing (7): 459-

464. https://doi.org/10.1016/j.promfg.2016.12.037

Admon, S., Green, M., & Avnimelech, Y., 2001. Biodegradation kinetics of hydrocarbons in soil during land treatment of oily sludge. Bioremediation Journal, 5(3): 193-209. https://doi.org/10.1080/20018891079285

Alegbeleye, O. O., Opeolu, B. O., & Jackson, V., 2017. Bioremediation of polycyclic aromatic hydrocarbon (PAH) compounds: (acenaphthene and fluorene) in water using indigenous bacterial species isolated from the Diep and Plankenburg rivers, Western Cape, South Africa. Brazilian Journal of Microbiology, 48(2): 314-325. https://doi.org/10.1016/j.bjm.2016.07.027

Allard, A.-S., & Neilson, A. H., 1997. Bioremediation of organic waste sites: A critical review of microbiological aspects. International Biodeterioration & Biodegradation, 39(4): 253-285. https://doi.org/10.1016/S0964-8305(97)00021-8

Alt, K., Sireesha, N. G., Akg, A., Sankar, G. G., & Lakshmi Tripura, A., 2014. Production optimization of rhamnolipid biosurfactant by streptomyces coelicoflavus (NBRC 15399 T) using Plackett-Burman design. European Journal of Biotechnology and Bioscience.

Annweiler, E., Richnow, H. H., Antranikian, G., Hebenbrock, S., Garms, C., Franke, S., ... Michaelis, W., 2000. Naphthalene degradation and incorporation of naphthalene-derived carbon into biomass by the thermophile bacillus thermoleovorans. Applied and Environmental Microbiology, 66(2): 518-523. https://doi.org/10.1128/AEM.66.2.518-523.2000

Appanna, V. D., & Pierre, M. S. T., 1996. Aluminum elicits exocellular phosphatidylethanolamine production in pseudomonas fluorescens. Applied and Environmental Microbiology, 62(8): 2778-2782. https://doi.org/10.1128/AEM.62.8.2778-2782.1996

Atlas, R. M., & Bartha, R., 1973. Stimulated biodegradation of oil slicks using oleophilic fertilizers. Environmental Science & Technology, 7(6): 538-541. https://doi.org/10.1021/es60078a005

Auger, C., Han, S., Appanna, V. P., Thomas, S. C., Ulibarri, G., & Appanna, V. D., 2013. Metabolic reengineering invoked by microbial systems to decontaminate aluminum: Implications for bioremediation technologies. Biotechnology Advances, 31(2): 266-273. https://doi.org/10.1016/j.biotechadv.2012.11.008

Austin, B., & Austin, D. A., 2012. Bacterial fish pathogens: disease of farmed and wild fish. https://doi.org/10.1007/978-94-007-4884-2

Bamforth, S. M., & Singleton, I., 2005. Bioremediation of polycyclic aromatic hydrocarbons: current knowledge and future directions. Journal of Chemical Technology & Biotechnology, 80(7): 723-736. https://doi.org/10.1002/jctb.1276

Berretta, N., Bernardi, G., & Mercuri, N. B., 2000. Alpha1-adrenoceptor-mediated excitation of substantia nigra pars reticulata neurons. Neuroscience, 98(3): 599-604. https://doi.org/10.1016/S0306—4522(00)00135-4

Birch, G. F., & Hutson, P., 2009. Use of sediment risk and ecological/conservation value for strategic management of estuarine environments: Sydney Estuary, Australia. Environmental Management. https://doi.org/10.1007/s00267—009-9362-0

Boonyatumanond, R., Wattayakorn, G., Togo, A., & Takada, H., 2006. Distribution and origins of polycyclic aromatic hydrocarbons (PAHs) in riverine, estuarine, and marine sediments in Thailand. Marine Pollution Bulletin, 52(8): 942-956. https://doi.org/10.1016/j.marpolbul.2005.12.015

Boopathy, R., 2000. Factors limiting bioremediation technologies. Bioresource Technology, 74(1): 63-67. https://doi.org/10.1016/S0960—8524(99)00144-3

Boro , M.-N., Micle, V., Flămînd, L., & Monica SUR, I., 2016. Phytoremediation planning in the case of former industrial sites. Studia Ubb Ambientum, LXI (1-2): 5-14. Retrieved from http://studia.ubbcluj.ro/download/pdf/Ambientum/2016_1_2/01.pdf

Botwe, B. O., Kelderman, P., Nyarko, E., & Lens, P. N. L., 2017. Assessment of DDT, HCH and PAH contamination and associated ecotoxicological risks in surface sediments of coastal Tema Harbour (Ghana). Marine Pollution Bulletin, 115(1-2): 480-488. https://doi.org/10.1016/j.marpolbul.2016.11.054

Bouloubassi, I., Fillaux, J., & Saliot, A., 2001. Hydrocarbons in surface sediments from the Changjiang (Yangtze River) Estuary, East China Sea. Marine Pollution Bulletin, 42(12): 1335-1346. https://doi.org/10.1016/S0025—326X(01)00149-7

Brigmon, R., Camper, D., & Stutzenberger, F., 2002. Bioremediation of compounds hazardous to health and the environment: An overview. Progress in Industrial Microbiology, 36(C): 1-28. https://doi.org/10.1016/S0079—6352(02)80005-4

Brown, D. M., Okoro, S., van Gils, J., van Spanning, R., Bonte, M., Hutchings, T., Smith, J. W. N., 2017. Comparison of landfarming amendments to improve bioremediation of petroleum hydrocarbons in Niger Delta soils. Science of The Total Environment (596-597): 284-292. https://doi.org/10.1016/j.scitotenv.2017.04.072

Cachot, J., Law, M., Pottier, D., Peluhet, L., Norris, M., Budzinski, H., & Winn, R., 2007. Characterization of toxic effects of sediment-associated organic pollutants using the λ transgenic medaka. Environmental Science & Technology, 41 (22): 7830-7836. https://doi.org/10.1021/es071082v

Caille, N., Tiffreau, C., Leyval, C., & Morel, J. L., 2003. Solubility of metals in an anoxic sediment during prolonged aeration. Science of the Total Environment.

https://doi.org/10.1016/S0048—9697(02)00289-9

Callén, M. S., López, J. M., Iturmendi, A., & Mastral, A. M., 2012. Nature and sources of particle associated polycyclic aromatic hydrocarbons (PAH) in the atmospheric environment of an urban area. Environmental Pollution, 1-9. https://doi.org/10.1016/j.envpol.2012.11.009

Chakraborty, S., Khopade, A., Kokare, C., Mahadik, K., & Chopade, B., 2009. Isolation and characterization of novel α-amylase from marine Streptomyces sp. D1. Journal of Molecular Catalysis B: Enzymatic, 58(1-4): 17-23. https://doi.org/10.1016/j.molcatb.2008.10.011

Chandra, S., Sharma, R., Singh, K., & Sharma, A., 2013. Application of bioremediation technology in the environment contaminated with petroleum hydrocarbon. Annals of Microbiology, 63(2): 417-431. https://doi.org/10.1007/s13213—012-0543-3

Chen, Y., Zhang, J., Zhang, F., Li, F., & Zhou, M.,2018. Polycyclic aromatic hydrocarbons in farmland soils around main reservoirs of Jilin Province, China: occurrence, sources and potential human health risk. Environmental Geochemistry and Health, 40(2): 791-802. https://doi.org/10.1007/s10653—017-0024-5

Chenier, D., Beriault, R., Mailloux, R., Baquie, M., Abramia, G., Lemire, J., & Appanna, V., 2008. Involvement of Fumarase C and NADH Oxidase in metabolic adaptation of pseudomonas fluorescens cells evoked by aluminum and gallium toxicity. Applied and Environmental Microbiology, 74(13): 3977-3984. https://doi.org/10.1128/AEM.02702-07

Cheung, K. H., & Gu, J. D., 2007. Mechanism of hexavalent chromium detoxification by microorganisms and bioremediation application potential: A review. International Biodeterioration and Biodegradation. https://doi.org/10.1016/j.ibiod.2006.05.002

Chizoba, C., Gwen, A. O., & Chike, J., 2012. Oil and gas resources management and environmental challenges in Nigeria. Journal of Environmental Science and Engineering B, 1(4). https://doi.org/10.17265/2162-5263/2012.04.012

Choi, J., & Valentine, R. L., 2002. Formation of N-nitrosodimethylamine (NDMA) from reaction of monochloramine: a new disinfection by-product. Water Research, 36(4): 817-824. https://doi.org/10.1016/S0043—1354(01)00303-7

Cunningham, J. A., Rahme, H., Hopkins, G. D., Lebron, C., & Reinhard, M., 2001. Enhanced in-situ bioremediation of BTEX-Contaminated groundwater by combined injection of nitrate and sulfate. Environmental Science & Technology, 35(8): 1663-1670. https://doi.org/10.1021/es001722t

De Luca, G., Furesi, A., Leardi, R., Micera, G., Panzanelli, A., Costantina Piu,

P., & Sanna, G., 2004. Polycyclic aromatic hydrocarbons assessment in the sediments of the Porto Torres Harbor (Northern Sardinia, Italy). Marine Chemistry, 86(1-2): 15-32. https://doi.org/10.1016/j.marchem.2003.11.001

de Nardi, I. R., Zaiat, M., & Foresti, E., 2007. Kinetics of BTEX degradation in a packed-bed anaerobic reactor. Biodegradation, 18(1): 83-90. https://doi.org/10.1007/s10532—005-9038-2

Dey, A. N., & Basak, P., 2015. Microgrid from an Indian perspective. 2015 IEEE 9th International Conference on Intelligent Systems and Control (ISCO), 1-7. https://doi.org/10.1109/ISCO.2015.7282271

Disdier, B., Arfi, C., Pastor, J., Pauli, A. M., & Portugal, H., 1999. Analysis by GC-MS of monocyclic and polycyclic aromatic hydrocarbons in thermolysed waste products. Analusis, 27(3): 235-240. https://doi.org/10.1051/analusis:1999112

Djozan, D., Pournaghi-Azar, M. H., & Bahar, S., 2004. Modified polypyrrole with tetrasulfonated nickel phthalocyanine as a fiber for solid-phase microextraction. Application to the Extraction of BTEX Compounds from Water Samples. Chromatographia, 59(9-10). https://doi.org/10.1365/s10337—004-0222-z

Dórea, H. S., Bispo, J. R. L., Aragão, K. A. S., Cunha, B. B., Navickiene, S., Alves, J. P. H., … Garcia, C. A. B., 2007. Analysis of BTEX, PAHs and metals in the oilfield produced water in the State of Sergipe, Brazil. Microchemical Journal. https://doi.org/10.1016/j.microc.2006.06.002

Elum, Z. A., Mopipi, K., & Henri-Ukoha, A., 2016. Oil exploitation and its socio-economic effects on the Niger Delta region of Nigeria. Environmental Science and Pollution Research, 23(13): 12880-12889. https://doi.org/10.1007/s11356—016-6864-1

Fagervold, S. K., Watts, J. E. M., May, H. D., & Sowers, K. R., 2011. Effects of bioaugmentation on indigenous PCB dechlorinating activity in sediment microcosms. Water Research, 45(13): 3899-3907. https://doi.org/10.1016/j.watres.2011.04.048

Fathollahzadeh, H., Kaczala, F., Bhatnagar, A., & Hogland, W., 2015. Significance of environmental dredging on metal mobility from contaminated sediments in the Oskarshamn Harbor, Sweden. Chemosphere (119): 445-451. https://doi.org/10.1016/j.chemosphere.2014.07.008

Feka, Z. N., & Morrison, I., 2017. Managing mangroves for coastal ecosystems change: A decade and beyond of conservation experiences and lessons for and from west-central Africa. Journal of Ecology and The Natural Environment.

Fentiman, A., & Zabbey, N., 2015. Environmental degradation and cultural erosion in Ogoniland: A case study of the oil spills in Bodo. The Extractive Industries and

Society, 2(4): 615-624. https://doi.org/10.1016/j.exis.2015.05.008

Fischer, A., & Werner, P., 2000. Phenylacetylene as a new surrogate standard for the determination of BTEX by GC/FID. Fresenius' Journal of Analytical Chemistry, 368(4): 424-425. https://doi.org/10.1007/s002160000479

Foght, J., 2008. Anaerobic biodegradation of aromatic hydrocarbons: pathways and prospects. Journal of Molecular Microbiology and Biotechnology, 15(2-3): 93-120. https://doi.org/10.1159/000121324

Fonti, V., Beolchini, F., Rocchetti, L., & Dell'Anno, A., 2015. Bioremediation of contaminated marine sediments can enhance metal mobility due to changes of bacterial diversity. Water Research (68): 637-650. https://doi.org/10.1016/j.watres.2014.10.035

Fraile, J., Niaerola, J. M., Olivella, L., Figueras, M., Ginebreda, A., Vilanova, M., & Barcela, D., 2002. Monitoring of the gasoline oxygenate MTBE and BTEX Compounds in groundwater in Catalonia (Northeast Spain). The Scientific World Journal (2): 1235-1242. https://doi.org/10.1100/tsw.2002.223

Fung, C. N., Zheng, G. J., Connell, D. W., Zhang, X., Wong, H. L., Giesy, J. P., ··· Lam, P. K. S., 2005. Risks posed by trace organic contaminants in coastal sediments in the Pearl River Delta, China. Marine Pollution Bulletin, 50 (10): 1036-1049. https://doi.org/10.1016/j.marpolbul.2005.02.040

Gavrilescu, M., 2004. Removal of heavy metals from the environment by biosorption. Engineering in Life Sciences, 4(3): 219-232. https://doi.org/10.1002/elsc.200420026

Ghosh, U., Gillette, J. S., Luthy, R. G., & Zare, R. N., 2000. Microscale location, characterization, and association of Polycyclic Aromatic Hydrocarbons on harbor sediment particles. Environmental Science & Technology, 34(9): 1729-1736. https://doi.org/10.1021/es991032t

Gidley, P. T., Kwon, S., Yakirevich, A., Magar, V. S., & Ghosh, U., 2012. Advection dominated transport of Polycyclic Aromatic Hydrocarbons in amended sediment caps. Environmental Science & Technology, 46(9): 5032-5039. https://doi.org/10.1021/es202910c

Grosser, R. J., Friedrich, M., Ward, D. M., & Inskeep, W. P., 2000. Effect of model sorptive phases on phenanthrene biodegradation: Different enrichment conditions influence bioavailability and selection of phenanthrene-degrading isolates. Applied and Environmental Microbiology, 66(7): 2695-2702. https://doi.org/10.1128/AEM.66.7.2695-2702.2000

Hassan, H. M., Castillo, A. B., Yigiterhan, O., Elobaid, E. A., Al-obaidly, A., & Al-ansari, E., 2018. Baseline concentrations and distributions of Polycyclic Aro-

matic Hydrocarbons in surface sediments from the Qatar marine environment. 126 (October 2017), 58-62. https://doi.org/10.1016/j.marpolbul.2017.10.093

He, Y., & Chi, J., 2016. Phytoremediation of sediments polluted with phenanthrene and pyrene by four submerged aquatic plants. Journal of Soils and Sediments, 16 (1): 309-317. https://doi.org/10.1007/s11368—015-1221-4

Heemken, O. P., Stachel, B., Theobald, N., & Wenclawiak, B. W., 2000. Temporal variability of organic micropollutants in suspended particulate matter of the River Elbe at Hamburg and the River Mulde at Dessau, Germany. Archives of Environmental Contamination and Toxicology, 38(1): 11-31. https://doi.org/10.1007/s002449910003

Heubeck, M., Camphuysen, K. C. J., Bao, R., Humple, D., Rey, A. S., Cadiou, B., ... Thomas, T., 2003. Assessing the impact of major oil spills on seabird populations. Marine Pollution Bulletin. https://doi.org/10.1016/S0025—326X(03)00098-5

Hong, W. J., Jia, H., Li, Y. F., Sun, Y., Liu, X., & Wang, L., 2016. Polycyclic aromatic hydrocarbons (PAHs) and alkylated PAHs in the coastal seawater, surface sediment and oyster from Dalian, Northeast China. Ecotoxicology and Environmental Safety (128): 11-20. https://doi.org/10.1016/j.ecoenv.2016.02.003

Hou, D., & Al-Tabbaa, A., 2014. Sustainability: A new imperative in contaminated land remediation. Environmental Science & Policy (39): 25-34. https://doi.org/10.1016/j.envsci.2014.02.003

Hou, D., Al-Tabbaa, A., & Guthrie, P., 2014. The adoption of sustainable remediation behaviour in the US and UK: A cross country comparison and determinant analysis. Science of the Total Environment. https://doi.org/10.1016/j.scitotenv.2014.05.059

Hu, W., Wang, T., Khim, J. S., Luo, W., Jiao, W., Lu, Y., ··· Giesy, J. P., 2010. HCH and DDT in sediments from marine and adjacent riverine areas of North Bohai Sea, China. Archives of Environmental Contamination and Toxicology, 59(1): 71-79. https://doi.org/10.1007/s00244—009-9455-z

Huang, X.-D., El-Alawi, Y., Penrose, D. M., Glick, B. R., & Greenberg, B. M., 2004. A multi-process phytoremediation system for removal of polycyclic aromatic hydrocarbons from contaminated soils. Environmental Pollution, 130(3): 465-476. https://doi.org/10.1016/j.envpol.2003.09.031

Ibrahim, M., Shuaibu, R., & Abdulsalam, S., 2016. Remediation of Escravous crude oil contaminated soil using activated carbon from coconut shell. Journal of Bioremediation & Biodegradation, 7(5). https://doi.org/10.4172/2155-6199.1000365

Ijah, U. J. J., & Antai, S. P., 2003. Removal of Nigerian light crude oil in soil over a 12-month period. International Biodeterioration and Biodegradation. https://doi.org/10.1016/S0964—8305(01)00131-7

Inam, E., Offiong, N.-A., Essien, J., Kang, S., Kang, S.-Y., & Antia, B., 2016. Polycyclic aromatic hydrocarbons loads and potential risks in freshwater ecosystem of the Ikpa River Basin, Niger Delta—Nigeria. Environmental Monitoring and Assessment, 188(1): 49. https://doi.org/10.1007/s10661—015-5038-9

Iwamoto, T., Nasu, M., 2001. Current bioremediation practice and perspective. Journal of Bioscience and Bioengineering, 92(1): 1-8. https://doi.org/10.1263/jbb.92.1

Janda, J. M., Abbott, S. L., 2010. The genus Aeromonas: taxonomy, pathogenicity, and infection. Clinical Microbiology Reviews, 23(1): 35-73. https://doi.org/10.1128/CMR.00039-09

Jia, Y., Yin, H., Ye, J.S., Peng, H., He, B.Y., Qin, H.M., … Qiang, J., 2008. Characteristics and pathway of naphthalene degradation by Pseudomonas sp. N7. Huan Jing Ke Xue = Huanjing Kexue, 29(3): 756-762. Retrieved from http://www.ncbi.nlm.nih.gov/pubmed/18649540

Jiang, Y.F., Wang, X.T., Wang, F., Jia, Y., Wu, M.H., Sheng, G.Y., & Fu, J.-M., 2009. Levels, composition profiles and sources of polycyclic aromatic hydrocarbons in urban soil of Shanghai, China. Chemosphere, 75(8): 1112-1118. https://doi.org/10.1016/j.chemosphere.2009.01.027

John, R. C., Ntino, E. S., & Itah, A. Y., 2016. Impact of crude oil on soil nitrogen dynamics and uptake by legumes grown in wetland ultisol of the Niger Delta, Nigeria. Journal of Environmental Protection, 07(04): 507-515. https://doi.org/10.4236/jep.2016.74046

Kabanza, A., Dondeyne, S., Tenga, J., Kimaro, D., Poesen, J., Kafiriti, E., & Deckers, J., 2013. More people, more trees in South Eastern Tanzania: local and global drivers of land-use/cover changes. African Geographical Review, 32(1): 44-58. https://doi.org/10.1080/19376812.2012.746093

Karačonji, B., Skender, L., & Karačić, V., 2006. Benzene, Toluene, Ethylbenzene, and Isomeric Xylenes in various water samples in Croatia. Bulletin of Environmental Contamination and Toxicology, 76(3): 458-462. https://doi.org/10.1007/s00128—006-0943-9

Karsa, D. R., Bailey, R. M., Shelmerdine, B., & McCann, S. A., 1999. Overview: A decade of change in the surfactant industry. Industrial Applications of Surfactants Ⅳ (pp. 1-22). https://doi.org/10.1533/9781845698614.1

Khan, R., & Al-nakhli, A. R., 2012. An overview of emerging technologies and in-

novations for tight gas reservoir development. SPE International Production and Operations Conference & Exhibition. https://doi.org/10.2118/155442-MS

King, A. J., Readman, J. W., & Zhou, J. L., 2004. Dynamic behaviour of polycyclic aromatic hydrocarbons in Brighton marina, UK. Marine Pollution Bulletin, 48 (3-4): 229-239. https://doi.org/10.1016/S0025—326X(03)00393-X

Kokare, C. R., Kadam, S. S., Mahadik, K. R., & Chopade, B. A., 2007. Studies on bioemulsifier production from marine Streptomyces sp. S1. Indian Journal of Biotechnology.

Korayem, A. S., Abdelhafez, A. A., Zaki, M. M., & Saleh, E. A., 2015. Optimization of biosurfactant production by Streptomyces isolated from Egyptian arid soil using Plackett-Burman design. Annals of Agricultural Sciences. https://doi.org/10.1016/j.aoas.2015.09.001

Kulshreshtha, A., Agrawal, R., Barar, M., & Saxena, S., 2014. A review on bioremediation of heavy metals in contaminated water. IOSR Journal of Environmental Science, Toxicology and Food Technology, 8(7): 44-50. https://doi.org/10.9790/2402-08714450

Kwon, H. K., Oh, S. J., & Yang, H. S., 2013. Growth and uptake kinetics of nitrate and phosphate by benthic microalgae for phytoremediation of eutrophic coastal sediments. Bioresource Technology. https://doi.org/10.1016/j.biortech.2012.11.078

Lavrova, S., & Koumanova, B., 2011. Landfill leachate purification in a vertical flow constructed wetland with/without preliminary aerobic treatment. Journal of the University of Chemical Technology and Metallurgy, 46(3): 299-304.

Lee, M.-R., Chang, C.-M., & Dou, J., 2007. Determination of benzene, toluene, ethylbenzene, xylenes in water at sub-ngl-1 levels by solid-phase microextraction coupled to cryo-trap gas chromatography-mass spectrometry. Chemosphere, 69(9): 1381-1387. https://doi.org/10.1016/j.chemosphere.2007.05.004

Léopold, E. N., Jung, M. C., Auguste, O., Ngatcha, N., Georges, E., & Lape, M., 2008. Metals pollution in freshly deposited sediments from river Mingoa, main tributary to the Municipal lake of Yaounde, Cameroon. Geosciences Journal, 12 (4): 337-347. https://doi.org/10.1007/s12303—008-0034-5

Lin, D., Cho, Y.-M., Werner, D., & Luthy, R. G., 2014. Bioturbation delays attenuation of DDT by clean sediment cap but promotes sequestration by thin-layered activated carbon. Environmental Science & Technology, 48(2): 1175-1183. https://doi.org/10.1021/es404108h

Lin, T., Hu, Z., Zhang, G., Li, X., Xu, W., Tang, J., & Li, J., 2009. Levels and mass burden of DDTs in sediments from fishing harbors: The importance of

DDT-containing antifouling paint to the coastal environment of China. Environmental Science & Technology, 43 (21): 8033-8038. https://doi.org/10.1021/es901827b

Lin, Y., Deng, W., Li, S., Li, J., Wang, G., Zhang, D., & Li, X., 2016. Science of the total environment congener profiles, distribution, sources and ecological risk of parent and alkyl-PAHs in surface sediments of Southern Yellow Sea, China. Science of the Total Environment. https://doi.org/10.1016/j.scitotenv.2016.12.094

Liu, Y., Yu, Y., Liu, M., Lu, M., Ge, R., Li, S.,... Qadeer, A., 2018. Science of the total environment characterization and source identification of PM 2.5-bound polycyclic aromatic hydrocarbons (PAHs) in different seasons from Shanghai, China. Science of the Total Environment (644): 725-735. https://doi.org/10.1016/j.scitotenv.2018.07.049

Lu, M., Zeng, D.-C., Liao, Y., & Tong, B., 2012. Distribution and characterization of organochlorine pesticides and polycyclic aromatic hydrocarbons in surface sediment from Poyang Lake, China. Science of The Total Environment (433): 491-497. https://doi.org/10.1016/j.scitotenv.2012.06.108

Ma, L. L., Chu, S. G., Wang, X. T., Cheng, H. X., Liu, X. F., & Xu, X. B., 2005. Polycyclic aromatic hydrocarbons in the surface soils from outskirts of Beijing, China. Chemosphere, 58(10): 1355-1363. https://doi.org/10.1016/j.chemosphere.2004.09.083

Malviya, R., & Chaudhary, R., 2006. Factors affecting hazardous waste solidification/stabilization: A review. Journal of Hazardous Materials. https://doi.org/10.1016/j.jhazmat.2006.01.065

Manap, N., & Voulvoulis, N., 2014. Risk-based decision-making framework for the selection of sediment dredging option. Science of The Total Environment (496): 607-623. https://doi.org/10.1016/j.scitotenv.2014.07.009

Margesin, R., & Schinner, F., 2001. Bioremediation (natural attenuation and biostimulation) of diesel-oil-contaminated soil in an Alpine Glacier skiing area. Applied and Environmental Microbiology, 67(7): 3127-3133. https://doi.org/10.1128/AEM.67.7.3127-3133.2001

Mari, M., Harrison, R. M., Schuhmacher, M., Domingo, J. L., & Pongpiachan, S., 2010. Inferences over the sources and processes affecting polycyclic aromatic hydrocarbons in the atmosphere derived from measured data. Science of The Total Environment, 408(11): 2387-2393. https://doi.org/10.1016/j.scitotenv.2010.01.054

Martin, T. A., & Ruby, M. V., 2004. Review of in-situ remediation technologies

for lead, zinc, and cadmium in soil. Remediation Journal, 14(3): 35-53. https://doi.org/10.1002/rem.20011

Maruya, K. A., Risebrough, R. W., & Horne, A. J., 1996. Partitioning of Polynuclear Aromatic Hydrocarbons between sediments from San Francisco Bay and their porewaters. Environmental Science & Technology, 30(10): 2942-2947. https://doi.org/10.1021/es950909v

Masih, A., & Taneja, A., 2006. Polycyclic aromatic hydrocarbons (PAHs) concentrations and related carcinogenic potencies in soil at a semi-arid region of India. Chemosphere, 65(3): 449-456. https://doi.org/10.1016/j.chemosphere.2006.01.062

Meng, F., & Chi, J., 2015. Interactions between Potamogeton crispus L. and phenanthrene and pyrene in sediments. Journal of Soils and Sediments, 15(5): 1256-1264. https://doi.org/10.1007/s11368—015-1080-z

Meng, F., Huang, J., Liu, H., & Chi, J., 2015. Remedial effects of Potamogeton crispus L. on PAH-contaminated sediments. Environmental Science and Pollution Research, 22(10): 7547-7556. https://doi.org/10.1007/s11356—015-4280-6

Mestres, M., Sierra, J. P., Mösso, C., & Sánchez-Arcilla, A., 2010. Sources of contamination and modelled pollutant trajectories in a Mediterranean harbour (Tarragona, Spain). Marine Pollution Bulletin, 60(6): 898-907. https://doi.org/10.1016/j.marpolbul.2010.01.002

Meylheuc, T., Herry, J.-M., & Bellon-Fontaine, M.-N., 2001. Les biosurfactants, des biomolécules à forte potentialité d'application. Sciences Des Aliments, 21(6): 591-649. https://doi.org/10.3166/sda.21.591-649

Mhlanga, S. D., Mamba, B. B., Krause, R. W., & Malefetse, T. J., 2007. Removal of organic contaminants from water using nanosponge cyclodextrin polyurethanes. Journal of Chemical Technology & Biotechnology, 82(4): 382-388. https://doi.org/10.1002/jctb.1681

Mhlongo, S. H., Mamba, B. B., & Krause, R. W., 2009. Monitoring the prevalence of nitrosamines in South African waters and their removal using cyclodextrin polyurethanes. Physics and Chemistry of the Earth, Parts A/B/C, 34(13-16): 819-824. https://doi.org/10.1016/j.pce.2009.07.008

Mittal, A., & Singh, P., 2009. Isolation of hydrocarbon degrading bacteria from soils contaminated with crude oil spills. Indian Journal of Experimental Biology, 47(9): 760-765. Retrieved from http://www.ncbi.nlm.nih.gov/pubmed/19957890

Modoi, O.-C., Roba, C., Torok, Z., & Ozunu, A., 2014. Environmental risks due to heavy metal pollution of water resulted from mining wastes in NW Romania. Environmental Engineering and Management Journal, 13(9): 2325-2336. https://

doi.org/10.30638/eemj.2014.260

Molnaa, B. (1999). A powerful and resilient companion technology. Pollution Engineering.

Moscoso, F., Deive, F. J., Longo, M. A., & Sanromán, M. A., 2015. Insights into polyaromatic hydrocarbon biodegradation by Pseudomonas stutzeri CECT 930: operation at bioreactor scale and metabolic pathways. International Journal of Environmental Science and Technology, 12(4): 1243-1252. https://doi.org/10.1007/s13762—014-0498-y

Moscoso, F., Teijiz, I., Deive, F. J., & Sanromán, M. A., 2012. Efficient PAHs biodegradation by a bacterial consortium at flask and bioreactor scale. Bioresource Technology (119): 270-276. https://doi.org/10.1016/j.biortech.2012.05.095

Mrozik, A., Piotrowska-Seget, Z., & Łabuzek, S. (2003). Bacterial degradation and bioremediation of polycyclic aromatic hydrocarbons. Polish Journal of Environmental Studies.

Nam, J. J., Song, B. H., Eom, K. C., Lee, S. H., & Smith, A., 2003. Distribution of polycyclic aromatic hydrocarbons in agricultural soils in Korea. Chemosphere, 50(10): 1281-1289. https://doi.org/10.1016/S0045—6535(02)00764-6

New center for Integrated studies of Land & Environment (NILE)., 2013. Annual report for solid waste management in Egypt, 2013. In Ministry of State for Environmental Affairs National Solid Waste Management Programme (NSWMP) (Vol. 2). Retrieved from http://www.wmra.gov.eg/en-us/ReportsandGuidelines/ReportsandIndicators/Documents/2013_Annual Report for SWM in Egypt_EN.pdf

Nyarko, E., Botwe, B. O., & Klubi, E., 2012. Polycyclic aromatic hydrocarbons (PAHs) levels in two commercially important fish species from the coastal waters of Ghana and their carcinogenic health risks. West African Journal of Applied Ecology.

Okumagba, P. O., & Okereka, O. P., 2013. The politics of oil and the Niger Delta regional development master plan: Its workability and the option of political goodwill. Global Advanced Research Journal of History Political Science and International Relations, 2(1): 2315-2506. Retrieved from http://garj.org/garjhpsir/index.htm

Okoh, A. I., & Trejo-Hernandez, M. R., 2006. Remediation of petroleum hydrocarbon polluted systems: Exploiting the bioremediation strategies. African Journal of Biotechnology. https://doi.org/10.5897/AJB2006.000—5108

Oluwafemi S. O., 2012. Degradation of weathered crude oil (Escravos Light) by bacterial strains from hydrocarbons-polluted site. African Journal of Microbiology Research, 6(26). https://doi.org/10.5897/AJMR10.026

Onwurah, I. N. E., Ogugua, V. N., Onyike, N. B., Ochonogor, A. E., & Otitoju, O. F., 2007. Crude oils spills in the environment, effects and some innovative clean-up biotechnologies. International Journal of Environmental Research.

OPEC. (2017). Nigeria facts and figures. Member Countries.

Orecchio, S., 2010. Contamination from polycyclic aromatic hydrocarbons (PAHs) in the soil of a botanic garden localized next to a former manufacturing gas plant in Palermo (Italy). Journal of Hazardous Materials, 180(1-3), 590-601. https://doi.org/10.1016/j.jhazmat.2010.04.074

Orji, F. A., Ibiene, A. A., & Dike, E. N., 2012. Laboratory scale bioremediation of petroleum hydrocarbon-polluted mangrove swamps in the Niger Delta using cow dung. Malaysian Journal of Microbiology. https://doi.org/10.21161/mjm.40312

Orozco, A. M. F., Contreras, E. M., & Zaritzky, N. E., 2008. Modelling Cr(VI) removal by a combined carbon-activated sludge system. Journal of Hazardous Materials, 150(1): 46-52. https://doi.org/10.1016/j.jhazmat.2007.04.043

Otitoju, O., Onwurah, I. N. E., Otitoju, G. T. O., Ndem, J. I., & Uwah, A. F., 2011. Effect of Bonny light crude oil contaminated diet on serum cholesterol and testosterone concentrations in wistar albino rats. African Journal of Biotechnology, 10(53): 10986-10990. https://doi.org/10.5897/AJB11.1025

Paria, S., & Yuet, P. K., 2006. Solidification-stabilization of organic and inorganic contaminants using portland cement: A literature review. Environmental Reviews. https://doi.org/10.1139/A06—004

Park, I.-S., & Park, J.-W., 2010. A novel total petroleum hydrocarbon fractionation strategy for human health risk assessment for petroleum hydrocarbon-contaminated site management. Journal of Hazardous Materials, 179(1-3): 1128-1135. https://doi.org/10.1016/j.jhazmat.2010.03.124

Pavel, V. L., Diaconu, M., Bulgariu, D., Statescu, F., & Gavrilescu, M., 2012. Evaluation of heavy metals toxicity on two microbial strains isolated from soil: Azotobacter sp. and Pichia sp. Environmental Engineering and Management Journal, 11(1): 165-168. https://doi.org/10.30638/eemj.2012.021

Payne, R. B., Fagervold, S. K., May, H. D., & Sowers, K. R., 2013. Remediation of polychlorinated biphenyl impacted sediment by concurrent bioaugmentation with anaerobic halorespiring and aerobic degrading bacteria. Environmental Science & Technology, 47(8): 3807-3815. https://doi.org/10.1021/es304372t

Peng, C., Chen, W., Liao, X., Wang, M., Ouyang, Z., Jiao, W., & Bai, Y., 2011. Polycyclic aromatic hydrocarbons in urban soils of Beijing: Status, sources, distribution and potential risk. Environmental Pollution, 159(3): 802-808. https://doi.org/10.1016/j.envpol.2010.11.003

Peng, C., Ouyang, Z., Wang, M., Chen, W., Li, X., & Crittenden, J. C., 2013. Assessing the combined risks of PAHs and metals in urban soils by urbanization indicators. Environmental Pollution (178): 426-432. https://doi.org/10.1016/j.envpol.2013.03.058

Peng, C., Wang, M., Zhao, Y., & Chen, W., 2016. Distribution and risks of polycyclic aromatic hydrocarbons in suburban and rural soils of Beijing with various land uses. Environmental Monitoring and Assessment, 188(3): 162. https://doi.org/10.1007/s10661—016-5156-z

Perelo, L. W., 2010. Review: In-situ and bioremediation of organic pollutants in aquatic sediments. Journal of Hazardous Materials, 177(1-3): 81-89. https://doi.org/10.1016/j.jhazmat.2009.12.090

Peter, O., 2011. Biological remediation of hydrocarbon and heavy metals contaminated soil. In Soil Contamination. https://doi.org/10.5772/24938

Pignatello, J. J., Oliveros, E., & MacKay, A., 2006. Advanced oxidation processes for organic contaminant destruction based on the Fenton Reaction and related chemistry. Critical Reviews in Environmental Science and Technology, 36(1): 1-84. https://doi.org/10.1080/10643380500326564

Rizzo, E., Bardos, P., Pizzol, L., Critto, A., Giubilato, E., Marcomini, A., … Smith, G., 2016. Comparison of international approaches to sustainable remediation. Journal of Environmental Management (184): 4-17. https://doi.org/10.1016/j.jenvman.2016.07.062

Rose, M., Holland, J., Dowding, A., Petch, S. R. G., White, S., Fernandes, A., & Mortimer, D., 2015. Investigation into the formation of PAHs in foods prepared in the home to determine the effects of frying, grilling, barbecuing, toasting and roasting. Food and Chemical Toxicology. https://doi.org/10.1016/j.fct.2014.12.018

Rosell, M., Lacorte, S., Forner, C., Rohns, H. P., Irmscher, R., & Barceló, D., 2005. Fate of gasoline oxygenates in conventional and multilevel wells of a contaminated groundwater table in Düsseldorf, Germany. Environmental Toxicology and Chemistry. https://doi.org/10.1897/05-080R.1

Rosell, M., Lacorte, S., Ginebreda, A., & Barcelo, D., 2003. Simultaneous determination of methyl tert-butyl ether and its degradation products, other gasoline oxygenates and benzene, toluene, ethylbenzene and xylenes in Catalonian groundwater by purge-and-trap-gas chromatography-mass spectrometry. Journal of Chromatography A, 995(1-2): 171-184. https://doi.org/10.1016/S0021—9673(03)00500-4

Roy, S., Hens, D., Biswas, D., Biswas, D., & Kumar, R., 2002. Survey of petro-

leum-degrading bacteria in coastal waters of Sunderban Biosphere Reserve. World Journal of Microbiology and Biotechnology. https://doi. org/10. 1023/A:1016362819746

Sam, K., & Zabbey, N., 2018. Contaminated land and wetland remediation in Nigeria: Opportunities for sustainable livelihood creation. Science of The Total Environment (639): 1560-1573. https://doi.org/10.1016/j.scitotenv.2018.05.266

Sam, Kabari, Coulon, F., & Prpich, G., 2017. A multi-attribute methodology for the prioritisation of oil contaminated sites in the Niger Delta. Science of The Total Environment (579): 1323-1332. https://doi.org/10.1016/j.scitotenv.2016.11.126

Sarria-Villa, R., Ocampo-Duque, W., Páez, M., & Schuhmacher, M., 2016. Presence of PAHs in water and sediments of the Colombian Cauca River during heavy rain episodes, and implications for risk assessment. Science of The Total Environment (540): 455-465. https://doi.org/10.1016/j.scitotenv.2015.07.020

Seklemova, E., Pavlova, A., & Kovacheva, K., 2001. Biostimulation-based bioremediation of diesel fuel: field demonstration. Biodegradation, 12(5): 311-316. https://doi.org/10.1023/a:1014356223118

Seo, J.-S., Keum, Y.-S., & Li, Q., 2009. Bacterial degradation of aromatic compounds. International Journal of Environmental Research and Public Health, 6(1): 278-309. https://doi.org/10.3390/ijerph6010278

Shahidul Islam, M., & Tanaka, M., 2004. Impacts of pollution on coastal and marine ecosystems including coastal and marine fisheries and approach for management: a review and synthesis. Marine Pollution Bulletin, 48(7-8): 624-649. https://doi.org/10.1016/j.marpolbul.2003.12.004

Singh, R., Lemire, J., Mailloux, R. J., Chénier, D., Hamel, R., & Appanna, V. D., 2009. An ATP and oxalate generating variant tricarboxylic acid cycle counters aluminum toxicity in Pseudomonas fluorescens. PLOS ONE. https://doi. org/10.1371/journal. pone. 0007344

Soclo, H. H., Garrigues, P. H., & Ewald, M., 2009. Origin of Polycyclic Aromatic Hydrocarbons (PAHs) in coastal marine sediments: Case studies in Cotonou (Benin) and Aquitaine (France) Areas, 40(5): 387-396.

Souza, F. A., Dziedzic, M., Cubas, S. A., & Maranho, L. T., 2013. Restoration of polluted waters by phytoremediation using Myriophyllum aquaticum (Vell.) Verdc., Haloragaceae. Journal of Environmental Management (120): 5-9. https://doi.org/10.1016/j.jenvman.2013.01.029

Surriya, O., Sarah Saleem, S., Waqar, K., & Gul Kazi, A., 2015. Phytoremediation of soils: Prospects and challenges. Soil Remediation and Plants: Prospects and Challenges. https://doi.org/10.1016/B978—0-12-799937-1.00001-2

Tang, L., Tang, X.-Y., Zhu, Y.-G., Zheng, M.-H., & Miao, Q.-L., 2005. Contamination of polycyclic aromatic hydrocarbons (PAHs) in urban soils in Beijing, China. Environment International, 31(6): 822-828. https://doi.org/10.1016/j.envint.2005.05.031

Tongo, I., Ezemonye, L., & Akpeh, K., 2017. Levels, distribution and characterization of Polycyclic Aromatic Hydrocarbons (PAHs) in Ovia river, Southern Nigeria. Journal of Environmental Chemical Engineering, 5(1): 504-512. https://doi.org/10.1016/j.jece.2016.12.035

UNEP., 2011. Environmental Assessment of Ogoniland United. Psychopharmacology Bulletin, 1-262. Retrieved from http://www.unep.org

Vane, C. H., Harrison, I., & Kim, A. W., 2007. Polycyclic aromatic hydrocarbons (PAHs) and polychlorinated biphenyls (PCBs) in sediments from the Mersey Estuary, U. K. (374): 112-126. https://doi.org/10.1016/j.scitotenv.2006.12.036

Varjani, S. J., Rana, D. P., Jain, A. K., Bateja, S., & Upasani, V. N., 2015. Synergistic ex-situ biodegradation of crude oil by halotolerant bacterial consortium of indigenous strains isolated from on shore sites of Gujarat, India. International Biodeterioration & Biodegradation (103): 116-124. https://doi.org/10.1016/j.ibiod.2015.03.030

Varjani, S. J., & Upasani, V. N., 2016. Biodegradation of petroleum hydrocarbons by oleophilic strain of Pseudomonas aeruginosa NCIM 5514. Bioresource Technology. https://doi.org/10.1016/j.biortech.2016.10.006

Wang, C. H., Wu, S. H., Zhou, S. L., Wang, H., Li, B. J., Chen, H., ... Shi, Y. X., 2015. Polycyclic aromatic hydrocarbons in soils from urban to rural areas in Nanjing: Concentration, source, spatial distribution, and potential human health risk. Science of the Total Environment (527-528): 375-383. https://doi.org/10.1016/j.scitotenv.2015.05.025

Wang, Cuiping, Sun, H., Chang, Y., Song, Z., & Qin, X., 2011. PAHs distribution in sediments associated with gas hydrate and oil seepage from the Gulf of Mexico. Marine Pollution Bulletin, 62(12): 2714-2723. https://doi.org/10.1016/j.marpolbul.2011.09.016

Wang, J., & Chen, C., 2006. Biosorption of heavy metals by Saccharomyces cerevisiae: A review. Biotechnology Advances, 24(5): 427-451. https://doi.org/10.1016/j.biotechadv.2006.03.001

Wang, L., 2006. Site remediation and groundwater decontamination. In hazardous industrial waste treatment (pp. 241 - 287). https://doi.org/10.1201/9780849375750.ch7

Wang, S.Y., Kuo, Y.C., Hong, A., Chang, Y.M., & Kao, C.M., 2016. Biore-

mediation of diesel and lubricant oil-contaminated soils using enhanced landfarming system. Chemosphere (164): 558-567. https://doi.org/10.1016/j.chemosphere.2016.08.128

Wang, X.C., Zhang, Y.X., & Chen, R. F., 2001. Distribution and partitioning of polycyclic aromatic hydrocarbons (PAHs) in different size fractions in sediments from Boston Harbor, United States. Marine Pollution Bulletin, 42(11): 1139-1149. https://doi.org/10.1016/S0025—326X(01)00129-1

Wang, Y.F., & Tam, N. F.Y., 2012. Natural attenuation of contaminated marine sediments from an old floating dock Part Ⅱ: Changes of sediment microbial community structure and its relationship with environmental variables. Science of The Total Environment (423): 95-103. https://doi.org/10.1016/j.scitotenv.2012.01.066

Wang, Y., Zhou, S., Xia, J., Xue, J., Xu, J., & Zhu, J., 2004. Trapping and degradation of volatile nitrosamines on cyclodextrin and zeolites. Microporous and Mesoporous Materials, 75(3): 247-254. https://doi.org/10.1016/j.micromeso.2004.07.025

Wang, Zhen, Chen, J., Yang, P., Qiao, X., & Tian, F., 2007. Polycyclic aromatic hydrocarbons in Dalian soils: distribution and toxicity assessment. J. Environ. Monit., 9(2): 199-204. https://doi.org/10.1039/B617338C

Wang, Zhendi, Li, K., Fingas, M., Sigouin, L., & Ménard, L., 2002. Characterization and source identification of hydrocarbons in water samples using multiple analytical techniques. Journal of Chromatography A, 971(1-2): 173-184. https://doi.org/10.1016/S0021—9673(02)01003-8

Widdel, F., & Rabus, R., 2001. Anaerobic biodegradation of saturated and aromatic hydrocarbons. Current Opinion in Biotechnology. https://doi.org/10.1016/S0958—1669(00)00209-3

Willett, K. L., Ulrich, E. M., & Hites, R. A., 1998. Differential toxicity and environmental fates of hexachlorocyclohexane isomers. Environmental Science & Technology, 32(15): 2197-2207. https://doi.org/10.1021/es9708530

Williams, P., Botes, E., Maleke, M., Ojo, A., DeFlaun, M., Howell, J., Van Heerden, E., 2014. Effective bioreduction of hexavalent chromium-contaminated water in fixed-film bioreactors. Water SA, 40(3): 549. https://doi.org/10.4314/wsa.v40i3.19

Wu, S., Liu, X., Liu, M., Chen, X., Liu, S., Cheng, L., Li, Y., 2018. Sources, influencing factors and environmental indications of PAH pollution in urban soil columns of Shanghai, China. Ecological Indicators(85): 1170-1180. https://doi.org/10.1016/j.ecolind.2017.11.067

Xiang, N., Jiang, C., Yang, T., Li, P., Wang, H., & Xie, Y., 2018. Ecotoxicology and environmental safety occurrence and distribution of Polycyclic aromatic hydrocarbons (PAHs) in seawater, sediments and corals from Hainan Island, China. Ecotoxicology and Environmental Safety, 152(December 2017):8-15. https://doi.org/10.1016/j.ecoenv.2018.01.006

Yang, R., Jiang, G., Zhou, Q., Yuan, C., & Shi, J., 2005. Occurrence and distribution of organochlorine pesticides (HCH and DDT) in sediments collected from East China Sea. Environment International, 31(6): 799-804. https://doi.org/10.1016/j.envint.2005.05.027

Yang, X., Ren, D., Sun, W., Li, X., Huang, B., Chen, R., Pan, X., 2015. Polycyclic aromatic hydrocarbons associated with total suspended particles and surface soils in Kunming, China: distribution, possible sources, and cancer risks. Environmental Science and Pollution Research, 22(9): 6696-6712. https://doi.org/10.1007/s11356—014-3858-8

Yang, Z., Feng, J., Niu, J., & Shen, Z., 2008. Release of polycyclic aromatic hydrocarbons from Yangtze River sediment cores during periods of simulated resuspension. Environmental Pollution, 155(2): 366-374. https://doi.org/10.1016/j.envpol.2007.11.007

Yelton, A. P., Williams, K. H., Fournelle, J., Wrighton, K. C., Handley, K. M., & Banfield, J. F., 2013. Vanadate and acetate biostimulation of contaminated sediments decreases diversity, selects for specific taxa, and decreases aqueous V 5+ concentration. Environmental Science & Technology, 47(12): 6500-6509. https://doi.org/10.1021/es4006674

Yin, C. Q., Jiang, X., Yang, X. L., Bian, Y. R., & Wang, F., 2008. Polycyclic aromatic hydrocarbons in soils in the vicinity of Nanjing, China. Chemosphere, 73(3): 389-394. https://doi.org/10.1016/j.chemosphere.2008.05.041

Zabbey, N., & Uyi, H., 2014. Community responses of intertidal soft-bottom macrozoobenthos to oil pollution in a tropical mangrove ecosystem, Niger Delta, Nigeria. Marine Pollution Bulletin, 82(1-2): 167-174. https://doi.org/10.1016/j.marpolbul.2014.03.002

Zhang, H. B., Luo, Y. M., Wong, M. H., Zhao, Q. G., & Zhang, G. L., 2006. Distributions and concentrations of PAHs in Hong Kong soils. Environmental Pollution, 141(1): 107-114. https://doi.org/10.1016/j.envpol.2005.08.031

Zhang, K., Zhang, B. Z., Li, S. M., & Zeng, E. Y., 2011. Regional dynamics of persistent organic pollutants (POPs) in the Pearl River Delta, China: Implications and perspectives. Environmental Pollution, 159(10): 2301-2309. https://doi.org/10.1016/j.envpol.2011.05.011

Zhao, Y., Yang, Z., Xia, X., & Wang, F., 2012. A shallow lake remediation regime with Phragmites australis: Incorporating nutrient removal and water evapotranspiration. Water Research, 46(17): 5635-5644. https://doi.org/10.1016/j.watres.2012.07.053

Zhao, Z., Qin, Z., Xia, L., Zhang, D., Margaret, S., & Li, Y., 2019. The responding and ecological contribution of bio film-leaves of submerged macrophytes on phenanthrene dissipation in sediments. Environmental Pollution (246): 357-365. https://doi.org/10.1016/j.envpol.2018.12.030

Prediction and assessment of the immersion of cascade reservoirs on the mountain rivers

Minglong Bai[1], Bin Lu[2], Xianzhong Chen[3], Xingwei Zheng[4], Honghao Fan[5], Weichen Qiu[6], Xinghua Xie[7]

[1,2,7] Nanjing Hydraulic Research Institute, Nanjing, China. e-mail: 970047646@qq.com; blu@nhri.cn; iamxiexh@163.com

[3] Changshan County Changshan River Channel Development and Construction headquarters, Changshan, China. e-mail: 526855643@qq.com

[4,5] Quzhou Jujiang Shipping Construction and Development Co. LTD, Changshan, China. e-mail: 49314063@qq.com; csjskglj@163.com

[6] Changshan County Dingyang Shipping Development Company, Changshan, China. e-mail: 753377046@qq.com

Abstract: Reservoir immersion is an environmental geological problem caused by the rise of groundwater level due to reservoir impoundment, and has adverse effects on low-lying farmland, building foundations and underground structures. The prediction and assessment of reservoir immersion hazard is very important for reservoir operation and surrounding environment protection. Aiming at the reservoir immersion problem caused by the impoundment of the cascade reservoirs in mountainous areas, taking the six cascade reservoirs of CSJ River Waterway Project as an example, based on the hydrogeological conceptual model of each reservoir area, a three-dimensional groundwater numerical simulation model of each cascade reservoir is established to simulate the groundwater flow field and water level before and after the completion of the project, and the reservoir immersion range of the six cascade reservoirs after completion is obtained. The results show that after the impoundment of the project, the groundwater level around the reservoir rises significantly, and the water head lines are densely distributed near the project, and the total immersion area of the reservoir reaches 6.456 km^2, in which the ZX reservoir area and BHT reservoir area are more seriously immersed. Appropriate anti-seepage or drainage measures shall be taken according to the actual conditions of the project.

Keywords: Reservoir immersion; Numerical simulation; Cascade reservoir; Critical depth of groundwater

1 Introduction

Reservoir immersion is widely distributed in China. Sun (2012) analyzed 108 pa-

pers on reservoir immersion in China, involving 38 reservoirs, distributed in more than 20 provinces and autonomous regions in China. Immersion of the reservoir will adversely affect crops and buildings around the reservoir. The groundwater level of Guanting Reservoir has risen since its impoundment in August 1955, resulting in salinization and swamping, as well as in crop reduction and house collapse around the reservoir (Ji, 2005). The submerged area of 180 hectares of cultivated land in Huaxian County near Sanmenxia Reservoir increased from 15 hectares in 1958 to 167 hectares in 1963, accounting for 93% of the total cultivated land area (Ling, 1992). Reservoir immersion has become one of the four major engineering geological problems (i.e., seepage, immersion, bank collapse and siltation) in the reservoir exploration and demonstration, and the immersion problem is the most common. The cost of reservoir immersion treatment is high, and in some projects, the cost of immersion treatment even exceeds 40% of the total project cost (Yu et al., 2008).

Tang (1957) and Kang (1958) studied the environmental geological problems caused by the immersion of Guanting Reservoir after its impoundment in 1955. In the 1990s, research on reservoir immersion prediction and management increased. Xing et al. (1996) and Li (2001) made a further study on the reservoir immersion of Guanting Reservoir. After 2000, the research trend is to use new technology to evaluate the problem of reservoir immersion and to study the mechanism of reservoir immersion. The prediction and evaluation methods of reservoir immersion are increasing, such as hydrodynamic principle (Li, 2008), geophysical exploration method (Ma, 2006; Dai et al., 2012), finite element method (Zhu et al., 2006; Wu et al., 2012; Ren et al., 2013) and so on, but the traditional analytical method is mostly used in practical engineering. The analytical method is convenient to be used in engineering (Wang, 2003; Wang, 2004), but its applicable conditions are limited, and it cannot describe the complex groundwater flow. The three-dimensional groundwater flow model based on a large number of data can adapt to more complex hydrogeological conditions and has higher accuracy for the prediction of groundwater level.

In the past, the research object of reservoir immersion was mostly a single reservoir, and the research on cascade reservoirs, which are common in waterway engineering, is still relatively scare. In this paper, six cascade reservoirs of CSJ River Channel Project are taken as the research objects. The three-dimensional groundwater numerical simulation model of each cascade reservoir is established. The groundwater level and flow field before and after the completion of the project are simulated, and the immersion range of the six cascade reservoirs after the completion of the project is obtained, and some suggestions for immersion control are put forward.

2 Background

The total length of the channel project of CSJ River is 51.1 km. Six low water head navigation and power generation hubs mainly for navigation and power generation will be built or reconstructed on CSJ River. Each power station is equipped with a ship lock for navigation. The locations of power stations are shown in Fig. 1.

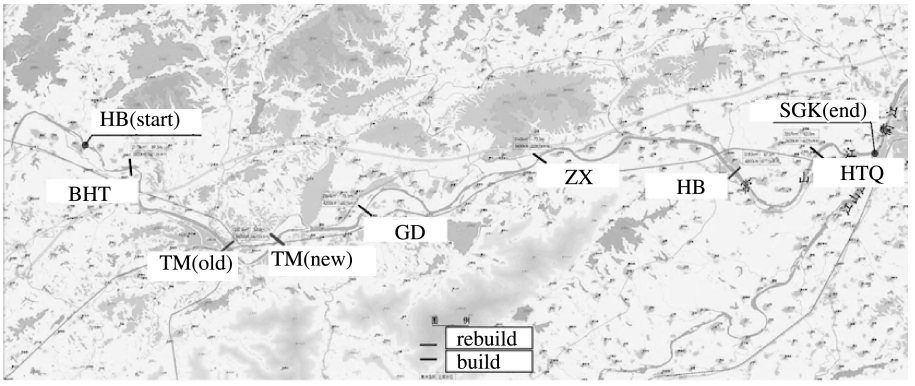

Fig. 1. Schematic diagram of the distribution of hydropower stations on CSJ River.

3 Materials and methods

3.1 Construction of 3D groundwater model

Accurately determining the distribution of groundwater level is the focus of this study, and the three-dimensional groundwater model has high accuracy. In this paper, the FEFLOW groundwater system simulation software is used to establish the physical model and conduct the numerical simulation experiment.

The total length of CSJ River waterway from HB to SGK is 51.1 km, and the cascade development involves a large area of influence. In order to improve the accuracy of the model, six models are established according to the layout of the navigation and power hubs. Because the modelling process of each model is similar, we only take the modelling of HB reservoir area as an example.

Firstly, determine the plane range of the model (Fig. 2(a)). The model selects the range of the ground elevation of the reservoir area within 2 m above the normal water level, and is expanded by 100 m upstream and downstream, so as to reduce the impact of upstream and downstream boundaries. Then, import the CAD graphics pro-

cessed by preliminary space division into FEFLOW to create a super-unit model (Fig. 2 (b)), and then use the triangle algorithm to perform two-dimensional grid division on the super-unit model (Fig. 2(c)), and finally use the parameter association function to assign values to the model parameters (Fig. 2(d)).

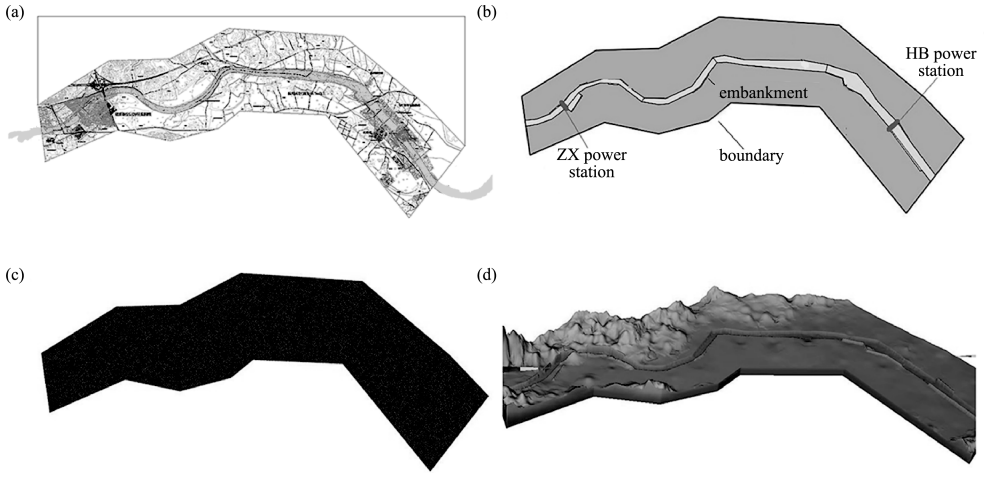

Fig. 2. (a)Calculation range of HB reservoir area; (b)HB reservoir super element model; (c) 2D finite element mesh; (d) 3D model of HB reservoir area (Z magnification 5 times display).

We assign the permeability coefficient to the three-dimensional model constructed in Fig. 2(d). According to the exploration data, the geological stratification of the project area can be divided into four types from top to bottom: artificial accumulation soil, muddy silty fine sand (with gravel) layer, (muddy) sand gravel layer and argillaceous sandstone layer.

In the model, the geological layering of the hub location is set according to the survey data, and the geological layering between hubs is interpolated according to the layering thickness of the hubs at both ends. The statistical average value of the permeability coefficient of each geological layer is taken as the value of the permeability coefficient of the geological layer. The final values of permeability coefficient are shown in Table 1 and Table 2, and the setting of permeability coefficient is shown in Fig. 3(a).

Table 1 ZX Reservoir Area geological stratification parameter statistics and model values.

Geological stratification	Layered thickness range on both sides(m)	Permeability range (cm/s)	The value of permeability coefficient (cm/s)
(Mud-containing) sand and gravel layer	1 - 2	1.7×10^{-4} - 7.7×10^{-3}	4.1×10^{-3}
Mud-bearing fine sand (with gravel) layer	5 - 8	1.0×10^{-3} - 1.3×10^{-2}	4.7×10^{-3}
Argillaceous sandstone	—	1.3×10^{-4}	1.3×10^{-4}

Table 2 HB Reservoir Area geological stratification parameter statistics and model values.

Geological stratification	Layered thickness range on both sides(m)	Permeability range (cm/s)	The value of permeability coefficient(cm/s)
Mud-bearing fine sand (with gravel) layer	3 - 4	6.5×10^{-4} - 7.4×10^{-3}	4.6×10^{-3}
(Mud-containing) sand and gravel layer	6 - 8	7.6×10^{-4} - 6.5×10^{-3}	2.0×10^{-3}
Argillaceous sandstone	—	1.3×10^{-4}	1.3×10^{-4}

3.2 Governing equations

The groundwater flow problem is described by the following three-dimensional seepage mathematical model:

$$\begin{cases} S\dfrac{\partial h}{\partial t}=\dfrac{\partial}{\partial x}\left(K_x\dfrac{\partial h}{\partial x}\right)+\dfrac{\partial}{\partial y}\left(K_y\dfrac{\partial h}{\partial y}\right)+\dfrac{\partial}{\partial z}\left(K_z\dfrac{\partial h}{\partial z}\right)+\varepsilon & x,y,z\in\Omega,t\geqslant 0 \\ \mu\dfrac{\partial y}{\partial t}=K_x\left(\dfrac{\partial h}{\partial x}\right)^2+K_y\left(\dfrac{\partial h}{\partial y}\right)^2+K_z\left(\dfrac{\partial h}{\partial z}\right)^2-\dfrac{\partial h}{\partial z}(K_z+p) & x,y,z\in\Omega,t\geqslant 0 \\ h(x,y,z,t)\mid_{t=0}=h_0 & x,y,z\in\Omega,t\geqslant 0 \\ K_n\dfrac{\partial h}{\partial \vec{n}}\mid_{\Gamma_1}=q(x,y,z,t) & x,y,z\in\Omega,t\geqslant 0 \\ K_n\dfrac{\partial h}{\partial \vec{n}}-\dfrac{h-h_s}{\sigma}\mid\Gamma_2=0 & x,y,z\in\Omega,t\geqslant 0 \end{cases} \tag{1}$$

where Ω (m) is the seepage area; h is the water level elevation of the aquifer; K_x, K_y and K_z (m/d) are the permeability coefficients in the x, y, and z directions; S (1/m) is the water storage in the aquifer below the free surface coefficient; μ is the gravity water supply of the phreatic aquifer on the phreatic surface; ε (1/d) is the source-sink term of the aquifer; p (1/d) is the evaporation and precipitation recharge of the diving surface; h_0 (m) is the initial water level distribution of the aquifer; Γ_1 is the second-class boundary of the seepage area, including the water-blocking boundary at the bottom of the confined aquifer and the side of the seepage area directional flow or water-proof boundary; n is the normal direction of the boundary surface; K_n (m/d) is the permeability coefficient of the normal direction of the boundary surface; $q(x,y,z,t)$ ($m^3/(d\cdot m^2)$) is the unit defined as the second-class boundary area flow, where inflow is positive, outflow is negative, and the water barrier is 0; Γ_2 is the mixed boundary; σ is the aquitard at the bottom of the river resistance coefficient, $\sigma=L/K_s$; L is the thickness of the aquitard at the bottom; K_s (m/d) is the vertical permeability coefficient of the aquitard at the bottom of the river.

3.3 Boundary conditions

In the model, the upstream and downstream boundaries and the river region are generalized as constant head boundary conditions, and two working conditions of normal water level before and after the completion of the project are considered. The water level at the pivot location is set according to the normal pool level at the location, the water level of each section of the river is set according to the interpolation of the normal pool level of the pivot at both ends of the reservoir, and the head node between the known sections of the river is calculated by interpolation. Fig. 3(b) shows the setting of water head boundary conditions for HB reservoir area model.

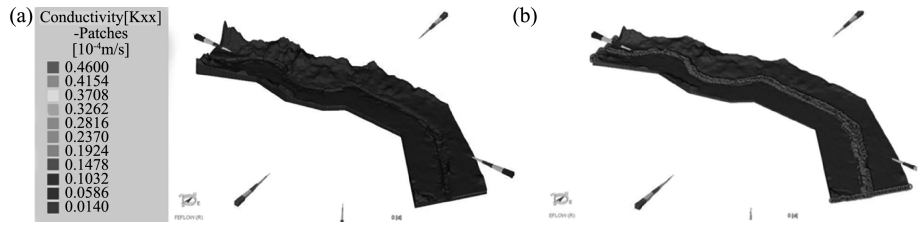

Fig. 3. (a) Geological stratification and permeability coefficient (magnified by 10 times in z direction); (b) Model boundary conditions (z-direction magnified 5 times).

3.4 Model validation

Six locations within the HB reservoir area are selected as verification points, including five drilling points (Z1 – Z5) and one field investigation point (D1). See Fig. 4 for the plane location of verification points and Table 3 for the specific information of verification points.

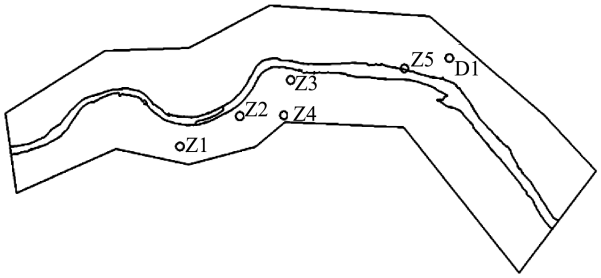

Fig. 4. Plane position of verification points.

The comparison between the groundwater numerical simulation results and the measured groundwater depth is shown in Table 3. From the table, we can see that the difference between the calculated value and the measured value of groundwater depth

at each observation point is between 0.07 m and 0.76 m, which is generally in good agreement. Therefore, we believe that the model can better reflect the distribution of groundwater level in the study area, and can be used to predict and analyze the impact of groundwater immersion in the reservoir area.

Table 3 Comparison between simulation results and measured data.

Observation Point	Orifice/Ground Elevation(m)	Measured burial depth(m)	Calculated groundwater level (m)	Calculated burial depth(m)
Z1	70.41	2.8	67.54	2.87
Z2	72.00	3.8	67.52	2.48
Z3	69.25	2.0	67.51	1.74
Z4	71.45	4.7	67.51	3.94
Z5	69.92	2.8	67.50	2.42
D1	69.78	2-3	67.46	2.32

3.5 Determination of immersion evaluation criteria

Sun et al. (2012) have analyzed the factors affecting the submergence of riparian reservoirs, up to 12 categories, and they can be further summarized into three aspects: groundwater level, soil texture (as the rising height of capillary water), crop tolerance and building foundation strength (as the safety superelevation).

We call the depth of groundwater burial at which submergence occurs the critical depth of groundwater. Immersion will not occur if the actual water table after impounding of the reservoir does not reach the immersion level; immersion may occur if the above level is exceeded. The formula for calculating the critical groundwater depth of submergence is:

$$H_{cr} = H_k + \Delta h \tag{2}$$

where H_{cr} (m) is the burial depth of the submerged critical groundwater; H_k (m) is the height of the capillary water rise zone of the soil above the groundwater level; Δh (m) is the safe ultra-high value.

We have calculated the depth of groundwater. The capillary rise height of soil is mainly obtained through field investigation or indoor test. The surface soil layer within the immersion influence range of the study area is mainly silty fine sand (with gravel) layer. Referring to the research results of Zhang et al. (1988) (Table 4), the capillary rise height of surface soil is taken as 1.00 m.

Table 4 Capillary rise value of different soils (by Zhang et al. 1988).

Soil type	h_c (m)	Soil type	h_c (m)
Gravel soil	0.05 - 0.10	Silt soil	1.00 - 2.00
Coarse sand	0.10 - 0.15	Sandy soil	2.00 - 3.00
Medium sand soil	0.15 - 0.25	Loam	1.00 - 2.00
Fine sand	0.25 - 0.50	Clay	0.50 - 1.00
Very fine sand	0.50 - 1.00		

The safety superelevation value is related to the evaluation object. The root depth of crops should be considered when taking crops as the evaluation object, and it depends on the bearing capacity of the foundation when taking buildings as the evaluation object. The crops planted in the study area are mainly grapefruit, citrus and other cash crops, and the root length is 0.50 m to 1.00 m. According to the theoretical derivation of the survey data above, the critical groundwater depth of immersion in the study area should be 2.00 m. At the same time, referring to the experience of each reservoir area of QJ river waterway project after impoundment, we finally get the critical groundwater depth of 0.5 m in farmland area and 1.0 m in building area to control.

4 Results

4.1 HB reservoir

The distribution of the groundwater level before and after the construction of HB reservoir is shown in Fig. 5(a) and Fig. 5(b). It can be seen from the figure that the distribution law of the underground water level at the location of HB hydroproject is similar under the two working conditions. After the reconstruction of the hydroproject, the underground water level increases as a whole, and the equal water head line at the hydroproject location is densely distributed.

The distribution of groundwater depth in HB reservoir area is shown in Fig. 5(c) and Fig. 5(d). It can be seen from the figure that there is no area with groundwater depth less than 1.0 m after the completion of HB reservoir. The villages and towns around the reservoir are arranged with observation points to monitor the groundwater level. The results show that the groundwater depth around the villages is more than 2.0 m after the completion of the reservoir, and there is no reservoir immersion in the villages and towns around the HB reservoir area.

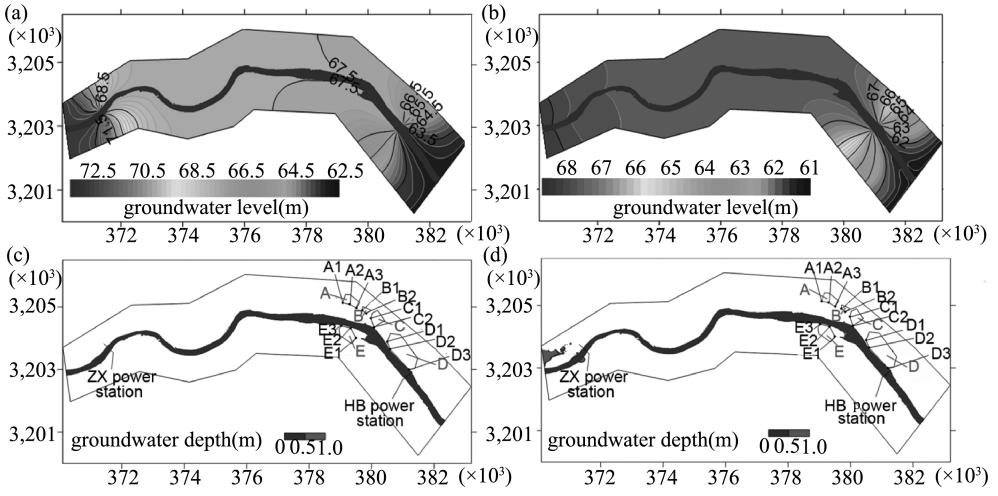

Fig. 5. (a) Groundwater level distribution before HB reservoir area completion; (b) Groundwater level distribution after HB reservoir area completion; (c) Groundwater depth distribution before HB reservoir area construction; (d) Groundwater depth distribution after HB reservoir area construction.

4.2 BHT reservoir

In order to observe the impact of the new hydropower station on the immersion of surrounding villages, we selected the new BHT reservoir area as the research object, and the results are as follows.

The distribution of the groundwater level before and after the construction of BHT reservoir is shown in Fig. 6(a) and Fig. 6(b). Before the completion of BHT project, the distribution of groundwater level on both banks is similar to that of river water level. However, after the completion of the BHT project, the water level in the reservoir area rises, and the distribution of the surrounding groundwater level has changed significantly. The groundwater level at the location of the project has risen from 84. 40 m to 89. 50 m, and the water head lines are densely distributed.

The distribution of groundwater depth in BHT reservoir area is shown in Fig. 6 (c) and Fig. 6(d). It can be seen from the figure that there is no area with groundwater depth less than 1.0 m on both sides of the river before the completion of the project. After the hydroproject is completed, there are areas with groundwater depth less than 1.0 m around villages A, B, D, E and F, with a total area of 1.382 km^2. The immersion location is about 788 – 2,842 m away from the BHT hydroproject dam site, and the maximum vertical distance from the riverway is about 858 m. The immersion influence range is relatively large.

The elevation distribution of river beaches around B and E villages is shown in Fig. 7(a). The elevation in this area is 89.50 m lower than the normal pool level, and

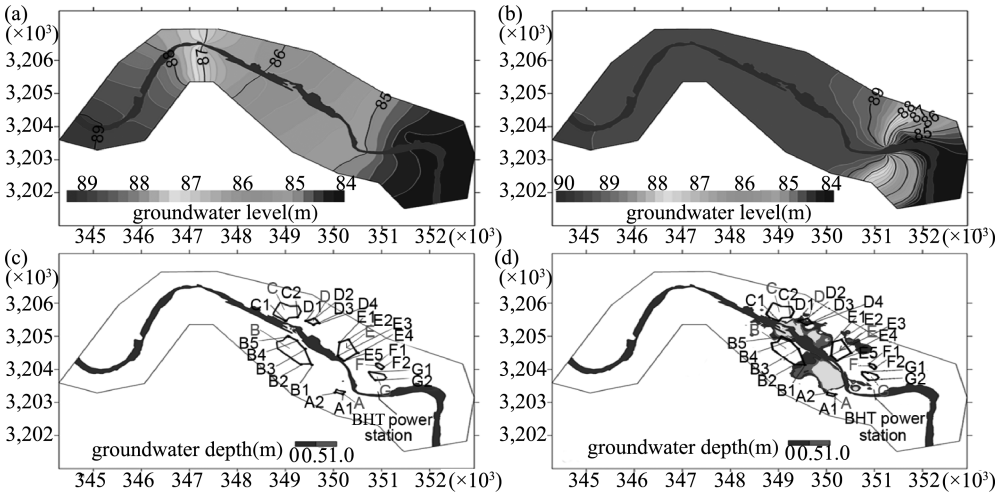

Fig. 6. (a) Groundwater level distribution before BHT reservoir area completion; (b) Groundwater level distribution after BHT reservoir area completion; (c) Groundwater depth distribution before BHT reservoir area construction; (d) Groundwater depth distribution after BHT reservoir area construction.

the lowest elevation is 86.10 m. The relationship between the buried depth of groundwater and the location of surrounding villages after the completion of the project is shown in Fig. 7(b). The range line of the buried depth of groundwater of 1.0 m is close to the edge of villages B, C and E.

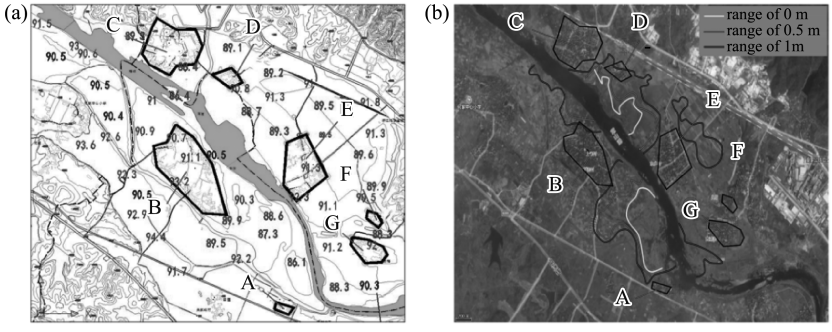

Fig. 7. (a) Surface elevation distribution of river shoals around B and E villages; (b) submerged area and moderately submerged area around B and E villages.

Arrange observation points in villages and towns around the reservoir to monitor the groundwater level. After the reservoir was filled, the groundwater level rose by at least 3.5 m. After the completion of the hydroproject, there are areas with groundwater depth less than 1.0 m in the north and south of B village, south of C village, west of D village and south of F village. The high groundwater level will have a certain impact on the foundation of buildings in this area.

4.3 Summary of immersion results for each reservoir

The immersion conditions of each reservoir area are summarized as shown in Table 5. The total area of land immersion along the two banks of the reservoir area reaches 6.456 km^2, and the immersion disasters of ZX reservoir area and BHT reservoir area are more serious.

Table 5 Summary of coastal immersion in reservoir area of each reservoir.

Reservoir	Immersion hazard level	Immersion zone conditions	
		Area	Maximum width of immersion zone
HTQ	Slight	0.145	178
HB	Medium	0.687	500
ZX	Serious	1.446	700
GD	Slight	0.119	150
TM	Medium	0.328	370
BHT	Serious	3.731	900
SUM		6.456	

5 Discussion

5.1 Influence of new construction and reconstruction on groundwater level distribution

By comparing and analyzing the groundwater levels before and after the construction of BHT Reservoir (Fig. 6(a) and Fig. 6(b)), we find that the distribution law of groundwater before the construction of the project is consistent with that of the river water level. When the reservoir is impounded, the groundwater level rises, and the distribution of groundwater level in the reservoir area tends to be consistent. This indicates that the reservoir hinders the discharge process of groundwater after impoundment, resulting in the rise of groundwater level and the change of groundwater flow direction. By analyzing the HB reservoir area (Fig. 5(a) and Fig. 5(b)), we find that the groundwater distribution in the HB reservoir area is similar before and after the reconstruction. Compared with the groundwater level distribution in the BHT reservoir area, the reconstructed HB hub has less disturbance to the groundwater than the newly built BHT hub. To sum up, we can find that both the building hub and the reconstruction hub will lead to the rise of groundwater level, and the new project will have a greater impact on the distribution of groundwater and change the flow direc-

tion of the original groundwater.

5.2 Analysis of influencing factors of reservoir immersion

Through the analysis of six cascade reservoirs, we found that there was no reservoir immersion before the completion of each reservoir. After the completion of each cascade reservoir, the surrounding villages and towns of each reservoir showed the situation of reservoir immersion. This indicates that reservoir impoundment can cause reservoir submergence.

From Fig. 6(c), we can see that the location of reservoir immersion is not only at the edge of the river, but also at the location far away from the river bank. In Fig. 6 (c), there is a separate immersion area in the east of E village. Comparing Fig. 7(a) and Fig. 7(b), we can see that the elevation of the reservoir immersion area is lower than areas where no reservoir flooding has occurred, which indicates that the topography has an impact on the distribution of groundwater and thus on the reservoir immersion.

Combining our modelling process, we can find that the influencing factors of reservoir immersion are groundwater depth, topographic conditions, stratum structure, permeability characteristics, building foundation strength and crop tolerance to groundwater.

5.3 Reservoir immersion control measures

Based on the other engineering cases and engineering practice, we believe that in the farmland area, the destructive impact caused by immersion can be avoided or reduced by changing the types of crops planted in the slightly immersed area and setting up intercepting ditches or drainage ditches in the moderately or severely immersed area. Necessary anti-seepage measures may be taken for the reservoir bank in cities and towns with serious submergence or in the river sections of the reservoir area where key buildings need to be protected. For example, anti-seepage grouting curtain and anti-seepage wall may be arranged near the side of the dike to block the basic seepage channel of the dike.

6 Conclusions

In this paper, the submergence of six cascade reservoirs on the CSJ River is analyzed and evaluated. Three-dimensional groundwater numerical simulation model is established to predict the inundation of each cascade reservoir. The inundation conditions of six cascade reservoirs before and after the completion of the project are calcu-

lated and compared. The results show that:

(1) According to the actual setting of the shipping hub, the CSJ River waterway is divided into several reservoir areas for calculation, which can reduce the difficulty of calculation and improve the accuracy.

(2) After the impoundment of the reservoir, the groundwater around the reservoir rises obviously, the equal water head line is densely distributed, and the reservoir immersion phenomenon occurs in some areas.

(3) Both the new project and the reconstruction project will cause the redistribution of groundwater level, both of which will lead to the increase of groundwater level, while the new project will change the direction of groundwater flow.

(4) The influencing factors of reservoir immersion include groundwater depth, stratum structure, permeability, topographic conditions, foundation strength of buildings and tolerance of crops to groundwater.

(5) It is verified that the 3D groundwater model generalized by geological and hydrological data in this paper has high accuracy and can accurately predict the immersion of CSJ River Reservoir.

Acknowledgements

This research was supported by the National Natural Science Foundation of China (grant numbers 42177079 and U1765202), the Central Public-Interest Scientific Institution Basal Research Fund (grant number Y1♯22001), the China Power Construction Group Project (grant number DJ-ZDXM-2019—44) and the Guizhou Science and Technology Planning Project (grant number [2020]4Y024).

References

Dai, C.L., Fan, Q.M., Li, H.M., et al., 2012. Critical groundwater depth of reservoir immersion hazard in cold region. Journal of Engineering of Heilongjiang University, 3(4): 9-14+20.

Ji, J.J., 2005. Evaluation and prediction on immersion problem of Guanting Reservoir. Water Resources and Hydropower Engineering (2): 18-21.

Kang, S.B., 1958. Some opinions on the submersion of Guanting Reservoir. China Water Resources (4): 36-38.

Li, N.X., 2008. Inundating problem in reservoir of low-head run-of-river plant in South China. Pearl River (2): 30-33.

Li, Z.F., 2001. Submersion compensation and thinking of Guanting Reservoir. Wa-

ter Sciences and Engineering Technology (2): 20-21.

Ling, K.Q., 1992. A preliminary discussion on the problem of reservoir immersion. Water Resources & Hydropower of Northeast (7): 26－29＋48.

Ma, T.W., 2006. Analysis of the current situation of immersion in the first-phase project of Taoshan Reservoir and prediction of the immersion of the second-phase project. Heilongjiang Hydraulic Science and Technology (3): 159.

Ren, Y.F., Cao, J.Z., and Wei, C.Q., 2013. Immersion analysis of Longhu Water Diversion Reservoir from Yellow River. Yangtze River, 44 (16): 90-94.

Sun, S.M., 2012. Experiment and modelling of the influence of reservoir inundation in cold regions. Heilongjiang University, Harbin, Heilongjiang.

Sun, S.M., Dai, C.L., and Lv, Y.J., 2012. Influencing factors and prevention measures of riverbank-type reservoir inundation. Water Resources and Power, 30 (4): 94-96.

Tang, S.F., 1957. Several problems in the flood prediction of Guanting Reservoir. Water Power (23): 16-21.

Wang, H.M., 2004. Analysis and research on immersion of reservoir in the plain. Hohai University, Nanjing, Jiangsu.

Wang, W.D., 2003. Brief analysis of engineering geological problems in Zhangfeng reservoir area. Journal of Electric Power (4): 304-306.

Wu, W.J., Mu, P., 2012. Research on the submergence of the reservoir area of a hydropower station on the Yellow River. Yellow River, 33 (4): 102－103＋106.

Xing, D.Z., Sun, W.H., Bi, Y.X., et al., 1996. Analysis on pumping test of well drainage project in submerged area of Guanting Reservoir. China Rural Water and Hydropower (7): 19-20.

Yu, J.K., and Huang, H., 2008. Discussion on immersion control measures of plain type reservoirs. Hunan Hydro & Power (5): 64-66.

Zhang, J.G., and Zhao, H.J., 1988. Groundwater capillary rise and determination. Ground Water (3): 135-139.

Zhu, J., and Wang, H.M., 2006. The application of two-dimensional seepage finite element method to the analysis of immersion of the Chaozhou Reservoir. Acta Geological Sichuan (2): 121-124.

Study on calculation method of water level and discharge relationship at cascade navigation-power junction dam site based on hydrodynamic calculation

Chunhui Yu[1], Ming Zhang[2], Xingwei Zheng[3], Honghao Fan[4], Qing Leng[5]

[1,5] Quzhou Highway Port and Shipping and Transportation Management Center, Quzhou, China. e-mail:583129184@qq.com

[2] Key Laboratory of Navigation Structures, Nanjing Institute of Hydraulic Sciences, Nanjing, China. e-mail: zhangm@nhri.cn

[3,4] Quzhou Xin'an Shipping Construction Development Co., Ltd., Quzhou, China. e-mail: 49314063@qq.com

Abstract: In order to rationally use hydraulic resources, multi cascade hydroproject development is often carried out for rivers. Physical model test is the main method to determine the hub layout scheme and key performance parameters. Determining the relationship between water level and discharge at the dam site of each cascade hydroproject is a necessary prerequisite for carrying out physical model test and ensuring the reliability of test results. However, the actual hydrological stations and their measured hydrological data often cannot directly meet the needs of analyzing and determining the relationship between water level and discharge at the dam site. In this paper, through the combination of hydrodynamic model and weir flow standard calculation formula, and through step-by-step recursive iterative calculation, the water level and flow relationship of each dam site of Changshan River Cascade Hydropower Junction is determined, so as to provide reasonable boundary control conditions for the physical model test of each junction.

Keywords: Cascade hydroproject; Boundary conditions; Hydrodynamic calculation; Weir flow calculation; Water level and discharge relationship

1 Introduction

In order to reasonably determine the layout type and design performance parameters of each cascade hydroproject, it is necessary to carry out the overall physical model test of the hydroproject, and the relationship between water level and dis-

charge at the dam site of each hydroproject is a necessary prerequisite for carrying out the corresponding model test conditions. Within the reach of this study, Changshan (Ⅲ) hydrological station is only located at the downstream of the second cascade (see Fig. 2). It is obviously difficult to accurately analyze the water level and discharge relationship of each cascade hydroproject dam site with the only data.

Hydraulic conditions of the Changshan River single-stage project are closely related to adjacent cascades. In this paper, through the combination of the whole river flow mathematical model and weir flow calculation formula, the flow conditions under the joint operation of the hub are calculated, and the water level and discharge relationship of each cascade hub dam site is reasonably determined.

2 Project overview

Changshan river channel is from Huibu to Intersection of two ports river section. The starting point of Changshan River (Huibu to Intersection of two ports) avionics hub project is located in the planned Huibu operation area, and the ending point is connected with the starting point of Qujiang channel (Quzhou section) (Intersection of two ports), with a total length of about 50.9 km. It is constructed according to the natural and channelized class Ⅳ channel standards, and the channel scale meets the navigation requirements of 1,000 ton ships. Channel scale: 3.4 m×60 m×480 m (water depth×navigation width×bending radius).

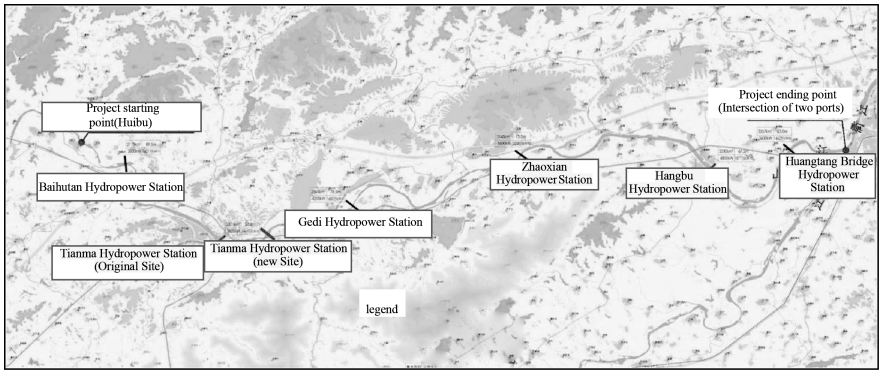

Fig. 1. Schematic diagram of cascade development of Changshan River Navigation Project.

The main stream of Changshan River (Huibu to Intersection of two ports) is divided into six levels of development, from downstream to upstream: Huangtang Bridge, Hangbu, Zhaoxian, Gedi, Tianma and Baihutan cascade hubs, and corresponding ship lock supporting facilities, channel dredging, embankment works, etc. The total installed capacity of the six cascade hydropower stations is 25.8 MW, and

the channel grade is grade Ⅳ. The task of each cascade is to focus on aviation, combine aviation with electricity, and give consideration to the comprehensive utilization functions of irrigation and water supply, flood control and improving the ecological environment. The distribution of Changshan River Cascade hubs is shown in Fig. 1, and the design performance parameters of each cascade hub are shown in Table 1.

Table 1 General layout parameters of Changshan River Cascade project.

Serial number	Project	Unit	Baihutan	Tianma	Gedi	Zhaoxian	Hangbu	Huangtang Bridge	Total
1	Catchment area of dam site	km^2	2,178	2,337	2,594	3,145	3,310	3,357	
2	Check flood level (P=1%)	m	93.83	85.90	82.70	78.02	71.40	69.17	
3	Design flood level (P=2%)	m	93.11	85.38	82.17	77.58	71.00	68.74	
4	Normal pool level	m	89.5	84	78.5	73	67.0	63	
5	Dead water level of power generation	m	89	83.5	78	72.5	66.5	62.5	
6	Installed capacity	10,000 kW	4.0	4.0	4.5	5.5	4.2	3.6	25.8
7	Design generation flow	m^3/s	102	116	116	130	161	162	787

3 One-dimensional numerical model of the whole river

The study area of the project is located in the section from Huibu to Intersection of two ports of the main stream of Changshan River, about 51 km. According to the topography of Changshan river channel and the distribution of cascade navigation and hydropower projects, a one-dimensional hydrodynamic simulation model of Changshan river channel based on cascade hub dispatching is constructed, and the model parameters are calibrated by using the measured flood data, which provides support for the calculation of water level and discharge relationship at the dam site of Changshan River Cascade hub and the numerical simulation of flow conditions of the whole river channel.

3.1 Model building

(1) Model scope

The upper boundary of the model is Changfeng hydrological station in the upper reaches of Changshan River and Macheli water level station in Jiangshan River, and the lower boundary is Quzhou hydrological station.

Fig. 2. Schematic diagram of one-dimensional flow simulation range of Changshan River.

(2) Boundary conditions

① Upper boundary

The upper boundary of the model provides the corresponding flow process for the model calculation.

Baihutan water control project is the most upstream level-1 hub of the project, and its upstream is the completed and operated Changfeng hub. About 300 m upstream of Changfeng hub, the right bank is the site of the original Changfeng hydrological station. In order to consider the impact of the operation of Changfeng power station on the downstream, it is necessary to ensure the accuracy of numerical simulation and reasonably extend the scope of numerical simulation. Therefore, the upper boundary of the one-dimensional flow – sediment simulation model of the whole reach is set as the site of the original Changfeng hydrological station, about 300 m upstream of Changfeng hub.

As rivers and mountains converge at the double ports upstream of Quzhou hydrological station, the jacking effect of rivers and mountains on the water level of Changshan River should be reasonably considered in the model calculation. The Macheli water level station about 2.2 km away from Intersection of two ports is taken as another upper boundary condition of the model.

② Lower boundary

The lower boundary of the model provides the water level process or flow – discharge process curve for the model calculation.

The lower boundary of the model is Quzhou hydrologic station, which is about 3 km away from the downstream of Intersection of two ports at Xi'an gate bridge. Quzhou hydrological station was established in 1930 and has rich measured sediment, flow and water level data.

③ Inner boundary

The cascade hubs of Huangtang Bridge, Hangbu, Zhaoxian, Gedi, Tianma and Baihutan within the simulation range will be used as the internal boundary control conditions of the model simulation.

(3) Model verification station

Xiayutou village, 3.9 km upstream of Changshan River Estuary, is equipped with Xiayutou water level station. The station is located near the last stage of Huangtang Bridge cascade hub of the project. The station will be used as a verification station for one-dimensional flow simulation model of the whole river section.

3.2 Model solving

(1) Basic equation

According to the relevant test regulations, specifications and relevant technical requirements, a one-dimensional flow mathematical model of the whole reach is established and solved.

Flow continuity equation: $$\frac{\partial Q}{\partial x}+\frac{\partial A}{\partial t}-q=0 \tag{1}$$

Momentum equation: $$\frac{\partial Q}{\partial t}+\frac{\partial}{\partial x}\left(\frac{Q^2}{A}\right)+gA\left(\frac{\partial h}{\partial x}+S_f-S_0\right)=0 \tag{2}$$

where: x、t are section distance and time; Q is the section flow, m^3/s; A is the sectional area, m^2; q is the side unit width flow, m^2/s; g is the acceleration of gravity, m/s^2; h is the average water depth of the section, m; S_f is the friction gradient; S_0 is the bottom slope of riverbed.

(2) Solution method

According to the technical specification for flow and sediment simulation of inland waterways and ports (JTJ/T232—98), the one-dimensional flow model adopted the Preissmann scheme for discrete difference solution.

3.3 Model verification

The accuracy of model roughness parameters determines the accuracy of model calculation results. The measured flood process should be used to calibrate the model parameters. The model construction adopted the measured river section in 2016. The flood in June 2017 was a major flood in Qujiang River Basin in recent years. The flood data are detailed and can be used to calibrate the model parameters. The measured water level processes of Changshan (Ⅲ) hydrological station, Xiayutou water level station, Macheli water level station and Quzhou hydrological station from 08:00 on June 11, 2017 to 05:00 on July 9, 2017 are collected, and the corresponding flood flow process of Changshan (Ⅲ) station is calculated and determined by using the annual calibrated water level and discharge relationship of Changshan (Ⅲ) station as the basic data for model parameter calibration. At the same time, referring to the on-site

investigation data of flood in 2017, the investigation flood level of characteristic locations such as Jujia, Tuan Village, Qingshi Town, Zhaoxian bridge, Hangbu bridge and Wanchuan is added as the basis for parameter calibration.

Simulated boundary conditions: the flow process of Changshan station and the water level process of Quzhou station and Macheli station are shown in Fig. 3 below.

Verification conditions: corresponding water level process of Xiayutou station.

Fig. 4 shows the measured water level and simulated water level process of the flood at Xiayutou station. It can be seen from the figure that the calculated flood process is basically consistent with the measured process, and the difference of flood peak water level is small, which shows that the model can better simulate the flood within the study range.

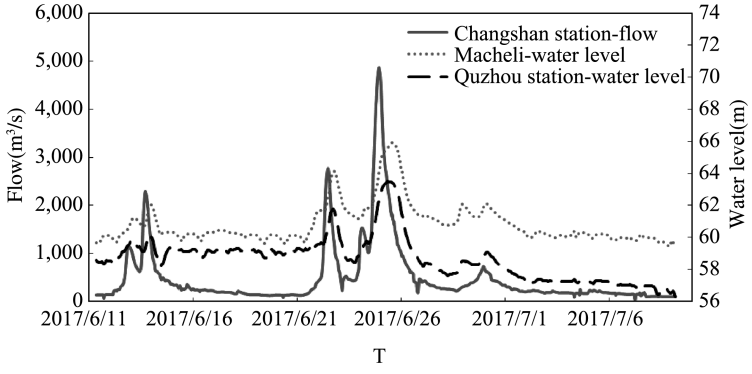

Fig. 3. Boundary conditions.

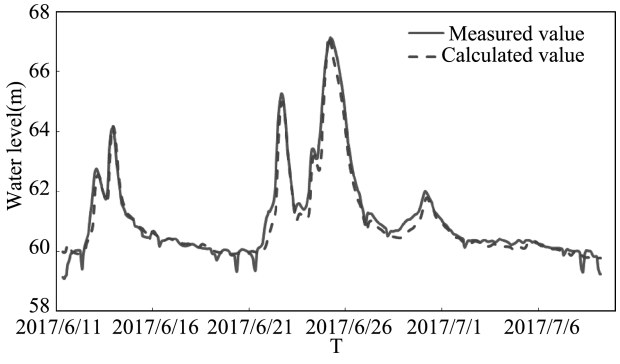

Fig. 4. Process of measured water level and calculated water level of Xiayutou water level station.

4 Relationship between water level and discharge at cascade dam sites of Changshan River

4.1 Computing method

The calculation method of segmented and graded constant flow is adopted to recur to the water level and discharge relationship between the upstream and downstream of the dam sites of various hydroprojects from bottom to top. According to the condition of "graded discharge + water level in front of the next cascade dam", firstly, the above one-dimensional numerical model (considering channel dredging, upstream and downstream dredging of the dam site and embankment design) is used for bottom-up flood calculation to determine the water level under the dam corresponding to each graded discharge of the upper cascade; secondly, the weir flow formula is used to determine the water level in front of the graded flood dam through iterative calculation according to the design parameters of each cascade sluice gate and considering the submerged water level under the dam. By analogy, the water level and discharge relationship of upstream and downstream of each cascade dam site are determined from bottom to top. The graded flood of each cascade includes the flood of different return periods at the corresponding dam site; at the same time, other floods of corresponding magnitude are reasonably interpolated or postponed upward and downward to ensure the representativeness and comprehensiveness of the drawing points of the relationship between water level and discharge.

The design parameters of each cascade gate shall be considered in the calculation, so as to determine the value of discharge coefficient of corresponding magnitude flood. See Table 2 for the statistics of design parameters of flood discharge gates of Changshan River cascade. When calculating the water level on the dam with different graded discharge, the design parameters of the gate and the water level under the dam will be considered, and the values of parameters such as submergence, discharge coefficient, lateral shrinkage coefficient and submergence coefficient will be calculated iteratively to determine the water level on the dam.

Table 2 Design parameters of cascade flood discharge gates.

	Huangtang Bridge	Hangbu	Zhaoxian	Gedi	Tianma	Baihutan
Top elevation of sluice floor (m)	58.5	60.5	66.0	72.5	76.5	83.0
Clear width of single hole (m)	14	14	14	14	14	14

continue

	Huangtang Bridge	Hangbu	Zhaoxian	Gedi	Tianma	Baihutan
Number of holes	16	16	18	17	14	15
Total clear width of flood gate (m)	224	224	252	238	196	210
Dredging elevation of upstream river (m)	58.0	60.0	65.5	72.0	76.0	82.5
Bottom elevation of stilling basin under dam (m)	56.0	58.0	64.5	70.0	74.0	80.5
Top elevation of stilling basin under dam (m)	58.5	60.5	66.0	72.5	76.5	83.0
Top elevation of downstream apron (m)	57.5	59.5	67.0	71.5	75.5	82.0
Downstream river dredging elevation (m)	57.5	59.5	65.0	71.5	75.5	82.0
Gate side pier type	Fillet shape	Fillet shape	Fillet shape	Fillet shape	Fillet shape	Fillet shape
Plane shape of pier head	Semicircle	Semicircle	Semicircle	Semicircle	Semicircle	Semicircle
Current river width at dam site (m)	190	230	212	230	175	164
River width after completion (m)	300	300	350	350	300	300

4.2 Relationship between water level and discharge at the downstream cascade dam site

As the most downstream cascade, the rationality and accuracy of the water level and discharge relationship at the dam site of Huangtang Bridge hydroproject determine the accuracy of the water level and discharge relationship at the dam sites of upstream cascade hydroprojects. Considering the actual jacking impact of the downstream river inflow on the water surface line along the Changshan River, the reach below Huangtang Bridge takes Quzhou hydrological station as the calculation lower boundary, and reasonably considers the corresponding river discharge under each calculation condition.

The flood combination of Changshan River, Jiangshan River and Qujiang River adopts the combination method of "Changshan River and Qujiang River have the same frequency, and rivers, mountains and rivers correspond", that is, the incoming flow of rivers, mountains and rivers is the difference between the flow of Quzhou hydrological station and that of Changshan River with the same frequency. The water level of Quzhou hydrometric station corresponding to different classified flows is determined by analyzing the water level and discharge relationship curve of Quzhou station site in 2017.

The downstream water level at the dam site of Huangtang Bridge hydroproject is

calculated by using the river hydraulic model, and the corresponding water level in front of the dam is obtained by using the weir flow formula. The water level and discharge relationship of Huangtang Bridge dam site is calculated by using the constant flow method. The design conditions are shown in Table 3.

Table 3 Calculation conditions.

Classification number	Huangtang Bridge flow(m^3/s)	Jiangshanjiang flow(m^3/s)	Quzhou Railway station flow (m^3/s)	Quzhou Railway station water level (m)
1	162	88	250	59.5
3	400	218	618	59.5
5	800	219	1,019	59.5
7	1,200	328	1,528	58.83
8	1,400	383	1,783	59.15
11	3,020	895	3,930	61.44
13	4,610	1,200	5,830	63.14
17	6,470	1,525	8,042	64.98
21	8,280	1,860	10,200	66.91
22	9,360	1,980	11,400	67.98

By calculating the step-by-step flow from the lower boundary to the water level under the dam through the hydraulic method, the water level and flow relationship downstream of the dam site of Huangtang Bridge hydroproject can be determined. Then, considering the design characteristic parameters of the sluice gate of the hydroproject, it is assumed that the water level in front of the dam is determined by the iterative calculation of the weir flow formula in the open discharge mode of the hydroproject. If the calculated water level in front of the dam is lower than the normal pool level, the water level in front of the dam shall be taken as the normal pool level, and the sluice gate shall discharge according to the discharge control mode. In the step-by-step and segmented flow calculation, the flow difference between the upstream and downstream steps, that is, the interval inflow, adopts the way of linear inflow along the way to participate in the model calculation.

$$Q = \sigma_s \varepsilon m B \sqrt{2g} H_0^{3/2} \tag{3}$$

where: Q—Gate flow (m^3/s); σ_s—Weir flow submergence coefficient; ε—Contraction coefficient of weir flow side; m—Weir flow coefficient, which can be 0.385; B—Total clear width of gate hole (m); H_0—Water depth on weir included in approaching velocity head (m); g—Gravitational acceleration.

The water level and discharge relationship between the upstream and downstream

of the dam site of Huangtang Bridge hydroproject determined by calculation is shown in Fig. 5 below.

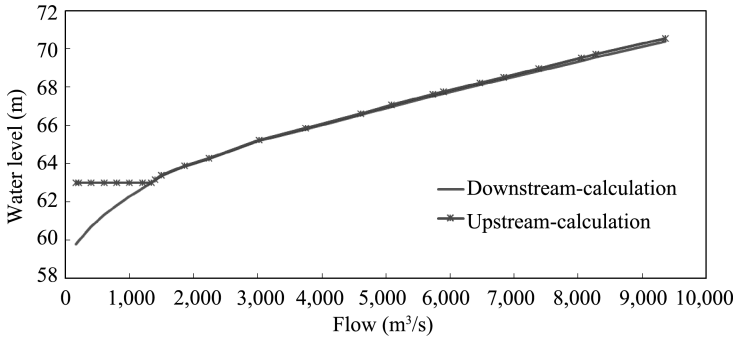

Fig. 5. Water level and discharge relationship between upstream and downstream of Huangtang Bridge hydroproject dam site.

4.3 Water level and discharge relationship of other cascade dam sites of Changshan River

After the water level and discharge relationship of the most downstream cascade Huangtang Bridge hydroproject dam site is determined through hierarchical calculation, the same method is used to calculate and determine the water level and discharge relationship of Hangbu, Zhaoxian, Gedi, Tianma and Baihutan hydroproject dam sites step by step and from bottom to top, as shown in Fig. 6 to Fig. 10 below. The calculation and determination of the relationship between water level and discharge at the dam site of cascade hydroproject can provide boundary conditions for the overall physical model test of the hydroproject.

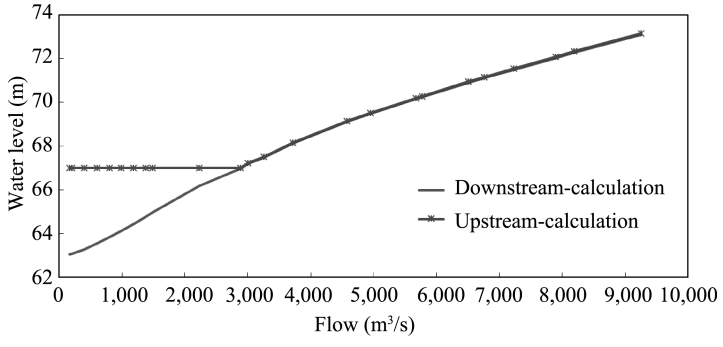

Fig. 6. Relationship between water level and flow at upstream and downstream of Hangbu hydroproject dam site.

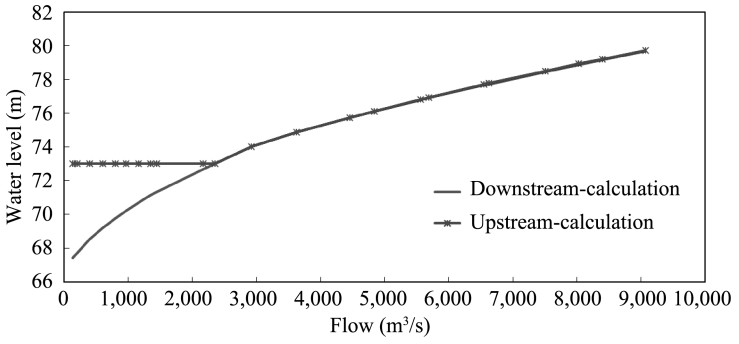

Fig. 7. Relationship between water level and flow at upstream and downstream dam sites of Zhaoxian hydroproject.

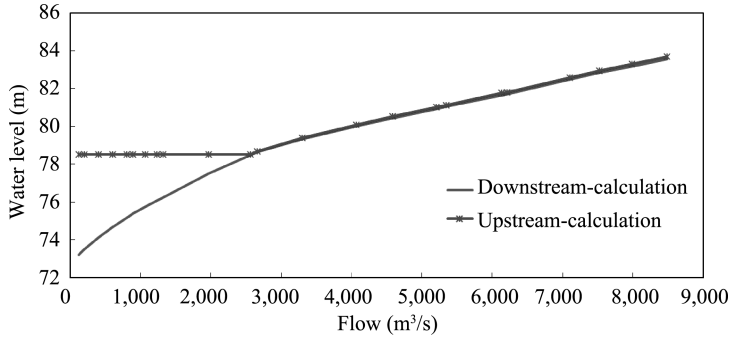

Fig. 8. Relationship between water level and flow at upstream and downstream of Gedi hydroproject dam site.

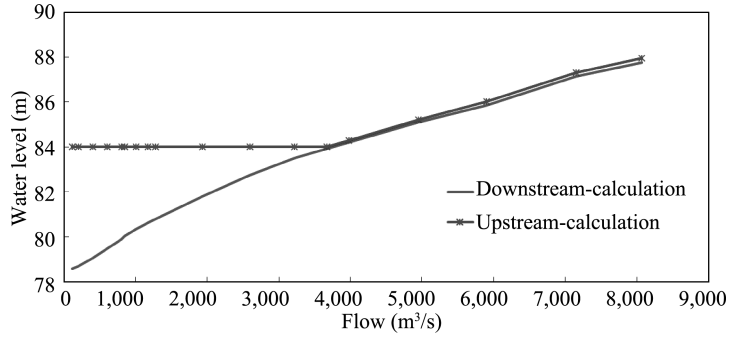

Fig. 9. Relationship between water level and flow at upstream and downstream of Tianma hydroproject dam site.

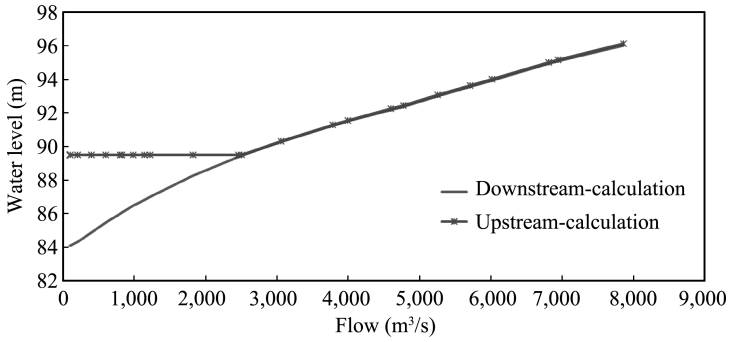

Fig. 10. Relationship between water level and flow at upstream and downstream of Baihutan hydroproject dam site.

5 Conclusions

The relationship between water level and discharge at the dam site of cascade hydroproject is a necessary boundary condition for the physical model test of hydroproject. The construction of cascade hubs divides the natural hydrological and hydraulic characteristics of the river, and the measured hydrological series of existing hydrological stations are difficult to meet the needs of stage – discharge relationship analysis of cascade dam sites. In this paper, by combining the hydrodynamic model with the calculation formula of weir flow specification, considering the influence of the confluence of rivers, mountains and rivers in the interval tributary, the model calculation boundary conditions are reasonably determined. Through step-by-step recursive iterative calculation, the water level and flow relationship of each dam site of Changshan River Cascade Hydropower Junction is analyzed and calculated, so as to provide reasonable boundary control conditions for the physical model test of each junction. It provides key technical support for the construction of Changshan River Cascade hubs.

Acknowledgements

This study is financially supported by the National Key R&D Program of China (2021YFC3200302).

References

Qu, Z. H. Research on Qujiang channel navigation condition. Hangzhou: Zhejiang University, 2014.

Zhang, M., Hu, Y. A., Fan, Z. W. Optimization of operation mode of cascade hub based on integration of navigation-power junction. Port & Waterway Engineering, 2016, 12:113-119.

Pre-feasibility study report on flood discharge sluice project of hydropower station of Changshan River main stream (Huibu to Intersection of two ports) navigation power junction project, Zhejiang Water Resources and Hydropower Survey and Design Institute Co., Ltd., 2019.

Pre-feasibility study report of Changshan River (Huibu to Intersection of two ports) avionics hub project, Zhejiang Shuzhi Jiaoyuan Technology Co., Ltd., 2019.

One of the relevant model test research reports of Qujiang (Quzhou section) navigation development project hub and ship lock in the middle and upper reaches of Qiantang River, one-dimensional numerical simulation of flow and sediment in the whole river, Nanjing Institute of Hydraulic Sciences, 2010.

Channel regulation model test of Yangfushan new port area of Oujiang River, Nanjing Institute of Water Resources, 2012.

Numerical simulation study on flow and sediment of channel regulation project in the engineering feasibility stage of Oujiang (Wenzhou section) shipping development project, Nanjing Institute of Hydraulic Sciences, 2013.

Study on Numerical Simulation of one-dimensional flow and sediment in the whole reach, Nanjing Institute of Hydraulic Sciences, 2009.

Simulation and analysis of the stability of vegetation-covered ecological river bank

Youzhi Hao[1], Dongdong Jia[2], Xingnong Zhang[3], Lei Wu[4], Jun Yang[5], Changying Chen[6]

[1,2,3,4,5,6] Key Laboratory of Port, Waterway and Sedimentation Engineering of Ministry of Transport, Nanjing Hydraulic Research Institute, Nanjing, China

[2] Yangtze Institute for Conservation and Development, Nanjing, China. e-mail: hao_youzhi@foxmail.com; ddjia@nhri.cn; xnzhang@nhri.cn; 1693260842@qq.com; yjun2021@163.com; 771958982@qq.com

Abstract: River bank collapse frequently occurs in rivers. In order to protect the river bank and stabilize the river situation, a large number of hard revetments have been applied to the river bank collapse zone in the past. However, the rigid bank protection structure is not conducive to the sustainable development of the ecological environment. Therefore, the vegetation-covered bank protection has become an important measure for modern ecological river management. So it is necessary to evaluate the stability of the vegetation-covered ecological bank slope and guide the design and application of the ecological bank protection project. In this paper, the finite element method based on the principle of strength reduction is adopted, and the stability of the bank slope is calculated by taking into account the reinforcement effect of the vegetation root system on the soil. For herbaceous vegetation, the root tensile strength is small but the distribution is relatively dense, so the root-containing area of the bank slope is treated as a root-soil complex. For arbor and shrub vegetation, the tensile strength of the root system is relatively large, and the relative distribution range is wide and sparse. Therefore, the root system of the arbor and shrub is considered as the anchor rod structure. At the same time, the hydrostatic pressure in the river channel and the pore water pressure caused by the seepage of the water body are also considered when calculating the stability of the bank slope. The results show that when the herb vegetation is distributed on the top of the river bank, its root system is more conducive to the stability of the bank. And when the tree and shrub vegetation is located on the bank slope, the effect of stabilizing the river bank is better.

Keywords: Vegetation; Roots; River bank; Stability

1 Introduction

The traditional river bank protection is mainly based on engineering protection

measures, such as the bank protection structure made of concrete, masonry and other materials. These types of bank protection can effectively avoid the collapse of the river bank, but they block the ecological connection of water and land, and seriously damage the waterfront ecological environment. At the same time, the hard protective components will be weathered and fall off over time, resulting in a decrease in protective performance. The use of vegetation for riparian protection can not only effectively maintain the ecological balance of the riparian zone, but also play a role in strengthening the beach and protecting the bank (Gasser et al., 2020; Andreoli et al., 2020). With the extension of time, the root system of the vegetation will become more developed, making the reinforcement effect on the riparian soil better and better (Docker et al., 2008; Gurnell et al., 2019). Therefore, vegetation revetment has received extensive attention in recent years. For a long time, the statement that vegetation enhances the stability of river banks and stabilizes river conditions has been generally recognized, but there are few quantitative studies on the effect of vegetation on river bank stability. Relevant researchers have explored the stabilizing effect of plant roots on bank slopes from experimental research methods (Gray et al., 1983; Wu et al., 1988). Generally, the shear strength of soil is measured by direct shear test of soil samples containing roots on bank slopes. Similar test results can determine the influence of root system on soil mechanical properties, but the soil strength parameters under the action of root system are not further used in the calculation of bank slope stability. In fact, for the evaluation of beach stability, based on the above research on the reinforcement and soil stabilization of the vegetation root system, an appropriate root-soil complex model can be established to calculate the safety factor of the banks, so as to quantitatively evaluate the stability of ecological banks. In addition, for the trees and shrubs whose roots are not densely distributed but widely distributed, the effect of gas bank protection is not considered.

In this paper, the finite element numerical analysis method is used for simulation. By analyzing the distribution of root systems of different types of vegetation, different root-soil interaction modes are selected respectively, and the influence of vegetation type and distribution location on the safety factor of river bank stability is discussed.

2 Methodology

2.1 Numerical simulation method

The herb roots are densely distributed, and the roots are tightly entangled with

the riparian soil, which enhances the mechanical strength parameters of the soil (Pollen et al., 2005). The root system of arbors and shrubs is not as dense as the root system of herbs, but the root system is developed, and the root length can reach several meters. When the root system goes deep into the ground, the shallow soil of the river bank can be anchored to the deep soil of the river bank, which can effectively improve the stability of the river bank. Therefore, as shown in Fig. 1, in the model, the action of herb roots is reflected by the mechanical strength of the shallow root-soil complex. In fact, the root system of trees and shrubs is not only a single rod-shaped distribution, but also has many lateral or oblique branches. However, the cohesion or supporting effect of these branches on the soil is less than its anti-slip effect. Therefore, the morphological characteristics of the root system are not considered in this paper, and only the root system of trees and shrubs is simplified as a rod-shaped distribution, and its role is approximated as an anchoring anti-sliding pile to study its bank-fixing effect.

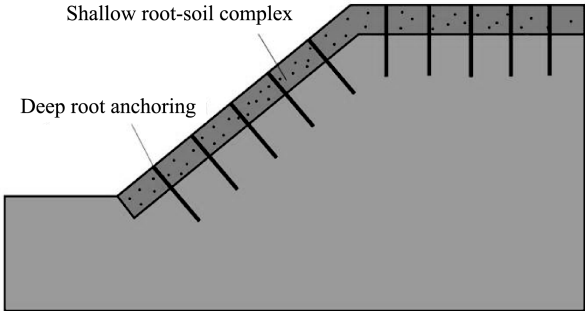

Fig. 1. Mechanism of stabilizing river bank by vegetation root system.

2.2 Numerical simulation method

Considering that the river bank is also affected by the infiltration of the channel water and the hydrostatic pressure, the direct coupling method is used to calculate the displacement and pore pressure of the element matrix or element load through the fluid-structure coupling equation. On this basis, the strength reduction principle applied to the bank stability calculation can be used to obtain the bank plastic strain and the bank slope stability safety factor.

The strength reduction method can directly obtain the bank slope stability safety factor through finite element numerical simulation calculation. It is relatively common in engineering applications. The reduced cohesion parameter expression is shown in Eq. (1), and the reduced internal friction angle parameter expression is shown in Eq. (2):

$$c_m = c/F_r \tag{1}$$

where c is the cohesion value that the soil can provide. c_m is the cohesion value required to maintain equilibrium. F_r is the strength reduction factor.

$$\varphi_m = \arctan(\tan\varphi/F_r) \tag{2}$$

where φ is the internal friction angle in the anti-reduction strength index that the soil can provide. φ_m is the internal friction angle in the decompression strength index required to maintain balance.

Different strength reduction coefficients are assumed in the calculation, and finite element analysis is performed according to the strength parameters after reduction to observe whether the calculation converges. It increase continuously throughout the calculation process, and the strength reduction factor when the critical failure is reached is the slope stability safety factor.

At present, the evaluation criteria for judging whether the soil slope has reached the critical failure are mainly as follows:

(1) Whether the bank slope will be unstable is judged by whether the numerical calculation converges or not. When the calculation results do not converge, it indicates that the maximum stress exerted by the soil is less than the strain caused by the external load exerting pressure on the soil. In this case the soil will be destroyed.

(2) Observe the plastic area of the bank slope to see if a continuous penetration area is formed in the slope body. If the plastic area is penetrated, it is considered that the soil is unstable and damaged.

(3) Select the feature points and observe the displacement changes of the feature points. The sudden change in the displacement of the characteristic part is used as the basis for instability. At the inflection point of the correlation curve between the safety factor and the displacement, the soil mass can be considered to be damaged.

2.3 Model parameters

The river bank geometric model takes the river bank height of 4 m, the slope of 45°, the water level of 2 m, the soil layer containing the herb root system of 0.5 m thick, and the root system of trees and shrubs is simplified as a single anchoring pile with a length of 1 m. The soil parameters and root system parameters are shown in Table 1. The ideal elastic-plastic model is used as the soil model, and the Mohr-Coulomb constitutive model is used to describe the soil properties. The root system is set as an elastic material, and the soil constraint on the root system is simulated by using embedded constraints.

Table 1 Soil and root parameters.

	Internal friction angle(°)	Cohesion (kPa)	Bulk density (kN • m^{-3})	Elastic modulus (MPa)	Poisson's ratio
Plain soil	30	15	23	20	0.3
Root-soil complex	30	38	23	20	0.3
Root system of trees and shrubs	——	——	——	400	0.25

3 Results

3.1 River bank stability safety factor

Fig. 2 shows the stability safety factor of the river bank under different cases. By comparing the stability safety factor of the plain soil river bank and the vegetation root system to reinforce the river bank, it is found that the vegetation root system can improve the stability of the river bank, but it depends on the type of vegetation and vegetation planting location.

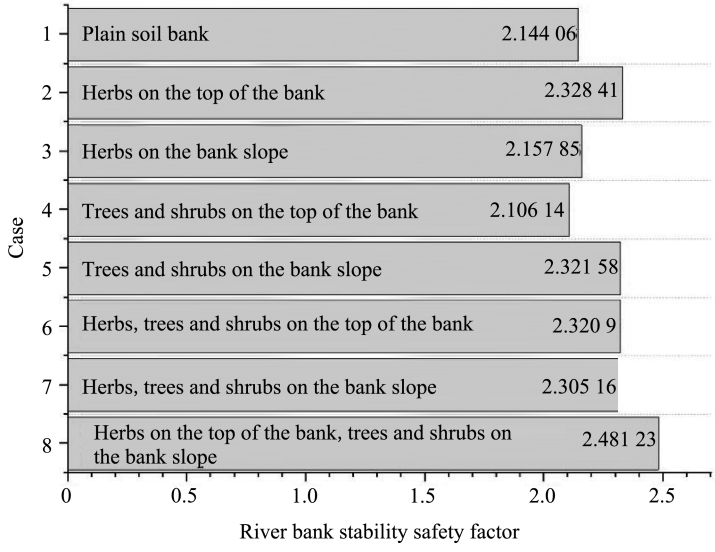

Fig. 2. River bank stability safety factor under different cases.

When the herb vegetation was planted on the top of the river bank, the bank fixing effect was better than that of planting on the bank slope, and the safety factor increased by 8.6% and 0.6% respectively compared with the plain soil bank. Trees and shrubs are better planted on the bank slope than on the top of the river bank. And when planted on the slope, the safety factor increased by 8.3% compared with the plain soil bank, while when planted on the top of the river bank, the safety factor

was smaller than that of the plain soil bank slope. When herbs, trees and shrubs were planted at the same time on the bank slope or the top of the bank, the effect of fixing the bank not much different, and the safety factor of the river bank increased by 7.5% and 8.2%, respectively. When the slopes were planted with arbor and shrub vegetation, and the top of the bank was planted with herbaceous vegetation, the maximum advantages of their respective root systems can be exerted, and the bank-fixing effect can be maximized. Compared with the plain soil bank, the safety factor increased by 15.7%.

3.2 River bank plastic strain

Fig. 3 shows the plastic strain map of the bank slope. It can be seen from the figure that when the herbaceous vegetation is planted on the bank top, the plastic strain value on the potential sliding surface of the bank slope decreases significantly compared with the plain soil river bank. This is because the herbaceous root system is dense and the soil cohesion is strong, which can significantly increase the shear strength of the top soil layer and effectively avoid the cracking of the top of the bank when the river bank is unstable. When planted on the bank slope, the root system of the bank slope can only slightly move the potential sliding surface of the river bank downwards, and the plastic strain value on the sliding surface decreases to a certain extent, but the plastic strain at the top of the slope increases. Therefore, herbaceous vegetation planted on the top of the bank has a better bank-fixing effect than planted on the bank slope.

For trees and shrubs, when the vegetation is planted on the top of the bank, the potential sliding surface does not form a penetration condition on the top of the bank. However, compared with the plain soil river bank, the potential sliding surface has a certain upward trend, which may easily lead to shallow landslides. When trees and shrubs are planted on the slope of the river bank, compared with the plain soil river bank, under the influence of the distribution of the vegetation root system, the potential sliding surface obviously moves to the deep soil body, which greatly increases the stability of the river bank. Therefore, the effect of the bank protection when the trees and shrubs are planted on the slope of the river bank is better than that when planted on the top of the bank.

When planting grass, shrub and tree at the same time, each type of vegetation will play its own advantages. When the vegetation is all distributed on the top of the bank, the herb vegetation mainly plays the role of stabilizing the bank, and the tree and shrub vegetation does not play a significant role. In the same way, when the vegetation is distributed on the slope of the river bank, the main function of bank-fixing

is the irrigated and arbor vegetation. Therefore, by making the roots of various types of vegetation play their respective advantages, the contribution to the stability of the river bank can reach the highest level. Trees and shrubs can be planted on the bank slope, and herb vegetation can be planted on the top of the bank. This combination of vegetation types can not only move the potential sliding surface down, but also reduce the penetration of the sliding surface.

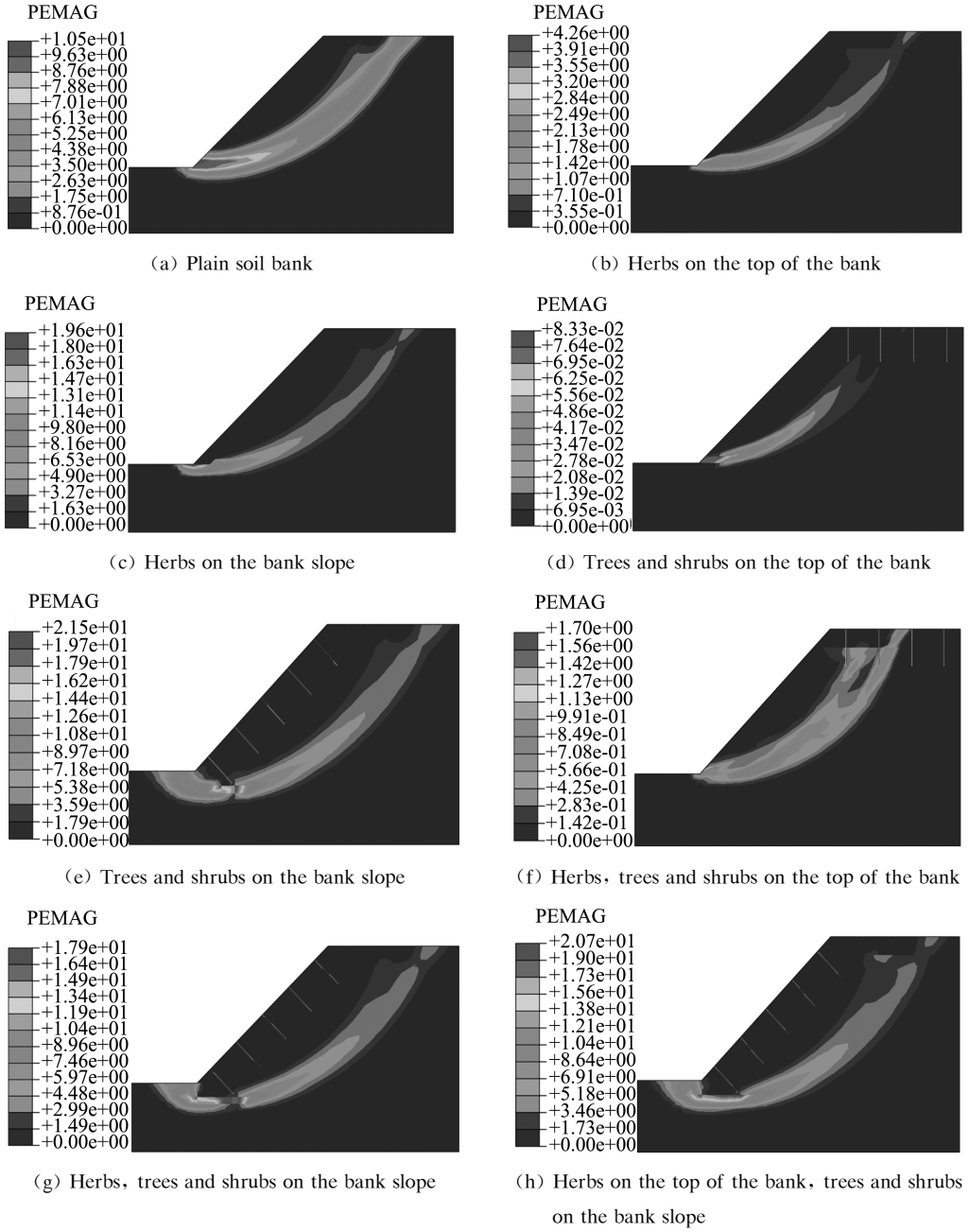

Fig. 3. Plastic strain diagram of bank slope under different cases.

4 Conclusions

When vegetation is planted in an appropriate location on the riparian zone, its root system can play a role in strengthening the riverbank. The best results are achieved when the herbaceous vegetation is located on the top of the bank. When the trees and shrubs are located on the bank slope, the bank fixing effect is the strongest. This conclusion can be used in river bank ecological restoration projects, which is of great significance to maintain the stability and safety of river banks and the sustainable development of waterfront environment ecology.

Acknowledgements

The work presented in this paper is financially supported by the National Natural Science Foundation of China (Nos. U2040215 and 52079080)

References

Andreoli, A., Chiaradia, E.A., Cislaghi, A., et al., 2020. Roots reinforcement by riparian trees in restored rivers. Geomorphology (370): 107389.

Docker, B.B., Hubble, T., 2008. Quantifying root-reinforcement of river bank soils by four Australian tree species. Geomorphology, 100(3-4): 401-418.

Gasser, E., Perona, P., Dorren, L., et al., 2020. A new framework to model hydraulic bank erosion considering the effects of roots. Water, 12 (3): 893.

Gurnell, A.M., Holloway, J.V., Liffen, T., et al., 2019. Plant root and rhizome strength: are there differences between and within species and rivers? Earth Surface Processes and Landforms, 44(1): 389-392.

Gray, D.H., Ohashi, H., 1983. Mechanics of fiber reinforcements in sand. Journal of Geotechnical Engineering, 109(3):335-353.

Pollen, N., Simon, A., 2005. Estimating the mechanical effects of riparian vegetation on stream bank stability using a fiber bundle model. Water Resources Research, 41(7): 226-244.

Wu, T.H., Mcomber, R.M., Erb, R.T., et al., 1988. Study of soil-root interaction. Journal of Geotechnical Engineering, 114(12): 1351-1375.

Study on calculation methods of ship carbon dioxide emissions

Yue Li[1], Yonglin Zhang[1], Chaohui Zheng[1], Mingjun Li[1], Jinxiang Chang [1], Renjie Wang[1], Honglei Xu[1], Rui Wu[1], Yuanyuan Song[1], Xiaoyi Li[1], Dongsheng Chen[2], Xiaotong Wang[2,3], Xinyi Fu[2], Yuehua Zhao[4]

[1] Transport Planning and Research Institute, Ministry of Transport, Laboratory of Transport Pollution Control and Monitoring Technology, Beijing, China. e-mail: lijiayue1107@163.com

[2] Beijing University of Technology, Beijing, China

[3] Tsinghua University, Beijing, China

[4] Shanxi Research Academy of Environmental Sciences, Taiyuan, China

Abstract: China, a major shipping power in the world, paints a shipping emission landscape that allows no underestimation. With the implementation of national strategies on the transportation industry with a focus on maritime and restructuring, ship activities in China will further increase. Reigning in ship-sourced carbon emissions is one of steppingstones to achieve a carbon neutral country. Having clarity on the baseline of carbon emissions serves as the foundation of emission reduction, policy prioritization and implementation of science-based endeavors. The study reviews the existing methods for the accounting of ship-based CO_2 emissions and proposes two new approaches that are based on ship-level fuel consumption and voyage-level engine power, respectively. By analysis of their data requirements, ease of application, result granularity, applicability with underpinning theories, formulas, parameters, the study offers references for researchers, policymakers, and emission management programs. Compared with conventional accounting methodologies, this repertoire of methods offers solutions to more scenarios and supports the systematic and scientific management of pollution and carbon reduction.

Keywords: Ship; Carbon Emissions; Emissions Inventory; Accounting Methods

1 Introduction

The ambition of emissions peaking and carbon neutrality pose new requirements to greenhouse gas emission reduction across all industries and sectors. Already a crucial contributor to emission reduction, the transportation industry also features water

transportation, an essential means of transport in China. With the implementation of national strategies on the transportation industry with a focus on maritime and restructuring, ship activities in China will further increase. Chinese Academy of Engineering forecasts that in the context of fast-growing green solutions in highways and railroads, ships will likely stand out as one of the key emission sources in the industry. Therefore, it is of great significance to curb shipping emissions effectively.

Having clarity on the baseline of carbon emissions provides the foundation of emission reduction and science-based policy making and implementation. At present, carbon accounting of the shipping industry mainly depends on total fuel consumption or conversion from passenger and cargo turnover, which, despite ease of application, have limitations in the calculation boundary, accuracy of results, spatial and temporal resolution, and ship-level information granularity, etc. Hence, the existing methods fail to fulfill the diversely complex research and policy requisites. The study systematically analyzes five accounting methods for ship-based CO_2 emissions, including the common practices by total fuel consumption and passenger/cargo turnover, a modification to the air pollutant emission inventory for calculations based on ship-level engine power, as well as accounting by ship-level fuel consumption and voyage-level engine power proposed in this study. By reviewing the characteristics and applicability of each method, the study establishes a system of accounting methods suitable to different principles, results, and scenarios for the benefit of researchers, policymakers, and emission management programs. Compared with conventional accounting approaches, this repertoire of methods offers applicability to more scenarios and supports the systematic and scientific management of pollution and carbon reduction, thus contributing to the carbon peaking and neutrality goals of China.

2 Carbon emissions: calculation methods

2.1 By regional fuel consumption

This method calculates CO_2 emissions by total fuel consumption in the study area obtained directly from surveys or statistics in combination with CO_2 emission factor per unit of fuel. See Eq. (1).

$$EM_{CO_2} = \sum_f (FC_f \cdot EF_f) \tag{1}$$

EM_{CO_2}—total CO_2 emissions from fuel consumption in the study area (t)

FC_f—total consumption of fuel type f (t)

EF_f—CO_2 emission factors of fuel type f (t-CO_2/t-fuel)

f—fuel type

2.2 By fuel consumption per ship

This study proposes a method based on the fuel consumption of individual ship to calculate CO_2 emissions. See Eq. (2).

$$EM_{CO_2} = \sum_s \sum_f \sum_e (FC_{e,f} \cdot EF_{e,f}) \quad (2)$$

EM_{CO_2}—total CO_2 emissions from fuel consumption in the study area (t)

$FC_{e,f}$—type-f fuel consumption of main engine, auxiliary engine and boiler (t)

$EF_{e,f}$—CO_2 emission factors of fuel type f for main engine, auxiliary engine and boiler (tCO_2/t)

s—the number of ships in the study area

f—fuel type

e—CO_2 emission sources onboard including main engine, auxiliary engine and boiler

2.3 By passenger/cargo turnover

This method converts the passenger and cargo turnover in the study area into fuel consumption by the empirical coefficient of energy consumption per unit of turnover, and then calculates CO_2 emissions by emission factors per unit of fuel. See Eq. (3).

$$EM_{CO_2} = \sum_f (CTO_f \cdot CFCUT_f \cdot EF_{p,f} + PTO_f \cdot PFCUT_f \cdot EF_{p,f}) \quad (3)$$

EM_{CO_2}—total CO_2 emissions from fuel consumption in the study area (t)

CTO_f— cargo turnover (t • km)

$CFCUT_f$—type-f fuel consumption per unit of cargo turnover (t fuel/t • km)

$EF_{p,f}$—CO_2 emission factors of fuel type f (t-CO_2/t-fuel)

PTO_f—cargo turnover (person • km)

$PFCUT_f$—type-f fuel consumption per unit of passenger turnover (t fuel/person • km)

f—fuel type

p—transportation type (cargo and passenger)

2.4 By engine power per ship

This method allows ship CO_2 emissions to be calculated by the work done by the engine using activity levels based on dynamic activity trajectory. See Eq. (4)-(7).

$$EM_{CO_2} = \sum_s (ME + AE + GE) \cdot 10^{-6} \quad (4)$$

EM_{CO_2}—total CO_2 emissions from fuel consumption in the study area (t)

ME—CO_2 emissions from main engine (g)

AE—CO_2 emissions of auxiliary engine (g)

GE—air pollutant emissions of boilers (g)

s—the number of ships in the study area

$$ME = \sum_{f} (MPR_f \cdot LF \cdot MT_f \cdot MCF \cdot EF_{e,f}) \tag{5}$$

ME—CO_2 emissions from main engine (g)

MPR_f—power of main engine using type *f* fuel (kW), obtained by multiplying main engine's rated power and its load factor.

LF—low-load adjustment factor of main engine (dimensionless quantity)

MT_f—hours of main engine using type *f* fuel, determined by the ship's AIS data and navigation state.

MCF—emission factors of main engine (dimensionless quantity)

$EF_{e,f}$—CO_2 emission factors of main engine using fuel type *f* (g/kWh)

f —fuel type

e—CO_2 emission sources onboard including main engine, auxiliary engine, boiler.

$$AE = \sum_{f} (APR_f \cdot AT_f \cdot ACF \cdot EF_{e,f}) \tag{6}$$

AE—CO_2 emissions of auxiliary engine (g)

APR_f—power of auxiliary engine using type *f* fuel (kW), obtained by multiplying auxiliary engine's rated power and its load factor, or from the boiler engine power ratio.

AT_f—hours of auxiliary engine using type *f* fuel, determined by AIS data and sailing state.

ACF—emission factors of auxiliary engine(dimensionless quantity). 0 for shore power and otherwise based on CO_2 reduction.

$EF_{e,f}$—CO_2 emission factors of auxiliary engine using fuel type *f* (g/kWh)

$$GE = \sum_{f} (GPR_f \cdot GT_f \cdot GCF \cdot EF_{e,f}) \tag{7}$$

GE—CO_2 emissions of boilers (g)

GPR_f—power of boiler using type *f* fuel (kW), derived by multiplying the rated power and load factor of the boiler, or from the boiler rated power ratio

GT_f—hours of boiler using type *f* fuel, determined by the AIS time data and navigation state, excluding hours using residual heat.

GCF—emission factors of boiler (dimensionless quantity)

$EF_{e,f}$—CO_2 emission factors of boiler using fuel type *f* (g/kWh)

2.5 By voyage-based engine power

This study proposes a method based on the engine power statistics of incoming and outgoing vessels. See Eq. (8)-(11).

$$EM_{CO_2} = \sum_m \sum_n \sum_f (\overline{ME} + \overline{AE} + \overline{GE}) \tag{8}$$

EM_{CO_2}—total CO_2 emissions from fuel consumption in the study area (t)

$\overline{ME}$—average CO_2 emissions(t) from main engine of ship type m, tonnage n, and fuel type f

$\overline{AE}$—average CO_2 emissions(t) from auxiliary engine of ship type m, tonnage n, and fuel type f

$\overline{GE}$—average CO_2 emissions(t) from boiler of ship type m, tonnage n, and fuel type f

m—the number of ship types

n—the number of ship tonnage class

f—fuel type

$$\overline{ME} = ST_{m,n,f} \cdot MPR_{m,n,f} \cdot LF \cdot \frac{L_{m,n,f}}{u_{m,n,f}} \cdot MCF \cdot EF_{m,n,e,f} \tag{9}$$

$\overline{ME}$—average CO_2 emissions(t) from main engine of ship type m, tonnage n, and fuel type f

$ST_{m,n,f}$—voyage of ship type m, tonnage n, and fuel type f

—Calculate incoming emissions by voyage entering ports

—Calculate outbound emissions by voyage exiting ports

—Calculate emissions at berth by average voyage entering and exiting ports

—Calculate emissions during sailing by the sum of ascending and descending voyage

$MPR_{m,n,f}$—average power (kW) of main engine of ship type m, tonnage n, and fuel type f

LF—low-load adjustment factors of main engine (dimensionless quantity)

L—average navigation distance of ship type m, tonnage n, and fuel type f; L of cargo ships are usually similar but different from working ships.

u—average speed of ship type m, tonnage n, and fuel type f

MCF—emission control factors (dimensionless quantity). Situations such as shore power and exhaust cleaning equipment should be considered.

$EF_{m,n,e,f}$—CO_2 emission control factors of main engine of ship type m, tonnage n, and fuel type f (g/kWh)

e—CO_2 emission sources onboard including main engine, auxiliary engine, boiler

$$\overline{AE} = ST_{m,n,f} \cdot APR_{m,n,f} \cdot AT_{m,n,f} \cdot ACF \cdot EF_{m,n,e,f} \tag{10}$$

$\overline{AE}$ —average CO_2 emissions(t) from auxiliary engine of ship type m, tonnage n, and fuel type f

$ST_{m,n,f}$—voyage of ship type m, tonnage n, and fuel type f

$APR_{m,n,f}$—average power of auxiliary engine of ship type m, tonnage n, and fuel type f (kW)

$AT_{m,n,f}$—average working hours of auxiliary engines of ship type m, tonnage n, and fuel type f (h)

—Derive T for ships sailing, entering and exiting ports by L/u calculation. Reference Eq. (9)

—T represents time at berth, which can be obtained from yearbooks and surveys

ACF—emission factors of auxiliary engine (dimensionless quantity). 0 for shore power and otherwise based on CO_2 reduction

$EF_{m,n,e,f}$—CO_2 emission control factors of auxiliary engine of ship type m, tonnage n, and fuel type f (g/kWh)

$$\overline{GE} = ST_{m,n,f} \cdot GPR_{m,n,f} \cdot GT_{m,n,f} \cdot GCF \cdot EF_{m,n,e,f} \tag{11}$$

$\overline{GE}$ —average CO_2 emissions(t) from boiler of ship type m, tonnage n, and fuel type f

$ST_{m,n,f}$—voyage of ship type m, tonnage n, and fuel type f

$GPR_{m,n,f}$—average power of boilers of ship type m, tonnage n, and fuel type f (kW)

$GT_{m,n,f}$—average working hours of boilers of ship type m, tonnage n, and fuel type f (h) excluding hours running on residual heat

GCF—emission control factors (dimensionless quantity)

$EF_{m,n,e,f}$—CO_2 emission control factors of boiler of ship type m, tonnage n, and fuel type f (g/kWh).

3 Calculation methods of emission factors

Emission factors have a decisive influence on the accuracy of calculation results. The 5 accounting methods proposed in this paper include two types of CO_2 emission factors, which are obtained as follows.

3.1 Fuel-based CO_2 emission factors

CO_2 emission factors differ markedly between fuels, among which the factors

powered by electricity, hydrogen and ammonia are recorded as 0 t-CO_2/t fuel. The CO_2 emission factors are calculated based on lower CV (calorific value), carbon content per unit CV, and the rate of carbon oxidation. See the method in Eq. (12). Refer to empirical data in Table 1 in case of lacking data availability. Indirect CO_2 emissions such as those from electricity usage are not included in this study.

$$EF_f = QDW_f \cdot CC_f \cdot COR_f \frac{M_{CO_2}}{M_C} \cdot 10^{-6} \tag{12}$$

EF_f—CO_2 emission factor of fuel type f (t-CO_2/t-fuel)

QDW_f—lower CV of fuel type f (kJ/kg)

CC_f—carbon content per unit CV of fuel type f (t-C/TJ)

COR_f—rate of carbon oxidation of fuel type f (%)

M_{CO_2}—molecular weight of CO_2(44)

M_C—molecular weight of C (12)

Table 1 Parameters in calculation of CO_2 emission factors.

Fuel	Carbon content per unit of volume or mass	Lower CV	Rate of carbon oxidation
Fuel oil	21.1t-C/TJ①	40.2×10³kJ/kg②	0.98①
Diesel	20.2t-C/TJ①	43.3×10³kJ/kg②	0.98①
Gasoline	18.9t-C/TJ①	44.8×10³kJ/kg②	0.98①
Natural gas	15.3t-C/TJ①	38.9×10³kJ/m³②	0.99①
LNG	17.2t-C/TJ①	41.9×10³kJ/kg②	0.98①
LPG	17.2t-C/TJ①	47.3×10³kJ/kg②	0.98①

① Department of climate change, National Development and Reform Commission. (2011). ② Office of the National Climate Change Response Coordination Group, Energy Research Institute of National Development and Reform Commission. (2007).

3.2 Power-based CO_2 emission factors

Methods 4 and 5 require power-based emission factors. Ocean-going ships can use test data from abroad, while measured data are recommended for domestic coastal and river ships in study areas. Power-based emission factors can also be converted from fuel consumption per unit power of the engine. See Eq. (13).

$$\mathrm{EF_P} = FC_P \cdot EF_f \tag{13}$$

EF_P—power-based CO_2 emission factor (g/kW-h)

FC_P—fuel consumption per unit power of engine (g fuel/kW-h)

EF_f—fuel-based CO_2 emission factor (g-CO_2/g-fuel).

4 Comparative analysis of calculation methods

This study proposes 5 calculation methods and their principles, types, and data requirements based on theoretical and statistical analysis. Readers can choose the most applicable solution when calculating ship-sourced CO_2 emissions according to data availability, purpose, usage, etc. It is to be noted that a relatively high precision of the temporal and spatial distribution of emissions is typically needed in the accounting of air pollutants from ships, but micro and medium-scaled accounting only require accuracy on the volume of emissions. Therefore, readers can choose the calculation method in accordance with the specific circumstances.

a) Method of regional fuel consumption. This method calculates CO_2 emissions by total fuel consumption in the study area obtained directly from surveys or statistics in combination with CO_2 emission factor per unit of fuel, which is typically applied to calculating emissions of a ship, port, city, province, or country, and widely used for ship-sourced carbon emissions. Fast and convenient, the method relies on the precision and granularity of fuel consumption data for its accuracy and ability to reveal ship-level information. Data requirements include fuel consumption and fuel-based CO_2 emission factors in the study area. Fuel consumption is mostly derived from either the study area (e.g., provinces, cities, ports, shipping companies, etc.), or sales data from petrol and gas stations, etc.

b) Method of fuel consumption per ship. This study proposes a method based on the fuel consumption of individual ship to calculate CO_2 emissions by fuel consumption per vessel and voyage in combination with CO_2 emission factors per unit of fuel, which requires detailed fuel consumption records of each ship and voyage in the study area. The method can also use coarse-grained fuel consumption data over a period of time. Compared with conventional accounting by regional consumption and the passenger/cargo turnover, this bottom-up approach offers more precision and support to systematic and scientific management of pollution and carbon reduction. Data requirements include fuel consumption by ship and voyage, fuel-based CO_2 emission factors, etc. A more coarse-grained alternative is using data such as oil(gas) refuel volume and time. According to the requirements of IMO and domestic maritime authorities, coastal vessels shall record and report fuel consumption of each voyage by segment, and river ships report fuel consumption by time, which is the foundation for applying this method. Given reliable data on fuel consumption, this method produces the highest accuracy and the capability to classify CO_2 emissions by vessel type, navigating zone, tonnage, etc.

c)Method of passenger/cargo turnover. This method converts the passenger and cargo turnover in the study area into fuel consumption by the empirical coefficient of energy consumption per unit of turnover, and then calculates CO_2 emissions by emission factors per unit of fuel. As a top-down variation of the fuel consumption approach, it is commonly used to calculate CO_2 emissions from shipping. Data requirements include passenger/cargo turnover, fuel consumption per unit of cargo/passenger turnover, and fuel-based emission factors in the study area. Passenger/cargo turnover can be obtained from yearbooks and communiques, fuel consumption per unit of cargo/passenger turnover from the energy balance sheet of the water transportation industry energy, which are published statistics in the country.

d)Method of engine power per ship. This method allows ship CO_2 emissions to be calculated by the work done by the engine using activity levels based on dynamic activity trajectory, which often has Automatic Identification System(AIS) data. It requires information on time, ship position, and navigation conditions (or speed), etc., which are regularly recorded and reported during the voyage. After matching the dynamic information with baselines such as engine power, the work done by the engine between two adjacent records can be derived. Subsequently, the CO_2 emissions and locations can be used to calculate the total ship emissions in the area, as well as an emission inventory of high tempo-spatial and vessel－level resolution. Compared with conventional accounting methods by total fuel consumption or passenger/cargo turnover, this method provides more visibility on ship type, tonnage and navigation zone, etc., as well as higher accuracy of results, thus supporting the systematic and scientific management of carbon and pollution reduction. As a bottom-up approach, it is mostly seen in the compilation of air pollutant emission inventory (Liu et al., 2016; Fan et al., 2016; Chen et al., 2017; Chen et al., 2017), and this study proposes its modified application for the calculation of CO_2 emissions. Carbon emission of a ship is the sum of main engine, auxiliary engine and boiler, and the regional emission is the total of all ships in the region. Data requirements include AIS data (or other activity trajectory data) of the study area, baseline information such as main/auxiliary engine power, power-based ship CO_2 emission factors (alternatives: fuel consumption per unit power; fuel-based CO_2 emission factors), engine load factor, low-load adjustment factor, and control measure adjustment factor, etc.

e)Method of voyage-based engine power. This study proposes a method based on the engine power statistics of incoming and outgoing vessels. In the case of absence of AIS and other dynamic trajectory data, the "engine power method based on dynamic trajectory data" can be generalized, i.e., the statistical data of ship arrivals and departures or voyages, the average engine power of a certain ship type and tonnage, and

the average engine usage time can be used to calculate CO_2 emissions, which is similar to accounting by "engine power per ship". However, the engine work and activity trajectory are generalized by ship type and tonnage. This method is an intermediate approach between bottom-up and top-down. Data requirements include incoming and outgoing voyage (or statistical data from a defined segment), average engine power and usage time by ship type and tonnage, and power-based CO_2 emission factors, which could be obtained from the voyage record in the national maritime statistics system, or from statistics of shipping lines, sample surveys, and cross-sectional observation.

See Table 2 for a comparative analysis of the accounting methods.

Table 2 Comparative analysis of the calculation methods.

		Method 1—regional fuel consumption	Method 2—fuel consumption by vessel	Method 3—passenger and cargo turnover	Method 4—engine power by vessel	Method 5—engine power by voyage
Methodology		Fuel consumption	Fuel consumption	Fuel consumption	Engine power	Engine power
Type		Top-down	Bottom-up	Top-down	Bottom-up	Between top-down and bottom-up
Application		Some	New (no application yet)	Common	Common in emission inventory for air pollutants but rare for carbon	New (no application yet)
Data requirements	Activity level	• Regional ship fuel consumption	• Fuel consumption by vessel and voyage, or oil (gas) fueled by vessel in a certain time • Navigation path or start & stop points	• Passenger/cargo turnover	• AIS and other vessel movement data	• Vessel voyages at ports or research segments
	Vessel information	/	/	• Fuel consumption by unit passenger/cargo turnover	• Engine and boiler power by ship • Load factors under the different engine operating conditions • Emissions reduction measures	• Average power of engines and boilers by vessel type and tonnage • Load factors under the different engine operating conditions • Engine operating time • Emissions reduction measures

continue

		Method 1—regional fuel consumption	Method 2—fuel consumption by vessel	Method 3—passenger and cargo turnover	Method 4—engine power by vessel	Method 5—engine power by voyage
Data requirements	Emission factors	Fuel-based CO_2 emission factors (g/kg fuel)	Fuel-based CO_2 emission factors (g/kg fuel)	Fuel-based CO_2 emission factors (g/kg fuel)	Power-based CO_2 emission factors (g/kW·h) or fuel-based CO_2 emission factors (g/kg fuel), fuel consumption by unit power (g fuel/kW·h)	Power-based CO_2 emission factors (g/kW·h) or fuel-based CO_2 emission factors (g/kg fuel), fuel consumption by unit power (g fuel/kW·h)
Ease of application		1	4	2	5	3
Accuracy		2 Depends on reliable energy consumption data	1 Depends on reliable energy consumption data	3	3	4
Accuracy of temporal distribution		3 No temporal distribution	2	3 No temporal distribution	1	3 No temporal distribution
Accuracy of spatial distribution		4 No spatial distribution	2 Low-precision spatial distribution	4 No spatial distribution	1 High-precision spatial distribution	3 No port spatial distribution. Low-precision regional and national spatial distribution
Distinguish vessel type		×	√	×	√	√
Distinguish operating condition		×	√	×	√	√
Distinguish emission source (main engine, auxiliary engine, boiler, etc.)		×	√	×	√	√
Scope of application		Quick results of CO_2 emissions from registered ships in a unit or area	CO_2 emissions from individual ship, unit and area that require precision on tempo-spatial distribution, ship information (e.g. ship type, tonnage) and sailing conditions	Quick results of CO_2 emissions from registered ships in a unit or area	CO_2 emissions from individual ship, unit and area that require precision on tempo-spatial distribution, ship information (e.g. ship type, tonnage) and sailing conditions	Quick results of CO_2 emissions from ships in ports/segments that require precision on tempo-spatial distribution and ship information (e.g. ship type, tonnage)

5 Conclusions

(1) At present, the accounting of ship-sourced CO_2 emissions mostly relies on fuel consumption and passenger/cargo turnover. This study proposes a modification to the technical pathway of air pollutant emission inventory for calculations based on ship-level engine power, ship-level fuel consumption, and voyage-level engine power. The five methods apply to different scenarios with their distinct methodologies, characteristics, and results.

(2) By core principles, the five methods are: a. regional fuel consumption, b. ship-level fuel consumption, c. passenger/cargo turnover by fuel consumption, d. ship-level engine power, e. voyage-level engine power, which by methodologies correspond to: a. regional fuel consumption, b. ship-level fuel consumption, c. top-down calculation of passenger/cargo turnover, d. top-down calculation of ship-level engine power, e. top-down and bottom-up calculation of voyage-level engine power.

(3) By ease of application, the five methods are ranked as follows: a. regional fuel consumption, c. passenger/cargo turnover by fuel consumption, e. voyage-level engine power, b. ship-level fuel consumption, d. ship-level engine power.

By accuracy of results, the ranking is: a. regional fuel consumption, b. ship-level fuel consumption, c. passenger/cargo turnover by fuel consumption, d. ship-level engine power, e. voyage-level engine power.

By accuracy of temporal distribution of results is ordered d. ship-level engine power, b. ship-level fuel consumption, a. regional fuel consumption, c. passenger/cargo turnover by fuel consumption, e. voyage-level engine power.

In terms of resolution of basic vessel information, b. ship-level fuel consumption, d. ship-level engine power, and e. voyage-level engine power support statistical analysis by vessel type, sailing conditions, emission sources, and tonnage, while a. regional fuel consumption and c. passenger/cargo turnover by fuel consumption fall short.

(4) In terms of applicability, a (regional fuel consumption) is more suitable for quick results of total CO_2 emissions of a unit or region, b (ship-level fuel consumption) for CO_2 emissions from individual ship, unit and area that require precision on tempo-spatial distribution, vessel information (e.g. ship type, tonnage) and sailing conditions, c (passenger/cargo turnover by fuel consumption) for total CO_2 emissions from registered ships in a unit or area, d (ship-level engine power) for CO_2 emissions from individual ship, unit and area that require precision on tempo-spatial distribution, ship information (e.g. ship type, tonnage) and sailing conditions, and e (voyage-level engine power) for quick results of CO_2 emissions from ships in ports/seg-

ments that require precision on tempo-spatial distribution and ship information (e.g. ship type, tonnage).

Acknowledgements

This work was supported by "Prototype development of methane escape control device for Marine dual fuel/gas engines", "Green Intelligent Inland Ship Innovation Programme", "Transportation Self-sufficient Energy System Infrastructure Planning and Design Technology" (2021YFB2601300) of the China National Key R&D Program, "R&D and Application of Active Monitoring Equipment for Ship Air Pollutant Emissions" (SQ2020YFF0426378) of the 2020 Key Project of Science and Technology as Economic Booster, "Research on Atmospheric Environmental Impact of Ships and Ports" of the "Young Science and Technology Talents" training program of the Transport Planning and Research Institute, Ministry of Transport, China.

References

Chen, D., Wang, X., Nelson, P., et al., 2017: Ship emission inventory and its impact on the $PM_{2.5}$ air pollution in Qingdao Port, North China. Atmospheric Environment (166).

Chen, D., Wang, X., Li, Y., et al., 2017. High spatiotemporal resolution ship emission inventory of China based on AIS data in 2014. Science of The Total Environment (609):776-787.

Department of climate change, China Development and Reform Commission, 2011. Guidelines for the preparation of provincial greenhouse gas inventories. CN.

Fan, Q., Zhang, Y., Ma, W., et al., 2016. Spatial and Seasonal Dynamics of Ship Emissions over the Yangtze River Delta and East China Sea and Their Potential Environmental Influence. Environmental Science & Technology, 50(3):1322-1329.

Li, Y., Li, M.J., Cheng, J.X., et al., 2019. Comparative analysis of inventory compilation methods for ship emissions. Materials Science and Engineering, 631.

Li, X.Y., Tan, X.Y., Wu, R., et al., 2021. Research on carbon peak and carbon neutralization path in transportation field. Chinese Academy of Engineering, 23(6):7.

Liu, H., Fu, M., Jin, X., et al., 2016. Health and climate impacts of ocean-going vessels in East Asia. Nature Climate Change.

Office of the National Climate Change Response Coordination Group, Energy Research Institute of National Development and Reform Commission, 2007. Study on China's greenhouse gas inventory. CN.

Topic 5
Logistics

A systematic tool for assessing quantitative relations across dissimilar stakeholder objectives: A case study on nature-based solutions to mitigate salt intrusion in a highly urbanized estuary

Sebastian Iglesias[1], Floor Bakker[2]

[1] Van Oord Dredging and Marine Contractors BV, Schaardijk 211, 3063 NH Rotterdam, the Netherlands

[2] Delft University of Technology, Stevinweg 1, 2628CN, Delft, the Netherlands

1 Introduction

In many system management challenges in hydraulic engineering, several parallel stakeholder objectives that often conflict with each other coexist. Consequently, if an intervention is deemed necessary in the system to improve one of its functions or values, hydraulic engineering solutions may comply with one objective that will go to the detriment of another objective. For example, to improve the navigability of a river, human interventions through river training or dredging activities are required that may negatively affect the ecology.

Nowadays in face of the global challenges that lie ahead (e.g. sustainable and resilient societies in a changing climate), society demands decision-makers and engineers to embrace an integrated perspective that strives for a desired state for a system that meets all stakeholder objectives. In hydraulic engineering, this new thinking resulted in the implementation of nature-based solutions (NBS). These types of solutions offer a sustainable, multi-functional, and multi-actor perspective that can be applied to water systems.

Because these solutions require cooperation among players, understanding their interactions and potential conflicts is essential. Moreover, its success rests on the compromises to be made in the trade-off between different stakeholder interests. The latter is not possible without stakeholders' information requirements as an explicit starting point for acquiring knowledge on the effects of a solution. Such knowledge can be

linked to end-users through systematic methods, such as the "Frame of Reference (FoR)" approach by Koningsveld (2003). This approach is commonly used to obtain performance indicators about a specific stakeholder. However, there is yet no straightforward method to obtain quantifiable knowledge to understand how multiple stakeholders interact, especially when interests affected by a solution originate from entirely different fields.

To bridge this gap, this work presents a new tool that is able to relate stakeholders' interests quantitatively. The tool's functionality is demonstrated through a case study of an application of a NBS in a highly urbanized estuary. These vulnerable coastal embayments are strongly subjected to new societal and ecological challenges as a consequence of newly imposed boundary conditions, mainly due to climate change and ever-changing societal needs. One of the main issues is the amplified upstream dispersion of salty seawater in the freshwater riverine areas of estuaries due to more frequent and extended periods of drought and sea level rise. This process, called salt intrusion, threatens freshwater availability for populations living in the delta and calls for new NBS. However, such measures should consider the necessary infrastructure for cargo supply to create sustainable and resilient societies where people can access their basic needs. The case study implemented in this research is a first approach to understand the conflicts that could emerge from this specific application, which reveals a complicated interaction between freshwater supply and port logistical objectives.

2 Methodology

An extensive review of available literature was conducted to identify methods to compare multiple stakeholder objectives affected by a NBS that causes alterations in the lay-out and dynamics of the estuarine system. It was found that Multi-Objective Decision-Making (MODM) and Multi-objective Optimisation (MO) methods suit this purpose, as these systematically relate quantifiable indicators and capture strong dissimilar indicators, i.e. expressed in different units. However, due to the high computational resources demanded by these methods, it was decided to develop a new tool (hereinafter the "comparison tool") which builds upon basic concepts about quantitative trade-offs found in MODM and MO sources. The comparison tool is founded on the objective-based assessment of Building with Nature (BwN) solutions according to the "Frame of Reference" (FoR) approach by Koningsveld (2003). This method enables the formulation of clear objectives systematically, while indicators are defined to quantify and evaluate the success in achieving those objectives. In this research, the

FoR decision recipe is replicated repeatedly to assess the effects on stakeholders individually. Then, the individual assessments are combined into one trade-off (Fig. 1). Typically, a trade-off curve exhibits an asymptotic behaviour. By delivering a visualization of such behaviour, the tool allows the decision-maker to quickly understand where the compromises are to be made.

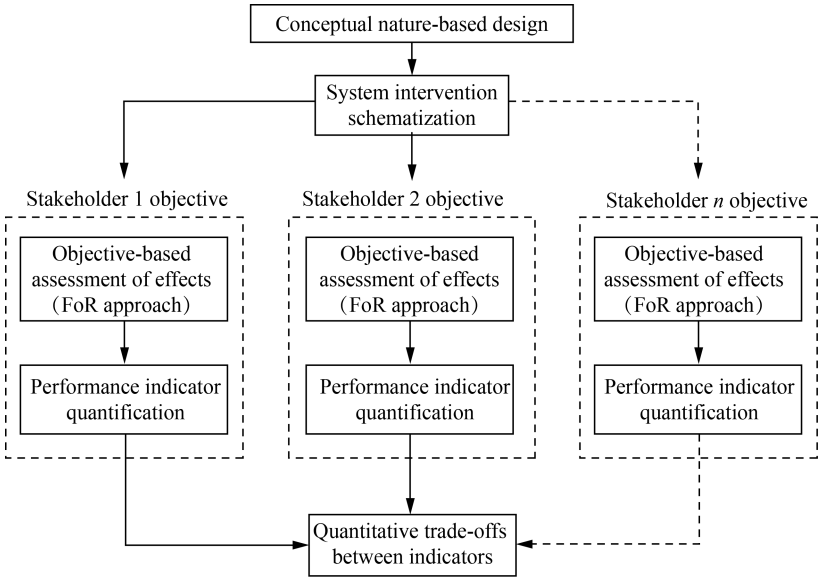

Fig. 1. Scheme of the comparison tool to find quantitative relations across dissimilar stakeholder objectives affected by a nature-based solution.

The comparison tool was tested for a potential nature-based solution to mitigate salt intrusion in the Rhine-Meuse Delta, in the Netherlands. This measure entails the river shallowing (i.e. bed increase) of the Rotterdam Waterways, i.e. the Nieuwe Waterweg and Nieuwe Maas (Fig. 2). This research used a model developed by the Port of Rotterdam Authority to study the effects of shallowing on hydrodynamics and salt transport. Based on the hydrodynamic model results, the impact on nautical traffic was addressed with an agent-based discrete－event model developed by TU Delft in a post-processing stage. For the effects on the availability of freshwater, no post-processing model was deemed necessary. The latter was assessed at two study locations in the Nieuwe Maas River, Boerengat and Brienenoordbrug, whereas the effects on nautical traffic flows were evaluated over a simplified network for seagoing vessels calling at a liquid bulk terminal in the Port of Rotterdam (Fig. 2).

The method used model results to derive and combined performance indicators in line with the two operational objectives of the availability of freshwater supply and the performance of the port network. The first objective was assessed through the

salinization days, which quantifies the duration in which normative standards of salinity concentration are exceeded during periods of freshwater demand. The second objective was assessed via the average waiting time of vessels over their total turnaround time (time of stay in the port).

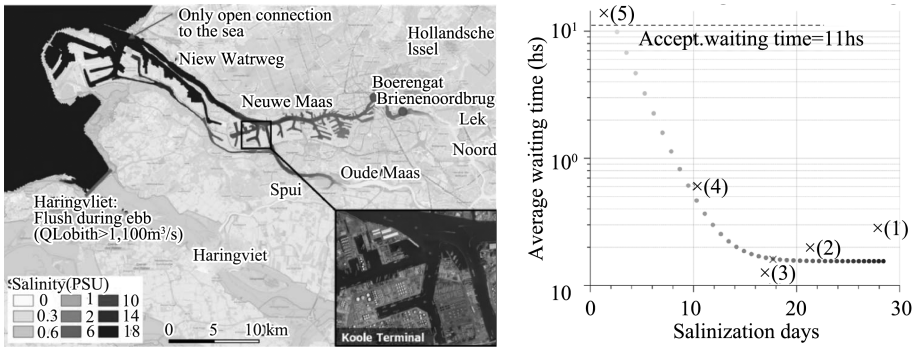

Fig. 2. Left: Rhine-Meuse Delta river streams, water inlet locations and port areas used in the case study. The figure shows a typical salinization event (High Water Slack salinity, in PSU) occurring during low river discharge and no storms. As seen, the Boerengat and Brienenoordbrug water inlets are inside the moderate-blue area, meaning that both are affected by salt intrusion. The liquid bulk terminal used in the nautical traffic assessment is shown in the bottom right part of the figure. Right: Trade-off visualization for port efficiency against freshwater supply at a water inlet in the Rhine-Meuse Delta. References in the figure: (1) Reference state +0.0 m; (2) Shallowing +1.4 m; (3) Shallowing +1.9 m; (4) Shallowing +2.9 m; (5) Shallowing +3.9 m.

3 Results analysis and discussion

The application of the comparison tool to the case study resulted in a trade-off curve between the average waiting time for vessels and the number of salinization days of the freshwater inlets, as presented in Fig. 2. The curve is based on the modelling outcomes, which are depicted in the figures by crosses. The bar on the right shows the increase in bed level with respect to the current situation (reference case). In addition, the figure presents the desired state for the two end-users (=0 in the x-axis and =11hs in the y-axis).

The results revealed that an increase in bed level in the Rotterdam Waterways leads to an increase in the availability of freshwater at the Boerengat and Brienenoord-brug water inlets due to a reduction in salt intrusion. In contrast, it leads to an exponential growth of the vessel's average waiting time due to heavier nautical traffic as deep-draughted vessels could not enter the port and their cargo had to be transferred to and divided over more lower-draughted vessels. In all four cases analysed, the resulting trade-off curves showed that, while increasing the bed level, the im-

provement towards the objective of port logistics always goes to the detriment of the freshwater supply objectives, and vice versa.

It should be noted that the uncertainty of the comparison tool can be significant due to the curve fitting procedure and the spread in the traffic model results. However, the comparison tool is still believed to be able to reproduce general trends of losses and gains in the trade-off curves. The relevance of these results is therefore not so much in the exact values but in the substantiation of an explicit asymptotic behaviour in the relationship between two stakeholder objectives. Moreover, the tool shows a great opportunity for expansion, as it should be suitable to handle more than two stakeholder objectives, resulting in a multi-variable visualization. This work highlights that a similar outcome can be obtained with Multi-Objective Decision-Making (MODM) and Multi-objective Optimisation (MO) concepts.

4 Conclusions

The most important outcome of this work entailed quantitative trade-offs across dissimilar stakeholder objectives, which decision-makers can use to understand the implications of interventions to the system from a multi-actor perspective. As a proof-of-concept, the "comparison tool" was successfully implemented for the shallowing of the Rotterdam Waterways in the Rhine-Meuse Delta. Here, the aim was not in the completeness and details but in the demonstration of the main principles in implementing the comparison tool for two stakeholders: freshwater supply and port logistics. It was concluded that the improvement towards the objective of port logistics always goes to the detriment of the freshwater supply objectives while increasing the river bed level. This case study was a first approach to demonstrating how the interaction between two objectives can be quantified. Then, it became clearer that the methodology offers great flexibility for including more than two stakeholders, even when their interests originate from totally different contexts. Furthermore, this work lays the groundwork for future research in exploring whether multiple variables can be merged altogether with the comparison tool. Finally, it was recognized that a natural step of this work is to include more aspects of Multi-Objective Decision-Making (MODM) and Multi-objective Optimisation (MO) methods.

Acknowledgement

This research is part of the SALTI Solutions Programme consortium and received support from the project Design and operation of nature-based SALTI Solutions led by

Prof. dr. ir. S. G. J. Aarninkhof. All activities were conducted at the Delft University of Technology. This research is a product of the MSc. Thesis Project chaired by Prof. dr. ir. M. van Koningsveld of the same educational institution.

References

Branke, J., Deb, K., Miettinen, K., et al., 2008. Multiobjective Optimization: Interactive and Evolutionary Approaches. Springer-Verlag GmbH.

Vriend, H. J., Koningsveld, M., 2012. Building with Nature: Thinking, acting and interacting differently. EcoShape, Building with Nature, Dordrecht, the Netherlands.

Vriend, H. J., Koningsveld, M., Aarninkhof, S. G. J., et al., 2015. Sustainable hydraulic engineering through building with nature. Hydro-environment research.

Dodgson, J. S., Spackman, M., Pearman, A., et al., 2009. Multi-criteria analysis: a manual. Communities and Local Government, Wetherby.

Eekelen, E., Bouw, M., Shapiro-Kline, J., et al. 2020. Building with nature: creating, implementing and upscaling nature-based solutions. EcoShape One Architecture Rotterdam publishers, Dordrecht New York.

Keeney, R. L., Howard, R., 2002. Decisions with Multiple Objectives. Cambridge University Press.

Kranenburg, W., Evaluatie, M., 2015. OSR-model voorzoutindringing in de Rijn-Maasmonding (Ⅰ). Technical report, Deltares.

Laboyrie, H. P., Konigsveld, M., Aarninkhof, S. G. J., et al., 2018. Dredging for sustainable infrastructure. CEDA, Central Dredging Association IADC, International Association of Dredging Companies, Delft Voorburg.

United Nations. The 2030 Agenda and the Sustainable Development Goals. United Nations, 2018.

Koningsveld, M., 2003. Matching specialist knowledge with end user needs.

Koningsveld, M., Uijl, J., OpenTNSim (Version 1. 0. 0), 2020. URL https://github. com/TUDelft5CITG/OpenTNSim.

Koningsveld, M., Verheij, H. J., Taneja, P., et al., Ports and Waterways-Navigating the changing world. TU Delft Open, 2021. doi: 10.5074/T.2021.004.

Vries, M., Koningsveld, M., Aarninkhof, S. G. J., et al., A systematic design approach for objectifying building with nature solutions. 7:29-50, feb 2021b. doi: 10.47982/rius. 7.124.

The crossing project on the Yellow River for the Grand (Jing-Hang) Canal

Chaobin Min[1]

[1] CCCC Water Transportation Planning and Design Institute Co., Ltd., Beijing, China

Abstract: The Grand Canal in China is the most inter-basin inland canal with the oldest history, the longest distance, the largest constructed scale and the most volume of cargo traffic in the world. This paper simply describe its history, its present situation and the existed problems on how to solve the problem that ships or fleets on the north and south banks of the Yellow River can directly reach the opposite bank through the Yellow River.

Keywords: Crossing project; Yellow River; Grand Canal

1 Introduction

The Grand Canal in China (GC) is an inland canal with a length of 1,754 km which is connected with five river basins as Haihe River, Yellow River, Huaihe River, Yangtze River and Qiantanjiang River, running through Beijing, Tianjin, Hebei, Shandong, Jiangsu, Zhejiang and other provinces and cities. Early as 486 BC, the 34th year of Emperors Jing of Zhou Dynasty, the King of Wu, Fuchai began to build a stretch of canal from Huai'an to Yangzhou by Yangtze River. Henceforth passing through many dynasties such as: Yuan, Ming and Qing the Grand Canal was finished at all.

The characteristics of the GC compared with the other inland canals of the world are as follows: (1) It was built earlier; (2) Its route was the longest; (3) Its route combined with river basins and passed through provinces and cities; (4) The volume of cargo traffic (T), the turnover volume of cargo traffic (T-km) as well as the traffic density per km (T-km / km) on the GC were the most; (5) The dimension of channel and the scale of ship locks were larger; (6) The comprehensive utilization of water resources on GC were more effective.

The situation of topography and hydrology of GC is related with the area and rivers where the route passed by. Based on a rough estimate with the low level of local

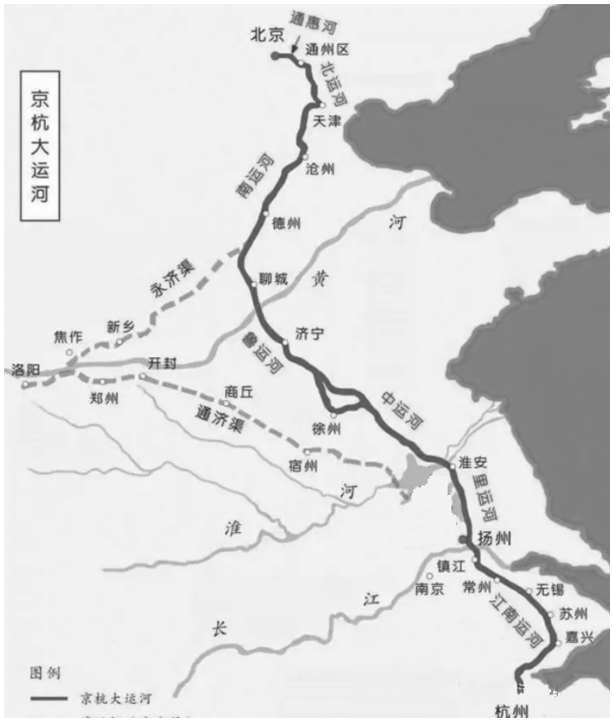

Fig. 1. Location of Beijing-Hangzhou Grand Canal.

point, the elevation difference between Beijing & Tianjin is almost 30 m and the former is higher. The elevation difference between Tianjin & Yangzhou, the middle of the Yellow River is 40 m, higher than both ends. The elevation difference between Jianbi ship lock (by Yangtze River) & Hangzhou is 10 cm, and the former is a little higher than the latter.

For overcoming the waterhead and saving water consumption, a checkgate as an embryonic form of ship lock was used in Ling Canal in the Qin Dynasty (221 BC) and was also widely used in the dynasties of Tang and Song in GC.

Owing to shortage of water resources in the area of northern China and other subjective and objective factors, the navigation activities on the northern canal as well as the southern canal of GC in the north side of the Yellow River were stopped for half a century.

At present, the 1st stage of the project (East line) of water regulation from Yangtze River to the area over Yellow River is finished already, and then 200 m^3/s discharges from Yangtze River will transit to northern China passing the tunnel with a diameter of 7.5 m and a length of 585 m. An inverted siphon tunnel with a diameter of 9.3 m is about 70 m from the bottom of the Yellow River in 2014.

Then GC could be navigable in all line. Under this premise this paper would pro-

vide some suggestion concerning the methods of how the ship and fleet of GC pass through the Yellow River.

2 The studying on the project of the Grand Canal crossing over

Generally there are two methods when a canal crosses over a river, i.e. horizontal crosses (affluence) and cubical crosses. In the light of the situation and problems of the Yellow River, the paper's opinion is as follows.

2.1 Horizontal / Level crossing

There are two plans. One is with a low dam on the Yellow River at the downstream of canal entrance for raising the water level of river on the crossing stretch and improving the flow pattern for sailing, while the other without.

When a canal meets a large river which is wider and deeper, the method of horizontally crossing is always used, no matter how much is the water level difference between them.

The typical example in GC is that on both banks of the downstream of the Yangtze River, there located separately entrances of GC with shiplock at northern bank (Yangzhou) and at southern bank (Jianbi).

During the early period (before 1950s) when small boats loaded less than 10 tons were sailing on the Yellow River and GC, the method of horizontally crossing with shiplock was also used. The entrance of GC with shiplock at northern bank is Zhangqiu, and at southern bank is Guonali.

But the navigation standard of GC at present is higher than that at early period in the Yellow River. Now the water depth needed in the GC is more than 3.0 m, and it is 3 times higher than that in the current Yellow River during the dry season. Especially in the Yellow River there exist many variable sand shoals among moving channels. Naturally the ship loaded over 1,000 t couldn't sail in the current Yellow River. Even if a lower dam at Weishan (downstream of GC entrances) is built for raising the lower water level and improving the sailing condition in the water area outside of entrance of GC on both banks, the sand content (37 kg/m^3) and the yearly sediment runoff (16×10^8 t) are too heavy. Under this condition, the channel dimension in the Yellow River and in the approach channel of both ship locks couldn't be ensured and the chamber of ship lock and channel of GC will be choked with silt from sand runoff surely, so the paper's conclusion is that the method of horizontal crossing is impossible to be used here.

During the last fifty years, the yearly sediment runoff has decreased to 3.0×10^8 t by

means of carrying out much work of water and soil conservation in the districts of Provinces of Shanxi and Shaanxi on both banks of the Yellow River.

Even so, the width of the Yellow River where the Grand Canal crosses is more than 10 km, and it is also the water surface width during the flood period. During the mid-water or dry season, the river channel and the line of water-side are several kilometers away from the bank and dyke. Under this condition, to construct a steady South-North navigation channel is impossible. So, this method of horizontal crossing is useless as well.

2.2 Cubical / Overhead crossing

The cubical crossing also has two plans. One is a navigable tunnel under the river bed, and the other is a canal bridge over the river.

1. Navigable tunnel plan

The navigable tunnel is used generally in the following cases:

a) The topographical condition of project position is high and steep, and this plan would surely decrease the engineering volume of cubic meter of earth and stone.

b) For avoiding the influence of the meeting river.

In China, there are few regular navigable tunnels. In the past, the diversion tunnel of a hydro junction in Hanjiang River was once used to pass through boats, which was extremely dangerous. Recently a Goupitan hydro junction of Wujiang River is under design. In addition to the arrangement of aqueduct, open channel is seen as an interval canal between two ship lifts with high water head and arranged as a navigable tunnel up to 371 m to reduce the amount of earthwork.

In the world, France and Britain have the most navigable tunnels, as well as Ukraine and Japan. The earliest navigable tunnel is Pouilly-en-Auxois in France. It was built in 1775 – 1832 with an arch and reinforced concrete structure. The thickness of the inverted arch is 0.3 m, the width of the side wall is 9.8 m to 1.25 m from top to bottom, the height is about 7.7 m, and the water depth is 3.0 m. The bottom width is 6.2 m. The other earlier one was built at Trent under the Bridge-water River in England. All tunnels are one-way navigation, and the reason is: two-way hole needs large scale, large engineering, high cost.

France has two two-way navigable tunnels, one of which is 7.119 km long from Marseille to Rhone River Rove built in 1927, 22 m wide, 4.0 m deep, sailing with self-propelled barge loaded 1,200 t.

The requirement of engineering-technical condition of tunnel structure for waterway is higher and more complicated than that for highway and railway. It is not only in the respects of lighting, ventilating, but also engineering geology and hydrologic

geology. The treatment of foundation for navigable tunnel is specially difficult, so, it is not allowed to build a navigable tunnel on the soft soil foundation with higher water-bearing layer in order to avoid leakage caused by non-uniform settlement. By the way, outside of the tunnel entrance, it needs a larger open area for layout of a long-distance straight line stretch and mooring area used for vessels dispatching and waiting.

Obviously, this plan is also not suitable here to be taken.

2. Canal bridge plan

From the international point of view, adopting canal bridge scheme is a universal and effective way to cross rivers. Germany uses canal bridge most in the world with its mature and advanced technology, and it has the largest canal bridge in the world located at Minding over Wessi River of Mitte-Land (Mid-Germany) Canal. It is 398 m long, 42 m wide, and the control water depth is 4.0 m. The weight of the steel trough of canal bridge with water is 60,000 t. It is a double channel for sailing a fleet formed with barge loaded up to 1,000 t (shown in Fig.2). By the building there also stands a self-controlled water pump room in which there are 4 pumps with capacity of 16 cubic meters per second discharges for all canal nets.

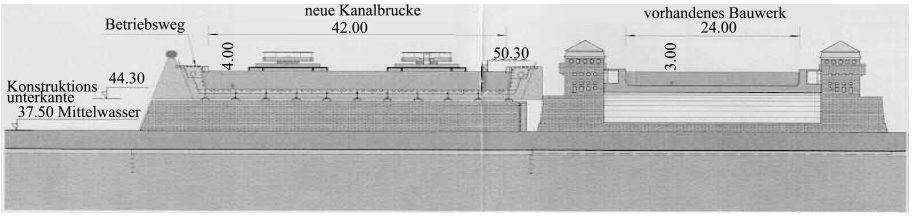

Fig. 2(a) Aqueduct cross section

The construction materials needed are 7,800 t of steel and 22,000 m^3 of concrete. The total investment is 85 million DM. The construction period lasted for 5 years from 1993 to 1998. And it operates normally for years. The antiseptic of negative pole for steel structure is the key technic in design. That means to build a long distance canal bridge is possible.

Fig. 2(b) Appearance drawing of aqueduct

Fig. 2(c) Aerial view of aqueduct

Recently we see another canal bridge at Magdeburg over Elbe River of Mittleland Canal which links Elbe-Harvel Canal from internet. Therefore, the Capital—Berlin could link cities along Rhine River and mid-part of Germany with waterborne transportation.

The length of the canal bridge is 1 km, of which 25% is over the Elbe River, and 75% is on the ground linked Mittleland Canal (shown in Fig.3). In Fig.3(b) we could see the training works with spur dikes group at the right bank of the Elbe River and some supporting seats group of canal bridge built on the ground.

Fig. 3(a) Crossing the Elbe River

Fig. 3(b) Overview of the Elbe River

Fig. 3(c)

Fig. 3(d)

The steel trough with U type is separately fixed with the supporting seat on the ground (Fig.3 (c)). At present it has been under operation for years, and you could see the vessels sailing on it. Many visitors stand around it to take a look with pleasure, and under canal bridge there is a boat passing through the bridge opening on the Elbe River (Fig.3 (d)).

Because the construction technique is advanced, the operation and technology are simple and the maintenance and administration are convenient, this paper believes surely that the canal bridge plan is suitable to be taken here. For overcoming the water difference between canal bridge and canal at the connecting place, the navigable building (ship lock / ship lift) ought to be arranged.

3. Wider rail gauge + moving ship-carrying chassis plan

In the downstream of the Yellow River the distance between two river banks (left/right) is almost 10 km, so it requires more investment for the plan above. In consideration of this case, the paper proposes to use wider rail gauge (over 6 m) + moving ship-carrying chassis plan. This plan is somewhat like a slope ship lift of 2,000 t vessel which is located in the river Yenisei of Fig. 4, ship-carrying chassis of Krasnoyarsk Russia, at the Krasnoyarsk hydro junction. The wider rail gauge is 9 m, and in each side of steel Ⅰ-beam there is a rack fixed on web plate. The moving steel ship-carrying chassis is shown in Fig. 3.

Fig. 4. 2,000 t Slope Ship Lift Box Car.

Owing to zero slope of the railway, the power needed is very small.

The difference between Plan 2 and Plan 3 is that: firstly, the barge in Plan 2 sails across the Yellow River by itself actively, but in Plan 3 the barge berths in chassis, and passes passively across the Yellow River depending upon the chassis; secondly, one line of Plan 2 could be one way or double way transportation depending on the width of navigation trough, but monotask railway of Plan 3 could only carry out for one way transportation, no matter how wide the chassis is. If it needs double way transportation, the route ought to be built as double track railway.

It is unknown before concrete analysis and calculation whether the construction investment will be lower if the traffic capacity is larger. So, this plan may be carried out with the canal bridge plan for comparison.

3 Conclusions

Since 1949, the construction and development of GC have been attached great importance to by the central and local governments, and great achievements have been made on the Southern stretch of the Yellow River:

From Jining (near south bank of the Yellow River) to Yangzhou (near north bank of the Yangtze River) 500 km has reached the standard of secondary channel. The ship lock dimension for 2,000 t vessels is 230×20/23×5.0 m, and the channel is 50/70×3.2/4.0×800 m (the east channel of Weishan Lake has only three levels: 2,000 t ships need to lighten the load to pass).

From Jianbi ship lock (by South bank of the Yangtze River) to Hangzhou (by Qiantangjiang River) 312 km has reached the 3rd class navigation standard. The ship lock dimension for 500 - 1,000 t self-driving barge with moving captain bridge is 230 m×20 m×4.0 m, and the dimension of Sanbao ship lock (On north bank of Qiantangjiang River) is 192 m×12 m×2.5 m, the dimension of channel is 45 m×3.2 m×480 m.

And the traffic volume of Lou Canal (canal stretch in Shandong Province) in the year 2009 was over 0.3×10^8 t. The canal stretch in the northern/southern Jiangsu province in the year 2013 was separately over 2.0×10^8 t.

The incomplete data shows that the traffic volume of part GC is the largest one in the inland canal of the world. By the way, based on the construction of the west dyke of north canal in Jiangsu Province, it protected 100×10^4 ha farmlands and 8 million people's life and property. The irrigated area enlarged to 56.2×10^4 ha, the drain waterlogged area reached 41.6×10^4 ha, and the flood discharge capacity enlarged. The effect of comprehensive utilization is obviously the best.

In 2014, the South-to-North Water Diversion Project allowed the Yangtze River overflowing to the Yellow River, making it possible to gradually solve the problems of industrial water use, farmland irrigation and shipping in the cities of Jing, Jin, Ji (three J) and other regions. Then the condition of recovering the navigation of North canal, South canal will surely be possessed. It will not only form a T type waterway trunk line pattern in the three J area, but also make navigation in the whole line of GC to enlarge the action of water transportation. But the key problem is the Project of the Grand Canal crossing over the Yellow River.

Based on the analysis of the similar situation at home and abroad and united with the concrete condition of the Yellow River, this paper confirms that Plan 2 and Plan 3 are suitable for selection.

Topic 6
Special Sessions

A new journey for the waterway transport on the Wujiang River

Wenwu Yang[1], Pengpeng Jia[2], Zhefei Jin[3]

[1] Wenwu Yang, Planning and Research Institute of the Ministry of Transport, Beijing, China. e-mail:634951278@qq.com

[2] Pengpeng Jia, Planning and Research Institute of the Ministry of Transport, Beijing, China. e-mail: jiapp@tpri.org.cn

[3] Zhefei Jin, Planning and Research Institute of the Ministry of Transport, Beijing, China. e-mail: jinzf@tpri.org.cn

Abstract: Wujiang River is the largest tributary on the south bank of the upper reaches of the Yangtze River. It is an important water transport passageway connecting regions of Guizhou and Chongqing with river and sea. However, the waterway transportation had been disconnected for 20 years since 2003 due to the hydropower cascade development of Goupitan, Silin, Shatuo, and Pengshui stations. In 2021, with the completion and operation of the navigation building of Goupitan hydroelectric hub, the passageway below Wujiangdu hydroelectric hub in the main stream of Wujiang River has the basic conditions for direct transportation of trunk and branch. At present, the development of Wujiang River water transportation is facing major strategic arrangements such as promoting the western development to form a new pattern, and comprehensively promoting the development of the Yangtze River Economic Belt, facing a consolidating and expanding the achievements of poverty alleviation and improving the overall development level of poverty alleviation areas, facing a new development situation of comprehensively improving the efficiency of resource utilization and promoting the harmonious coexistence between man and nature, requiring to deepen the supply side structural reform of Wujiang water transportation, building a new development pattern. This paper summarizes the current development of waterway, port, hydropower cascade construction, and waterway transportation along the Wujiang River, analyzes the main problems facing Wujiang waterway transport, the socio-economic and development requirements for waterway transport in general, and proposes a development blueprint and policy measures for the future Wujiang River waterway transportation.

Keywords: Wujiang; Water transport; New journey

Wujiang River is the largest tributary on the south bank of the upper reaches of the Yangtze River, originating from the eastern foot of Wumeng Mountain in the

northwest of Guizhou Province (referred to as "Qian"), with Sancha River in the south and Liuchong River in the north. After they converge in Huawuji, Qianxi City, Guizhou Province, it is called Wujing River. It flows through the central and northeastern parts of Guizhou Province and the central and southeastern parts of Chongqing (referred to as "Yu"), and joins the Yangtze River in Fuling District, Chongqing. Wujiang River is an important water transport channel connecting regions of Guizhou and Chongqing with river and sea. However, the waterway transportation had been disconnected for 20 years since 2003 due to the hydropower cascade development. In 2021, with the completion and operation of the navigation building of Goupitan hydroelectric hub, basic conditions have been created for Wujiang water transportation to start a new journey.

1 Current situation of development and utilization of Wujiang River

1.1 The downstream channel of Wujiangdu junction has been fully connected

Since the 12th Five-Year Plan period, with the completion and operation of 500 ton navigation buildings of Goupitan, Silin, Shatuo, Pengshui and other hydropower hubs, and the completion of Wujiangdu to Gongtan shipping construction project, the channel from Wujiangdu to Pengshui junction has reached the class Ⅳ channel standard for 500 ton ships, the reach from Pengshui junction to Baima junction under construction meets the class Ⅴ channel standard for 300 ton ships, and the channel from Baima hydroelectric hub to Fuling estuary meets the class Ⅲ channel standard for 1,000 ton ships. The waterway at the lower reaches of Wujiangdu is fully connected, realizing communication and connection with the waterway of the main stream of the Yangtze River, creating basic conditions for the development of trunk and branch direct transportation.

1.2 Port infrastructure conditions continued to improve

The completion of the Wujiang River water elevator stage for water storage has greatly improved the channel conditions, so the channel water depth has increased, the water flows gently, and the water area of some river sections has widened, creating good conditions for port construction. Since the 12th Five-Year Plan period, Guizhou Province has increased investment in the reconstruction of Wujiang wharf infrastructure, and built eight cargo terminals, including Wujiangdu, Nanmudu, Luowang River, Jiangjie River, Yanjiangdu, Heshandu, Sinan Taiping and Gonghe, the cargo throughput capacity reaches 8 million tons per year. At the same time, 14 small

passenger stops have been built in Yanjiangdu, Heshandu, Dejiang and other shoreline. The port infrastructure along the Wujiang River has been continuously improved, which has laid a foundation for building a new pattern of water and land intermodal transport.

1.3 Cascade development is coming to an end

Wujiang River is planned to have nine hubs, including Dongfeng, Suofengying, Wujiangdu, Goupitan, Silin, Shatuo, Pengshui, Yinpan and Baima. At present, except that Baima hydroelectric hub is under construction, all the other eight hydroelectric hubs have been completed and put into operation. The existing Dongfeng hydroelectric hub, Suofengying hydroelectric hub and Wujiangdu hydroelectric hub have not built navigable buildings, while five hydroelectric hubs including Goupitan, Silin, Shatuo, Pengshui and Yinpan have been constructed and a navigation building for 500 ton ships has been constructed for Baima hydroelectric hub under construction. The Navigable building of Yinpan hydroelectric hub and Baima hydroelectric hub can meet the navigation requirements of 1,000 ton motor single ship. The cascade hydropower development of Wujiang is drawing to a close, which has laid a solid foundation for Wujiang water transportation to start a new journey.

1.4 Waterway transportation is gradually restored

In recent years, cities and counties along the Wujiang River have increased the pace of ship construction. By the end of 2021, Guizhou Avionics Development and Investment Co., Ltd. had built ten 500-ton ships and now is building three 500-ton ships. At present, there are seven waterway transportation enterprises in Wujiang, including Guizhou Avionics Development and Investment Co., Ltd., Guizhou Yanhe Wujiang Shipping Co., Ltd., Guizhou Juchang Water Transportation Logistics Co., Ltd. and Chongqing Zhongyuan Shipping Co., Ltd., and there are 35 cargo ships with a capacity of about 20,000 tons. In January 2021, two cargo ships carrying 1,000 tons of phosphate rock were transported from Yuqing Port in Guizhou Province to Zhicheng Port in Hubei Province. In November 2021, 14 freighters carrying 6,800 tons of phosphate rock were transported from Kaiyang Port in Guizhou Province to Wuhu Port in Anhui Province. In February 2022, four cargo ships carrying extra large components for bridges were transported from Yanhe Port to Sinan Port. The road of Wujiang River water transportation revival has been opened, which will become an important support for the in-depth implementation of the regional coordinated development strategy and the construction of a new development pattern.

2 Main existing problems

2.1 The water elevator stage has a bottleneck restriction on the ship passing the dam

Firstly, the water level between some hydroelectric hubs is not connected, affecting the smooth flow of the channel. Due to insufficient consideration of water transportation in hydropower development, the water level between some hydroelectric hubs is not connected in the dry season, affecting the normal navigation of ships. For example, the water levels of Shatuo hydroelectric hub and Silin hydroelectric hub are not connected, which makes the water depth of the channel under the dam of Silin hydroelectric hub shallow in dry season, affecting the safety of ship navigation.

Secondly, the unstable flow discharged from the power station affects the navigation efficiency of the ship. Pengshui junction is the largest peak shaving and frequency modulation backbone power station in Chongqing power system. The unsteady flow discharged during peak shaving of the power station causes the instability of downstream river flow and the increase of instantaneous water level variation, which affects the safety and efficiency of ship navigation.

2.2 The whole channel does not reach the unified navigation standard

At present, waterway of Wujiangdu to Pengshui hydroelectric hub reaches Ⅳ channel standard, waterway of Pengshui to Baima hydroelectric hub reaches Ⅴ channel standard, waterway of Baima to Fuling estuary reaches Ⅲ channel standard, but the Wujiang River channel has not yet achieved the continuous and unobstructed navigation state of the unified standard of the whole channel during low water level operation of the hydroproject. Some ships need to be unloaded for navigation, since that affects the navigation efficiency of the channel and the transportation efficiency of ships.

2.3 The overall development level of the port is low

Firstly, there is a lack of overall planning guidance for port development. At present, Wujiang Port lacks a unified overall port planning, and there is no unified overall planning for the length of wharf coastline, development scale, production and living auxiliary facilities layout of each port. Thus, the role of ports in guiding the industrial layout of the hinterland and regional economic development is not prominent.

Secondly, the overall development level of the port is low. Wujiang Port is in its

infancy, and each port has not yet formed an intensive and large-scale port area. The port terminal has simple loading and unloading equipment, backward loading and unloading technology and single function, so it can only carry out simple loading and unloading business. Port construction and hinterland industrial development layout failed to form an effective connection. Incomplete port production and living facilities affect the operation efficiency and service level of the terminal. There are no container terminals along the Wujiang River.

2.4 Supporting facilities need to be improved

Firstly, the Internet of things, mobile network, cloud computing, artificial intelligence and other information technologies have not been organically connected with Wujiang water transportation, and the water transportation service level and service efficiency are low.

Secondly, there is a lack of necessary facilities along the Wujiang River, such as ship pollutant receiving and transfer, chemical tank washing station and so on, and the wharf environmental protection facilities need to be improved.

Thirdly, port terminals along the Wujiang River need to further improve ship berthing and shore power facilities and promote LNG filling services.

Fourthly, the joint dispatching information service platform for ship crossing has not been established along the Wujiang River, and the efficiency of ship crossing needs to be improved.

3 Facing the situation and development requirements

3.1 In-depth implementation of major regional strategies, requiring Wujiang water transportation to become a major external transportation channel in the hinterland

China has entered a new stage of development, promoting the western development to form a new pattern, and comprehensively promoted the development of the Yangtze River Economic Belt, which provides a new historical opportunities for the further development of Bijie, Liupanshui, Anshun, Zunyi, Guiyang, Qiannan and Tongren in Guizhou Province along the Wujiang River and Pengshui, Wulong and Fuling counties (districts) in Chongqing. Local governments of the regions along the Wujiang River will develop characteristic industries according to local conditions and the natural resource endowment conditions, deeply implement the strategy of Rural Revitalization and green development, vigorously promote new industrialization, new urbanization, agricultural modernization and tourism industrialization, deeply in-

tegrate into the construction of the Yangtze River Economic Belt, and form a new pattern of complementary advantages and coordinated industrial development with the regions along the Yangtze River. The Wujiang River is required to become a major transportation channel for materials, industrial raw materials and finished products required for economic and social development in the hinterland, and fully support the formation of a new development pattern along the Wujiang River, with the domestic cycle as the main body and the domestic and international double cycles promoting each other. According to the analysis of relevant units, the demand for external transportation of phosphorus ore, coal and stone materials along the Wujiang River is very strong. Among them, the demand for water transportation of characteristic stones can reach 5 million tons per year, and the transportation demand of raw materials of cement industry along the river can reach 3 million tons per year(Chongqing Transportation Bureau, 2001).

3.2 Consolidate and expand the achievements of poverty alleviation, and require Wujiang water transportation to give full play to its comparative advantages

The areas along the Wujiang River are rich in biological, energy, mineral, tourism and other resources and have great development potential. However, due to the complex terrain, imperfect transportation infrastructure network and serious lag in the economic and social development of the basin, the task of consolidating and expanding the achievements in poverty alleviation and protecting the ecological environment is very arduous. Local governments along the Wujiang River will concentrate their efforts on consolidating the achievements of poverty alleviation, actively undertake the industrial transfer in the East based on their own location and resource conditions, and vigorously develop industries such as new materials, special food, equipment manufacturing and tourism handicraft processing, cultivate a number of large leading enterprises, enhance self-development ability, gradually narrow the development gap with the eastern and central regions, requiring to give full play to the comparative advantages of Wujiang River water transportation in terms of large transportation capacity, low transportation cost, less adverse impact on the environment and less land occupation, expand the capacity supply of comprehensive transportation system in the region, make up for the capacity gap of medium and long-distance transportation of bulk goods by railways and highways in the region, provide transportation guarantee for promoting the sustainable development of resource-based areas. According to the analysis of relevant departments, Wujiang River water transportation has obvious advantages in medium and long-distance transportation of bulk goods. From Kaiyang Port in Guizhou Province to Suzhou Port in Jiangsu Province,

waterway transportation saves nearly 100 yuan per ton compared with railway transportation and nearly 1,900 yuan per ton compared with highway transportation. From Kaiyang Port in Guizhou Province to Fuling Port and Changshou Port in Chongqing, the water transportation cost is equivalent to 50% of the automobile transportation cost(Guizhou Department of Transportation, 2012).

3.3 The development of industrial agglomeration along the river requires Wujiang water transportation to play a leading role

To comprehensively improve the efficiency of resource utilization and promote the deepening of the new development concept of harmonious coexistence between man and nature, the local governments along the Wujiang River have made great efforts to optimize the industrial layout and strive to build an industrial agglomeration development pattern with industrial parks as the carrier. They also focus on resource conditions, build a number of industrial bases and industrial chains with high agglomeration, strong relevance and high output rate, and cultivate large enterprises with an income of more than 10 billion yuan and industrial parks with an income of 100 billion yuan. It is also required to speed up the construction of Wujiang national high-grade waterway connecting rivers and seas, improve the intensive and large-scale development level of ports, improve port storage facilities, distribution network and collection and distribution system, expand the functions of modern logistics, business services and bulk commodity trade of the port, lead the layout of hinterland industrial parks relying on ports, achieve a high-level dynamic balance between port and industrial development,such as the large-scale development of the port area that leads the layout of industrial agglomeration, and port industry development providing sufficient supply of goods for the port, effectively reduce the transportation costs of industrial production enterprises, and to provide important support for high-quality economic development and high-quality protection of ecological environment along the Wujiang River.

3.4 Building a new pattern of tourism development requires Wujiang water transportation to provide good services for the development of water tourism

There are abundant natural landscapes, ethnic customs, historical towns and other tourism resources along the Wujiang River, Wujiangyuan Baili Gallery tourist area, Wujiang Baima Mountain Scenic Area and Wulong karst landscape attracts a large number of tourists every year. Based on the new development stage, it is necessary to thoroughly implement the concept of integrated development of transportation and tourism, promote the development of tourist routes and improve the functions of

transportation facilities and tourism services. Wujiang water transportation is required to improve the wharf, tourism service function and safety supervision supporting facilities for water tourism, and provide good services for the development of water tourism in the Wujiang River.

4 General conception of water transport development

4.1 Basic principle

Firstly, adhere to the principle of a new stage of development, improve the quality and efficiency of Wujiang water transport supply system, meet the requirements of high-quality economic and social development.

Secondly, adhere to the principle of overall planning and coordination, rationally develop and scientifically protect Wujiang River water transport resources, comprehensively promote the coordinated development of waterways, ports and ships, comprehensively promote the coordinated development of ports, industries and cities.

Thirdly, adhere to the principle of building a comprehensive transportation system, replenish the short board of water transportation, give full play to the comparative advantages of Wujiang water transportation, build a safe, convenient, efficient, green and economic modern comprehensive transportation system.

4.2 General conception of Wujiang River water transportation development

Guided by the construction of a new pattern of Wujiang River water transportation development, it is required to deepen the structural reform of water transport supply side, improve the effective capacity supply of waterways, ports and other infrastructure, provide basic support for optimizing transportation structure and improving water transportation efficiency and benefits, improve the adaptability and leadership of water transportation to the economic and social development needs of the hinterland, and provide transportation guarantee for the areas along the Wujiang River to build a socialist modern country in an all-round way.

The development ideas of Wujiang River in terms of channel, port, transport ship and support guarantee are as follows.

4.2.1 Build a high-grade channel that can reach the trunk line of the Yangtze River

In the near future, the whole line from Wujiangdu junction to Fuling estuary will be built into a four-level channel to meet the needs of 500-ton ships to carry out trunk and branch direct transportation. In the long term, in order to meet the needs of the continuous growth of cargo transportation in the hinterland of Wujiang River, it is

necessary to implement the capacity expansion project of water elevator class navigable buildings and regulate the channel of key river sections that hinders navigation, namely, to build the second line of navigation buildings for five hydroelectric hubs, including Goupitan, Silin, Shatuo, Pengshui and Yinpan, according to the standard of 1,000 ton ships, and the waterway regulation project at the end of the reservoir shall be implemented according to the standard of 1,000-ton ships. It is also required to improve the channel support system, build the channel from Wujiang River crossing to Fuling estuary into a high-grade channel that can accommodate 1,000-ton ships, better serve the economic and social development needs of the new development stage along the Wujiang River and promote the formation and development of the Wujiang Industrial Belt.

4.2.2 Build a perfect layout, and a intensive and efficient port group

Build a modern port group with Kaiyang, Sinan, Yanhe, Wulong, Fuling and other ports as the backbone, and Weng'an, Zunyi, Yuqing, Dejiang, Pengshui and other ports as the important components, with reasonable layout, perfect functions, intensive efficiency, green intelligence and suitable for the economic and social development of the hinterland. Build a number of large-scale and intensive port areas, promote the construction of intensive and large-scale port area collection and distribution system, so as to make the port an important support for the intensive industrial layout along the Wujiang River and a water and land material transfer hub, strengthen economic ties and material exchanges between the areas along the Wujiang River and the upper, middle and lower reaches of the Yangtze River, and enhance regional economic competitiveness. Improve the terminal facilities and service functions of tourism passenger transport ports along the Wujiang River, so as to provide safety guarantee for the development of water tourism passenger transport. Promote the construction and operation of ship pollutant receiving and transfer facilities in ports along the Wujiang River to ensure that the Wujiang River water transportation realizes zero discharge of ship pollutants to water bodies.

4.2.3 Improve the specialization, energy conservation and environmental protection level of transport ships

In order to meet the transportation demand of resource goods in the hinterland of Wujiang River, improve the service level and competitiveness of shipping enterprises, and accelerate the development of professional transportation ships, combined with the development trend of ships in the Yangtze River system, we will vigorously develop motorized single ships. In order to meet the development requirements of Wujiang River of becoming a continuous channelized channel and to reduce or avoid the impact of transportation ship pollution on water quality, Wujiang ship power should gradual-

ly realize green transformation, gradually expand the scale of environmentally friendly ships powered by LNG clean energy and pure electricity.

4.2.4 Build a smart security support system

Build a traffic safety supervision and rescue system covering the navigable waters of the Wujiang River with dynamic perception, rapid response and efficient disposal. The water transportation support system widely applies the new generation of information technologies such as Internet of things and artificial intelligence to realize the digitization of government affairs, intelligent service and modernization of supervision. Promote the construction of comprehensive information service platform for ship crossing dispatching, shorten the ship crossing time, improve the operation efficiency of hydroelectric hub navigation buildings and increase the benefits of ship transportation.

5 Policy measures

5.1 Raise construction funds through multiple channels

Firstly, Guizhou Province and Chongqing Municipality will increase financial support and allocate a certain amount of financial funds every year for the construction of Wujiang River water transportation infrastructure, and at the same time, actively strive for the subsidy funds for inland water transport construction projects, so as to provide stable capital channels and capital scale for the development of Wujiang water transport.

Secondly, in accordance with the principles of marketization and rule of law, research the development and increase policy financial support for Wujiang water transportation construction project.

Thirdly, cities along the river according to their respective water transport development needs financial resources, and a certain scale of special financial funds shall be arranged in the annual budget to support the construction of local port projects.

5.2 Cultivate Wujiang water transportation market

Firstly, while strengthening the construction of Wujiang River water transportation infrastructure and improving service functions, government departments need to do a good job in publicizing the restoration of navigation of Wujiang River water transportation, so to promote the transfer of bulk goods and medium and long-distance goods in the hinterland to water transportation.

Secondly, water transport enterprises need to establish a good connection with

the transportation needs of industrial production enterprises in the hinterland, improve the efficiency of goods source organization, improve the water transportation logistics network, and effectively reduce the logistics costs of production enterprises to gradually establish and cultivate a unified, open, competitive and orderly water transport market system.

5.3 Strengthen the preliminary research work of water transportation projects

Firstly, the construction of Wujiang River waterway, the second line of navigable buildings and port projects is facing complex external conditions and technical problems of comprehensive utilization of water resources, involving the arduous task of cross regional and cross sectoral coordination. In order to ensure the smooth implementation of Wujiang River water transportation construction project, it suggests to speed up the preliminary research work of the second line 1,000-ton navigable buildings, channel regulation and other projects of Wujiang hydroelectric hub, and coordinate with relevant departments to provide technical support for the construction of 1,000 ton high-grade channel.

Secondly, cities along the river need to pay close attention to the planning and site selection of large-scale port shoreline under the condition of water storage, to the preliminary research work of port and wharf construction, so as to provide planning basis and technical support for port construction along the line.

5.4 Supplement the short board of water transportation public service facilities

Firstly, strengthen the capacity-building of waters safety supervision in the navigable waters of the Wujiang River, and form a modern water transport safety supervision and emergency rescue system with all-round coverage, all-weather operation and rapid response capability, improve the Wujiang River navigable waters to support the layout of the base, wharf facilities, mobile forces and service functions.

Secondly, establish the network framework of "three networks and one database" for water transportation management to realize the informatization, networking and intelligence of water transportation management.

Thirdly, promote the construction of water service areas in the navigable waters of the Wujiang River and facilities for receiving and transferring sewage and garbage from transport ships, realize zero discharge of transport ships to water bodies.

Fourthly, improve the construction of ship LNG filling stations and shore power facilities, realize the green transformation of water transportation mode.

Reference

Chongqing Transportation Bureau. Chongqing inland shipping development plan (2001—2020).

Guizhou Department of Transportation. Guizhou shipping development plan(2012—2030).

Deformation characteristics of channel regulation structures in Yizheng Waterway

Qianqian Shang[1], Hui Xu[2], Jian Zhang[3], Qilin Yang[4]

[1,2,4] Nanjing Hydraulic Research Institution, Nanjing, China. e-mail: [1] qqshang@nhri.cn, [2] huixu@nhri.cn, [4] 1246062029@qq.com

[3] Hohai University, Nanjing, China, e-mail: 1405817401@qq.com

Abstract: In the period 2015—2018, the 12.5 m deepwater channel regulation project downstream of Nanjing in the Yangtze River was constructed. Yizheng Waterway is one of the key regulated shallow waterways. Channel regulation structures in Yizheng Waterway are located at the head and the right edge of Shiyezhou Bar. The main types of the structures include spur dikes and bed protection mattresses. During the first few years, with the implement of the regulation structures, areas where the structures protected were generally silted up as the project was designed for. But the integrity of some structures, was influenced due to deformation caused by the flood events of the 2020 hydrological year. Deposited sediment on the structures at the right edge of Shiyezhou Bar, especially Y1# spur dike and SR2# spur dike, was flushed away during the flood season in 2020. In this paper, take Y1# spur dike as an example, the structural deformation characteristics are analyzed and the causes are discussed. Comparisons show that, in 2020, the spur dike body was kept free from damage, but the edge of the bottom protection mattress under the dike body deformed obviously and the deep trough moved towards the edge of protection mattress, which can lead to further deformation encountering flood events in the future. According to the investigation of recent measured data, fluvial processes and local bed deformation near the structures, a maintenance suggestion is proposed. Since scouring mainly occurred at the edge of the bed protection mattress, it is suggested that special attention should be paid on the bottom protection mattress of Y1# spur dike.

Keywords: Yizheng Waterway; Riverbed evolution; Channel regulation structures; Deformation; Bottom protection mattress

1 Introduction

Yizheng Waterway is a slightly bent and branched reach (Fig. 1), extending from the upstream Sanjiangkou to the downstream Guazhou, with a total length of 31 km (NHRI, 2021). Separated by Shi'erwei as the border, the upper segment is

straight and slightly bent, and the lower segment is slightly bent and branched. Shiyezhou Bar in the Yangtze River divides this waterway into left and right branches. The right branch is the main branch where the 12.5 m deep-water channel is located, and the left branch is a secondary branch.

The shallow area of the 12.5 m deep-water channel in Yizheng Waterway is located at the inlet segment of the right branch. With the scouring development of the left branch, the right branch shrinks at an obviously accelerated speed, which is disadvantageous to the channel conditions. According to the construction goals of the upper Nanjing reach of the 12.5 m deep-water channel, the deep-water channel regulation project was commenced by the deep-water channel construction headquarters on the lower Nanjing reach on June 29, 2015. The regulating structures were completed in May 2017, formally put into trial operation in May 2018, and passed the completion acceptance in May 2019. After the project was implemented, the channel maintenance scale was enlarged from 10.5 m × 500 m × 1,050 m to 12.5 m × 500 m × 1,050 m.

The channel regulating structures of Yizheng Waterway are mainly seated at the head of Shiyezhou Bar, including the head submerged dike, spur dikes at the south and north sides of the submerged dyke, spur dikes at the right edge of Shiyezhou Bar, left-branch bed protection mattress, and the bank protection design within the range of embankment body.

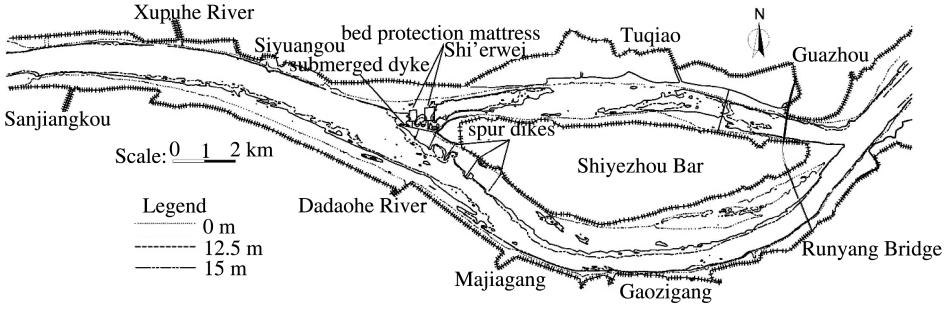

Fig. 1. Sketch of Yizheng Waterway (drawing base is local navigation base, in Jan. 2020).

2 River evolution and local scouring-silting

According to the recent riverbed deformation, the range of scouring and silting was small in normal hydrological years, but that in the flood years was large (Yu et al., 2019; Kou, 2019). After the project was completed (April 2019—January 2021), silting played a dominant role near the protective area where the project was construc-

ted. Due to the floods in 2020, the mainstream shifted closely to the right edge of Shiyezhou Bar, the dike-protecting area of SR2# - Y1# spur dikes was subjected to wide-range scouring, with a scouring amplitude of 1 - 5 m, which could reach close to 10 m locally. The dike-protecting area of the Y2# - Y3# spur dikes was silted up, accompanied by slight scouring at the right edge of the structures. Silting occurred within the channel at the right side of the Dadaohe River-Gaozigang, and the silting amplitude was about 1 - 3 m. The overall left branch was dominated by silting, the silting amplitude was 2 - 3 m, and local scouring still existed at the downstream side of YD2# bed protection mattress (Fig. 2).

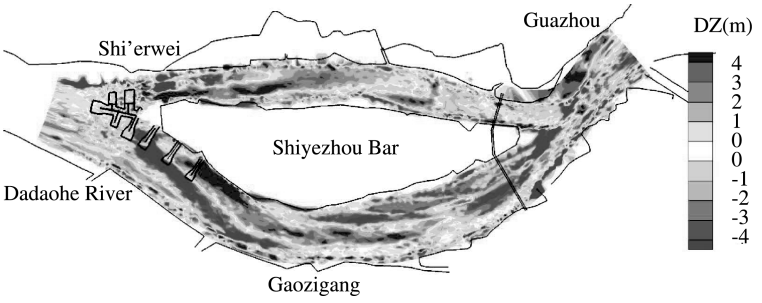

Fig. 2. Riverbed scouring-silting changes after project completion (Apr. 2019—Jan. 2021).

Scouring mainly occurred nearby Y1# spur dike, since Y1# structure was located in the mainstream scouring zone (Fig. 3). The most severe scouring appeared at the edge of Y1# spur dike structure, but the local scouring amplitude was generally small for other regulating structures.

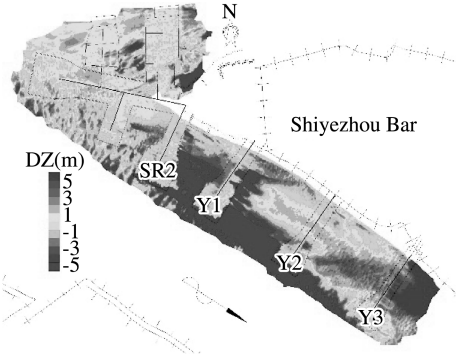

Fig. 3. Local scouring-silting near structures (Aug. 2019—Sept. 2020).

3 Y1# spur dike destruction characteristics

3.1 Destruction characteristics

Given that the scouring was the most severe nearby Y1# spur dike, the destruction characteristics of this structure was mainly analyzed. Based on the field survey and fixed cross-sectional monitoring charts (Fig. 4), the dike body of the Y1# spur dike was basically nondestructive, and the destruction mainly took place on the bottom protection mattress.

(1) Deformed parts

The bottom protection mattress of the Y1# spur dike generally silted up in the period 2016—2019 (i.e., from construction to completion). But in 2020, influenced by big floods, sediment silted on the mattress surface was almost all washed out, causing local deformation of the bottom protection mattress. The main destructed part was at the right edge of the mattress, with a maximum scouring depth of 8.0 m. The edge of the mattress at the upstream and downstream sides was also destructed, with a scouring depth of 1–3 m (Fig. 4).

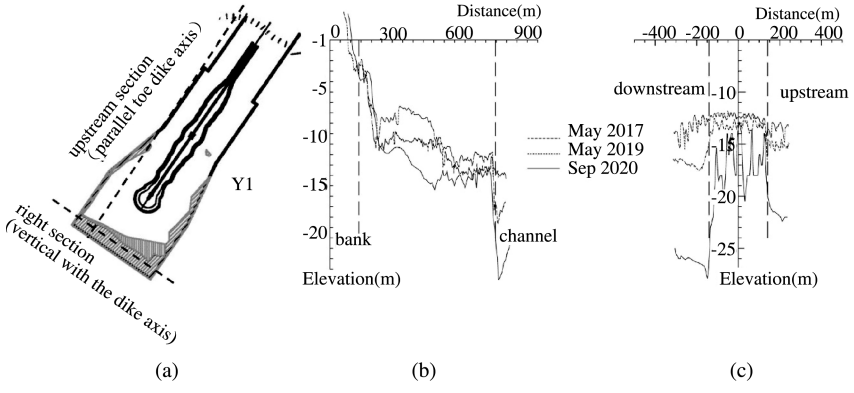

Fig. 4. Deformation of Y1# spur dike structure: (a) deformation area and section position; (b) variation of the upstream section; (c) variation of the right section.

(2) Deformation degree

The destructed area of the bottom protection and mattress at the Y1# spur dike accounted for 15.4% of the total mattress area. At the upstream side, scouring intruded into the mattress body by 30 m at most, and the slope was relatively gentle. At the downstream side, scouring intruded into the mattress body by 35 m at most, the scour pit at the mattress side was steep, with the slope gradient of 1∶4.2–1∶5,

which was close to the design stable slope gradient. The scouring at the mattress side of the dike head intruded into the mattress body by about 50 m, while outside the mattress was the deep river channel of right branch, and the slope gradient ranged from 1∶4.2 to 1∶4.5, which was approximate to the design stable slope gradient.

3.2 Destruction cause analysis

(1) In 2020, big floods continuously burst out in the Yangtze River basin, and the upstream incoming flow exceeded the design rechecked discharge of construction structures.

In 2020, the Yangtze River basin encountered continuous heavy rainfall processes, and the rainy season lasted for 62 days, which was the longest since 1961. Influenced by the heavy rainfalls, a big flood just second only to 1954 flood and 1998 flood took place in the whole Yangtze River basin. Along the main course of the middle and lower Yangtze River, the maximum flood levels from Jianli to Datong ranked 2–5 in the observation records, and the tide level of Ma'anshan-to-Zhenjiang exceeded the historical record (Feng, 2020).

In 2020, the crest discharge at Datong station was at 84,700 m^3/s, which was the maximum discharge ever since the 175 m impoundment of the Three Gorges Project (TGP) (Fig. 5), and exceeded the rechecked discharge of 82,300 m^3/s (in 1998) when designing the channel regulating structures. In addition, flood peaks were large with a long duration, e.g., discharge higher than 50,000 m^3/s and 60,000 m^3/s lasted for 89 days and 43 days respectively. The big floods generated adverse impacts on the structural stability.

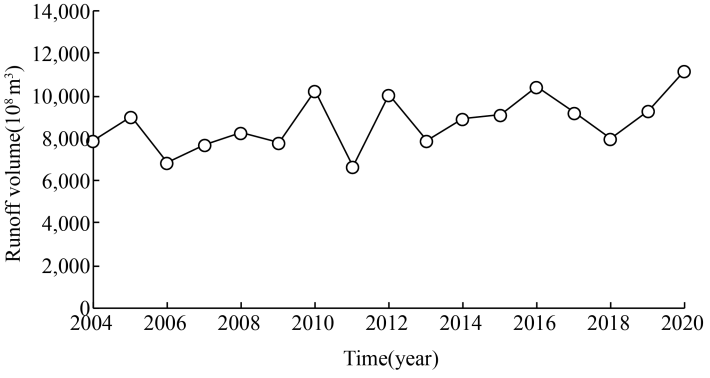

Fig. 5. Variation of annual runoff at Datong hydrological station.

(2) Y1# spur dike is located in the mainstream scouring zone, making it prone to deformation and destruction.

The mainstream shifted to the head and also the right edge of Shiyezhou Bar dur-

ing flood season. Located at the right edge of Shiyezhou, Y1# spur dike is the primary spur dike resisting floods and guarding the side shoals at the right edge of Shiyezhou. Under a high flow rate, the downstream side of the dike was scoured by the flow over the dike and the flow around the dike head, meanwhile, the right edge of the dike was scoured by the mainstream, and the scour holes around the mattress developed larger. When the flow rate was low, the mattress was slightly silted up (about 1 m). In summary, both scouring and silting took place within the year, but floods exerted much more significant action, leading to more severe scouring invasion into the mattress.

3.3 Future focus

According to the variation of topography and river regime near the dike structure, the bottom protection mattress of the Y1# spur dike had the trend and possibility of further scouring-induced deformation.

(1) The scour hole downstream the dike was bound to exist for a long time, and scouring would develop somehow when big flood occurs. Both annual and inter-annual scouring and silting occurred in the scour hole downstream the dike, which did not intrude into the mattress before 2020. However, the scour hole developed into the mattress due to big floods in 2020, the slope of the scour hole was generally steeper after scouring in flood season, and it became gentler after silting in dry season (Table 1).

(2) For the deep channel outside the mattress at the right edge of Y1# spur dike, sediment load was reduced sharply under the operating of the Three Gorges Project (TGP) and its upstream reservoirs. The mainstream was at the right edge of Y1# spur dike, where sediment could hardly be desilted. Therefore, the structure might be further scoured if encountering a big flood.

Accordingly, attention should be paid to the change trend at the edge of the bottom protection mattress of Y1# structure.

Table 1 Slope of scour holes nearby Y1# spur dike structure.

	Feb. 2018	Aug. 2019	Nov. 2019	Sept. 2020	Mar. 2021
slope of the downstream scour hole	1∶18.5	1∶4.0—1∶6.3	1∶5.0—1∶6.5	1∶4.2—1∶11.4	1∶5.6—1∶11.4
slope at the right edge of bottom protection mattress	—	—	—	1∶4.5	1∶5.3

4 Conclusions

(1) After being implemented, the 12.5 m deep-water channel regulation project

of Yizheng Waterway effectively guarded the head and the right edge of Shiyezhou Bar, achieving an evident regulation effect. The channel regulating structures were generally silted up after construction. However, big floods in 2020 rushed towards the head and the right edge of Shiyezhou Bar, causing severe scouring nearby Y1# spur dike at the right edge of Shiyezhou.

(2) The edge of the bottom protection mattress of Y1# spur dike was deformed, and a large-scale scour hole existed around the mattress, which might be further scoured. Therefore, it is suggested that emphasis should be laid on the bottom protection mattress of the Y1# spur dike and the nearby riverbed deformation.

Acknowledgements

This research is supported by the Subsequent Work of the Three Gorges Project (No. SXHXGZ-2020-3) and Central Public-Interest Scientific Institution Basal Research Fund (No. Y222013).

References

Nanjing Hydraulic Research Institute (NHRI), 2020. Study on water and sediment mathematical model of Yizheng Waterway of 12.5 m deep water channel below Nanjing.

Feng, Y., 2020. Analysis and reflection on characteristics of dikes dangers in middle and lower reaches of the Yangtze River in 2020. Yangtze River, 51(12):31-33+51.

Nanjing Hydraulic Research Institute (NHRI), 2021. Evaluation on technical status of channel regulation structures at Zhenjiang Section of the Yangtze River.

Yu, M.Q., Luo, J., Wu, L.B., 2019. Analysis of branching evolution characteristics and regulation countermeasures in the lower reaches of the Yangtze River. Science & Technology for Waterway, 4:10-16.

Kou, J., 2019. Regulation effect at Yizheng Waterway of 12.5 m deep-water channel project in the Yangtze River below Nanjing. China Harbor Engineering, 39(6):41-47.

Development of inland water transport over the Xijiang River in Guangxi: Achievements and inspirations

Ning Wu

(Guangxi Beibu Gulf Port Group International Co., Ltd., Nanning 530200, China)

Abstract: Ship lock is a key part of inland waterways, thus solving its various technical issues in the three stages of planning, design and operation management is conducive to fully exerting the function of inland waterway navigation and maximizing the shipping benefits of navigable rivers. This paper combines the experience and lessons learned from the planning, design and operation management of locks in the Xijiang River basin over the past forty years, systematically summarizes the technical issues that need to be solved at each stage and puts forward correspondingly reasonable suggestions, which are of referential significance to the planning, design and operation management of inland river cascade development and locks projects in Guangxi and even in China.

Keywords: Xijiang River basin; Ship lock; Technical issues

Guangxi is a major inland river shipping region in China. The Xijiang River basin, with the Xijiang River shipping trunk line and the national high-grade channels such as the Youjiang River, Hongshui River and Liuqian River as its core, and other regional major waterways as its important components, forms an inland navigation channel system that stretches from the east to west, connects the trunk and branches, and leads the water to the sea.

Since the reform and opening up, the cause of inland water transportation in Guangxi has been fruitful: a large number of shipping junctions and high-grade channels have been built, and the capacity of inland waterway vessels has increased significantly, from 500,000 DWT in 1996 to 10.68 million DWT by the end of 2020; the development of large-scale vessels has been rapid, and the average tonnage of vessels passing the locks in the Xijiang River trunk line has increased from 48 tons in 1989 to 2,020 tons by the end of 2020, with the largest one reaching 6,300 tons; the cargo throughput of the locks has grown rapidly, with that of the Changzhou Hydro Complex, Wuzhou, increasing from 39.28 million tons in 2010 to 151 million tons by the

end of 2020, making it the world's largest lock in natural waterways in terms of cargo throughput; a new model of navigation management in the river basin has been innovated, firstly realizing joint operation and centralized control of river basin locks in China. It has greatly exerted the function of inland river navigation and its advantage on water transportation of the Xijiang River, significantly promoting the social and economic development in the region.

Ship lock is a controlling link of the inland waterway, whose technical issues in the planning, design and operation stages must be systematically tackled in order to fully exert the shipping function of the inland river and maximize the benefits of inland river shipping. Combining the experience and lessons learned from the construction and navigation management of inland waterways in the Xijiang River basin in recent years, this paper systematically summarizes the technical issues of the locks there at various stages and puts forward feasible suggestions.

1 Technical issues in the planning stage

Cascade canalization of rivers in mountainous areas is a remarkable feature of Xijiang River waterways. The technical issues in the early planning stage mainly include the functional positioning of cascade junctions, and the scale and standard of the ship locks, all of which are the key factors affecting the ship locks' capacity, safety and accessibility, as well as the development of inland navigation and its overall benefits.

1.1 Emphasis on shipping in the functional positioning of the cascade junctions

The functional positioning of projects largely determines the necessity and scale of the cascade ship locks, and should be determined with an eye for development and based on the principle of maximizing the benefits of comprehensive utilization of water resource. The navigational function should not be limited by the original navigational status and the channel grade of the river reach in which the junction is located. The extension of the channel and its connection with high-grade waterways must be considered in an integrated manner.

For comprehensive hydro projects, power generation brings the most direct economic benefits, and the function of flood control can also be fully exerted and valued. However, the shipping function requires additional construction and operating costs and does not bring direct economic benefits, so it is not given sufficient attention. Yet delaying or not building ship locks, or reducing its scale are not conducive to river navigation and the maximization of the comprehensive use of water resources.

Certain cascade junctions in the Xijiang River basin did not build navigation facil-

ities during construction, resulting in their inability to connect with high-grade navigation channels. Practice has proven that emphasizing and strengthening the role of shipping in the functional positioning of the cascade junctions help to maximize the comprehensive benefits of the hydro projects. The Baise Hydro Complex in Guangxi is an example of increasing the shipping function, which thus successfully extends the high-grade navigation channel of the Youjiang River into Yunnan. The Datengxia Hydro Complex adjusted shipping from the third place to the second in its functional positioning, and the scale of the lock rose from 1,000 tons class to 3,000 tons, which is a good example for strengthening shipping functions.

1.2 Pay full attention to water level connection among cascades and the overall arrangement of locks.

The connection of the water levels among cascades largely determines whether the entire river can achieve the planned channel grade, whether it can meet the guarantee rate of navigation stage, and whether it can leave room for further development of the channel upgrading. During the construction of the cascade junctions and the whole project, it is essential to ensure that the water levels among the cascades are connected.

Water level connection means that when the downstream cascade junction is operating at dead water level, its backwater returns to the dam of its upper junction; and the water level connection is easily achieved when the downstream cascade junction is operating at normal water level.

In order to realize water level connection, full consideration must be given to the dam site selection and the water level analysis during the early planning stage. When the project is under progress, problems affecting the water level connection must be fully resolved. In order to reduce the inundation of the reservoir area, Yuliang Hydro Complex of the Youjiang River reduced the normal water level from 100 meters in elevation to 99.5 meters, and correspondingly reduced the dead water level in the reservoir area from 99.5 meters to 99 meters, which caused a disconnection with the water level of the Naji Hydro Complex in the upstream. The construction of the Naji Lock was decisively suspended and the design was modified by lowering the lock chamber and the lower gate head threshold. The problem was thus solved. Despite the resulting increase in investment of approximately RMB 40 million, it is highly beneficial for improving the guarantee rate of navigation stage and promoting the development of large vessels.

At present, there are 10 shipping cascades in the Xijiang River basin from the Baise Hydro Complex upstream to the Changzhou Hydro Complex downstream which

connect each other when operating at dead water level. When the junctions are operating at normal water levels, it is more conducive to the upgrading of the waterway and the development of larger vessels.

Meanwhile, the layout of ship locks should be fully considered in the site selection of the junction. While satisfying the function of flood discharge and matching the layout of other hydraulic structures, the layout between ship locks, power houses flood discharge gates should be properly handled. In principle, the ship locks should be arranged near the shore, not between power houses or discharge gates, and it should reserve space for second line and third line ship locks in the future.

1.3 The grade and scale of locks on high-grade channels should be moderately better than they are at the moment.

Locks belong to permanent hydraulic buildings, which are difficult to expand and transform after completion. Therefore, in determining the grade and scale of locks on high-grade waterways, it is appropriate to moderately build larger locks according to the freight volume and the ship types in future development, as well as reserve the construction conditions of second and third line locks.

For the lock construction in the Xijiang River basin, the completed Changzhou third line lock and fourth line lock, Guiping second line lock, Guigang second line lock, Yongning lock and the under-construction Xijin second line lock and Honghua second line lock are all based on the standard of 3,000-ton class, whose level of locks is higher than the planned waterway level at that time; the completed Yuliang lock, the under-construction Baise ship lift and the upcoming Yangxi lock and Meilin lock are all considered to be moderately advanced and there is reserved space. It has effectively promoted and adapted to the development of water transportation and the mega vessel trend, and is conducive to the full play of inland river shipping.

However, conservative decisions also left some regrets for the development of water transportation. Changzhou first line lock and second line lock basically reached the freight volume capacity just one year after completion; Jinji Hydro Complex reached the capacity in just two years after Youjiang 1,000-ton class waterway opened; the accumulated freight throughput of the rock beach ship lift in the Hongshui River has been less than 100,000 tons in the past 20 years since its completion due to its small scale.

1.4 The water depth on sill needs to be adapted to the upgrading of waterways and the mega vessel trend.

For rivers whose channel levels are upgraded by canalization with fully connected

cascade water levels (for instance, the Xijiang River shipping trunk line), there is great potential for long-term waterway upgrading through further waterway regulations and other measures. And the water depth on sill should leave enough room for waterway upgrading and the mega vessel trend.

The minimum design water depth on sill depends on the lowest navigable water level, ship draft, and the factor of under keel clearance.

Determining scientifically the minimum navigable water level both on the upstream and downstream of the locks (junctions) is a prerequisite for determining the minimum design water depth on sill. The determination of the minimum design navigable water level in the downstream is often more complex than the upstream. In view of the uncertainty of the downstream riverbed undercutting after the completion and operation of the junction, the determination of the downstream minimum navigable water level should be based on the principle of "extreme caution". This is especially true for junctions where there are dehydrated section in the downstream river, otherwise it will reduce the guarantee rate of navigation stage of the locks, or even cause the locks to stop working and paralyse the navigation on the whole river.

In this regard, Guangxi has much to say. The design minimum navigable water level in the downstream of the first and second line locks at the Changzhou junction in Wuzhou, Guangxi, was determined to be 5.05 meters in elevation (with a 0.5 meter allowance for the riverbed undercutting). Three years after the junction was put into operation, the riverbed scour depth in the downstream of the junction dropped far more than expected, reaching about 1.4 meters. When the flow is insufficient during the dry season, it causes insufficient water depth in the lock chamber, the lower gate head threshold and the lower approach channel of the first and second line locks, forcing vessels to reduce their loads significantly and lower their drafts to cross the locks. In severe cases, the operating water head of the locks exceeds the designed maximum (16.05 meters), forcing the locks to close and resulting in the paralysis of the entire Xijiang River shipping line.

In view of the problems arising from the first and second line locks, a very scientific and cautious approach was taken in the construction of the third and fourth line locks at Changzhou and Wuzhou, to determine their downstream minimum navigable water level, which was first reduced to 2.4 meters (in elevation) and then to 1.4 meters (in elevation) based on observations, analytical calculations and digital to analog studies after taking into account various unfavourable factors. From the operation condition of the third and fourth line locks in Changzhou since they were put into operation in 2015 to date, it is a correct and more reliable choice to adopt 1.4 meters as the design low water level.

The low navigable water level in the upstream of the locks occurs at different times with that in the downstream, which often happens in the flood season when the channel depth is generally deeper due to the large flow. However, according to the reservoir operation rules, in order to prevent flooding and not to increase the risks of reservoir area inundation, the water level before the dam shall be lowered. Although the water depth of the upper gate head threshold determined according to the specification meets the design minimum water depth requirements, it actually becomes a "shallow point" in the waterway, which is not conducive to the navigation of ships with larger tonnage by utilizing the water depth in the flood season, nor is it conducive to the full play of inland river shipping. The locks on the main line of the Xijiang River, the Youjiang River, the Liujiang River and the Qianjiang River in Guangxi have a deeper water depth at the upper lock head threshold and in the upper approach channel than required by the standard. This is so because of the need to address navigational issues during construction. After the second phase of the cofferdam (the dam has not yet completed construction), the lock will be put into operation. At this time, the upstream water level is lower than the dead water level of the reservoir (after the completion of the junction) and the lowest water level in flood season. Take the Guigang junction as an example, the minimum operating water level of the reservoir during the flood season is 41.1 meters in elevation and the normal operating dead water level is 42.6 meters in elevation. According to the standards, the threshold elevation would suffice with 37.6 meters in elevation (41.1 meters down by 3.5 meters), but in reality it was built to 35.3 meters in elevation. In the flood season, when the water level in front of the dam is reduced to 41.1 meters, the water depth of the upper gate head threshold and the upper approach channel is 5.8 meters, which avoids becoming a "shallow point" in the channel during the period and creates the basic conditions for navigating larger vessels with higher tonnage at the time. Therefore, in determining the minimum design navigable water level upstream, it is also necessary to take into account the characteristics of the river where the locks are located, and to appropriately reduce the elevation of the upper gate head threshold and the upper approach channel under the premise of meeting the current lock design standards and from the perspective of giving full play to inland navigation.

The determination of the design minimum water depth on sill, in addition to the scientific determination of the minimum navigable water level, also depends on the factor of under keel clearance, the ship draft and the typical vessels passing through. From the practical effect of Guangxi cases, the factor of under keel clearance of 1.6 is very successful, and the design minimum water depth on sill should unshakably adhere to it, which would not only ensure the safe operation of the locks, but also leave

space for the development of large vessels.

Another factor that should be considered when determining the design minimum water depth on sill is the draft of the design vessel type. The determination of the design vessel type should be based on the actual draft of the corresponding class of vessels in the market. Since 2015, the lock design in Guangxi are all based on operating vessels in the market to determine the draft of the design vessel type. For example, the full load draft of 1,000-ton class ships in Guangxi is between 2.7 and 3.0 meters. When calculating the minimum water depth on sill of the 1,000-ton class locks, the full load draft of the design vessel type takes 3.0 meters. This is the reason for the 1,000-ton class locks taking minimum water depth on sill as 4.8 meters at the Yangxi and Meilin junctions in the upper reaches of the Liujiang River, which is significantly larger than the 3.5 meters of the past 1,000-ton class locks, and also larger than the past 2,000-ton class of 4.5 meters.

According to years of experience, the total investment on the locks is not sensitive to the increase in the water depth on sills which nonetheless provides the basic conditions for giving full play to the river navigation. At present, the 1,000-ton class channel of the Youjiang River is able to navigate 2,000-ton vessels; the 2,000-ton class channel of the Xijiang River trunk line is able to navigate 3,000-ton class and above vessels thanks to their water depth on sills.

1.5 Overall consideration should be given to the coordination of the levels and scales of each cascade lock in the basin

The levels and scales of ship locks on the same high-grade channel should be coordinated with each other. The principal dimensions of those locks should be consistent as far as possible, and the coordination of lock throughput capacity between upstream and downstream cascades should be considered as a whole.

All the locks built after 2010 on the trunk line of the Xijiang River have adopted the 3,000-ton class, and the principal dimensions are basically identical. With the lock throughput capacity in the upstream and the downstream being relatively small and large, it is generally suited to the actual conditions of freight frequency in the basin, and the lock throughput capacity among the basin's cascade junctions is basically coordinated.

There are two junctions in the Liuqian River, namely Honghua and Datengxia. Honghua junction has a 1,000-ton class built lock and a 3,000-ton class lock under construction, while Datengxia junction in the downstream currently has only one 3,000-ton class lock. The navigational capacity of upstream and downstream cascades is obviously unbalanced. Preliminary work has been initiated on the second and third

lines of locks at the Datengxia junction, and the issue of the uncoordinated navigational capacity will be properly addressed upon completion. The lock throughput capacity of Jinji lock in the lower reaches of the Youjiang River is only about half that of Yuliang lock in the upper reaches. The preliminary work of Jinji second line lock has started, and this problem will be properly solved upon completion as well.

1.6 The navigability of locks (junctions) on important waterways during their construction should be ensured.

It usually takes a long time for building a junction or lock. However, navigable rivers where there are junctions or locks under construction should not be cut off for long, otherwise goods will switch to land transportation, terminal enterprises will be demobilized, ship enterprises will seek other businesses and the shipping function of the river will shrink or even be disabled. The navigation of Dahua Hydro Complex in the middle reaches of the Hongshui River in Guangxi was cut off during its construction due to the slow building of the facilities for ships passing the lock. The subsequent construction of cascade locks on the Hongshui River followed the example of the Dahua junction, resulting in a prolonged break in navigation on the Hongshui River.

The locks (junctions) on the Xijiang River trunk line, the Youjiang River and the Liuqian River all allowed navigation during the construction period, which only stopped navigation for a short time during the period from the river closure to the second phase of the cofferdam to retain and store water. The suspension time is usually about 30 to 40 days, and it would not exceed 3 months even for large water conservancy projects with high dams and large reservoirs like the Datengxia junction. After the second phase of the cofferdam impounding water to the water level to the first phase, the locks are put into operation so that the adverse impact on shipping is reduced to a minimum and there is no shrinking effect on the shipping function of the inland river. Therefore, it is necessary to protect the navigability of the locks (junctions) on important waterways during the construction period.

1.7 Construction sequence of cascade junctions

The construction sequence of the junctions determines whether they and the pertinent waterways can bring benefits into play in time. Improper arrangement of construction sequence will cause the lock to be idle after completion and waste channel resources. Therefore, in the development and construction of inland river cascade junctions, we should build the downstream cascade first, and push it upstream gradually. By building each cascade lock, the high-grade channel is supposed to be extended a section upstream.

The trunk line of the Xijiang River is a model of rational construction sequence of cascade junctions. In 1978, Guangxi and Guangdong jointly proposed to develop the shipping resources of the Xijiang River. Through the construction of Guiping and Guigang junctions, the channel grade of the Xijiang River trunk line was raised from Class Ⅵ at the time to Class Ⅲ. The construction of Guiping junction, which was started first in 1986, was completed and began the impoundment in 1992. The return water of the reservoir area returned to the Guigang shipping center in the middle reaches of the Xijiang River. Combined with local channel improvement, the reservoir area reached Class Ⅲ. Below the Guiping junction, the flow rate has increased significantly due to the tributaries' convergence into the Liuqian River, and after local channel improvement, it has also basically reached the standard of Class Ⅲ. Since then, the development of large-scale ships in the Xijiang navigation area began to speed up, and the freight volume of water transportation also began to rise. Then, the construction of Guigang junction in the upstream was started in 1995 and the locks were put into operation in 1998, whose backwater returned to the Xijin junction in the upstream which had already been put into operation. Combined with related waterway improvement, the target of building the 1,000-ton class waterway of the Xijiang River trunk line was achieved, which opened a new chapter of the modern water transportation of the Xijiang River and made it develop rapidly.

It is worth mentioning that the benefits brought by power generation of the Guigang junction on the Xijiang River trunk line are much greater than that of the Guiping junction. Nonetheless, Guiping shipping junction in the downstream was still prioritized in terms of construction sequence considering the comprehensive shipping benefits and to promote the entire project upstream-wise gradually.

2 Technical issues in design and construction

Based on years of experience in the construction of locks in the Xijiang River basin, the following is a review on several typical technical issues in the design and construction of locks in terms of layout, structural design, equipment selection and innovative concepts of construction.

2.1 The lock entrance area and the main channel should be connected as smoothly as possible.

Whether the entrance area is smoothly connected with the main channel will directly affect the safety and efficiency of passing the lock. The layout of the ship lock should take into account the topography and river course near the dam site to ensure

the smooth connection between the entrance area and the main channel. If necessary, engineering measures should be taken to meet that end. Large-angle connection or locks crossing the mainstream of the river at a wide angle should be avoided as far as possible to ensure the safety and efficiency of ships' passing the lock.

It will affect ships' safe entry when the connection between the entrance area and the main channel is not smooth enough. The encounter angle between the entrance area of the first line lock in the downstream approach channel of Guigang junction and the main channel of the Xijiang River trunk line is large, and ships getting into the entrance area in flood season need to cross the mainstream obliquely at a wide angle. In case of insufficient power of ship or captain's lack of experience, it would be difficult to pass the lock.

One of the main reasons for finally choosing the right bank instead of adopting the original Zhongjiang Scheme for building the third and fourth line locks of Changzhou in the Xijiang River trunk line is that ships in the Zhongjiang Scheme have to cross the mainstream to get into the lock entrance area. Model tests showed that it would be difficult for ships to enter the locks under certain flood discharge, and there are potential safety hazards.

2.2 Coordination of lock berthing facilities

The anchorage should be coordinated with the breasting dolphins of berthing facilities in the approach channel. When the anchorage is far away from the lock, the number of breasting dolphins should be reasonably increased near the lock for improving the efficiency and throughput capacity of the lock.

As the downstream anchorage of the Changzhou third and fourth line locks is located far away from the lock, in addition to the regular breasting dolphins in the upper and lower approach channels of the locks, secondary breasting dolphins capable of accommodating about three ships have also been creatively added, which significantly improve the efficiency and throughput capacity of the locks (preliminary analysis calculates an increase in throughput capacity of approximately 6%). Inspired by the valuable experience of the third and fourth line locks at the Changzhou junction, the Xijin and Honghua second line locks currently under construction have increased the number of near-lock breasting dolphins to enhance the efficiency of the locks.

2.3 Structural design should take full account of the mega vessel trend.

Some locks in the Xijiang River basin are designed according to the 1,000-ton class standard, however, they are accessible to ships of above 3,000-ton class as well. Although hydraulic structures such as mooring post have not been fractured or exces-

sively deformed due to overload, it is still an issue that deserves attention. There has been a case where a 300-ton class lock in the lower reaches of the Guijiang River "collapsed" during flood season due to the overloading of 1,000-ton class vessels berthing against the breasting dolphin.

When designing and constructing a ship lock, under the condition that the cost does not increase significantly, a certain safety margin should be considered in the structural design to increase the "toughness" of the ship lock operation, so that the ship lock can better adapt to the mega vessel trend, especially in the structures and facilities such as breasting dolphins, mooring posts and floating mooring posts in lock chambers, which are often under the action of ships.

2.4 The navigation clearance of ship lock cross-river buildings should fully consider the future development of the waterway.

The river-crossing structures of ship lock mainly include supporting facilities like lock-crossing bridge, maintenance bridge, cable bridge, bulkhead gate, etc. The navigation clearance of the river-crossing structures should fully consider the future development of the waterway and the mega vessel trend. Among those structures, the navigation clearance of upstream dam outlets and the cable bridge is often compromised. The navigation clearance of most locks in the Xijiang River meets its requirements of waterway grade. In a 300-ton class small lock in the Xijiang River basin, the clearance of cable bridge at the upper lock head is only 6.5 meters, where even 300-ton class ships have to put down the mast before they can pass, while those with larger tonnage can hardly pass, which restricts the benefits of inland navigation.

2.5 Operational reliability of the key lock equipment should be improved.

The hydraulic hoist system of the ship lock, miter gate (especially the pintle), main electrical equipment and monitoring system are the key equipment to ensure the safe and reliable operation of the lock. These equipment account for a small proportion (about 6%) of the investment in the lock construction, but they largely determine the stability and reliability of the lock operation. In the design and construction of the lock, new technologies and new processes should be adopted, and advanced, reliable, mature and stable equipment should be purchased, which can greatly reduce the maintenance personnel and the cost, the time needed for and the frequency of lock overhaul as well as ensure the safe, stable and reliable operation of the ship lock. At present, the average time interval of ship lock outage for overhauling of in the Xijiang River is 11.5 years. Besides scientific maintenance, the reliability of key equipment also plays an important role.

2.6 New development concept should be implemented for building green and ecological ship locks.

The reservoir area and arable land should be protected. The construction of the Guigang junction, which began in 1995, involved the construction of 26 pumping stations and the adoption of reservoir protection to protect high-quality arable land on both sides of the reservoir's tributaries, avoiding the permanent inundation of more than 6,500 mu (about 433 hectares) of high-yielding paddy fields and benefiting more than 90,000 mu (about 6,000 hectares) of arable land.

Land was reclaimed and given to the people. The Naji junction in Baise, which started construction in 2005, used the waste residue of the project to fill 340 mu (about 22.7 hectares) of land in the shallow water area of the flood plain of the reservoir area, and transformed it into a fertile land and demonstration area for ecological agriculture, which reduced the social contradictions caused by the inundation of the reservoir area and was well received by the villagers nearby.

Poverty alleviation was achieved by utilizing water photovoltaic system. In 2017, by making use of the water surface of the river bay in the reservoir area of the Yuliang junction of the Youjiang River, the local government jointly installed a 30 MW water photovoltaic power station whose annual profits amounted to RMB 13 million and were distributed to poor households, helping 1,200 poor households to get out of poverty and live in relative comfort.

3 Technical issues in the operation

After the completion of the lock, it is important to keep pace with the time and technological development, apply new technologies, innovate management modes, and improve the service level, management level and operational efficiency of the locks.

3.1 Joint operation of reservoirs in multi-dimensions to improve guarantee rate of navigation stage

The upgrading of the channel level in the Xijiang River basin in Guangxi is mainly achieved by means of canalization, and the navigable water level among the cascades is based on the fact that the water level before the dam is not lower than the low water level for shipping. The avoiding of large and frequent fluctuations in the water level must be achieved in order to ensure the connection of the water levels among cascades and the sufficient water depth on sill. The navigation channel under the Honghua and Datengxia junctions requires a certain base flow to maintain the water depth

of the channel. The section under the Changzhou junction in Wuzhou is a natural channel and the water discharge is the decisive factor in the water depth of the channel.

In recent years, by carrying out research on the key technology of the joint management of reservoirs in the basin based on multiple dimensions such as flood control, power generation, shipping, ecology and water transfer, the joint management regulations of inland river reservoirs were compiled and implemented by Guangxi Power Dispatch Control Center. The regulations aim to strengthen the function of inland river shipping, ensure the shipping water level and downstream shipping base flow, as well as enhance the guarantee rate of navigation stage of locks and waterways.

3.2 Use of advanced technology to enhance safety monitoring of hydraulic structures

In order to improve the safety management of locks and other hydraulic structures and avoid major accidents, the safety monitoring center of locks and other hydraulic structures is built to integrate sensor signals and safety monitoring information and realize real-time and online monitoring; at the same time, the online monitoring system of hydraulic structures deformation based on high-precision Beidou positioning technology is established. With the monitoring signals being transmitted to the monitoring center in real time, the automatic and intelligent safety diagnosis and early warning could be achieved.

3.3 A forecast system for complex river sections was established and the navigation of ships was accurately scheduled.

The section below the Changzhou junction is a natural waterway, whose water condition is complex due to the discharge of the junction, the Guijiang River and Hejiang River tributaries and the ocean tide. By developing a system for measuring and forecasting the water level below the junction, it provides a reliable basis for the reasonable allocation of vessel loads, for the accurate management of vessels passing the lock, and for navigation.

3.4 The shipping information services were vigorously enhanced.

By building the shipping and logistics information platform of the Xijiang River, it provides real-time information on water conditions, lock operations, ship waiting for passing locks, cargo types, current direction, terminal operations, cargo sources, etc. for ship owners, shipping companies and the department of port and navigation management, facilitating reasonable ship allocation and navigation planning, impro-

ving the service and supervision of shipping management department, as well as contributing to the improvement of the overall operational efficiency of inland water transportation and the full play of shipping.

3.5 Joint operation and centralized control of inland river locks

At present, the cascade locks in the Xijiang River basin have been completed and put into operation, and the freight throughput of locks has increased rapidly. Through the empowerment of Beidou positioning technology, cloud technology, big data, advanced perception and other information technologies, the platform for joint operation and intelligent control of ship locks in the Xijiang River Basin had been developed and was applied in 12 cascade junctions and 17 ship locks belonging to different management units. Among them, 8 ship locks have been operated remotely with no one being on duty at the site. The ships passing the lock could report and pay fees without stopping nor their staff leaving the ship and "only one report is needed for the whole voyage", which significantly improves the efficiency and service.

4 Conclusion

During the "14th Five-Year Plan" period, Guangxi inland water transportation will carry out a series of engineering constructions to develop the cause of inland water transportation in the new era, focusing on the Pinglu Canal, the expansion of ship locks, the upgrading and extension of waterways, and the green and intelligent water transportation. It is hoped that this paper will provide inspiration and help to the planning, design, construction and operation management of inland waterway cascade development and locks projects in the Xijiang River basin of Guangxi and even in the entire country.

Experimental study on discharge capacity optimizing for navigation junction on narrow river channel

Xingwei Zheng[1], Yu Wang[2], Jianguo Ye[3], Honghao Fan[4], Jianjun Zhao[5], Jintao Fang[6]

[1,4] Quzhou Jujiang River Shipping Construction and Development Co., Ltd., Quzhou, China. e-mail: 49314063@qq.com

[2,5,6] State Key Laboratory of Hydrology-Water Resources and Hydraulic Engineering, Nanjing Hydraulic Research Institute, Nanjing, China. e-mail: wangy@nhri.cn

[3] Quzhou Communications Investment Group, Quzhou, China

Abstract: Discharge capacity was the primary indicator for evaluating the layout of the shipping hub. The large width of ship lock approach channel would narrow the river bed and influence the discharge capacity of sluice, especially the multi-line ship locks approach channel. Narrow river channels, unlike wide and shallow channels, need to be further explored in the optimization measures of flow capacity due to their characteristics and layout difficulty with large discharge. Based on Huangtangqiao Project, a hydraulic model with 1/80 scale is employed to investigate the effect of optimized measures on discharge capacity, including moving the sluice to the right, increasing the width of sluice pore and dredging the downstream channel. Optimizations could meet the discharge capacity requirements, and the research results could be used as reference for related projects.

Keywords: Discharge capacity; Navigation junction; Entrance area; Model test

1 Introduction

The issues of discharge capacity play a vital role on water conservancy project construction. Discharging enough flood under flood conditions is an important indicator for evaluating the construction of navigation junction (Davis, 1989). The widely constructed low-head navigation junctions perform small water level difference between upstream and downstream during flood season, especially for narrow river channels in mountainous areas where the terrain difference between upstream and downstream is large. The river channel occupancy of the navigation structures aggravates the difficulty of sluice layout, and discharge capacity is even more difficult to

meet the design requirements (Huang, 1996).

So far, the research on the discharge capacity of navigation junction mostly adopted physical model test, by which the optimization of discharge capacity was carried out (Yu et al., 2014). Based on Dadingzishan Junction located on Songhua River, Li et al. (2006) proposed the plan layout to meet the discharge capacity by various effective improvement measures such as the change of sluice gate numbers, weir type and the elevation of the weir top. The inundation degree effect showed that measures such as reducing bed surface elevations between junction upstream and downstream, adjusting the dam axis to be perpendicular to the river trend, and bank-division operation between shipping hub and power station could increase discharge capacity of low-head junction (Zhang et al., 2005).

The discharge capacity tests of Naji Junction in Guangxi stated that the comprehensive flow coefficient, related to the overall junction arrangement and the number of full openings for the sluice holes, increases with the decrease of the sluice holes openings (Li et al., 2002). Wan et al. (2010) considered that the shape of pier head and the guide wall between the sluice gate and power house seriously influence the flow discharge capacity, therefore, the height and length of the guide wall should be minimized and streamlined pier head was designed. In terms of the difference between the discharge capacity results of the overall hydraulic model and the cross-section hydraulic model, some studies have also obtained the effect of roughness on the discharge capacity (Shi et al., 2021).

The previous literatures have a relatively deep understanding of discharge capacity optimization for the wide and shallow channel. Circular arc guide walls could be built on both sides of the discharge structure in order to better connect flow when the total width of the discharge structure is smaller comparing with the river width (Fang et al., 2008). Furthermore, water level difference for wide and shallow channels had a significant impact on discharge capacity (Liu et al., 2003). However, the present research on discharge capacity of navigation junction on narrow river is relatively lacking, particularly under the flood condition with the maximum unit discharge 40 m^3/s, it was inevitable to employ engineering measures to optimize discharge capacity. By carrying out overall hydraulic model test of the Huangtangqiao Junction on the Changshan River, this paper analyzed discharge capacity of narrow rivers in different cases, and proposed optimized engineering measures.

2 Project summary

Huangtangqiao Junction, the sixth cascade project of the Changshan River cas-

cade development in the upper reaches of the Qiantang River, was located in Kecheng District, Quzhou. The engineering layout from left to right was: power station, sluice, and ship lock, as shown in Fig. 1. The approach channels upstream and downstream were arranged in a straight line, and their total length and bottom width were 320.0 m and 60.0 m, respectively. The channel grade was Ⅳ. The sluice was arranged in the upstream section, the gate chamber section and the downstream section along the flow direction. The dredging elevation of upstream of sluice was 58.00 m, and the upstream side of the gate chamber was provided with an 8 m concrete pavement with the elevation of 58.00 m which was the same as the dredging elevation. The sluice baseboard was 58.50 m. The sluice, with a total of 18 holes, was 216 m in width with 12 m net width of a single hole. Energy dissipation with hydraulic jump was adopted, and the gate chamber downstream was connected to stilling basin with 39 m length.

The river width of Huangtangqiao Junction was about 200 m, the characteristics embodied: (1) The power station protruded to the left bank embankment (see the dotted line in Fig. 1), and the total discharge width was relatively narrow, which affected discharge capacity. (2) There were dense houses in vicinity of upstream of sluice, and the engineering layout was difficult. (3) The narrow channel in vicinity of the entrance area of the downstream approach channel restricted discharge capacity. Therefore, it was necessary to further demonstrate and optimize the discharge capacity and propose improvement measures.

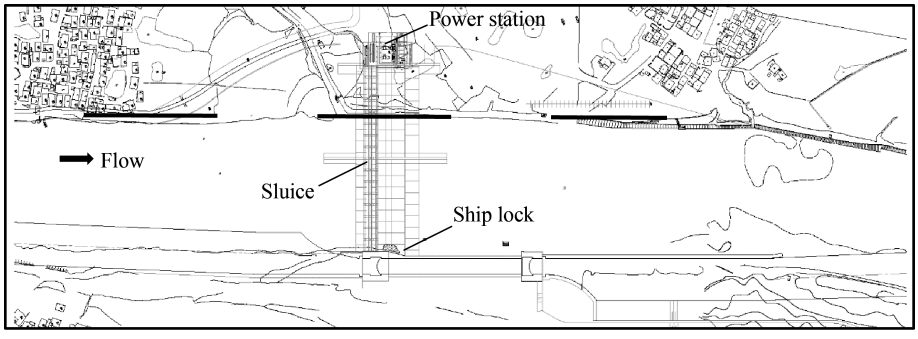

Fig. 1. Layout of Huangtangqiao Junction.

3 Experimental setup and methodology

3.1 Experimental setup

The test model was designed at the geometric scale of 1/80 on basis of Froude

similarity criterion according to the similarity law of model, the terrain conditions of the junction upstream and downstream and the laboratory site. The upstream and downstream river of Huangtangqiao Junction were relatively straight, therefore, the upper boundary of physical model was arranged at 1,020 m upstream of sluice taking into account of the smooth inflow and navigable flow conditions. The presence of bends in the downstream contributed to complex upstream flow conditions, consequently, the lower boundary of physical model should be taken to 2,160 m downstream of sluice considering the length of sufficient flow adjustment.

The section method is used for terrain production, and the triangulation wire system is employed for plane stakeout where the triangle closure error hardly exceeded $\pm 1'$. The model elevation was measured by a level and checked during the production process, and the installation elevation error of the section was controlled within ± 1 mm. For complex terrain, the intensive section was added and processed separately in order to improve the production accuracy. The junction, including sluice, ship lock and power station, was made of PMMA. The surface of the river was made of cement mortar. The overall model was photographed in Fig. 2.

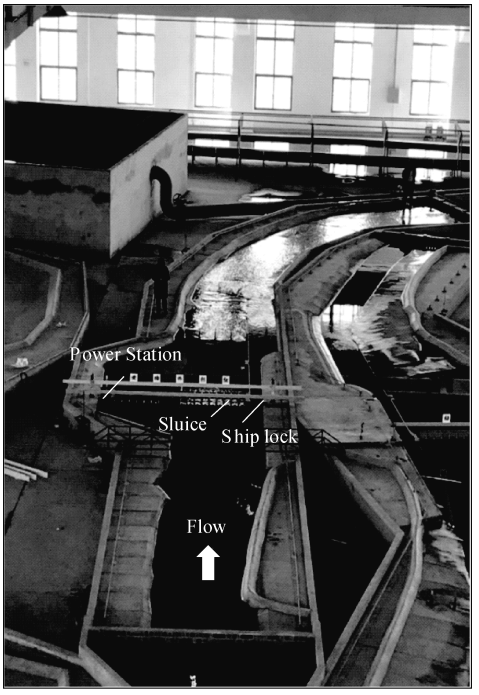

Fig. 2. Model photo of Huangtangqiao Junction

A total of six measuring points were arranged along flow direction, and the sluice axis was set as 0 m. Therefore, the sites of six measuring points were −555.20 m(#1), −319.20 m(#2), −112.00 m(#3),218.40 m(#4),940.60 m(#5), and 1526.30 m(#6) respectively (the negative sign represents the upstream of sluice axis). The water levels of the upstream and downstream of sluice were controlled by #2 and #3 measuring point respectively. It should be noted that, in order to further clarify water level evolution of sluice downstream, some cases carried out the encrypted measurement for water level evolution of sluice downstream. The flow discharge was measured by a standard rectangular thin-walled weir with an error of less than 1%; the water level was measured by a water level stylus with an accuracy of 0.02 mm.

3.2 Experimental cases

Table 1 lists the experimental cases for the flood conditions of the Huangtangqiao Junction. During the test, the power station was shut down, the ship lock was not in operation, and the sluice gate was fully opened for flood discharge. Additionally, the water level of downstream of sluice was controlled based on the designed value of the flood regulation results, and the designed data were shown in Table 2.

Table 1 Experimental cases of Huangtangqiao Junction.

Cases No.	Flow discharge (m^3/s)	Water level (m)	Note
1	8,050	69.62	$P=1\%$
2	7,380	69.11	$P=2\%$
3	6,470	68.41	$P=5\%$
4	5,900	67.77	$P=10\%$
5	5,090	66.92	$P=20\%$

Table 2 Discharge capacity of initial layout.

Flood frequency	Discharge (m^3/s)	Downstream water level (m)	Upstream water level (m)		Heading up value (m)	
			Designed value	Experimental value	Designed value	Experimental value
1%	8,050	69.62	69.80	69.90	0.18	0.28
2%	7,380	69.11	69.26	69.42	0.15	0.31
5%	6,470	68.41	68.57	68.83	0.16	0.36
10%	5,900	67.77	67.89	68.10	0.12	0.33
20%	5,090	66.92	67.07	67.08	0.15	0.16

4 Results and discussions

4.1 Discharge capacity of initial layout

The experimental observation noted that the regime gradient of the upstream of sluice was relatively small, and there was no obvious overfall or local stagnation. Thanks to the local topography in sluice downstream, obvious overfall occurred in the range of 0 – 330 m of the sluice axis downstream, and flow surface line was slowly lowered in the range of 330 – 700 m of the sluice axis downstream. Table 2 listed the discharge capacity data of the initial layout, which showed that the experimental value was significantly greater than the designed value for heading up of water level of upstream of sluice under each discharge. For comparison of discharge capacity be-

tween the experimental value and the designed value, see Fig. 3. Flow discharge was calculated by Eq. (1) and Eq. (2). It could be seen that discharge capacity of the initial layout was obviously insufficient, which is about 10% less than the designed value.

$$Q = \mu_0 h_s B_0 \sqrt{2g(H_0 - h_s)} \tag{1}$$

$$\mu_0 = 0.877 + \left(\frac{h_s}{H_0} - 0.65\right)^2 \tag{2}$$

Here, Q: flow discharge (m^3/s); B_0: the width of sluice hole(m); H_0: weir head including approach velocity(m); h_s: flow depth calculated from weir crest(m); μ_0: comprehensive discharge coefficient of submerged weir flow.

The reason for the insufficient discharge capacity lied in the obviously less discharge of the sluice hole #1-#3 in the left area, and the river mainstream was more concentrated in the right area of sluice, as shown in Fig. 4. Firstly, the left area of the Huangtangqiao Junction extends into the bank embankment, and the bank influence inclined to form a backflow area in front of the left area of sluice, which may contribute to less discharge capacity comparing with the designed value. Secondly, the narrow channel of downstream of sluice may also be an important reason for less discharge capacity. Narrow channel, owing to the downstream separation levee of ship lock, decreased the cross-sectional area of sluice downstream, increased the local resistance and reduced discharge capacity, which headed up both upstream and downstream water levels. Thirdly, narrow channel in the entrance area of the downstream of sluice increased flow velocity and precipitated local overfall, resulting in a decrease of the discharge capacity.

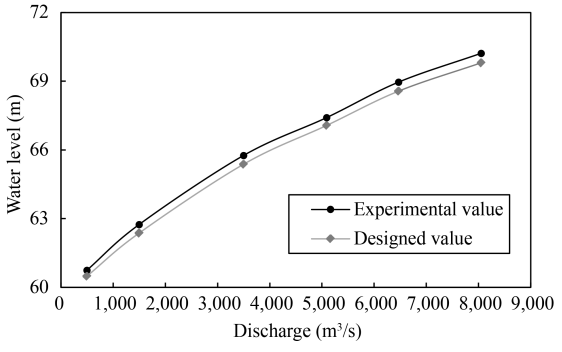

Fig. 3. Comparison of discharge capacity between the experimental value and the designed value.

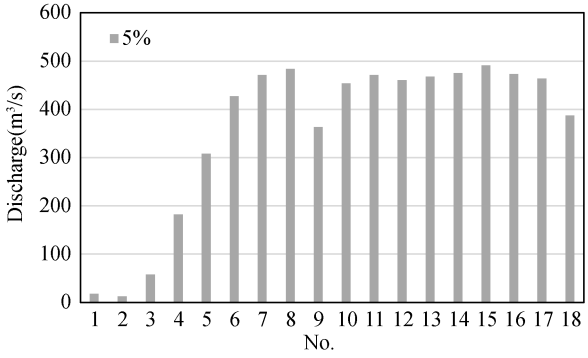

Fig. 4. Discharge distribution of sluice holes for initial layout (P=5%).

4.2 Discharge capacity after sluice moving and downstream dredging

Considering the insufficient discharge capacity in the left area due to sluice protruding into the left bank embankment for initial layout, the sluice was moved to the right by 50 m. In addition, local dredging was carried out in order to increase the discharge capacity due to the narrow channel of downstream entrance area of ship lock, the dredging scope was 420 – 860 m downstream of sluice, and the dredging elevation of the river channel was 56 m.

Fig. 5 plotted variations of water level along flow direction under various working conditions after sluice moving to the right and dredging. It could be seen that there was no obvious water level stagnation and overfall for the upstream and downstream of sluice, and upstream and downstream flow regime was smooth. Table 3 gave the water level difference between the upstream and downstream of sluice after sluice moving to the right by 50 m and dredging. The data showed that water level difference between the upstream and downstream of sluice is significantly reduced comparing with initial layout, which might be attributed to the dredging measures of downstream river channels. Additionally, the discharge suppression of sluice hole #1 – #3 by the left bank slope was significantly weakened after sluice moving, as shown in Fig. 6. Fig. 6 showed that the discharge of sluice hole #1 – #3 increased significantly comparing with the initial layout, and the increasing range is about 2 – 3 times. However, the discharge of #1 – #3 is still small comparing with other sluice holes, therefore, the optimization of sluice structure could be further considered.

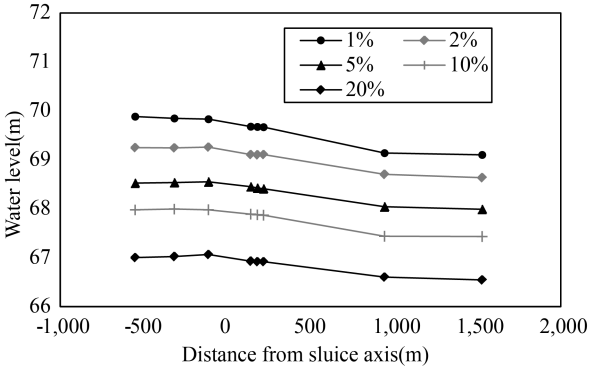

Fig. 5. Water level along flow direction.

Table 3 Water level difference between upstream and downstream after sluice moving and dredging(m).

Water level difference	P=1%	P=2%	P=5%	P=10%	P=20%
Designed	0.18	0.15	0.16	0.12	0.15
Initial layout	0.28	0.31	0.36	0.33	0.16
Sluice moving and dredging	0.19	0.15	0.16	0.13	0.13

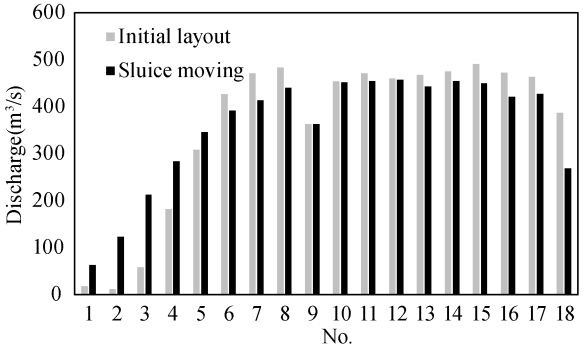

Fig. 6. Discharge distribution of sluice holes after sluice moving (P=5%).

4.3 Discharge capacity after increasing the width of sluice pore

In order to further increase the discharge capacity, sluice hole was widened and the initial layout of 12 m×18 holes was optimized to 14 m×16 holes. That was to say, the net width of a single hole was increased, and the net width of the flood discharge was increased from 216 m to 224 m. The downstream dredging measures (dredging 56 m elevation of the river channel for 420 – 860 m downstream of the sluice axis) were still reserved.

Table 4 listed water level difference between the upstream and downstream of sluice after the sluice holes were widened to 14 m. It could be seen that the widened

sluice holes played a positive effect on increasing the discharge capacity. The water level difference of experimental value was less than the designed value, and the discharge capacity met the requirements. Fig. 7 plotted flow distribution of each gate hole after the sluice holes were widened. In Fig. 7, the discharge capacity of the #1 hole was still smaller than other holes, but it reached 200 m^3/s, which could meet the requirements. Discharge capacity with sluice holes widened exceeds about 2% comparing with the designed value.

Table 4 Water level difference with sluice holes widened.

Water level difference	$P=1\%$	$P=2\%$	$P=5\%$	$P=10\%$	$P=20\%$
Designed value	0.18	0.15	0.16	0.12	0.15
Holes widened to 14 m	0.15	0.13	0.12	0.12	0.10

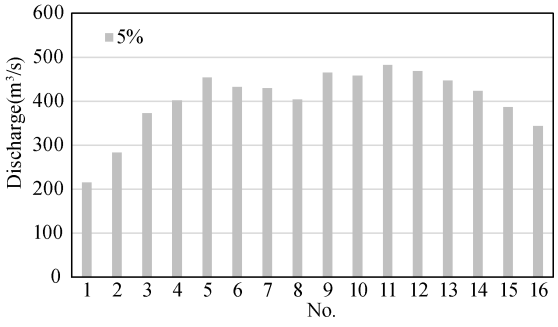

Fig. 7. Discharge distribution with sluice holes widened ($P=5\%$).

5 Conclusions

(1) The river width of the Huangtangqiao Junction was about 200 m. The maximum unit discharge was 40 m^3/s, and the left area of sluice stretched into the embankment. Moreover, the river channel in vicinity of downstream entrance area was narrower, which contributed to the severe conditions for meeting the flow capacity.

(2) The flow capacity significantly increased by engineering measures such as moving sluice to the right, dredging the narrow downstream area, and widening the sluice holes. The experimental results showed that discharge capacity of the initial layout is far from the design value due to less discharge for the left three holes. Discharge capacity exceeded the design value by about 2% by effective measures.

(3) For narrow river channels, reasonable downstream dredging combined with sluice holes optimization could be used as an important measure to optimize the flow capacity of narrow river channels due to small amount of engineering and easy construction. This paper could provide reference for similar design and research.

Acknowledgements

This research has been financially supported by the National Natural Science Foundation of China (Grant No. 52009083) and the Natural Science Foundation of Jiangsu Province (Grant No. BK20200159).

References

Davis, J.P., 1989. Hydraulic design of navigation locks. Vicksburg: Army Engineer Waterways Experiment Station Vicksburg MS Hydraulics Lab.

Fang, X.D., Diao, M.J., Li, B.H., et al., 2008. Hydraulic model test of junction engineering for wide river. Sichuan Water Power, 27 (1): 60-63. (in Chinese)

Huang, G.Q., 1996. Research on the design of energy dissipation for spillway of low head project with large flow. Pearl River, 17 (5): 23-27. (in Chinese)

Li, J.H., Cao Y.F., Zhou, H.X., 2002. Test on discharging capacity and downstream scour of Naji Hydro-junction. Journal of Waterway and Harbour, 27 (3): 170-174. (in Chinese)

Li, J.H., Du, Z.K., Zhang, R.H., 2006. Test on discharge capacity of Dadingzishan Hydro-junction of Songhuajiang River. Journal of Waterway and Harbour, 27 (3): 170-174. (in Chinese)

Liu, S.J., Xu, W.L., Wang, W., et al., 2003. The influence of water level differences on discharge of water-release structures of wide-shallow reservoir. Journal of Sichuan University (Engineering Science Edition), 35 (3): 18-20. (in Chinese)

Shi, D.B., Li, N., Jiao, T.L., 2021. Model test study on the discharge capacity of sluice gates in Nianpanshan Water Conservancy Project. Hydropower and New Energy, 35 (2): 15-16. (in Chinese)

Wan, X.M., Zhan, Q.W., Zhang, J.H., 2010. Study on the discharge capacity and energy dissipation of Xiajiang Hydro-junction. Jiangxi Hydraulic Science & Technology, 36 (4): 259-261. (in Chinese)

Yu, Z.G., Han, C.H., Peng, C.B., et al., 2014. Overview of bent waterway navigation hub layout research. Pearl River, 35 (6): 102-105. (in Chinese)

Zhang, X.J., Fan, W.P., Zhang, H.Q., 2005. Discharge capacity of low sluice. Journal of Hydraulic Engineering, 36 (10): 1246-1251. (in Chinese)

Research on problems and countermeasures of high-quality development in main ports of the Yangtze River

Jinpeng Lyu[1], Jinxiang Cheng [2], Zhaoxing Han [3], Yujian Gao [4]

[1,4] Zhonglugang Engineering Consultants, Beijing, China

[1,2,3,4] Transport Planning and Research Institute of Ministry of Transport, Beijing, China

[1,2,3,4] Transport Planning and Research Institute, Ministry of Transport, Laboratory of Transport Pollution Control and Monitoring Technology, Beijing, China

Abstract: The Yangtze River waterway is the "Golden Waterway" that traverses the eastern, central and western regions of China. It is the main framework of the comprehensive transportation system of the Yangtze River Economic Belt. After years of construction and development, the Yangtze River Golden Waterway has played an important role in the overall pattern of regional development. However, it still falls short of the requirements for developing the Yangtze River Economic Belt and building traffic transportation capacity of China in the new era. On the one hand, insufficient guarantee of land and sea resources has a greater impact on the normal development of ports and even the exertion of comparative advantages of water transportation. On the other hand, the inland river collecting and distributing capacity needs to be further improved, and the inland river distributing channels suitable for container development have not been effectively opened in the Yangshan Port Area of Shanghai Port and the Tongzhou Bay Port Area of Nantong Port. Considering these problems, we first recommend supporting dredging of waterway and land-reclamation ports that were clearly planned. Port and waterway projects in line with the national strategy and plan will be regarded as major projects and normally accepted for reclamation. Furthermore, it is essential to improve the operation efficiency of multimodal transport equipment, promote the research, development and application of standardized pallets, rapidly transfer equipment and new loading and unloading machinery for multimodal transport, and speed up the efficiency of transshipment and reloading of container goods.

Keywords: Yangtze River waterway; Golden Waterway; Port; Land-reclamation; Multimodal transport

1 Introduction

The Yangtze River waterway is the "Golden Waterway" that traverses the east-

ern, central and western regions of China. It is the main waterway of economic development along the Yangtze River and the main framework of the comprehensive transportation system of the Yangtze River Economic Belt. It has a very important strategic position in the overall pattern of regional development. After years of construction and development, the Yangtze River Golden Waterway has played an important role in improving the comprehensive transportation system, promoting regional ecological and green development, and promoting the implementation of national strategies, but it still falls short of the requirements for developing the Yangtze River Economic Belt and building a transportation power in the new era.

1.1 Raise the scale level in ports

The Yangtze River has formed a port development pattern with clear levels and reasonable distribution, and a specialized transportation system with containers, ores, coal, liquid chemicals and other key cargo categories (Song et al., 2020; Zhang et al., 2018). A number of large-scale and intensive port areas such as Nanjing Longtan, Wuhan Yangluo, and Chongqing Guoyuan have become important regional comprehensive transportation hubs. At the end of 2020, there were 5,249 productive terminal berths in ports along the Yangtze River, with a comprehensive cargo throughput capacity of 2.78 billion tons, including 31.53 million TEU containers, with a throughput of 3.3 billion tons and approximately 35 million TEU containers.

1.2 Improve the utilization efficiency of resources in port shoreline

Port shoreline resource is an important support for the implementation of the national strategy of the Yangtze River Economic Belt, the sustainable economic and social development, the optimal allocation of land and space resources, and the construction of ports (Wang, 2021; Cheng et al., 2020; Shu, 2020). Since 2016, a series of documents have been issued to clarify the general thinking and measures of "controlling the total amount, adjusting the stock, optimizing the increase, and improving the efficiency" of port shoreline resources along the Yangtze River. Special rectification of illegal docks on the main and tributaries of the Yangtze River has been carried out, and the upgrading of old docks and the integration of resources have been accelerated (Jiang et al., 2017). At present, the planned port coastline of the Yangtze River is 770 kilometers, a decrease of 706 kilometers compared with 2015. The unit freight coastline throughput of the Yangtze River reached 9.16 million tons/km, which is about three times that of 2010.

1.3 Increase railway-water combined transportation

Multimodal transport is an important carrier for the construction of a modern

comprehensive transportation system, and an important support for a new development pattern in which services support the domestic cycle as the main body, and the domestic and international dual cycles promote each other (Almotairi et al., 2009; Sun et al., 2017). In recent years, 14 port-railway-water combined transport projects on the Yangtze River have been fully launched. After the completion of the project, the main ports on the Yangtze River will achieve full coverage of railway access to ports. From January to October 2021, the combined transport volume of railway and water in inland ports along the Yangtze River completed 185,700 TEU, a year-on-year increase of 43.68%.

The ports along the Yangtze River have made great efforts to prevent and control pollution (Chen et al., 2020). Through the one-year special rectification of prominent pollution problems caused by ships and ports in the Yangtze River Economic Belt, the 11 provinces and province-level cities in the Yangtze River Economic Belt have basically achieved full coverage of newly built pollutant receiving facilities from fixed and mobile ships, and they are continuously promoting effective connection with urban public transport and disposal facilities. 13 water-washing stations on the Yangtze River included in the layout plan have been completed and put into operation (Wang et al., 2021). From 2016 to 2018, the central government provided 295 million yuan of financial support for 139 coastal power projects in the Yangtze River Economic Belt. It has issued and promoted the implementation of the Plan for Electricity Distribution at Ports of Hong Kong, and promoted the upgrading of shore power facilities at specialized berths. By the end of September 2021, more than 6,200 shore power berths have been built in the Yangtze River Economic Belt, and ships calling at ports have used shore power for about 310,000 times and 3.1 million hours, an increase of about 12 percent over the same period in 2020.

2 Main problems and causes

2.1 Guarantee of land and sea resources in port planning and construction

The problem of land and sea area seriously restricted the construction of waterways and ports (Rosoff et al., 2007). Water transportation projects are not included in the "Notice on the Pre-examination of Land Use for Major Construction Projects of Occupying Permanent Basic Farmland" of Ministry of Natural Resources of the People's Republic of China, and land use cannot accept pre-examination. The approval of sea reclamation construction project was almost completely stopped when the policy was implemented (Wang et al., 2014), and it was also extended to the port

planning where no additional sea use was allowed. The dredging of waterways and land reclamation are basically stagnated, and it is very difficult to select and delineate areas for dredging and reclamation (Costa et al., 2010). Insufficient guarantee of land and sea resources has a greater impact on the normal development of ports and even the exertion of comparative advantages of water transportation.

2.2 Improvement in collecting and dispatching system of port

The connection of multimodal transportation facilities and equipment is not smooth (Fang et al., 2020). The 35-ton railway open-top container is about 10 cm wider than the international standard container for water transportation, and it cannot be unloaded into the compartment grille during shipment. Dangerous goods are defined differently in different standards. Some ordinary waterway container goods are classified as dangerous goods by railway transportation. It is necessary to further strengthen the connection and implement inventory management. The operating rules of departments are very different. The transportation of sulfur and other goods allowed on the water is not allowed by the railway department because they are defined as dangerous goods. Inadequate opening of railway information, high cost and poor timeliness for enterprises to obtain information, affect the efficiency of railway-water combined transportation operations. The inland river collecting and distributing capacity needs to be further improved, and the inland river distributing channels suitable for container development have not been effectively opened in the Yangshan Port Area of Shanghai Port and the Tongzhou Bay Port Area of Nantong Port.

2.3 Construction level of green ports

Some urban sewage pipe networks in some areas are not effectively connected with ports and need to be transferred and disposed by tank trucks. The use of joint supervision and service information system of ship pollutants in transport and disposal links needs to be further improved (Xiong et al., 2015). The liquefied natural gas (LNG) price fluctuates greatly, the periodic supply guarantee is insufficient, and the LNG powered ship cost is high, so the enthusiasm of the ship owners to apply LNG is not high. The cost of upgrading the power receiving facilities of ships is high, and the use of shore power is charged high in some areas, which lead to the lack of willingness of ships to use shore power voluntarily (Vaishnav et al., 2016).

3 Countermeasures

3.1 Further improve the collecting and dispatching system of port

The green, low-carbon and high-quality development of the shipping industry is very important to help achieve the national goal of "carbon peak and carbon neutrality", and is related to national resource security, energy security and economic security (Prokopenko et al., 2018; Wu et al., 2022). Port and waterway projects in line with the national strategy and plan will be regarded as major projects and normally accepted for reclamation (Van Ham et al., 2001).

Further improve the operation efficiency of intermodal transport equipment, promote the research, development and application of standardized pallets (Horn et al., 2005). Rapidly transfer equipment and new loading and unloading machinery for intermodal transport, and speed up the efficiency of transshipment and reloading of container goods (Steenken et al., 2004). Focus on the convergence of railway and water transportation rules, and speed up the establishment of rule coordination and mutual recognition mechanisms that are suitable for the integrated operation of multimodal transport, encourage railway department to open up information on freight train plans and actual departure and arrival stations, open data interfaces, and realize real-time information interconnection and timely information push with enterprises (Huang et al., 2020). In accordance with the "14th Five-Year Development Plan for Water Transportation" of the Ministry of Transport of the People's Republic of China, guide and support local governments to promote the construction of inland river collecting and distributing channel projects such as the renovation project of the east extension of Dalu waterway of Shanghai Port and the inland river collecting and distributing channel project of Nantong Port.

3.2 Continue to promote the construction of green ports

Continue to promote the implementation of a long-term mechanism for preventing and controlling pollution from ships and ports along the Yangtze River Economic Belt (Sun, 2021), strengthen dispatching and supervision, promote in-depth implementation of the ship-to-shore exchange and joint inspection system for pollutants from ships, and effectively link port reception facilities with urban public transit and treatment facilities (Giuliano et al., 2008). Actively support the development of clean energy vessels. Study and formulate financial support policies for the application of new energy and clean energy in the construction of new LNG-powered ships and

LNG filling stations, and improve policies for ensuring the supply of LNG and stabilizing gas prices in the waterway industry. These need make it normal for ships to use shore power when they call at ports, and accelerate coordinated upgrading of power facilities between ships and ports (Kanellos et al., 2017). Optimize and enhance shore power service level, strengthen ship-shore information sharing, promote port enterprises, shore power supply enterprises and waterway transport operators to strengthen communication and cooperation, and promote the linkage of ship-shore power.

Acknowledgements

We appreciate the cooperation and efforts of all authors in producing the proceedings. This will be a great conference following the tradition of our sponsoring organizations.

References

Almotairi, B., Lumsden, K., 2009. Port logistics platform integration in supply chain management. International Journal of Shipping and Transport Logistics, 1 (2): 194-210.

Chen, T., Wang, Y., Gardner, C., et al., 2020. Threats and protection policies of the aquatic biodiversity in the Yangtze River. Journal for Nature Conservation (58): 125931.

Cheng, C., Yang, F., 2020. Strategies for Jiangsu in the coordinated and balanced development along Yangtze River Economic Belt.// Toward a coordinated and balanced development. Springer, Singapore: 77-92.

Costa, C. B., Ribeiro, S. P., Castro, P. T. A., 2010. Ants as bioindicators of natural succession in savanna and riparian vegetation impacted by dredging in the Jequitinhonha river basin, Brazil. Restoration Ecology, 18(S1): 148-157.

Fang, X., Ji, Z., Chen, Z., et al., 2020. Synergy degree evaluation of container multimodal transport system. Sustainability, 12(4): 1487.

Giuliano, G., Hayden, S.,Dell'aquila, P., et al., 2008. Evaluation of the terminal gate appointment system at the Los Angeles/Long Beach ports. METRANS Project, 4-6.

Horn, B. E., Nemoto, T., 2005. Intermodal logistics policies in the EU, the U. S. and Japan. Transport Policy Studies' Review, 7(4): 2-14.

Huang, Q., Yin, W., An, J., et al., 2020. A China railway express-based model

for designing a cross-border logistics information cloud platform scheme. Applied Sciences, 10(12): 4110.

Jiang, L., Tao, T., Zhang, C., et al., 2017. Summary of the port shoreline resource evaluation based on triangular fuzzy analytic hierarchy process. Polish Maritime Research,24(S3): 16-22.

Kanellos, F. D., Anvari-Moghaddam, A., Guerrero, J. M., 2017. A cost-effective and emission-aware power management system for ships with integrated full electric propulsion. Electric Power Systems Research (150): 63-75.

Prokopenko, O., Omelyanenko, V., Klisinski, J., 2018. Innovation policy development conceptual framework for national resource security providing. Journal of Environmental Management and Tourism, 9(5): 1099-1107.

Rosoff, H., Von Winterfeldt, D., 2007. A risk and economic analysis of dirty bomb attacks on the ports of Los Angeles and Long Beach. Risk Analysis: An International Journal, 27(3): 533-546.

Shu, X., 2020. An empirical analysis for the promoting effect of marine economy on sustainable development of inland economy. Journal of Coastal Research, 110(SI): 287-290.

Song, Y., Liu, H., 2020. Internet development, economic level, and port total factor productivity: an empirical study of Yangtze River ports. International Journal of Logistics Research and Applications, 23(4): 375-389.

Steenken, D., Voß, S., Stahlbock, R., 2004. Container terminal operation and operations research—a classification and literature review. OR Spectrum, 26(1): 3-49.

Sun, L., 2021. Coordinated development of ecological environment in Yangtze River Economic Belt.// Development of the Yangtze River Economic Belt in China. Springer, Singapore:107-146.

Sun, X., Zhang, Y., Wandelt, S., 2017. Air transport versus high-speed rail: an overview and research agenda. Journal of Advanced Transportation (3): 1-18.

Vaishnav, P., Fischbeck, P. S., Morgan, M. G., et al., 2016. Shore power for vessels calling at U.S. ports: benefits and costs. Environmental Science & Technology, 50(3): 1102-1110.

Van Ham, H., Koppenjan, J., 2001. Building public-private partnerships: assessing and managing risks in port development. Public Management Review, 3(4): 593-616.

Wang, W., Liu, H., Li, Y., et al., 2014. Development and management of land reclamation in China. Ocean & Coastal Management (102): 415-425.

Wang, X., 2021. Coordinated development of ports in the Yangtze River Economic

Belt.// Development of the Yangtze River Economic Belt in China. Springer, Singapore: 183-210.

Wang, Z.T., Duan, P.X., Akamatsu, T., et al., 2021. Riverside underwater noise pollution threaten porpoises and fish along the middle and lower reaches of the Yangtze River, China. Ecotoxicology and Environmental Safety (226): 112860.

Wu, X., Tian, Z., Guo, J., 2022. A review of the theoretical research and practical progress of carbon neutrality. Sustainable Operations and Computers (3): 54-66.

Xiong, S., Long, H., Tang, G., et al., 2015. The management in response to marine oil spill from ships in China: a systematic review. Marine Pollution Bulletin, 96(1-2): 7-17.

Zhang, M., Xiao, H., Sun, D., et al., 2018. Spatial differences in and influences upon the sustainable development level of the Yangtze River Delta urban agglomeration in China. Sustainability, 10(2): 411.

Study on navigable flow conditions and optimization measures in the confluence area of large-angle main stream and tributary

Wei Wang[1], Senhao Mao[2], Zhongshan Tong[3]

[1] Nanjing Hydraulic Research Institute, Nanjing, China. e-mail: suiningwangwei@163.com
[2] Nanjing Hydraulic Research Institute, Nanjing, China. e-mail: 913833325@qq.com
[3] Nanjing Hydraulic Research Institute, Nanjing, China. e-mail: 776051686@163.com

Abstract: The flow pattern of high-drop, steep-slope, large-angle mainstream and tributary confluence zone is complex, and it is easy to produce transverse flow, threatening navigation safety, which is an urgent technical problem in the current navigation field. In this paper, the normal physical model with a geometric scale of 1∶50 is established based on the Shutou River drop project in the Yangtze-Huaihe River Diversion Project. The model is designed by gravity similarity criterion, and the navigation flow conditions in the intersection area of the large angle mainstream and tributary are studied. The flow velocity conditions in the intersection area under different optimization schemes are analyzed. It is pointed out that the topography of the outlet of the Shutou River drop has the characteristics of short export diffusion section, concentrated mainstream and higher transverse flow velocity in the intersection area than the navigation requirements. The results show that the symmetric diffusion in the outlet section of drop water and the multi-stage diversion measures with two-stage diffluent piers in the transition section can significantly improve the flow velocity distribution in the confluence zone, reduce the lateral flow velocity in the confluence zone. When the minimum control water level of the channel encounters flood once in five years, the transverse velocity is not greater than 0.15 m/s (navigable water edge, vertical channel center line). The flow velocity index meets the navigation requirements to ensure the normal passage of ships and the safety of engineering operation. This achievement enriches the technology of multi-level diversion measures, which has the important theory value to promote the application of multi-level diversion measures into the actual project.

Keywords: Physical model; Confluence zone; Multi-level diversion measures; Transverse velocity

1 Introduction

The Yangtze-Huaihe River Diversion Project consists of three sections: the Yangtze River-Chaohu Lake Diversion Project, the Yangtze-Huaihe River Diversion

Project and the North Water Diversion Project. The total length of the water conveyance line is 1,048.68 km main stream. After the excavation of the river channel, the existing water system is interrupted, and it is necessary to build a new drop at the confluence of the main stream and the tributaries of the river, so that the existing water system can smoothly flow into the water conveyance channel without affecting navigation. The drop and the main stream form the characteristics of high drop difference, steep slope, intersection angle of large-angle main stream and tributaries, and complex flow pattern in multi-stage drop.

The water conveyance channel and waterway of the Yangtze-Huaihe River communication section are the navigation channels, and the navigation standard is level Ⅱ. According to the review opinions of water conservancy and shipping, the control conditions of the lateral flow velocity at the intersection of the Yangtze-Huaihe River Diversion Project are as follows: the minimum control water level of the waterway meets the flood once in five years, and the transverse velocity is not more than 0.15 m/s (the edge line of the navigation water area, perpendicular to the center line of the waterway). The navigation standard is much higher than the 0.3 m/s transverse velocity requirement required by the specification. Taylor (1944) found that the inflow angle had certain influence on the transverse velocity in the confluence zone; Li (2012) found that when inflow angle and the confluence ratio increased, the flow separation phenomenon in the downstream of the confluence area would be enhanced, and the backflow area was easy to form. Weber et al. (2001) studied the effect of confluence ratio on 90-degree inflow. Liu et al. (2009) found that when the confluence angle of tributaries was 90°, the confluence ratio increased, and the degree of tributaries supporting the main stream increased. The downstream flow in the confluence zone would form obvious high and low velocity zones. At present, a large number of studies have been carried out on the navigable flow conditions in the confluence zone of main and tributaries in China and abroad. However, this project is the first case of study on the navigable flow conditions in the confluence zone of main stream and tributaries with large angle, small confluence ratio of main and tributaries and strict navigation standards.

2 Project profile

A rolling dam with a weir height of 1.2 m is set up in the upper reaches of the Shutou River. The elevation of the dam top is 11.40 m, and the drop from the dam top to the water conveyance channel is 9.6 m. The water level drop is 7.72 m, 3.63 m and 2.51 m under 10-year energy dissipation condition, 20-year energy dissipation

condition, and flat flow energy dissipation condition respectively, and the drop is large. It is necessary to set a drop or steep slope to make the incoming water safely flow into the downstream water conveyance channel and adopt a multi-stage drop pattern to realize the drop.

The multi-stage drop scheme adopts three-stage drop. The net width of the rolling dam is 13.0 m, which is determined by the energy dissipation need of water drop and arranged at the head of water drop. The roller dam is connected with three stages of drop, and the drop difference of each stage is equal, which is 3.2 m. The floor elevation of the last stage of drop stilling basin is 1.80 m, and the total drop difference is 9.6 m. From the upstream to the downstream, the lengths of all levels of drop are 19.0 m 20.0 m and 19.0 m respectively. A continuous stilling basin is set at the end of the first and second levels of drop, and the heights are 1.8 m and 1.9 m respectively.

3 Experimental design

The Shutou River drop project is located in the Pai River, using a three-level waterfall structure, and the discharge flow enters the main stream at 90°. The overall layout of the water drop project is shown in Fig.1.

The overall model of the confluence zone adopts the normal model with a geometric scale of 1∶50 and is designed according to the gravity similarity criterion. In order to fully reflect the flow pattern of the project section, the upstream boundary of the model is arranged at 150 m before the intake of the drop project, and the total length of the downstream simulation channel is 1,000 m. The upstream section of the intersection center line of the drop and the river channel is 400 m, and the downstream section is 600 m. A total of 21 flow velocity observation sections are arranged in the model, 4－8 flow velocity measuring points are arranged in each section, and the distance between measuring points is 20 m (prototype distance).

The river channel topography is made by section method according to the measured data of the project, plastered by cement mortar, and the drainage buildings are made by organic glass. The flow is measured and controlled by standard rectangular weir and ultrasonic flowmeter, and the error range is ≤1%; the velocity of river section is measured by three-dimensional ADV. The water depth along the river is measured by a measuring needle with a precision of 0.1 mm.

4 Test result analysis

4.1 Flow pattern and velocity distribution in confluence zone

The confluence area of the main stream and the tributaries forms a reflux diversion area under the inertial effect. The mutual lifting of the flow in the intersection area leads to the bending of the streamline and the generation of spiral flow. The distinct separation zone, maximum velocity zone, stagnation zone, velocity bias area, shear layer and flow recovery region are formed in the confluence zone, as shown in Fig. 2.

Fig. 3 is the transverse velocity distribution of the confluence area when the flood peak flow occurs in five years, in which the mainstream flow $Q1 = 163\ m^3/s$, tributary flow $Q2 = 61.5\ m^3/s$, confluence ratio $Q1/Q2 \approx 2.65$. From Fig. 3, it can be seen that the flow discharges through the drop outlet, and the flow diffusion is uneven at the bell mouth, and the flow diversion on both sides is uneven. Multi-point transverse velocity in navigable waters is greater than 0.15 m/s, the maximum transverse velocity $U_{max} = 0.35$ m/s.

4.2 Bias analysis and scheme optimization

The engineering measures to improve the navigable flow conditions of tributaries are usually increasing the navigable net width, dredging and drainage, and adjusting the inlet angle or inlet ratio of tributaries. Through case a (see Table 1), it can be seen that the main reason for the serious flow deviation in the outlet section of the drop and the excessive lateral flow velocity in the confluence zone is that the overcurrent sections on both sides of the outlet section cannot be fully utilized and the outflow is uneven. Therefore, this test improves the phenomenon of insufficient diffusion of discharge water by optimizing the layout of the plane structure of the outlet section of the drop project.

This test adopts the method of increasing the angle of the diffusion section of the outlet chute and arranging the diversion pier to improve the flow condition. According to the "Design Specification of Water Conservancy and Hydropower Project Inlet", the diffusion angle is generally $6^\circ - 12^\circ$. When the diffusion angle is too large, the flow stability will decrease, resulting in uneven flow velocity distribution and reduced flow capacity. Zhang points out that the diversion pier divided the flow into several water tongues, which can reduce the oblique flow angle and lateral flow velocity, and effectively improve the adverse flow pattern of the flow in the discharge

building.

In order to quantitatively analyze the flow bias flow phenomenon in the outlet section, this paper introduces λ as the bias flow coefficient and defines it as the ratio of the flow velocity U_L at the left end of section 2# to the flow velocity U_R at the right end of section 2#. For formula see Eq. (1).

When the main stream is on the left side of the river, $\lambda > 1$, and when the main stream is on the right side, $\lambda < 1$. In this paper, a variety of layout optimization schemes are proposed based on five-year navigation conditions. Table 1 is the shape optimization scheme of the outlet section of the drop.

Case e(see Table 1) increases the angle of the diffusion section of the chute to 10°, and the diversion pier is still used after the outlet of the drop, as shown in Fig. 4. The results show that the flow in the transition section is drained by multiple streams of water. The partial flow coefficient in the transition section is close to 1, and there is no obvious partial flow. The overall flow channel is good, and the maximum lateral velocity in the intersection area is 0.15 m/s, which meets the navigation requirements, as shown in Fig.5.

5 Equation, table, figures, and footnotes

5.1 Equation

$$\lambda = \frac{U_L}{U_R} \tag{1}$$

5.2 Table and figures

Table 1 Shape optimization scheme of drop outlet.

Case	Export diffusion angle	Stage of diversion pier	Excavation depth of exit section (m)	U_{max} (m/s)	λ
a	0°	/	/	0.35	5.75
b	7°	/	/	0.33	4.12
c	10°	/	/	0.30	3.95
d	10°	one-order	/	0.25	3.05
e	10°	two-order	/	0.15	1.93
f	10°	one-order	5	0.24	2.88

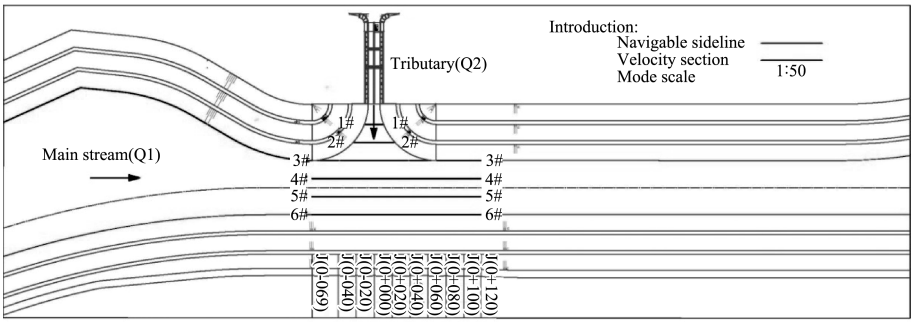

Fig. 1. Model plane diagram.

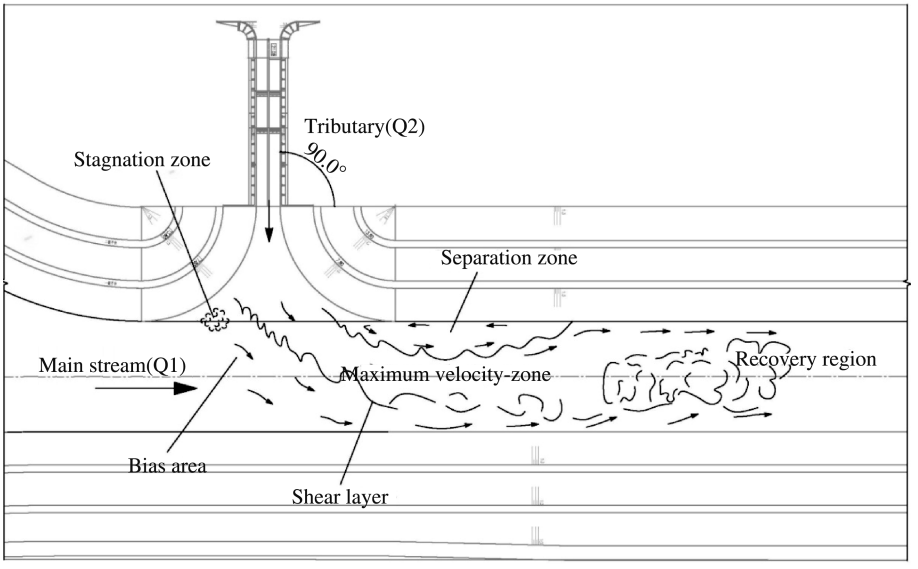

Fig. 2. Flow pattern diagram of confluence zone of main stream and tributary.

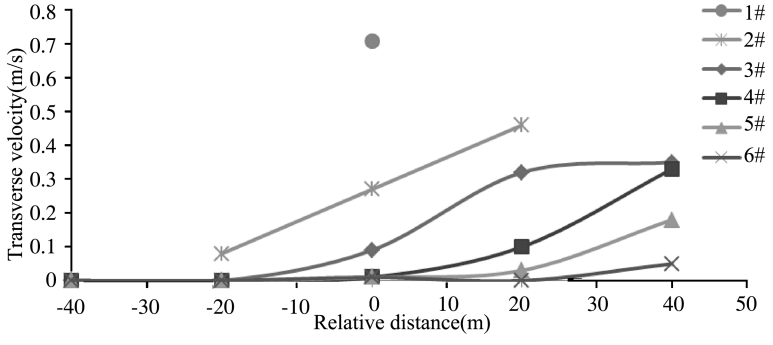

Fig. 3. Distribution of transverse velocity of confluence zone.

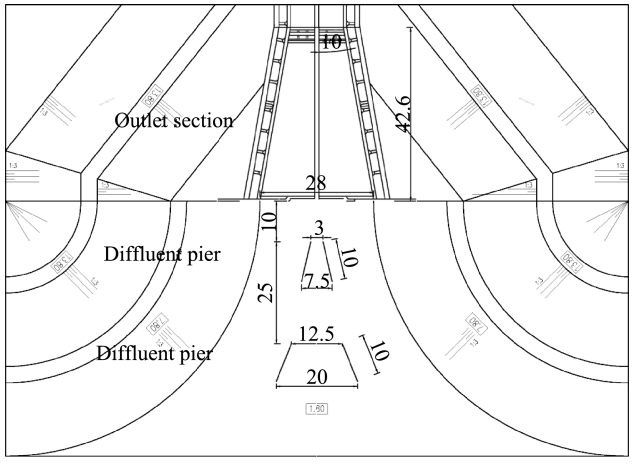

Fig. 4. The plan layout of multi-level diversion measures.

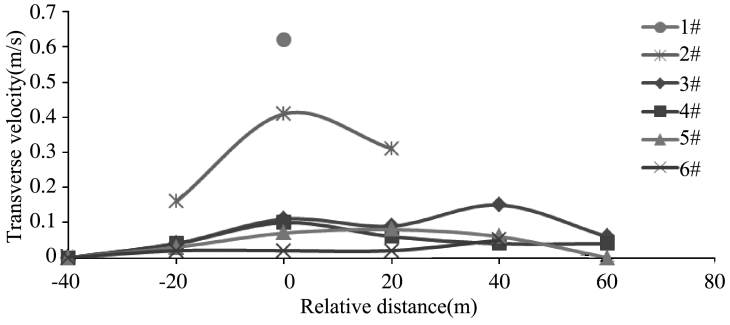

Fig. 5. Distribution of transverse velocity of confluence zone (Case e).

5.3 Footnotes

In this paper, U_L is defined as the flow transverse velocity at the left end of section 2 #, and U_R is the flow transverse velocity at the right end of section 2 #. U_{max} is the maximum velocity of each section.

6 Conclusion

In this paper, the normal physical model with a geometric scale of 1∶50 is established based on the Shutou River drop project in the Yangtze-Huaihe River Diversion Project. The model is designed by gravity similarity criterion, and the navigation flow conditions in the intersection area of the large-angle main stream and tributary are studied. The flow velocity conditions in the intersection area under different optimization schemes are analyzed. The results show that the symmetric diffusion in the out-

let section of drop water and the multi-stage diversion measures with two-stage diffluent piers in the transition section can significantly improve the flow velocity distribution in the confluence zone, reduce the lateral flow velocity in the confluence zone. When the minimum control water level of the channel encounters flood once in five years, the transverse velocity is not greater than 0.15 m/s.

Acknowledgements

Thanks for the project support provided by Anhui Institute of Water Resources and Hydropower Survey and Design.

References

Li, W., 2012. Experimental study on the flow characteristics in the bend section of tributaries. Port & Waterway Engineering (10): 62-68.

Liu, T., Guo, W., Zhan, L., 2009. Experimental study on the distribution characteristics of time-averaged velocity in the inflow region of 90° tributary. Advances in Water Science, 20(4): 485-489.

Nanjing Hydraulic Research Institute. Jianghuai communication section of Yangtze-Huaihe River diversion project.

Taylor E. H., 1944. Flow characteristics at rectangular open channel junction. Trans ASCE, 109(1): 893-902.

Weber, L. J., Schumate, E. D., Mawer, N., 2001. Experiments on flow at a 90° open-channel junction. Journal of Hydraulic Engineering, ASCE, 127(5): 351-368.

Xu, L., Huang, G., Shi, W., et al., 2020. Influence of guide plate on hydraulic performance of outlet channel of large inclined pump device. Chinese Journal of Hydrodynamics, 35(4): 479-487.

Suggestions on measures to enhance the resilience of the Three Gorges ship lock

Qiong Yang, Honglin Feng, Wentao Ding,
Wenwu Yang, Pengpeng Jia

(Transport Planning and Research Institute, Ministry of Transport, Beijing, China. e-mail: 83946442@qq.com)

Abstract: A safe and stable logistics supply chain is an important guarantee for the construction of a new development pattern, which is of great significance to promote the formation of a smooth domestic economic cycle and attract better global resources. "The Outline of Building a Strong Transport Country" and "The Outline of National Comprehensive Three-dimensional Network Planning" issued by the CPC Central Committee and the State Council clearly put forward enhancing the flexibility of the system, improving the resilience and safety of the transport network system, and building resilient transport. At present, China is faced with the severe test of insufficient safety resilience of water transport channel. For example, the Three Gorges Lock has been overloaded for more than ten years. It is urgent to improve the safety resilience of the national key water transport channel. The research and practice of resilient transportation construction are still in the initial stage in China, and mainly focus on the road transportation field. Based on the new requirements on constructing a new development pattern and resilient transport for a country with strong transportation, this paper, taking the Three Gorges Project as its research focus, deconstructs the connotation of water transport safety resilience, focuses on the key hubs on national major waterway channels, analyzes and identifies the critical factors affecting safety resilience from multiple dimensions. It proposes replicable and promotable measures and suggestions to improve the locks' resilience from the perspectives of strengthening top-level design, strengthening infrastructure construction, scientific operation and management, and improving policy fund guarantee, providing references for the industry to formulate science-based strategies and measures.

Keywords: Resilience; The Three Gorges Project; Suggestions

1 Connotation of resilience and resilient ship lock

1.1 Origin and connotation of resilience

The word "resilience" means to return to the original state. In 1973, Holling, a

Canadian ecologist, first introduced the concept of resilience into the study of ecosystem. The social-ecological resilience theory regards resilience as an important part of sustainable development. Because it is committed to improving the flexibility and adaptability of the social-ecological environment system in the long run. In recent years, the concept of resilience has been extended to the fields of economy, environment, urban construction and urban disaster prevention. In 1990, Hansen studied the effects of road closures caused by the Loma Prieta Earthquake, which ushered in a new era of research in the field of transportation system resilience. The study of transportation system resilience in foreign countries has gone through three stages: conceptual framework, index system, and quantitative evaluation. Bruneau et al. (2003) defined resilience as the ability of the system to mitigate the impact of disasters and maintain its own functions, and measured it by the resilience triangle composed of the degree of system function loss, the degree of disaster interference, and the time for the system to restore normal functions. Cutter et al. (2008) defined resilience as the ability of the system to cope with and recover from disasters, including the system to absorb and resist adverse effects of disasters and promote the adaptive process of self-organization, change and learning of the system in the process of coping with disasters. Judith Y. T. considered the quality of resilience, reliability and sustainability as the comprehensive resilience of transportation system. China has also made active exploration in the field of resilient transportation construction. In August 2019, the Ministry of Transport issued "The National Comprehensive Three-dimensional Transport Network Index Framework", which is used to scientifically evaluate the development level of China's comprehensive transport infrastructure network and reasonably determine the planning objectives of the transport network. The index framework sets up 16 indicators around six criteria, including reasonable scale, coordinated mode, safety and reliability, convenience and efficiency, greenness and intensiveness, and economic benefits to the people, among which the resilience index of the transportation network is used to reflect the reliability level of the transportation network, with emphasis on the substitution of comprehensive transport corridors and key sections under emergencies. The connectivity reliability, time reliability and capacity reliability of the transport network are comprehensively evaluated.

According to the theoretical research and construction practice of resilient transportation at home and abroad, resilient transportation refers to the ability of transportation infrastructure to have high robustness and redundancy, to predict the changes of the traffic environment, and to operate continuously and steadily or to achieve rapid recovery in the event of emergencies.

1.2 Connotation of resilient ship lock

"The Outline of Building a Strong Transport Country" and "The Outline of National Comprehensive Three-dimensional Network Planning" put forward the development requirements of resilient transportation, but the research on resilience has not yet been solved at the methodological level of connotation, extension, characteristics and measures. At present, the research on the resilience of inland waterways and locks is basically in a blank state. Most of the existing studies focus on inland navigation safety or shipping carrying capacity, and few studies consider the impact of inland waterway interruption on the entire transportation network from the perspective of the network.

Through the analysis of resilience and resilient transportation, we believe that the resilience of lock can be understood as having high robustness and necessary redundancy, which can warn and adapt to the changing external environment on the basis of maintaining stable operation under conventional interference. It has the ability to resist and withstand drastic changes in supply and demand caused by emergencies (natural disasters, accident disasters, public health incidents, social security incidents, etc.) and to achieve rapid recovery. The key features of resilient ship lock include:

Robustness: the ability to resist and respond to conventional external interference.

Redundancy: there are alternative or replacement transport channels, with a certain amount of rich capacity reserves.

Resilience: the ability to quickly identify problems and make use of existing resources, funds, information, technology and manpower to formulate emergency plans in a timely manner.

Recovery: after the impact of external shocks is reduced, the channel function can be quickly restored; the function of the lock can be quickly restored after the external impact is reduced.

Adaptability: self-organizing ability and the ability to learn and adapt.

2 Status of the Three Gorges ship lock

2.1 Overview of the Three Gorges Project

The Three Gorges Project is a large-scale water conservancy project constructed in the upper and middle reaches of the Yangtze River in China, and it is also the largest hydropower station in the world. The project is located in the main stream of the

Yangtze River from Chongqing to Yichang. The hub consists of a dam, a hydropower plant and navigable buildings, including the Three Gorges ship lock and vertical ship lift, which are arranged on the left bank. Among them, the Three Gorges ship lock is the main facility for ships to pass through the dam. It is a double-line five-step ship lock and the water level drop between the upstream and downstream of the ship lock is 113 meters. The one-way annual cargo volume is designed to be 50 million tons in 2030. The ship lock and approach channel can pass through a fleet of 10,000 tons, with a maximum single ship of 3,000 tons. The ship lift is a fast dam-crossing channel for passenger ships and special ships. It can effectively improve the navigation quality of the hub and the passing capacity of the lock. On December 27, 2019, the Three Gorges ship lift project was officially opened to navigation. For layout plan of the Three Gorges Project, see Fig. 1.

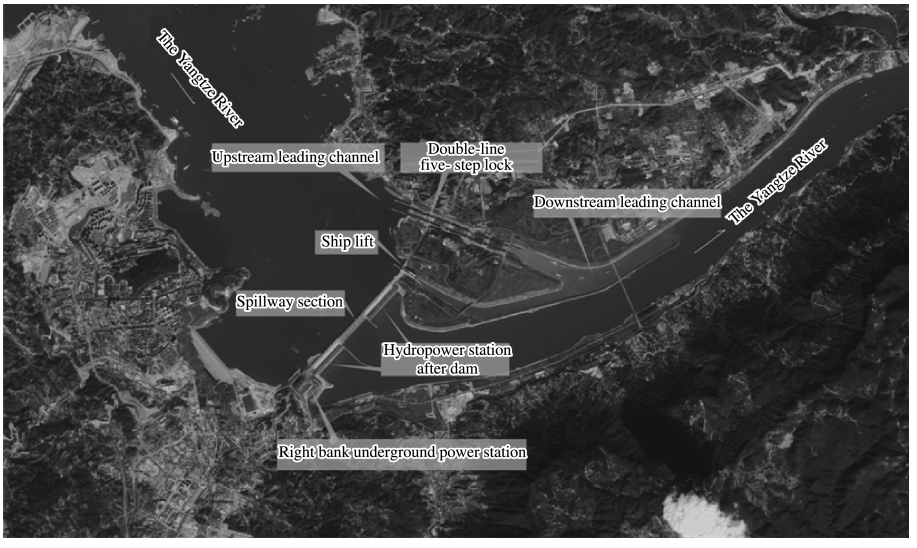

Fig. 1. Layout plan of the Three Gorges Project.

2.2 Navigation operation status of lock

2.2.1 The navigation of the Three Gorges ship lock is generally safe, and the operation of navigation structures is stable.

The Three Gorges Navigation Administration is responsible for the daily operation, maintenance and repair of the Three Gorges ship lock and ship lift. At present, the water safety situation of "zero death, zero shipwreck and zero pollution" has been realized in the Three Gorges Project for ten consecutive years, and 100% of the ships passing through the dam have passed the security inspection. In the past ten years, the lowest annual operation hours of the lock are 8,132 hours, exceeding the design index

by more than 762 hours. In addition to the suspension time due to maintenance and abnormal weather, it has been running continuously and steadily, the intact rate of main equipment is more than 99.8%, and the failure rate of equipment and the hours of obstruction of navigation due to failure are far below the design index, which reflects the high level of navigation management and operation maintenance.

2.2.2 The volume of bulk cargo is dominant, and the volume of passenger traffic is decreasing year by year.

Ore, mineral construction materials, steel, coal, oil, and other bulk goods and containers have been in the top six of the volume of goods passing through the dam for ten years, and their total volume has stabilized at more than 77% of the total volume of goods passing through the dam, which fully reflects the advantages of bulk cargo waterway transportation. During the peak period around 2016, the annual conversion volume of passenger transport accounted for about 9% of the total volume. Since 2018, short-term passenger ships have no longer been given priority to crossing the lock, and the growth of passenger demand for crossing the dam has been restrained, which has been less than 1% in recent years and was only 0.03% in 2020. In addition, since the implementation of dam-turning transportation in 2004, the volume of dam crossing has gradually increased, and reached a peak of 422,000 vehicles in 2008. After 2009, with the completion of expressways, the volume of dam crossing has decreased and stabilized, and decreased to 60,000 vehicles in 2020.

2.2.3 The Three Gorges Project operates efficiently and has limited space for further exploitation.

In 2011, the cargo volume of the Three Gorges Reach increased to 100 million tons, and the one-way cargo volume exceeded 50 million tons, reaching the designed capacity 19 years ahead of schedule. Over the past decade, the total freight volume of the Three Gorges ship lock increased from 100.3 million tons in 2011 to 146 million tons in 2019, with an annual growth rate of 3.83%. In 2020, affected by the epidemic, the freight volume decreased slightly to nearly 137 million tons. The navigation management department has carried out a series of measures to tap the potential. In the past ten years, the actual annual operation hours of the Three Gorges ship lock have far exceeded the designed annual operation hours, and the average daily number of operating locks has stabilized at more than 30. The volume of dam crossing has reached a high level. Although the volume of dam crossing has increased, the growth rate has slowed down significantly compared with the first eight years of operation of the Three Gorges Project, indicating that the space for further expansion of capacity and tapping potential is very limited. For freight volume through the Three Gorges ship lock, see Fig. 2.

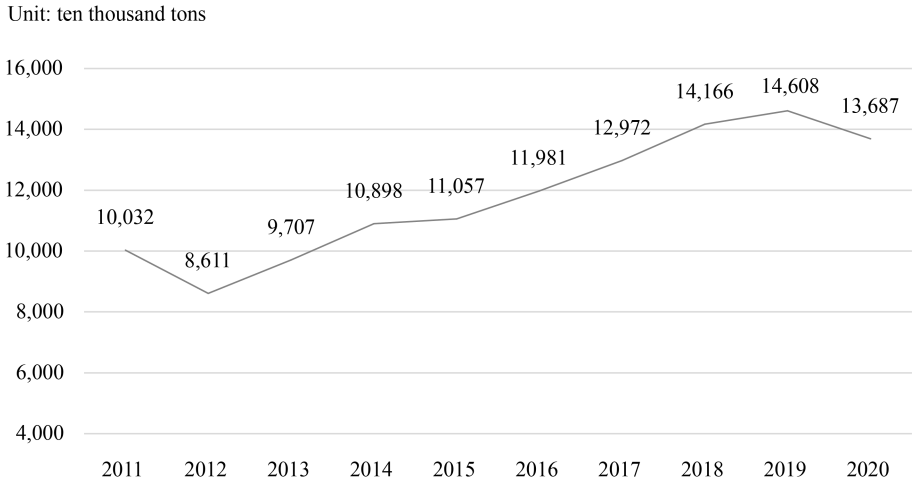

Fig. 2. Freight volume through the Three Gorges ship lock.

2.3 Existing problems

2.3.1 The insufficient passing capacity is still prominent.

With the rapid development of the cargo volume through the Three Gorges ship lock, the current cargo volume has far exceeded the design capacity, and the situation of ship waiting for lock is becoming more and more serious. In the past ten years, the daily average number of ships waiting for locks has increased from 300 per day in 2011 to 883 per day in 2018, and to 951 per day in the first ten months of 2021. The average waiting time has increased from about 40 hours to 151 hours in 2018, and has reached 187 hours in the first ten months of 2021. According to relevant studies, it is predicted that the potential demand for dam-crossing transportation of the Three Gorges Project will be 230 million tons in 2035 and 290 million tons in 2050, and the contradiction between the capacity and demand of the Three Gorges ship lock will be further highlighted.

2.3.2 The resilience of the ship lock is insufficient under bad weather, maintenance and sudden accidents.

Because the capacity of the hub has been saturated, there is a problem of insufficient resilience of the lock under special conditions such as bad weather, lock maintenance and sudden accidents. From 2009 to 2011, the average suspension time of the Three Gorges lock and Gezhouba lock due to strong wind, fog and excessive flow was 1,242 hours, including 1,754 hours in 2009. In the second half of 2012, due to the severe flood situation in the Yangtze River, despite the adoption of management measures such as control of drainage, the maximum number of ships waiting for the lock due to the restriction of navigable flow reached 941, and the longest waiting time was

nearly 40 days. During the repair period of the Three Gorges lock, especially the scheduled repair period of nearly 40 days, navigation was greatly affected.

3 Factors influencing the resilience of ship lock

The resilience of the Three Gorges ship lock is closely related to the passing capacity of the lock, and the direct factors include the operation efficiency of the ship lock and the transportation efficiency of ships passing through the lock. Among them, the intuitive measurement indicators of lock operation efficiency mainly include annual navigation days, daily operation times, navigation guarantee rate, lock chamber utilization rate, etc. The intuitionistic indexes to measure the efficiency of lockage ship transportation mainly include the average tonnage of lockage at one time, the coefficient of ship loading, the coefficient of unbalanced transportation volume, etc.

The resilience of the Three Gorges ship lock is triggered by external emergencies, and the indirect factors include macro-industrial policy and shipping policy, natural disasters and accidents, economic operation environment, dispatching management level, navigation suspension and maintenance plan, safety emergency response ability, etc. These indirect factors have an impact on the relevant indicators of direct factors from different levels, and the impact can even be a main one. As a result, the safety and resilience of the Three Gorges ship lock and even the Yangtze River waterway are facing a major test.

Generally speaking, the resilience of the Three Gorges ship lock includes not only the ability to operate steadily and safely under normal conditions, but also the ability to withstand and respond to short-term demand fluctuations in emergencies. At present, the Three Gorges ship lock has the basic ability to deal with the "high frequency and low loss" emergencies such as bad weather and routine maintenance. However, resilience tests the process of prevention, absorption, recovery and adaptation to the extreme situation of "low frequency and high loss". The maintenance and navigation interruption caused by natural disasters, accidents, public health events and other major emergencies should be the focus of attention in the future.

4 Suggestions on measures to enhance the resilience of ship lock

4.1 Strengthen the top-level design

4.1.1 Overall planning of regional comprehensive transportation system

Plan the comprehensive transportation system of the Three Gorges area as a

whole, promote the combination of water transport with highway, railway and pipeline transport, integrate the comprehensive transportation planning indicators of the Three Gorges ship lock, consider the transport capacity of alternative transport corridors in case of emergencies, make strategic reservations for traffic and dispatching capacity, and further improve the comprehensive transport capacity of the Three Gorges dam area. Promote the adjustment of the layout of economic industries along the Yangtze River, scientifically guide the dam-crossing logistics, promote the balance of dam-crossing upstream and downstream traffic volume, effectively improve the loading coefficient of ships passing through the lock, and further enhance the capacity of the Three Gorges Project.

4.1.2 Establishing a cross-sectoral comprehensive coordination and early warning mechanism

Coordinate the establishment of a national coordination mechanism involving the comprehensive benefits of the Three Gorges Project (such as shipping, flood control and power generation), formulate and improve management measures and major emergency plans, and build an efficient and smooth communication mechanism based on the results of risk analysis and evaluation. Improve the consultation system for flood control and further clarify the coordination and early warning mechanism for navigation management in flood season. It is suggested that the navigation management department should participate in the formulation of the annual flood season dispatching scheme and dispatching plan of the Three Gorges-Gezhouba Water Conservancy Project, establish the basic principle of giving consideration to navigation in flood season dispatching and operation of the Three Gorges-Gezhouba Water Conservancy Project, clarify the boundary conditions for controlling the outflow of the Three Gorges Reservoir and the emergency dispatching plan, and fully guarantee the traffic capacity of the Three Gorges Project in flood season.

4.2 Strengthen infrastructure construction to improve robustness and avoid redundancy

4.2.1 Accelerate the research, planning and construction of the new Three Gorges Corridor

The next 15 years are the fastest period of industrialization and urbanization in the upper reaches of the Yangtze River. It is also a period of accelerating the construction of tributaries such as Jialing River, Wujiang River and Minjiang River and accelerating the development of water transport. The introduction of large industrial projects along the Yangtze River will lead to a sudden increase of tens of millions of tons of water transport. It is urgent to speed up the research and planning of the new

Three Gorges Corridor. To make up for the shortage of shipping capacity of the Three Gorges Project, we should give full play to the comparative advantages of the Yangtze River Golden Waterway and promote the high-quality development of the Yangtze River Economic Zone.

4.2.2 Continue to implement the regulation of navigation-obstructing river sections

In order to improve the function of the golden waterway of the Yangtze River in an all-round way, the construction of the new Three Gorges Corridor should be considered as a whole with the regulation, construction and planning of the Yangtze River waterway. In addition to expanding the dam-crossing capacity of the Three Gorges and Gezhouba projects, it is also necessary to regulate the navigation-obstructing river sections between the two dams and Jingjiang River sections in a planned and targeted manner so as to give full play to the capacity of the key structures. We will continue to harness navigation-obstructing sections of the Yangtze River trunk line, strengthen coordination among relevant protected areas, promote the process of waterway regulation in relevant sections, and enhance the overall capacity of the Yangtze River trunk line.

4.2.3 Strengthen daily maintenance and support capacity

Do better in infrastructure maintenance and normal security inspection to ensure reliable operation under normal conditions. Renovate navigation facilities, speed up the construction of anchorage and maintenance base, and enhance the ability of the waterway to quickly restore the traffic flow of ships in the region after being affected by strong wind, heavy fog or large flow. We will further improve the navigation management information system and safety supervision facilities in the dam area, build new ship draft safety detection facilities, hydrological and meteorological monitoring and reporting systems, monitor the discharge wave of the ship lock in the lower approach channel, and monitor the changes of peak water level in Gezhouba and Three Gorges Dam power stations, so as to grasp the changes of water level caused by peak regulation in real time. Make reasonable arrangement of ship lockage plan to enhance safety and security capabilities. We will further increase investment in the purchase of rapid maintenance equipment. We will increase the optimization of waterway maintenance terminal stations, the renewal and mechanization of boats, emergency dredging, search and rescue facilities and equipment.

4.3 Scientific operation and management to improve operational efficiency and early warning and disposal capabilities

4.3.1 Further optimize and improve the efficiency of lock operation and ship transportation

Optimize the conditions for ships to enter the lock, study the fast ship lockage

technology suitable for the specific environment of the Three Gorges ship lockage, and realize the synchronous lockage of the same type of ships. We will continue to optimize the dispatch of ships passing through the lock, carry out joint dispatch of the Three Gorges ship lift and the Three Gorges and Gezhouba ship locks, improve the dispatching process and improve the efficiency of the navigation facilities of the two dams. We will further optimize the standard ship type in the Three Gorges Reservoir area and increase the tonnage of ships passing through the lock at one time. We will further improve the standard of ship draft control and implement the dynamic control of ship draft at the Three Gorges ship lock.

4.3.2 Enhance monitoring, early warning and emergency response capabilities

By means of information technology and big data, the monitoring and early warning capabilities of the lock operation system are improved, and the ship dispatch is predicted in advance considering possible emergencies. Establish stable, reliable and timely multi-source real-time forecasting channels for natural disasters such as floods, and timely access to early warning information. The regional risk model is established by using satellite, UAV remote sensing and GIS technology. The early warning mechanism of severe weather will provide effective information support for port, shipping enterprises and relevant management departments, and enhance the ability of ship locks to cope with extreme severe weather. Enhance the emergency response capability of hub suspension, organize and coordinate shipping enterprises to establish cooperation mechanism, realize the rational allocation of emergency resources, ensure the normal passage of alternative channels, coordinate relevant units to carry out accident investigation, maintenance and other related work, so as to timely control or eliminate the potential risk of suspension. Formulate, implement, evaluate and improve disaster emergency rescue plans, in order to enhance the service ability of the Three Gorges ship lock for economic and social operation under special circumstances.

4.3.3 Strengthen key technical research

We will carry out technical research on rapid overhaul of ship locks with minimal shipping impact, formulate work plans and measures to achieve rapid overhaul of ship locks, shorten the period of suspension and overhaul, and ensure navigation, so as to achieve the goal of further shortening the period of suspension of ship lock overhaul, give full play to the capacity of the overhaul period and control the backlog of ships. We will ensure the safe and orderly organization of shipping in the hub waters during the overhaul period, and reduce the social impact and the loss of shipping enterprises. We will carry out the research on the influence of the peak regulation of the key power station on the navigation of ships between the two dams, formulate reasonable, economic and reliable safety management measures in combination with the real-time

changes of various ships passing through the Three Gorges section and their loading conditions, and take timely and effective engineering measures to improve the navigation conditions between the two dams, so as to provide a safe navigation environment for ships.

4.4 Improve the guarantee of policies and funds

Strengthen the fund guarantee for the construction of resilient locks, incorporate the goal of resilience into the relevant planning and project design, ensure the investment of funds and establish the resilience standard of transportation assets. To study and set up a special fund for the construction of ship lock resilience capacity for operation, maintenance, management and emergency support, we will improve the dynamic guarantee mechanism for waterway maintenance funds and increase investment in ship lock maintenance funds. Establish a reasonable investment guarantee mechanism for ship lock maintenance funds.

References

Pendall, R., Foster, K. A., Cowell, M. Resilience and regions: building understanding of the metaphor. Cambridge Journal of Regions, Economy and Society, 2010, 3(1): 71-84.

Bruneau, M., Chang, S., Eguchi, R., et al. A framework to quantitatively assess and enhance the seismic resilience of communities. Earthquake Spectra, 2003, 19 (4): 733-752.

Cutter, S. L., Barnes, L., Berry, M., et al. A place-based model for understanding community resilience to natural disasters. Global Environmental Change, 2008, 18 (4): 598-606.

Ministry of Transport. Indicator Framework of National Integrated Three-dimensional Transportation Network. 2019.

Chen, C., Zhang, Q., Yin, Y., et al. Research on the Yangtze River shipping safety monitoring model based on Bayesian network. Transportation Research, 2017, 3 (6): 32-39.

Kou, W. Evaluation of shipping carrying capacity in the upper reaches of Yangtze River based on ArcGIS Engine. Chongqing Jiaotong University, 2018.

Liu, C. Development status of passenger and freight transport in Three Gorges Project. Planning and Research Institute of Ministry of Transport, 2021.

The analysis of the recent evolution mechanism of the morphology in the Yangtze River Estuary and the future trend estimation

Siqi Li[1], Huiming Huang[2], Yigang Wang[3]

[1,3] College of Harbour, Coastal and Offshore Engineering, Hohai University, Nanjing, China. e-mail: 1240050283@qq.com

Abstract: As currently the importance of maintaining the steady state of the significant tidal shoals in a bifurcated estuary standing out, mainly due to the consideration for both environmental protection and economic development, the urgency of the research for the inner evolution mechanism of the morphodynamics in a large-scale estuary with sophisticated natural and anthropogenic forces has been increased, especially in the Yangtze River Estuary. This study focuses on the bathymetric evolution mechanism of the Yangtze River Estuary, aimed to explore the relationship between the main control factors and the estuarine bathymetry variation in recent years and in the next few decades. The methods used in this study include the analysis of the recent bathymetric data of the tidal shoals, and the establishment of a large-scale two-dimensional mathematical model which is fully calibrated and verified on the bases of the recent measurement data. Firstly, the comparisons were made between the bathymetric data of different periods gathered in recent years and it is clarified that different change modes really exist along the estuary, which mainly result from the different positions of the shoals and channels spread in the estuary. Especially, the distinctness show how the forces of the tide and riverine current are balanced along the estuary from the upper reach to the lower reach and finally to the mouth part. Although the man-made engineering buildings such as the jet and sea walls surely have exerted certain influences on the morphological variation in their protection areas, the mouth area shows most deposition trend comparing with other parts. Secondly, the two-dimensional mathematical model stimulated both the short term and the long term of the estuary, and the results showed that in the short term erosion and deposition are nearly balanced in the mouth area, however, in the long term, the estuary presents a trend of general erosion. This research further explores the evolution mechanism of the shoals in an estuary influenced both from river and tide, clarifies the relationship of the bathymetric changes between different parts, and offers certain useful suggestions and thoughts for the further integrated management of the estuary.

Keywords: Yangtze River Estuary; Numerical stimulation; Evolution mechanism

1 Introduction

The estuaries, mainly generated by the ocean transgressive and regressive movement in the Holocene period, are the interfaces between the land fluvial system and the ocean systems. Due to the influence exerted by the interaction of both the runoff and the current from the two systems, a complicated hydraulic environment and sediment transportation mechanism have formed and made the morphodynamic of the estuaries changeable, which means the geomorphic equilibrium is prone to be affected by exertional forces and it is difficult to catch the evolution law of the estuarine geography accurately. Besides, as most estuaries are featured with abundant cultivated land and biological resources, they have become the economical and population centers of the countries in which they locate such as the Nile River Estuary in Egypt, the Mississippi River Estuary in the United States, the Mekong River Estuary in Vietnam. The Yangtze River Estuary is the largest estuary in China, known as the golden waterway, and scattered with important tidal shoals and submerged delta, as can be seen in Fig. 1. And because of the importance of those shoals to both the economical development of Shanghai and the life safety of the residents, artificial buildings such as dikes, groins and seawalls have been built to prevent those shoals from being eroded by the waves, currents and even the catastrophic flood. Therefore, studying the evolution mechanism of the channels and shoals is of great significance to the economy and the people's livelihood. However, most current studies are based on the analysis and comparison of certain areas of the topography in the Yangtze River Estuary, or all the topography in a relatively short time scale, mainly based on the analysis of measured data and remote sensing. While in a geomorphic system, the change of input conditions, or the change of the internal environment of the system, especially the continuous change, requires a long time scale and a large spatial scale to reflect the destruction of the original equilibrium state of the geomorphic system and the establishment of the new equilibrium state of the geomorphic system, which is difficult to be realized by remote sensing or measured data analysis at present. As a result, the usage of the large-scale numerical stimulation of the estuarine morphology has the advantage to study the evolution mechanism of an estuary in broader temporal and spatial scales. The research of this paper focuses on the current evolution mechanism of the existing important tidal shoals and the evolution trend of erosion and deposition in the next 20 years under the condition of sharp reduction of sediment from the upstream and intensified human intervention in the Yangtze River Estuary.

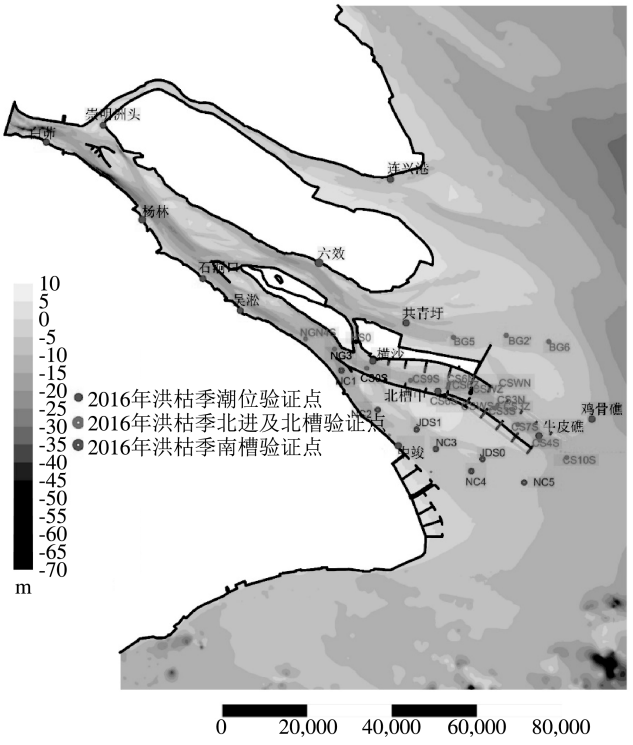

Fig. 1. Topographic map of the study area.

2 Methods and data

2.1 Yangtze River Estuary model

2.1.1 Model settings

The research mainly focuses on the Yangtze River Estuary (Qingcaosha Reservoir, East Hengsha Shoal, Nanhui Shoal). Therefore, the scope of the model includes the Yangtze River Estuary and Hangzhou Bay. The upstream river boundary is taken to Datong and the outer sea boundary is taken to about −50 m isobath, so as to eliminate the influence of the outer sea boundary on the calculation to the greatest extent. The grid of the model adopts orthogonal curve grid, which can better fit the shoreline, as shown in Fig. 2. The grid scale is about 10 m in the mouth and about 5,000 m in the open sea. The bathymetric data used in the model calculation is the latest version measured in Hangzhou Bay and the Yangtze River Estuary in 2016, and the latest working conditions in 2016 are considered for all the artificial buildings. The model grid is densified at the buildings and at the three key tidal flats. The upper boundary of

the model is controlled by the hydrological and sediment process of Datong, the outer sea boundary is provided by the China Sea model driven by 8 main tidal components, and the sediment transport is controlled by flux conservation. The roughness of the model is selected according to the data verification, which is between 0.015 - 0.020. The viscosity coefficient is calculated according to the formula and the model is driven by cold start. As the tidal flat in the Yangtze River Estuary is still dominated by silt and fine silt, the sediment particle size refers to the statistical analysis results of suspended sediment particle size in the Yangtze River Estuary. According to the calculation of sediment particle size and starting shear stress, the critical starting shear stress is selected between 0.16 - 0.2. In the selection of sedimentation rate, the influence of salinity in the Yangtze River Estuary on sediment flocculation is considered, and the value is taken with reference to the analysis results of large-scale suspended sediment sedimentation rate in the Yangtze River Estuary. During the landform calculation, the landform will be updated at each time step. Since the change of landform lags far behind the change of hydrodynamic force, the landform acceleration factor is introduced into the model to multiply the change of bed surface in each time step by the acceleration factor to improve the calculation efficiency.

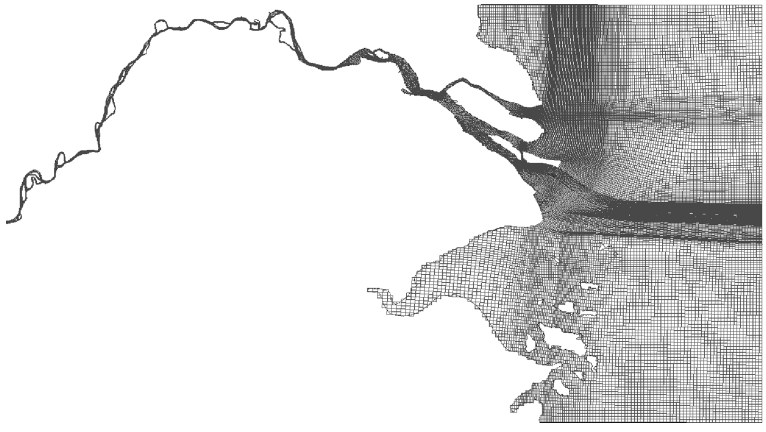

Fig. 2. Computational grid.

2.1.2 Model validation

The model verification includes hydrodynamic verification, sediment concentration verification and erosion and deposition verification in three areas. The model is verified by using the data of tide level, velocity, flow direction and sediment concentration measured in the flood season (July to August) and dry season (February to March) of the Yangtze River Estuary in 2016, and the erosion and deposition of three key areas of concern (Qingcaosha Reservoir, East Hengsha Shoal, Nanhui Shoal) are verified in combination with the historical data of previous years.

2.2 Analysis of measured topographic data

This study collected the recent topographic measurements of several important tidal flats or in the Yangtze River Estuary (including the East Hengsha Shoal, the Nanhui Shoal, the shoals around the Qingcaosha Reservoir). The data are processed by the Kriging interpolation and generate the DEMs of deposition and erosion. Those DEMs are pictured through the Surfer software, as can be seen in Fig. 3 to Fig. 5, and each picture has shown the accurate measured years that are made comparison for different tidal flats. In this part, the measured deposition and erosion DEMs are put with the calculated DEMs from the models to verify the accuracy of the model for further predicting the evolution trend of these key tidal flats in the future.

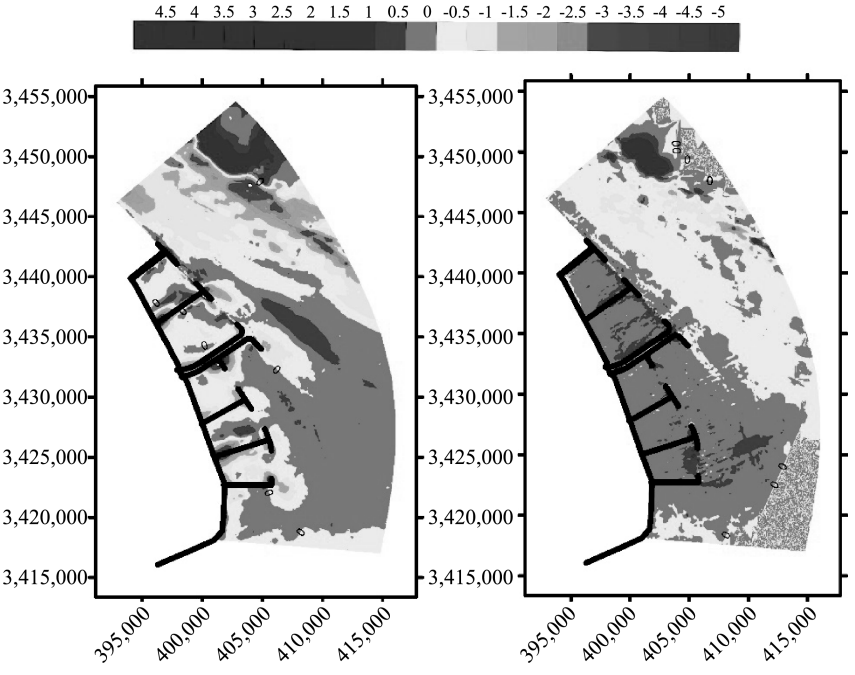

Fig. 3. 2015 – 2016 Nanhui erosion and deposition (calculation on the left and measurement on the right).

3 Construction and simulation of the long term scouring and silting model

Based on the verification of the flow, sediment and bathymetry model of the Yangtze River Estuary, the simulation of the evolution of estuarine erosion and deposition in the next 20 years is carried out. Because the Yangtze River Estuary belongs to the area where runoff and tidal current interact together, the water and sediment from the upstream and the boundary conditions of the open sea are very important for

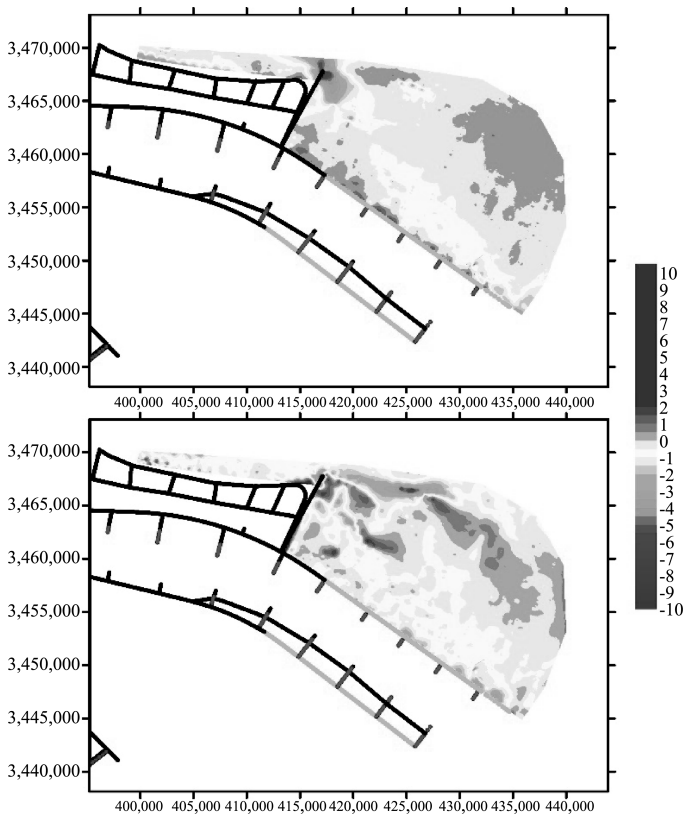

Fig. 4. 2013–2016 Hengsha erosion and deposition (calculation above and measurement below).

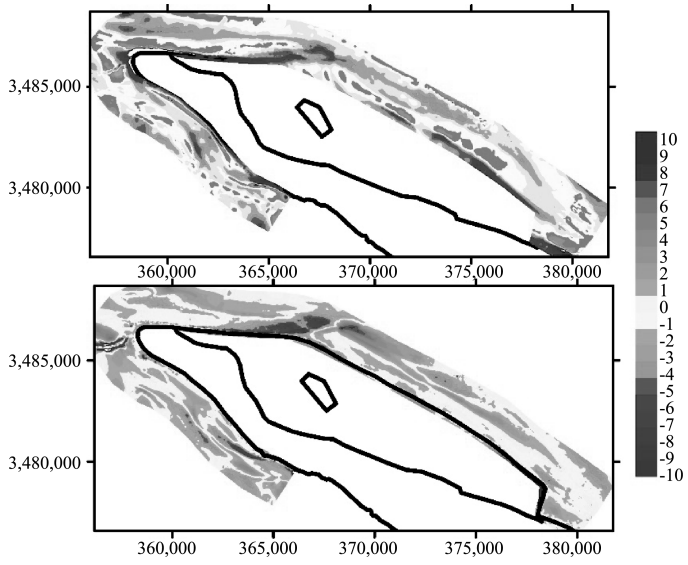

Fig. 5. 2007–2009 Qingcaosha erosion and deposition (calculation above and measurement below).

the simulation of estuarine erosion and deposition evolution in the next 20 years. Therefore, this paper focuses on the selection of water and sediment from the upstream and the boundary conditions of the open sea, and aims to fully reflect the impact of the operation of the Three Gorges Reservoir on the adjustment of water and sediment from the upstream after 2003. However, considering that the flow and sediment concentration process after the closure and operation of the Three Gorges Project from 2003 to 2009 are still in the adjustment stage, the regulation effect on the water and sediment from the Yangtze River Estuary has not been stable. Therefore, the measured flow and sediment concentration data of Datong hydrological station from 2009 to 2018 are selected as the upstream water and sediment inflow conditions in the next 20 years. The East China Sea model driven by eight main tidal components directly predicts the tidal dynamic process in the next 20 years. In addition, considering the relatively large area of the Yangtze River Estuary, the role of large-scale wind and wave in the mouth bar area cannot be ignored. Therefore, in the simulation and prediction of the next 20 years, the model considers the joint action of wind and wave fields. The large-scale wind field is provided by the monthly average wind field averaged by the multi-year wind data downloaded from the European Meteorological Center, and the large-scale wave field is provided by the Swan model combined with the wind data simulation. For average monthly flow of Datong from 2009 to 2018, see Fig. 6.

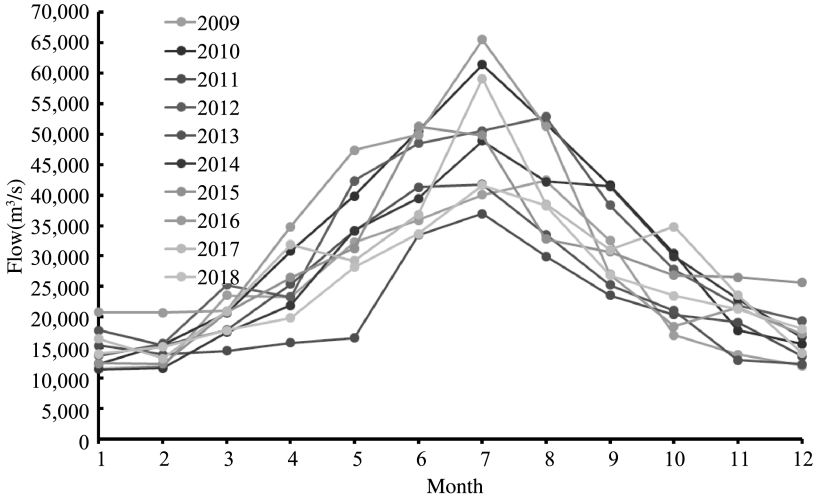

Fig. 6. Average monthly flow of Datong from 2009 to 2018.

4 Results and discussion

4.1 The Nanhui Shoal

From the field survey shown in Fig. 3, it can be proven that the Nanhui protection project effectively influenced the deposition process of the Nanhui Shoal from the year 2015 to the year 2016. And the deposition rates were relatively high not only within the Nanhui protection project, but also in the adjacent area. However from the next 20 years' stimulation in Fig. 7, the Nanhui Shoal is dominated by slight siltation compared with the measured current years' deposition rate, and the main siltation range is concentrated in the cover range of Nanhui protection project and there is slight scouring within the siltation area, but just scouring of nearly 1 m near some internal dams and external embankments.

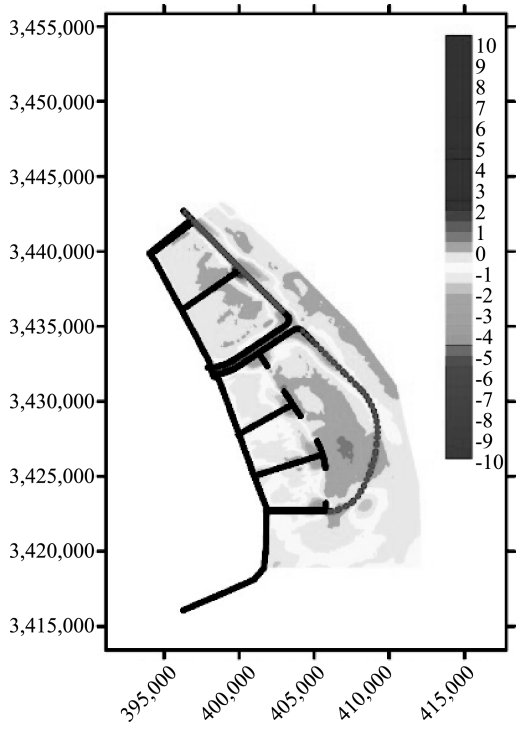

Fig. 7. Erosion and deposition prediction of Nanhui Shoal from 2019 to 2039.

4.2 The East Hengsha Shoal

From Fig. 4, it can be deduced that the submerged dike of the East Hengsha Shoal has contributed a lot to the siltation within the East Hengsha Shoal during the

three years from 2013 to 2016. From the long-term morphology stimulation in the next 20 years shown in Fig. 8, however, the scouring and silting characteristics of Hengsha east beach are directly related to the location characteristics of this area. This area is located in the ebb tide protection area of Hengsha silting promoting dike. During ebb tide, the backflow of the protection area causes a certain amount of back siltation, but during flood tide, the tidal beach is submerged and directly affected by the ocean tide and waves, and the sediment on the beach surface and bed surface is easy to start and resuspend. Therefore, although the sediment on Hengsha east beach is mainly silted, the siltation amplitude is not large.

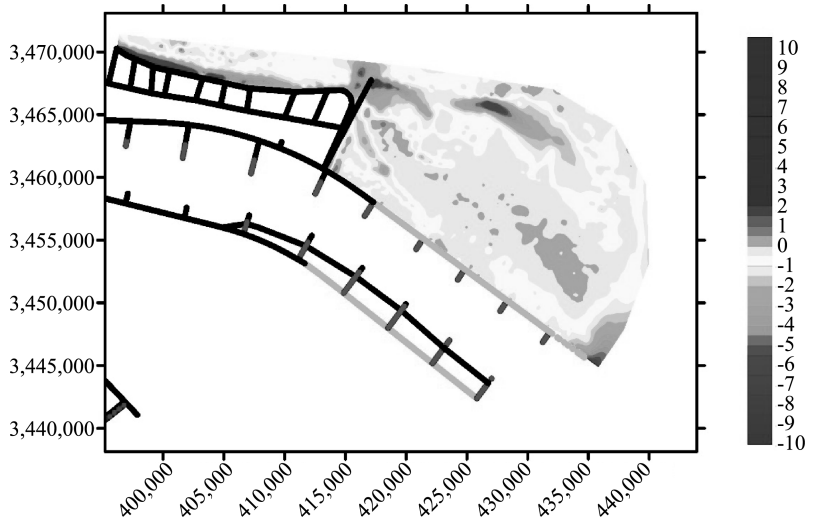

Fig. 8. Erosion and deposition prediction of Hengsha Shoal from 2019 to 2039.

4.3 The Qingcaosha Reservoir

As the field survey results shown in Fig. 5, the shoals or the submerged delta around the Qingcaosha Reservoir showed a trend of slight deposition during the period from 2007 to 2009. Then from the numerical stimulation of the next 20 years shown in Fig. 9, the Qingcaosha tidal flat is dominated by strong scouring trend, especially at the north embankment. The main siltation range exists in the cover of central sand head and south embankment buildings, but the siltation range is very small.

5 Conclusion

From the recent years' observation of the important tidal flat bathymetries, one regulation is clear that in the finite time around the establishment of the artificial

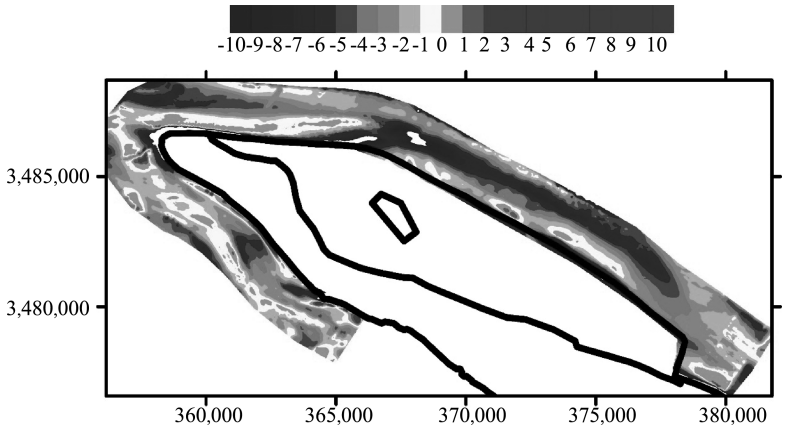

Fig. 9. Erosion and deposition prediction around the Qingcaosha reservoir from 2019 to 2039.

buildings, the influence of the human-made buildings weighs more in the geographical aspect of the estuarine than both the runoff and the currents, and have contributed to a general trend of siltation to the whole area. And from the entrance part of the estuary to the outside part of the estuary, the degree of deposition is decreased with the currents slowing down during the estuaries expansion.

However, from results calculated by the large-scale morphological stimulation in the next 20 years, as long as the new geographical equilibrium with the artificial buildings has emerged, the landform mechanism of the estuary is no longer influenced mainly by the human activity but by the sediment load from the runoff and the current from the ocean. This paper shows that in the near future, the upstream runoff with fewer sediment (due to the continuous decrease in upstream sediment measured in Datong station in recent years) will rebuild the estuarine geomorphology, resulting in strong scour among the tidal flat and the erosion extent will be stronger when the tidal flat is near the entrance of the estuarine and will become weaker when it is near the mouth of the estuary. Therefore, it is absolutely necessary and urgent to supervise the extent of the erosion before the artificial buildings in case of dangerous situations resulted from stronger scour in the future.

Acknowledgements

This study was supported by the National Natural Science Foundation of China (Nos. 51979096 and U2040203), and the Fundamental Research Funds for the Central Public Welfare Research Institutes, Nanjing Hydraulic Research Institute (YN912001).

References

Stanley, D.J., Warne, A.G., Worldwide initiation of Holocene marine deltas by deceleration of sea-level rise. Science (New York, NY), 1994,265(5169):228-231.

Sanchez-Arcilla, A., Jimenez, J.A., Valdemoro H.I. The Ebro delta: Morphodynamics and vulnerability. J Coast Res., 1998,14(3):754-772.

Stanley, D.J., Nile delta: Extreme case of sediment entrapment on a delta plainand consequent coastal land loss. Mar Geol., 1996,129(3-4):189-195.

Syvitski, J.P.M., Kettner, A.J., Overeem, I., et al. Sinking deltas due to human activities. Nat Geosci., 2009,2(10):681-686.

Eelkema, M., Wang, Z.B., Hibma, A., et al. Morphological effects of the eastern scheldt storm surge barrier on the ebb-tidal delta. Coast Eng J., 2013,55(3):26.

De Vriend, H.J., Wang, Z.B., Ysebaert, T., et al. Eco-morphological problems in the Yangtze Estuary and the western scheldt. Wetlands., 2011,31(6):1033-1042.

Ericson, J.P., Vorosmarty, C.J., Dingman, S.L., et al. Effective sea-level rise and deltas: Causes of change and human dimension implications. Glob Planet Change., 2006,50(1-2):63-82.

Blum, M.D., Roberts, H.H., Drowning of the Mississippi Delta due to insufficient sediment supply and global sea-level rise. Nat Geosci., 2009,2(7):488-491.

Yang, S.L., Milliman, J.D., Xu, K.H., et al. Downstream sedimentary and geomorphic impacts of the Three Gorges Dam on the Yangtze River. Earth-Sci Rev., 2014(138):469-486.

Roelvink, J.A., Coastal morphodynamic evolution techniques. Coast Eng., 2006,53(2-3):277-287.

Yang, H.F., Yang, S.L., Meng, Y., et al. Recent coarsening of sediments on the southern Yangtze subaqueous delta front: A response to river damming. Cont Shelf Res., 2018(155):45-51.

Lanzoni, S., Seminara, G. Long-term evolution and morphodynamic equilibrium of tidal channels. Journal of Geophysical Research: Oceans., 2002,107(C1):1-13.

Luan, H.L., Ding, P.X., Wang, Z.B., et al. Process-based morphodynamic modelling of the Yangtze Estuary at a decadal timescale: Controls on estuarine evolution and future trends. Geomorphology, 2017(290):347-364.

Cooper, N.J., Hooke, J.M., Bray, M.J. Predicting coastal evolution using a sediment budget approach: a case study from southern England. Ocean & Coastal Management, 2001,44(11-12):711-728.

French, J., Payo, A., Murray, B., et al. Appropriate complexity for the prediction

of coastal and estuarine geomorphic behaviour at decadal to centennial scales. Geomorphology, 2016(256):3-16.

Luo, X.X., Yang, S.L., Zhang, J. The impact of the Three Gorges Dam on the downstream distribution and texture of sediments along the middle and lower Yangtze River (Changjiang) and its estuary, and subsequent sediment dispersal in the East China Sea. Geomorphology, 2012(179):126-140.

Luan, H.L., Ding, P.X., Wang, Z.B., et al. Morphodynamic impacts of large-scale engineering projects in the Yangtze River delta. Coast Eng., 2018(141):1-11.

沈焕庭，潘定安. 长江河口潮流特性及其对河槽演变的影响. 华东师范大学学报(自然科学版),1979(1):131-144.

Li, Y., Li, X. Remote sensing observations and numerical studies of a super typhoon-induced suspended sediment concentration variation in the East China Sea. Ocean Modelling, 2016(104):187-202.

Yang, S.L., Milliman, J.D., Li, P., et al. 50,000 dams later: Erosion of the Yangtze River and its delta. Glob Planet Change, 2011,75(1-2):14-20.

Luo, X.X., Yang, S.L., Wang, R.S., et al. New evidence of Yangtze delta recession after closing of the Three Gorges Dam. Sci Rep., 2017(7).

Dai, Z., Liu, J.T., Wei, W., et al. Detection of the Three Gorges Dam influence on the Changjiang (Yangtze River) submerged delta. Sci Rep., 2014(4).

Yang, H.F., Yang, S.L., Xu, K.H., et al. Erosion potential of the Yangtze Delta under sediment starvation and climate change. Sci Rep., 2017(7).

Yang, S.L., Belkin, I.M., Belkina, A.I., et al. Delta response to decline in sediment supply from the Yangtze River: evidence of the recent four decades and expectations for the next half-century. Estuar Coast Shelf Sci., 2003,57(4):689-699.

Cayocca, F. Long-term morphological modelling of a tidal inlet: the Arcachon Basin, France. Coast Eng., 2001,42(2):115-142.

张飞，王义刚，黄惠明，等. 长江口主要水道洪季悬沙有效沉速分布研究,2011.

唐树涛，黄惠明，王义刚，等. 台风路径对长江口各汊道波高的影响. 水运工程，2019(1):48-54.

Process and reflection of the Yangtze River waterway regulation and development

Honglin Feng, Sensong Fang, Qiong Yang,
Pengpeng Jia, Wenwu Yang

Transport Planning and Research Institute, Ministry of Transport, Beijing, China. e-mail: fenghl@tpri.org.cn

Abstract: This paper reviews the status of Yangtze River waterway regulation since the 9th Five-Year Plan, and summarizes the major results and experiences of the waterway regulation and development. By analyzing the main problems facing the Yangtze River waterway, such as the inconsistent standards of the waterway sections, changes in water and sand conditions, and the requirements for the grand protection of the Yangtze River, the paper proposes countermeasures and suggestions such as strategies implementation, overall planning, collaborations strengthening and increase in research investment.

Keywords: Yangtze River waterway; Management and development; Experience and knowledge; Countermeasures and suggestions

1 Introduction

The Yangtze River waterway is a grand waterway transport corridor that runs through China's eastern, central and western regions and is known as the "Golden Waterway". It is considered a major national strategy to promote the Yangtze River Economic Belt development through the "Golden Waterway". The Yangtze River waterway management and development have achieved prominent results after years of research and practice. Practical experience has been accumulated on management rules, management philosophy, and development measures. This paper reviews and summarizes the course and experience of the regulation and development of the Yangtze River waterway, analyzes the main problems faced by the development of the Yangtze River waterway, and puts forward countermeasures and suggestions, hoping to provide reference for the regulation and development of the Yangtze River waterway.

2 Course of the Yangtze River waterway regulation and development

2.1 Before the 9th Five-Year Plan, the conditions of the upstream channel were preliminarily improved.

From the founding of the People's Republic of China to the 9th Five-Year Plan period, the waterway regulation projects in the upper reaches of the Yangtze River from Yibin to Lanjiatuo, from Lanjiatuo to Chongqing and from Chongqing to Yichang were mainly implemented, with a total of more than 150 beach risks and 115 sporadic obstacles cleared, and the upstream waterway conditions were preliminarily improved. The channel below Yichang was mainly navigable by using the natural water depth, and maintenance measures were mainly taken in some river sections to ensure safety and no impediment. From the founding of the People's Republic of China to the 9th Five-Year Plan, 236 million yuan was invested in the construction of the Yangtze River waterway.

2.2 During the 9th Five-Year Plan and the 10th Five-Year Plan, the regulation projects of the middle and lower reaches of the Yangtze River waterway started.

Since the 9th Five-Year Plan, marked by the comprehensive treatment project of Jiepai reach in the middle reaches of the Yangtze River, the construction of the channel in the middle and lower reaches of the Yangtze River started. During the 9th Five-Year Plan and the 10th Five-Year Plan, projects such as the comprehensive regulation of Jiepai river section, the regulation of Taiziji waterway, the salvage of sunken ships in Madang waterway, the regulation of Zhangjiazhou South Port waterway, the regulation of Nianziwan river section and desilting emergency were successively implemented, which effectively alleviated the tension of "fighting dry water" in the middle reaches of the Yangtze River every year. The first and second phases of the Yangtze Estuary Deepwater Channel Regulation Project have been completed, and the channel water depth has been increased from 7 m to 10 m, which can meet the navigation requirements of 30,000 ton seagoing ships entering and leaving the Yangtze Estuary all day. Combined with the construction of the Three Gorges water control project, the submerged reconstruction project of channel facilities in the reservoir area has been implemented, and the channel conditions in the reservoir area have been improved accordingly. During the 9th Five-Year Plan and the 10th Five-Year Plan, 7.354 billion yuan was invested in the main channel of the Yangtze River, of which 6.02 billion

yuan was invested in the regulation of the deepwater channel of the Yangtze River Estuary.

2.3 During the 11th Five-Year Plan period, waterway regulation entered a large-scale stage.

During the 11th Five-Year Plan period, the investment in the main channel of the Yangtze River was further increased and began to enter the stage of large-scale governance. The upstream has successively implemented the three-level channel regulation projects from Yibin to Luzhou and Luzhou to Chongqing, the reef-blasting project in Fuling-Tongluoxia reach and the Letianxi channel regulation project between two dams. In the middle reaches, the waterway regulation projects of Zhijiang-Jiangkou, Shashi, Majiazui, Zhoutian, Ouchikou, Yaojian, Jiayu-Yanziwo, Daijiazhou and Guniusha have been implemented successively. The downstream has focused on the regulation of Dongliu, Anqing, Tuqiao, Heishazhou, Kou'anzhi, Shuangjiansha and other waterways, and completed the third phase of the regulation of the Yangtze Estuary deep-water channel and the upward extension to Taicang project. During the 11th Five-Year Plan period, the investment in the main channel of the Yangtze River is 9.064 billion yuan, including 5.43 billion yuan for the regulation of the deepwater channel of the Yangtze Estuary.

2.4 During the 12th Five-Year Plan period, waterway regulation was comprehensively accelerated.

In 2011, the State Council issued the guiding opinions on comprehensively accelerating the development of inland water transportation such as the Yangtze River, and the construction and development of the main channel of the Yangtze River faced the opportunity of comprehensively accelerating the development. In the upstream, the first phase of the project the fluctuating backwater area in the Three Gorges Reservoir and the channel regulation project of Letianxi section between the Three Gorges and Gezhouba dams have been implemented, which further improved the channel conditions at the tail of the Three Gorges Reservoir and between the Three Gorges and Gezhouba dams. Focusing on the regulation of Jingjiang river channel, the middle reaches have successively implemented channel regulation projects such as Yichang-Changmenxi Phase Ⅰ, Jingjiang-Changmenxi-Xiongjiazhou Section, Jiepai Phase Ⅱ, Chibi-Panjiawan, Wuqiao Waterway, Tianxingzhou, Huguang-Luohuzhou and Xinzhou-Jiujiang sections, significantly improving the navigation conditions of the middle reaches. Focusing on the construction project of 12.5 m deepwater channel below Nanjing, the downstream has successively implemented the waterway regulation

projects such as Manan, Dongliu Phase Ⅱ, Liyushan and Dongbei waterway, so as to further consolidate and improve the downstream waterway conditions. During the 12th Five-Year Plan period, the investment in the main channel of the Yangtze River was 16.2 billion yuan, including 520 million yuan in the Yangtze River Estuary.

2.5 During the 13th Five-Year Plan period, the systematic management of navigation channels and the construction of green ecological navigation channels have been coordinated.

During the 13th Five-Year Plan period, under the guidance of the development strategy of the Yangtze River Economic Belt, with the goal of comprehensively improving the function of the golden waterway of the Yangtze River, the systematic management of trunk waterways has been accelerated and the construction of green ecological waterways has been actively promoted. Relying on the implementation of the waterway regulation project of Jingjiang river section and the 6 m deep waterway regulation project from Wuhan to Anqing section, the research and practice of the combination of waterway regulation and ecological protection and restoration have been comprehensively promoted, which has promoted the coordinated development of waterway construction and ecological environment, and the implementation of the national strategy of the Yangtze River Economic Belt. During the 13th Five-Year Plan period, the investment in the main channel of the Yangtze River is 7.5 billion yuan.

Up to now, the navigation conditions of the Yangtze River waterway have been significantly improved. The minimum maintenance water depth of the channel from Yibin to Chongqing in the upstream is raised to 2.9 m, the minimum maintenance water depth from Yichang to Wuhan in the middle reaches is raised to 3.5－4.2 m, the minimum maintenance water depth from Wuhan to Anqing is raised to 6.0 m, and the 12.5 m deepwater channel below Nanjing is fully connected. 3,000 tonnage ships can go directly to Chongqing, 10,000 ton ships can go directly to Wuhan, and 50,000 ton seagoing ships can go directly to Nanjing. In 2020, the freight volume of the Yangtze River waterway will reach 3.06 billion tons, undertaking more than 80% of the transportation of iron ore and electric coal, 90% of the foreign trade container transportation required by the areas along the river. It plays an important supporting role in the construction of comprehensive three-dimensional transportation network of the Yangtze River Economic Belt and the economic and social development along the river. For the minimum maintenance scale of the Yangtze River trunk channel, see Table 1. For development of freight volume in the Yangtze River waterway from 2015 to 2020, see Fig. 1.

Table 1 The minimum maintenance scale of the Yangtze River trunk channel.

reach	mileage (km)	minimum maintenance standard scale (depth × width × bending radius) (m)	guarantee rate
Shuifu—Yibin	30	1.8×40×320	98%
Yibin—Chongqing	384	2.9×50×560	98%
Chongqing—Fuling	112.4	3.5×100×800	98%
Fuling—Yichang Xialinjiangping	558.6	4.5×(100-150)×(750-1,000)	98%
Yichang Xialinjiangping—Jingzhou Fourth Wharf	137	3.5×(100-150)×750	98%
Jingzhou Fourth Wharf—Yueyang Chenglingji	248	3.8×150×750	98%
Yueyang Chenglingji—Wuhan	227.5	4.2×150×1,000	98%
Wuhan—Wuhu	607.2	6.0×200×1,050	98%
Wuhu—Nanjing	101.3	9.0×500×1,050	98%
Nanjing—the Yangtze River Estuary	431.6	12.5×(350-500)×(1,050-1,500)	95%

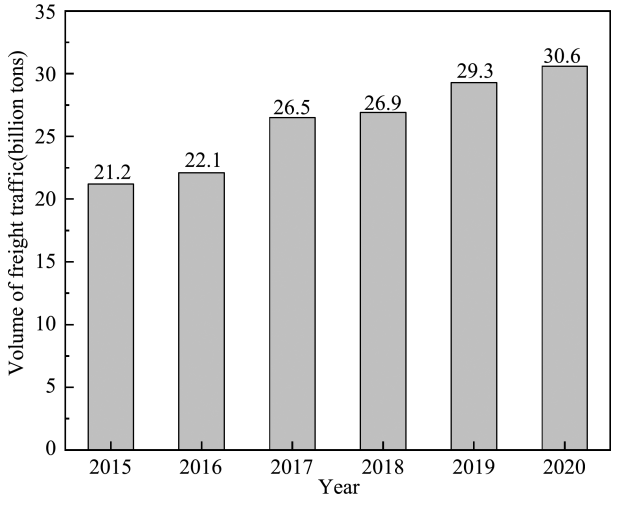

Fig. 1. Development of freight volume in the Yangtze River waterway from 2015 to 2020.

3 Main experience and knowledge

3.1 The Yangtze River waterway is in the stage of optimization and improvement of system governance.

With a great deal of practice in waterway regulation engineering, the construction concept of Yangtze River waterway regulation has improved, which gradually transforms from single beach regulation into systematic study and management of long

reaches. At the same time, the Yangtze River waterway and the water conservancy departments control water jointly, and they have effectively responded to the changes of river regime and channel pattern in the middle and lower reaches caused by the water storage operation of the Three Gorges Project.

In recent years, the waterway management of the Jingjiang River section, the 12.5 m deepwater channel at lower reaches of Nanjing, and the 6 m water depth channel from Wuhan to Anqing have achieved satisfactory results, improving the navigation capacity of the Yangtze River waterway. The theoretical level, depth of understanding, and research methods of channel regulation in the Yangtze River have been comprehensively improved, a number of key technologies for channel regulation have been formed, a number of new materials, new structures, and new processes have been explored, and rich experience in channel regulation has been accumulated. The scientific research has gradually expanded, and the construction technology has been continuously improved, and a number of talent teams have also been trained, which has laid a solid foundation for further implementing higher-level governance, breaking the bottleneck, and optimizing and improving the scale of the Yangtze River waterway.

3.2 The regulation of the Yangtze River waterway must follow the natural law of the river channel, grasp the opportunity and make good use of the situation.

The purpose of channel regulation and development is to rectify the navigation-obstructing hazardous rapids and improve the navigation conditions of ships. There are certain natural mechanisms in the transportation of water and sediment, and the formation of riverbed in natural rivers. Both river channel and channel regulation should follow the river characteristics and the laws of river channel evolution. The Yangtze River is a large natural river. The characteristics of the upper, middle and lower reaches of the river are different, and the water and sediment conditions and river evolution are complex. In recent years, the construction of the Three Gorges and a series of other hydropower projects in its upper reaches has had a new and sustainable impact on the incoming water and sediment conditions of the Yangtze River. The Yangtze River waterway will still be in the process of adjustment and change for a long time. The practice of channel regulation engineering shows that we need to constantly study and understand the water and sediment situations and laws of river channel change of the Yangtze River. Grasping the opportunity, conforming to the river regime and making good use of the situations are the key to the success of the Yangtze River waterway regulation.

3.3 The management and development of the Yangtze River waterway should adhere to the principle of comprehensive utilization of water resources, and adhere to unity in water control, overall consideration and comprehensive strategy.

The Yangtze River has comprehensive functions such as ecological conservation, flood control, power generation, water supply and irrigation, navigation and tourism. The regulation and development of the Yangtze River waterway is not only related to the development of the shipping and the economic and industrial development of the Yangtze River basin, but also related to flood control, ecological environmental protection and other water-related rights and interests. As an important part of the comprehensive development and utilization of water resources, shipping should always coordinate the relationship with the various tasks of water resources development and utilization, and the rights and interests of relevant water-related departments.

3.4 The construction and operation of the Three Gorges and other large hydropower projects in the upper reaches have both advantages and disadvantages on the Yangtze River waterway, so it is necessary to actively study those projects and take appropriate control measures.

In the upper reaches of the Yangtze River, large-scale water conservancy and hydropower projects such as the Three Gorges, Xiangjiaba, Xiluodu and Wudongde have been constructed and put into operation. These water conservancy projects can increase the flow of the channel in the dry season, increase the channel depth in the shoal, and reduce the incoming sediment, which can reduce the sedimentation in the shoal in the flood season, so as to create favorable conditions for the maintenance of the Yangtze River waterway and further improve the channel scale. However, water conservancy projects have also brought adverse effects such as release of clear water, shoal brushing and silt water troughs, local riverbed undercut, water level drop, and unstable shoal and trough patterns. Research and practice in recent years have shown that the upper reaches of the Yangtze River are large mountain rivers with stable river conditions, small changes in scouring and silting between years, and the riverbed is dominated by sand and pebbles. Rapids can be regulated by a combination method of regulation and dredging, and in combination with the drain flow of upstream water conservancy to increase water supply, the channel dimension can be increased. The middle and lower reaches of the Yangtze River are characterized by plain alluvial rivers. In view of the unfavorable influences such as release of clear water, the channel management has formed the idea of "guarding the beach, stabilizing the trough, and

integrating dredging and regulation". On the basis of controlling the key water level and guarding the important beaches, the scale of the channel can be improved through regulation and dredging to achieve the goal of channel management.

3.5 The implementation of the Yangtze River Economic Belt strategy requires waterway governance to implement the construction concepts of ecological priority and green development.

Relying on the golden waterway of the Yangtze River to advance the Yangtze River Economic Belt is one of the major regional strategies that China is implementing. Xi Jinping has repeatedly emphasized that the restoration of the ecological environment of the Yangtze River should be placed in an overwhelming position, that we should focus on large-scale protection instead of large-scale development and adhere to the path of ecological priority and green development. These emphasized contents put forward new and higher requirements for the scientific governance and appropriate development of the Yangtze River waterway. During the 13th Five-Year Plan period, the Yangtze River waterway vigorously promoted the construction of ecological channels in accordance with the national strategic requirements, and organically combined channel regulation and ecological restoration. In the practice of waterway system governance projects in Jingjiang, Wuhan and Anqing, the research and application of eco-friendly structures and processes have been strengthened, and ecological and environmental protection measures such as ecological wetlands, ecological conservation area construction and aquatic ecological monitoring have been incorporated, which has promoted green, coordinated and sustainable development of channel governance and the ecological environment of the Yangtze River.

4 Existing problems

After large-scale system governance, the navigation capacity and service level of the Yangtze River waterway have been significantly improved. However, compared with the national strategic requirements of the Yangtze River Economic Belt, the following problems still exist:

Firstly, there are many ecologically sensitive areas in the upper reaches of the Yangtze River. The velocity of channel regulation in the upper section of Chongqing is slow, and the channel level is low. During the dry season, a large number of 2,000-3,000 tonnage ships need load reduction for general navigation, which is inconsistent with the navigation standards of the entire Yangtze River waterway.

Secondly, the middle reaches of the Yangtze River are restricted by factors such as

riverbed evolution and urban flood control. The standard of the channel from Yichang to Wuhan is not connected with the upper and lower reaches, because of the shape of the channel with deep depth in upper Yichang and lower Wuhan, but shallow depth from Yichang to Wuhan. Therefore, 5,000 tonnage ships are forced to transfer to reduce load, which restricts the overall advantages and benefits of Yangtze River shipping.

Thirdly, the Yangtze River waterway conditions in the lower reaches are not stable enough, and the maintenance pressure after the completion and operation of the 12.5-meter deepwater waterway at the Yangtze River Estuary and lower reaches of Nanjing has become increasingly heavy. The annual silting volume of the Yangtze River Estuary is nearly 60 million cubic meters.

5 Countermeasures and suggestions

(1) Take overall planning to promote the unification of the standards of the Yangtze River waterway in different reaches.

In accordance with the requirements of the upper reaches of the Yangtze River combined with water replenishment of stepped hydro-junction and ecological protection, focus on promoting the construction of the ecological waterway from Yibin to Chongqing, and speed up the improvement of waterway conditions. In the middle reaches, the Three Gorges-Gezhouba Reservoir will be optimized and dispatched, and measures such as integration of regulation and dredging, equal emphasis on construction and maintenance, and ecological environmental protection will be adopted. Focus on the implementation of the second phase of Jingjiang channel management project, and gradually increase the water depth of the channel to 4.5 m. The lower reaches continue to strengthen the protection of key beaches, shape local excellent beach and trough forms, and focus on ensuring the safe and stable operation of the 12.5 m deep-water channel through measures such as sediment reduction and erosion prevention.

(2) Actively coordinate and strive for the support of water conservancy and environmental protection departments.

Adhere to unity in water control, strengthen communication and coordination with water conservancy and hydropower, ecological and environmental protection, natural resources, agriculture and fishery and other departments, and promote the establishment of comprehensive utilization of water resources and comprehensive dispatching mechanism of stepped hydro-junction. Comply with the requirements of the Yangtze River Protection Law. For the channel regulation projects that really need to be implemented in the red line of ecological protection, nature reserves and important habitat waters of aquatic organisms, it is necessary to handle relevant procedures according to law, strive for the support of rele-

vant departments, strictly implement environmental protection measures, and accelerate the preliminary work of key construction projects of the Yangtze River waterway.

(3) Increase investment to promote the green and sustainable development of the Yangtze River waterway.

In the planning, construction, maintenance and management of the channel, we should fully integrate the ecological and green concepts, further increase capital and research investment, and coordinate the relationship between the regulation of the Yangtze River waterway and the needs of economic and social development and the carrying capacity of the ecological environment. In addition, we should constantly improve the ecological and green level of design and construction in the process of channel construction and maintenance, actively participate in ecological restoration and environmental protection, improve the level of channel ecological monitoring and management, and promote the green and sustainable development of the Yangtze River waterway.

References

Feng, H.L., 2017. Research on revision of development plan of Yangtze River waterway. Beijing: Transport Planning and Research Institute, Ministry of Transport: 42-51.

He, C. J., 2015. Waterway regulation ideas, countermeasures and initial effects for Jingjiang reach in middle Yangtze River. Port & Waterway Engineering, 500(2): 173-181.

Liu, H. H., Liu, Q., Lei, G. P., et al., 2020. Research progress and prospect of ecological waterway technology in Yangtze River. Yangtze River, 51(1): 11-15.

Zhang, Y., Liu, X.Q., 2019. Research on the transition of the Yangtze River waterway to green and low-carbon during the 13th Five-Year Plan. China Water Transport (9): 37-38.